THE NEURONAL FUNCTIONS OF EF-HAND Ca^{2+}-BINDING PROTEINS

2nd EDITION

EDITED BY: Michael R. Kreutz, José R. Naranjo, Karl-Wilhelm Koch and Beat Schwaller

PUBLISHED IN: Frontiers in Molecular Neuroscience

frontiers Research Topics

ISSN 1664-8714
ISBN 978-2-88945-003-9
DOI 10.3389/978-2-88945-003-9

About Frontiers

Frontiers is more than just an open-access publisher of scholarly articles: it is a pioneering approach to the world of academia, radically improving the way scholarly research is managed. The grand vision of Frontiers is a world where all people have an equal opportunity to seek, share and generate knowledge. Frontiers provides immediate and permanent online open access to all its publications, but this alone is not enough to realize our grand goals.

Frontiers Journal Series

The Frontiers Journal Series is a multi-tier and interdisciplinary set of open-access, online journals, promising a paradigm shift from the current review, selection and dissemination processes in academic publishing. All Frontiers journals are driven by researchers for researchers; therefore, they constitute a service to the scholarly community. At the same time, the Frontiers Journal Series operates on a revolutionary invention, the tiered publishing system, initially addressing specific communities of scholars, and gradually climbing up to broader public understanding, thus serving the interests of the lay society, too.

Dedication to Quality

Each Frontiers article is a landmark of the highest quality, thanks to genuinely collaborative interactions between authors and review editors, who include some of the world's best academicians. Research must be certified by peers before entering a stream of knowledge that may eventually reach the public - and shape society; therefore, Frontiers only applies the most rigorous and unbiased reviews.
Frontiers revolutionizes research publishing by freely delivering the most outstanding research, evaluated with no bias from both the academic and social point of view.
By applying the most advanced information technologies, Frontiers is catapulting scholarly publishing into a new generation.

What are Frontiers Research Topics?

Frontiers Research Topics are very popular trademarks of the Frontiers Journals Series: they are collections of at least ten articles, all centered on a particular subject. With their unique mix of varied contributions from Original Research to Review Articles, Frontiers Research Topics unify the most influential researchers, the latest key findings and historical advances in a hot research area! Find out more on how to host your own Frontiers Research Topic or contribute to one as an author by contacting the Frontiers Editorial Office: **researchtopics@frontiersin.org**

THE NEURONAL FUNCTIONS OF EF-HAND Ca^{2+}-BINDING PROTEINS

2nd Edition

Topic Editors:
Michael R. Kreutz, Leibniz Institute for Neurobiology, Germany
José R. Naranjo, Centro Nacional de Biotecnología/Consejo Superior de Investigaciones Científicas, Spain
Karl-Wilhelm Koch, Carl von Ossietzky University Oldenburg, Germany
Beat Schwaller, University of Fribourg, Switzerland

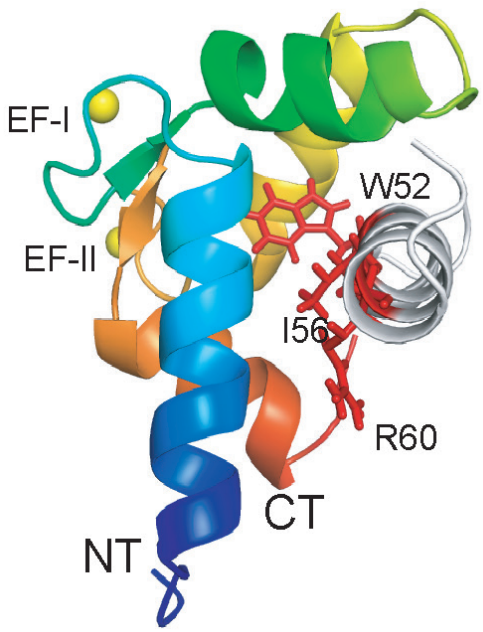

Ca^{2+} signaling in neurons is characterized by highly restricted and dynamic gradients called Ca^{2+} waves, spikes, transients and puffs depending upon their corresponding spatial and temporal features. Based on this strict segmentation the Ca^{2+} ion provides a versatile basis for complex signaling in neuronal subcompartments with a spatial resolution of micro- and nanodomains. The multitude of Ca^{2+}-regulated processes requires specialized downstream processing machinery, translating the Ca^{2+} signal into alterations of cellular processes. The broad range of different Ca^{2+}-triggered phenomena in neurons, ranging from neurotransmission to gene expression, is reflected by the existence of a multitude of different Ca^{2+}-binding proteins (CaBPs) from which numerous belong to the EF-hand super-family. EF-hand proteins can be subdivided into Ca^{2+}

buffer and Ca^{2+} sensor proteins. Whereas the first group has a very high affinity for Ca^{2+}, exhibits little conformational change in the Ca^{2+}-bound state and is thought to mainly chelate Ca^{2+}, the second group has a lower affinity for Ca^{2+} and shows considerable conformational changes upon Ca^{2+}-binding, which usually triggers a target interaction. Neuronal calcium sensor (NCS) proteins and the related Caldendrin/CaBP/Calneuron (nCaBPs) proteins are members of this latter group. They resemble the structure of their common ancestor Calmodulin (CaM) with four EF-hand Ca^{2+}-binding motifs, of which not all are functional. However, despite their structural homology with CaM, NCS as well as nCaBPs are quite diverse in amino acid sequence. It is therefore surprising that relatively few binding partners have been identified that are not CaM targets and this raises the question of the specificity and function of these interactions. In terms of function, binding of NCS and nCaBP has frequently different consequences than binding of CaM, which substantially increases the versatility of the Ca^{2+} tool kit. The general idea of this special issue is to provide an overview on the function of neuronal EF-hand calcium-binding proteins in health and disease. But we will not just provide a mere collection of articles to stress the function of each protein. The issue will mainly deal with emerging concepts on Ca^{2+}-signaling/buffering mediated by EF-hand Ca^{2+}-binding proteins. This includes questions like features that define the functional role of a EF-hand calcium sensor in neurons, the conditions that make physiological relevance of a given interaction of a CaBP with its target plausible, the emerging synaptic role of these proteins, and mounting evidence for their role in the regulation of protein trafficking. Structural aspects and biophysical studies will be covered. Another aspect will be the role of CaBPs in brain disease states. This aspect includes studies showing that CaBPs are targets of drugs in clinical use, studies showing that expression levels of calcium-binding proteins are frequently altered in brain disease states as well as reports on mutations in EF-hand calcium sensors linked to human disease.

Citation: Kreutz, M. R., Naranjo, J. R., Koch, K- W., Schwaller, B., eds. (2016). The Neuronal Functions of EF-hand Ca^{2+}-binding Proteins, 2nd Edition. Lausanne: Frontiers Media.
doi: 10.3389/978-2-88945-003-9

Table of Contents

frontiers in
MOLECULAR NEUROSCIENCE

EDITORIAL
published: 11 September 2012
doi: 10.3389/fnmol.2012.00092

The neuronal functions of EF-hand Ca^{2+}-binding proteins

Michael R. Kreutz[1]*, Jose R. Naranjo[2], Karl-Wilhelm Koch[3] and Beat Schwaller[4]

[1] *Leibniz-Institute for Neurobiology, Magdeburg, Germany*
[2] *Centro Nacional de Biotecnología, Consejo Superior de Investigaciones Científicas, Madrid, Spain*
[3] *Institute of Biology and Environmental Science, Carl von Ossietzky University Oldenburg, Oldenburg, Germany*
[4] *Department of Medicine, University of Fribourg, Fribourg, Switzerland*
**Correspondence: kreutz@ifn-magdeburg.de*

Edited by:
Jochen C. Meier, Max Delbrück Center for Molecular Medicine, Germany

Reviewed by:
Jochen C. Meier, Max Delbrück Center for Molecular Medicine, Germany

Neuronal Ca^{2+} signaling exhibits highly restricted and dynamic gradients called Ca^{2+} waves, spikes, transients, and puffs depending upon their corresponding spatial and temporal features. The central role of Ca^{2+} in cellular physiology of neurons is based on a Ca^{2+}-signaling toolkit that assembles intracellular signaling systems with different spatial and temporal dynamics (Berridge, 2000). The cytosolic Ca^{2+} concentration is tightly regulated by binding and chelation of the ion by various Ca^{2+}-binding proteins (CaBPs) and by transport of the ion across plasma and intracellular membranes. The complex regulation of cytosolic Ca^{2+} concentrations is the subject of an increasing number of investigations, because this regulation is intimately linked to the function of Ca^{2+} in neurotransmitter release, synaptic plasticity, neurosensory signaling, activity-dependent gene transcription, intracellular trafficking, and many other cellular processes. The multitude of Ca^{2+}-regulated processes requires specialized downstream processing machinery, translating the Ca^{2+} signal into alterations of cellular functions. It is generally believed that the versatile basis for the complex signaling in micro- and nanodomains of neuronal subcompartments is provided by the existence of a multitude of different CaBPs from which numerous belong to the EF-hand super-family. EF-hand proteins are traditionally subdivided into Ca^{2+} buffer and Ca^{2+} sensor proteins. This distinction is however not really valid, because Ca^{2+}-binding to EF-hand proteins can serve both functions, even at the same time. Nonetheless, whereas the first group is characterized by a rather high affinity for Ca^{2+}, exhibits little conformational change upon Ca^{2+}-binding and is thought to mainly chelate Ca^{2+}, the second group has a somewhat lower affinity for Ca^{2+} (often in the 1–10 μM range) and shows considerable conformational changes upon Ca^{2+}-binding, which usually triggers a target interaction.

Members of the latter group belong either to the Neuronal calcium sensor (NCS) proteins or the related Caldendrin/CaBP/Calneuron (nCaBPs) family. All of these proteins resemble to a varying degree to the structure of their common ancestor Calmodulin (CaM), but they are quite diverse in amino acid sequence in comparison to CaM. It is therefore surprising that relatively few binding partners for NCS/nCaBP proteins have been identified that are not also CaM targets and this raises the question on the specificity and function of these interactions. Interestingly, binding of target proteins to NCS proteins and nCaBP has frequently different consequences than binding to CaM, which substantially increases the versatility of the Ca^{2+} signaling toolkit. The general idea of this special issue was to provide an overview on the function of neuronal EF-hand CaBPs in health and disease. The issue contains reviews that summarize the state-of-the-art in the field, as well as experimental and theoretical papers dealing with emerging concepts on Ca^{2+}-signaling/buffering mediated by EF-hand CaBPs. Questions like which features define the functional role of a EF-hand Ca^{2+} sensor in neurons, the conditions under which a given interaction of a CaBP with its target is of physiological relevance, the emerging synaptic role of these proteins, and mounting evidence for their role in the regulation of protein trafficking are covered. Structural aspects and biophysical studies are included and provocative new ideas based on numerical modeling are part of this issue. Another interesting aspect covered in the research topic is the emerging role of CaBPs in brain disease states. Several papers have shown that CaBPs are targets of drugs in clinical use, that expression levels of CaBPs are frequently altered in brain disease states, and more recently reports on mutations in EF-hand Ca^{2+} sensors linked to human disease were published. We want to thank all authors for the high quality of the papers that they have submitted and the efforts that they have made to provide an excellent overview of this interesting field. It was a pleasure to edit this research topic.

REFERENCE

Berridge, M. J., Lipp, P., and Bootman, M. D. (2000). The versatility and universality of calcium signaling. *Nat. Rev. Mol. Cell Biol.* 1, 11–21.

Received: 22 August 2012; accepted: 23 August 2012; published online: 11 September 2012.
*Citation: Kreutz MR, Naranjo JR, Koch K-W and Schwaller B (2012) The neuronal functions of EF-hand Ca^{2+}-binding proteins. Front. Mol. Neurosci. **5**:92. doi: 10.3389/fnmol.2012.00092*

frontiers in
MOLECULAR NEUROSCIENCE

GENERAL COMMENTARY
published: 02 April 2012
doi: 10.3389/fnmol.2012.00041

Neuronal calcium sensor proteins – recognizing a face in a crowd

Robert H. Kretsinger*

University of Virginia, Charlottesville, VA, USA
**Correspondence: rhk5i@virginia.edu*

A commentary on

Molecular structure and target recognition of neuronal calcium sensor proteins
by Ames, J. B., Lim, S., and Ikura, M. (2012). *Front. Mol. Neurosci.* 5:10. doi: 10.3389/fnmol.2012.00010

Ames, Lin, and Ikura in "Molecular structures and target recognition of neuronal calcium sensor proteins" describe the wide range of functions performed by the neuronal calcium sensor proteins in various nervous tissues. These NCS proteins are closely related in amino acid sequence and comprise 1 of over 70 subfamilies of proteins that contain 2–12 EF-hands. The N-termini of the NCS's are myristoylated and in their apo-forms this hydrophobic tail is discretely tucked into a cavity that differs among recoverin, NCS1, and GCAP1 – all of whose solutions structures have been determined by nuclear magnetic resonance spectroscopy. Ames et al. conclude that "Ca^{2+} induced extrusion of the myristoyl group exposes unique hydrophobic binding sites in each protein that in turn interact with distinct target proteins."

The calci-structures of seven NCS's, two with peptides from their respective targets bound, clearly revealed that the calci-structures differ significantly from one another and from their respective apo-structures. Therein lie their specificities for diverse targets within various cells of the nervous system. The EF-hands 1, 2 and EF-hands 3, 4 retain their approximate canonical shapes and relationships; however, the binding cavities between the two pairs of EF-hands vary to suit their chosen targets. These NCS structures reveal how small differences in amino sequences of close homologs can be amplified to major changes in cell function.

Received: 02 March 2012; accepted: 18 March 2012; published online: 02 April 2012.
*Citation: Kretsinger RH (2012) Neuronal calcium sensor proteins – recognizing a face in a crowd. Front. Mol. Neurosci. **5**:41. doi: 10.3389/fnmol.2012.00041*

frontiers in
MOLECULAR NEUROSCIENCE

REVIEW ARTICLE
published: 21 February 2012
doi: 10.3389/fnmol.2012.00009

Evolution and functional diversity of the Calcium Binding Proteins (CaBPs)

Lee P. Haynes*, Hannah V. McCue and Robert D. Burgoyne

The Physiological Laboratory, Department of Cellular and Molecular Physiology, Institute of Translational Medicine, University of Liverpool, Liverpool, UK

Edited by:
Karl-Wilhelm Koch, Carl von Ossietzky University Oldenburg, Germany

Reviewed by:
Michael R. Kreutz, Leibniz-Institute for Neurobiology, Germany
Karl H. Braunewell, Southern Research Institute, USA

****Correspondence:***
Lee P. Haynes, The Physiological Laboratory, Department of Cellular and Molecular Physiology, Institute of Translational Medicine, University of Liverpool, Crown Street, Liverpool L69 3BX, UK.
e-mail: leeh@liv.ac.uk

The mammalian central nervous system (CNS) exhibits a remarkable ability to process, store, and transfer information. Key to these activities is the use of highly regulated and unique patterns of calcium signals encoded by calcium channels and decoded by families of specific calcium-sensing proteins. The largest family of eukaryotic calcium sensors is those related to the small EF-hand containing protein calmodulin (CaM). In order to maximize the usefulness of calcium as a signaling species and to permit the evolution and fine tuning of the mammalian CNS, families of related proteins have arisen that exhibit characteristic calcium binding properties and tissue-, cellular-, and sub-cellular distribution profiles. The Calcium Binding Proteins (CaBPs) represent one such family of vertebrate specific CaM like proteins that have emerged in recent years as important regulators of essential neuronal target proteins. Bioinformatic analyses indicate that the CaBPs consist of two subfamilies and that the ancestral members of these are CaBP1 and CaBP8. The CaBPs have distinct intracellular localizations based on different targeting mechanisms including a novel type-II transmembrane domain in CaBPs 7 and 8 (otherwise known as calneuron II and calneuron I, respectively). Recent work has led to the identification of new target interactions and possible functions for the CaBPs suggesting that they have multiple physiological roles with relevance for the normal functioning of the CNS.

Keywords: calcium, Calcium Binding Protein, bioinformatics, protein evolution, protein targeting, protein-protein interaction

INTRODUCTION

Communication between neurons lies at the heart of abstract higher level cognitive processes including memory acquisition, learning, and complex reasoning. Fundamental to the mechanism by which all mammalian neurons communicate is intracellular calcium signaling (Berridge, 1998; Lohmann, 2009). Complex patterns of spatial and temporal calcium signals drive alterations in synaptic plasticity and neuronal gene expression which in turn affect neuronal architecture and connectivity to influence higher brain function (Catterall and Few, 2008; Greer and Greenberg, 2008). At the single neuron level, unique pre- and post-synaptic calcium signals generated by the opening of plasma membrane (PM) voltage sensitive- or ligand gated-ion channels are initially decoded by families of small calcium sensing proteins that exhibit distinct calcium binding characteristics in combination with specific patterns of cellular expression and sub-cellular localization (Haeseleer et al., 2000; Burgoyne and Weiss, 2001; Burgoyne et al., 2004; Burgoyne, 2007). Calcium binding typically elicits a conformational switch in the sensor (Haynes and Burgoyne, 2008; Ames and Lim, 2011) which in turn permits association with specific downstream effectors to modulate intracellular signaling cascades and ultimately neuronal activity and local synaptic structure.

In mammals, the largest class of calcium sensing proteins are those belonging to the calmodulin (CaM) superfamily that is defined by the EF-hand calcium binding motif (Kawasaki et al., 1998). CaM is expressed in all plants and animals and exerts essential functions in many aspects of normal cellular physiology (Klee et al., 1980). One CaM-related sub-family of calcium sensors, the Calcium Binding Proteins or CaBPs, has recently been shown to have co-evolved with vertebrate animals (McCue et al., 2010a). The CaBPs share a similar domain organization with CaM and have four EF-hand motifs (Haeseleer et al., 2000; Mikhaylova et al., 2006) however, they exhibit significant sequence divergence from their common ancestor and this is reflected in unique structural and functional properties (McCue et al., 2010b; Mikhaylova et al., 2011). The CaBPs are enriched in neuronal tissues where they have been shown to act as important regulators of key calcium influx channels. Coupled to their vertebrate specific expression profile the available evidence implicates CaBPs specifically as mediators of central nervous system (CNS) behavior in higher animals. Perhaps not unexpectedly members of the CaBP family regulate target effectors in common with CaM however, in every instance thus far examined there has been no detectable redundancy and CaBP target regulation appears distinct to that exerted by CaM (Lee et al., 2002; Haynes et al., 2004; Kinoshita-Kawada et al., 2005; Zhou et al., 2005; Tang et al., 2007; Li et al., 2009; Findeisen and Minor, 2010; Minor and Findeisen, 2010; Few et al., 2011; Oz et al., 2011). The importance and specificity of CaBP function is further highlighted by the distinct phenotypes exhibited by CaBP4 and CaBP5 knock-out mice and the visual impairment observed in human patients carrying mutations in the CaBP4 gene (Jeziorski et al., 2000; Williams, 2006; Zeitz et al., 2006; Rieke et al., 2008; Littink et al., 2009; Aldahmesh et al., 2010). It has also been discovered that the CaBPs exhibit specific

target interactions independent of CaM and intriguingly some of these appear to have co-evolved with the CaBP family during the emergence of vertebrates (McCue et al., 2010a).

A picture is now emerging whereby the CaBP family can be viewed as providing an expansion in CaM functionality by exerting additional levels of target regulation for shared effectors in addition to executing novel functions through unique effector interactions. This increase in signaling complexity maximizes the range of physiological calcium signals that can be utilized and may have been instrumental in the evolution of complex vertebrate nervous systems that we observe today (Williams, 2006). This paper will focus on the evolution, mechanisms of targeting, and emerging roles of the CaBP protein family and discuss the importance of recent experimental findings in the context of mammalian CNS function.

METHODS

Hela cells were cultured in 75 cm^2 flasks at 37°C in a humidified atmosphere of 5% CO_2/95% air. Cells for transfection were seeded onto coverslips in a 24-well tray at a density of $\sim 4 \times 10^5$ cells/well. 1 μg of mCherry-TM7 [residues 188–215 of human CaBP7 (transmembrane domain: residues 189–205)] or mCherry-CaBP7 plasmid was transfected per well using Genejuice transfection reagent (Novagen) according to manufacturer's instructions. Cells were maintained for 24 h post-transfection before fixation. Cells were washed three times in phosphate buffered saline (PBS; 137 mM NaCl, 2.7 mM KCl, 10 mM Na_2PO_4, 2 mM NaH_2PO_4, pH 7.4) then fixed in 4% formaldehyde in PBS at room temperature for 10 min. Cells were then washed a further three times in PBS then permeabilized using 0.2% triton X-100 in PBS for 6 min at room temperature. Cells were washed three times in PBS to remove detergent then twice in PBS containing 5% (w/v) BSA (PBSB). Cells were incubated with anti-TOM20 (1:1000, BD Biosciences) or anti-Calnexin (1:200, Sigma) primary antibodies for 1 h at room temperature in PBSB. Cells were washed three times in PBS and twice in PBSB prior to incubation with the relevant species specific fluorophore conjugated secondary antibody for 1 h at room temperature. Cells were washed again three times in PBS, rinsed with deionized H_2O, dried, and mounted onto glass slides using ProLong Gold antifade reagent (Invitrogen). Imaging of transfected and immunostained cells was carried out using a Leica AOBS SP2 microscope (Leica microsystems, Heidelberg, Germany) using a 63x oil immersion objective with a 1.4 numerical aperture. In most cases the pinhole was set to Airy1 to give the optimum signal to noise ratio and hence minimum thickness confocal section for the excitation laser used.

CaBP EVOLUTION

The CaBP family in humans comprises six proteins: Caldendrin/CaBP1, 2, 4, 5, 7, and 8 (Haeseleer et al., 2000; Wu et al., 2001; Mikhaylova et al., 2006). The CaBP3 that was originally identified is likely to be a pseudogene and no CaBP6 gene exists. CaBP7 and CaBP8 have been referred to by the alternative names calneuron II and calneuron I, respectively, in other studies (Wu et al., 2001; Mikhaylova et al., 2006, 2009; Hradsky et al., 2011) but will henceforth be referred to as CaBP7 and CaBP8 in this paper. We have taken this approach for self-consistency (our previously published work has used these protein identifiers) and also because bioinformatics analyses links CaBP 7 and 8 to CaBPs 1–5 more than to any other small EF-hand Ca^{2+}-sensors (McCue et al., 2010a). Alternative splicing of the CaBP1 and 2 genes generates additional novel transcripts so that the final complement of CaBPs numbers nine distinct proteins in humans (McCue et al., 2010a). These proteins share a core domain comprised of four EF-hand motifs but differ in unique regions located at the extreme N- or C-termini (McCue et al., 2010b). The EF-hand core represents the region with greatest similarity to CaM however, the most closely related family member, CaBP2-Short, only shares 37.8% total sequence identity with its primordial ancestor suggesting that the unique N- and C-terminal domains of the CaBPs are highly divergent and likely confer specific cellular functions and target regulation distinct from that exerted by CaM (McCue et al., 2010a). The EF-hand core additionally exhibits divergence within the CaBP family and there are unique patterns of EF-hand inactivation coupled to sequence substitutions conferring binding specificity preferentially toward either Ca^{2+} or Mg^{2+} ions (McCue et al., 2010a). The unique cation binding properties of individual CaBP proteins will further influence their biological activity and increase the specificity of cellular Ca^{2+}-signals to which they are able to respond.

How these proteins evolved from their CaM ancestor was unclear until a recent bioinformatic analyses examined available invertebrate and vertebrate genome sequence databases in an effort to locate CaBP-related transcripts (McCue et al., 2010a). From these analyses it was determined that the oldest species harboring CaBP-related genomic DNA sequences was the cartilaginous fish, the elephant shark (*Callorhincus milli*). No invertebrate genomes analyzed, including the widely used experimental model organisms *Drosophila melanogaster* and *Caenorhabditis elegans*, where genome coverage is >10X, contained CaBP like sequences (C.elegans, 1998; Adams et al., 2000; McCue et al., 2010a). The elephant shark genome sequencing project currently stands at 1.4X coverage however, sequences with homology to CaBPs 1, 2, 5, 7, and 8 are clearly present based on BLAST searches against the human coding sequences [(McCue et al., 2010a) and **Table 1**].

Further detailed analysis of protein alignment data showed that the elephant shark genome contains a CaBP1 like sequence having 46% sequence coverage of the human orthologue and 90% identity (**Figure 1A**). The coverage for elephant shark CaBP7 and CaBP8 sequences was found to be significantly greater and these again shared considerable identity with the corresponding human sequences (**Figure 1B**). In the study of McCue et al. (McCue et al., 2010a) no CaBP like sequences were discovered in the jawless fish, lamprey which is thought to represent the oldest living organism related to the human vertebrate ancestor. Coverage of the Lamprey genome has since improved and a new series of specific BLAT and BLAST searches performed here has uncovered two partial CaBP like sequences with highest homology to human CaBP1 and CaBP8 (**Figures 1A,B**). It would appear, therefore, that there were two ancestral members of the CaBP family, CaBP1 and CaBP8. This observation is consistent with the

Table 1 | Protein sequence fragments identified in BLAST searches against the elephant shark genome (left column) along with the sequence of the corresponding CaBP exon in the human genome (right column) and the percentage identity between the two sequences.

Contig	Sequence	Homology	Exon	Human exon sequence	%Identity
AAVX01573327.1	FDRDRDGLISCRDLGNLMRTMG YMPTEMELIELSQQINMN	CaBP5	3	ELREAFLEFDKDRDGFISCKDL GNLMRTMGYMPTEMELI ELGQQIRMN	87
AAVX01478821.1	VGGHVDFDDFVELMGPKLLAETADM IGVKELRDAFKE	CaBP1	4	LGGHVDFDDFVELMGPKLLAETADMIGVK ELRDAFRE	94
AAV01407556.1	VGGRVNFEDFVE*MAPKLLAETADMIGIK	CaBP2	5	SGGKVDFEDFVELMGPKLLAETADM IGVRELRDAFRE	78
AAVX01108357.1	EIRKAFKVFDRDGNGFISKQELG MAMRSLGYMPNEVELEVIIQRLDMD	CaBP7	2	EIREAFKVFDRDGNGFISKQE LGTAM'RSLGYMPN EVELEVIIQRLDMD	95
AAVX01059912.1	GDGQVDFEEFVSLLGPRLSSAA IPEKFHGTEFDNVFWK	CaBP7	3	GDGQVDFEEFVTLLGPKLSTSGIPEKFHGT DFDTVFWK	81
AAVX01059912.1	CDMQRMTVEELKRLLYEAFCEHLSMKDEI NIIMTEEEGHVDNPDECPVDIDSK	CaBP7	4	CDMQKLTVDELKRLLYDT FCEHL SMKDIENIIMTEEESHLGTAEECPVDVET	71
AAVX01124961.1	STQQIKQTCLRKSLICAFAIAFIIS VMLIAANQVLRSGMK	CaBP7	5	CSNQQIRQTCVRKSLICAFAIAFII SVMLIAANQVRSGMK	80
AAVX01563725.1	MPFHPVHGSLLYKGSFLSESLSDTSET EQLANISEEELD	CaBP8	1	MPFHHVTAGLLYKGNYLNRSLSA GSDSEQLANISVEELD	66
AAVX01190659.1	EIREAFRVLDRDGNGFISKQELGMAMRSL GYMPSEVELAIIMQRLDMDG	CaBP8	2	EIREAFRVLDRDGNGFISKQELGMA MRSLGY MPSEVELAIIMQRLDMDG	98
AAVX01097552.1	DGQVDFEEFMTILGPKLLTSEV REGFHGSAIDSIFW	CaBP8	3	DGQVDFDEFMTILGPKLVSSEGR DGFLGNTIDSIFWQ	77
AAVX01062942.1	QFDMQRITLEELKHILFHAFRDHLTMKD IENIIINEEESLNENSNSCQTEFEG	CaBP8	4	FDMQRITLEELKHILYHAFRDHLT MKDIENIIINEEESLNETSGNCQTEFEG	90
AAVX01282372.1	VHSQKQNRQTCVRKSLICAFGVA FIISVMLIAANQILRNGME	CaBP8	5	VHSQKQNRQTCVRKSLICAFAMAFIIS VMLIAA NQILRSGME	92

CaBP family forming two distinct sub-families based on unique sequence characteristics, the first comprising CaBPs1–5 and the second consisting of CaBP7 and CaBP8 (McCue et al., 2010a). Collectively, these results suggest that the CaBP protein family arose specifically with the emergence of vertebrate species and that whole genome duplication event, acting initially on CaBP1- and CaBP8-like genes present in the jawless fish, likely gave rise to the full complement of CaBP proteins found from the bony fish onwards through vertebrate evolution (McCue et al., 2010a).

In addition to examining the evolution of CaBP proteins by performing searches based on the full-length human coding sequences (McCue et al., 2010a), domains unique to individual CaBPs were also analyzed to examine if there was evolutionary conservation or divergence which might indicate correspondingly conserved or unique cellular functions. It was determined that the novel N-terminal domain of CaBP1-Long (residues 16–75) was relatively well conserved from amphibians to humans which may correlate with an important vertebrate specific activity in the inhibition of Ca^{2+}-release from ER resident inositol 1, 4, 5-trisphosphate (IP_3) receptors (IP_3Rs) (Haynes et al., 2004; Kasri et al., 2004; Li et al., 2009; McCue et al., 2010a). In contrast, the variable N-terminal regions of CaBP2 and CaBP4 both exhibited a progressive increase in sequence similarity from the bony fish to humans. As both of these proteins are expressed in sensory neurons these observations may correspond to an increase in the complexity of the audio-visual sensory system during vertebrate evolution. Specific domains of CaBP7 and CaBP8 were not included in this analysis but recent evidence characterizing the unique functional properties of the hydrophobic C-termini of both of these family members (McCue et al., 2011) led us to evaluate the evolutionary conservation of these regions (**Figure 1B**). The hydrophobic C-terminal 38 residues of both CaBP7 (residues 177–215) and CaBP8 (residues 181–219) exhibit significant sequence conservation across vertebrate evolution. There is 92% sequence similarity between lamprey and human CaBP8 sequences in the C-terminal region and 94% similarity between elephant shark and human CaBP7 in the corresponding region. This high degree of domain conservation is indicative of a conserved function and is consistent with this region of CaBP7 and CaBP8 controlling the normal sub-cellular targeting of both proteins to the trans-Golgi network (TGN) and post-TGN vesicles (McCue et al., 2009; Mikhaylova et al., 2009; Hradsky et al., 2011).

The conservation of CaBP family members throughout vertebrate evolution raised a further interesting question regarding the potential co-evolution of specific interacting proteins (McCue et al., 2010a) which might shed light on vertebrate specific functions for this protein family. There are numerous documented interactions between CaBPs and various classes of cellular calcium channels including IP_3Rs (Haynes et al., 2004; Kasri et al., 2004) and voltage gated calcium channels (VGCCs) (Lee et al., 2002; Haeseleer et al., 2004; Zhou et al., 2004, 2005; Cui et al., 2007; Lee et al., 2007b; Tippens and Lee, 2007; Few et al., 2011). These channels are also targets of CaM, however, in mammalian

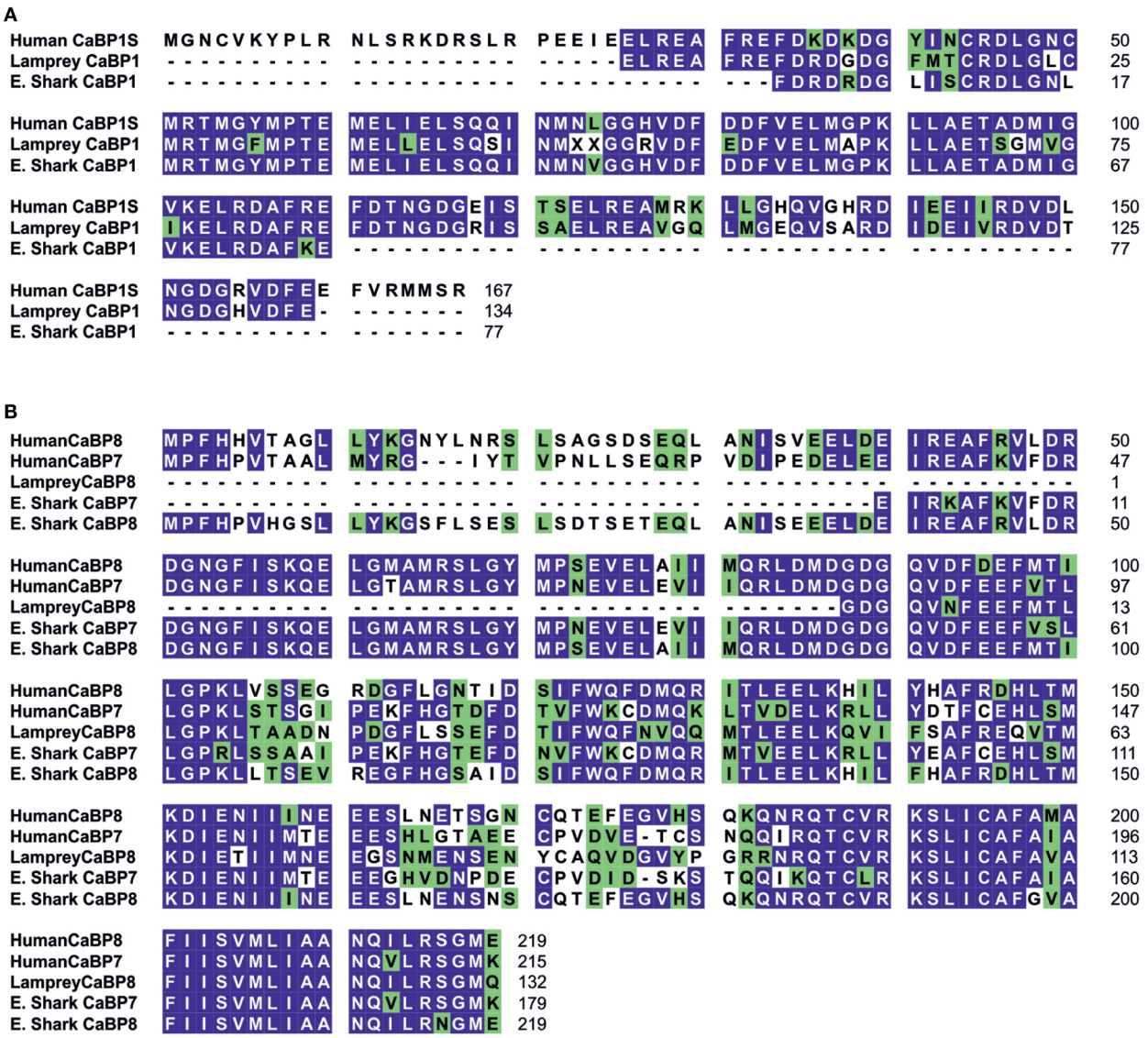

FIGURE 1 | Bioinformatic analysis of CaBP1, 7, and 8 proteins during vertebrate evolution. (A) Protein sequence alignment for human CaBP1-Short (Genbank accession: NM_004276) with related protein sequences identified from BLAT/BLAST searches of Lamprey and Elephant Shark (E. Shark) genomes. Identical residues between = 50% aligned sequences are highlighted in blue, similar residues are highlighted in green. Lamprey CaBP1 shares 80% coverage and 76% identity with human CaBP1-Short. Elephant Shark CaBP1 shares 46% coverage and 90% identity with human CaBP1-Short. **(B)** Protein sequence alignment for human CaBP7 (Genbank accession: NM_182527) and CaBP8 (Genbank accession: AY007302) with BLAT/BLAST identified related sequences from Lamprey (CaBP8) and Elephant Shark (CaBP7 and CaBP8). Identical residues between = 50% aligned sequences are highlighted in blue, similar residues are highlighted in green. Lamprey CaBP8 exhibited 61% and 60% coverage and 56% and 65% identity with human CaBP7 and human CaBP8, respectively. Elephant Shark CaBP7 exhibited 83% and 82% coverage and 84% and 66% identity with human CaBP7 and human CaBP8, respectively. Elephant Shark CaBP8 exhibited 102% and 100% coverage and 63% and 87% identity with human CaBP7 and human CaBP8, respectively.

systems it would appear that the CaBPs and CaM have the capacity to differentially regulate common channel targets (Lee et al., 2002; Haynes et al., 2004; Kasri et al., 2006; Minor and Findeisen, 2010). Within the CaBP family further examples of regulatory diversity exist and both Caldendrin and CaBP1-Short modulate L-type VGCCs in distinct ways even though they share a common C-terminal EF-hand domain (Tippens and Lee, 2007). VGCCs and IP_3Rs are present in invertebrates, however, the number of specific isoforms has increased with the appearance of vertebrates (Jeziorski et al., 2000; Iwasaki et al., 2002; Zhang et al., 2007; McCue et al., 2010a). It seems likely that the co-evolution of key calcium channels tailored to discrete functions within the mammalian CNS in conjunction with new types of calcium sensor proteins including the CaBPs has been instrumental in permitting vertebrates to generate and utilize an extended repertoire of spatio-temporal calcium signals. This in turn has

likely influenced the evolution of increasingly complex modes of neuronal communication and enhanced CNS processing power.

CaBP TARGETING

CaM is a cytosolic protein that lacks primary sequence information or post-translational modifications which would mediate its specific localization to subcellular organelles (Mikhaylova et al., 2006). This feature of CaM perhaps underlies its versatility as a Ca^{2+}-sensor and helps explain its ability to interact with a wide spectrum of cellular effectors, only becoming recruited to specific cellular domains at specific time points through formation of multiple distinct complexes. The cellular activity of CaM consequently often relies on Ca^{2+} increases that are generated globally throughout the cytoplasm (Parekh, 2011). In order to maximize the usefulness of Ca^{2+} as a second messenger, mechanisms have evolved for the generation Ca^{2+}-signals that are highly restricted in both space and time to ensure that only specific cell signaling pathways are activated or inhibited without perturbing other Ca^{2+}-sensitive events within the cell. For Ca^{2+} to be used in this manner it follows that calcium sensing proteins dedicated to the detection of such specific signals must be similarly localized or harbor the ability to become localized in response to the signal. A variety of mechanisms are employed by the CaBPs to restrict their localization to particular cellular organelles and domains. Like CaM, a number of the CaBP proteins (Caldendrin, CaBP4 and CaBP5) contain no inherent primary sequence targeting information or consensus sequences for post translational modification that might influence their retention at specific subcellular locations (Haeseleer et al., 2000). The strategy employed in these instances relies on interactions with target effectors that in turn are specifically localized (Haeseleer et al., 2004; Rieke et al., 2008).

Caldendrin is enriched in post-synaptic density protein fractions (Seidenbecher et al., 1998) and specifically interacts with a light chain of the microtubule associated protein MAP1A/B (Seidenbecher et al., 2004). More recently a novel interaction between Caldendrin and a retinal specific small EF-hand containing calcium sensor, recoverin, was reported (Fries et al., 2010). Recoverin is a photoreceptor-enriched, myristoylated protein that exhibits a so called Ca^{2+}-myristoyl switch mechanism (Tanaka et al., 1995; Ames et al., 1997; Ames and Ikura, 2002) whereby the acyl group is sequestered within the protein core in the absence of Ca^{2+} and, on Ca^{2+}-binding and a conformational rearrangement (Yap et al., 1999), is extruded to permit dynamic association with cellular membranes. Caldendrin interacted with recoverin in a calcium dependent manner and this was reported to traffic the normally cytosolic Caldendrin protein to Golgi membranes (Fries et al., 2010). This mechanism of targeting is potentially interesting since many neuronal populations often express multiple different Ca^{2+}-sensing proteins. Further investigations will be required to validate this targeting mechanism for the endogenous proteins, in particular it would be of interest to examine what effect depletion of recoverin has on the ability of Caldendrin to redistribute in response to elevations in cytoplasmic Ca^{2+} concentration. Since the C-terminal EF-hand containing domain of Caldendrin and not its variable N-terminal region was able to bind to recoverin (Fries et al., 2010) and because this domain is identical in the other CaBP1 splice isoforms, CaBP1-Long and CaBP1-Short, it would also be of interest to test the promiscuity of recoverin binding with respect to other CaBP1 interactions.

Shorter splice variants of the Caldendrin/CaBP1 gene, CaBP1-Long, and CaBP1-Short (Landwehr et al., 2003; Haynes et al., 2004; Kasri et al., 2004) incorporate a distinct exon, not present in the Caldendrin transcript, that encodes for an N-terminal myristoylation consensus site (Landwehr et al., 2003). *N*-myristoylation of both proteins has been proven essential for localization to the PM and membranes of the Golgi apparatus and for functional inhibition of IP_3Rs (Haynes et al., 2004; Kasri et al., 2004).

The remaining two members of the CaBP family, CaBP7 and CaBP8, like CaM, Caldendrin, CaBP4 and CaBP5 contain no consensus motifs for post-translational modifications that are known to mediate association with cellular membranes (Wu et al., 2001; Mikhaylova et al., 2006). Surprisingly, when the localization of these proteins was examined in mammalian cell lines, they were found to specifically localize to membranes of the TGN and vesicular compartments of the constitutive secretory pathway (McCue et al., 2009; Mikhaylova et al., 2009). Closer inspection of the CaBP7 and CaBP8 primary sequences (McCue et al., 2009) using transmembrane domain prediction tools uncovered the presence of a highly hydrophobic 38 residue C-terminal extension not present in the other CaBPs that was strongly predicted to form a transmembrane domain. Cellular and biochemical characterization of these sequences determined that they do indeed operate as transmembrane domains which are essential for normal CaBP7 and CaBP8 localization (McCue et al., 2009). Furthermore it was demonstrated that chimeric constructs encoding normally cytosolic proteins fused to the CaBP7 and CaBP8 transmembrane domains were efficiently targeted to membranes of the secretory pathway (McCue et al., 2009).

The CaBP7 and CaBP8 transmembrane domains are located 10 residues from the C-terminus in each protein and this topology is consistent with that of the tail-anchor class of type-II transmembrane proteins that have cytosolically oriented N-terminal functional domains, a transmembrane domain and a short lumenal C-terminal tail (Borgese et al., 2003, 2007; Brambillasca et al., 2006; McCue et al., 2011). Tail-anchor proteins are defined by their post-translational insertion into biological membranes through a series of novel pathways, the molecular details of which remain to be fully resolved (Abell et al., 2004; Stefanovic and Hegde, 2007; Borgese and Fasana, 2011). CaBP7 and CaBP8 have recently been shown to adopt the expected tail-anchor protein topology (Hradsky et al., 2011; McCue et al., 2011) and to interact with the ATPase TRC40/Asna1 (Hradsky et al., 2011) (**Figure 3**) a protein implicated in the post-translational membrane insertion of other tail-anchored proteins (Stefanovic and Hegde, 2007; Rabu et al., 2008). Tail-anchor proteins are initially post-translationally inserted either into the endoplasmic reticulum, outer mitochondrial- or peroxisomal-membranes (Borgese et al., 2007; Borgese and Fasana, 2011). Peroxisomes and mitochondria represent terminal destinations, however, ER targeted tail-anchor proteins can subsequently traffic along the secretory pathway and access a number of possible cellular membranes. Analysis of the CaBP7 and CaBP8 transmembrane domains explains why these proteins are observed at the TGN and on transport vesicles (McCue et al., 2009, 2011; Hradsky et al., 2011).

When fused to the normally cytosolic fluorescent tag protein mCherry, a C-terminal domain fragment of CaBP7 incorporating the predicted transmembrane domain [residues 188–215 (transmembrane domain: residues 189–205)] showed no colocalization with the outer mitochondrial membrane tail-anchored protein TOM20 (**Figure 2A**). In contrast, it exhibited a reticular distribution in a proportion of HeLa cells where it colocalized extensively with the ER marker calnexin (**Figure 2B**). This construct is also competent for correct traffic to the TGN in another proportion of HeLa cells (data not shown) as has been observed in the neuronal like N2A cell line (McCue et al., 2009). This observation may be consistent with differential expression levels between cells: in low to moderate expressing situations the CaBP7 transmembrane domain fusion remains ER-trapped, however, at higher expression levels ER-based retention mechanisms are likely saturated and the construct escapes to latter compartments of the secretory pathway. Collectively these data illustrate that the transmembrane domain of CaBP7 is of the class that

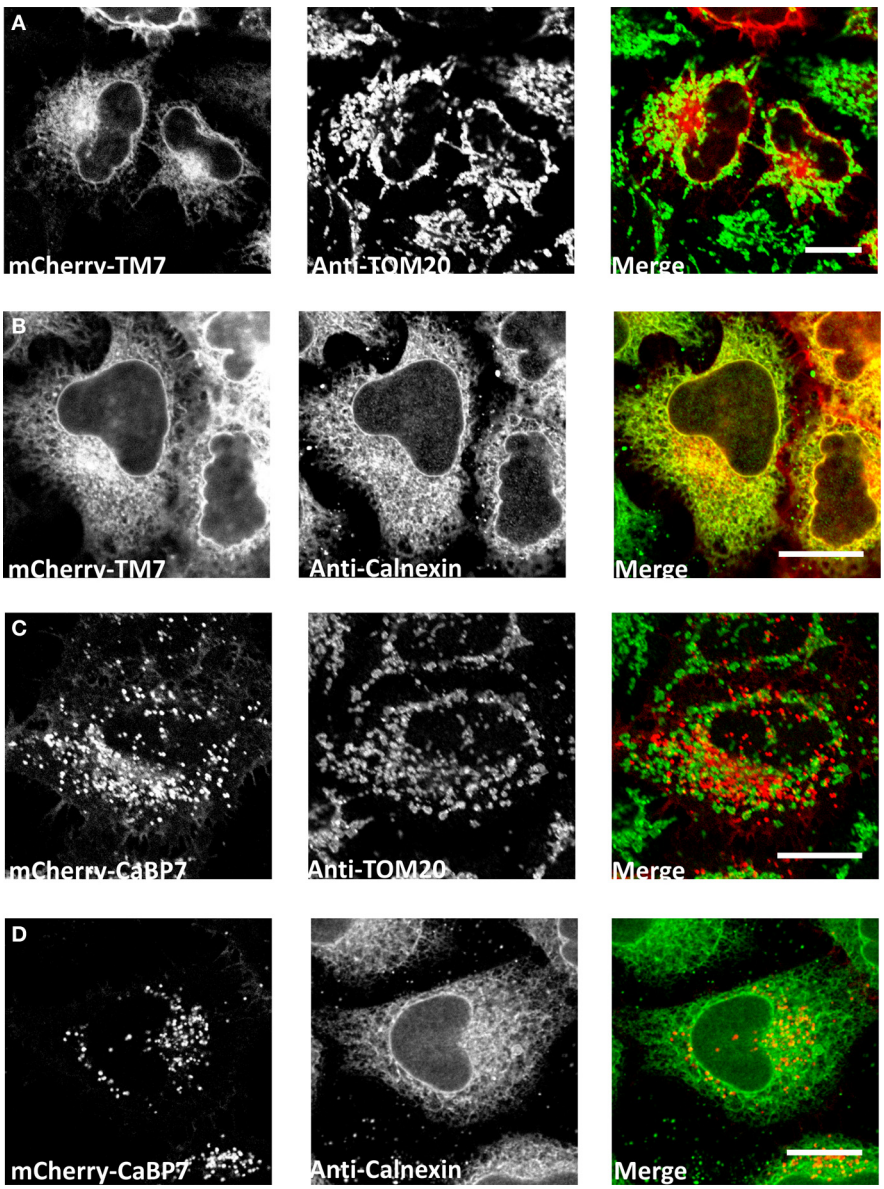

FIGURE 2 | Analysis of localization of mCherry-CaBP7 or mCherry-CaBP7 transmembrane containing domain (residues 188–215) fusion (mCherry-TM7) compared with markers of the mitochondria (TOM20) and the ER (Calnexin). (A and **B)** mCherry-TM7 expression in HeLa cells (red) and co-staining with antibodies against endogenous TOM20 (**A**, green) or Calnexin (**B**, green). Cells with low to moderate levels of mCherry-TM7 were analyzed in this experiment, more highly expressing cells exhibit a localization pattern more consistent with the full-length CaBP7 protein (see text for further discussion). **(C** and **D)** mCherry-CaBP7 expression in HeLa cells (red) and co-staining with antibodies against endogenous TOM20 (**C**, green) or Calnexin (**D**, green). Regions of colocalization appear yellow in overlay images. Scale bars = 10 μm.

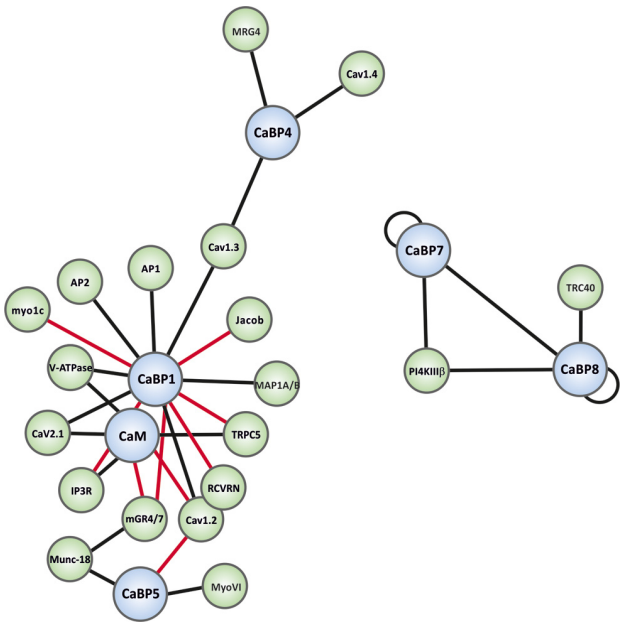

FIGURE 3 | Interaction map of the known binding partners for the CaBP family. CaBP proteins are shown in blue spheres and specific effectors in green spheres. Black connecting lines indicate Ca^{2+}-independent interactions and red connecting lines Ca^{2+}-dependent interactions. Binding partner abbreviations are: MRG4 (Unc-119), $Ca_V1.4$ (L-type Ca^{2+}-channel), $Ca_V1.3$ (L-type Ca^{2+}-channel), Jacob, AP1 (Clathrin adaptor complex 1), AP2 (Clathrin adaptor complex 2), Myo1c (Myosin1c), V-ATPase (Vacuolar ATPase), $Ca_V2.1$ (P/Q-type Ca^{2+}-channel), IP3R (Inositol 1,4,5-trisphosphate Receptor), $Ca_V1.2$ (L-type Ca^{2+}-channel), RCVRN (Recoverin), TRPC5 (Transient receptor potential channel 5), MAP1A/B (Microtubule associated protein light chain 3 isoform A and B, LC3α/β), PI4KIIIβ (Phosphatidylinositol4-kinaseIIIβ), TRC40 (Transmembrane domain recognition complex-40), mGR4/7 (Group III metabotropic glutamate receptor 4/7), Munc-18 (nSec1), MyoVI (myosinVI).

directs initial insertion into the ER membrane. Additional intrinsic targeting information or specific protein-protein interactions must be required for the efficient direction of CaBP7 and CaBP8 for forward traffic through the secretory pathway to the TGN and beyond as can be observed for full-length CaBP7 protein which exhibits a punctate distribution that does not significantly overlap with either calnexin or TOM20 (**Figure 2C,D**).

CaBP7 and CaBP8 represent the only known CaM-related small EF-hand containing calcium sensors that have adopted the use of a tail-anchor targeting strategy. Tail-anchor proteins perform highly conserved and essential functions in mammalian cells and include SNARE proteins required for membrane fusion events throughout the secretory pathway (Borgese and Fasana, 2011). A number of issues remain to be resolved with regards to the precise targeting of CaBP7 and CaBP8. Although CaBP8 was shown to associate with TRC40 (Hradsky et al., 2011) it remains to be demonstrated that this chaperone is capable of post-translationally inserting recombinantly expressed or *in vitro* translated CaBP7 or CaBP8 across endoplasmic reticulum/microsomal membranes. It will also be of interest to understand the exact molecular determinants and protein-protein or protein-lipid interactions that control the final targeting of CaBP7 and CaBP8 to latter compartments of the secretory pathway. This information will further our understanding of the emerging functions of CaBP7 and CaBP8 as regulatory factors of protein trafficking from the TGN (Mikhaylova et al., 2009).

CaBP-EFFECTOR INTERACTIONS

As noted above, CaBPs along with CaM have been found to be able to regulate several types of VGCCs (Lee et al., 2002; Zhou et al., 2005; Cui et al., 2007; Findeisen and Minor, 2010; Minor and Findeisen, 2010). For a detailed overview of these and other well-characterized CaBP-effector interactions readers are directed to the recent comprehensive review articles (McCue et al., 2010b; Mikhaylova et al., 2011). The current article will focus on novel CaBP interactions that have been reported only in the past few years and which hint at further important physiological functions for the CaBP family in the mammalian CNS. A graphical overview of all presently characterized CaBP interactions is presented in network diagram form in **Figure 3**.

CALDENDRIN/CaBP1

GROUP III METABOTROPIC GLUTAMATE RECEPTORS (mGluRs)

Group III mGluRs function presynaptically to modulate synaptic vesicle exocytosis and neurotransmitter release (Pinheiro and Mulle, 2008). A recent study by Nakajima (Nakajima, 2011) reported an *in vitro* Ca^{2+}-dependent interaction between rat CaBP1-Long and the membrane proximal portion of the cytoplasmic C-terminal tail of mGluR4 and mGluR7. This interaction was sensitive to phosphorylation of the mGluR fragment by protein kinase C mimicking the characterized binding of CaM to these receptors (Nakajima et al., 1999; O'Connor et al., 1999; Nakajima et al., 2009). There was competitive binding between CaM and CaBP1-Long suggesting that both proteins could regulate this receptor type through interaction with the same target motif. This is reminiscent of CaBP1/CaM dual regulation of VGCCs (Lee et al., 2002; Few et al., 2005, 2011) and it will be fascinating to examine whether, in the case of mGluR regulation, both Ca^{2+}-sensors exert identical or differential modulation of these important neuronal receptors. CaM binding to mGluRs is able to displace the regulatory protein Munc-18 (Nakajima et al., 2009) and it will of interest to test if CaBP1 can elicit the same loss of Munc-18 binding.

The study of Nakajima (Nakajima, 2011) was conducted entirely using *in vitro* biochemical techniques and there is currently no information validating these findings in intact cells. The biochemical characteristics reported in this paper are, however, consistent with documented CaM/CaBP1 *in vivo* interactions (Lee et al., 2002; Few et al., 2005, 2011) and this work remains of great potential interest as Ca^{2+}-influx downstream of mGluR activation is known to influence short term facilitation and higher level neuronal function (Cosgrove et al., 2011; Fioravante and Regehr, 2011).

UNCONVENTIONAL MYOSIN 1c

Class I unconventional myosins organize the cortical actin cytoskeleton and are involved in processes encompassing membrane trafficking and cell migration (Soldati, 2003). Myosin1c (myo1c), a protein essential for inner hair cell (IHC) adaptation

in the inner ear (Gillespie and Cyr, 2004), has been shown to interact with CaBP1 through its IQ motif containing regulatory domain (Tang et al., 2007). CaBP1 binding was found to be competitive with that of CaM suggesting that myo1c may represent yet another example of a target protein regulated by multiple small EF-hand Ca^{2+}-sensors. No functional data was presented in this study to confirm a physiological role for the CaBP1/myo1c interaction and further work is required to clarify this issue. Intriguingly, CaBP1 expression in rat and chicken auditory IHCs has been confirmed by both reverse transcription PCR and immunostaining (Yang et al., 2006; Lee et al., 2007b) and these may represent prime cellular models to study the functional implications of a putative CaBP1/myo1c interaction. IHCs have also been demonstrated to express CaBP4 (Yang et al., 2006; Lee et al., 2007b and CaBP7 Lee et al., 2007b) and, therefore, an analysis of myo1c binding by these family members might also further our understanding of potential mechanisms of cytoskeleton organization and regulation by multiple CaBPs in a key special sensory tissue.

JACOB

The interplay of calcium signaling through synaptic and extra-synaptic NMDA receptors influences complex aspects of neuronal function including synaptic connectivity and survival (Hardingham and Bading, 2003). These changes are brought about by alterations in neuronal gene expression (Greer and Greenberg, 2008; Lyons and West, 2011) and one pathway involved in such regulation in mammalian neurons is controlled by Caldendrin (Dieterich et al., 2008). This detailed study isolated and characterized a brain specific Caldendrin binding protein, Jacob, and demonstrated a role for this interaction in modulating activity of the CREB transcription factor to ultimately influence neuronal gene expression. Activation of synaptic NMDA receptors and subsequent Ca^{2+}-binding by Caldendrin localized at the post-synaptic density was shown to drive its interaction with the Jacob nuclear localization signal thereby preventing import of Jacob into the nucleus. Conversely, activation of extra-synaptic NMDA receptors was shown to induce Jacob redistribution to the nucleus where it was able to induce CREB dephosphorylation and inactivation (Dieterich et al., 2008). Jacob mediated inhibition of CREB dependent gene expression elicited a loss of synaptic contacts and extensive simplification of dendritic architecture. This mechanism, therefore, couples synaptic activity to maintenance/loss of synaptic contacts through Ca^{2+}-signaling via Caldendrin. Intriguingly, Jacob is a vertebrate specific protein (McCue et al., 2010a) that may have co-evolved specifically with the CaBP family to regulate this important aspect of synaptic plasticity.

CaBP4

Unc-119 (MRG4)

CaBP4 is the only CaBP member thus far characterized that has a proven role in human disease and mutations in the gene lead to rod and cone dysfunction and visual impairments of varying severity (Zeitz et al., 2006; Littink et al., 2009; Aldahmesh et al., 2010). CaBP4 regulates $Ca_v1.4$ channels in the retina (Haeseleer et al., 2004) and $Ca_v1.3$ channels in auditory IHCs (Yang et al., 2006; Cui et al., 2007; Lee et al., 2007b), however, non-channel binding partners are also emerging (Lee et al., 2007a).

Vertebrate orthologues of the *C. elegans* Unc-119 protein (also known as MRG4), like CaBP4, exhibit retinal specific expression profiles (Higashide et al., 1998; Higashide and Inana, 1999). Functional deficits due to mutations in MRG4 mirror those observed for CaB4 mutations and have been found to lead to rod/cone dystrophy in animal models and humans (Kobayashi et al., 2000). Unc-119 orthologues are expressed from invertebrates onwards (Maduro et al., 2000) and appear to have a nervous system specific function in *C. elegans* and *D. melanogaster* (Maduro and Pilgrim, 1995, 1996) which has apparently become restricted to the visual system in vertebrate animals.

MRG4 was found to interact with CaBP4 in a calcium independent manner consistent with binding to the variable N-terminal domain of CaBP4 (Haeseleer, 2008). This observation itself is intriguing as the vast majority of CaBP target effectors characterized to date have been shown to bind to the conserved C-terminal EF-hand containing core of the CaBP under investigation. An interaction with the novel N-terminus of CaBP4 seems to be important for stabilizing MRG4 protein (Haeseleer, 2008) and further hints at a co-evolution of tissue expression and cellular function between these proteins which has likely been important for the development and normal function of vertebrate visual systems. Further investigations into the molecular pathway linking CaBP4 and MRG4 to normal retinal activity are required to gain a complete understanding regarding the roles that both proteins play in human disease pathologies and to ascertain whether this retinal signaling system might provide a useful therapeutic target in the future treatment of some visual impairments.

CaBP5

Munc-18 (nSec-1) AND MYOSIN VI

CaBP5 has been shown to be expressed in IHCs, however, the available data suggests that, in this particular cell type, it is CaBP1 and CaBP4 that functionally regulate $Ca_v1.3$ channels (Cui et al., 2007). CaBP5 is able to modulate the activity of both $Ca_v1.2$ and $Ca_v1.3$ channels when co-expressed in HEK293 cells (Cui et al., 2007; Rieke et al., 2008) and CaBP5 knock-out mice exhibit a reduction in light sensitivity of their retinal ganglion cells suggesting that CaBP5 may instead perform an important modulatory function in the visual system (Rieke et al., 2008).

Munc-18 is a highly conserved protein related to yeast Sec1 that is critical for neurotransmission throughout the mammalian CNS where it interacts with multiple effectors to control membrane fusion. Originally isolated as a syntaxin1 binding partner, Munc-18 has since been shown to interact with the synaptic SNARE complex in multiple unique "modes" to regulate synaptic vesicle fusion with the presynaptic PM (Burgoyne et al., 2009; Sudhof and Rothman, 2009). New, SNARE independent, Munc-18 binding proteins have been discovered suggesting that this protein itself is tightly regulated through multiple routes perhaps to further modulate SNARE complex activity and ultimately neurotransmission (Okamoto and Sudhof, 1997; Verhage et al., 1997; Graham et al., 2008; Hikita et al., 2009; Nakajima et al., 2009; Huang et al., 2011). Recently, a calcium independent

interaction has been described between Munc-18 and CaBP5 in the retina establishing a potential new mechanism of linking calcium sensor function to SNARE activity in the visual system (Sokal and Haeseleer, 2011). CaBP5 was also shown to influence neurotransmitter release when overexpressed in a model neuroendocrine cell line, further implicating it as a regulator of secretion in selected regions of the nervous system (Sokal and Haeseleer, 2011).

In the same study, myosin VI was identified as a second specific binding partner for CaBP5 (Sokal and Haeseleer, 2011). Myosin VI has been implicated in endocytic processes. The related myosin V, a protein associated with synaptic vesicles and involved in their movement to the PM, was also detected in CaBP5 affinity chromatography pull-downs. For technical reasons a myosin V interaction was not characterized further in this study, however, these observations hint at a possible role for CaBP5 in synaptic vesicle recruitment to the presynaptic membrane of retinal neurons, a potentially important role which warrants further investigation. The CaBP5 knock-out mouse is available and it would be interesting to examine if there are defects in synaptic vesicle recruitment to the presynaptic active zone (myosin V pathway) or retrieval of exocytosed synaptic membrane components (myosin VI pathway) in retinal neurons from these animals. It would also be of interest to examine whether CaBP5 mediated stimulation of neurotransmitter release and neurite outgrowth (Sokal and Haeseleer, 2011) can be supported by a CaBP5 EF-hand mutant incapable of binding to Ca^{2+}.

CaBP7 AND CaBP8

PHOSPHATIDYLINOSITOL 4-KINASEIIIβ (PI4Kβ)

PI4Kβ is a lipid modifying enzyme that associates with the TGN to generate phosphatidylinositol 4-phosphate (PI4P) from phosphatidylinositol (Graham and Burd, 2011). PI4P is an essential lipid for budding of transport vesicles from the TGN and, therefore, regulation of PI4Kβ is a key control checkpoint of the secretory pathway. Known regulators of PI4Kβ activity include the small GTPase ARF1 and the small calcium sensing protein NCS-1 (Hendricks et al., 1999; Audhya et al., 2000; Haynes et al., 2005, 2007; Burgoyne and Haynes, 2010). NCS-1 modulation of PI4Kβ has been reported to be both Ca^{2+}-independent (Zhao et al., 2001) and Ca^{2+}-dependent (Haynes et al., 2005). It is known, however, that the Golgi complex stores luminal Ca^{2+} and uses this to generate local Ca^{2+}-signals suggesting a link between Ca^{2+}-release and membrane trafficking events (Dolman and Tepikin, 2006). A further level of regulation in this system was reported with the finding that both CaBP7 and CaBP8 could also interact with and inhibit the activity of PI4Kβ in mammalian cells to influence trafficking of specific secretory cargo to the PM (Mikhaylova et al., 2009).

The study of Mikhaylova et al. (Mikhaylova et al., 2009) uncovered an inhibitory interaction of CaBP7 and CaBP8 with PI4Kβ at resting (∼100 nM) cytosolic calcium concentrations [$(Ca^{2+})_i$] that was competitively displaced by NCS-1 at increasing free [$Ca^{2+}]_i$ to elicit stimulation of kinase activity. The interplay between NCS-1 and CaBP7 and CaBP8, therefore, permits dual control of TGN transport events over a range of physiological [$Ca^{2+}]_i$ and importantly prevents activation of the enzyme in the absence of a threshold Ca^{2+}-signal. The interaction of CaBP7 and CaBP8 with PI4Kβ was specific and was not observed with Caldendrin, however, it would be of interest to test PI4Kβ regulation with CaBP5, the family member exhibiting highest homology to CaBP7 and CaBP8 (McCue et al., 2010a).

Crosstalk between ARF1 and NCS-1/CaBP7 and CaBP8 was not examined in this study and since the NCS-1-PI4K-ARF1 network has been implicated in a developmental setting (Petko et al., 2009) it would be of interest to examine if CaBP7 and CaBP8 repression of PI4K activity can be linked to a similar physiological model.

VGCCs?

Until recently, the only documented regulatory role for CaBP7 and CaBP8 was that involving the interaction with PI4K discussed in the previous section. As small EF-hand Ca^{2+}-sensing proteins often display promiscuity in their target interactions (Haynes et al., 2006; Burgoyne, 2007) it seems reasonable to expect further binding partners for CaBP7 and CaBP8 to appear in future studies. A new potential interaction between CaBP8 and various VGCC's has been reported which may provide the first clues regarding additional CaBP7 and CaBP8 cellular functions (Shih et al., 2009). This study examined the effect of CaBP8 over-expression in bovine adrenal chromaffin cells on PM Ca^{2+}-channel activity and found that wild-type protein or a mutant deficient in Ca^{2+}-binding both inhibited currents generated through N-, L-, and P/Q-type channels (Shih et al., 2009). A mutant CaBP8 lacking the hydrophobic C-terminal domain mislocalized in this cell type and did not support inhibition of channel currents reinforcing the idea that correct sub-cellular targeting on this Ca^{2+}-sensor is critical for its normal cellular function.

The most profound inhibitory phenotype was observed on N-type currents and N-type channels are widely expressed in the mammalian CNS where they operate presynaptically to regulate neurotransmitter release (Delcour et al., 1993). No direct interaction between CaBP8 and the various Ca^{2+}-channels analyzed was reported in the study of Shih et al. (Shih et al., 2009), however, this merits examination in future investigations in view of the importance of N-type channels, coupled to the widespread expression of CaBP7 and CaBP8, in the mammalian CNS.

Since CaBP7 and CaBP8 regulate PI4K, the possibility exists that these Ca^{2+}-sensors are able to inhibit Ca^{2+}-currents not by direct channel gating but rather by restricting the traffic of Ca^{2+}-channels to the PM (Shih et al., 2009). Other small EF-hand Ca^{2+}-sensors are known to modulate channel activity in this manner, the most well characterized example being the regulation of Kv4 potassium channel traffic to the PM by the KChIP family of Ca^{2+}-sensors (Burgoyne, 2007; Flowerdew and Burgoyne, 2009). Since a mutant CaBP8 incapable of Ca^{2+}-binding was able to inhibit N-type currents and since PI4K activity is inhibited at resting [$Ca^{2+}]_i$, these observations are consistent with this regulatory model. Distinguishing between channel traffic and direct channel modulation mechanisms should prove straightforward and will provide further insights into the role of CaBP7 and CaBP8 in the normal function of the mammalian CNS.

DISCUSSION

Calcium sensing in the vertebrate CNS is of fundamental importance in establishing and maintaining normal neuronal activity. The complexity of Ca^{2+}-signals generated in the mammalian brain is only just beginning to be understood, however, the identity of many of the protein factors involved in decoding them is already known. The CaM superfamily of small EF-hand containing Ca^{2+}-sensors have emerged as key regulators of multiple important neuronal Ca^{2+}-channels that influence all aspects of neuronal plasticity. Sub-groups of vertebrate specific CaM-related proteins including the CaBPs have seemingly evolved in parallel with increasing levels of CNS complexity in higher animals. These proteins exhibit diversity in patterns of expression, sub-cellular localization and Ca^{2+}-sensing dynamics and are, therefore, well suited to functioning as transducers of the highly specific Ca^{2+}-signals that underpin complex neuronal activity.

We are now aware that the CaBPs not only regulate neuronal specific Ca^{2+}-channels but also targets involved in membrane trafficking, the organization of the cytoskeleton and proteins that influence neuronal gene expression and synaptic connectivity. The list of CaBP effector interactions is steadily increasing as is our appreciation of CaBP functionality. Testing the importance of CaBP activity in the mammalian CNS is largely restricted to studies utilizing cell lines and would benefit greatly from the generation of transgenic animal models. In particular, the application of Cre-Lox approaches (Sauer, 1998; Nickerson et al., 2011) to test loss of function of CaBPs in particular tissues and cell types during both development and in the adult animal will significantly enhance our understanding of the key physiological functions performed by these multifunctional signaling molecules.

ACKNOWLEDGMENTS

This work was supported by a Wellcome Trust Prize Studentship to Hannah V. McCue.

REFERENCES

Abell, B. M., Pool, M. R., Schlenker, O., Sinning, I., and High, S. (2004). Signal recognition particle mediates post-translational targeting in eukaryotes. *EMBO J.* 23, 2755–2764.

Adams, M. D., Celniker, S. E., Holt, R. A., Evans, C. A., Gocayne, J. D., Amanatides, P. G., Scherer, S. E., Li, P. W., Hoskins, R. A., Galle, R. F., George, R. A., Lewis, S. E., Richards, S., Ashburner, M., Henderson, S. N., Sutton, G. G., Wortman, J. R., Yandell, M. D., Zhang, Q., Chen, L. X., Brandon, R. C., Rogers, Y. H., Blazej, R. G., Champe, M., Pfeiffer, B. D., Wan, K. H., Doyle, C., Baxter, E. G., Helt, G., Nelson, C. R., Gabor, G. L., Abril, J. F., Agbayani, A., An, H. J., Andrews-Pfannkoch, C., Baldwin, D., Ballew, R. M., Basu, A., Baxendale, J., Bayraktaroglu, L., Beasley, E. M., Beeson, K. Y., Benos, P. V., Berman, B. P., Bhandari, D., Bolshakov, S., Borkova, D., Botchan, M. R., Bouck, J., Brokstein, P., Brottier, P., Burtis, K. C., Busam, D. A., Butler, H., Cadieu, E., Center, A., Chandra, I., Cherry, J. M., Cawley, S., Dahlke, C., Davenport, L. B., Davies, P., de Pablos, B., Delcher, A., Deng, Z., Mays, A. D., Dew, I., Dietz, S. M., Dodson, K., Doup, L. E., Downes, M., Dugan-Rocha, S., Dunkov, B. C., Dunn, P., Durbin, K. J., Evangelista, C. C., Ferraz, C., Ferriera, S., Fleischmann, W., Fosler, C., Gabrielian, A. E., Garg, N. S., Gelbart, W. M., Glasser, K., Glodek, A., Gong, F., Gorrell, J. H., Gu, Z., Guan, P., Harris, M., Harris, N. L., Harvey, D., Heiman, T. J., Hernandez, J. R., Houck, J., Hostin, D., Houston, K. A., Howland, T. J., Wei, M. H., Ibegwam, C., Jalali, M., Kalush, F., Karpen, G. H., Ke, Z., Kennison, J. A., Ketchum, K. A., Kimmel, B. E., Kodira, C. D., Kraft, C., Kravitz, S., Kulp, D., Lai, Z., Lasko, P., Lei, Y., Levitsky, A. A., Li, J., Li, Z., Liang, Y., Lin, X., Liu, X., Mattei, B., McIntosh, T. C., McLeod, M. P., McPherson, D., Merkulov, G., Milshina, N. V., Mobarry, C., Morris, J., Moshrefi, A., Mount, S. M., Moy, M., Murphy, B., Murphy, L., Muzny, D. M., Nelson, D. L., Nelson, D. R., Nelson, K. A., Nixon, K., Nusskern, D. R., Pacleb, J. M., Palazzolo, M., Pittman, G. S., Pan, S., Pollard, J., Puri, V., Reese, M. G., Reinert, K., Remington, K., Saunders, R. D., Scheeler, F., Shen, H., Shue, B. C., Siden-Kiamos, I., Simpson, M., Skupski, M. P., Smith, T., Spier, E., Spradling, A. C., Stapleton, M., Strong, R., Sun, E., Svirskas, R., Tector, C., Turner, R., Venter, E., Wang, A. H., Wang, X., Wang, Z. Y., Wassarman, D. A., Weinstock, G. M., Weissenbach, J., Williams, S. M., Woodage, T., Worley, K. C., Wu, D., Yang, S., Yao, Q. A., Ye, J., Yeh, R. F., Zaveri, J. S., Zhan, M., Zhang, G., Zhao, Q., Zheng, L., Zheng, X. H., Zhong, F. N., Zhong, W., Zhou, X., Zhu, S., Zhu, X., Smith, H. O., Gibbs, R. A., Myers, E. W., Rubin, G. M., and Venter, J. C. (2000). The genome sequence of *Drosophila melanogaster*. *Science* 287, 2185–2195.

Aldahmesh, M. A., Al-Owain, M., Alqahtani, F., Hazzaa, S., and Alkuraya, F. S. (2010). A null mutation in CABP4 causes Leber's congenital amaurosis-like phenotype. *Mol. Vis.* 16, 207–212.

Ames, J. B., and Ikura, M. (2002). Structure and membrane-targeting mechanism of retinal Ca2+-binding proteins, recoverin and GCAP-2. *Adv. Exp. Med. Biol.* 514, 333–348.

Ames, J. B., Ishima, R., Tanaka, T., Gordon, J. I., Stryer, L., and Ikura, M. (1997). Molecular mechanics of calcium-myristoyl switches. *Nature* 389, 198–202.

Ames, J. B., and Lim, S. (2011). Molecular structure and target recognition of neuronal calcium sensor proteins. *Biochim. Biophys. Acta*. [Epub ahead of print].

Audhya, A., Foti, M., and Emr, S. D. (2000). Distinct roles for the yeast phosphatidylinositol 4-kinases, Stt4p and Pik1p, in secretion, cell growth, and organelle membrane dynamics. *Mol. Biol. Cell* 11, 2673–2689.

Berridge, M. J. (1998). Neuronal calcium signaling. *Neuron* 21, 13–26.

Borgese, N., Brambillasca, S., and Colombo, S. (2007). How tails guide tail-anchored proteins to their destinations. *Curr. Opin. Cell Biol.* 19, 368–375.

Borgese, N., Brambillasca, S., Soffientini, P., Yabal, M., and Makarow, M. (2003). Biogenesis of tail-anchored proteins. *Biochem. Soc. Trans.* 31 (Pt 6), 1238–1242.

Borgese, N., and Fasana, E. (2011). Targeting pathways of C-tail-anchored proteins. *Biochim. Biophys. Acta* 1808, 937–946.

Brambillasca, S., Yabal, M., Makarow, M., and Borgese, N. (2006). Unassisted translocation of large polypeptide domains across phospholipid bilayers. *J. Cell Biol.* 175, 767–777.

Burgoyne, R. D. (2007). Neuronal calcium sensor proteins: generating diversity in neuronal Ca2+ signalling. *Nat. Rev. Neurosci.* 8, 182–193.

Burgoyne, R. D., Barclay, J. W., Ciufo, L. F., Graham, M. E., Handley, M. T., and Morgan, A. (2009). The functions of Munc18-1 in regulated exocytosis. *Ann. N.Y. Acad. Sci.* 1152, 76–86.

Burgoyne, R. D., and Haynes, L. P. (2010). Neuronal calcium sensor proteins: emerging roles in membrane traffic and synaptic plasticity. *F1000 Biol. Rep.* 2, 5.

Burgoyne, R. D., O'Callaghan, D. W., Hasdemir, B., Haynes, L. P., and Tepikin, A. V. (2004). Neuronal Ca2+-sensor proteins: multitalented regulators of neuronal function. *Trends Neurosci.* 27, 203–209.

Burgoyne, R. D., and Weiss, J. L. (2001). The neuronal calcium sensor family of Ca2+-binding proteins. *Biochem. J.* 353(Pt 1), 1–12.

C.elegans, S. C. (1998). Genome sequence of the nematode *C. elegans*: a platform for investigating biology. *Science* 282, 2012–2018.

Catterall, W. A., and Few, A. P. (2008). Calcium channel regulation and presynaptic plasticity. *Neuron* 59, 882–901.

Cosgrove, K. E., Galvan, E. J., Barrionuevo, G., and Meriney, S. D. (2011). mGluRs modulate strength and timing of excitatory transmission in hippocampal area CA3. *Mol. Neurobiol.* 44, 93–101.

Cui, G., Meyer, A. C., Calin-Jageman, I., Neef, J., Haeseleer, F., Moser, T., and Lee, A. (2007). Ca2+-binding proteins tune Ca2+-feedback to Cav1.3 channels in mouse auditory hair cells. *J. Physiol.* 585(Pt 3), 791–803.

Delcour, A. H., Lipscombe, D., and Tsien, R. W. (1993). Multiple modes of N-type calcium channel activity distinguished by differences in gating kinetics. *J. Neurosci.* 13, 181–194.

Dieterich, D. C., Karpova, A., Mikhaylova, M., Zdobnova, I., Konig, I., Landwehr, M., Kreutz, M., Smalla, K. H., Richter, K., Landgraf, P., Reissner, C., Boeckers, T. M., Zuschratter, W., Spilker, C., Seidenbecher, C. I., Garner, C. C., Gundelfinger, E. D., and Kreutz, M. R. (2008). Caldendrin-Jacob: a protein liaison that couples NMDA receptor signalling to the nucleus. *PLoS Biol.* 6, e34. doi: 10.1371/journal.pbio.0060034

Dolman, N. J., and Tepikin, A. V. (2006). Calcium gradients and the Golgi. *Cell Calcium* 40, 505–512.

Few, A. P., Lautermilch, N. J., Westenbroek, R. E., Scheuer, T., and Catterall, W. A. (2005). Differential regulation of CaV2.1 channels by calcium-binding protein 1 and visinin-like protein-2 requires N-terminal myristoylation. *J. Neurosci.* 25, 7071–7080.

Few, A. P., Nanou, E., Scheuer, T., and Catterall, W. A. (2011). Molecular determinants of CaV2.1 channel regulation by calcium-binding protein-1. *J. Biol. Chem.* 286, 41917–41923.

Findeisen, F., and Minor, D. L. Jr. (2010). Structural basis for the differential effects of CaBP1 and calmodulin on Ca(V)1.2 calcium-dependent inactivation. *Structure* 18, 1617–1631.

Fioravante, D., and Regehr, W. G. (2011). Short-term forms of presynaptic plasticity. *Curr. Opin. Neurobiol.* 21, 269–274.

Flowerdew, S. E., and Burgoyne, R. D. (2009). A VAMP7/Vti1a SNARE complex distinguishes a non-conventional traffic route to the cell surface used by KChIP1 and Kv4 potassium channels. *Biochem. J.* 418, 529–540.

Fries, R., Reddy, P. P., Mikhaylova, M., Haverkamp, S., Wei, T., Muller, M., Kreutz, M. R., and Koch, K. W. (2010). Dynamic cellular translocation of caldendrin is facilitated by the Ca2+-myristoyl switch of recoverin. *J. Neurochem.* 113, 1150–1162.

Gillespie, P. G., and Cyr, J. L. (2004). Myosin-1c, the hair cell's adaptation motor. *Annu. Rev. Physiol.* 66, 521–545.

Graham, M. E., Handley, M. T., Barclay, J. W., Ciufo, L. F., Barrow, S. L., Morgan, A., and Burgoyne, R. D. (2008). A gain-of-function mutant of Munc18-1 stimulates secretory granule recruitment and exocytosis and reveals a direct interaction of Munc18-1 with Rab3. *Biochem. J.* 409, 407–416.

Graham, T. R., and Burd, C. G. (2011). Coordination of Golgi functions by phosphatidylinositol 4-kinases. *Trends Cell Biol.* 21, 113–121.

Greer, P. L., and Greenberg, M. E. (2008). From synapse to nucleus: calcium-dependent gene transcription in the control of synapse development and function. *Neuron* 59, 846–860.

Haeseleer, F. (2008). Interaction and colocalization of CaBP4 and Unc119 (MRG4) in photoreceptors. *Invest. Ophthalmol. Vis. Sci.* 49, 2366–2375.

Haeseleer, F., Imanishi, Y., Maeda, T., Possin, D. E., Maeda, A., Lee, A., Rieke, F., and Palczewski, K. (2004). Essential role of Ca2+-binding protein 4, a Cav1.4 channel regulator, in photoreceptor synaptic function. *Nat. Neurosci.* 7, 1079–1087.

Haeseleer, F., Sokal, I., Verlinde, C. L., Erdjument-Bromage, H., Tempst, P., Pronin, A. N., Benovic, J. L., Fariss, R. N., and Palczewski, K. (2000). Five members of a novel Ca(2+)-binding protein (CABP) subfamily with similarity to calmodulin. *J. Biol. Chem.* 275, 1247–1260.

Hardingham, G. E., and Bading, H. (2003). The Yin and Yang of NMDA receptor signalling. *Trends Neurosci.* 26, 81–89.

Haynes, L. P., and Burgoyne, R. D. (2008). Unexpected tails of a Ca2+ sensor. *Nat. Chem. Biol.* 4, 90–91.

Haynes, L. P., Fitzgerald, D. J., Wareing, B., O'Callaghan, D. W., Morgan, A., and Burgoyne, R. D. (2006). Analysis of the interacting partners of the neuronal calcium-binding proteins L-CaBP1, hippocalcin, NCS-1 and neurocalcin delta. *Proteomics* 6, 1822–1832.

Haynes, L. P., Sherwood, M. W., Dolman, N. J., and Burgoyne, R. D. (2007). Specificity, promiscuity and localization of ARF protein interactions with NCS-1 and phosphatidylinositol-4 kinase-III beta. *Traffic* 8, 1080–1092.

Haynes, L. P., Tepikin, A. V., and Burgoyne, R. D. (2004). Calcium-binding protein 1 is an inhibitor of agonist-evoked, inositol 1,4,5-trisphosphate-mediated calcium signaling. *J. Biol. Chem.* 279, 547–555.

Haynes, L. P., Thomas, G. M., and Burgoyne, R. D. (2005). Interaction of neuronal calcium sensor-1 and ADP-ribosylation factor 1 allows bidirectional control of phosphatidylinositol 4-kinase beta and trans-Golgi network-plasma membrane traffic. *J. Biol. Chem.* 280, 6047–6054.

Hendricks, K. B., Wang, B. Q., Schnieders, E. A., and Thorner, J. (1999). Yeast homologue of neuronal frequenin is a regulator of phosphatidylinositol-4-OH kinase. *Nat. Cell Biol.* 1, 234–241.

Higashide, T., and Inana, G. (1999). Characterization of the gene for HRG4 (UNC119), a novel photoreceptor synaptic protein homologous to unc-119. *Genomics* 57, 446–450.

Higashide, T., McLaren, M. J., and Inana, G. (1998). Localization of HRG4, a photoreceptor protein homologous to Unc-119, in ribbon synapse. *Invest. Ophthalmol. Vis. Sci.* 39, 690–698.

Hikita, T., Taya, S., Fujino, Y., Taneichi-Kuroda, S., Ohta, K., Tsuboi, D., Shinoda, T., Kuroda, K., Funahashi, Y., Uraguchi-Asaki, J., Hashimoto, R., and Kaibuchi, K. (2009). Proteomic analysis reveals novel binding partners of dysbindin, a schizophrenia-related protein. *J. Neurochem.* 110, 1567–1574.

Hradsky, J., Raghuram, V., Reddy, P. P., Navarro, G., Hupe, M., Casado, V., McCormick, P. J., Sharma, Y., Kreutz, M. R., and Mikhaylova, M. (2011). Post-translational membrane insertion of tail-anchored transmembrane EF-hand Ca2+ sensor calneurons requires the TRC40/Asna1 rrotein chaperone. *J. Biol. Chem.* 286, 36762–36776.

Huang, C. C., Yang, D. M., Lin, C. C., and Kao, L. S. (2011). Involvement of Rab3A in vesicle priming during exocytosis: interaction with Munc13-1 and Munc18-1. *Traffic* 12, 1356–1370.

Iwasaki, H., Chiba, K., Uchiyama, T., Yoshikawa, F., Suzuki, F., Ikeda, M., Furuichi, T., and Mikoshiba, K. (2002). Molecular characterization of the starfish inositol 1,4,5-trisphosphate receptor and its role during oocyte maturation and fertilization. *J. Biol. Chem.* 277, 2763–2772.

Jeziorski, M. C., Greenberg, R. M., and Anderson, P. A. (2000). The molecular biology of invertebrate voltage-gated Ca(2+) channels. *J. Exp. Biol.* 203(Pt 5), 841–856.

Kasri, N. N., Holmes, A. M., Bultynck, G., Parys, J. B., Bootman, M. D., Rietdorf, K., Missiaen, L., McDonald, F., De Smedt, H., Conway, S. J., Holmes, A. B., Berridge, M. J., and Roderick, H. L. (2004). Regulation of InsP3 receptor activity by neuronal Ca2+-binding proteins. *EMBO J.* 23, 312–321.

Kasri, N. N., Torok, K., Galione, A., Garnham, C., Callewaert, G., Missiaen, L., Parys, J. B., and De Smedt, H. (2006). Endogenously bound calmodulin is essential for the function of the inositol 1,4,5-trisphosphate receptor. *J. Biol. Chem.* 281, 8332–8338.

Kawasaki, H., Nakayama, S., and Kretsinger, R. H. (1998). Classification and evolution of EF-hand proteins. *Biometals* 11, 277–295.

Kinoshita-Kawada, M., Tang, J., Xiao, R., Kaneko, S., Foskett, J. K., and Zhu, M. X. (2005). Inhibition of TRPC5 channels by Ca2+-binding protein 1 in Xenopus oocytes. *Pflugers Arch.* 450, 345–354.

Klee, C. B., Crouch, T. H., and Richman, P. G. (1980). Calmodulin. *Annu. Rev. Biochem.* 49, 489–515.

Kobayashi, A., Higashide, T., Hamasaki, D., Kubota, S., Sakuma, H., An, W., Fujimaki, T., McLaren, M. J., Weleber, R. G., and Inana, G. (2000). HRG4 (UNC119) mutation found in cone-rod dystrophy causes retinal degeneration in a transgenic model. *Invest. Ophthalmol. Vis. Sci.* 41, 3268–3277.

Landwehr, M., Redecker, P., Dieterich, D. C., Richter, K., Bockers, T. M., Gundelfinger, E. D., and Kreutz, M. R. (2003). Association of Caldendrin splice isoforms with secretory vesicles in neurohypophyseal axons and the pituitary. *FEBS Lett.* 547, 189–192.

Lee, A., Jimenez, A., Cui, G., and Haeseleer, F. (2007a). Phosphorylation of the Ca2+-binding protein CaBP4 by protein kinase C zeta in photoreceptors. *J. Neurosci.* 27, 12743–12754.

Lee, A., Westenbroek, R. E., Haeseleer, F., Palczewski, K., Scheuer, T., and Catterall, W. A. (2002). Differential modulation of Ca(v)2.1 channels by calmodulin and Ca2+-binding protein 1. *Nat. Neurosci.* 5, 210–217.

Lee, S., Briklin, O., Hiel, H., and Fuchs, P. (2007b). Calcium-dependent inactivation of calcium channels in cochlear hair cells of the chicken. *J. Physiol.* 583(Pt 3), 909–922.

Li, C., Chan, J., Haeseleer, F., Mikoshiba, K., Palczewski, K., Ikura, M., and Ames, J. B. (2009). Structural insights into Ca2+-dependent regulation of inositol

1,4,5-trisphosphate receptors by CaBP1. *J. Biol. Chem.* 284, 2472–2481.

Littink, K. W., van Genderen, M. M., Collin, R. W., Roosing, S., de Brouwer, A. P., Riemslag, F. C., Venselaar, H., Thiadens, A. A., Hoyng, C. B., Rohrschneider, K., den Hollander, A. I., Cremers, F. P., and van den Born, L. I. (2009). A novel homozygous nonsense mutation in CABP4 causes congenital cone-rod synaptic disorder. *Invest. Ophthalmol. Vis. Sci.* 50, 2344–2350.

Lohmann, C. (2009). Calcium signaling and the development of specific neuronal connections. *Prog. Brain Res.* 175, 443–452.

Lyons, M. R., and West, A. E. (2011). Mechanisms of specificity in neuronal activity-regulated gene transcription. *Prog. Neurobiol.* 94, 259–295.

Maduro, M., and Pilgrim, D. (1995). Identification and cloning of unc-119, a gene expressed in the *Caenorhabditis elegans* nervous system. *Genetics* 141, 977–988.

Maduro, M., and Pilgrim, D. (1996). Conservation of function and expression of unc-119 from two Caenorhabditis species despite divergence of non-coding DNA. *Gene* 183, 77–85.

Maduro, M. F., Gordon, M., Jacobs, R., and Pilgrim, D. B. (2000). The UNC-119 family of neural proteins is functionally conserved between humans, Drosophila and *C. elegans*. *J. Neurogenet.* 13, 191–212.

McCue, H. V., Burgoyne, R. D., and Haynes, L. P. (2009). Membrane targeting of the EF-hand containing calcium-sensing proteins CaBP7 and CaBP8. *Biochem. Biophys. Res. Commun.* 380, 825–831.

McCue, H. V., Burgoyne, R. D., and Haynes, L. P. (2011). Determination of the membrane topology of the small EF-Hand Ca^{2+}-sensing proteins CaBP7 and CaBP8. *PLoS One* 6, e17853. doi: 10.1371/journal.pone.0017853

McCue, H. V., Haynes, L. P., and Burgoyne, R. D. (2010a). Bioinformatic analysis of CaBP/calneuron proteins reveals a family of highly conserved vertebrate Ca2+-binding proteins. *BMC Res. Notes* 3, 118.

McCue, H. V., Haynes, L. P., and Burgoyne, R. D. (2010b). The diversity of calcium sensor proteins in the regulation of neuronal function. *Cold Spring Harb. Perspect. Biol.* 2, a004085.

Mikhaylova, M., Hradsky, J., and Kreutz, M. R. (2011). Between promiscuity and specificity: novel roles of EF-hand calcium sensors in neuronal Ca2+ signalling. *J. Neurochem.* 118, 695–713.

Mikhaylova, M., Reddy, P. P., Munsch, T., Landgraf, P., Suman, S. K., Smalla, K. H., Gundelfinger, E. D., Sharma, Y., and Kreutz, M. R. (2009). Calneurons provide a calcium threshold for trans-Golgi network to plasma membrane trafficking. *Proc. Natl. Acad. Sci. U.S.A.* 106, 9093–9098.

Mikhaylova, M., Sharma, Y., Reissner, C., Nagel, F., Aravind, P., Rajini, B., Smalla, K. H., Gundelfinger, E. D., and Kreutz, M. R. (2006). Neuronal Ca2+ signaling via caldendrin and calneurons. *Biochim. Biophys. Acta* 1763, 1229–1237.

Minor, D. L. Jr., and Findeisen, F. (2010). Progress in the structural understanding of voltage-gated calcium channel (CaV) function and modulation. *Channels (Austin)* 4, 459–474.

Nakajima, Y. (2011). Ca2+-dependent binding of calcium-binding protein 1 to presynaptic group III metabotropic glutamate receptors and blockage by phosphorylation of the receptors. *Biochem. Biophys. Res. Commun.* 412, 602–605.

Nakajima, Y., Mochida, S., Okawa, K., and Nakanishi, S. (2009). Ca2+-dependent release of Munc18-1 from presynaptic mGluRs in short-term facilitation. *Proc. Natl. Acad. Sci. U.S.A.* 106, 18385–18389.

Nakajima, Y., Yamamoto, T., Nakayama, T., and Nakanishi, S. (1999). A relationship between protein kinase C phosphorylation and calmodulin binding to the metabotropic glutamate receptor subtype 7. *J. Biol. Chem.* 274, 27573–27577.

Nickerson, P. E., Ronellenfitch, K., McEwan, J., Kim, H., McInnes, R. R., and Chow, R. L. (2011). A transgenic mouse line expressing cre recombinase in undifferentiated postmitotic mouse retinal bipolar cell precursors. *PLoS One* 6, e27145. doi: 10.1371/journal.pone.0027145

O'Connor, V., El Far, O., Bofill-Cardona, E., Nanoff, C., Freissmuth, M., Karschin, A., Airas, J. M., Betz, H., and Boehm, S. (1999). Calmodulin dependence of presynaptic metabotropic glutamate receptor signaling. *Science* 286, 1180–1184.

Okamoto, M., and Sudhof, T. C. (1997). Mints, Munc18-interacting proteins in synaptic vesicle exocytosis. *J. Biol. Chem.* 272, 31459–31464.

Oz, S., Tsemakhovich, V., Christel, C. J., Lee, A., and Dascal, N. (2011). CaBP1 regulates voltage-dependent inactivation and activation of Ca(V)1.2 (L-type) calcium channels. *J. Biol. Chem.* 286, 13945–13953.

Parekh, A. B. (2011). Decoding cytosolic Ca2+ oscillations. *Trends Biochem. Sci.* 36, 78–87.

Petko, J. A., Kabbani, N., Frey, C., Woll, M., Hickey, K., Craig, M., Canfield, V. A., and Levenson, R. (2009). Proteomic and functional analysis of NCS-1 binding proteins reveals novel signaling pathways required for inner ear development in zebrafish. *BMC Neurosci.* 10, 27.

Pinheiro, P. S., and Mulle, C. (2008). Presynaptic glutamate receptors: physiological functions and mechanisms of action. *Nat. Rev. Neurosci.* 9, 423–436.

Rabu, C., Wipf, P., Brodsky, J. L., and High, S. (2008). A precursor-specific role for Hsp40/Hsc70 during tail-anchored protein integration at the endoplasmic reticulum. *J. Biol. Chem.* 283, 27504–27513.

Rieke, F., Lee, A., and Haeseleer, F. (2008). Characterization of Ca2+-binding protein 5 knockout mouse retina. *Invest. Ophthalmol. Vis. Sci.* 49, 5126–5135.

Sauer, B. (1998). Inducible gene targeting in mice using the Cre/lox system. *Methods* 14, 381–392.

Seidenbecher, C. I., Landwehr, M., Smalla, K. H., Kreutz, M., Dieterich, D. C., Zuschratter, W., Reissner, C., Hammarback, J. A., Bockers, T. M., Gundelfinger, E. D., and Kreutz, M. R. (2004). Caldendrin but not calmodulin binds to light chain 3 of MAP1A/B: an association with the microtubule cytoskeleton highlighting exclusive binding partners for neuronal Ca(2+)-sensor proteins. *J. Mol. Biol.* 336, 957–970.

Seidenbecher, C. I., Langnaese, K., Sanmarti-Vila, L., Boeckers, T. M., Smalla, K. H., Sabel, B. A., Garner, C. C., Gundelfinger, E. D., and Kreutz, M. R. (1998). Caldendrin, a novel neuronal calcium-binding protein confined to the somatodendritic compartment. *J. Biol. Chem.* 273, 21324–21331.

Shih, P. Y., Lin, C. L., Cheng, P. W., Liao, J. H., and Pan, C. Y. (2009). Calneuron I inhibits Ca(2+) channel activity in bovine chromaffin cells. *Biochem. Biophys. Res. Commun.* 388, 549–553.

Sokal, I., and Haeseleer, F. (2011). Insight into the role of Ca2+-binding protein 5 in vesicle exocytosis. *Invest. Ophthalmol. Vis. Sci.* 52, 9131–9141.

Soldati, T. (2003). Unconventional myosins, actin dynamics and endocytosis: a menage a trois? *Traffic* 4, 358–366.

Stefanovic, S., and Hegde, R. S. (2007). Identification of a targeting factor for posttranslational membrane protein insertion into the ER. *Cell* 128, 1147–1159.

Sudhof, T. C., and Rothman, J. E. (2009). Membrane fusion: grappling with SNARE and SM proteins. *Science* 323, 474–477.

Tanaka, T., Ames, J. B., Harvey, T. S., Stryer, L., and Ikura, M. (1995). Sequestration of the membrane-targeting myristoyl group of recoverin in the calcium-free state. *Nature* 376, 444–447.

Tang, N., Lin, T., Yang, J., Foskett, J. K., and Ostap, E. M. (2007). CIB1 and CaBP1 bind to the myo1c regulatory domain. *J. Muscle Res. Cell Motil.* 28, 285–291.

Tippens, A. L., and Lee, A. (2007). Caldendrin, a neuron-specific modulator of Cav/1.2 (L-type) Ca2+ channels. *J. Biol. Chem.* 282, 8464–8473.

Verhage, M., de Vries, K. J., Roshol, H., Burbach, J. P., Gispen, W. H., and Sudhof, T. C. (1997). DOC2 proteins in rat brain: complementary distribution and proposed function as vesicular adapter proteins in early stages of secretion. *Neuron* 18, 453–461.

Williams, R. J. (2006). The evolution of calcium biochemistry. *Biochim. Biophys. Acta* 1763, 1139–1146.

Wu, Y. Q., Lin, X., Liu, C. M., Jamrich, M., and Shaffer, L. G. (2001). Identification of a human brain-specific gene, calneuron 1, a new member of the calmodulin superfamily. *Mol. Genet. Metab.* 72, 343–350.

Yang, P. S., Alseikhan, B. A., Hiel, H., Grant, L., Mori, M. X., Yang, W., Fuchs, P. A., and Yue, D. T. (2006). Switching of Ca2+-dependent inactivation of Ca(v)1.3 channels by calcium binding proteins of auditory hair cells. *J. Neurosci.* 26, 10677–10689.

Yap, K. L., Ames, J. B., Swindells, M. B., and Ikura, M. (1999). Diversity of conformational states and changes within the EF-hand protein superfamily. *Proteins* 37, 499–507.

Zeitz, C., Kloeckener-Gruissem, B., Forster, U., Kohl, S., Magyar, I., Wissinger, B., Matyas, G., Borruat, F. X., Schorderet, D. F., Zrenner, E., Munier, F. L., and Berger, W. (2006). Mutations in CABP4, the gene encoding the Ca2+-binding protein 4, cause autosomal recessive

night blindness. *Am. J. Hum. Genet.* 79, 657–667.

Zhang, D., Boulware, M. J., Pendleton, M. R., Nogi, T., and Marchant, J. S. (2007). The inositol 1,4,5-trisphosphate receptor (Itpr) gene family in Xenopus: identification of type 2 and type 3 inositol 1,4,5-trisphosphate receptor subtypes. *Biochem. J.* 404, 383–391.

Zhao, X., Varnai, P., Tuymetova, G., Balla, A., Toth, Z. E., Oker-Blom, C., Roder, J., Jeromin, A., and Balla, T. (2001). Interaction of neuronal calcium sensor-1 (NCS-1) with phosphatidylinositol 4-kinase beta stimulates lipid kinase activity and affects membrane trafficking in COS-7 cells. *J. Biol. Chem.* 276, 40183–40189.

Zhou, H., Kim, S. A., Kirk, E. A., Tippens, A. L., Sun, H., Haeseleer, F., and Lee, A. (2004). Ca2+-binding protein-1 facilitates and forms a postsynaptic complex with Cav1.2 (L-type) Ca2+ channels. *J. Neurosci.* 24, 4698–4708.

Zhou, H., Yu, K., McCoy, K. L., and Lee, A. (2005). Molecular mechanism for divergent regulation of Cav1.2 Ca2+ channels by calmodulin and Ca2+-binding protein-1. *J. Biol. Chem.* 280, 29612–29619.

Conflict of Interest Statement: The authors declare that the research was conducted in the absence of any commercial or financial relationships that could be construed as a potential conflict of interest.

Received: 09 January 2012; paper pending published: 23 January 2012; accepted: 25 January 2012; published online: 21 February 2012.

Citation: Haynes LP, McCue HV and Burgoyne RD (2012) Evolution and functional diversity of the Calcium Binding Proteins (CaBPs). Front. Mol. Neurosci. 5:9. doi: 10.3389/fnmol.2012.00009

frontiers in
MOLECULAR NEUROSCIENCE

REVIEW ARTICLE
published: 14 May 2012
doi: 10.3389/fnmol.2012.00064

The calcium: an early signal that initiates the formation of the nervous system during embryogenesis

Catherine Leclerc*, Isabelle Néant and Marc Moreau

Centre de Biologie du Développement, Université de Toulouse, CNRS UMR 5547, Toulouse, France and GDRE n° 731, "Ca^{2+} toolkit coded proteins as drug targets in animal and plant cells"

Edited by:
Jose R. Naranjo, Centro Nalcional De Biotecnologia/Consejo Superior De Investigaciones Cientificas, Spain

Reviewed by:
Jose R. Naranjo, Centro Nalcional De Biotecnologia/Consejo Superior De Investigaciones Cientificas, Spain
Andrew L. Miller, The Hong Kong University of Science and Technology, China

****Correspondence:***
Catherine Leclerc, Centre de Biologie du Développement, UMR CNRS 5547 and GDRE 731, Université Toulouse III, 118 route de Narbonne, 31062 Toulouse, France.
e-mail: catherine.leclerc@univ-tlse3.fr

The calcium (Ca^{2+}) signaling pathways have crucial roles in development from fertilization through differentiation to organogenesis. In the nervous system, Ca^{2+} signals are important regulators for various neuronal functions, including formation and maturation of neuronal circuits and long-term memory. However, Ca^{2+} signals are also involved in the earliest steps of neurogenesis including neural induction, differentiation of neural progenitors into neurons, and the neuro-glial switch. This review examines when and how Ca^{2+} signals are generated during each of these steps with examples taken from *in vivo* studies in vertebrate embryos and from *in vitro* assays using embryonic and neural stem cells (NSCs). During the early phases of neurogenesis few investigations have been performed to study the downstream targets of Ca^{2+} which posses EF-hand in their structure. This opens an entire field of research. We also discuss the highly specific nature of the Ca^{2+} signaling pathway and its interaction with the other signaling pathways involved in early neural development.

Keywords: calcium signaling, EF-hand, neural induction, early neural development, stem cell, neural progenitor, neuro-glial switch

INTRODUCTION

The formation of the vertebrate nervous system requires the temporally and spatially controlled production of a large number of neuronal and glial cell types. This starts with neural induction, an inductive interaction between the dorsal mesoderm and the dorsal ectoderm which occurs during gastrulation. As a result of this interaction, the dorsal ectoderm adopts a neural fate. This is the pioneer work of Spemann and Mangold in the 1920s (Spemann and Mangold, 1924) in the newt embryo which identified the dorsal mesoderm as the neural organizing center. Equivalent regions were then found in most vertebrates (Waddington, 1933, 1936; Oppenheimer, 1936).

Following neural induction, the dorsal ectoderm or neuroectoderm forms the neural plate which consists of undifferentiated dividing neuroepithelial cells that later during development will exit the cell cycle and will differentiate into neurons and glial cells. Differentiation occurs in defined temporal sequences with neurons generated first and glial cells second. These temporal sequences of early neural development are widely conserved across vertebrate species (Bayer and Altman, 1991). Numerous studies have detailed the diverse signaling pathways that control each sequence (Rowitch, 2004; Stern, 2005; Okano and Temple, 2009; Rogers et al., 2009).

Spontaneous Ca^{2+} events appear to be common features of developing brain. Ca^{2+} transients have been observed in dorsal region of embryos as early as gastrulation. In Zebrafish embryo as well as in amphibians, localized Ca^{2+} transients have been imaged during gastrulation in dorsal region of the embryos, and correlate both temporally and spatially to neural induction (Webb and Miller, 2007). Later on, spontaneous Ca^{2+} oscillations have been associated with the expansion of the neural progenitors pool.

This review describes how Ca^{2+} signaling participates in the control of the earliest steps of neural development, including neural induction, followed by the differentiation of neural progenitors into neurons, and the neuro-glial switch. We call these two last steps early neurogenesis (**Figure 1**). Our goal is to highlight how through the combination of specific Ca^{2+} toolkit elements (Berridge et al., 2000) calcium can achieve specific functions.

Ca^{2+} SIGNALING DURING NEURAL INDUCTION

Neural and epidermal tissues have the same embryonic origin, the ectoderm. In vertebrates, during gastrulation, the cells of the embryonic ectoderm give rise to epidermal progenitors in the ventral side and to neural progenitors in the dorsal side. This binary choice of cell fate is controlled by complex mechanisms that involve positive effectors (Fibroblast Growth Factors, FGFs) and negative effectors (Bone morphogenetic proteins, BMPs; Wingless/Int proteins, Wnts, and Nodal) of neural induction (De Robertis and Kuroda, 2004; Stern, 2005; Gaspard and Vanderhaeghen, 2010). One key regulatory mechanism involved in the conversion of the ectoderm into neuroectoderm is the inhibition of the BMP pathway by noggin, chordin, and follistatin, which are factors secreted by the dorsal mesoderm.

Direct evidence that Ca^{2+} plays an important role in the choice of fate between neural versus epidermal has emerged through data obtained in the amphibians. In the newt *Pleurodeles waltl* and in

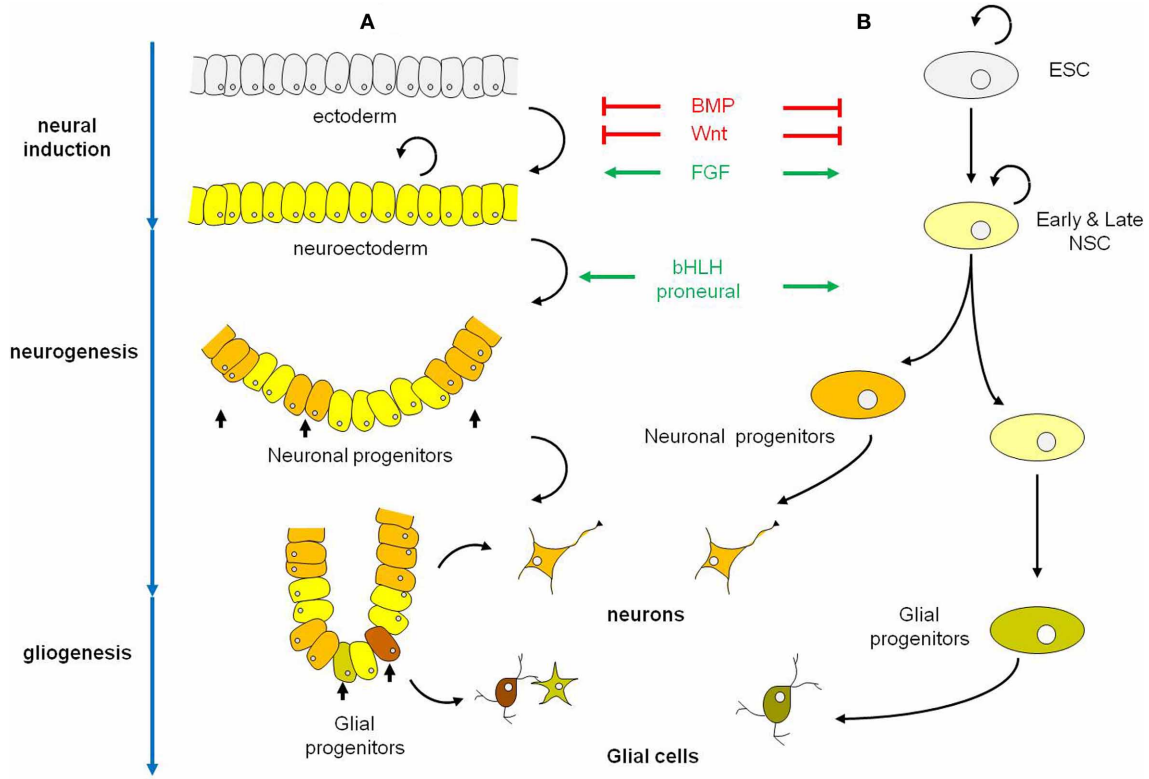

FIGURE 1 | Schematic representations of the early phases of neural development in the embryo (A) and in Esc (B). (A) Neural induction which converts ectoderm into neuroectoderm is regulated by the coordinated actions of BMP, Wnt, and FGF signaling pathways. Neuroectodermal cells are undifferentiated dividing neuroepithelial cells that will latter differentiate into neurons (neurogenesis period) and in a second phase into glial cells (gliogenesis period). Among the factors that control the selection of neuronal progenitors from the neuroectodermal cells and their commitment to differentiate along the neuronal lineage are the proneural bHLH genes. In vertebrates, proneural bHLH genes are first expressed in the neuroectodermal cells, already committed to the neural fate. The neuronal progenitors have a limited mitotic potential. Differentiation occurs in a defined temporal sequence, neurons being generated first, followed by glial cells. The switch from neurogenesis to gliogenesis is controlled by both extrinsic and intrinsic signals and is the result of changes in the progenitor properties within the same pool of neuronal progenitors. **(B)** In ESC neural induction and specification of ES-derived neural progenitors follow the same cues as in the embryo to give rise to populations of neurons and glial cells. Black curved arrows indicate self-renewing cells. *Abbreviations:* BMP, bone morphogenetic protein; bHLH genes, basic helix-loop-helix genes; ESC, embryonic stem cell; NSC, neural stem cell.

Xenopus laevis embryos, spontaneous elevations of intracellular Ca^{2+} ($[Ca^{2+}]_i$) are restricted to the dorsal ectoderm cells (the tissue where neural induction takes place) and never occurs in ventral ectoderm cells, which are at the origin of the epidermis (Leclerc et al., 1997, 2000). As gastrulation proceeds, Ca^{2+} transients increase both in number and intensity, to reach a peak activity by mid-gastrulation, a stage where neural determination is thought to have occurred (Leclerc et al., 2000). The onset of these spontaneous Ca^{2+} events occurs at the blastula stage, long before the start of gastrulation (i.e., before mesoderm invagination). These observations are in agreement with other results obtained in *Xenopus* (Sharpe et al., 1987) and in Chick (Streit et al., 2000) suggesting that neural induction starts before gastrulation. At the late blastula stage, the dorsal ectoderm is already biased toward dorsal fate and is more responsive to neural-inducing signals than the ventral ectoderm (Sharpe et al., 1987). Furthermore, direct visualization of the Ca^{2+} dynamics in *Xenopus laevis* reveals that the Ca^{2+} transients are localized in the most anterior part of the dorsal ectoderm. The accumulation of these Ca^{2+} transients versus time correlates with the prospective neuroectoderm and the Ca^{2+} transients are probably the first directly visualized events linked to neural induction. Later, during gastrulation, Ca^{2+} transients are always restricted to the dorsal ectoderm (the prospective forebrain-midbrain) and never occur in the non involuting marginal zone (NIMZ; i.e., the prospective hindbrain-spinal cord).

The ability of the ectoderm cells to be induced and to differentiate toward neural tissue, called neural competence, is acquired shortly before gastrulation and lost during late gastrula stages. In *Xenopus*, as in *Pleurodeles* embryos, neural competence is associated with the expression of functional dihydropyridine sensitive Ca^{2+} channels (DHP-Ca^{2+} channels) in the plasma membrane (Drean et al., 1995; Leclerc et al., 1995). Functional DHP-Ca^{2+} channels first appear in the ectoderm cells at blastula stage. The highest density of DHP-Ca^{2+} channels is reached at mid-gastrula, when competence of the ectoderm is optimal. The decrease of

the DHP-Ca^{2+} channel density occurs simultaneously with the normal loss of competence, at the end of gastrulation. This temporal pattern of DHP-Ca^{2+} channels expression correlates with the dynamic pattern of Ca^{2+} transients. DHP-Ca^{2+} channels belong to the large family of voltage-operated Ca^{2+} channels (VOCCs) composed of a pore forming Ca_v subunit, associated with regulatory subunits. The Ca_v subunit is encoded by four genes; $Ca_v1.1$, $Ca_v1.2$, $Ca_v1.3$, $Ca_v1.4$ (Catterall et al., 2005). In *Xenopus laevis* gastrula embryo, the expression of $Ca_v1.2$ transcripts is restricted to the dorsal mesoderm and to the inner layer of the ectoderm (Leclerc et al., unpublished data); i.e., the first ectoderm layer to be induced toward neural fate during gastrulation (Chalmers et al., 2002).

The inhibition of DHP-Ca^{2+} channels function by specific antagonists during gastrulation completely abolishes the patterns of Ca^{2+} transients and decreases the intracellular Ca^{2+} resting level, suggesting that the patterns of Ca^{2+} transients are generated via the activation of DHP-Ca^{2+} channels (Leclerc et al., 1997, 2000). The abolition of these Ca^{2+} transients induces both the downregulation of at least two early neural genes (*Zic3* and *geminin*) and the presence of severe abnormalities in the anterior nervous system. The most apparent defects are a deformation of the head, a reduction in the size or the total disappearance of the eyes, and lack of melanophores (Leclerc et al., 2000, 2001). Acquisition of the neural fate in amphibians therefore requires the expression of functional DHP-Ca^{2+} channels in the ectoderm. Since these channels are VOCCs, this raises the question about the mechanism by which the DHP-Ca^{2+} channels are specifically activated in the dorsal ectoderm during the process of neural induction. Other questions concern the identification of the Ca^{2+}-target genes and the persistence of the role of Ca^{2+} during neural induction in vertebrates. Some clues will be given in the following paragraphs.

Ex vivo MODELS OF NEURAL INDUCTION

Two *ex vivo* models have been particularly useful to decipher the molecular mechanisms involved during neural induction. We will discuss data obtained from mouse embryonic stem cells (ESCs) and from naïve ectoderm (animal caps) isolated from *Xenopus laevis* blastula. Although the spatial and temporal influences of early vertebrate embryogenesis are missing from these *ex vivo* assays, the same signals affecting neural induction in developing embryos also regulate neurogenesis in these models (**Figure 1**). Indeed, FGFs and antagonists of BMP, Nodal and Wnt signaling pathways (for reviews see Cai and Grabel, 2007; Gaulden and Reiter, 2008) have been shown to promote commitment of ESC to Neural stem cells (NSCs). This is also true for *Xenopus* ectoderm cells. Particularly, any manipulation that reduces BMP signaling neuralizes the animal cap cells. The Noggin protein, a BMP antagonist rapidly induces the expression of neural specific markers in animal cap cells at the expense of epidermal markers (Lamb et al., 1993; Hemmati-Brivanlou and Melton, 1997; Stern, 2005).

THE EMBRYONIC STEM CELLS

Neural induction studies in mammals have mainly involved the use of ESC due to difficulties in accessing and manipulating early embryos. ESCs are self-renewing and pluripotent cells that give rise to derivatives of all three germ layers (endoderm, ectoderm, and mesoderm). The derivation of specific neuronal and glial cell types from ESC results from different protocols but invariably proceeds through similar steps: (1) induction and production of NSCs, (2) stabilization of cell fate and appearance of radial-glial-like progenitor cells and (3) differentiation of progenitors into a variety of specific neuronal and glial cells derivatives, including dopaminergic, glutamatergic, or GABAergic neurons and oligodendrocytes, respectively (**Figure 1**).

Evidences indicate that the control of Ca^{2+} homeostasis is an important regulator of neural fate in mammals. A proteomic analysis to determine the global protein expression changes between mouse ESC and differentiated dopaminergic neurons identified about 20 proteins differentially regulated during neural differentiation (Wang and Gao, 2005). Among these proteins, Wang and Gao identified three Ca^{2+}-related proteins: calreticulin and pyruvate dehydrogenase E1/E2 subunits which are up-regulated, and the *T*ranslationally *C*ontrolled *T*umor *P*rotein (TCTP) which is down-regulated in neurons. TCTP is a Ca^{2+}- and microtubule-binding protein involved in the control of cell proliferation and cell cycle. It is up-regulated upon entry into cell cycle, bound to microtubules during mitosis and detached from the spindle after metaphase (Bommer and Thiele, 2004). TCTP has been shown to regulate Ca^{2+} uptake and Ca^{2+} homeostasis in trophoblast cells (Arcuri et al., 2005) and to negatively regulate the Na, K-ATPase activity in HeLa cells (Yoon et al., 2006). Calreticulin is an endoplasmic reticulum luminal Ca^{2+} buffering protein involved in the regulation of intracellular Ca^{2+} homeostasis (Michalak et al., 2009) and the E1/E2 subunits of the mitochondrial pyruvate dehydrogenase are activated by Ca^{2+} (Denton, 2009). Additional studies have started to decipher the role of Ca^{2+} signaling in neuronal fate induction. Electrical stimulation of embryoid bodies (EBs) induces the differentiation of cells expressing TuJ1, a marker for early committed neuronal cells. The mechanism of this electrical induction requires an influx of Ca^{2+} that does not involve VOCCs (Yamada et al., 2007).

More recently, a screen to identify genes involved in neural induction in mammals identified Neuronatin (Nnat) (Lin et al., 2010). Nnat is a membrane protein from the endoplasmic reticulum that belongs to the proteolipid family, strongly expressed in specific developing brain structures (Wijnholds et al., 1995). During *ex vivo* neural differentiation, Nnat is expressed in all steps from ESC to neurons, and reaches a maximum of expression in early neuroectodermal cells. Nnat has been shown to physically interact with the sarco/endoplasmic reticulum Ca^{2+}-ATPase isoform 2 (SERCA2) and to regulate the intracellular Ca^{2+} level by antagonizing SERCA2 activity. The modulation of Ca^{2+} homeostasis controls neural induction (i.e., the ability of ESC to produce NSC). While the overexpression of Nnat is associated with an increase in $[Ca^{2+}]_i$ and the generation of neuroectodermal cells and neurons, knocking down of Nnat reduces the level of intracellular Ca^{2+} and inhibits neural induction in ESCs (Lin et al., 2010). This latter effect can be rescued with thapsigargin, an inhibitor of the SERCA pump. Furthermore, high $[Ca^{2+}]_i$ conditions inhibit BMP signaling and interact with the FGF/Erk signaling pathway by increasing the phosphorylation of Erk.

THE ANIMAL CAP ASSAY IN XENOPUS LAEVIS

In *Xenopus laevis* embryo, the ectoderm cells isolated at blastula stage retain their pluripotentiality and upon exposure to specific inducers can differentiate into neural, mesodermal, or endodermal tissues. In this sense, although not self-renewing, the isolated ectoderm cells (or animal cap cells) display behavior similar to mammalian ESCs (Okabayashi and Asashima, 2003).

Barth and Barth (1964) were the first to suggest that in *Rana pipiens* embryos, Ca^{2+} is required to induce neuralisation of the ectoderm cells. Following on this early report, it was shown that dissociation of *Xenopus laevis* and *Pleurodeles waltl* animal caps in Ca^{2+}- and Mg^{2+}-free medium directed cells towards a neural fate (Grunz and Tacke, 1989; Saint-Jeannet et al., 1990) and was associated with an increase in $[Ca^{2+}]_i$ (Leclerc et al., 2001). This increase is due to a release of Ca^{2+} from internal stores, resulting from the reverse gradient of concentration of Ca^{2+} between intra and extracellular compartments. Dissociation of animal caps preloaded with the Ca^{2+} chelator BAPTA both abolishes the Ca^{2+} increase and neural induction (Leclerc et al., 2001). It has been shown that Noggin is one of the endogenous neural inducer by interacting BMP proteins (Zimmerman et al., 1996). Noggin is also able to trigger an increase in $[Ca^{2+}]_i$ via an influx through DHP-Ca^{2+} channels (Leclerc et al., 1997, 1999, 2000). The direct activation of DHP-Ca^{2+} channels by specific agonists such as S(-)Bay K 8644, generates a transient increase in $[Ca^{2+}]_i$. This increase is sufficient, even in an active BMP context, to trigger not only the expression of neural markers but also the formation of neurons and glial cells (Moreau et al., 1994). In addition, methylxanthines, such as caffeine or theophyline, which are known to stimulate the release of Ca^{2+} from internal stores, are also potent neural inducers (Moreau et al., 1994; Batut et al., 2005). These data strongly suggest that Ca^{2+} is a necessary and sufficient signal to initiate neural induction and to promote neural differentiation.

Recent studies suggest that the mechanism by which DHP-Ca^{2+} channels are activated in the ectoderm during neural induction might be via membrane depolarization induced by BMP antagonist and/or FGF signaling (Lee et al., 2009). Both FGF-4 and Noggin depolarize the membrane of ectoderm cells. Furthermore, FGF-4 induces an increase in $[Ca^{2+}]_i$ which can be blocked by SU5402, an FGF receptor inhibitor, and by DHP-Ca^{2+} channel antagonists. SU5402 also blocks the induction of neural genes induced by Noggin. The proposed mechanism involves that (1) FGFR activation, most likely *via* FGFR1 and/or FGFR4, triggers an influx of Ca^{2+} through non specific cationic channels (namely TRP channels). (2) This initial Ca^{2+} increase is then able to depolarize the cell membrane (Puro and Mano, 1991; Distasi et al., 1995, 1998; Fiorio Pla et al., 2005), which in turn activates DHP-Ca^{2+} channels. (3) This subsequent influx of Ca^{2+} amplifies the initial Ca^{2+} increase and leads to the expression of neural genes (Lee et al., 2009). However, the question regarding how the inhibition of BMP4 signaling by noggin might induce an influx of Ca^{2+} influx remains to be clarified.

Ca^{2+} SIGNALING DURING NEURAL INDUCTION IN VERTEBRATES: AN EMERGING MODEL

Altogether the results obtained from *Xenopus* and mouse models reveal that the mechanisms that govern neural induction involve the cross-talk between several signaling pathways and specially require the inhibition of BMP pathway, the activation of the FGF/Erk pathway and the control of Ca^{2+} homeostasis. The general model of neural induction, presented in **Figure 2**, highlights the similarities and the differences between mammals and amphibians.

The phosphorylation of Erk is a common event that mediates neural fate in vertebrates. In mouse ESC Ca^{2+} signaling increases the phosphorylation of Erk and triggers neural induction (Lin et al., 2010). In the amphibian the same mechanism is likely to control Erk phosphorylation. It has been shown that dissociation of ectoderm cells triggers a large increase in $[Ca^{2+}]_i$ (Leclerc et al., 2001) and causes the phosphorylation of Erk (Kuroda et al., 2005). An increase in intracellular Ca^{2+} concentration appears to be the core signal that controls neural fate determination in vertebrates. This increase in $[Ca^{2+}]_i$ may result from an influx of Ca^{2+} through plasma membrane Ca^{2+} channels and/or release from endoplasmic reticulum Ca^{2+} stores. However, the route for Ca^{2+} increase seems different between the amphibian and the mammal models. On the one hand, in *Xenopus* naïve ectoderm cells an influx of Ca^{2+} through DHP-Ca^{2+} channels is likely to be the main component of the changes in $[Ca^{2+}]_i$ observed both *in vivo* and *ex vivo* during neural induction (Moreau et al., 2008). Members of the TRP (*T*ransient *R*eceptor *P*otential) channels family, particularly TRPC1, are probably also involved (Lee et al., 2009). On the other hand, in mouse ESC, investigations to identify the Ca^{2+} channels and transporters that are expressed in plasma membrane and internal stores reveal the absence of VOCCs. The only plasma membrane Ca^{2+} channels expressed are TRPC1 and TRPC2 (Yanagida et al., 2004; Wang et al., 2005). Ca^{2+} release from the endoplasmic reticulum (ER) are mediated by the inositol triphosphate receptors (IP_3Rs) but not by the ryanodine receptors (RyRs). Both plasma membrane Ca^{2+}-ATPase (PMCA-1) and Na^+/Ca^{2+} exchanger (NCX-1, -2, -3) contribute to the extrusion of Ca^{2+} from the cytoplasm (Yanagida et al., 2004). Therefore, in mouse ESC, the main source of Ca^{2+} comes from internal stores. This is further supported by the identification and the characterization of Nnat function during neural induction in ESC (Lin et al., 2010). However, in amphibians, caffeine has been shown to trigger the expression of specific neural genes in naive ectoderm (Moreau et al., 1994; Batut et al., 2005). This suggests that internal stores may participate in Ca^{2+} signaling during neural induction in the amphibians. Finally, results obtained from both models suggest a cross-talk between Ca^{2+} signaling and the BMP pathway. The release of Ca^{2+} from internal stores via caffeine (Batut et al., 2005) or through inhibition of SERCA2 (Lin et al., 2010) suppresses the expression of BMP4. Whether this cross-talk is direct or involves Erk signaling is still an open question.

Ca^{2+} SIGNALING DURING EARLY NEUROGENESIS

The next step in neural development involves the differentiation of neural progenitors into neurons (**Figure 3**). This step occurs during the radial differentiation of the neural tube. At the time of its closure, the neural progenitors are localized in a single layer of proliferative cells, the ventricular zone (VZ) (**Figure 3A**). Then during development, two other zones are successively formed.

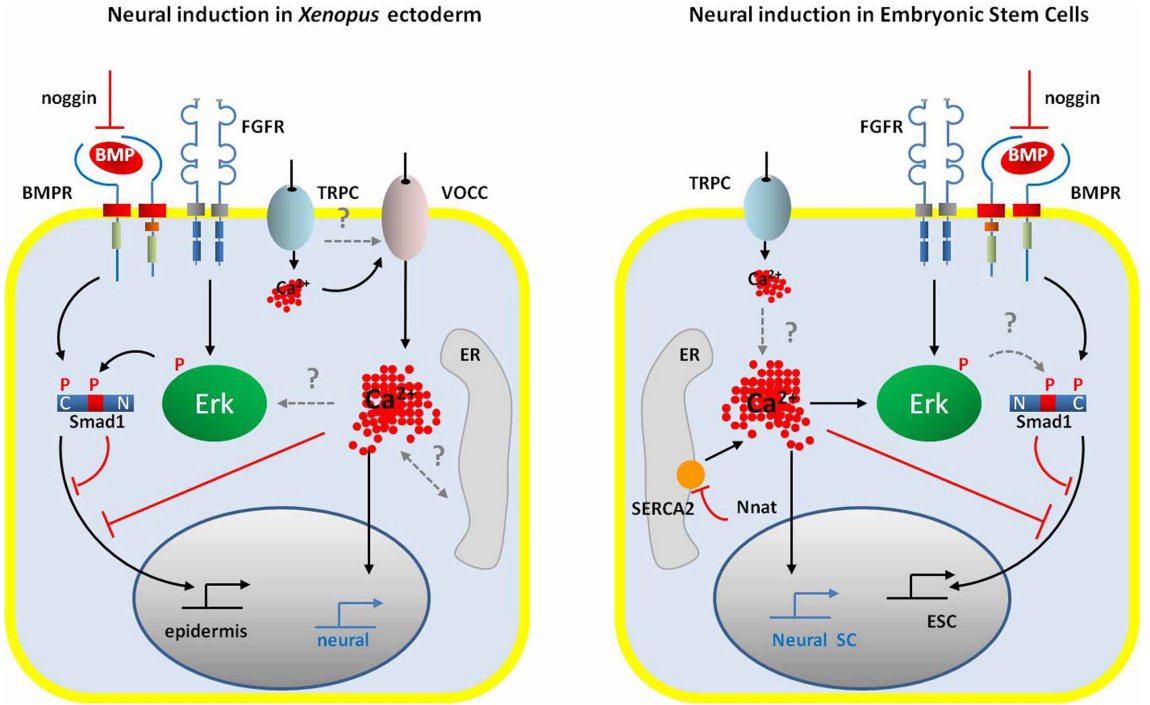

FIGURE 2 | Schematic representation of the signaling pathways occurring during neural induction in the amphibian ectoderm cells (left panel) and in the ESCs (right panel). In both systems, neural commitment of naïve cells requires the activation of FGF/ERK signaling and the inhibition of BMP signaling by noggin and via the Erk-dependent phosphorylation of Smad1 at linker domain. An increase in intracellular Ca^{2+} concentration is also a common signal that drives embryonic cells toward the neural fate. However, the control of Ca^{2+} homeostasis differs between amphibian ectodermal cells and ESCs. While in amphibian, the main source of Ca^{2+} increase appears to rely on an influx through VOCCs (likely DHP-Ca^{2+} channels), ESCs do not express VOCC. In ESCs, the regulation of intracellular Ca^{2+} level depends on the activity of the SERCA2 pump, negatively regulated by neuronatin. Both cell types expressed TRP channels, probably TRPC, which could contribute to the Ca^{2+} signals. Gating of the VOCC in ectodermal cells could be due to membrane depolarization induced by the activation of TRPC. In ESCs, a direct link between intracellular Ca^{2+} increase and Erk phosphorylation has been established; in ectodermal cells the question of the amplification of the initial Ca^{2+} influx by the release of Ca^{2+} from the ER remains open. However, in both models Ca^{2+} signals participate in the inhibition of the BMP signaling pathway, either directly or indirectly via Erk-dependent phosphorylation of Smad1. *Abbreviations:* BMP, bone morphogenetic protein; BMPR, BMP receptor; ER, endoplasmic reticulum; ESC, embryonic stem cell; FGFR, fibroblast growth factor receptor; Nnat, neuronatin; Neural SC, neural stem cell; SERCA2, sarco/endoplasmic reticulum Ca^{2+}-ATPase, isoform2; TRPC, class C transient potential receptor; VOCC, voltage-operated Ca^{2+} channels.

The marginal zone (MZ) located between the VZ and the outer surface of the neural tube, followed by the intermediate zone (IZ), between the VZ and the MZ. The VZ contains neuronal progenitors with a more restricted fate than neuroepithelial cells called the radial glial cells (Gotz and Huttner, 2005) and the IZ contains the first postmitotic neurons (**Figure 3B**). At later stages, different parts of the neural tube display specific organizations. In the spinal cord, the neural progenitors will differentiate into postmitotic neurons, distributed laterally into the IZ. In the cerebral cortex, in birds and mammals, a second proliferative zone, the subventricular zone (SVZ), appears adjacent to the VZ (**Figure 3C**); the postmitotic neurons arise from both the ventricular and the SVZ zones (Nowakowski and Hayes, 2005). Neural progenitors are produced by asymmetric division of neuroepithelial cells. Self-renewing divisions of the progenitors, such as radial glial cells, can be either symmetric, generating two progenitors or asymmetric, producing a neural progenitor and a neuron (Fish et al., 2008). In the VZ, neuroepithelial cells and neuronal precursor cells undergo interkinetic nuclear migration in which cells in S phase of the cell cycle have their nuclei in the upper third of the VZ. When cells pass from S to G_2, the nuclei migrate toward the neural tube lumen where mitosis occurs (**Figure 3** and review in Nowakowski and Hayes, 2005).

Ca^{2+}-imaging investigations during the development of embryonic cortex reveals distinct pattern of Ca^{2+} activities between the proliferative VZ, which contains the neural progenitors, and the IZ and MZ, which contains the postmitotic neurons. In the proliferative VZ, the Ca^{2+} signals are mediated by the activation of metabotropic ATP receptors, most likely the purinergic P2Y1 receptor and the release of Ca^{2+} through IP_3R. In the VZ there is no requirement of extracellular Ca^{2+} while the Ca^{2+} activities observed in the IZ and the MZ require Ca^{2+} influx through VOCCs (Owens and Kriegstein, 1998; Weissman et al., 2004). This discrepancy illustrates the differential expression of intracellular Ca^{2+} releasing channels, Ca^{2+} channels and receptors in the neocortex during early neurogenesis. Transcripts for the three main isoforms of the intracellular Ca^{2+} release channels the IP_3Rs and the RyRs were detected in the mouse neocortex

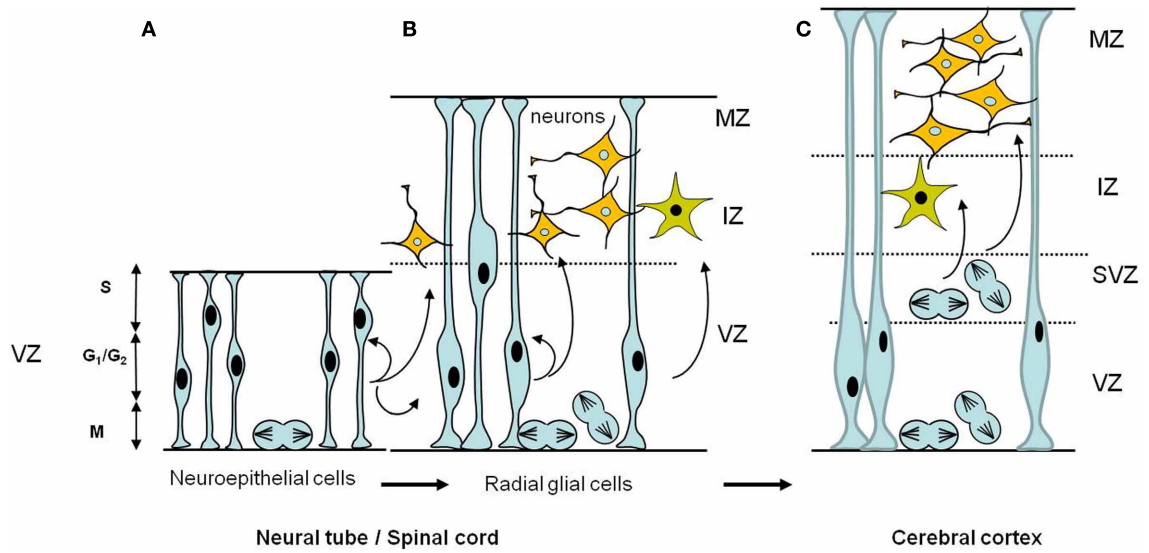

FIGURE 3 | Schematic diagrams of the temporal development of neural progenitors in the early stages of CNS formation. (A) Early neuroepithelial progenitors of the ventricular zone are columnar cells self-renewing by symmetric divisions. These cells can generate some neurons. **(B)** As neurogenesis proceeds, neuroepithelial cells are transformed into radial glial cells which ultimately will give rise to neurons and glial cells. Radial glia cells can undergo either symmetric divisions, generating two progenitors or asymmetric divisions, producing a neural progenitor and a neuron. Also illustrated is the interkinetic nuclear migration of the nuclei during the cell cycle in the VZ. The nucleus of a single neuroepithelial cell moves during the G_1 phase, from the ventricular surface to the border of the VZ where it enters S phase. During G_2, the nucleus moves down to the ventricular surface where it enter mitosis (M phase). Interkinetic nuclear migration in radial glial cells is confined to the VZ portion, does not extend to the border of the MZ. **(C)** In the cerebral cortex a second proliferative zone, the subventricular zone (SVZ), appears adjacent to the VZ; the postmitotic neurons and glia arise from both the ventricular and the subventricular zones. In the SVZ interkinetic nuclear migration does not occur, mitotic cells are found throughout the SVZ. *Abbreviations:* CNS, central nervous system; IZ, intermediate zone; MZ, marginal zone; SVZ, subventricular zone; VZ, ventricular zone.

as early as embryonic day 11 (E11) and at the protein level, the IP3R-1 and RyR-2 are predominant at E13. The expression of these two isoforms increases progressively throughout development up to the adult age (Maric et al., 2000a; Rowitch, 2004; Mori et al., 2000; Faure et al., 2001). Moreover, while the expression of IP3R-1 is ubiquitous in proliferative VZ and neuronal zone, the expression of RyR-2 is mainly restricted to the neuronal cells population (Faure et al., 2001). Other works indicate that non-VOCCs Ca^{2+} channels are differentially regulated during neurogenesis. The neuroepithelial cells at E13 also express TRPC1 channels, whereas the expression of TRPC1 decreases in more fate-restricted cells such as radial glial cells which expressed TRPC5 and TRPC6 at high level (Fiorio Pla et al., 2005; Shin et al., 2010). Altogether these data raise the question of the function of these distinct Ca^{2+} transients in the control of the symmetric, proliferative division versus the asymmetric neurogenic division.

Accumulating evidences indicate that the kinetic of the cell cycle can directly influence the switch from proliferation to differentiation of the neural progenitors with the lengthening of the G1 phase acting as a trigger for differentiation while a shortened G1 phase is associated with the expansion of the neural progenitor pool (review in Salomoni and Calegari, 2010). Interestingly, Ca^{2+} signaling appears to control neuronal progenitor cells proliferation (Weissman et al., 2004; Lin et al., 2007) but also to be an important regulator of the switch from proliferation to neuronal differentiation. For instance, the Ca^{2+} waves observed in the VZ have been shown to control the entry in S phase of radial glial cells organized in clusters (Weissman et al., 2004). The requirement of Ca^{2+} for cell cycle progression through G_1/S phase was confirmed in mouse NSCs (Kapur et al., 2007; Resende et al., 2010). Another work indicates that bFGF-induced Ca^{2+} influx through TRPC1 is also involved in self-renewal of embryonic rat NSCs (Fiorio Pla et al., 2005). Using ESCs deficient in the RyR-2, it has been shown that RyR-2 activity is required to mediate the differentiation of neural precursors into neurons after activation of $GABA_A$ receptors or DHP-Ca^{2+} channels (Yu et al., 2008). This mechanism of excitation-neurogenesis coupling involving activation of DHP-Ca^{2+} channels has also been described in adult NSCs (Deisseroth et al., 2004). Finally, the TRPC5 channel has recently been shown to play a key role in the induction of neuronal differentiation from radial glial cells (Shin et al., 2010). However, the mechanisms involved in the activation of these channels remain to be elucidated. Likely mechanisms may involve the activity of the secreted signaling molecules, including Sonic hedgehog (Shh), Wnts, BMPs, FGFs, and retinoic acid known to pattern the vertebrate developing central nervous system (Borello and Pierani, 2010; Ulloa and Marti, 2010).

Recent data came to fill the gap between the spontaneous Ca^{2+} transients, the lengthening of G1 and the activity of cell cycle modulators during neurogenesis. Neuronal differentiation induced from P19 embryonic carcinoma cells is associated with spontaneous Ca^{2+} transients regulated by IP3R and RYR stores occurring during the G1/S transition. Furthermore, in the neural progenitor cells, ATP-evoked Ca^{2+} release from IP3R both

increases proliferation and decreases the levels of the cell cycle regulators cyclin A and E bound to the cyclin-dependent kinase inhibitor p27 (Resende et al., 2010). A similar role for Ca^{2+} events has been found in primary human neural progenitor cells where mobilization of IP3-dependent Ca^{2+} stores lengthens the cell cycle and increases the number of intermediate neural progenitors. In this model, Ca^{2+} controls the duration of the cell cycle by increasing of the level of the p53 protein, a known regulator of the cyclin-dependent kinase inhibitor p21 (Garcia-Garcia et al., 2012). These new data raise additional questions about the mechanisms linking Ca^{2+} oscillations and the duration of G1 phase. One likely mechanism could involve the multifunctional Serine/threonine Ca^{2+}/Calmodulin stimulated protein kinases (CaMKs), particularly the CaMKI which has been shown to control G1 progression (Skelding et al., 2011). Although, numerous studies have implicated CaMKs in neuronal functions such as synaptic development and plasticity or learning and memory (Wayman et al., 2008; Fukunaga et al., 2009), their expression and function during early neurogenesis need to be explored.

Once neurons are specified, they undergo a process of maturation which includes the specification of neurotransmitters, the elaboration of axons, neurites, and synaptic connections to form functional networks. A number of excellent reviews illustrate the pivotal role played by intracellular Ca^{2+} signaling in these aspects (Lohmann, 2009; Michaelsen and Lohmann, 2010; Takemoto-Kimura et al., 2010; Spitzer, 2012). However, increasing evidences also point to the role of extracellular Ca^{2+} via activation of the Extracellular Ca^{2+}-Sensing receptor (CaSR). CaSR which is constantly monitoring the level of extracellular Ca^{2+}, belongs to the family C of GPCRs (*G-p*rotein-*c*oupled *r*eceptor), along with the metabotropic glutamate receptors (mGluRs) and the γ-aminobutyric acid $(GABA)_B$ receptors (Hofer and Brown, 2003). *CaSR* is localized in almost all areas of the brain including the circumventricular organs, the olfactory bulbs, the striatum, the orbital cortex, the cerebellum, and the hippocampus (Ruat et al., 1995; Yano et al., 2004; Bandyopadhyay et al., 2010). Furthermore, its expression in the central and peripheral nervous system is developmentally regulated (Ferry et al., 2000; Vizard et al., 2008). Interestingly, the highest levels of expression of *CaSR* correlate with a window of development during which neurite extension and branching occurs. Recently it has been shown that CaSR regulates the growth and the branching of developing sympathetic ganglion neurons and of hippocampal pyramidal neurons in mice (Vizard et al., 2008). The Extracellular CaSR has also been implicated in controlling other important functions in the nervous system including the migration of neurons synthesizing gonadotropin-releasing hormone (GnRH neurons), and the regulation of neuronal excitability via the control of ion channels activity (review in Brown and Macleod, 2001; Bandyopadhyay et al., 2010). These data highlight the importance of the regulation of the extracellular Ca^{2+} homeostasis during neural development.

Ca^{2+} TARGET GENES AND EARLY NEUROGENESIS

The transcriptional control of early neurogenesis involves a large number of transcription factors which can act as positive or negative regulators. These include the *Zic* (Aruga, 2004; Aruga and Mikoshiba, 2011), *Sox* (Wegner and Stolt, 2005), *Xiro* (Gomez-Skarmeta and Modolell, 2002), and *bHLH* (Bertrand et al., 2002; Sugimori et al., 2007) gene families. Control of gene expression by Ca^{2+} signaling may either be indirect through changes in the transactivating properties of transcription factors following the activation of Ca^{2+}-dependent kinases and phosphatases (Dolmetsch et al., 2001; West et al., 2001; Kornhauser et al., 2002; Spotts et al., 2002) or direct through nuclear Ca^{2+} sensors. To date, DREAM (*D*ownstream *R*egulatory *E*lement (DRE) *A*ntogonist *M*odulator) is the only Ca^{2+} sensor, which is known to bind specifically to DNA and to directly regulate transcription in a Ca^{2+}-dependent manner. DREAM is a Ca^{2+}-binding protein of the recoverin subfamily containing 4 EF-hands. In the absence of Ca^{2+} DREAM binds DNA on specific DRE site, located downstream from the TATA box, and represses transcription (Carrion et al., 1999; Mellstrom and Naranjo, 2001). Recently, a novel concept emerged around the idea that Ca^{2+} channel domains may act as transcription factor. The C-terminal fragment of the $Ca_v1.2$ channel, called Ca^{2+} channel associated transcriptional regulator (CCAT) has been shown to have a nuclear localization and to be able to regulate gene expression. CCAT overexpression in neurons increases dendritic length (Gomez-Ospina et al., 2006).

Ca^{2+} TARGET GENES AND NEURAL INDUCTION IN THE AMPHIBIANS

The embryo of the amphibian *Xenopus laevis* and the animal cap cells have been extensively used to elucidate how the aforementioned transcription factors interact to regulate early neurogenesis (Rogers et al., 2009). Animal cap cells are also a good assay for screening downstream target genes of Ca^{2+} signaling during neural induction.

It has been previously shown that Ca^{2+} controls the expression of the immediate early gene *c-fos* and of two other transcription factors: *XlPou2* and *Zic3* (Leclerc et al., 1999). While Fos is a ubiquitous transcription factor, XlPou2 and Zic3 are specific to neural determination and primary neural regulators (Witta et al., 1995; Nakata et al., 1997). Furthermore, the expression of *XlPou2* in response to noggin in animal caps and the expression of *Zic3* in the whole embryo require the presence of functional DHP-Ca^{2+} channels (Leclerc et al., 2000). In an attempt to correlate the Ca^{2+} pattern with the expression pattern of early neural genes, a two-dimensional system of neural induction was used, the Keller explants (Keller and Danilchik, 1988). These explants extend from the blastopore lip up toward the animal pole and therefore contain the prospective neuroectoderm associated with the dorsal mesoderm (Keller et al., 1992). In such explants the accumulated pattern of Ca^{2+} transients correlates with the expression of *Zic3*, and treatment with nifedipine, a DHP-Ca^{2+} channel antagonist, blocks the Ca^{2+} transients and reduces the level of *Zic3* expression (Leclerc et al., 2003). These results suggest that the function of the localized increase in $[Ca^{2+}]_i$ that occurs in the dorsal ectoderm during neural induction might be to activate locally genes with proneural activity.

To identify new Ca^{2+} target genes involved in neural induction, a subtractive cDNA library was constructed between untreated (i.e., ectodermal cells fated to become epidermis) and caffeine-treated animal caps (15–45 min) (i.e., ectodermal cells

fated to become neural) (Batut et al., 2003). Caffeine triggers neural induction via an increase in $[Ca^{2+}]_i$ (Moreau et al., 1994), and thus allows the differential isolation of the earliest Ca^{2+}-dependent genes involved in neural determination (Batut et al., 2003). A total of about 400 clones were screened, and about 30 clones were found to selectively hybridize to the neural-subtracted probe and not to the epidermis-subtracted probe. Among these clones, *xMLP* encodes a MARCKS-like protein, a substrate for PKC (Zhao et al., 2001; Batut et al., 2003); *xPRMT1b* is the *Xenopus* homologue of the mammalian arginine methyltransferase *PRMT1* gene (Batut et al., 2005); *xId3* (Wilson and Mohun, 1995), encodes HLH protein that acts as dominant negative inhibitor of bHLH transcription factors; and *Xp54nrb* encodes a protein which exhibits the RRM domains characteristic of RNA binding proteins, and implicated in pre-mRNA splicing steps (Neant et al., 2011). The spatio-temporal expression pattern of these genes is restricted to neural territories and their expression is triggered following the inhibition of BMP signaling by noggin. In addition, the expression of *xMLP* and of *xPRMT1b* is an early response to an increase in Ca^{2+} that does not require *de novo* protein synthesis and that the early expression of *xPRMT1b* at the gastrula stage also occurs via a Ca^{2+}-dependent mechanism mediated by the activation of DHP-sensitive Ca^{2+} channels.

Functional analysis of *xPRMT1b* in *Xenopus* embryo demonstrates that it is required for neural induction. Overexpression of *xPRMT1b* in the neural territories activates the expression of the neural precursor gene *Zic3*. Conversely, the utilization of a Morpholino-based approach, to block xPRMT1b translation, inhibits the expression of *Zic3* in animal caps, and impairs anterior neural development in the whole embryo (Batut et al., 2005). Identical phenotypes were obtained with antagonists of DHP-Ca^{2+} channels (Leclerc et al., 2000). These results suggest that during neural induction, *xPRMT1b* provides a direct link between the $[Ca^{2+}]_i$ increase and downstream events; a likely mechanism could involve methylation of early neural factors.

PRONEURAL bHLH GENES AND Ca^{2+}

The bHLH proneural genes, which encode transcription factors of the basic *H*elix-*L*oop-*H*elix class, have been shown to be key regulators of neurogenesis. In vertebrates, proneural bHLH genes are first expressed in neuroepithelial cells that are already committed to neural fate (Bertrand et al., 2002). Proneural bHLH proteins bind DNA as heterodimeric complexes that are formed with another class of ubiquitously bHLH proteins, called E-proteins. Regulation of proneural bHLH may occur at different levels, including regulation of gene expression, transcriptional activities, subcellular localization, or post-translational modifications.

In adult neural precursor cells, the excitation-neurogenesis coupling via activation of DHP-Ca^{2+} channels rapidly induces the expression of the neuronal differentiation regulator, *NeuroD*, and inhibits the expression of two proneural gene inhibitors, *Hes1* and *Id2* (Deisseroth et al., 2004). Furthermore, over-expression of the Ca^{2+} binding protein, calbindin-D_{28K} (Kim et al., 2006) in neural precursor cells promotes neurogenesis, induces the expression of the bHLH neuronal differentiation regulators, *NeuroD* and *Mash1*, and inhibits the expression of the proneural gene inhibitors, *Hes1, Hes5,* and *Id2*. The exact Ca^{2+}-dependent mechanism that regulates *NeuroD* expression is not yet identified. However, possible mechanisms may involve the *Hes1* transcriptional repressor. *Hes1* has been shown to repress the transcription of *Mash1* by binding to *Mash1* promoter; Hes1 may also form heterodimers with Mash1 that do not bind to DNA (review in Kageyama et al., 2008). In addition to their abilities to form heterodimers with other bHLH proteins, there are evidences that some bHLH proteins, like E-protein and MyoD a myogenic bHLH regulator, may physically interact with Ca^{2+}-loaded calmodulin but also with S-100 Ca^{2+} binding proteins; this interaction masks their DNA binding site (review in Hermann et al., 1998). To what extent this Ca^{2+}-dependent mechanism may also regulate the transcriptional activity of proneural bHLH proteins remains to be established. However, proneural bHLH proteins have been shown to be post-translationally modified in a Ca^{2+}-dependent manner. In rat hippocampal neural progenitors, the modulation of Ca^{2+} signaling by calbindin-D_{28K} induces the phosphorylation of Ca^{2+}- and Calmodulin-dependent protein kinases (CaMKs), possibly CaMKII and of NeuroD at serine^{336} (Kim et al., 2006). This post-translational modification of NeuroD which has been described during neuronal differentiation of embryonic and adult neuronal progenitors is also involved in the control of dendritic outgrowth in granule neurons (Gaudilliere et al., 2004).

THE NEUROGENIC TO GLIOGENIC SWITCH

After neurons, the radial glial progenitors switch to generate glial cells. Macroglial cells of the central nervous system (CNS) comprise two major cell types; astrocytes and oligodendrocytes. The molecular mechanisms that underlie the specification of glial cells appear strikingly similar to those that regulate neurons specification (Rowitch and Kriegstein, 2010). Here we will exclusively consider the implication of Ca^{2+} signaling in the specification of astrocytes and oligodendrocytes during early development.

The mechanisms by which macroglial cells are generated from neural precursors involve different levels of regulation. One level of regulation occurs during the neurogenic period and renders the neuroepithelial precursors unable to generate glial cells, even in the presence of gliogenic signals. This could be achieved via the transcriptional repression of glial-specific genes by proneural bHLH genes. Another mechanism involves the repression of gliogenesis by neuregulin-1, a neurogenic factor. Activation of the receptor tyrosine kinase (RTK) Erb4 by neuregulin-1 induces the presenilin-dependent cleavage of the RTK. The cleaved intracellular domain of Erb4 translocates to the nucleus of undifferentiated neural precursors and represses the transcription of two astrocyte specific genes, *GFAP* (*g*lial *f*ibrillary *a*cidic *p*rotein) and *S100*β which encodes a Ca^{2+}-binding protein, thereby inhibiting the differentiation of the neural progenitors into astrocytes (Sardi et al., 2006). Despite the fact that presenilin forms the catalytic subunit of the γ-secretase complex, increasing evidences suggest that presenilin is part of a mechanism that control Ca^{2+} homeostasis. Presenilin is an integral membrane protein of the ER (Annaert et al., 1999) that has been shown to function as a passive ER Ca^{2+} leak channels (Tu et al., 2006). Other works have shown that presenilin can interact with the IP_3R Ca^{2+} release channel and modulates its gating (Cheung et al., 2008); presenilin can also regulate the activity of the SERCA pump (Green

et al., 2008). The function of presenilin both in regulating Ca^{2+} homeostasis and in the inhibition of astrocytic fate raised the possibility that the Ca^{2+} waves observed in the radial glial progenitors cells during the neurogenic period not only promote neurogenesis but also repress gliogenesis. Conversely, a positive neuronal feedback mechanism has been shown to promote gliogenesis. The neurotrophic cytokine CT-1 generated by embryonic cortical neurons is a powerful astrocytic signal, which activates the JAK-STAT signaling pathway (Barnabe-Heider et al., 2005). However, in cortical neuronal precursors another pathway able to promote astrocytes differentiation involves the activation of the seven transmembrane-spanning domains receptor PAC1 by the Pituitary Adenylate Cyclase Activating Peptide (PACAP). PAC1 activation by PACAP triggers the production of cAMP, and a cAMP-dependent Ca^{2+} influx. Cebolla et al, have shown that the transcriptional activation of *GFAP* in response to PACAP is mediated by DREAM and requires the functional integrity of the Ca^{2+}-binding EF-hand domains of DREAM (Cebolla et al., 2008). Unexpectedly, during astrocytes differentiation, DREAM is acting as a transcriptional transactivator of the *GFAP* gene and not as a repressor (Scsucova et al., 2005). In fact, two binding sites for DREAM have been identified on the *GFAP* promoter, located upstream of the TATA box rather than downstream (Cebolla et al., 2008). The mechanism by which DREAM controls the expression of *GFAP* may involve changes in DREAM protein conformation, interactions with other gliogenic specific transcription factors, and cross-talk with the JAK-STAT signaling pathway (review in Vallejo, 2009).

There are some evidences indicating that Ca^{2+} signaling may also regulate the specification of the oligodendrocyte lineage. A subtractive approach to characterize genes expressed in the ventral neuroepithelium of chick spinal cord at the time of oligodendrocyte specification identify several elements of the Ca^{2+} toolkit, including a specific auxiliary subunit (α2–δ1) of a voltage-dependent Ca^{2+} channel; Ankyrin-2, α2, a membrane adaptor protein, requires to anchor ion channels, exchangers, and pumps to the plasma membrane; and slow troponin C, a Ca^{2+}-binding protein, expressed in cardiac muscle (Braquart-Varnier et al., 2004). Other works identify the Extracellular CaSR as a key element for oligodendrocyte specification. *CaSR* is expressed in all cells of the CNS with predominance in oligodendrocyte lineage (Chattopadhyay et al., 2008). *CaSR* is up-regulated when NSCs are specified to oligodendrocyte progenitor cells (OPCs) its expression remains at a high level in pre-oligodendrocyte cells, and then decreases in mature oligodendrocytes. Furthermore, activation of CaSR with high extracellular Ca^{2+} or with spermine, an agonist of CaSR present in the CNS, promotes OPCs proliferation and induces the expression of Myelin Basic Protein, a marker for oligodendrocyte maturation (Chattopadhyay et al., 2008; Bandyopadhyay et al., 2010). This work provides the demonstration that Ca^{2+}, in addition to a role as second messenger, acting intracellularly, may also act extracellularly as a first messenger.

CONCLUSION AND PERSPECTIVES

In this review, we have briefly summarized the recent advances in early neurogenesis, a rapidly moving field, and then focused specifically on several regulatory events that are modulated by Ca^{2+}, including short term effects or long-lasting modifications. The different functions of Ca^{2+} signaling during neurogenesis illustrate the versatility of Ca^{2+} both as a second and a first messenger.

While much is known about how the different Ca^{2+} signals are generated during the initial phases of nervous system formation, much less is known about the EF-hand calcium proteins involved in the transmission of these Ca^{2+} signals. The members of the EF-hand superfamily can be divided into two main categories according to their calcium affinity or their ability to change conformation following Ca^{2+} binding (Leclerc et al., 2009). Calmodulins (CaM), the S100 superfamily, and the neuronal calcium sensors such as DREAM constitute the first group of calcium sensors involved in Ca^{2+} signaling. The second group is constituted by Ca^{2+} buffering proteins such as calbindin.

The role of Ca^{2+} during neural induction in the amphibians is mainly focused on the triggering of Ca^{2+} signaling via the activation of Ca^{2+} channels and the downstream genes whose expression is controlled directly or indirectly by Ca^{2+} (Moreau et al., 2009). However, some evidences indicate that EF-hand Ca^{2+} proteins may be involved in signal transduction. The upregulation of FOS-related protein by Noggin or a DHP-Ca^{2+} channels agonist is inhibited by KN62, a specific inhibitor of CaMKinase, suggesting that CaMs and CaMKs are candidates to decode the Ca^{2+} signals during amphibian neural induction (Leclerc et al., 1999). Calcineurin, a Ca^{2+}/CaM-dependent phosphatase (CaN or PP2B) is maternally expressed and throughout development including neural induction (Saint-Saneyoshi et al., 2000). Finally, the expression of the calcium sensor DREAM has been found to be restricted to neuroectoderm during early development in *Xenopus laevis* (I. Neant unpublished results).

During early neurogenesis, EF-hand proteins such as CaMs and CaMKs are also involved (Skelding et al., 2011). In rat hippocampal neural progenitors, Ca^{2+} signaling is modulated by Calbindin-D28K (Kim et al., 2006), during the neurogenic to gliogenic switch the S100β protein is important for the differentiation of neural progenitors into astrocytes (Sardi et al., 2006) and during astrocyte differentiation triggered by the pituitary adenylate cyclase activating peptide, it has been shown that transcriptional activation of GFAP is mediated by DREAM (Cebolla et al., 2008).

Specific Ca^{2+} signals which are decoded by different Ca^{2+} sensors proteins and the different Ca^{2+} binding properties of these sensors (affinity, conformational changes) allow a fine tuning of the Ca^{2+} signaling. Among the Ca^{2+} sensors proteins more EF-hand Ca^{2+} proteins play certainly essential roles during early neural development. This field of research needs more development in the future.

ACKNOWLEDGMENTS

We apologize to those whose work we could not cite owing to space limitations. Work in our laboratory is supported by CNRS (Centre National de la Recherche Scientifique), GDRE 731, Procore/Ministère des Affaires Etrangères/RGC grants (Hong Kong, PRC) and the LIA "Rocade" (Laboratoire International Associé from CNRS).

REFERENCES

Annaert, W. G., Levesque, L., Craessaerts, K., Dierinck, I., Snellings, G., Westaway, D., George-Hyslop, P. S., Cordell, B., Fraser, P., and De Strooper, B. (1999). Presenilin 1 controls gamma-secretase processing of amyloid precursor protein in pre-golgi compartments of hippocampal neurons. *J. Cell Biol.* 147, 277–294.

Arcuri, F., Papa, S., Meini, A., Carducci, A., Romagnoli, R., Bianchi, L., Riparbelli, M. G., Sanchez, J. C., Palmi, M., Tosi, P., and Cintorino, M. (2005). The translationally controlled tumor protein is a novel calcium binding protein of the human placenta and regulates calcium handling in trophoblast cells. *Biol. Reprod.* 73, 745–751.

Aruga, J. (2004). The role of Zic genes in neural development. *Mol. Cell. Neurosci.* 26, 205–221.

Aruga, J., and Mikoshiba, K. (2011). Role of BMP, FGF, calcium signaling, and zic proteins in vertebrate neuroectodermal differentiation. *Neurochem. Res.* 36, 1286–1292.

Bandyopadhyay, S., Tfelt-Hansen, J., and Chattopadhyay, N. (2010). Diverse roles of extracellular calcium-sensing receptor in the central nervous system. *J. Neurosci. Res.* 88, 2073–2082.

Barnabe-Heider, F., Wasylnka, J. A., Fernandes, K. J., Porsche, C., Sendtner, M., Kaplan, D. R., and Miller, F. D. (2005). Evidence that embryonic neurons regulate the onset of cortical gliogenesis via cardiotrophin-1. *Neuron* 48, 253–265.

Barth, L. G., and Barth, L. J. (1964). Sequential induction of the presumptive epidermis of the Rana pipiens gastrula. *Biol. Bull.* 127, 413–427.

Batut, J., Neant, I., Leclerc, C., and Moreau, M. (2003). xMLP is an early response calcium target gene in neural determination in Xenopus laevis. *J. Soc. Biol.* 197, 283–289.

Batut, J., Vandel, L., Leclerc, C., Daguzan, C., Moreau, M., and Neant, I. (2005). The Ca^{2+}-induced methyltransferase xPRMT1b controls neural fate in amphibian embryo. *Proc. Natl. Acad. Sci. U.S.A.* 102, 15128–15133.

Bayer, S. A., and Altman, J. (1991). *Neocortical Development*. New York: Raven Press.

Berridge, M. J., Lipp, P., and Bootman, M. D. (2000). The versatility and universality of calcium signalling. *Nat. Rev. Mol. Cell Biol.* 1, 11–21.

Bertrand, N., Castro, D. S., and Guillemot, F. (2002). Proneural genes and the specification of neural cell types. *Nat. Rev. Neurosci.* 3, 517–530.

Bommer, U. A., and Thiele, B. J. (2004). The translationally controlled tumour protein (TCTP). *Int. J. Biochem. Cell Biol.* 36, 379–385.

Borello, U., and Pierani, A. (2010). Patterning the cerebral cortex: traveling with morphogens. *Curr. Opin. Genet. Dev.* 20, 408–415.

Braquart-Varnier, C., Danesin, C., Clouscard-Martinato, C., Agius, E., Escalas, N., Benazeraf, B., Ai, X., Emerson, C., Cochard, P., and Soula, C. (2004). A subtractive approach to characterize genes with regionalized expression in the gliogenic ventral neuroepithelium: Identification of chick sulfatase 1 as a new oligodendrocyte lineage gene. *Mol. Cell. Neurosci.* 25, 612–628.

Brown, E. M., and Macleod, R. J. (2001). Extracellular calcium sensing and extracellular calcium signaling. *Physiol. Rev.* 81, 239–297.

Cai, C., and Grabel, L. (2007). Directing the differentiation of embryonic stem cells to neural stem cells. *Dev. Dyn.* 236, 3255–3266.

Carrion, A. M., Link, W. A., Ledo, F., Mellstrom, B., and Naranjo, J. R. (1999). DREAM is a Ca^{2+}-regulated transcriptional repressor. *Nature* 398, 80–84.

Catterall, W. A., Perez-Reyes, E., Snutch, T. P., and Striessnig, J. (2005). International Union of Pharmacology. XLVIII. Nomenclature and structure-function relationships of voltage-gated calcium channels. *Pharmacol. Rev.* 57, 411–425.

Cebolla, B., Fernandez-Perez, A., Perea, G., Araque, A., and Vallejo, M. (2008). DREAM mediates cAMP-dependent, Ca^{2+}-induced stimulation of GFAP gene expression and regulates cortical astrogliogenesis. *J. Neurosci.* 28, 6703–6713.

Chalmers, A. D., Welchman, D., and Papalopulu, N. (2002). Intrinsic differences between the superficial and deep layers of the Xenopus ectoderm control primary neuronal differentiation. *Dev. Cell* 2, 171–182.

Chattopadhyay, N., Espinosa-Jeffrey, A., Tfelt-Hansen, J., Yano, S., Bandyopadhyay, S., Brown, E. M., and De Vellis, J. (2008). Calcium receptor expression and function in oligodendrocyte commitment and lineage progression: Potential impact on reduced myelin basic protein in CaR-null mice. *J. Neurosci. Res.* 86, 2159–2167.

Cheung, K. H., Shineman, D., Muller, M., Cardenas, C., Mei, L., Yang, J., Tomita, T., Iwatsubo, T., Lee, V. M., and Foskett, J. K. (2008). Mechanism of Ca^{2+} disruption in Alzheimer's disease by presenilin regulation of InsP3 receptor channel gating. *Neuron* 58, 871–883.

De Robertis, E. M., and Kuroda, H. (2004). Dorsal-ventral patterning and neural induction in Xenopus embryos. *Annu. Rev. Cell Dev. Biol.* 20, 285–308.

Deisseroth, K., Singla, S., Toda, H., Monje, M., Palmer, T. D., and Malenka, R. C. (2004). Excitation-neurogenesis coupling in adult neural stem/progenitor cells. *Neuron* 42, 535–552.

Denton, R. M. (2009). Regulation of mitochondrial dehydrogenases by calcium ions. *Biochim. Biophys. Acta* 1787, 1309–1316.

Distasi, C., Munaron, L., Laezza, F., and Lovisolo, D. (1995). Basic fibroblast growth factor opens calcium-permeable channels in quail mesencephalic neural crest neurons. *Eur. J. Neurosci.* 7, 516–520.

Distasi, C., Torre, M., Antoniotti, S., Munaron, L., and Lovisolo, D. (1998). Neuronal survival and calcium influx induced by basic fibroblast growth factor in chick ciliary ganglion neurons. *Eur. J. Neurosci.* 10, 2276–2286.

Dolmetsch, R. E., Pajvani, U., Fife, K., Spotts, J. M., and Greenberg, M. E. (2001). Signaling to the nucleus by an L-type calcium channel-calmodulin complex through the MAP kinase pathway. *Science* 294, 333–339.

Drean, G., Leclerc, C., Duprat, A. M., and Moreau, M. (1995). Expression of L-type Ca^{2+} channel during early embryogenesis in Xenopus laevis. *Int. J. Dev. Biol.* 39, 1027–1032.

Faure, A. V., Grunwald, D., Moutin, M. J., Hilly, M., Mauger, J. P., Marty, I., De Waard, M., Villaz, M., and Albrieux, M. (2001). Developmental expression of the calcium release channels during early neurogenesis of the mouse cerebral cortex. *Eur. J. Neurosci.* 14, 1613–1622.

Ferry, S., Traiffort, E., Stinnakre, J., and Ruat, M. (2000). Developmental and adult expression of rat calcium-sensing receptor transcripts in neurons and oligodendrocytes. *Eur. J. Neurosci.* 12, 872–884.

Fiorio Pla, A., Maric, D., Brazer, S. C., Giacobini, P., Liu, X., Chang, Y. H., Ambudkar, I. S., and Barker, J. L. (2005). Canonical transient receptor potential 1 plays a role in basic fibroblast growth factor (bFGF)/FGF receptor-1-induced Ca^{2+} entry and embryonic rat neural stem cell proliferation. *J. Neurosci.* 25, 2687–2701.

Fish, J. L., Dehay, C., Kennedy, H., and Huttner, W. B. (2008). Making bigger brains-the evolution of neural-progenitor-cell division. *J. Cell Sci.* 121, 2783–2793.

Fukunaga, K., Shioda, N., and Miyamoto, E. (2009). "The function of CaM kinase II in synaptic plasticity and spine formation," in *Handbook of Neurochemistry and Molecular Neurobiology,*ed K. Mikoshiba (New York, NY: Springer Science), 163–183.

Garcia-Garcia, E., Pino-Barrio, M. J., Lopez-Medina, L., and Martinez-Serrano, A. (2012). Intermediate progenitors are increased by lengthening of cell cycle through calcium signaling and p53 expression in human Neural Progenitors. *Mol. Biol. Cell.* 23, 1167–1180.

Gaspard, N., and Vanderhaeghen, P. (2010). Mechanisms of neural specification from embryonic stem cells. *Curr. Opin. Neurobiol.* 20, 37–43.

Gaudilliere, B., Konishi, Y., De La Iglesia, N., Yao, G., and Bonni, A. (2004). A CaMKII-NeuroD signaling pathway specifies dendritic morphogenesis. *Neuron* 41, 229–241.

Gaulden, J., and Reiter, J. F. (2008). Neur-ons and neur-offs: Regulators of neural induction in vertebrate embryos and embryonic stem cells. *Hum. Mol. Genet.* 17, R60–R66.

Gomez-Ospina, N., Tsuruta, F., Barreto-Chang, O., Hu, L., and Dolmetsch, R. (2006). The C terminus of the L-type voltage-gated calcium channel Ca(V)1.2 encodes a transcription factor. *Cell* 127, 591–606.

Gomez-Skarmeta, J. L., and Modolell, J. (2002). Iroquois genes: genomic organization and function in vertebrate neural development. *Curr. Opin. Genet. Dev.* 12, 403–408.

Gotz, M., and Huttner, W. B. (2005). The cell biology of neurogenesis. *Nat. Rev. Mol. Cell Biol.* 6, 777–788.

Green, K. N., Demuro, A., Akbari, Y., Hitt, B. D., Smith, I. F., Parker, I., and Laferla, F. M. (2008). SERCA pump activity is physiologically regulated by presenilin and regulates amyloid beta production. *J. Cell Biol.* 181, 1107–1116.

Grunz, H., and Tacke, L. (1989). Neural differentiation of Xenopus laevis ectoderm takes place after disaggregation and delayed reaggregation without inducer. *Cell Differ. Dev.* 28, 211–217.

Hemmati-Brivanlou, A., and Melton, D. (1997). Vertebrate neural induction. *Annu. Rev. Neurosci.* 20, 43–60.

Hermann, S., Saarikettu, J., Onions, J., Hughes, K., and Grundstrom, T. (1998). Calcium regulation of basic helix-loop-helix transcription factors. *Cell Calcium* 23, 135–142.

Hofer, A. M., and Brown, E. M. (2003). Extracellular calcium sensing and signalling. *Nat. Rev. Mol. Cell Biol.* 4, 530–538.

Kageyama, R., Ohtsuka, T., and Kobayashi, T. (2008). Roles of Hes genes in neural development. *Dev. Growth Differ.* 50(Suppl. 1), S97–S103.

Kapur, N., Mignery, G. A., and Banach, K. (2007). Cell cycle-dependent calcium oscillations in mouse embryonic stem cells. *Am. J. Physiol. Cell Physiol.* 292, C1510–C1518.

Keller, R., and Danilchik, M. (1988). Regional expression, pattern and timing of convergence and extension during gastrulation of Xenopus laevis. *Development* 103, 193–209.

Keller, R., Shih, J., Sater, A. K., and Moreno, C. (1992). Planar induction of convergence and extension of the neural plate by the organizer of Xenopus. *Dev. Dyn.* 193, 218–234.

Kim, J. H., Lee, J. A., Song, Y. M., Park, C. H., Hwang, S. J., Kim, Y. S., Kaang, B. K., and Son, H. (2006). Overexpression of calbindin-D28K in hippocampal progenitor cells increases neuronal differentiation and neurite outgrowth. *FASEB J.* 20, 109–111.

Kornhauser, J. M., Cowan, C. W., Shaywitz, A. J., Dolmetsch, R. E., Griffith, E. C., Hu, L. S., Haddad, C., Xia, Z., and Greenberg, M. E. (2002). CREB transcriptional activity in neurons is regulated by multiple, calcium-specific phosphorylation events. *Neuron* 34, 221–233.

Kuroda, H., Fuentealba, L., Ikeda, A., Reversade, B., and De Robertis, E. M. (2005). Default neural induction: Neuralization of dissociated Xenopus cells is mediated by Ras/MAPK activation. *Genes Dev.* 19, 1022–1027.

Lamb, T. M., Knecht, A. K., Smith, W. C., Stachel, S. E., Economides, A. N., Stahl, N., Yancopolous, G. D., and Harland, R. M. (1993). Neural induction by the secreted polypeptide noggin. *Science* 262, 713–718.

Leclerc, C., Daguzan, C., Nicolas, M. T., Chabret, C., Duprat, A. M., and Moreau, M. (1997). L-type calcium channel activation controls the *in vivo* transduction of the neuralizing signal in the amphibian embryos. *Mech. Dev.* 64, 105–110.

Leclerc, C., Duprat, A. M., and Moreau, M. (1995). *In vivo* labelling of L-type Ca^{2+} channels by fluorescent dihydropyridine: Correlation between ontogenesis of the channels and the acquisition of neural competence in ecotderm cells from Pleurodeles waltl embryos. *Cell Calcium* 17, 216–224.

Leclerc, C., Duprat, A. M., and Moreau, M. (1999). Noggin upregulates Fos expression by a calcium-mediated pathway in amphibian embryos. *Dev. Growth Differ.* 41, 227–238.

Leclerc, C., Lee, M., Webb, S. E., Moreau, M., and Miller, A. L. (2003). Calcium transients triggered by planar signals induce the expression of ZIC3 gene during neural induction in Xenopus. *Dev. Biol.* 261, 381–390.

Leclerc, C., Rizzo, C., Daguzan, C., Neant, I., Batut, J., Auge, B., and Moreau, M. (2001). Neural determination in Xenopus laevis embryos: Control of early neural gene expression by calcium. *J. Soc. Biol.* 195, 327–337.

Leclerc, E., Sturchler, E., and Heizmann, C. W. (2009). "Calcium regulation by EF-hand protein in the brain," in *Handbook of Neurochemistry and Molecular Neurobiology,* ed K. Mikoshiba (New York, NY: Springer Science), 510–532.

Leclerc, C., Webb, S. E., Daguzan, C., Moreau, M., and Miller, A. L. (2000). Imaging patterns of calcium transients during neural induction in Xenopus laevis embryos. *J. Cell Sci.* 113(Pt 19), 3519–3529.

Lee, K. W., Moreau, M., Neant, I., Bibonne, A., and Leclerc, C. (2009). FGF-activated calcium channels control neural gene expression in Xenopus. *Biochim. Biophys. Acta* 1793, 1033–1040.

Lin, H. H., Bell, E., Uwanogho, D., Perfect, L. W., Noristani, H., Bates, T. J., Snetkov, V., Price, J., and Sun, Y. M. (2010). Neuronatin promotes neural lineage in ESCs via Ca(2+) signaling. *Stem Cells* 28, 1950–1960.

Lin, J. H., Takano, T., Arcuino, G., Wang, X., Hu, F., Darzynkiewicz, Z., Nunes, M., Goldman, S. A., and Nedergaard, M. (2007). Purinergic signaling regulates neural progenitor cell expansion and neurogenesis. *Dev. Biol.* 302, 356–366.

Lohmann, C. (2009). Calcium signaling and the development of specific neuronal connections. *Prog. Brain Res.* 175, 443–452.

Maric, D., Maric, I., and Barker, J. L. (2000). Developmental changes in cell calcium homeostasis during neurogenesis of the embryonic rat cerebral cortex. *Cereb. Cortex* 10, 561–573.

Maric, D., Maric, I., Chang, Y. H., and Barker, J. L. (2000). Stereotypical physiological properties emerge during early neuronal and glial lineage development in the embryonic rat neocortex. *Cereb. Cortex* 10, 729–747.

Mellstrom, B., and Naranjo, J. R. (2001). Ca(2+)-dependent transcriptional repression and derepression: DREAM, a direct effector. *Semin. Cell Dev. Biol.* 12, 59–63.

Michaelsen, K., and Lohmann, C. (2010). Calcium dynamics at developing synapses: Mechanisms and functions. *Eur. J. Neurosci.* 32, 218–223.

Michalak, M., Groenendyk, J., Szabo, E., Gold, L. I., and Opas, M. (2009). Calreticulin, a multi-process calcium-buffering chaperone of the endoplasmic reticulum. *Biochem. J.* 417, 651–666.

Moreau, M., Leclerc, C., Gualandris-Parisot, L., and Duprat, A.-M. (1994). Increased internal Ca^{2+} mediates neural induction in the amphibian embryo. *Proc. Natl. Acad. Sci. U.S.A.* 91, 12639–12643.

Moreau, M., Neant, I., Webb, S. E., Miller, A. L., and Leclerc, C. (2008). Calcium signalling during neural induction in Xenopus laevis embryos. *Philos. Trans. R. Soc. Lond. B Biol. Sci.* 363, 1371–1375.

Moreau, M., Webb, S. E., Neant, I., Miller, A. L., and Leclerc, C. (2009). "Calcium signalling and cell fate determination during neural induction in amphibian embryos," in *Handbook of Neurochemistry and Molecular Neurobioloy,* ed K. Mikoshiba (New York, NY: Springer Science), 3–14.

Mori, F., Fukaya, M., Abe, H., Wakabayashi, K., and Watanabe, M. (2000). Developmental changes in expression of the three ryanodine receptor mRNAs in the mouse brain. *Neurosci. Lett.* 285, 57–60.

Nakata, K., Nagai, T., Aruga, J., and Mikoshiba, K. (1997). *Xenopus Zic* 3, a primary regulator both in neural and neural crest developement. *Proc. Natl. Acad. Sci. U.S.A.* 94, 11980–11985.

Neant, I., Deisig, N., Scerbo, P., Leclerc, C., and Moreau, M. (2011). The RNA-binding protein Xp54nrb isolated from a Ca(2)-dependent screen is expressed in neural structures during Xenopus laevis development. *Int. J. Dev. Biol.* 55, 923–931.

Nowakowski, R., and Hayes, N. (2005). "Cell proliferation in the developing mammalian brain," in *Developmental Neurobiology,* 4th edn., eds M. S. Rao and M. Jacobson (New York, NY: Plenum Publishers), 21–39.

Okabayashi, K., and Asashima, M. (2003). Tissue generation from amphibian animal caps. *Curr. Opin. Genet. Dev.* 13, 502–507.

Okano, H., and Temple, S. (2009). Cell types to order: temporal specification of CNS stem cells. *Curr. Opin. Neurobiol.* 19, 112–119.

Oppenheimer, J. M. (1936). Transplantation experiments on developing teleosts (*Fundulus* and *Perca*). *J. Exp. Zool.* 72, 409–437.

Owens, D. F., and Kriegstein, A. R. (1998). Patterns of intracellular calcium fluctuation in precursor cells of the neocortical ventricular zone. *J. Neurosci.* 18, 5374–5388.

Puro, D. G., and Mano, T. (1991). Modulation of calcium channels in human retinal glial cells by basic fibroblast growth factor: a possible role in retinal pathobiology. *J. Neurosci.* 11, 1873–1880.

Resende, R. R., Adhikari, A., Da Costa, J. L., Lorencon, E., Ladeira, M. S., Guatimosim, S., Kihara, A. H., and Ladeira, L. O. (2010). Influence of spontaneous calcium events on cell-cycle progression in embryonal carcinoma and adult stem cells. *Biochim. Biophys. Acta* 1803, 246–260.

Rogers, C. D., Moody, S. A., and Casey, E. S. (2009). Neural induction and factors that stabilize a neural fate. *Birth Defects Res. C Embryo Today* 87, 249–262.

Rowitch, D. H. (2004). Glial specification in the vertebrate neural tube. *Nat. Rev. Neurosci.* 5, 409–419.

Rowitch, D. H., and Kriegstein, A. R. (2010). Developmental genetics of vertebrate glial-cell specification. *Nature* 468, 214–222.

Ruat, M., Molliver, M. E., Snowman, A. M., and Snyder, S. H. (1995). Calcium sensing receptor: Molecular cloning in rat and localization to nerve terminals. *Proc. Natl. Acad. Sci. U.S.A.* 92, 3161–3165.

Saint-Jeannet, J. P., Huang, S., and Duprat, A. M. (1990). Modulation of neural commitment by changes in target cell contacts in Pleurodeles waltl. *Dev. Biol.* 141, 93–103.

Saneyoshi, T., Kume, S., Natsume, T., and Mikoshiba, K. (2000). Molecular cloning and expression profile of Xenopus calcineurin A subunit(1). *Biochim Biophys Acta* 1499, 164–170.

Salomoni, P., and Calegari, F. (2010). Cell cycle control of mammalian neural stem cells: Putting a speed limit on G1. *Trends Cell Biol.* 20, 233–243.

Sardi, S. P., Murtie, J., Koirala, S., Patten, B. A., and Corfas, G. (2006). Presenilin-dependent ErbB4 nuclear signaling regulates the timing of astrogenesis in the developing brain. *Cell* 127, 185–197.

Scsucova, S., Palacios, D., Savignac, M., Mellstrom, B., Naranjo, J. R., and Aranda, A. (2005). The repressor DREAM acts as a transcriptional activator on Vitamin D and retinoic acid response elements. *Nucleic Acids Res.* 33, 2269–2279.

Sharpe, C. R., Fritz, A., De Robertis, E. M., and Gurdon, J. B. (1987). A homeobox-containing marker of posterior neural differentiation shows the importance of predetermination in neural induction. *Cell* 50, 749–758.

Shin, H. Y., Hong, Y. H., Jang, S. S., Chae, H. G., Paek, S. L., Moon, H. E., Kim, D. G., Kim, J., Paek, S. H., and Kim, S. J. (2010). A role of canonical transient receptor potential 5 channel in neuronal differentiation from A2B5 neural progenitor cells. *PLoS One* 5, e10359.

Skelding, K. A., Rostas, J. A., and Verrills, N. M. (2011). Controlling the cell cycle: the role of calcium/calmodulin-stimulated protein kinases I and II. *Cell Cycle* 10, 631–639.

Spemann, H., and Mangold, H. (1924). Über die induktion von embryonalanlagen durch implantation artfremder organisatoren. *Wilhelm Roux Arch Entwickl. Mech. Org.* 100, 599–638.

Spitzer, N. C. (2012). Activity-dependent neurotransmitter respecification. *Nat. Rev. Neurosci.* 13, 94–106.

Spotts, J. M., Dolmetsch, R. E., and Greenberg, M. E. (2002). Time-lapse imaging of a dynamic phosphorylation-dependent protein-protein interaction in mammalian cells. *Proc. Natl. Acad. Sci. U.S.A.* 99, 15142–15147.

Stern, C. D. (2005). Neural induction: Old problem, new findings, yet more questions. *Development* 132, 2007–2021.

Streit, A., Berliner, A. J., Papanayotou, C., Sirulnik, A., and Stern, C. D. (2000). Initiation of neural induction by FGF signalling before gastrulation. *Nature* 406, 74–78.

Sugimori, M., Nagao, M., Bertrand, N., Parras, C. M., Guillemot, F., and Nakafuku, M. (2007). Combinatorial actions of patterning and HLH transcription factors in the spatiotemporal control of neurogenesis and gliogenesis in the developing spinal cord. *Development* 134, 1617–1629.

Takemoto-Kimura, S., Suzuki, K., Kamijo, S., Ageta-Ishihara, N., Fujii, H., Okuno, H., and Bito, H. (2010). Differential roles for CaM kinases in mediating excitation-morphogenesis coupling during formation and maturation of neuronal circuits. *Eur. J. Neurosci.* 32, 224–230.

Tu, H., Nelson, O., Bezprozvanny, A., Wang, Z., Lee, S. F., Hao, Y. H., Serneels, L., De Strooper, B., Yu, G., and Bezprozvanny, I. (2006). Presenilins form ER Ca^{2+} leak channels, a function disrupted by familial Alzheimer's disease-linked mutations. *Cell* 126, 981–993.

Ulloa, F., and Marti, E. (2010). Wnt won the war: Antagonistic role of Wnt over Shh controls dorso-ventral patterning of the vertebrate neural tube. *Dev. Dyn.* 239, 69–76.

Vallejo, M. (2009). PACAP signaling to DREAM: A cAMP-dependent pathway that regulates cortical astrogliogenesis. *Mol. Neurobiol.* 39, 90–100.

Vizard, T. N., O'Keeffe, G. W., Gutierrez, H., Kos, C. H., Riccardi, D., and Davies, A. M. (2008). Regulation of axonal and dendritic growth by the extracellular calcium-sensing receptor. *Nat. Neurosci.* 11, 285–291.

Waddington, C. H. (1933). Induction of the primitive streak and its derivatives in the chick. *J. Exp. Biol.* 10, 38–46.

Waddington, C. H. (1936). Organizers in mammalian development. *Nature* 138, 125.

Wang, D., and Gao, L. (2005). Proteomic analysis of neural differentiation of mouse embryonic stem cells. *Proteomics* 5, 4414–4426.

Wang, K., Xue, T., Tsang, S. Y., Van Huizen, R., Wong, C. W., Lai, K. W., Ye, Z., Cheng, L., Au, K. W., Zhang, J., Li, G. R., Lau, C. P., Tse, H. F., and Li, R. A. (2005). Electrophysiological properties of pluripotent human and mouse embryonic stem cells. *Stem Cells* 23, 1526–1534.

Wayman, G. A., Lee, Y. S., Tokumitsu, H., Silva, A. J., and Soderling, T. R. (2008). Calmodulin-kinases: Modulators of neuronal development and plasticity. *Neuron* 59, 914–931.

Webb, S. E., and Miller, A. L. (2007). Ca^{2+} signalling and early embryonic patterning during zebrafish development. *Clin. Exp. Pharmacol. Physiol.* 34, 897–904.

Wegner, M., and Stolt, C. C. (2005). From stem cells to neurons and glia: a Soxist's view of neural development. *Trends Neurosci.* 28, 583–588.

Weissman, T. A., Riquelme, P. A., Ivic, L., Flint, A. C., and Kriegstein, A. R. (2004). Calcium waves propagate through radial glial cells and modulate proliferation in the developing neocortex. *Neuron* 43, 647–661.

West, A. E., Chen, W. G., Dalva, M. B., Dolmetsch, R. E., Kornhauser, J. M., Shaywitz, A. J., Takasu, M. A., Tao, X., and Greenberg, M. E. (2001). Calcium regulation of neuronal gene expression. *Proc. Natl. Acad. Sci. U.S.A.* 98, 11024–11031.

Wijnholds, J., Chowdhury, K., Wehr, R., and Gruss, P. (1995). Segment-specific expression of the neuronatin gene during early hindbrain development. *Dev. Biol.* 171, 73–84.

Wilson, R., and Mohun, T. (1995). XIdx, a dominant negative regulator of bHLH function in early Xenopus embryos. *Mech. Dev.* 49, 211–222.

Witta, S. E., Agarwal, V. R., and Sato, S. M. (1995). XIPOU 2, a noggin-inducible gene, has direct neuralizing activity. *Development* 121, 721–730.

Yamada, M., Tanemura, K., Okada, S., Iwanami, A., Nakamura, M., Mizuno, H., Ozawa, M., Ohyama-Goto, R., Kitamura, N., Kawano, M., Tan-Takeuchi, K., Ohtsuka, C., Miyawaki, A., Takashima, A., Ogawa, M., Toyama, Y., Okano, H., and Kondo, T. (2007). Electrical stimulation modulates fate determination of differentiating embryonic stem cells. *Stem Cells* 25, 562–570.

Yanagida, E., Shoji, S., Hirayama, Y., Yoshikawa, F., Otsu, K., Uematsu, H., Hiraoka, M., Furuichi, T., and Kawano, S. (2004). Functional expression of Ca^{2+} signaling pathways in mouse embryonic stem cells. *Cell Calcium* 36, 135–146.

Yano, S., Brown, E. M., and Chattopadhyay, N. (2004). Calcium-sensing receptor in the brain. *Cell Calcium* 35, 257–264.

Yoon, T., Kim, M., and Lee, K. (2006). Inhibition of Na, K-ATPase-suppressive activity of translationally controlled tumor protein by sorting nexin 6. *FEBS Lett.* 580, 3558–3564.

Yu, H. M., Wen, J., Wang, R., Shen, W. H., Duan, S., and Yang, H. T. (2008). Critical role of type 2 ryanodine receptor in mediating activity-dependent neurogenesis from embryonic stem cells. *Cell Calcium* 43, 417–431.

Zhao, H., Cao, Y., and Grunz, H. (2001). Isolation and characterization of a Xenopus gene (XMLP) encoding a MARCKS-like protein. *Int. J. Dev. Biol.* 45, 817–826.

Zimmerman, L. B., De Jesus-Escobar, J. M., and Harland, R. M. (1996). The Spemann organizer signal noggin binds and inactivates bone morphogenetic protein 4. *Cell* 86, 599–606.

Conflict of Interest Statement: The authors declare that the research was conducted in the absence of any commercial or financial relationships that could be construed as a potential conflict of interest.

Received: 12 March 2012; accepted: 25 April 2012; published online: 14 May 2012.

Citation: Leclerc C, Néant I and Moreau M (2012) The calcium: an early signal that initiates the formation of the nervous system during embryogenesis. Front. Mol. Neurosci. 5:64. doi: 10.3389/fnmol.2012.00064

frontiers in
MOLECULAR NEUROSCIENCE

MINI REVIEW ARTICLE
published: 04 May 2012
doi: 10.3389/fnmol.2012.00057

The role of neuronal calcium sensors in balancing synaptic plasticity and synaptic dysfunction

Talitha L. Kerrigan[1], Daniel J. Whitcomb[1]*, Philip L. Regan[1,2] and Kwangwook Cho[1,2]*

[1] Henry Wellcome Laboratories for Integrative Neuroscience and Endocrinology, School of Clinical Sciences, Faculty of Medicine and Dentistry, University of Bristol, Bristol, UK

[2] MRC Centre for Synaptic Plasticity, University of Bristol, Bristol, UK

Edited by:
Michael R. Kreutz, Leibniz-Institute for Neurobiology, Germany

Reviewed by:
Michael R. Kreutz, Leibniz-Institute for Neurobiology, Germany
Jose R. Naranjo, Centro Nalcional de Biotecnologia/Consejo Superior de Investigaciones Cientificas, Spain

***Correspondence:**
Daniel J. Whitcomb and Kwangwook Cho, Henry Wellcome Laboratories for Integrative Neuroscience and Endocrinology, School of Clinical Sciences, Faculty of Medicine and Dentistry, University of Bristol, Whitson Street, Bristol BS1 3NY, Bristol, UK. e-mail: d.j.whitcomb@bristol.ac.uk; kei.cho@bristol.ac.uk

Neuronal calcium sensors (NCS) readily bind calcium and undergo conformational changes enabling them to interact and regulate specific target molecules. These interactions lead to dynamic alterations in protein trafficking that significantly impact upon synaptic function. Emerging evidence suggests that NCS and alterations in Ca^{2+} mobilization modulate glutamate receptor trafficking, subsequently determining the expression of different forms of synaptic plasticity. In this review, we aim to discuss the functional relevance of NCS in protein trafficking and their emerging role in synaptic plasticity. Their significance within the concept of "translational neuroscience" will also be highlighted, by assessing their potential as key molecules in neurodegeneration.

Keywords: neuronal calcium sensor, long-term synaptic plasticity, Alzheimer's disease

INTRODUCTION

Ca^{2+} signaling plays an important role in diverse biological processes, ranging from gene expression to cellular development (Sheng et al., 1991; Means, 1994; Park et al., 2007). Cellular Ca^{2+} sources are abundant and include the mitochondria, endoplasmic reticulum, lysosome, and extracellular environment. Changes in Ca^{2+} mobilization from this array of "Ca^{2+} stores" serve as the primary factor in the regulation of Ca^{2+} sensors and the subsequent activity of various substrates (Rosen et al., 1994; Moldoveanu et al., 2002; Burgoyne, 2007). Accordingly, uncovering the mechanisms underlying the activation and function of various Ca^{2+} sensors is fundamental to developing our understanding of dynamic neuronal responses to Ca^{2+}; controlling synaptic transmission, modulating neuronal excitability, and, the particular focus of this review, regulating synaptic plasticity (Berridge, 2000).

Although a few exceptional cases of Ca^{2+}-independent forms of synaptic plasticity have been reported (Fitzjohn et al., 2001; Dickinson et al., 2009), it is widely accepted that the majority of synaptic long-term plasticity operates through Ca^{2+}-dependent mechanisms. Tetanic high frequency stimulation of presynaptic regions in the hippocampus induces a rise in postsynaptic Ca^{2+}, leading to long-term potentiation (LTP) (Malenka et al., 1986; Lisman, 1989). Conversely, low frequency stimulation induces a low-to-moderate rise in free intracellular Ca^{2+}, producing long-term depression (LTD) (Mulkey et al., 1994). These different and specific effects suggest that Ca^{2+} is involved in the induction of LTP as well as LTD, and that the magnitudes of activity-dependent rises in free Ca^{2+} and Ca^{2+} mobilization from different sources determines the induction of LTP and LTD (Lisman, 1989; Artola and Singer, 1993; Cho et al., 2001).

Thought to be central to this functional dichotomy are Ca^{2+}-regulated enzymes. For example, LTP-inducing Ca^{2+} rises are detected by calmodulin (CaM; Mulkey et al., 1993) and activate Ca^{2+}/calmodulin-dependent kinases (CaMKs; Malenka et al., 1986), while LTD-inducing Ca^{2+} signals activate a calcineurin/inhibitor-1 phosphatase cascade (Mulkey et al., 1994). These Ca^{2+}-sensitive molecules play a key role in neuronal function through the regulation of glutamate receptor trafficking and synaptic plasticity in various regions of the brain (Palmer et al., 2005; Burgoyne, 2007; Jo et al., 2008, 2010). This is achieved either through direct interaction with cargo molecules, or through regulation of protein membrane trafficking (Palmer et al., 2005; Jo et al., 2008, 2010).

Recently, neuronal calcium sensors (NCS) have been shown to interact with endocytic molecules involved in glutamate receptor trafficking (**Figures 1A,B**; Palmer et al., 2005; Jo et al., 2008, 2010). More specifically, these Ca^{2+} sensors interact with several downstream effectors involved in AMPAR trafficking, including ABP/GRIP (Chung et al., 2000), adaptor protein 2 (AP2; Lee et al., 2002; Palmer et al., 2005), the Arp2/3 complex (Rocca et al., 2008), and PSD-95 (Kim et al., 2007). Here we will discuss how NCS proteins serve to orchestrate LTD signaling, and what makes them unique to one another in their roles in synaptic plasticity.

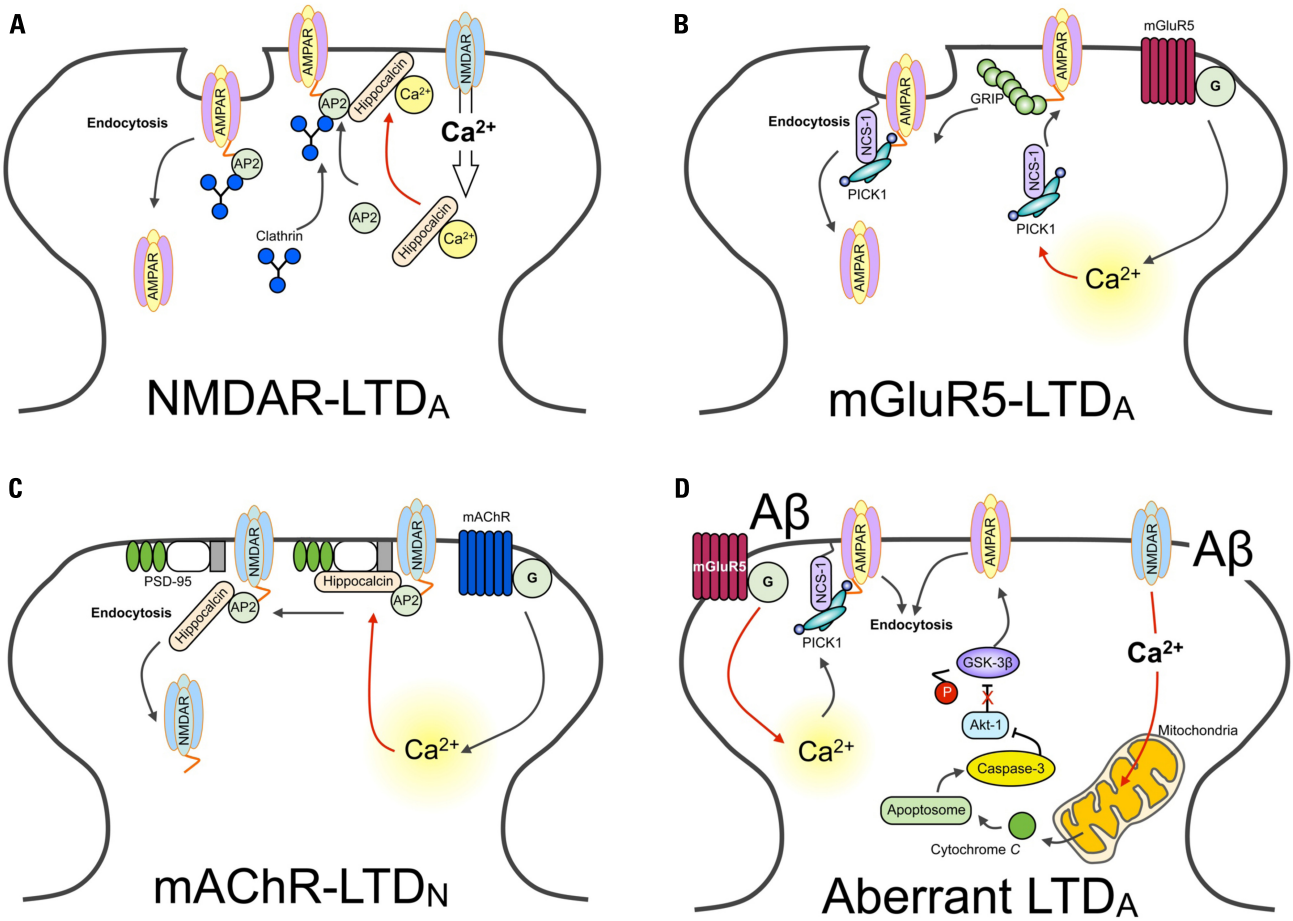

FIGURE 1 | Ca^{2+} sensors and LTD. Schematic diagram showing different Ca^{2+} sensors regulate distinct forms of LTD. **(A)** The activation of NMDARs results in Ca^{2+} entry in the neuron. Ca^{2+} entry through NMDARs is sensed by hippocalcin, activating the myristoyl switch and stimulating the binding to β-adaptin of the AP2 complex, resulting in its translocation to the plasma membrane. AP2 is then able to bind with the GluA2 subunit of AMPARs, recruiting clathrin. Finally, hippocalcin is displaced by clathrin, and AMPARs are internalized. **(B)** AMPARs are stabilized at the synapse through interactions with GRIP. Activation of the G-protein coupled metabotropic glutamate receptor (mGluR), specifically the mGluR5-isoform containing receptor, induces the release of Ca^{2+} from intracellular stores. Increased levels of Ca^{2+} trigger the association of PICK1 with NCS-1. PICK1 interacts with PKC. NCS-1 localizes PICK1 in close proximity with AMPARs, facilitating the PKC-mediated phosphorylation of GluA2. This releases AMPARs from the GRIP interaction, mobilizing them for synaptic removal via endocytosis. **(C)** Hippocalcin in bound with the SH3 domain of PSD-95. This interacts with the NMDAR subunit GluN2B. These interactions prevent the binding of AP2, required for dynamin and clathrin-dependent endocytosis. Activation of the G-protein coupled mAChR induces the release of Ca^{2+} from intracellular stores. Increased levels of Ca^{2+} are sensed by hippocalcin. As a consequence of this, PSD-95 disassociates from NMDARs. AP2 is now free to bind with NMDARs and initiate their endocytosis. **(D)** The hypothetical model of Ca^{2+}-mediated Aβ toxicity. The aberrant activation of synaptic receptors leads to enhanced Ca^{2+} influx from both extracellular sites and intracellular Ca^{2+} stores. Ca^{2+} entry via NMDARs can impair mitochondrial function, leading to the release of cytochrome *c* and the formation of the apoptosome. This activates caspase-3, which cleaves and inhibits Akt-1. Given that Akt-1 ordinarily functions to phosphorylate GSK-3β and thereby downregulate the activity of GSK-3β, without this constitutive inhibition GSK-3β is now able to induce AMPAR endocytosis (Lopez et al., 2008; Li et al., 2009; Jo et al., 2011). Similarly, sustained release of Ca^{2+} from intracellular stores is likely to be sensed by, for example, PICK1. One likely consequence of this is the induction of LTD-signaling mechanisms and the endocytosis of AMPARs.

NEURONAL CALCIUM SENSORS

Neuronal calcium sensors proteins are a subgroup of proteins belonging to the EF-hand super family (Pongs et al., 1993; for detail of their structural and functional properties, we refer the reader to a number of excellent comprehensive reviews that cover these issues in great depth; Burgoyne, 2007; Ames et al., 2012; Burgoyne and Haynes, 2012). NCS proteins are widely expressed in neurons throughout the nervous system, and are able to regulate axonal outgrowth and synaptic transmission (Pongs et al., 1993; Olafsson et al., 1997). Upon Ca^{2+} binding, they exhibit the distinct property of being able to associate with the plasma membrane, via the post-translational addition of a myristoyl group (Ames et al., 1997). Such functional characteristics (among others to be discussed) render these proteins particularly adept at regulating synaptic receptor movement in response to neuronal activation, a fundamental prerequisite for the regulation of synaptic plasticity.

NCS AND LTD

Activation of NMDAR and metabotropic glutamate receptor (mGluR) induces both NMDAR-dependent and mGluR-dependent

LTD (NMDAR-LTD, mGluR-LTD respectively; see review Anwyl, 2006). Importantly, induction mechanisms of NMDAR- and mGluR-LTD are mediated by different Ca^{2+}-dependent signaling pathways, involving different Ca^{2+} sensors (Jo et al., 2008; **Figure 1B**). These two distinct forms of LTD are conferred by different Ca^{2+} sensitivities and/or conformational changes of particular intracellular Ca^{2+} binding proteins. Accordingly, whilst NMDAR-LTD requires CaM and hippocalcin, mGluR-LTD involves NCS-1, protein kinase C (PKC), and IP3 (Jo et al., 2008). This suggests that distinct properties of Ca^{2+} sensors not only control the induction of LTD, but also maintain and regulate specificity of various signaling cascades. Given the physiological importance of different forms of Ca^{2+} sensors in LTD, the selective behavior of these proteins is undoubtedly significant in receptor trafficking, particularly receptor endocytosis.

NCS-1, PICK1, AND AMPA RECEPTOR ENDOCYTOSIS

Neuronal calcium sensor-1, first described as a regulator of synaptic transmission at the neuromuscular junction in *Drosophila* and *Xenopus* (Pongs et al., 1993; Olafsson et al., 1997), is highly expressed throughout the brain (Paterlini et al., 2000). NCS-1 interacts with protein kinase interacting with C kinase 1 (PICK1) and regulates synaptic plasticity in the perirhinal cortex (Jo et al., 2008). NCS-1 binds directly to PICK1 via its Bin/Amphiphysin/Rvs (BAR) domain, in a Ca^{2+}-dependent manner. The PICK1-BAR domain dimerizes, forming a concave arrangement. This unique conformation is thought to act as a "curvature sensor" (Peter et al., 2004), serving as a means of interaction between PICK1 and curved lipid membranes, like those of endocytic vesicles (He et al., 2011). The surface of the PICK1-BAR domain consists of positively charged regions, which mediate non-covalent interactions with negatively charged lipids. Accordingly, changes in membrane charges could dynamically regulate the membrane-localization of PICK1 (Jin et al., 2006), a possible crucial factor in synaptic plasticity.

PICK1 plays a key role in mediating the interaction between GluA2/3 of AMPARs and synaptic stabilizing structures, and accordingly can function to promote receptor endocytosis (Chung et al., 2000; Xia et al., 2000; Hanley and Henley, 2005). Again, the BAR domain plays a central part here; PICK1 binds with phosphoinositide lipids through the BAR domain, and this lipid/BAR interaction is essential for the synaptic targeting of PICK1 (Jin et al., 2006). Specifically, the BAR domain interacts with lipids of endocytic vesicles, mediating the internalization of PICK1 and associated synaptic receptors. Accordingly, it was shown that expression of a mutant BAR domain-containing PICK1 (K266, 268E) prevented the endocytosis of GluA2-containing AMPARs and enhanced AMPAR-mediated synaptic transmission (Jin et al., 2006). Interestingly, PICK1 itself is also a Ca^{2+} sensor (Hanley and Henley, 2005), and can regulate AMPAR endocytosis through actin depolymerization (Rocca et al., 2008). Thus, it is thought that the association of PICK1 with NCS-1 might serve to target PICK1 to the vicinity of AMPARs to initiate their removal from the synapse, providing a distinctive role for NCS-1 in LTD (Jo et al., 2008).

HIPPOCALCIN AND LTD

Emerging findings have outlined an important role for hippocalcin, a member of the visinin-like (VSNL) family proteins (VSNLs), in regulating dynamic neuronal synaptic change. It has previously been shown that NMDAR-mediated Ca^{2+} entry into neurons results in the hippocalcin-dependent internalization of AMPARs (Palmer et al., 2005). Here, it was shown that hippocalcin interacts with the AP2 adaptor complex subunit β2-adaptin (**Figure 1A**). This, in turn, binds with the GluA2/3 AMPAR subunit – an interaction that is Ca^{2+}-dependent – and promotes its clathrin-mediated endocytosis. In this study, the infusion of a dominant negative truncated form of hippocalcin (Hip^{2-72}), an N-terminal region of the protein that does not include Ca^{2+} binding domains and is required for β2-adaptin interaction, inhibits the induction of LTD. Critically, this hippocalcin-mediated mechanism appears to be specific for LTD, as there was no effect found on the induction of LTP, though the same NMDAR-mediated Ca^{2+} influx is involved in LTP and LTD.

A more recent study has found evidence to suggest that under basal conditions, hippocalcin binds with the SH3 region of PSD-95, and that muscarinic acetylcholine receptor (mAChR)-induced intracellular Ca^{2+} release induces the translocation of hippocalcin to the plasma membrane (**Figure 1C**). This leads to the dissociation of PSD-95 from NMDARs, allowing for the binding of AP2 to NMDARs to result in their endocytosis (Jo et al., 2010). Therefore, given the associate relationship between hippocalcin and the endocytosis of AMPARs, it is likely that hippocalcin could discriminate and respond to two distinct forms of intracellular Ca^{2+} mobilization (i.e., NMDAR- and mAChR-mediated). It is clear, therefore, that NCS-1 and hippocalcin are central regulators of receptor trafficking, pivotal in the expression of physiological LTD. Here, these NCS proteins activate key LTD molecules to induce both AMPAR and NMDAR internalization. Further work is required, however, to fully characterize how the same Ca^{2+} sensor can detect two distinct Ca^{2+} mobilizations and induce distinct receptor trafficking.

Ca^{2+} DYSREGULATION AND NEURODEGENERATION: ARE CALCIUM SENSORS THE KEY?

Dysregulation of Ca^{2+} is well documented in the "Ca^{2+} theory of neurodegenerative disease," involving excitatory toxicity and mitochondria-mediated apoptosis (Khachaturian, 1987; Schneider et al., 2001). For example, changes in $[Ca^{2+}]_i$ can induce a concomitant change in mitochondrial Ca^{2+} ($[Ca^{2+}]_m$), leading to an increase of reactive oxygen species (ROS) production and the release of cytochrome *c* (Jiang et al., 2001; Brustovetsky et al., 2003). Released cytochrome *c* binds apoptotic protease activating factor 1 (Apaf-1) and triggers the caspase cascade and cell death (Hengartner, 2000). Given the significance of disrupted Ca^{2+} homeostasis to enhanced oxidative stress and neuronal loss evident in neurodegenerative diseases, here we discuss how Ca^{2+} and Ca^{2+} sensor-mediated receptor trafficking may affect synaptic function during Alzheimer's disease (AD).

Large bodies of evidence support that amyloid-beta peptide (Aβ) induces the dysregulation of Ca^{2+} homeostasis and leads to activation of pro-apoptotic signal cascades (Ekinci et al., 2000;

Smith et al., 2005; Lopez et al., 2008). Surprisingly however, a role for Ca^{2+} sensors in this pathogenesis has not yet been unambiguously demonstrated. Aβ-induced $[Ca^{2+}]_i$ rises have been shown to regulate calsenilin, a KChIP subfamily of NCS, and its binding with the pro-apoptotic C-terminus of presenilin-2 (PS2; Buxbaum et al., 1998; Jo et al., 2005). The calsenilin–PS2 association leads to an increase in apoptosis and APP production (Jo et al., 2005; Jang et al., 2011). Additionally, the Ca^{2+} sensor visinin-like protein (VILIP) has been shown to associate with amyloid plaques and its expression enhances phosphorylation of tau, an additional hallmark of AD brains (Schnurra et al., 2001). In contrast to this finding, however, expression of VILIP-1 was reduced in AD brains compared with age-matched brain samples (Braunewell et al., 2001). Together, such studies currently paint a somewhat undefined picture as the exact role of NCS in AD pathology. Nevertheless, these studies do indicate that the aberrant regulation of Ca^{2+} sensors could underlie the development of AD, and this concept certainly warrants future investigation.

Caspase has been implicated as a key LTD molecule in the hippocampus and is involved in Aβ-mediated synaptic dysfunction (Li et al., 2010; Jo et al., 2011). Recently, it has been revealed that synaptic impairment caused by Aβ is mediated by a caspase–Akt-1–GSK3β signal cascade (termed the CAG cascade; Li et al., 2010; Jo et al., 2011). Interestingly, Aβ induces aberrant synaptic plasticity, leads to the inhibition of LTP but facilitation of LTD, and causes AMPAR endocytosis (Kim et al., 2001; Walsh et al., 2002; Hsieh et al., 2006; Shankar et al., 2007, 2008; Li et al., 2009). Thus, it is perhaps not surprising that the Aβ-mediated activation of the CAG cascade leads to the facilitation of LTD (**Figure 1D**). As we have described in this review, NCS-1, hippocalcin, and PICK1 are key molecules in the signaling underlying the induction of LTD and AMPAR and NMDAR endocytosis (Hanley and Henley, 2005; Citri et al., 2010; Jo et al., 2010). It would therefore be of great interest to investigate whether NCS could be aberrantly regulated during AD pathology.

As suggested in **Figure 1C**, activation of mAChR regulates NMDAR trafficking through a hippocalcin and PSD-95-mediated mechanism. Given the importance of enhancing cholinergic transmission and downregulating NMDAR transmission – strategies used as clinically approved AD treatments (e.g., memantine) – the role played by this NCS in receptor trafficking could provide a potential therapeutic target for Aβ-mediated synaptic dysfunction.

CONCLUDING REMARKS

Ca^{2+} signals can be "detected (sensor)" and "translated (switch)" to effectors. "Sensing" and "switching" should be tightly controlled to maintain effective homeostatic regulation in neurons. Growing evidence supports the notion that NSC and PICK1 have a key role in the endocytosis of glutamate receptors, a major molecular mechanism of LTD at excitatory synapses. Interestingly, Aβ-mediated neurotoxicity has been linked with excessive intracellular Ca^{2+} and aberrant synaptic plasticity. Thus our assumption is that overactive AMPAR endocytosis (or excessive LTD) caused by hyperactive NCS is likely to be found in AD or Aβ-induced neurotoxicity models. Therefore, it is of great interest to examine how NCS are involved in neurotoxicity and synaptic dysfunction. What is evident is the fact that intracellular Ca^{2+} mobilization, which includes mitochondrial Ca^{2+} flux and Ca^{2+} sensing, is a fundamental process in both physiological and pathological states. Through this review, we have aimed to bring new insight into NCS and synaptic plasticity, and provide a potential translation to synaptic disease models.

ACKNOWLEDGMENTS

This work was supported by BBSRC, Wellcome Trust, MRC, and Alzheimer's Research UK (to Kwangwook Cho).

REFERENCES

Ames, J. B., Ishima, R., Tanaka, T., Gordon, J. I., Stryer, L., and Ikura, M. (1997). Molecular mechanics of calcium-myristoyl switches. *Nature* 389, 198–202.

Ames, J. B., Sunghyuk, L., and Ikura, M. (2012). Molecular structure and target recognition of neuronal calcium sensor proteins. *Front. Mol. Neurosci.* 5:10. doi: 10.3389/fnmol.2012.00010

Anwyl, R. (2006). Induction and expression mechanisms of postsynaptic NMDA receptor-independent homosynaptic long-term depression. *Prog. Neurobiol.* 78, 17–37.

Artola, A., and Singer, W. (1993). Long-term depression of excitatory synaptic transmission and its relationship to long-term potentiation. *Trends Neurosci.* 16, 480–487.

Berridge, M. J. (2000). Neuronal calcium signaling. *Neuron* 21, 13–26.

Braunewell, K., Riederer, P., Spilker, C., Gundelfinger, E. D., Bogerts, B., and Bernstein, H. G. (2001). Abnormal localization of two neuronal calcium sensor proteins, visinin-like proteins (vilips)-1 and -3, in neocortical brain areas of Alzheimer disease patients. *Dement. Geriatr. Cogn. Disord.* 12, 110–116.

Brustovetsky, N., Dubinsky, J. M., Antonsson, B., and Jemmerson, R. (2003). Two pathways for tBID-induced cytochrome *c* release from rat brain mitochondria: BAK- versus BAX-dependence. *J. Neurochem.* 84, 196–207.

Burgoyne, R. D. (2007). Neuronal calcium sensor proteins: generating diversity in neuronal signalling. *Nat. Rev. Neurosci.* 8, 182–193.

Burgoyne, R. D., and Haynes, L. P. (2012). Understanding the physiological roles of the neuronal calcium sensor proteins. *Mol. Brain* 5, 2.

Buxbaum, J. D., Choi, E. K., Luo, Y., Lilliehook, C., Crowley, A. C., Merriam, D. E., and Wasco, W. (1998). Calsenilin: a calcium-binding protein that interacts with the presenilins and regulates the levels of a presenilin fragment. *Nat. Med.* 4, 1177–1181.

Cho, K., Aggleton, J. P., Brown, M. W., and Bashir, Z. I. (2001). An experimental test of the role of postsynaptic calcium levels in determining synaptic strength using perirhinal cortex of rat. *J. Physiol.* 532, 459–466.

Chung, H. J., Xia, J., Scannevin, R. H., Zhang, X., and Huganir, R. L. (2000). Phosphorylation of the AMPA receptor subunit GluR2 differentially regulates its interaction with PDZ domain-containing proteins. *J. Neurosci.* 20, 7258–7267.

Citri, A., Bhattacharyya, S., Ma, C., Morishita, W., Fang, S., Rizo, J., and Malenka, R. C. (2010). Calcium binding to PICK1 is essential for the intracellular retention of AMPA receptors underlying long-term depression. *J. Neurosci.* 30, 16437–16452.

Dickinson, B. A., Jo, J., Seok, H., Son, G. H., Whitcomb, D. J., Davies, C. H., Sheng, M., Collingridge, G. L., and Cho, K. (2009). A novel mechanism of hippocampal LTD involving muscarinic receptor-triggered interactions between AMPARs, GRIP and liprin-alpha. *Mol. Brain* 2, 18.

Ekinci, F. J., Linsley, M. D., and Shea, T. B. (2000). Beta-amyloid-induced calcium influx induces apoptosis in culture by oxidative stress rather than tau phosphorylation. *Brain Res. Mol. Brain Res.* 76, 389–395.

Fitzjohn, S. M., Palmer, M. J., May, J. E., Neeson, A., Morris, S. A., and Collingridge, G. L. (2001). A characterisation of long-term depression induced by metabotropic glutamate receptor activation in the rat hippocampus *in vitro*. *J. Physiol.* 537, 421–430.

Hanley, J. G., and Henley, J. M. (2005). PICK1 is a calcium-sensor

for NMDA-induced AMPA receptor trafficking. *Embo. J.* 24, 3266–3278.

He, Y., Liwo, A., Weinstein, H., and Scheraga, H. A. (2011). PDZ binding to the BAR domain of PICK1 is elucidated by coarse-grained molecular dynamics. *J. Mol. Biol.* 405, 298–314.

Hengartner, M. O. (2000). The biochemistry of apoptosis. *Nature* 407, 770–776.

Hsieh, H., Boehm, J., Sato, C., Iwatsubo, T., Tomita, T., Sisodia, S., and Malinow, R. (2006). AMPAR removal underlies Abeta-induced synaptic depression and dendritic spine loss. *Neuron* 52, 831–843.

Jang, C., Choi, J. K., Na, Y. J., Jang, B., Wasco, W., Buxbaum, J. D., Kim, Y. S., and Choi, E. K. (2011). Calsenilin regulates presenilin 1/gamma-secretase-mediated N-cadherin epsilon-cleavage and beta-catenin signaling. *FASEB J.* 25, 4174–4183.

Jiang, D., Sullivan, P. G., Sensi, S. L., Steward, O., and Weiss, J. H. (2001). Zn^2 induces permeability transition pore opening and release of pro-apoptotic peptides from neuronal mitochondria. *J. Biol. Chem.* 276, 47524–47529.

Jin, W., Ge, W. P., Xu, J., Cao, M., Peng, L., Yung, W., Liao, D., Duan, S., Zhang, M., and Xia, J. (2006). Lipid binding regulates synaptic targeting of PICK1, AMPA receptor trafficking, and synaptic plasticity. *J. Neurosci.* 26, 2380–2390.

Jo, D. G., Jang, J., Kim, B. J., Lundkvist, J., and Jung, Y. K. (2005). Overexpression of calsenilin enhances gamma-secretase activity. *Neurosci. Lett.* 378, 59–64.

Jo, J., Heon, S., Kim, M. J., Son, G. H., Park, Y., Henley, J. M., Weiss, J. L., Sheng, M., Collingridge, G. L., and Cho, K. (2008). Metabotropic glutamate receptor-mediated LTD involves two interacting Ca^{2+} sensors, NCS-1 and PICK1. *Neuron* 60, 1095–1111.

Jo, J., Son, G. H., Winters, B. L., Kim, M. J., Whitcomb, D. J., Dickinson, B. A., Lee, Y. B., Futai, K., Amici, M., Sheng, M., Collingridge, G. L., and Cho, K. (2010). Muscarinic receptors induce LTD of NMDAR EPSCs via a mechanism involving hippocalcin, AP2 and PSD-95. *Nat. Neurosci.* 13, 1216–1224.

Jo, J., Whitcomb, D. J., Olsen, K. M., Kerrigan, T. L., Lo, S. C., Bru-Mercier, G., Dickinson, B., Scullion, S., Sheng, M., Collingridge, G., and Cho, K. (2011). Abeta(1–42) inhibition of LTP is mediated by a signaling pathway involving caspase-3, Akt1 and GSK-3beta. *Nat. Neurosci.* 14, 545–547.

Khachaturian, Z. S. (1987). Hypothesis on the regulation of cytosol calcium concentration and the aging brain. *Neurobiol. Aging* 8, 345–346.

Kim, J. H., Anwyl, R., Suh, Y. H., Djamgoz, M. B., and Rowan, M. J. (2001). Use-dependent effects of amyloidogenic fragments of (beta)-amyloid precursor protein on synaptic plasticity in rat hippocampus *in vivo*. *J. Neurosci.* 21, 1327–1333.

Kim, M. J., Futai, K., Jo, J., Hayashi, Y., Cho, K., and Sheng, M. (2007). Synaptic accumulation of PSD-95 and synaptic function regulated by phosphorylation of serine-295 of PSD-95. *Neuron* 56, 488–502.

Lee, S. H., Liu, L., Wang, Y. T., and Sheng, M. (2002). Clathrin adaptor AP2 and NSF interact with overlapping sites of GluR2 and play distinct roles in AMPA receptor trafficking and hippocampal LTD. *Neuron* 36, 661–674.

Li, S., Hong, S., Shepardson, N. E., Walsh, D. M., Shankar, G. M., and Selkoe, D. (2009). Soluble oligomers of amyloid Beta protein facilitate hippocampal long-term depression by disrupting neuronal glutamate uptake. *Neuron* 62, 788–801.

Li, Z., Jo, J., Jia, J. M., Lo, S. C., Whitcomb, D. J., Jiao, S., Cho, K., and Sheng, M. (2010). Caspase-3 activation via mitochondria is required for long-term depression and AMPA receptor internalization. *Cell* 141, 859–871.

Lisman, J. (1989). A mechanism for the Hebb and the anti-Hebb processes underlying learning and memory. *Proc. Natl. Acad. Sci. U.S.A.* 86, 9574–9578.

Lopez, J. R., Lyckman, A., Oddo, S., Laferla, F. M., Querfurth, H. W., and Shtifman, A. (2008). Increased intraneuronal resting Ca^{2+} in adult Alzheimer's disease mice. *J. Neurochem.* 105, 262–271.

Malenka, R. C., Madison, D. V., and Nicoll, R. A. (1986). Potentiation of synaptic transmission in the hippocampus by phorbol esters. *Nature* 321, 175–177.

Means, A. R. (1994). Calcium, calmodulin and cell cycle regulation. *FEBS Lett.* 347, 1–4.

Moldoveanu, T., Hosfield, C. M., Lim, D., Elce, J. S., Jia, Z., and Davies, P. L. (2002). A Ca^{2+} switch aligns the active site of calpain. *Cell* 108, 649–660.

Mulkey, R. M., Endo, S., Shenolikar, S., and Malenka, R. C. (1994). Involvement of a calcineurin/inhibitor-1 phosphatase cascade in hippocampal long-term depression. *Nature* 369, 486–488.

Mulkey, R. M., Herron, C. E., and Malenka, R. C. (1993). An essential role for protein phosphatases in hippocampal long-term depression. *Science* 261, 1051–1055.

Olafsson, P., Soares, H. D., Herzog, K. H., Wang, T., Morgan, J. I., and Lu, B. (1997). The Ca^{2+} binding protein, frequenin is a nervous system-specific protein in mouse preferentially localized in neurites. *Brain Res. Mol. Brain Res.* 44, 73–82.

Palmer, C. L., Lim, W., Hastie, P. G., Toward, M., Korolchuk, V. I., Burbidge, S. A., Banting, G., Collingridge, G. L., Isaac, J. T., and Henley, J. M. (2005). Hippocalcin functions as a calcium sensor in hippocampal LTD. *Neuron* 47, 487–494.

Park, H., Varadi, A., Seok, H., Jo, J., Gilpin, H., Liew, C. G., Jung, S., Andrews, P. W., Molnar, E., and Cho, K. (2007). mGluR5 is involved in dendrite differentiation and excitatory synaptic transmission in NTERA2 human embryonic carcinoma cell-derived neurons. *Neuropharmacology* 52, 1403–1414.

Paterlini, M., Revilla, V., Grant, A. L., and Wisden, W. (2000). Expression of the neuronal calcium sensor protein family in the rat brain. *Neuroscience* 99, 205–216.

Peter, B. J., Kent, H. M., Mills, I. G., Vallis, Y., Butler, P. J., Evans, P. R., and McMahon, H. T. (2004). BAR domains as sensors of membrane curvature: the amphiphysin BAR structure. *Science* 303, 495–499.

Pongs, O., Lindemeier, J., Zhu, X. R., Theil, T., Engelkamp, D., Krah-Jentgens, I., Lambrecht, H. G., Koch, K. W., Schwemer, J., Rivosecchi, R., Mallart, A., Galceran, J., Canal, I., Barbas, J. A., and Ferrús, A. (1993). Frequenin – a novel calcium-binding protein that modulates synaptic efficacy in the *Drosophila* nervous system. *Neuron* 11, 15–28.

Rocca, D. L., Martin, S., Jenkins, E. L., and Hanley, J. G. (2008). Inhibition of Arp2/3-mediated actin polymerization by PICK1 regulates neuronal morphology and AMPA receptor endocytosis. *Nat. Cell Biol.* 10, 259–271.

Rosen, L. B., Ginty, D. D., Weber, M. J., and Greenberg, M. E. (1994). Membrane depolarization and calcium influx stimulate MEK and MAP kinase via activation of Ras. *Neuron* 12, 1207–1221.

Schneider, I., Reverse, D., Dewachter, I., Ris, L., Caluwaerts, N., Kuiperi, C., Gilis, M., Geerts, H., Kretzschmar, H., Godaux, E., Moechars, D., Van Leuven, F., and Herms, J. (2001). Mutant presenilins disturb neuronal calcium homeostasis in the brain of transgenic mice, decreasing the threshold for excitotoxicity and facilitating long-term potentiation. *J. Biol. Chem.* 276, 11539–11544.

Schnurra, I., Bernstein, H. G., Riederer, P., and Braunewell, K. H. (2001). The neuronal calcium sensor protein VILIP-1 is associated with amyloid plaques and extracellular tangles in Alzheimer's disease and promotes cell death and tau phosphorylation *in vitro*: a link between calcium sensors and Alzheimer's disease? *Neurobiol. Dis.* 8, 900–909.

Shankar, G. M., Bloodgood, B. L., Townsend, M., Walsh, D. M., Selkoe, D. J., and Sabatini, B. L. (2007). Natural oligomers of the Alzheimer amyloid-beta protein induce reversible synapse loss by modulating an NMDA-type glutamate receptor-dependent signaling pathway. *J. Neurosci.* 27, 2866–2875.

Shankar, G. M., Li, S., Mehta, T. H., Garcia-Munoz, A., Shepardson, N. E., Smith, I., Brett, F. M., Farrell, M. A., Rowan, M. J., Lemere, C. A., Regan, C. M., Walsh, D. M., Sabatini, B. L., and Selkoe, D. J. (2008). Amyloid-beta protein dimers isolated directly from Alzheimer's brains impair synaptic plasticity and memory. *Nat. Med.* 14, 837–842.

Sheng, M., Thompson, M. A., and Greenberg, M. E. (1991). CREB: a Ca^2-regulated transcription factor phosphorylated by calmodulin-dependent kinases. *Science* 252, 1427–1430.

Smith, I. F., Green, K. N., and LaFerla, F. M. (2005). Calcium dysregulation in Alzheimer's disease: recent advances gained from genetically modified animals. *Cell Calcium* 38, 427–437.

Walsh, D. M., Klyubin, I., Fadeeva, J. V., Cullen, W. K., Anwyl, R., Wolfe, M. S., Rowan, M. J., and Selkoe, D. J. (2002). Naturally secreted oligomers of amyloid beta protein potently inhibit hippocampal long-term potentiation *in vivo*. *Nature* 416, 535–539.

Xia, J., Chung, H. J., Wihler, C., Huganir, R. L., and Linden, D. J. (2000). Cerebellar long-term depression requires PKC-regulated interactions between GluR2/3 and PDZ domain-containing proteins. *Neuron* 28, 499–510.

Conflict of Interest Statement: The authors declare that the research was conducted in the absence of any commercial or financial relationships that could be construed as a potential conflict of interest.

Received: 01 March 2012; accepted: 07 April 2012; published online: 04 May 2012.
*Citation: Kerrigan TL, Whitcomb DJ, Regan PL and Cho K. (2012) The role of neuronal calcium sensors in balancing synaptic plasticity and synaptic dysfunction. Front. Mol. Neurosci. **5**:57. doi: 10.3389/fnmol.2012.00057*

frontiers in
MOLECULAR NEUROSCIENCE

MINI REVIEW ARTICLE
published: 13 April 2012
doi: 10.3389/fnmol.2012.00039

Negative modulation of NMDA receptor channel function by DREAM/calsenilin/KChIP3 provides neuroprotection?

KeWei Wang*[1,2] *and* ***Yun Wang*[2]***

[1] *Department of Molecular and Cellular Pharmacology, State Key Laboratory of Natural and Biomimetic Drugs, Peking University School of Pharmaceutical Sciences, Beijing, China*
[2] *Department of Neurobiology, Neuroscience Research Institute, Key Laboratory for Neuroscience, Ministry of Education, Peking University School of Basic Medical Sciences, Beijing, China*

Edited by:
Jose R. Naranjo, Centro Nalcional de Biotecnologia/Consejo Superior de Investigaciones Cientificas, Spain

Reviewed by:
Felix Hernandez, Universiad Autonoma de Madrid, Spain
Laura Mateos, Karolinska Institutet, Sweden

****Correspondence:***
KeWei Wang, Department of Molecular and Cellular Pharmacology, State Key Laboratory of Natural and Biomimetic Drugs, Peking University School of Pharmaceutical Sciences, Beijing, China.
e-mail: wangkw@bjmu.edu.cn
Yun Wang, Department of Neurobiology, Neuroscience Research Institute, Key Laboratory for Neuroscience, Ministry of Education, Peking University School of Basic Medical Sciences, Beijing, China.
e-mail: wangy66@bjmu.edu.cn

N-methyl-D-aspartate receptors (NMDARs) are glutamate-gated ion channels highly permeable to calcium and essential to excitatory neurotransmission. The NMDARs have attracted much attention because of their role in synaptic plasticity and excitotoxicity. Evidence has recently accumulated that NMDARs are negatively regulated by intracellular calcium binding proteins. The calcium-dependent suppression of NMDAR function serves as a feedback mechanism capable of regulating subsequent Ca^{2+} entry into the postsynaptic cell, and may offer an alternative approach to treating NMDAR-mediated excitotoxic injury. This short review summarizes the recent progress made in understanding the negative modulation of NMDAR function by DREAM/calsenilin/KChIP3, a neuronal calcium sensor (NCS) protein.

Keywords: calcium, excitotoxicity, neuroprotection, NMDA, NR1, NR2B, glutamate, neuronal calcium sensor (NCS) proteins

INTRODUCTION

Glutamate functions as the major excitatory neurotransmitter by binding to *N*-methyl-D-aspartate receptors (NMDARs) that are widespread in the central nervous system. The NMDARs constitute a major class of ionotropic glutamate receptors and play an essential role in synaptic transmission, plasticity, and memory. Activation of NMDARs results in cell membrane depolarization with an equilibrium potential near 0 mV, producing the excitatory postsynaptic potential (EPSP) and leading to an increase of Ca^{2+} influx into the cell. The intracellular Ca^{2+} can in turn function as a second messenger, mediating a variety of signaling cascades. Excessive activation of NMDARs by glutamate mediates neuronal damage in many neurological disorders including ischemia and neurodegenerative diseases (Choi et al., 1988; Sattler and Tymianski, 2001).

The NMDARs have long been considered the main target for the treatment of excitotoxicity-related neuronal injury, and a variety of antagonists or blockers of NMDARs have been developed. Unfortunately, the results of clinical trials have been disappointing because of the obvious side effects associated with blocking the physiological roles of NMDARs (Chen and Lipton, 2006). Therefore, a better understanding of the mechanism of how NMDARs can be modulated by regulatory proteins should help in the development of new therapeutic agents to counteract overactive NMDA receptor function, and may represent an alternative to treating NMDAR-mediated excitotoxic injury. This short review focuses on the specific negative modulation of NMDARs by a neuronal calcium sensor (NCS) protein, DREAM/calsenilin/KChIP3.

STRUCTURAL AND FUNCTIONAL FEATURES OF NMDA RECEPTOR CHANNELS

NMDARs are believed to be heterotetrameric complexes composed of combinations of the obligatory NR1 subunit and NR2 and/or NR3 subunits (Chazot and Stephenson, 1997; Laube et al., 1998; Schorge and Colquhoun, 2003; Furukawa et al., 2005). The NR1 subunit is encoded by a single gene but exists as eight functional splice variants, while the NR2 (NR2A-B) and NR3 (NR3A-B) subunits are encoded by four and two different genes, respectively. The NMDAR subunits form a central ion conductance pathway selective for cations such as Na^{+}, K^{+}, and Ca^{2+}, and share a common membrane topology, with each subunit consisting of four transmembrane (TM) domains (M1–M4). The long extracellular N-terminal regions of NMDAR subunits are organized as a tandem of two domains. The first domain, called the N-terminal domain (NTD) that includes the first 380 amino

acids, is involved in tetrameric assembly (Mayer, 2006; Paoletti and Neyton, 2007; Stroebel et al., 2011). The second domain of about 300 amino acids is known as the agonist-binding domain (ABD) that precedes the TM1 domain. The ABD binds glycine (or D-serine) in the NR1 and NR3 subunits, whereas the NR2 ABD binds glutamate (Furukawa et al., 2005; Yao and Mayer, 2006). The pore loop (P loop), or the M2 region, forms the narrowest constriction of the channel ion conductance pathway and determines the permeation properties of NMDARs. The NMDARs feature an intracellular C-terminal tail of about 400–600 residues that has a strong diversity in its amino acid sequence. The C-terminal tails of NMDAR subunits contain a series of short motifs that interact with intracellular factors or binding partners involved in receptor trafficking, anchoring and signaling (Skeberdis et al., 2006; Ryan et al., 2008; Lau et al., 2010).

Activation of NMDARs requires a simultaneous binding of two co-agonists, glutamate, and glycine with different biophysical properties of ion permeation. The typical NMDARs contain NR2 subunits with properties of high permeability to Ca^{2+} and extracellular Mg^{2+} block at hyperpolarized membrane potentials (Wrighton et al., 2008; Singh et al., 2012). Different from conventional NR1/NR2 heterotetramers, NR3-containing NMDARs have unique properties with a five to tenfold decrease of Ca^{2+} permeability, insensitivity to Mg^{2+} block, and reduced single-channel conductance and open probability, functioning as a negative modulator for NMDA receptor channel function (Das et al., 1998; Sasaki et al., 2002; Nakanishi et al., 2009; Cavara et al., 2010; Henson et al., 2010).

MODULATION OF NMDAR FUNCTION BY INTRACELLULAR BINDING PARTNERS

NMDA receptors are also regulated by other intracellular signals and proteins, including calcium, protein kinases, protein phosphatase calcineurin, and calcium-sensitive proteins such as calmodulin (Legendre et al., 1993; Vyklicky, 1993; Lieberman and Mody, 1994; Tong et al., 1995; Ehlers et al., 1996). Calcium-dependent NMDA receptor desensitization and inactivation provides a feedback mechanism capable of regulating subsequent Ca^{2+} entry into the postsynaptic cell through NMDA channels (**Figure 1**).

So far, a number of NR1 or NR2 subunit binding partners have been identified in the postsynaptic density. The NR1 binding proteins include calmodulin (CaM) (Ehlers et al., 1996; Akyol et al., 2004), Ca^{2+}/CaM-dependent protein kinase II (CaMKII) (Leonard et al., 2002), α-actinin (Wyszynski et al., 1997; Merrill et al., 2007), tubulin (van Rossum et al., 1999), spectrin (Wechsler and Teichberg, 1998), neurofilament (Ehlers et al., 1998), and Yotiao (Lin et al., 1998). Calmodulin binding to the NR1 subunit is Ca^{2+} dependent and occurs with homomeric NR1 complexes, heteromeric NR1/NR2 subunit complexes from expression systems, and NMDA receptors from the brain. Calmodulin binding to NR1 causes a fourfold reduction in NMDA channel open probability, mediating the negative modulation of NMDAR function (Ehlers et al., 1998).

DREAM/calsenilin/KChIP3, A NEURONAL CALCIUM SENSOR AND CALCIUM BINDING EF-HAND PROTEIN

DREAM/calsenilin/KChIP3 is encoded by the same gene locus. The downstream regulatory element antagonist modulator (DREAM) protein, first identified in the nucleus as a Ca^{2+}-regulated transcriptional repressor through its binding to DNA at specific regulatory elements, contains four Ca^{2+}-binding EF-hand domains and belongs to the NCS family (Carrion et al., 1999; Burgoyne, 2007). DREAM was named for its ability to block gene expression in its Ca^{2+}-free form via direct binding with the downstream regulatory element (DRE) sequence in target genes such as preprodynorphin (PPD), c-fos, Hrk, Na^{+}, and Ca^{2+} exchanger NCX3 (Carrion et al., 1999; Sanz et al., 2001; Gomez-Villafuertes et al., 2005). DREAM was also named calsenilin or Kv channel interacting protein 3 (KChIP3) (Buxbaum et al., 1998; An et al., 2000), indicating that DREAM/calsenilin/KChIP3 has multifunctional properties. In the nucleus the DREAM protein functions as a dimer, whereas outside the nucleus KChIP3 is a monomer and regulates the surface expression and gating kinetics of Kv4 channels (An et al., 2000; Kim and Sheng, 2004;

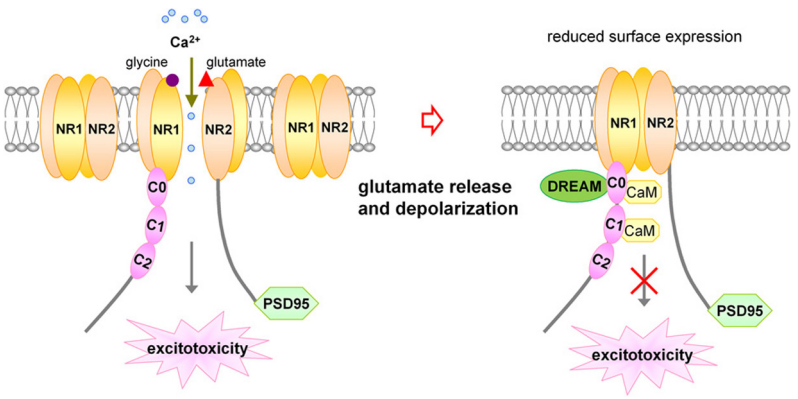

FIGURE 1 | Schematic representation for inhibitory effect of DREAM/calsenilin/KChIP3 on NMDARs in a Ca^{2+}-sensitive manner. Upon activation of NMDARs by glutamate binding, Ca^{2+} influx through NMDARs increases the association between DREAM and NR1 subunits, resulting in reduced surface expression of NMDARs, and subsequent inhibition of NMDARs-mediated Ca^{2+} influx and excitotoxicity. DREAM functions as a Ca^{2+}-sensitive modulator for the negative feedback control of NMDAR function.

Scannevin et al., 2004; Pioletti et al., 2006; Wang et al., 2007; Wang, 2008).

DREAM/calsenilin/KChIP3 is preferentially expressed in the central nervous system, as well as in non-neuronal tissues (Link et al., 2004; D'Andrea et al., 2005; Savignac et al., 2005). DREAM/calsenilin/KChIP3 knock-out mice display a hypoalgesic phenotype, suggesting a critical role of DREAM/calsenilin/KChIP3 in pain modulation (Cheng et al., 2002). In addition, emerging evidence reveals the role of DREAM/calsenilin/KChIP3 in long-term potentiation (LTP) (Lilliehook et al., 2003) and learning and memory (Alexander et al., 2009; Fontan-Lozano et al., 2009), suggesting a possible connection between DREAM and NMDA function.

KChIP1–3 were initially identified from a rat brain library in yeast two-hybrid (YTH) screens using the cytoplasmic N-terminal domain (amino acids 1–180) of rat Kv4.3 as a bait (An et al., 2000). Similarly, KChIP4 from mouse and human was accidentally cloned using the C-terminal 43 amino acid residues of presenilin 2 (PS2, amino acids 406–448) as a bait in the YTH system (Morohashi et al., 2002). KChIP4, also known as calsenilin-like protein (CALP), binds to PS2 which is known to facilitate intramembranous γ-cleavage of γ-amyloid protein precursor (βAPP) (Morohashi et al., 2002).

KChIP1–4 (216 ∼ 256 amino acids) can co-immunoprecipitate and co-localize with either Kv4 from co-transfected cells or Kv4 α-subunits from tissues, and thus constitute integral components of native Kv4 channel complexes (Wang, 2008). KChIP1–4 all share a conserved carboxy-terminal core region that contains four EF-hand-like calcium binding motifs, but have a variable amino-terminal region that causes diverse modulation of Kv4 trafficking and channel function (An et al., 2000; Holmqvist et al., 2002; Scannevin et al., 2004; Cui et al., 2008; Liang et al., 2009, 2010).

FUNCTIONAL INTERACTIONS BETWEEN DREAM AND NMDA RECEPTORS

We and others have investigated mechanisms underlying the functional interactions between DREAM and NMDARs. Findings from co-immunoprecipitation experiments show that DREAM antibody can immunoprecipitate endogenous NR1 subunit and DREAM protein from rat hippocampal tissue (Zhang et al., 2010). In the reciprocal co-IP studies in HEK 293 cells expressing DREAM and NR1-1a (NR1a) proteins, NR1 antibody can also immunoprecipitate DREAM along with the NR1 subunit. GST pull-down assays reveal that the N-terminus of DREAM directly interacts with the NR1a C-terminus, and that the DREAM-NR1 interaction is sensitive to Ca^{2+} and depends on the EF hand domains of DREAM (Zhang et al., 2010).

PSD-95 is a major scaffolding protein in the postsynaptic density, tethering NMDARs to signaling proteins, and is critical for NMDA receptor function (Kim and Sheng, 2004). Wu et al. generated a line of transgenic mice (TgDREAM) overexpressing a dominant active DREAM mutant, and compared NMDA receptor-mediated EPSCs in TgDREAM and wild-type mice under conditions of various stimulation intensities (Wu et al., 2010). They found that the amplitude of NMDA receptor-mediated EPSCs in TgDREAM mice is significantly reduced compared to that in wild-type mice (Wu et al., 2010). In addition, LTD is significantly reduced in TgDREAM mice whereas LTP is not affected by DREAM, demonstrating that DREAM interacts with PSD-95, and that the interaction is negatively regulated by calcium (Wu et al., 2010). In Xenopus oocytes expressing NR2B-containing NMDARs alone or together with DREAM, two-electrode voltage clamp recordings show that, in the absence of DREAM, the peak currents of NMDA channels activated by glutamate (plus glycine) are suppressed by DREAM, and the current decrease is caused by a reduction in the density of NMDARs at the cell surface (**Figure 1**; Zhang et al., 2010).

Fontan-Lozano et al. recently provided another piece of evidence that DREAM negatively regulates the function of NMDA receptors (Fontan-Lozano et al., 2011). By taking advantage of mice lacking the DREAM protein, they demonstrated that the facilitated learning induced by decreased expression of Kv4.2 in *dream*$^{-/-}$ mice requires the activation of NMDA receptors containing the NR2B subunit (Fontan-Lozano et al., 2011). This study not only indicates the significance of the balance between Kv4 channel function and NMDAR activity, but also suggests the formation of a functional complex between DREAM/Kv4.2/NMDARs that regulates the synaptic efficacy mediating synaptic plasticity and learning.

NEUROPROTECTIVE EFFECT OF DREAM/calsenilin/KChIP3 OVER-EXPRESSION ON NEURONAL EXCITOTOXIC INJURY

Excitotoxicity is caused by overactivation of NMDA receptor function, and inhibition of NMDARs can reverse the neuronal toxicity. The data available so far support both the pro-apoptotic and anti-apoptotic roles of DREAM. In general, the pro-apoptotic role of DREAM closely correlates with its interaction with presenilins, the production of amyloid beta (Aβ) and the modulation in Ca^{2+} signaling, whereas the anti-apoptotic role of DREAM is conferred by its transcriptional repressor activity on the apoptotic protein Hrk. Jo et al. reported that HeLa cells transiently transfected with DREAM exhibit the morphological and biochemical features of apoptosis and that expression of presenilin potentiates DREAM-induced apoptosis (Jo et al., 2001). Jo et al. also reported that DREAM expression increases in either human neuroblastoma SK-N-BE2(c) cells or rat neuroblastoma B103 cells after exposure to Aβ, but no other apoptotic inducers such as staurosporine, thapsigargin, and calcium ionophore A23187. The pro-apoptotic role of DREAM is selectively induced during Ab toxicity. Because of the involvement of presenilins/γ-secretase in Aβ formation and neuronal death, DREAM coordinates with presenilin activity to play a crucial role in these processes through binding with the C-terminus of presenilins (Jo et al., 2003, 2004). Lilliehook et al. stably expressed DREAM in H4 neuroglioma cells which showed no initiation of apoptosis in the absence of apoptosis triggers, and the apoptosis-associated caspase and calpain activities were not affected by DREAM (Lilliehook et al., 2002). On the other hand, binding of the transcriptional repressor DREAM to the hrk gene avoids inappropriate Hrk expression and apoptosis in hematopoietic progenitor cell lines (Sanz et al., 2001, 2002). Nevertheless, the precise function of DREAM in pro-apoptosis and anti-apoptosis remains to be explored.

From our previous observations, we noticed that cell viability is affected by the amount of exogenous DREAM gene and the method of transfection. However, we could not observe any obvious morphological changes associated with cell death after the transfection of DREAM. To prove the cytoprotective role of DREAM, we utilized cell lines and primary cultured hippocampal neurons with DREAM overexpression or siRNA-mediated knockdown, and evaluated lactate dehydrogenase (LDH) leakage and propidium iodide (PI) uptake both in NMDA and oxygen-glucose deprivation (OGD) -induced excitotoxic injury models (Zhang et al., 2010). Administration of NMDA markedly increases the number of PI-positive cells (dead cells) in NMDAR-transfected CHO cells, whereas co-expression of DREAM greatly reduces PI-positive cells (Zhang et al., 2010). LDH leakage measurement is a sensitive index reflecting the extent of cell damage. Over-expression of DREAM suppresses the NMDA-induced LDH release. OGD is commonly used *in vitro* to mimic ischemia-reperfusion insult to the brain, and OGD treatment induces a significant increase of LDH release (Dawson et al., 1994). With over-expression of DREAM, however, OGD treatment induces a smaller increase in LDH release. These results indicate that the over-expression of DREAM attenuates NMDAR-mediated excitotoxicity (Zhang et al., 2010).

We have previously tested the effect of DREAM siRNA on NMDA-induced current and excitotoxic injury in hippocampal neurons (Zhang et al., 2010). Knockdown of endogenous DREAM with siRNA results in an increased amplitude of NMDA current recorded by whole-cell patch-clamp assays. DREAM siRNA also significantly exacerbates NMDA-induced cell death in hippocampal neurons. After NMDA exposure, PI-positive cells in the DREAM siRNA group increase compared with control siRNA, indicating the inhibitory effect of DREAM on NMDAR-mediated current and excitotoxic injury (Zhang et al., 2010).

CONCLUSIONS

The NCS protein DREAM/calsenilin/KChIP3 acts as an auxiliary subunit and suppresses NMDA receptor channel function. This negative modulation of NMDA receptor function by DREAM likely provides a feedback mechanism by which overactive NMDA receptors are inhibited. Therefore, targeting regulatory proteins of NMDARs may represent an alternative approach to treating NMDAR-mediated excitotoxic damage and providing neuroprotection.

ACKNOWLEDGMENTS

We would like to thank the members of our laboratories for their comments and Greg Vatcher for his careful proof-reading of this manuscript. This work was supported by research grants from the National Science Foundation of China to KeWei Wang (30970919) and to Yun Wang (81161120497, 30830044, and 30925015).

REFERENCES

Akyol, Z., Bartos, J. A., Merrill, M. A., Faga, L. A., Jaren, O. R., Shea, M. A., and Hell, J. W. (2004). Apo-calmodulin binds with its C-terminal domain to the *N*-methyl-D-aspartate receptor NR1 C0 region. *J. Biol. Chem.* 279, 2166–2175.

Alexander, J. C., McDermott, C. M., Tunur, T., Rands, V., Stelly, C., Karhson, D., Bowlby, M. R., An, W. F., Sweatt, J. D., and Schrader, L. A. (2009). The role of calsenilin/DREAM/KChIP3 in contextual fear conditioning. *Learn. Mem.* 16, 167–177.

An, W. F., Bowlby, M. R., Betty, M., Cao, J., Ling, H. P., Mendoza, G., Hinson, J. W., Mattsson, K. I., Strassle, B. W., Trimmer, J. S., and Rhodes, K. J. (2000). Modulation of A-type potassium channels by a family of calcium sensors. *Nature* 403, 553–556.

Burgoyne, R. D. (2007). Neuronal calcium sensor proteins: generating diversity in neuronal Ca^{2+} signalling. *Nat. Rev. Neurosci.* 8, 182–193.

Buxbaum, J. D., Choi, E. K., Luo, Y., Lilliehook, C., Crowley, A. C., Merriam, D. E., and Wasco, W. (1998). Calsenilin: a calcium-binding protein that interacts with the presenilins and regulates the levels of a presenilin fragment. *Nat. Med.* 4, 1177–1181.

Carrion, A. M., Link, W. A., Ledo, F., Mellstrom, B., and Naranjo, J. R. (1999). DREAM is a Ca^{2+}-regulated transcriptional repressor. *Nature* 398, 80–84.

Cavara, N. A., Orth, A., Hicking, G., Seebohm, G., and Hollmann, M. (2010). Residues at the tip of the pore loop of NR3B-containing NMDA receptors determine Ca^{2+} permeability and Mg^{2+} block. *BMC Neurosci.* 11, 133.

Chazot, P. L., and Stephenson, F. A. (1997). Molecular dissection of native mammalian forebrain NMDA receptors containing the NR1 C2 exon: direct demonstration of NMDA receptors comprising NR1, NR2A, and NR2B subunits within the same complex. *J. Neurochem.* 69, 2138–2144.

Chen, H. S., and Lipton, S. A. (2006). The chemical biology of clinically tolerated NMDA receptor antagonists. *J. Neurochem.* 97, 1611–1626.

Cheng, H. Y., Pitcher, G. M., Laviolette, S. R., Whishaw, I. Q., Tong, K. I., Kockeritz, L. K., Wada, T., Joza, N. A., Crackower, M., Goncalves, J., Sarosi, I., Woodgett, J. R., Oliveira-dos-Santos, A. J., Ikura, M., van der Kooy, D., Salter, M. W., and Penninger, J. M. (2002). DREAM is a critical transcriptional repressor for pain modulation. *Cell* 108, 31–43.

Choi, D. W., Koh, J. Y., and Peters, S. (1988). Pharmacology of glutamate neurotoxicity in cortical cell culture: attenuation by NMDA antagonists. *J. Neurosci.* 8, 185–196.

Cui, Y. Y., Liang, P., and Wang, K. W. (2008). Enhanced trafficking of tetrameric Kv4.3 channels by KChIP1 clamping. *Neurochem. Res.* 33, 2078–2084.

D'Andrea, B., Di Palma, T., Mascia, A., Motti, M. L., Viglietto, G., Nitsch, L., and Zannini, M. (2005). The transcriptional repressor DREAM is involved in thyroid gene expression. *Exp. Cell Res.* 305, 166–178.

Das, S., Sasaki, Y. F., Rothe, T., Premkumar, L. S., Takasu, M., Crandall, J. E., Dikkes, P., Conner, D. A., Rayudu, P. V., Cheung, W., Chen, H. S., Lipton, S. A., and Nakanishi, N. (1998). Increased NMDA current and spine density in mice lacking the NMDA receptor subunit NR3A. *Nature* 393, 377–381.

Dawson, T. M., Zhang, J., Dawson, V. L., and Snyder, S. H. (1994). Nitric oxide: cellular regulation and neuronal injury. *Prog. Brain Res.* 103, 365–369.

Ehlers, M. D., Fung, E. T., O'Brien, R. J., and Huganir, R. L. (1998). Splice variant-specific interaction of the NMDA receptor subunit NR1 with neuronal intermediate filaments. *J. Neurosci.* 18, 720–730.

Ehlers, M. D., Zhang, S., Bernhadt, J. P., and Huganir, R. L. (1996). Inactivation of NMDA receptors by direct interaction of calmodulin with the NR1 subunit. *Cell* 84, 745–755.

Fontan-Lozano, A., Romero-Granados, R., del-Pozo-Martin, Y., Suarez-Pereira, I., Delgado-Garcia, J. M., Penninger, J. M., and Carrion, A. M. (2009). Lack of DREAM protein enhances learning and memory and slows brain aging. *Curr. Biol.* 19, 54–60.

Fontan-Lozano, A., Suarez-Pereira, I., Gonzalez-Forero, D., and Carrion, A. M. (2011). The A-current modulates learning via NMDA receptors containing the NR2B subunit. *PLoS One* 6:e24915. doi: 10.1371/journal.pone.0024915

Furukawa, H., Singh, S. K., Mancusso, R., and Gouaux, E. (2005). Subunit arrangement and function in NMDA receptors. *Nature* 438, 185–192.

Gomez-Villafuertes, R., Torres, B., Barrio, J., Savignac, M., Gabellini, N., Rizzato, F., Pintado, B.,

Gutierrez-Adan, A., Mellstrom, B., Carafoli, E., and Naranjo, J. R. (2005). Downstream regulatory element antagonist modulator regulates Ca^{2+} homeostasis and viability in cerebellar neurons. *J. Neurosci.* 25, 10822–10830.

Henson, M. A., Roberts, A. C., Perez-Otano, I., and Philpot, B. D. (2010). Influence of the NR3A subunit on NMDA receptor functions. *Prog. Neurobiol.* 91, 23–37.

Holmqvist, M. H., Cao, J., Hernandez-Pineda, R., Jacobson, M. D., Carroll, K. I., Sung, M. A., Betty, M., Ge, P., Gilbride, K. J., Brown, M. E., Jurman, M. E., Lawson, D., Silos-Santiago, I., Xie, Y., Covarrubias, M., Rhodes, K. J., Distefano, P. S., and An, W. F. (2002). Elimination of fast inactivation in Kv4 A-type potassium channels by an auxiliary subunit domain. *Proc. Natl. Acad. Sci. U.S.A.* 99, 1035–1040.

Jo, D. G., Chang, J. W., Hong, H. S., Mook-Jung, I., and Jung, Y. K. (2003). Contribution of presenilin/gamma-secretase to calsenilin-mediated apoptosis. *Biochem. Biophys. Res. Commun.* 305, 62–66.

Jo, D. G., Lee, J. Y., Hong, Y. M., Song, S., Mook-Jung, I., Koh, J. Y., and Jung, Y. K. (2004). Induction of pro-apoptotic calsenilin/DREAM/KChIP3 in Alzheimer's disease and cultured neurons after amyloid-beta exposure. *J. Neurochem.* 88, 604–611.

Jo, D. G., Kim, M. J., Choi, Y. H., Kim, I. K., Song, Y. H., Woo, H. N., Chung, C. W., and Jung, Y. K. (2001). Pro-apoptotic function of calsenilin/DREAM/KChIP3. *FASEB J.* 15, 589–591.

Kim, E., and Sheng, M. (2004). PDZ domain proteins of synapses. *Nat. Rev. Neurosci.* 5, 771–781.

Lau, C. G., Takayasu, Y., Rodenas-Ruano, A., Paternain, A. V., Lerma, J., Bennett, M. V., and Zukin, R. S. (2010). SNAP-25 is a target of protein kinase C phosphorylation critical to NMDA receptor trafficking. *J. Neurosci.* 30, 242–254.

Laube, B., Kuhse, J., and Betz, H. (1998). Evidence for a tetrameric structure of recombinant NMDA receptors. *J. Neurosci.* 18, 2954–2961.

Legendre, P., Rosenmund, C., and Westbrook, G. L. (1993). Inactivation of NMDA channels in cultured hippocampal neurons by intracellular calcium. *J. Neurosci.* 13, 674–684.

Leonard, A. S., Bayer, K. U., Merrill, M. A., Lim, I. A., Shea, M. A., Schulman, H., and Hell, J. W. (2002). Regulation of calcium/calmodulin-dependent protein kinase II docking to *N*-methyl-D-aspartate receptors by calcium/calmodulin and alpha-actinin. *J. Biol. Chem.* 277, 48441–48448.

Liang, P., Chen, H., Cui, Y., Lei, L., and Wang, K. (2010). Functional rescue of Kv4.3 channel tetramerization mutants by KChIP4a. *Biophys. J.* 98, 2867–2876.

Liang, P., Wang, H., Chen, H., Cui, Y., Gu, L., Chai, J., and Wang, K. (2009). Structural Insights into KChIP4a Modulation of Kv4.3 Inactivation. *J. Biol. Chem.* 284, 4960–4967.

Lieberman, D. N., and Mody, I. (1994). Regulation of NMDA channel function by endogenous Ca(2+)-dependent phosphatase. *Nature* 369, 235–239.

Lilliehook, C., Bozdagi, O., Yao, J., Gomez-Ramirez, M., Zaidi, N. F., Wasco, W., Gandy, S., Santucci, A. C., Haroutunian, V., Huntley, G. W., and Buxbaum, J. D. (2003). Altered Abeta formation and long-term potentiation in a calsenilin knock-out. *J. Neurosci.* 23, 9097–9106.

Lilliehook, C., Chan, S., Choi, E. K., Zaidi, N. F., Wasco, W., Mattson, M. P., and Buxbaum, J. D. (2002). Calsenilin enhances apoptosis by altering endoplasmic reticulum calcium signaling. *Mol. Cell. Neurosci.* 19, 552–559.

Lin, J. W., Wyszynski, M., Madhavan, R., Sealock, R., Kim, J. U., and Sheng, M. (1998). Yotiao, a novel protein of neuromuscular junction and brain that interacts with specific splice variants of NMDA receptor subunit NR1. *J. Neurosci.* 18, 2017–2027.

Link, W. A., Ledo, F., Torres, B., Palczewska, M., Madsen, T. M., Savignac, M., Albar, J. P., Mellstrom, B., and Naranjo, J. R. (2004). Day-night changes in downstream regulatory element antagonist modulator/potassium channel interacting protein activity contribute to circadian gene expression in pineal gland. *J. Neurosci.* 24, 5346–5355.

Mayer, M. L. (2006). Glutamate receptors at atomic resolution. *Nature* 440, 456–462.

Merrill, M. A., Malik, Z., Akyol, Z., Bartos, J. A., Leonard, A. S., Hudmon, A., Shea, M. A., and Hell, J. W. (2007). Displacement of alpha-actinin from the NMDA receptor NR1 C0 domain By Ca^{2+}/calmodulin promotes CaMKII binding. *Biochemistry* 46, 8485–8497.

Morohashi, Y., Hatano, N., Ohya, S., Takikawa, R., Watabiki, T., Takasugi, N., Imaizumi, Y., Tomita, T., and Iwatsubo, T. (2002). Molecular cloning and characterization of CALP/KChIP4, a novel EF-hand protein interacting with presenilin 2 and voltage-gated potassium channel subunit Kv4. *J. Biol. Chem.* 277, 14965–14975.

Nakanishi, N., Tu, S., Shin, Y., Cui, J., Kurokawa, T., Zhang, D., Chen, H. S., Tong, G., and Lipton, S. A. (2009). Neuroprotection by the NR3A subunit of the NMDA receptor. *J. Neurosci.* 29, 5260–5265.

Paoletti, P., and Neyton, J. (2007). NMDA receptor subunits: function and pharmacology. *Curr. Opin. Pharmacol.* 7, 39–47.

Pioletti, M., Findeisen, F., Hura, G. L., and Minor, D. L. Jr. (2006). Three-dimensional structure of the KChIP1-Kv4.3 T1 complex reveals a cross-shaped octamer. *Nat. Struct. Mol. Biol.* 13, 987–995.

Ryan, T. J., Emes, R. D., Grant, S. G., and Komiyama, N. H. (2008). Evolution of NMDA receptor cytoplasmic interaction domains: implications for organisation of synaptic signalling complexes. *BMC Neurosci.* 9, 6.

Sanz, C., Horita, M., and Fernandez-Luna, J. L. (2002). Fas signaling and blockade of Bcr-Abl kinase induce apoptotic Hrk protein via DREAM inhibition in human leukemia cells. *Haematologica* 87, 903–907.

Sanz, C., Mellstrom, B., Link, W. A., Naranjo, J. R., and Fernandez-Luna, J. L. (2001). Interleukin 3-dependent activation of DREAM is involved in transcriptional silencing of the apoptotic Hrk gene in hematopoietic progenitor cells. *EMBO J.* 20, 2286–2292.

Sasaki, Y. F., Rothe, T., Premkumar, L. S., Das, S., Cui, J., Talantova, M. V., Wong, H. K., Gong, X., Chan, S. F., Zhang, D., Nakanishi, N., Sucher, N. J., and Lipton, S. A. (2002). Characterization and comparison of the NR3A subunit of the NMDA receptor in recombinant systems and primary cortical neurons. *J. Neurophysiol.* 87, 2052–2063.

Sattler, R., and Tymianski, M. (2001). Molecular mechanisms of glutamate receptor-mediated excitotoxic neuronal cell death. *Mol. Neurobiol.* 24, 107–129.

Savignac, M., Pintado, B., Gutierrez-Adan, A., Palczewska, M., Mellstrom, B., and Naranjo, J. R. (2005). Transcriptional repressor DREAM regulates T-lymphocyte proliferation and cytokine gene expression. *EMBO J.* 24, 3555–3564.

Scannevin, R. H., Wang, K., Jow, F., Megules, J., Kopsco, D. C., Edris, W., Carroll, K. C., Lü, Q., Xu, W., Xu, Z., Katz, A. H., Olland, S., Lin, L., Taylor, M., Stahl, M., Malakian, K., Somers, W., Mosyak, L., Bowlby, M. R., Chanda, P., and Rhodes, K. J. (2004). Two N-terminal domains of Kv4 K(+) channels regulate binding to and modulation by KChIP1. *Neuron* 41, 587–598.

Schorge, S., and Colquhoun, D. (2003). Studies of NMDA receptor function and stoichiometry with truncated and tandem subunits. *J. Neurosci.* 23, 1151–1158.

Singh, P., Doshi, S., Spaethling, J. M., Hockenberry, A. J., Patel, T. P., Geddes-Klein, D. M., Lynch, D. R., and Meaney, D. F. (2012). N-methyl-D-aspartate receptor mechanosensitivity is governed by C terminus of NR2B subunit. *J. Biol. Chem.* 287, 4348–4359.

Skeberdis, V. A., Chevaleyre, V., Lau, C. G., Goldberg, J. H., Pettit, D. L., Suadicani, S. O., Lin, Y., Bennett, M. V., Yuste, R., Castillo, P. E., and Zukin, R. S. (2006). Protein kinase A regulates calcium permeability of NMDA receptors. *Nat. Neurosci.* 9, 501–510.

Stroebel, D., Carvalho, S., and Paoletti, P. (2011). Functional evidence for a twisted conformation of the NMDA receptor GluN2A subunit N-terminal domain. *Neuropharmacology* 60, 151–158.

Tong, G., Shepherd, D., and Jahr, C. E. (1995). Synaptic desensitization of NMDA receptors by calcineurin. *Science* 267, 1510–1512.

van Rossum, D., Kuhse, J., and Betz, H. (1999). Dynamic interaction between soluble tubulin and C-terminal domains of *N*-methyl-D-aspartate receptor subunits. *J. Neurochem.* 72, 962–973.

Vyklicky, L. Jr. (1993). Calcium-mediated modulation of *N*-methyl-D-aspartate (NMDA) responses in cultured rat hippocampal neurones. *J. Physiol.* 470, 575–600.

Wang, H., Yan, Y., Liu, Q., Huang, Y., Shen, Y., Chen, L., Chen, Y., Yang, Q., Hao, Q., Wang, K., and Chai, J. (2007). Structural basis for modulation of Kv4 K^+ channels by auxiliary KChIP subunits. *Nat. Neurosci.* 10, 32–39.

Wang, K. (2008). Modulation by clamping: Kv4 and KChIP interactions. *Neurochem. Res.* 33, 1964–1969.

Wechsler, A., and Teichberg, V. I. (1998). Brain spectrin binding to the NMDA receptor is regulated by phosphorylation, calcium and calmodulin. *EMBO J.* 17, 3931–3939.

Wrighton, D. C., Baker, E. J., Chen, P. E., and Wyllie, D. J. (2008). Mg^{2+} and memantine block of rat recombinant NMDA receptors containing chimeric NR2A/2D

subunits expressed in Xenopus laevis oocytes. *J. Physiol.* 586, 211–225.

Wu, L. J., Mellstrom, B., Wang, H., Ren, M., Domingo, S., Kim, S. S., Li, X. Y., Chen, T., Naranjo, J. R., and Zhuo, M. (2010). DREAM (downstream regulatory element antagonist modulator) contributes to synaptic depression and contextual fear memory. *Mol. Brain* 3, 3.

Wyszynski, M., Lin, J., Rao, A., Nigh, E., Beggs, A. H., Craig, A. M., and Sheng, M. (1997). Competitive binding of alpha-actinin and calmodulin to the NMDA receptor. *Nature* 385, 439–442.

Yao, Y., and Mayer, M. L. (2006). Characterization of a soluble ligand binding domain of the NMDA receptor regulatory subunit NR3A. *J. Neurosci.* 26, 4559–4566.

Zhang, Y., Su, P., Liang, P., Liu, T., Liu, X., Liu, X. Y., Zhang, B., Han, T., Zhu, Y. B., Yin, D. M., Li, J., Zhou, Z., Wang, K. W., and Wang, Y. (2010). The DREAM protein negatively regulates the NMDA receptor through interaction with the NR1 subunit. *J. Neurosci.* 30, 7575–7586.

Conflict of Interest Statement: The authors declare that the research was conducted in the absence of any commercial or financial relationships that could be construed as a potential conflict of interest.

Received: 16 February 2012; paper pending published: 01 March 2012; accepted: 15 March 2012; published online: 13 April 2012.

Citation: Wang K and Wang Y (2012) Negative modulation of NMDA receptor channel function by DREAM/calsenilin/KChIP3 provides neuroprotection?. Front. Mol. Neurosci. 5:39. doi: 10.3389/fnmol.2012.00039

frontiers in
MOLECULAR NEUROSCIENCE

REVIEW ARTICLE
published: 08 May 2012
doi: 10.3389/fnmol.2012.00061

Ca^{2+} sensor proteins in dendritic spines: a race for Ca^{2+}

Vijeta Raghuram*[1,2], *Yogendra Sharma*[1] and *Michael R. Kreutz*[2]

[1] *Centre for Cellular and Molecular Biology, CSIR, Hyderabad, India*
[2] *RG Neuroplasticity, Leibniz Institute for Neurobiology, Magdeburg, Germany*

Edited by:
Beat Schwaller, University of Fribourg, Switzerland

Reviewed by:
Miou Zhou, University of California, Los Angeles, USA
Guido C. Faas, University of California, Los Angeles, USA
Hartmut Schmidt, University of Leipzig, Germany

***Correspondence:**
Michael R. Kreutz, RG Neuroplasticity, Leibniz Institute for Neurobiology, Brenneckestr. 6, 39118 Magdeburg, Germany.
e-mail: kreutz@lin-magdeburg.de

Dendritic spines are believed to be micro-compartments of Ca^{2+} regulation. In a recent study, it was suggested that the ubiquitous and evolutionarily conserved Ca^{2+} sensor, calmodulin (CaM), is the first to intercept Ca^{2+} entering the spine and might be responsible for the fast decay of Ca^{2+} transients in spines. Neuronal calcium sensor (NCS) and neuronal calcium-binding protein (nCaBP) families consist of Ca^{2+} sensors with largely unknown synaptic functions despite an increasing number of interaction partners. Particularly how these sensors operate in spines in the presence of CaM has not been discussed in detail before. The limited Ca^{2+} resources and the existence of common targets create a highly competitive environment where Ca^{2+} sensors compete with each other for Ca^{2+} and target binding. In this review, we take a simple numerical approach to put forth possible scenarios and their impact on signaling via Ca^{2+} sensors of the NCS and nCaBP families. We also discuss the ways in which spine geometry and properties of ion channels, their kinetics and distribution, alter the spatio-temporal aspects of Ca^{2+} transients in dendritic spines, whose interplay with Ca^{2+} sensors in turn influences the race for Ca^{2+}.

Keywords: Ca^{2+}, neuronal calcium signaling, neuronal calcium sensor, calcium-binding protein, dendritic spine, binding affinity, calcium dynamics, protein-protein interaction

INTRODUCTION

In the human brain, spinous synapses on pyramidal neurons are the most abundant synapse type in the cerebrum and Ca^{2+} signaling in spines has been extensively studied. A largely overlooked area of neuronal Ca^{2+} signaling, though, is the functional role of EF-hand Ca^{2+}-binding proteins of the calmodulin (CaM) superfamily in dendritic spines. Traditionally, these proteins have been assigned to the neuronal calcium sensor (NCS) and neuronal calcium-binding protein (nCaBP) families, all of which are evolutionarily related to the ancestral CaM (**Figure 1**). Being particularly abundant in brain and retina, members of the NCS and nCaBP family have been implicated in a plethora of different cellular events (see Burgoyne, 2007; and Mikhaylova et al., 2011), although their exact synaptic function is largely unknown.

EVOLUTION OF NCS AND nCaBP FAMILIES OF PROTEINS

The NCS family of Ca^{2+} sensors (**Figure 1**) has been named after a group of proteins initially thought to be specifically expressed in neurons (De Castro et al., 1995). This group originated from the ancestral frequenin/NCS-1 and has diversified during evolution. Several reviews cover the topics of evolution and function of the NCS family of proteins (Burgoyne, 2007; Mikhaylova et al., 2011). Briefly, on the basis of sequence analysis, these proteins have been grouped into five classes, labeled in the order of their appearance during evolution (Burgoyne and Weiss, 2001; Burgoyne, 2007). Class A consists of NCS-1 or frequenin which appeared first in yeast. Visinin-like proteins or VILIPs evolved first in *Caenorhabditis elegans* and constitute the class B. With the evolution of the vertebrate eye, two new classes—C and D arose which comprise recoverin and guanylate cyclase activating proteins (GCAPs). Class E includes the voltage-gated K^+ channel (K_v) interacting proteins or KChIPs and appeared first in insects. The mammalian genome encodes a single NCS-1, five VILIPS (hippocalcin, neurocalcin-δ, VILIPs1-3), a single recoverin, three GCAPs (GCAP1–3) and four KChIPs (KChIP 1–4) which exist in multiple isoforms. The various proteins of the NCS family show roughly <20% sequence identity with CaM. They possess four EF-hands out of which only two or three are capable of binding Ca^{2+}. All of the members except KChIP2 and KChIP3 show an N-terminal myristoylation consensus sequence (**Figure 1**). This post-translational modification is important for their membrane localization. The Ca^{2+} binding is generally cooperative in most of the members and they show a much higher affinity for Ca^{2+} compared to CaM, while many of them also bind Mg^{2+} (Mikhaylova et al., 2011).

The nCaBP family of proteins (Seidenbecher et al., 1998; Haeseleer et al., 2000; Wu et al., 2001; Laube et al., 2002; Mikhaylova et al., 2006, 2009, 2011; McCue et al., 2010a,b) comprising caldendrin/CaBPs 1–5 and calneurons-1 and -2 arose much later during evolution and are found only in vertebrates (**Figure 1**). With respect to their EF-hands, they show a greater similarity to CaM than the NCS-1 family. It is, therefore, believed that the nCaBP family has evolved directly from the ancestral CaM (Seidenbecher et al., 1998; Haeseleer et al., 2000; Wu et al., 2001; Mikhaylova et al., 2006, 2011; McCue et al., 2010a). Like the NCS family, the nCaBPs too possess cryptic EF-hands and a few members are also N-myristoylated (CaBPs 1 and 2). A common distinctive feature is the presence of four extra amino

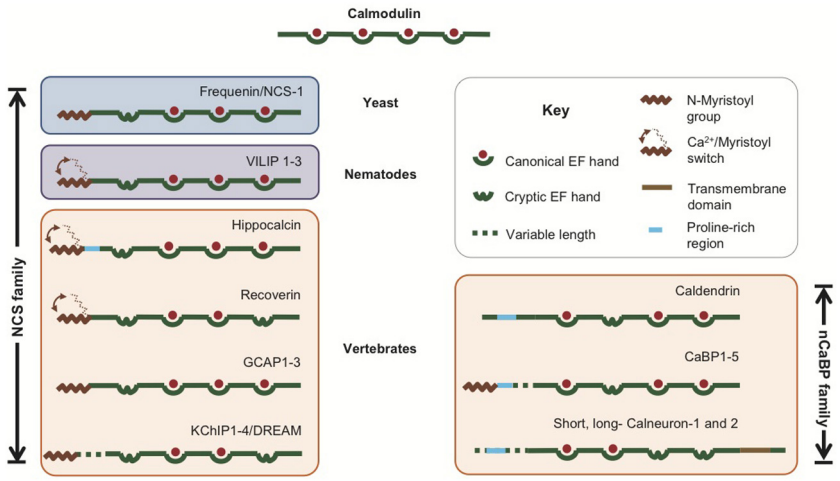

FIGURE 1 | The NCS and nCaBP families of Ca^{2+} sensors. A cartoon representation of the different proteins of these families and the various motifs present in them are shown. The proteins have been placed in boxes based on the group of organisms where they first evolved. The ancestral CaM is also shown for comparison.

acids in the linker region between the two EF-hand pairs in Caldendrin/CaBPs (Haeseleer et al., 2000). Besides this common feature, the family members show diversity in the N-terminal region, which, in case of caldendrin, CaBP1 and CaBP2, is due to alternate splicing (Haeseleer et al., 2000; Laube et al., 2002; Mikhaylova et al., 2011). Calneurons (also called CaBP7 and 8) are a subfamily that has evolved independently from caldendrin/CaBPs with a different EF-hand organization, much higher Ca^{2+}-binding affinities and a carboxy-terminal transmembrane domain (Wu et al., 2001; Mikhaylova et al., 2006, 2009; McCue et al., 2009, 2011; Hradsky et al., 2011). They have been assigned to the nCaBP family largely based on sequence similarity (Mikhaylova et al., 2006, 2011; McCue et al., 2010a).

THE RACE FOR Ca^{2+}: NCS AND nCaBPs IN DENDRITIC SPINES

Dendritic spines are considered as microcompartments of Ca^{2+} signaling (Yuste and Denk, 1995; Yuste et al., 2000; Sabatini et al., 2001) with faster Ca^{2+} decay kinetics than their parent dendrites (Cornelisse et al., 2007). "Fast" Ca^{2+} buffers such as calbindin D28K are thought to be important for this increased rate of decay of Ca^{2+}-transients in spines immediately after the closing of Ca^{2+} channels (Keller et al., 2008). It has also been assumed that these fast buffers are the first to intercept Ca^{2+} entering the spine. In a landmark study by Faas et al. (2011), it was found utilizing 1-(2-Nitro-4,5-dimethoxyphenyl)-N,N,N′,N′-tetrakis[(oxycarbonyl)methyl]-1,2 ethanediamine (DM-nitrophen)-Ca^{2+} uncaging experiments, that CaM binds Ca^{2+} at a faster rate than previously thought and the Ca^{2+}-association to the N-terminal lobe turned out to be even faster than those of calbindin. Notably, calbindin D28K is absent in CA3 pyramidal cells and is expressed only at very low levels in a sub-population of CA1 pyramidal cells (Sloviter, 1989; Czarnecki et al., 2005; Jinno and Kosaka, 2010). Other important Ca^{2+} buffers, like parvalbumin and calretinin are also not expressed in CA1 and CA3 pyramidal neurons of the hippocampus (Sloviter, 1989; Baimbridge et al., 1992; Résibois and Rogers, 1992; Czarnecki et al., 2005). Thus, CaM, with its fast Ca^{2+}-binding ability, high abundance, and ubiquitous expression, is most likely the principal buffer in these neurons (also discussed in Kubota et al., 2008). Its Ca^{2+}-dependent targets are numerous and regulate diverse cellular events, making it a very important Ca^{2+} sensor as well. An important question thus arises—how do other NCS and nCaBP proteins function in the presence of CaM? With respect to the abundance and fast association rate of CaM and the steep and short Ca^{2+} transients in spines, would other sensors have a chance at all to compete for Ca^{2+} binding? In many cases, CaM and NCS/nCaBP proteins associate with the same target with different functional outcomes (**Figure 2**). However, it is still essentially unclear how they can compete with CaM and with each other for target interactions particularly in dendritic spines. In this opinion type review, we focus on these questions and provide some numerical reasoning which might be useful for future experiments. Keeping non-specialist readers in mind, we approach these questions in a step-wise manner and although some of the initial assumptions present an over-simplified view of this very complex and dynamic system, we hope that this approach will help to better appreciate the complexity of neuronal Ca^{2+} signaling and the race for Ca^{2+}.

ABUNDANCE AND AFFINITIES OF Ca^{2+} SENSORS

Table 1A provides an estimate of the abundance and Ca^{2+}-binding affinity of five important EF-hand Ca^{2+} sensors found in dendritic spines of hippocampal pyramidal neurons. The precise protein concentrations of these sensors in neuronal subcompartments such as the synapse are unknown. A detailed discussion on the concentration of CaM in spines is available in Faas et al., 2011. For most brain regions including cerebral cortex, hippocampus, caudate nucleus, striatum, and amygdala, an average CaM

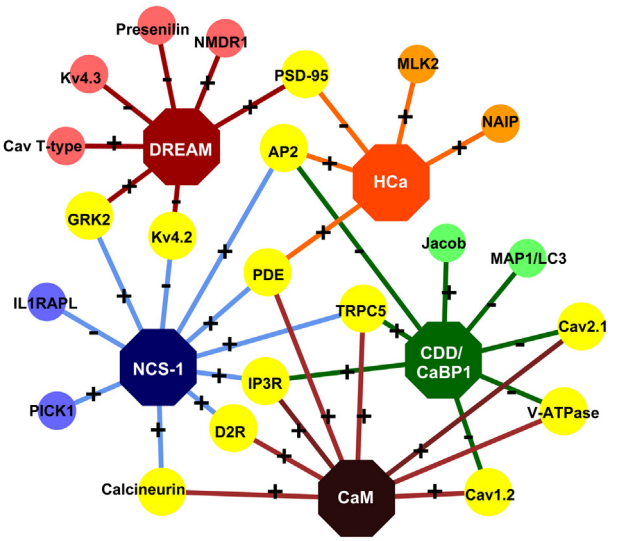

FIGURE 2 | The NCS/nCaBP interactome. Some of the known targets of the NCS and nCaBP family members in the spine are shown. Specific interaction partners are color-coded according to the color of the sensor. Common interaction partners are shown in yellow. "+" and "−" indicate Ca^{2+} -dependence and -independence of an interaction, respectively. AP2: Clathrin adaptor protein 2 [Haynes et al. (2006)]; Calcineurin [Schaad et al. (1996); Xia and Storm (2005)]; Cav1.2: Voltage-gated (L-type) Ca^{2+} channel [Zhou et al. (2004), (2005); Tippens and Lee (2007); Dick et al. (2008)]; Cav2.1: Voltage-gated (P/Q-type) Ca^{2+} channel [Lee et al. (2000), (2006); Few et al. (2005)]; CavT-type: Voltage-gated (T-type) Ca^{2+} channel [Anderson et al. (2010)]; CDD: Caldendrin; D2R: Dopamine D2 receptor [Bofill-Cardona et al. (2000); Kabbani et al. (2002); Woll et al. (2011)]; GRK2: G protein-coupled receptor kinase 2 [Kabbani et al. (2002); Ruiz-Gomez et al. (2007)]; HCa: Hippocalcin; IL1RAPL: Interleukin like-1 receptor accessory protein-like protein [Bahi et al. (2003)]; IP3R: Inositol 1,4,5-Trisphosphate Receptor [Hirota et al. (1999); Yang et al. (2002); Schlecker et al. (2006)]; Jacob [Dieterich et al. (2008)]; Kv4.2: Voltage-gated potassium channel 4.2 [An et al. (2000); Nakamura et al. (2001)]; Kv4.3: Voltage-gated potassium channel 4.3 [An et al. (2000)]; MAP1/LC3: microtubule-associated protein 1A/1B light chain 3 [Seidenbecher et al. (2004)]; MLK2: Mixed-Lineage Kinase 2 [Nagata et al. (1998)]; NAIP: Neuronal apoptosis inhibitory protein [Mercer et al. (2000); Lindholm et al. (2002)]; NMDR1: NMDA Receptor NR1 subunit [Zhang et al. (2010)]; PDE: cyclic nucleotide phosphodiesterase [Schaad et al. (1996); Haynes et al. (2006)]; PICK1: Protein Interacting with C-Kinase 1 [Jo et al. (2008)]; Presenilin [Buxbaum et al. (1998)]; PSD-95: postsynaptic density-95 protein [Jo et al. (2010); Wu et al. (2010)]; TRPC5: Transient receptor potential channel 5 [Kinoshita-Kawada et al. (2005); Ordaz et al. (2005); Hui et al. (2006)]; V-ATPase: Vacuolar Type H+-Adenosine 5-Triphosphatase [Haynes et al. (2006)]. The figure was created with the help of Cytoscape 2.8 [Cline et al. (2007)].

concentration of about 100 μM has been reported (Vargas and Guidotti, 1980; Kakiuchi et al., 1982; Klee and Vanaman, 1982; Kitajima et al., 1983; Sano and Kitajima, 1983; Teolato et al., 1983; Biber et al., 1984). The values reported for the hippocampus range from 74 to 156 μM (Kakiuchi et al., 1982; Klee and Vanaman, 1982; Biber et al., 1984). With the exception of hippocalcin, which is very abundant in hippocampus (**Table 1**), other sensors will most likely be expressed at much lower levels with an average cellular concentration that is estimated to range between 1 and 10 μM (Furuta et al., 1999; Burgoyne, 2007; Mikhaylova et al., 2011).

Following excessive synaptic activity, the induction of back-propagating dendritic action potentials (bAPs) may result in Ca^{2+} levels up to 50 μM within a dendritic spine (Faas et al., 2011). As a starting point, we therefore, considered a hypothetical situation in which Ca^{2+} sensors equilibrate with the 50 μM Ca^{2+} that enters the spine. This assumption is most likely not valid for all sensors as Ca^{2+} transients occurring during a single action potential are very brief and favor fast buffers (Markram et al., 1998). The actual time required for equilibration depends on the association and dissociation rates of Ca^{2+} binding (Markram et al., 1998) and this has to be correlated with the rate of Ca^{2+} influx. We discuss this aspect in detail in a later section. Thus, an equilibrium will possibly even not be reached during slower transients and high frequency dendritic spiking. In addition, since the structural unit that binds Ca^{2+} is a single EF-hand motif, we have initially treated the spine as a bag full of many EF-hands with different affinities for Ca^{2+}, corresponding to the global affinity of the parent protein. This is also not a realistic assumption as EF-hand motifs pair up to form EF-hand domains and these domains, even within a single protein, show distinct affinities, binding and dissociation rates as well as cooperativity in Ca^{2+}-binding (Grabarek, 2006; Gifford et al., 2007). Based on these simplistic assumptions, we calculated the parameters, E_b, which is the concentration of Ca^{2+}-bound EF hands of a particular protein, and P_{sat}, the maximum concentration of that protein that can possibly get saturated with Ca^{2+}. These calculations were done for each protein separately and independent of the others. We have also calculated the buffer capacities (κ_B; Neher and Augustine, 1992) of these proteins at resting [Ca^{2+}] of 100 nM in order to give a general idea about the steady state distribution of their Ca^{2+}-bound forms during smaller Ca^{2+} transients. The Ca^{2+} buffer capacity of a spine, which is a function of the cumulative buffer capacities of its Ca^{2+}-binding proteins, determines the peak amplitude and the decay rate of its Ca^{2+} transients. The kinetic profile of a Ca^{2+} transient in the spine with a higher buffer capacity has a smaller peak amplitude and a lower decay rate than the spine with lower buffer capacity. Based on the calculations in **Table 1A**, we ranked the sensors in different categories, shown in **Table 1B**. Since this review focuses mainly on the rising phase of Ca^{2+} transients, we have skipped the category of buffer capacity in **Table 1B**.

Dendritic spine heads of hippocampal pyramidal neurons have an average diameter of 0.5 μm and a volume of 0.062 fL (Harris and Stevens, 1989), and contain Ca^{2+} buffers at 210 μM concentration (Cornelisse et al., 2007). If [Ca^{2+}] increases up to 50 μM in the spine, this means that ∼2000 Ca^{2+} ions enter the spine at which point, >6000 Ca^{2+} binding protein molecules, roughly accounting for >20,000 EF hands, out of which ∼4000 belong to CaM alone, must compete with each other to bind Ca^{2+}. Under the category of total abundance (P_t) in **Table 1B**, CaM appears to be a clear winner in the race for Ca^{2+} by a very large margin, followed by hippocalcin. However, owing to its much greater affinity to Ca^{2+}, the concentration of Ca^{2+}-saturated hippocalcin exceeds that of Ca^{2+}-saturated CaM (given as parameter P_{sat}). Provided Ca^{2+} saturation is essential for the activation of a sensor, in the competition for binding a low abundant Ca^{2+}-dependent target having the same affinity for all the sensors, hippocalcin would out-compete CaM. Other sensors,

Table 1A | Concentration, affinity, and other parameters of selected neuronal Ca^{2+} sensors and CaM.

Protein	P_t(μM)	N	K_{dCa} (μM)	E_t (μM)	E_b (μM)	P_{sat} (μM)	κ_B at 100 nM Ca^{2+}	References
Hippocalcin	35.6	3	0.324	106.8	49.72	16.57	192.48	Furuta et al., 1999; O'Callaghan et al., 2003.
NCS-1	$10^{\#}$	3	0.440^{δ}	30	29.37	9.79	45.27	Aravind et al., 2008
DREAM	$10^{\#}$	$2^{\S}$	∼1	20	19.37	9.68	16.53	Osawa et al., 2005
Caldendrin	$10^{\#}$	$2^{\S,\alpha}$	$7^{\alpha,\delta}$	20	16.54	8.27	2.78	Wingard et al., 2005
CaM	100	4	5.85^{δ}	400	49.18	12.29	66.10	Faas et al., 2011

$^{\#}$Estimated approximate cellular levels; $^{\alpha}$Value published for the isoform, S-CaBP1; P_t, Total protein concentration; N, §number of functional EF hands. Those that bind Mg^{2+} constitutively have been excluded (e.g., DREAM, Caldendrin); K_{dCa}, $^{\delta}$Global dissociation constant, which is the geometric mean of dissociation constants of individual sites of Ca^{2+} binding. In case of NCS-1 and Caldendrin, the dissociation constant of Mg^{2+}-bound protein/isoform is shown. In case of CaM, the geometric mean of the global dissociation constants (geometric mean of the T- and R- forms of an individual EF- hand domain) of the N- and C- terminal EF- hand domains [Faas et al. (2011)] is shown. E_t, Concentration of functional EF-hands $= P_t^* N$; E_b, Concentration of Ca^{2+}-bound EF-hands obtained by solving the equation, $E_b(K_d + Ca_t + E_t - E_b) - (E_t \times Ca_t) = 0$, where Ca_t = total Ca^{2+} concentration = 50 μM. P_{sat}, maximum concentration of Ca^{2+}-saturated Protein $= E_b/N$; κ_B Buffer capacity $= K_a[E_t]/(1 + [Ca^{2+}]K_a)^2$, where $K_a = 1/K_{dCa}$ [Neher and Augustine (1992)].

Table 1B | Ranking of various Ca^{2+} sensors under different categories (Absolute values calculated in Table 1A are shown in brackets).

Rank	P_t (μM)	E_t (μM)	K_{dCa} (μM) in decreasing order	E_b (μM)	P_{sat} (μM)
1	CaM (100)	CaM (400)	Hippocalcin (0.324)	Hippocalcin (49.72)	Hippocalcin (16.57)
2	Hippocalcin (35.6)	Hippocalcin (106.8)	NCS-1 (0.44)	CaM (49.18)	CaM (12.29)
3	NCS-1, Caldendrin and DREAM (10)	NCS-1 (30)	DREAM (1)	NCS-1 (29.375)	NCS-1 (9.79)
4		Caldendrin and DREAM (20)	CaM (5.85)	DREAM (19.37)	DREAM (9.68)
5			Caldendrin (7)	Caldendrin (16.54)	Caldendrin (8.27)

which include NCS-1, DREAM, and caldendrin with a low P_{sat} value, would have a much lesser chance to interact with this target under these conditions.

As stated earlier, the validity of the equilibrium assumption made above depends on the Ca^{2+} binding kinetics of the Ca^{2+} sensors (or their EF-hands) and the Ca^{2+} influx rate. Differences in the binding kinetics of Ca^{2+} sensors could result in a non-equilibrium concentration distribution of Ca^{2+}-bound proteins leading to P_{sat} values different from those in **Table 1A**. Obtaining this non-equilibrium concentration distribution necessitates a thorough understanding of the kinetics of all these sensors. Unfortunately, the kinetic data for most of these sensors is not available in the literature.

ENRICHMENT AND SEQUESTRATION OF Ca^{2+} SENSORS

While CaM is soluble and probably uniformly distributed in the cytosol (but see below), most NCS and nCaBP proteins are enriched in specific sub-cellular compartments, such as plasma membrane, golgi, endoplasmic reticulum (ER), and post-synaptic density (PSD; an electron-dense region with post-synaptic membrane thickening and enriched with cytoskeletal elements, scaffolding proteins and neurotransmitter receptors). The mechanism for membrane attachment is largely based on an N-terminal myristoyl group that provides a lipid anchor that interacts with certain phospholipids unique to the membranes of the organelle (O'Callaghan et al., 2005; Mikhaylova et al., 2011). While in case of hippocalcin, this myristoyl group is buried in the apo protein and gets exposed in a Ca^{2+}-dependent manner—the so called Ca^{2+}-myristoyl switch-, the myristoyl group in NCS-1 is probably constitutively exposed and membrane-bound. Caldendrin gets enriched at the PSD by a yet unknown mechanism (Seidenbecher et al., 1998; Laube et al., 2002).

The protein concentration (P_t) stated in **Table 1A** estimates the global concentration of the proteins in neurons. Could accumulation at a specific organelle be effective enough to increase the concentration of these proteins to levels greater than CaM? In general, a diffusible Ca^{2+} sensor with at least two canonical EF-hands and at a global concentration of 10 μM (which is thought to be roughly the expression level of major EF-hand Ca^{2+} sensors other than CaM in brain), would have to get enriched at synapses by at least a factor of 20 in order to match the abundance of CaM. Is this degree of accumulation achievable? The PSD has a thickness of ∼40 nm (Takashima et al., 2011) and an area of 0.08 μm^2 (Arellano et al., 2007). The average volume of the PSD and the postsynaptic membrane is therefore ∼0.003 μm^3, which is ∼20 times lesser than the spine head volume. Caldendrin, which gets enriched at the PSD in an activity-dependent manner (Smalla et al., 2003) probably meets this criterion in the PSD but not in the entire spine. Hippocalcin, which is already more abundant in the hippocampus than other EF-hand sensors, can get concentrated by dozens of times upon translocation to the membrane and as a consequence might even surpass the abundance of CaM at synaptic membranes (Dovgan et al., 2010).

In parallel to the above enrichment, sequestration of CaM might be another way to increase the relative abundance of NCS and nCaBPs as compared to CaM. RC3/neurogranin is a protein belonging to the IQ-motif family of CaM binding proteins with an estimated abundance of ∼60 μM (Huang et al., 2004) in dendritic spines of CA1 pyramidal neurons. It preferentially binds to apo-CaM with a high affinity and, therefore, sequesters it at low [Ca^{2+}] (Gerendasy et al., 1994) and upon binding it reduces the affinity of CaM for Ca^{2+} (Gaertner et al., 2004). The affinity of RC3 and CaM binding reduces significantly at higher [Ca^{2+}] and gets completely abolished upon phosphorylation of RC3 by protein kinase C (Gerendasy et al., 1994). Due to these properties, the interaction between RC3 and CaM at low resting [Ca^{2+}] has important implications on the availability of free CaM for Ca^{2+} dependent as well as independent targets (Gerendasy et al., 1994). Ca^{2+}/calmodulin-dependent protein kinase II (CaMKII) is one of the most abundant proteins in the PSD that might similarly sequester CaM. The concentration of its subunits ranges from 100 to 200 μM (Lisman and Zhabotinsky, 2001). It has been shown that autophosphorylation of CaMKII causes a 100-fold reduction in dissociation rate of CaM due to which CaM stays bound to phosphorylated CaMKII long after [Ca^{2+}] returns to basal levels (Meyer et al., 1992). Since NCS and nCaBPS have not been reported to associate with CaMKII, it will be interesting to experimentally test if chelation of CaM by CaMKII could create open slots for target interactions of other Ca^{2+} sensors.

Ca^{2+}-INDEPENDENT PRE-ASSOCIATION OF NCS AND nCaBPs WITH TARGET MOLECULES

Another way to circumvent the problem of limited Ca^{2+} resources for target interactions is a Ca^{2+}-independent pre-association with a binding partner. Caldendrin is the best example for this mode of operation. Regarding its EF-hand containing C-terminal domains it is the closest relative of CaM and shares this region with its shorter splice isoforms. Interestingly, caldendrin modulates the activity of $Ca_v1.2$ (L-type) Ca^{2+} channels *via* different molecular determinants than the shorter splice isoform, caldendrin-S1 (also called S-CaBP1), which is, however, barely expressed in brain (Laube et al., 2002; Zhou et al., 2005; Tippens and Lee, 2007), indicating that the structures of the isoforms may be very different. An important feature of caldendrin and S-CaBP1 is that they bind many of their targets, e.g., $Ca_v1.2$, $Ca_v2.1$ Ca^{2+}-channels, LC3, V-ATPase, and Inositol 1,4,5-trisphosphate receptors (InsP(3)Rs) in a Ca^{2+}-independent manner (**Figure 2**; Kasri et al., 2004; Seidenbecher et al., 2004; Zhou et al., 2004, 2005; Few et al., 2005; Haynes et al., 2006; Lee et al., 2006; Tippens and Lee, 2007) whereas Ca^{2+}-binding increases the affinity of the association and triggers the actual signaling event. Although CaM is also a subunit of complexes with many enzymes and ion channels, such a pre-association would be very advantageous to convey a signal faster than other Ca^{2+} sensors, given that there is no other pre-association with another sensor at the target site and thereby could provide a molecular mechanism by which signals can be transduced to a specific target interaction irrespective of Ca^{2+}-concentrations and CaM levels.

The idea of a signalosome-like protein preassembly that provides a clear advantage in terms of accessibility of a target site within Ca^{2+}-nanodomains is not experimentally supported yet. A Ca^{2+}-dependent increase in the binding affinity for a target within such a pre-associated signalosome could overrule all advantages of CaM in the race of Ca^{2+}-binding in spines. This is clearly conceivable since Ca^{2+}-affinities of EF-hand domains can increase in the target-bound form (Dukhanina et al., 1997; Peersen et al., 1997). In this respect, it is also worth mentioning that levels of macromolecular crowding impact the conformation of EF-hand domains and potentially their Ca^{2+}-affinity (Wang et al., 2011). The impact of macromolecular complexes in spines could be substantial, given the high protein content and the compact structure of the PSD.

VARIABILITY AND INHOMOGENEITY OF DENDRITIC SPINES AND THEIR INFLUENCE ON THE RACE

Dendritic spines display spatio-temporal gradients in cytosolic Ca^{2+} concentration and Ca^{2+} amplitudes. This variability reflects the diversity of various factors including the kind, number, and distribution of Ca^{2+}-channels and pumps, the mechanisms that regulate their activity, and the diffusability of Ca^{2+} and Ca^{2+}-bound buffers. These factors can influence the race for Ca^{2+} and will be described in more detail below.

THE INTERPLAY BETWEEN Ca^{2+} ION CHANNELS AND Ca^{2+} SENSORS

The principal sources of Ca^{2+} in spines are voltage-gated Ca^{2+} channels (VGCCs), InsP(3)Rs, ryanodine receptors (RyRs), and Ca^{2+} permeable glutamate receptors, such as α-amino-3-hydroxy-5-methyl-4-isoxazolepropionic acid receptors (AMPAR) and N-methyl-D-aspartate receptors (NMDARs). VGCCs, NMDARs, and AMPARs are located on the plasma membrane, whereas, InsP(3)Rs and RyRs line the membranes of smooth ER invading the spine.

The opening of VGCCs leads to a fast rise in Ca^{2+} concentration with a rise time constant of 3.24 ms (Cornelisse et al., 2007) which decays slowly with a time constant of ∼15 ms (Sabatini et al., 2002). On the other hand, NMDARs open slowly (rise time of Ca^{2+} >100 ms) and allow for longer-lasting and much larger Ca^{2+} influxes. Kubota and Waxham (2010) elegantly described the critical impact of Ca^{2+} injection rates of VGCCs and NMDARs on Ca^{2+} dynamics. VGCCs have a high injection rate (∼1.4 ions/μs) but stay open for a very short time. Therefore, the opening of a VGCC leads to an accumulation of Ca^{2+} very close to the mouth of the channel before it diffuses away (**Figure 3A**). On the other hand, NMDARs have a much lower injection rate (∼0.07 ions/μs) and remain open for a longer time. Ca^{2+} that enters the spine following the opening of these receptors can diffuse to a considerable distance (∼140 nm from the channel) before the next ion enters (Kubota and Waxham, 2010). What properties should a Ca^{2+} sensor have, in order to respond to these diverse signals? The answer lies in the binding kinetics of the individual EF-hands.

In the previous paragraphs, we considered only the global Ca^{2+} affinity of a Ca^{2+}-binding protein which indicates only an average of affinities of its individual EF-hands. The dissociation

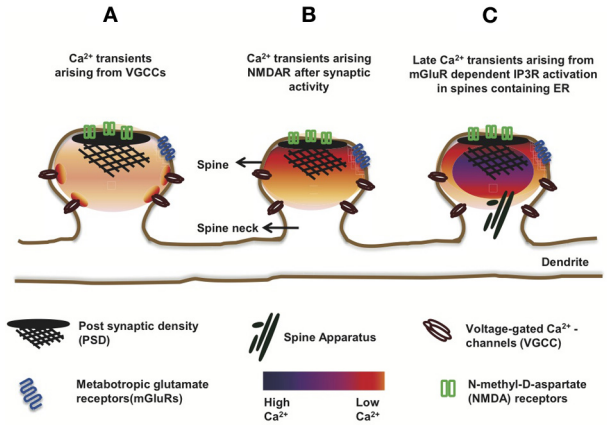

FIGURE 3 | Ca^{2+} transients in dendritic spines. The schematic shows mushroom spines displaying variability in the amplitudes and spatial patterns of Ca^{2+} transients, depending on the type of ion channels involved. **(A)** Opening of VGCCs leads to a fast rise and decay of Ca^{2+}-transients in the spine. Except near the mouth of the channel where $[Ca^{2+}]$ reaches a very high level, the distribution of the ion is largely uniform, reflecting the uniform distribution of VGCCs over the spine membrane. **(B)** Activated NMDARs allow slower, larger, and longer-lasting Ca^{2+}-transients than the VGCCs. Unlike the latter, NMDARs are clustered at the PSD. Therefore, the Ca^{2+}-transients arising from NMDARs show a stronger spatial gradient than the transients arising from open VGCCs. **(C)** In a subset of ER-containing spines, delayed Ca^{2+}-transients with several folds higher amplitude than the NMDAR-mediated ones, have been observed and attributed to mGluR-dependent Ca^{2+}-induced Ca^{2+} release (CICR) from IP3Rs, located on ER membranes.

constant (inverse of affinity) is an equilibrium constant, given by the ratio between the OFF and ON rate constants of a reversible reaction.

$$E + Ca^{2+} \underset{k_{OFF}}{\overset{k_{ON}}{\rightleftarrows}} ECa \quad \text{(where } E \text{ is an individual EF hand)}$$

Due to subtle variations in structure, individual EF-hands have different ON and OFF rates of Ca^{2+}-binding and, therefore, are fine-tuned to different Ca^{2+}-binding affinities (Grabarek, 2006; Gifford et al., 2007). To be able to respond to a Ca^{2+} signal, the binding kinetics of EF-hands must match the rate of Ca^{2+} entry. CaM has four EF hands organized into two domains. These EF-hands display cooperativity and allosterism in Ca^{2+}-binding. An apo-EF hand is in the tensed or T-state, which binds the first ion to change to the relaxed or R-state. Although it was previously estimated that the N-terminal domain has a faster ON-rate of Ca^{2+} binding than the C-terminal domain (Kubota et al., 2007), an important finding by Faas et al. (2011) was that the ON-rate of Ca^{2+} binding of the N-terminal lobe of CaM $[k_{on(T)} = 7.7 \times 10^8 M^{-1}s^{-1}]$ was faster than important Ca^{2+} buffers like calbindin $[k_{on(T)} = 7.5 \times 10^7 M^{-1}s^{-1}]$ and calretinin $[1.8 \times 10^6 M^{-1}s^{-1}$; Faas et al., 2007], making it the prime "fast" buffer. In spite of the fast binding rate, this domain has a much lower affinity ($K_d = 12.7\,\mu M$) than the C-terminal domain ($K_d = 2.7\,\mu M$) owing to its faster OFF-rate. When a VGCC opens, the instantaneous rise in Ca^{2+} concentration and the short duration for which the channel stays open would enable only those sensors with a fast binding capacity without much regard to their affinity since the Ca^{2+} levels attained are reasonably high. These features match perfectly with the fast binding N-terminal EF-hands of CaM. Along these lines, the N-terminal EF-hand domain could also be important for the role of CaM in long-term potentiation (LTP), which is associated with a steep rise in $[Ca^{2+}]$ to high amplitudes (Byrne et al., 2009). However, the function of CaM or its individual domains as Ca^{2+} sensors also depends on the kinetics of downstream target interaction. Only those targets are physiologically relevant whose association rate with CaM or one of its EF-hand domains is greater than the dissociation rate of Ca^{2+} from that domain. This is especially important in the case of the N-terminal domain of CaM, since it has a faster dissociation rate $[k_{off(R)} = 2.2 \times 10^4 s^{-1}]$ than the C-terminal domain $[k_{off(R)} = 6.5\,s^{-1}]$ (Faas et al., 2011). Unfortunately, although a number of Ca^{2+}-dependent targets of CaM have been reported in the literature, the interaction kinetics of only a few of them is known.

The C-terminal lobe is unlikely to participate during the fast Ca^{2+} transients described above, due to its slow association rate. The possibility of a selective participation of the C-terminal domain during longer-lasting Ca^{2+} transients of long-term depression has been pointed out earlier (Byrne et al., 2009). The fast-binding of the N-terminal EF hands of CaM would be of no particular advantage in case of NMDAR-mediated Ca^{2+} influx. Their fast OFF-rates make CaM a low affinity sensor, rendering it less sensitive toward changes in Ca^{2+} concentration during NMDAR-mediated Ca^{2+} transients. The slow kinetics of NMDARs would not only engage the slower Ca^{2+} binding EF-hands/proteins, but might preferentially activate those Ca^{2+}-binding proteins which are more sensitive to gradual changes in $[Ca^{2+}]$, such as the high affinity proteins of the NCS family, e.g., NCS-1 ($K_{dCa} = 440$ nM; Aravind et al., 2008) and hippocalcin ($K_{dCa} = 324$ nM; O'Callaghan et al., 2003), assuming that their Ca^{2+} association rate is not lower than the diffusion rate of Ca^{2+}. Though their binding rates have not been determined, an advantage remains with these sensitive proteins even if they are slower in binding Ca^{2+} than CaM. It is hence not surprising that these two proteins play a crucial role in mGluR-dependent and NMDAR-dependent synaptic plasticity (Palmer et al., 2005; Jo et al., 2008, 2010). Importantly, it has also been shown that the Ca^{2+} influx through NMDARs, and not through VGCCs, is mainly responsible for the translocation of hippocalcin (Dovgan et al., 2010).

The VGCCs and NMDARs also differ in their distribution over the spine membrane. Based on a model by Keller et al. (2008), the VGCCs are uniformly distributed over the membrane. Therefore, their opening results in a uniform distribution of Ca^{2+} over the entire spine volume (**Figure 3A**). Although $[Ca^{2+}]$ can reach more than $10\,\mu M$ at the mouth of an open VGCC (Simon and Llinás, 1985), these microdomains of high Ca^{2+} exist only within a few nanometer around the channel and dissipate within microseconds of channel closing (Sabatini et al., 2002). Intriguingly, the N- and C-terminal domains of CaM complexed to a VGCC (Ca_v1–2) might show distinct selectivity toward these local (nano domain of the complex) and global changes

in [Ca^{2+}] arising from the "host" VGCC (Tadross et al., 2008). The C-terminal domain might transduce local (nano domain) Ca^{2+} signals and the N-terminal domain global signals and is reportedly also capable of switching its selectivity between local (Ca_v1) and global(Ca_v2) changes in [Ca^{2+}] (Dick et al., 2008; Tadross et al., 2008).

In contrast to VGCCs, NMDARs are clustered at the PSD. This leads to a longer lasting Ca^{2+} gradient extended across the spine during an excitatory post-synaptic potential (EPSP) (Keller et al., 2008; **Figure 3B**). This scenario might favor caldendrin, which is also enriched in the PSD. Although caldendrin and CaM bind Ca^{2+} with similar affinity, it is conceivable that the greater physical proximity of caldendrin might render it a strong competitor for CaM.

Interaction partners can influence the Ca^{2+} binding kinetics and affinity of Ca^{2+}-binding proteins. RC3/Neurogranin interacts with apo-CaM (discussed in an earlier section) and increases the k_{off} of the C-terminal lobe of CaM (Gaertner et al., 2004), thereby reducing its affinity. On the other hand, another CaM target- CaMKII decreases the k_{off} of both N- and C-terminal lobes of CaM (Gaertner et al., 2004). The regulation of Ca^{2+}-binding kinetics of CaM by its targets could explain how it is able to decode a variety of Ca^{2+} signals. Alteration of Ca^{2+}- binding kinetics and affinity of CaM can not only influence Ca^{2+}/CaM-dependent signaling pathways, but also regulate the amounts and duration for which free [Ca^{2+}] is available for other Ca^{2+} sensors; an idea that is supported by mathematical models (Kubota et al., 2007, 2008).

Depolarization of spines is the key event that regulates the Ca^{2+} entry via VGCCs and NMDARs, which, as discussed above, is very influential in the race for Ca^{2+}. During synaptic activity, AMPARs function as the major source of spine depolarization, necessary to activate VGCCs as well as to remove the Mg^{2+} blockage of NMDARs (Bloodgood et al., 2009; Holbro et al., 2010). The arrival of bAPs to a spine is another source of spine depolarization. Co-incident pre- and post-synaptic activity which involves glutamate release at the synapse preceding the arrival of bAPs in a millisecond time window, is responsible for the non-linear amplification of Ca^{2+} transients that underlie LTP (Helias et al., 2008; Holbro et al., 2010; Hao and Oertner, 2011). NMDARs, with their dependence on both glutamate binding and voltage-dependent unblocking have been considered to play the role of a co-incidence detector for the induction of LTP. However, it has also been suggested that NMDARs alone are not sufficient for co-incidence detection, but that it is the spine that acts as a co-incident detector of pre- and post-synaptic activity and the degree of depolarization of the whole spine is the key element for the induction of LTP (Hao and Oertner, 2011). The depolarizing currents from AMPARs sensitize the NMDARs and VGCCs, so that their I-V curves reach the steepest zone where even a slight further depolarization drastically increases Ca^{2+} influx into the spine (Holbro et al., 2010). A negative feedback loop provided by small conductance Ca^{2+}-activated K^+ (SK) channels controls the depolarization of spines. The Cav2.3 class of VGCCs activate SK channels, which shunt the synaptic current and dampen Ca^{2+} fluxes through NMDARs by promoting Mg^{2+} blockage of these receptors (Ngo-Anh et al., 2005; Bloodgood and Sabatini, 2007; Bloodgood et al., 2009). Spine head depolarization and the non-linear amplification of Ca^{2+} transients upon co-incident pre- and post-synaptic activity have been observed to be sharpest in spines that were well isolated from the dendrite (Holbro et al., 2010). This suggests the importance of spine neck dimensions in synaptic plasticity. The spine geometry also correlates well with the number of ion channels present on its membrane. Both the AMPAR and NMDAR-mediated currents increase with increase in the size of spine head. Intriguingly, the postsynaptic Ca^{2+} increase is lower in larger spines (Nimchinsky et al., 2004; Hayashi and Majewska, 2005; Noguchi et al., 2005). The importance of spine geometry in biochemical and electrical compartmentalization of spine heads is discussed in detail later.

THE ROLE OF SMOOTH ENDOPLASMIC RETICULUM (SER)

The smooth endoplasmic reticulum (SER), which is also called spine apparatus in spines, is a major internal store of Ca^{2+} and houses Ca^{2+} pumps such as sarco/ER Ca^{2+}-ATPase (SERCA) and Ca^{2+}- sensitive Ca^{2+} channels, namely, InsP(3)Rs and RyRs. While the SER is, undoubtedly, a major player in the regulation of cytosolic Ca^{2+} in a cell in general, its precise role in shaping the Ca^{2+} dynamics in dendritic spines in particular, is a matter of debate.

Emptage et al. (1999) found that although SER does not play any role in bAP-stimulated Ca^{2+} transients, they have a significant contribution in NMDAR-dependent Ca^{2+} dynamics. Upon depletion of the internal Ca^{2+} store by SERCA blockers and by application of RyR antagonists, a significant reduction in NMDAR-dependent Ca^{2+} transients was observed. This led the authors to conclude that during a single synaptic event, the Ca^{2+} current through activated NMDARs is too small in itself to be detected. What is actually detected is a much larger Ca^{2+} influx through RyRs that were triggered by the small Ca^{2+} currents coming from the NMDARs (Emptage et al., 1999). This phenomenon in which the SER releases the stored Ca^{2+} through its Ca^{2+}-sensitive channels, is known as Ca^{2+}-induced Ca^{2+} release or CICR (for review, see Rose and Konnerth, 2001).

Contradictory to this observation, other groups later found no significant role of CICR in either bAP- or NMDAR-dependent Ca^{2+} transients (Sabatini et al., 2002; Holbro et al., 2009). Both spines, that contained or lacked ER, showed no difference in NMDAR-dependent Ca^{2+} signals (Holbro et al., 2009); however, the authors observed delayed Ca^{2+} transients in a subset of ER-positive spines with more than five-fold larger amplitude arising in the order of 100 ms later than the NMDAR-dependent transient (**Figure 3C**). These large Ca^{2+} waves were abolished in the presence of group I metabotropic glutamate receptor (mGluR) or InsP(3)R blockers as well as upon depletion of Ca^{2+} stores, but persisted even in the presence of NMDAR blockers. Group I mGluRs are located in a perisynaptic zone surrounding the AMPARs and NMDARs and their role in mGluR-dependent long-term depression (mGluR-LTD) has been well studied (Lüscher and Huber, 2010). Holbro et al. (2009) observed that the induction of mGluR-dependent LTD was limited to ER-positive spines. Therefore, they suggested that the ER plays a role in mGluR-dependent LTD which involves CICR by activated IP3Rs.

Notably, only about 20% of the CA1 dendritic spines contain SER (Spacek and Harris, 1997; Toresson and Grant, 2005; Holbro et al., 2009). One can, therefore, speculate that in ER containing spines, upon the arrival of large Ca^{2+} waves, the concentration of Ca^{2+} might rise to a level where all Ca^{2+} sensors can be completely saturated, probably obsoleting the race for Ca^{2+}, albeit further intensifying the race for targets.

SPINE GEOMETRY AND THE RACE FOR Ca^{2+}

A spine is considered to be a micro-compartment of depolarization and Ca^{2+}-dynamics distinct from the dendrite owing to the diffusional resistance of the spine neck. The idea that the spine neck acts as an electrical resistor is supported by the finding that (1) VGCCs present on the spines get activated by synaptic but not dendritic depolarization (Bloodgood et al., 2009); (2) voltage pulses arriving at a spine head from the soma get attenuated linearly with increasing length of the spine neck (Araya et al., 2006); (3) potential changes arising in a spine due to synaptic activity are largely restricted to its volume and their invasion into the parent dendrite are limited by the spine neck (Araya et al., 2006; Bloodgood et al., 2009). Therefore, an electrical resistance to movement of ions provided by the spine neck controls the activation of depolarization-dependent Ca^{2+} channels and thereby controls the amplitude of Ca^{2+} transients within the spine boundaries.

Besides electrical resistance, the spine neck also provides a diffusional barrier for ions and other molecules (Hayashi and Majewska, 2005; Biess et al., 2007; Grunditz et al., 2008; Schmidt and Eilers, 2009; Sabatini et al., 2002). The residing actin meshwork within the neck could, therefore, act as a molecular sieve for the entry and exit of NCS and nCaBPs from spines in a manner similar to CaMKII (Byrne et al., 2011). The spine neck diameter has been found to be correlated with spine head volume and it has been observed that Ca^{2+} dynamics varies with spine volume, in part due to the faster diffusion allowed by wider spine necks, and in part because of the relationship between the number of AMPA and NMDA receptors and the spine head size (discussed above; Hayashi and Majewska, 2005). Neuronal activity has been shown to regulate the diffusional properties of the spine neck (Bloodgood and Sabatini, 2005), the plasticity of which, can further control the spatio-temporal aspects of Ca^{2+} dynamics in spines (Segal, 2001; Grunditz et al., 2008). Future studies with super-resolution microscopy and live-imaging will resolve these issues and potentially also answer the question how dynamic the spine geometry actually is.

CONCLUSIONS AND FUTURE DIRECTIONS

In the next coming years, it will be imperative to learn more about the biophysical features including their precise ion binding properties, their actual concentration in spines and the sequence of filling of EF-hand motifs of NCS and nCaBPs, to judge the physiological relevance of their synaptic protein interactions. How the presence of one Ca^{2+} sensor would influence the Ca^{2+}-binding to another sensor or target is another interesting question to be addressed. Super resolution microscopy to identify nanodomains, fast spectroscopic methods to study *in vitro* protein kinetics and advanced modeling might also help to address at least some of the unresolved issues. Finally, a systematic analysis of the synaptic interactome of NCS and nCaBPs will help to appreciate their synaptic role. Compelling evidence for this synaptic role is, with the exception of hippocalcin, caldendrin, and NCS-1, still lacking and the conditions under which these proteins will eventually "meet" Ca^{2+} in the synapse still remain to be established.

ACKNOWLEDGMENTS

This work was supported by grants from the Deutsche Forschungsgemeinschaft (DFG/Kr1879/3-1; SFB 779 TPB8; SFB 854 TP7), DIP grant and the MC-ITN NPlast (EU-FP7). Vijeta Raghuram thanks Indian Council of Medical Research, India for senior research fellowship (SRF). Yogendra Sharma thanks for a neuroscience grant from the DBT, India.

REFERENCES

An, W. F., Bowlby, M. R., Betty, M., Cao, J., Ling, H. P., Mendoza, G., Hinson, J. W., Mattsson, K. I., Strassle, B. W., Trimmer, J. S., and Rhodes, K. J. (2000). Modulation of A-type potassium channels by a family of calcium sensors. *Nature* 403, 553–556.

Anderson, D., Mehaffey, W. H., Iftinca, M., Rehak, R., Engbers, J. D., Hameed, S., Zamponi, G. W., and Turner, R. W. (2010). Regulation of neuronal activity by Cav3-Kv4 channel signaling complexes. *Nat. Neurosci.* 13, 333–337.

Aravind, P., Chandra, K., Reddy, P. P., Jeromin, A., Chary, K. V., and Sharma, Y. (2008). Regulatory and structural EF-hand motifs of neuronal calcium sensor-1, Mg^{2+} modulates Ca^{2+} binding, Ca^{2+} -induced conformational changes, and equilibrium unfolding transitions. *J. Mol. Biol.* 376, 1100–1115.

Araya, R., Jiang, J., Eisenthal, K. B., and Yuste, R. (2006). The spine neck filters membrane potentials. *Proc. Natl. Acad. Sci. U.S.A.* 103, 17961–17966.

Arellano, J. I., Benavides-Piccione, R., Defelipe, J., and Yuste, R. (2007). Ultrastructure of dendritic spines: correlation between synaptic and spine morphologies. *Front. Neurosci.* 1:10. doi: 10.3389/neuro.01.1.1.010.2007

Bahi, N., Friocourt, G., Carrié, A., Graham, M. E., Weiss, J. L., Chafey, P., Fauchereau, F., Burgoyne, R. D., and Chelly, J. (2003). IL1 receptor accessory protein like, a protein involved in X-linked mental retardation, interacts with Neuronal Calcium Sensor-1 and regulates exocytosis. *Hum. Mol. Genet.* 12, 1415–1425.

Baimbridge, K. G., Celio, M. R., and Rogers, J. H. (1992). Calcium-binding proteins in the nervous system. *Trends Neurosci.* 15, 303–308.

Berridge, M. J., Lipp, P., and Bootman, M. D. (2000). The versatility and universality of calcium signalling. *Nat. Rev. Mol. Cell. Biol.* 1, 11–21.

Biber, A., Schmid, G., and Hempel, K. (1984). Calmodulin content in specific brain areas. *Exp. Brain Res.* 56, 323–326.

Biess, A., Korkotian, E., and Holcman, D. (2007). Diffusion in a dendritic spine: the role of geometry. *Phys. Rev. E Stat. Nonlin. Soft Matter Phys.* 76, 021922.

Bloodgood, B. L., Giessel, A. J., and Sabatini, B. L. (2009). Biphasic synaptic Ca influx arising from compartmentalized electrical signals in dendritic spines. *PLoS Biol.* 7:e1000190. doi: 10.1371/journal.pbio.1000190

Bloodgood, B. L., and Sabatini, B. L. (2005). Neuronal activity regulates diffusion across the neck of dendritic spines. *Science* 310, 866–869.

Bloodgood, B. L., and Sabatini, B. L. (2007). Nonlinear regulation of unitary synaptic signals by CaV(2.3) voltage-sensitive calcium channels located in dendritic spines. *Neuron* 53, 249–260.

Bofill-Cardona, E., Kudlacek, O., Yang, Q., Ahorn, H., Freissmuth, M., and Nanoff, C. (2000). Binding of calmodulin to the D2-dopamine

receptor reduces receptor signaling by arresting the G protein activation switch. *J. Biol. Chem.* 275, 32672–32680.

Burgoyne, R. D. (2007). Neuronal calcium sensor proteins: generating diversity in neuronal Ca^{2+} signalling. *Nat. Rev. Neurosci.* 8, 182–193.

Burgoyne, R. D., and Weiss, J. L. (2001). The neuronal calcium sensor family of Ca^{2+}-binding proteins. *Biochem. J.* 353, 1–12.

Buxbaum, J. D., Choi, E. K., Luo, Y., Lilliehook, C., Crowley, A. C., Merriam, D. E., and Wasco, W. (1998). Calsenilin: a calcium-binding protein that interacts with the presenilins and regulates the levels of a presenilin fragment. *Nat. Med.* 4, 1177–1181.

Byrne, M. J., Putkey, J. A., Waxham, M. N., and Kubota, Y. (2009). Dissecting cooperative calmodulin binding to CaM kinase II: a detailed stochastic model. *J. Comput. Neurosci.* 27, 621–638.

Byrne, M. J., Waxham, M. N., and Kubota, Y. (2011). The impacts of geometry and binding on CaMKII diffusion and retention in dendritic spines. *J. Comput. Neurosci.* 31, 1–12.

Clapham, D. E. (2007). Calcium signaling. *Cell* 131, 1047–1058.

Cline, M. S., Smoot, M., Cerami, E., Kuchinsky, A., Landys, N., Workman, C., Christmas, R., Avila-Campilo, I., Creech, M., Gross, B., Hanspers, K., Isserlin, R., Kelley, R., Killcoyne, S., Lotia, S., Maere, S., Morris, J., Ono, K., Pavlovic, V., Pico, A. R., Vailaya, A., Wang, P. L., Adler, A., Conklin, B. R., Hood, L., Kuiper, M., Sander, C., Schmulevich, I., Schwikowski, B., Warner, G. J., Ideker, T., and Bader, G. D. (2007). Integration of biological networks and gene expression data using Cytoscape. *Nat. Protoc.* 2, 2366–2382.

Cornelisse, L. N., van Elburg, R. A., Meredith, R. M., Yuste, R., and Mansvelder, H. D. (2007). High speed two-photon imaging of calcium dynamics in dendritic spines: consequences for spine calcium kinetics and buffer capacity. *PLoS One* 2:e1073. doi: 10.1371/journal.pone.0001073

Czarnecki, K., Haas, C. A., Bas Orth, C., Deller, T., and Frotscher, M. (2005). Postnatal development of synaptopodin expression in the rodent hippocampus. *J. Comp. Neurol.* 490, 133–144.

De Castro, E., Nef, S., Fiumelli, H., Lenz, S. E., Kawamura, S., and Nef, P. (1995). Regulation of rhodopsin phosphorylation by a family of neuronal calcium sensors. *Biochem. Biophys. Res. Commun.* 216, 133–140.

Dick, I. E., Tadross, M. R., Liang, H., Tay, L. H., Yang, W., and Yue, D. T. (2008). A modular switch for spatial Ca^{2+} selectivity in the calmodulin regulation of CaV channels. *Nature* 451, 830–834.

Dieterich, D. C., Karpova, A., Mikhaylova, M., Zdobnova, I., König, I., Landwehr, M., Kreutz, M., Smalla, K. H., Richter, K., Landgraf, P., Reissner, C., Boeckers, T. M., Zuschratter, W., Spilker, C., Seidenbecher, C. I., Garner, C. C., Gundelfinger, E. D., and Kreutz, M. R. (2008). Caldendrin-Jacob: a protein liaison that couples NMDA receptor signalling to the nucleus. *PLoS Biol.* 6:e34. doi: 10.1371/journal.pbio.0060034

Dovgan, A. V., Cherkas, V. P., Stepanyuk, A. R., Fitzgerald, D. J., Haynes, L. P., Tepikin, A. V., Burgoyne, R. D., and Belan, P. V. (2010). Decoding glutamate receptor activation by the Ca^{2+} sensor protein hippocalcin in rat hippocampal neurons. *Eur. J. Neurosci.* 32, 347–358.

Dukhanina, E. A., Dukhanin, A. S., Lomonosov, M. Y., Lukanidin, E. M., and Georgiev, G. P. (1997). Spectral studies on the calcium-binding properties of Mtsl protein and its interaction with target protein. *FEBS Lett.* 410, 403–406.

Emptage, N., Bliss, T. V., and Fine, A. (1999). Single synaptic events evoke NMDA receptor-mediated release of calcium from internal stores in hippocampal dendritic spines. *Neuron* 22, 115–124.

Faas, G. C., Raghavachari, S., Lisman, J. E., and Mody, I. (2011). Calmodulin as a direct detector of Ca^{2+} signals. *Nat. Neurosci.* 14, 301–304.

Faas, G. C., Schwaller, B., Vergara, J. L., and Mody, I. (2007). Resolving the fast kinetics of cooperative binding: Ca^{2+} buffering by calretinin. *PLoS Biol.* 5:e311. doi: 10.1371/journal.pbio.0050311

Few, A. P., Lautermilch, N. J., Westenbroek, R. E., Scheuer, T., and Catterall, W. A. (2005). Differential regulation of CaV2.1 channels by calcium-binding protein 1 and visinin-like protein-2 requires N-terminal myristoylation. *J. Neurosci.* 25, 7071–7080.

Furuta, Y., Kobayashi, M., Masaki, T., and Takamatsu, K. (1999). Age-related changes in expression of hippocalcin and NVP2 in rat brain. *Neurochem. Res.* 24, 651–658.

Gaertner, T. R., Putkey, J. A., and Waxham, M. N. (2004). RC3/Neurogranin and Ca2+/calmodulin dependent protein kinase II produce opposing effects on the affinity of calmodulin for calcium. *J. Biol. Chem.* 279, 39374–39382.

Gerendasy, D. D., Herron, S. R., Watson, J. B., and Sutcliffe, J. G. (1994). Mutational and biophysical studies suggest C3/neurogranin regulates calmodulin availability. *J. Biol. Chem.* 269, 22420–22426.

Gierke, P., Zhao, C., Brackmann, M., Linke, B., Heinemann, U., and Braunewell, K. H. (2004). Expression analysis of members of the neuronal calcium sensor protein family: combining bioinformatics and Western Blot analysis. *Biochem. Biophys. Res. Commun.* 323, 38–43.

Gifford, J. L., Walsh, M. P., and Vogel, H. J. (2007). Structures and metal-ion-binding properties of the Ca^{2+}-binding helix-loop-helix EF-hand motifs. *Biochem. J.* 405, 199–221.

Grabarek, Z. (2006). Structural basis for diversity of the EF-hand calcium-binding proteins. *J. Mol. Biol.* 359, 509–525.

Grunditz, A., Holbro, N., Tian, L., Zuo, Y., and Oertner, T. G. (2008). Spine neck plasticity controls postsynaptic calcium signals through electrical compartmentalization. *J. Neurosci.* 28, 13457–13466.

Haeseleer, F., Sokal, I., Verlinde, C. L., Erdjument-Bromage, H., Tempst, P., Pronin, A. N., Benovic, J. L., Fariss, R. N., and Palczewski, K. (2000). Five members of a novel Ca^{2+}-binding protein (CABP) subfamily with similarity to calmodulin. *J. Biol. Chem.* 275, 1247–1260.

Hao, J., and Oertner, T. G. (2011). Depolarization gates spine calcium transients and spike-timing-dependent potentiation. *Curr. Opin. Neurobiol.* doi: 10.1016/j.conb.2011.10.004. [Epub ahead of print].

Harris, K. M., and Stevens, J. K. (1989). Dendritic spines of CA1 pyramidal cells in the rat hippocampus: serial electron microscopy with reference to their biophysical characteristics. *J. Neurosci.* 9, 2982–2997.

Hayashi, Y., and Majewska, A. K. (2005). Dendritic spine geometry: functional implication and regulation. *Neuron* 46, 529–532.

Haynes, L. P., Fitzgerald, D. J., Wareing, B., O'Callaghan, D. W., Morgan, A., and Burgoyne, R. D. (2006). Analysis of the interacting partners of the neuronal calcium-binding proteins L-CaBP1, hippocalcin, NCS-1 and neurocalcin delta. *Proteomics* 6, 1822–1832.

Helias, M., Rotter, S., Gewaltig, M. O., and Diesmann, M. (2008). Structural plasticity controlled by calcium based correlation detection. *Front. Comput. Neurosci.* 2:7. doi: 10.3389/neuro.10.007.2008

Henzl, M. T., and Tanner, J. J. (2007). Solution structure of Ca^{2+}-free rat beta-parvalbumin (oncomodulin). *Protein Sci.* 16, 1914–1926.

Hirota, J., Michikawa, T., Natsume, M., Furuichi, T., and Mikoshiba, K. (1999). Calmodulin inhibits inositol 1,4,5-trisphosphate-induced calcium release through the purified and reconstituted inositol 1,4,5-trisphosphate receptor type 1. *FEBS Lett.* 456, 322–326.

Holbro, N., Grunditz, A., and Oertner, T. G. (2009). Differential distribution of endoplasmic reticulum controls metabotropic signaling and plasticity at hippocampal synapses. *Proc. Natl. Acad. Sci. U.S.A.* 106, 15055–15060.

Holbro, N., Grunditz, A., Wiegert, J. S., and Oertner, T. G. (2010). AMPA receptors gate spine Ca(2+) transients and spike-timing-dependent potentiation. *Proc. Natl. Acad. Sci. U.S.A.* 107, 15975–15980.

Hradsky, J., Raghuram, V., Reddy, P. P., Navarro, G., Hupe, M., Casado, V., McCormick, P. J., Sharma, Y., Kreutz, M. R., and Mikhaylova, M. (2011). Post-translational membrane insertion of tail-anchored transmembrane EF-hand Ca^{2+} sensor calneurons requires the TRC40/Asna1 protein chaperone. *J. Biol. Chem.* 286, 36762–36776.

Huang, K. P., Huang, F. L., Jäger, T., Li, J., Reymann, K. G., and Balschun, D. (2004). Neurogranin/RC3 enhances long-term potentiation and learning by promoting calcium-mediated signaling. *J. Neurosci.* 24, 10660–10669.

Hui, H., McHugh, D., Hannan, M., Zeng, F., Xu, S. Z., Khan, S. H., Levenson, R., Beech, D. J., and Weiss, J. L. (2006). Calcium-sensing mechanism in TRPC5 channels contributing to retardation of neurite outgrowth. *J. Physiol.* 572, 165–172.

Jinno, S., and Kosaka, T. (2010). Stereological estimation of numerical densities of glutamatergic principal neurons in the mouse hippocampus. *Hippocampus* 20, 829–840.

Jo, J., Heon, S., Kim, M. J., Son, G. H., Park, Y., Henley, J. M., Weiss, J. L., Sheng, M., Collingridge, G. L., and Cho, K. (2008). Metabotropic

glutamate receptor-mediated LTD involves two interacting Ca^{2+} sensors, NCS-1 and PICK1. *Neuron* 60, 1095–1111.

Jo, J., Son, G. H., Winters, B. L., Kim, M. J., Whitcomb, D. J., Dickinson, B. A., Lee, Y. B., Futai, K., Amici, M., Sheng, M., Collingridge, G. L., and Cho, K. (2010). Muscarinic receptors induce LTD of NMDAR EPSCs via a mechanism involving hippocalcin, AP2 and PSD-95. *Nat. Neurosci.* 13, 1216–1224.

Kabbani, N., Negyessy, L., Lin, R., Goldman-Rakic, P., and Levenson, R. (2002). Interaction with neuronal calcium sensor NCS-1 mediates desensitization of the D2 dopamine receptor. *J. Neurosci.* 22, 8476–8486.

Kakiuchi, S., Yasuda, S., Yamazaki, R., Teshima, Y., Kanda, K., Kakiuchi, R., and Sobue, K. (1982). Quantitative determinations of calmodulin in the supernatant and particulate fractions of mammalian tissues. *J. Biochem.* 92, 1041–1048.

Kapp-Barnea, Y., Melnikov, S., Shefler, I., Jeromin, A., and Sagi-Eisenberg, R. (2003). Neuronal calcium sensor-1 and phosphatidylinositol 4-kinase β regulate IgE receptor-triggered exocytosis in cultured mast cells. *J. Immunol.* 171, 5320–5327.

Kasri, N. N., Holmes, A. M., Bultynck, G., Parys, J. B., Bootman, M. D., Rietdorf, K., Missiaen, L., McDonald, F., De Smedt, H., Conway, S. J., Holmes, A. B., Berridge, M. J., and Roderick, H. L. (2004). Regulation of InsP3 receptor activity by neuronal Ca2+-binding proteins. *EMBO J.* 23, 312–321.

Keller, D. X., Franks, K. M., Bartol, T. M. Jr., and Sejnowski, T. J. (2008). Calmodulin activation by calcium transients in the postsynaptic density of dendritic spines. *PLoS One* 3:e2045. doi: 10.1371/journal.pone.0002045

Kinoshita-Kawada, M., Tang, J., Xiao, R., Kaneko, S., Foskett, J. K., and Zhu, M. X. (2005). Inhibition of TRPC5 channels by Ca^{2+}-binding protein 1 in Xenopus oocytes. *Pflugers Arch.* 450, 345–354.

Kitajima, S., Seto-Ohshima, A., Sano, M., and Kato, K. (1983). Production of antibodies to calmodulin in rabbits and enzyme immunoassays for calmodulin and anti-calmodulin. *J. Biochem.* 94, 559–564.

Klee, C. B., and Vanaman, T. C. (1982). Calmodulin. *Adv. Protein Chem.* 35, 213–321.

Kubota, Y., Putkey, J. A., Shouval, H. Z., and Waxham, M. N. (2008). IQ-motif proteins influence intracellular free Ca2+ in hippocampal neurons through their interactions with calmodulin. *J. Neurophysiol.* 99, 264–276.

Kubota, Y., Putkey, J. A., and Waxham, M. N. (2007). Neurogranin controls the spatiotemporal pattern of postsynaptic Ca^{2+}/CaM signaling. *Biophys. J.* 93, 3848–3859.

Kubota, Y., and Waxham, M. N. (2010). Lobe specific Ca^{2+}-calmodulin nano-domain in neuronal spines: a single molecule level analysis. *PLoS Comput. Biol.* 6:e1000987. doi: 10.1371/journal.pcbi.1000987

Kuo, H. C., Cheng, C. F., Clark, R. B., Lin, J. J., Lin, J. L., Hoshijima, M., Nguyên-Trân, V. T., Gu, Y., Ikeda, Y., Chu, P. H., Ross, J., Giles, W. R., and Chien, K. R. (2001). A defect in the Kv channel-interacting protein 2 (KChIP2) gene leads to a complete loss of I(to) and confers susceptibility to ventricular tachycardia. *Cell* 107, 801–813.

Laube, G., Seidenbecher, C. I., Richter, K., Dieterich, D. C., Hoffmann, B., Landwehr, M., Smalla, K. H., Winter, C., Böckers, T. M., Wolf, G., Gundelfinger, E. D., and Kreutz, M. R. (2002). The neuron-specific Ca^{2+}- binding protein caldendrin: gene structure, splice isoforms and expression in the rat central nervous system. *Mol. Cell. Neurosci.* 19, 459–475.

Lee, A., Scheuer, T., and Catterall, W. A. (2000). Ca^{2+}/calmodulin dependent facilitation and inactivation of P/Q-type Ca^{2+} channels. *J. Neurosci.* 20, 6830–6838.

Lee, A., Westenbroek, R. E., Haeseleer, F., Palczewski, K., Scheuer, T., and Catterall, W. A. (2006). Differential modulation of Cav2.1 channels by calmodulin and Ca^{2+}-binding protein 1. *Nat. Neurosci.* 5, 210–217.

Lindholm, D., Mercer, E. A., Yu, L. Y., Chen, Y., Kukkonen, J., Korhonen, L., and Arumäe, U. (2002). Neuronal apoptosis inhibitory protein: structural requirements for hippocalcin binding and effects on survival of NGF-dependent sympathetic neurons. *Biochim. Biophys. Acta* 1600, 138–147.

Lisman, J. E., and Zhabotinsky, A. M. (2001). A model of synaptic memory: a CaMKII/PP1 switch that potentiates transmission by organizing an AMPA receptor anchoring assembly. *Neuron* 31, 191–201.

Lüscher, C., and Huber, K. M. (2010). Group 1 mGluR-dependent synaptic long-term depression: mechanisms and implications for circuitry and disease. *Neuron* 65, 445–459.

Markram, H., Roth, A., and Helmchen, F. (1998). Competitive calcium binding: implications for dendritic calcium signaling. *J. Comput. Neurosci.* 5, 331–348.

McCue, H. V., Burgoyne, R. D., and Haynes, L. P. (2009). Membrane targeting of the EF-hand containing calcium-sensing proteins CaBP7 and CaBP8. *Biochem. Biophys. Res. Commun.* 380, 825–831.

McCue, H. V., Burgoyne, R. D., and Haynes, L. P. (2011). Determination of the membrane topology of the small EF-hand Ca^{2+}-sensing proteins CaBP7 and CaBP8. *PLoS One* 6:e17853. doi: 10.1371/journal.pone.0017853

McCue, H. V., Haynes, L. P., and Burgoyne, R. D. (2010a). Bioinformatic analysis of CaBP/calneuron proteins reveals a family of highly conserved vertebrate Ca^{2+}-binding proteins. *BMC Res. Notes* 3, 118.

McCue, H. V., Haynes, L. P., and Burgoyne, R. D. (2010b). The diversity of calcium sensor proteins in the regulation of neuronal function. *Cold Spring Harb. Perspect. Biol.* 2, a004085.

McFerran, B. W., Graham, M. E., and Burgoyne, R. D. (1998). Neuronal Ca^{2+} sensor 1, the mammalian homologue of frequenin, is expressed in chromaffin and PC12 cells and regulates neurosecretion from dense-core granules. *J. Biol. Chem.* 273, 22768–22772.

Mercer, E. A., Korhonen, L., Skoglösa, Y., Olsson, P. A., Kukkonen, J. P., and Lindholm, D. (2000). NAIP interacts with hippocalcin and protects neurons against calcium-induced cell death through caspase-3-dependent and -independent pathways. *EMBO J.* 19, 3597–3607.

Meyer, T., Hanson, P. I., Stryer, L., and Schulman, H. (1992). Calmodulin trapping by calcium-calmodulin-dependent protein kinase. *Science* 256, 1199–1202.

Mikhaylova, M., Hradsky, J., and Kreutz, M. R. (2011). Between promiscuity and specificity: novel roles of EF-hand calcium sensors in neuronal Ca^{2+} signalling. *J. Neurochem.* 118, 695–713.

Mikhaylova, M., Reddy, P. P., Munsch, T., Landgraf, P., Suman, S. K., Smalla, K. H., Gundelfinger, E. D., Sharma, Y., and Kreutz, M. R. (2009). Calneurons provide a calcium threshold for trans-Golgi network to plasma membrane trafficking. *Proc. Natl. Acad. Sci. U.S.A.* 106, 9093–9098.

Mikhaylova, M., Sharma, Y., Reissner, C., Nagel, F., Aravind, P., Rajini, B., Smalla, K. H., Gundelfinger, E. D., and Kreutz, M. R. (2006). Neuronal Ca^{2+} signaling via caldendrin and calneurons. *Biochim. Biophys. Acta* 1763, 1229–1237.

Nagata, K., Puls, A., Futter, C. l., Aspenstrom, P., Schaefer, E., Nakata, T., Hirokawa, N., and Hall, A. (1998).The MAP kinase kinase kinase MLK2 co-localizes with activated JNK along microtubules and associates with kinesin superfamily motor KIF3. *EMBO J.* 17, 149–158.

Nakamura, T. Y., Pountney, D. J., Ozaita, A., Nandi, S., Ueda, S., Rudy, B., and Coetzee, W. A. (2001). A role for frequenin, a Ca^{2+}-binding protein, as a regulator of Kv4 K-currents. *Proc. Natl. Acad. Sci. U.S.A.* 98, 12808–12813.

Neher, E., and Augustine, G. J. (1992). Calcium gradients and buffers in bovine chromaffin cells. *J. Physiol.* 450, 273–301.

Ngo-Anh, T. J., Bloodgood, B. L., Lin, M., Sabatini, B. L., Maylie, J., and Adelman, J. P. (2005). SK channels and NMDA receptors form a Ca^{2+}-mediated feedback loop in dendritic spines. *Nat. Neurosci.* 8, 642–649.

Nimchinsky, E. A., Yasuda, R., Oertner, T. G., and Svoboda, K. (2004). The number of glutamate receptors opened by synaptic stimulation in single hippocampal spines. *J. Neurosci.* 24, 2054–2064.

Noguchi, J., Matsuzaki, M., Ellis-Davies, G. C., and Kasai, H. (2005). Spine-neck geometry determines NMDA receptor-dependent Ca^{2+} signaling in dendrites. *Neuron* 46, 609–622.

O'Callaghan, D. W., Haynes, L. P., and Burgoyne, R. D. (2005). High-affinity interaction of the N-terminal myristoylation motif of the neuronal calcium sensor protein hippocalcin with phosphatidylinositol 4,5-bisphosphate. *Biochem. J.* 391, 231–238.

O'Callaghan, D. W., Tepikin, A. V., and Burgoyne, R. D. (2003). Dynamics and calcium sensitivity of the Ca^{2+}/myristoyl switch protein hippocalcin in living cells. *J. Cell. Biol.* 163, 715–721.

Ordaz, B., Tang, J., Xiao, R., Salgado, A., Sampieri, A., Zhu, M. X., and Vaca, L. (2005). Calmodulin and calcium interplay in the modulation

of TRPC5 channel activity. *J. Biol. Chem.* 280, 30788–30796.

Osawa, M., Dace, A., Tong, K. I., Valiveti, A., Ikura, M., and Ames, J. B. (2005). Mg^{2+} and Ca^{2+} differentially regulate DNA binding and dimerization of DREAM. *J. Biol. Chem.* 280, 18008–18014.

Palmer, C. L., Lim, W., Hastie, P. G., Toward, M., Korolchuk, V. I., Burbidge, S. A., Banting, G., Collingridge, G. L., Isaac, J. T., and Henley, J. M. (2005). Hippocalcin functions as a calcium sensor in hippocampal LTD. *Neuron* 47, 487–494.

Peersen, O. B., Madsen, T. S., and Falke, J. J. (1997). Intermolecular tuning of calmodulin by target peptides and proteins: differential effects on Ca^{2+} binding and implications for kinase activation. *Protein Sci.* 6, 794–807.

Redecker, P., Kreutz, M. R., Bockmann, J., Gundelfinger, E. D., and Boeckers, T. M. (2003). Brain synaptic junctional proteins at the acrosome of rat testicular germ cells. *J. Histochem. Cytochem.* 51, 809–819.

Résibois, A., and Rogers, J. H. (1992). Calretinin in rat brain: an immunohistochemical study. *Neuroscience* 46, 101–134.

Rose, C. R., and Konnerth, A. (2001). Stores not just for storage: intracellular calcium release and synaptic plasticity. *Neuron* 31, 519–522.

Ruiz-Gomez, A., Mellström, B., Tornero, D., Morato, E., Savignac, M., Holguín, H., Aurrekoetxea, K., González, P., González-García, C., Ceña, V., Mayor, F. Jr., and Naranjo, J. R. (2007). G protein-coupled receptor kinase 2-mediated phosphorylation of downstream regulatory element antagonist modulator regulates membrane trafficking of Kv4.2 potassium channel. *J. Biol. Chem.* 282, 1205–1215.

Sabatini, B. L., Maravall, M., and Svoboda, K. (2001). Ca^{2+} signaling in dendritic spines. *Curr. Opin. Neurobiol.* 11, 349–356.

Sabatini, B. L., Oertner, T. G., and Svoboda, K. (2002). The life cycle of Ca^{2+} ions in dendritic spines. *Neuron* 33, 439–452.

Sano, M., and Kitajima, S. (1983). Ontogeny of calmodulin and calmodulin-dependent adenylate cyclase in rat brain. *Brain Res.* 283, 215–220.

Schaad, N. C., De Castro, E., Nef, S., Hegi, S., Hinrichsen, R., Martone, M. E., Ellisman, M. H., Sikkink, R., Rusnak, F., Sygush, J., and Nef, P. (1996). Direct modulation of calmodulin targets by the neuronal calcium sensor NCS-1. *Proc. Natl. Acad. Sci. U.S.A.* 93, 9253–9258.

Schlecker, C., Boehmerle, W., Jeromin, A., DeGray, B., Varshney, A., Sharma, Y., Szigeti-Buck, K., and Ehrlich, B. E. (2006). Neuronal calcium sensor-1 enhancement of InsP3 receptor activity is inhibited by therapeutic levels of lithium. *J. Clin. Invest.* 116, 1668–1674.

Schmidt, H., and Eilers, J. (2009). Spine neck geometry determines spino-dendritic cross-talk in the presence of mobile endogenous calcium binding proteins. *J. Comput. Neurosci.* 27, 229–243.

Schmidt, H., Schwaller, B., and Eilers, J. (2005). Calbindin D28k targets myo-inositol monophosphatase in spines and dendrites of cerebellar Purkinje neurons. *Proc. Natl. Acad. Sci. U.S.A.* 102, 5850–5855.

Schwaller, B. (2010). Cytosolic Ca^{2+} buffers. *Cold Spring Harb. Perspect. Biol.* 2, a004051.

Schwaller, B. (2011). The use of transgenic mouse models to reveal the functions of Ca(2+) buffer proteins in excitable cells. *Biochim. Biophys. Acta* doi: 10.1016/j.bbagen.2011.11.008. [Epub ahead of print].

Segal, M. (2001). Rapid plasticity of dendritic spine: hints to possible functions? *Prog. Neurobiol.* 63, 61–70.

Seidenbecher, C. I., Landwehr, M., Smalla, K. H., Kreutz, M., Dieterich, D. C., Zuschratter, W., Reissner, C., Hammarback, J. A., Böckers, T. M., Gundelfinger, E. D., and Kreutz, M. R. (2004). Caldendrin but not calmodulin binds to light chain 3 of MAP1A/B: an association with the microtubule cytoskeleton highlighting exclusive binding partners for neuronal Ca^{2+}-sensor proteins. *J. Mol. Biol.* 336, 957–970.

Seidenbecher, C. I., Langnaese, K., Sanmartí-Vila, L., Boeckers, T. M., Smalla, K. H., Sabel, B. A., Garner, C. C., Gundelfinger, E. D., and Kreutz, M. R. (1998). Caldendrin, a novel neuronal calcium-binding protein confined to the somato-dendritic compartment. *J. Biol. Chem.* 273, 21324–21331.

Simon, S. M., and Llinás, R. R. (1985). Compartmentalization of the submembrane calcium activity during calcium influx and its significance in transmitter release. *Biophys. J.* 48, 485–498.

Sloviter, R. S. (1989). Calcium-binding protein (calbindin-D28k) and parvalbumin immunocytochemistry: localization in the rat hippocampus with specific reference to the selective vulnerability of hippocampal neurons to seizure activity. *J. Comp. Neurol.* 280, 183–196.

Smalla, K. H., Seidenbecher, C. I., Tischmeyer, W., Schicknick, H., Wyneken, U., Böckers, T. M., Gundelfinger, E. D., and Kreutz, M. R. (2003). Kainate-induced epileptic seizures induce a recruitment of caldendrin to the postsynaptic density in rat brain. *Mol. Brain Res.* 116, 159–162.

Spacek, J., and Harris, K. M. (1997). Three-dimensional organization of smooth endoplasmic reticulum in hippocampal CA1 dendrites and dendritic spines of the immature and mature rat. *J. Neurosci.* 17, 190–203.

Stuart, R. O., Bush, K. T., and Nigam, S. K. (2003). Changes in gene expression patterns in the ureteric bud and metanephric mesenchyme in models of kidney development. *Kidney Int.* 64, 1997–2008.

Tadross, M. R., Dick, I. E., and Yue, D. T. (2008). Mechanism of local and global Ca2+ sensing by calmodulin in complex with a Ca2+ channel. *Cell* 133, 1228–1240.

Takashima, N., Odaka, Y. S., Sakoori, K., Akagi, T., Hashikawa, T., Morimura, N., Yamada, K., and Aruga, J. (2011). Impaired cognitive function and altered hippocampal synapse morphology in mice lacking Lrrtm1, a gene associated with schizophrenia. *PLoS One* 6:e22716. doi: 10.1371/journal.pone.0022716

Teolato, S., Calderini, G., Bonetti, A. C., and Toffano, G. (1983). Calmodulin content in different brain areas of aging rats. *Neurosci. Lett.* 38, 57–60.

Tippens, A. L., and Lee, A. (2007). Caldendrin, a neuron-specific modulator of Cav/1.2 (L-type) Ca^{2+} channels. *J. Biol. Chem.* 282, 8464–8473.

Toresson, H., and Grant, S. G. (2005). Dynamic distribution of endoplasmic reticulum in hippocampal neuron dendritic spines. *Eur. J. Neurosci.* 22, 1793–1798.

Vargas, F., and Guidotti, A. (1980). Calmodulin in brain of schizophrenics. *Neurochem. Res.* 5, 673–681.

Wang, Q., Liang, K. C., Czader, A., Waxham, M. N., and Cheung, M. S. (2011). The effect of macromolecular crowding, ionic strength and calcium binding on calmodulin dynamics. *PLoS Comput. Biol.* 7:e1002114. doi: 10.1371/journal.pcbi.1002114

Wingard, J. N., Chan, J., Bosanac, I., Haeseleer, F., Palczewski, K., Ikura, M., and Ames, J. B. (2005). Structural analysis of Mg^{2+} and Ca^{2+} binding to CaBP1, a neuron-specific regulator of calcium channels. *J. Biol. Chem.* 280, 37461–37470.

Woll, M. P., De Cotiis, D. A., Bewley, M. C., Tacelosky, D. M., Levenson, R., and Flanagan, J. M. (2011). Interaction between the D2 dopamine receptor and neuronal calcium sensor-1 analyzed by fluorescence anisotropy. *Biochemistry* 50, 8780–8791.

Wu, L. J., Mellström, B., Wang, H., Ren, M., Domingo, S., Kim, S. S., Li, X. Y., Chen, T., Naranjo, J. R., and Zhuo, M. (2010). DREAM (Downstream Regulatory Element Antagonist Modulator) contributes to synaptic depression and contextual fear memory. *Mol. Brain* 3, 3.

Wu, Y. Q., Lin, X., Liu, C. M., Jamrich, M., and Shaffer, L. G. (2001). Identification of a human brain-specific gene, calneuron 1, a new member of the calmodulin superfamily. *Mol. Genet. Metab.* 72, 343–350.

Xia, Z., and Storm, D. R. (2005). The role of calmodulin as a signal integrator for synaptic plasticity. *Nat. Rev. Neurosci.* 6, 267–276.

Yang, J., McBride, S., Mak, D. O., Vardi, N., Palczewski, K., Haeseleer, F., and Foskett, J. K. (2002). Identification of a family of calcium sensors as protein ligands of inositol trisphosphate receptor Ca^{2+} release channels. *Proc. Natl. Acad. Sci. U.S.A.* 99, 7711–7716.

Yuste, R., Majewska, A., and Holthoff, K. (2000). From form to function: calcium compartmentalization in dendritic spines. *Nat. Neurosci.* 3, 653–659.

Yuste, R., and Denk, W. (1995). Dendritic spines as basic functional units of neuronal integration. *Nature* 375, 682–684.

Zhang, Y., Su, P., Liang, P., Liu, T., Liu, X., Liu, X. Y., Zhang, B., Han, T., Zhu, Y. B., Yin, D. M., Li, J., Zhou, Z., Wang, K. W., and Wang, Y. (2010). The DREAM protein negatively regulates the NMDA receptor through interaction with the NR1 subunit. *J. Neurosci.* 30, 7575–7586.

Zhou, H., Kim, S. A., Kirk, E. A., Tippens, A. L., Sun, H., Haeseleer, F., and Lee, A. (2004). Ca^{2+}-binding protein-1 facilitates and forms a postsynaptic complex with Cav1.2 (L-type) Ca^{2+} channels. *J. Neurosci.* 24, 4698–4708.

Zhou, H., Yu, K., McCoy, K. L., and Lee, A. (2005). Molecular mechanism for divergent regulation of Cav1.2 Ca^{2+} channels by calmodulin and Ca^{2+}-binding protein-1. *J. Biol. Chem.* 280, 29612–29619.

Conflict of Interest Statement: The authors declare that the research was conducted in the absence of any commercial or financial relationships that could be construed as a potential conflict of interest.

Received: 12 February 2012; accepted: 18 April 2012; published online: 08 May 2012.

Citation: Raghuram V, Sharma Y and Kreutz MR (2012) Ca^{2+} sensor proteins in dendritic spines: a race for Ca^{2+}. Front. Mol. Neurosci. ***5****:61. doi: 10.3389/fnmol.2012.00061*

frontiers in
MOLECULAR NEUROSCIENCE

REVIEW ARTICLE
published: 09 April 2012
doi: 10.3389/fnmol.2012.00042

Ca^{2+}-sensors and ROS-GC: interlocked sensory transduction elements: a review

Rameshwar K. Sharma* and Teresa Duda

Research Divisions of Biochemistry and Molecular Biology, The Unit of Regulatory and Molecular Biology, Salus University, Elkins Park, PA, USA

Edited by:
Michael R. Kreutz, Leibniz-Institute for Neurobiology, Germany

Reviewed by:
Karl-Wilhelm Koch, Carl von Ossietzky University Oldenburg, Germany
Ivan I. Senin, A. N. Belozersky Institute Lomonosov Moscow State University, Russia

****Correspondence:***
Distinguished Professor Rameshwar K. Sharma, Research Divisions of Biochemistry and Molecular Biology, The Unit of Regulatory and Molecular Biology, Salus University, 8360 Old York Road, Elkins Park, PA 19027, USA.
e-mail: rsharma@salus.edu

From its initial discovery that ROS-GC membrane guanylate cyclase is a mono-modal Ca^{2+}-transduction system linked exclusively with the photo-transduction machinery to the successive finding that it embodies a remarkable bimodal Ca^{2+} signaling device, its widened transduction role in the general signaling mechanisms of the sensory neuron cells was envisioned. A theoretical concept was proposed where Ca^{2+}-modulates ROS-GC through its generated cyclic GMP via a nearby cyclic nucleotide gated channel and creates a hyper- or depolarized sate in the neuron membrane (Ca^{2+} Binding Proteins 1:1, 7–11, 2006). The generated electric potential then becomes a mode of transmission of the parent $[Ca^{2+}]_i$ signal. Ca^{2+} and ROS-GC are interlocked messengers in multiple sensory transduction mechanisms. This comprehensive review discusses the developmental stages to the present status of this concept and demonstrates how neuronal Ca^{2+}-sensor (NCS) proteins are the interconnected elements of this elegant ROS-GC transduction system. The focus is on the dynamism of the structural composition of this system, and how it accommodates selectivity and elasticity for the Ca^{2+} signals to perform multiple tasks linked with the SENSES of vision, smell, and possibly of taste and the pineal gland. An intriguing illustration is provided for the Ca^{2+} sensor GCAP1 which displays its remarkable ability for its flexibility in function from being a photoreceptor sensor to an odorant receptor sensor. In doing so it reverses its function from an inhibitor of ROS-GC to the stimulator of ONE-GC membrane guanylate cyclase.

Keywords: ROS-GC guanylate cyclase, Ca^{2+} sensors, cyclic GMP, sensory transductions

INTRODUCTION

The discovery and molecular characterization of the photoreceptor ROS-GC is a land mark event in the photo-transduction field (reviewed in Pugh et al., 1997; Koch et al., 2010). It filled in the gap on the identity of the source of cyclic GMP that serves as a second messenger of the LIGHT signal; and made it possible to explain the principles of photo-transduction machinery in molecular and physiological terms.

It also impacted the core membrane guanylate cyclase field by the branching of the guanylate cyclase family into two subfamilies. The family became a transducer of both the extracellular peptide hormonal and the intracellularly genearted $[Ca^{2+}]_i$ signals. Before, it was believed to be the sole transducer of the peptide hormone signals (reviewed in: Sharma, 2010).

Prior to its discovery in 1994, an intense search was on the identification of a guanylate cyclase unique to photo-transduction. It was known that both $[Ca^{2+}]_i$ and cyclic GMP are the critical messengers of the photon signal in the vertebrate photoreceptors. How these signals are generated and interact with each other was not recognized, however, (early reviews: Pugh and Cobbs, 1986; Stryer, 1986). Early reports on the successful identification of photoreceptor ROS-GC contradicted each other, and created a lot of confusion. One of these reports even suggested that this Ca^{2+}-sensitive membrane guanylate cyclase is nitric oxide sensitive, and its molecular mass is 67 kDa (Horio and Murad, 1991a,b). Another major perception was that the photo-transduction-linked membrane guanylate cyclase consists of "separate regulatory and catalytic subunits" (Stryer, 1991). In yet another report it was reported to be cloned from the human retina library (Shyjan et al., 1992). It was named retGC and via *in situ* hybridization was detected only in the inner segments and outer nuclear layers of the monkey's retina, the segments and the layers not linked with photo-transduction.

ROS-GC DISCOVERY

These contradictions on the true identity of the photoreceptor ROS-GC were resolved by establishing its direct purification from the bovine outer segments (OS) (Margulis et al., 1993), the site of photo-transduction. Its protein-sequence-based molecular cloning, structure, and function demonstrated that it is not any of the earlier, including retGC, membrane guanylate cyclases (Goraczniak et al., 1994). Its theoretical molecular mass is 120, 360 Da, in general agreement with the earlier 110 kDa value reported for the biochemically purified forms of bovine and frog forms (Hayashi and Yamazaki, 1991; Koch, 1991). It was settled that unlike other family members, it is not a natriuretic peptide hormone surface receptor membrane guanylate cyclase.

The molecular identities of the photoreceptor ROS-GC from the rod outer segments (ROS) and two other members of the natriuretic peptide receptor family, ANF-RGC (Kutty et al., 1992)

from the rat retina and CNP-RGC (Duda et al., 1993) from the human retina, demonstrated that the retinal neurons contain both the surface receptor and ROS-GC sub-families, but only ROS-GC is potentially linked with the photo-transduction machinery. Two important conspicuous structural differences were noted between the two sub-families. One was that ROS-GC beyond the catalytic domain contains a C-terminal extension tail of 90 amino acids, Y^{965}-K^{1054}; the second was that the signature ATP-regulated domain, Gly-X-X-X-Gly of the natriuretic peptide hormone receptors, CNP-RGC and ANF-RGC, is missing in ROS-GC. These differences play a key role in determining the cellular and functional specificity of the ROS-GC containing neurons.

Significantly, among all the family members, ROS-GC is the only membrane guanylate cyclase that has been cloned on the basis of its protein sequence. This approach experimentally validated the position of the N-terminus amino acid of the mature protein and demonstrated that the immature protein contains a 56 amino acid N-terminus hydrophobic signal peptide. The theoretical molecular mass of the protein with its signal peptide is 120, 361 Da and without it is 114, 360 Da.

This approach of its identification also played a key role in demonstrating that the structure of the originally cloned human retGC (Shyjan et al., 1992) was a cloning artifact. Consistent with this fact, in the January 1995 GenBank data (Accession number M92432) the structure of human retGC was revised to match it with the bovine ROS-GC. Thereby, the revised retGC became a human counter part of the bovine ROS-GC.

ROS-GC, A TWO-COMPONENT TRANSDUCTION SYSTEM

Before the characterization of photoreceptor ROS-GC and the coined-terminology for the guanylate cyclase activating protein as GCAP, a key observation showed that a GCAP stimulates a membrane guanylate cyclase in the bovine ROS in a Ca^{2+}-dependent fashion (Koch and Stryer, 1988). An essential feature of this GCAP was that it was a cytosolic factor. Ca^{2+}-bound, it inhibited the membrane guanylate cyclase activity. This was the first hint that ROS-GC is a two-component $[Ca^{2+}]_i$ transduction system and that the system had an unusual property of being inhibited by the $[Ca^{2+}]_i$ signal. With the availability of the recombinant (r)ROS-GC, it was now possible to test and study this unusual feature of the native photoreceptor ROS-GC in its isolated form. All prior membrane guanylate cyclases were only stimulated by their peptide hormone signals.

Fortuitously, at almost the same time the cloning of ROS-GC was reported (Goraczniak et al., 1994), the cloning of two forms of GCAP, GCAP1 (Palczewski et al., 1994; Subbaraya et al., 1994; Frins et al., 1996) and GCAP2 (Dizhoor et al., 1995) was also reported. They were the Ca^{2+} modulators of one, or more, native ROS guanylate cyclase/s with undetermined identities. Their relationship with the cloned ROS-GC was not known.

The availabilities of the cloned forms of ROS-GC1 and GCAP1 made it possible to test if these two Ca^{2+} transduction elements were linked, together constituting one ROS-GC transduction system.

They indeed were (Duda et al., 1996). ROS-GC1 expressing heterologous system of COS cells responded at 10 nM $[Ca^{2+}]_i$ to the GCAP1 stimulation in a dose dependent manner. The stimulation was incrementally inhibited by free Ca^{2+} with a $K_{1/2}$ of 100 nM. In contrast, under identical conditions, GCAP1 had no effect on the recombinant ANF-RGC, the peptide hormone receptor. An additional important characteristic of the transduction system was that the GCAP remained bound to ROS-GC at the low and high Ca^{2+} levels, consistent with the physiological observations (Koutalos et al., 1995). These results demonstrated that (1) rROS-GC mimicked the native ROS-GC present in the ROS in its Ca^{2+}-modulation, and, therefore, functionally it was identical to the native enzyme; (2) It received its Ca^{2+} signals through GCAP1; therefore, the GCAP was its $[Ca^{2+}]_i$ sensor and the transmitter component; and ROS-GC was the signal receiver and the transducer component; (3) GCAP always remains bound to ROS-GC regardless of the $[Ca^{2+}]_i$ concentration; and (4) the ROS-GC transduction system differed from the peptide hormone receptor family members in being solely the transducer of the intracellularly generated Ca^{2+} signals within the light-sensitive OS.

In this manner the biochemical and physiological identity of the native with its cloned form photoreceptor ROS-GC1 was established, and also its linkage with photo-transduction. It was concluded that the ROS-GC is a two-component transduction system where the Ca^{2+}-sensor GCAP element is interlocked with the ROS-GC transducer element and the change in $[Ca^{2+}]_i$ level defines the activity state of ROS-GC. This interlocked transduction system represented a new paradigm of the fields of membrane guanylate cyclase and the NCS proteins.

Similar conclusions based on the reconstitution studies with retGC established that GCAP2 is another NCS protein linked with photo-transduction (Dizhoor et al., 1994, 1995). In addition, the molecular identity of the second member of the ROS-GC subfamily, retGC2, from the ROS of the human and bovine retinas was established (Lowe et al., 1995; Goraczniak et al., 1997). To distinguish between the two ROS-GCs, the original ROS-GC was termed ROS-GC1 and the second as ROS-GC2.

Thus, two GCAPs and two ROS-GCs, bound to each other, reside in the OS of the rods. Because only ROS-GC1 was able to be purified directly from the ROS, it was perceived that ROS-GC1 was the dominant guanylate cyclase in ROS. This perception was validated by the direct quantitative estimation of the two isozymes in the bovine ROS. Their ratios are 96% ROS-GC1 and 4% ROS-GC2 (Helten et al., 2007). The latest estimation in the mouse shows the same pattern, yet, slightly higher concentration of ROS-GC2, 76% ROS-GC1, and 24% ROS-GC2 (Peshenko et al., 2011). However, in contrast to the bovine, the mouse study was made with the total OS instead of the isolated membrane fractions.

Because most of the studies have been conducted with ROS-GC1, the following discussion will deal with this transduction system only. It is, however, noted that GCAP2 appears to be the only natural sensor of ROS-GC2 and its target site resides between the aa736–1010 domain, quite different from the corresponding domain for the GCAP1 site in ROS-GC1 domain (Goraczniak et al., 1997). In contrast, the discussion below will indicate that both GCAP1 and GCAP2 are critical Ca^{2+} sensor elements of ROS-GC1.

PHOTO-TRANSDUCTION MODEL

Photo-transduction is the biochemical process by which the rods and cones convert the incoming LIGHT signal into the electrical signal. Enlightened by the ROS specific features of the interlocked GCAP/ROS-GC transduction system, a model for its role in operation of the photo-transduction machinery was proposed (Pugh et al., 1997; this review covers the historical development of the membrane guanylate cyclase related photo-transduction field up to June 1997; others subsequently published are: (Pugh et al., 1999; Burns and Baylor, 2001; Koch et al., 2002, 2010; Sharma, 2002; Sharma et al., 2004; Luo et al., 2008; Stephen et al., 2008; Wensel, 2008).

This model with some advanced features is presented in **Figure 1**.

In this model ROS-GC is the central component of the photo-transduction machinery. It generates cyclic GMP, the second messenger of the LIGHT signal. Its key feature is that it regulates and is regulated by the produced $[Ca^{2+}]_i$ signal. Thereby, the accelerated production of $[Ca^{2+}]_i$ inhibits and the decelerated production accelerates its operation. Cyclic GMP and $[Ca^{2+}]_i$ create a feedback loop in the photo-transduction machinery. The machinery operates in the decelerated mode within 50 nM to the 250 nM $[Ca^{2+}]_i$ range.

For almost two decades this model has served as a template in advancing the molecular, biochemical and physiological principles of the photo-transduction operation. These advancements in the model are briefly outlined below; their details are available in the cited references.

ADVANCEMENTS

GCAPs

As the entry of the molecular form of ROS-GC dawned on the era of decoding the molecular principles of photo-transduction machinery, so was the entrance of recoverin for the age of NCS protein field. First reported on its presence in the rods and cones of photoreceptors and its direct Ca^{2+}-dependent regulation of guanylate cyclase, it was named recoverin referring to its function "because it promotes recovery of the dark state" (Dizhoor et al., 1991). Its linkage with true ROS-GC was concluded because it reportedly inhibited the catalytic activity of guanylate cyclase in the range of 450–40 nM of free Ca^{2+}. However, this conclusion and its role in recovery was withdrawn (Hurley et al., 1993), yet it represents the first member of the NCS protein family. It is present in the photoreceptors; in its new role, it senses Ca^{2+} signals, inhibits rhodopsin kinase, and thereby, plays a role in light adaptation (Makino et al., 2004; Philippov et al., 2007).

An important contribution of recoverin's entry into the field of NCS proteins is related to the identification of its four Ca^{2+}-specific structural motifs, these EF hands define the general Ca^{2+} sensor property of the NCS family. Only two are functional in recoverin, however.

The GCAPs, 1 and 2, constitute a sub-family of the NCS proteins (reviewed in Koch et al., 2010). The NCS superfamily is grouped into five subfamilies of recoverins, VILIPs, frequenins, KCHIPs, and GCAPs (reviewed in: Nef, 1996; Braunewell and Gundelfinger, 1999; McCue et al., 2010). These subfamilies perform diverse regulatory processes, which include gene expression, ion channel function, enzyme modulations like that of kinases, guanylate cyclases, and adenylate cyclases, membrane trafficking of ion channels and receptors, and control of apoptosis.

This section focuses only on the GCAPs, 1 and 2: expression, properties, and physiological functions, the reader is referred to a recent review for the details (Koch et al., 2010). However, it is noted that the number of GCAPs has expanded with their findings in several mammalian, amphibian, and teleost species. While mammals express only 2–3 GCAP isoforms, 6–8 isoforms are found in the retina of teleost fish (Rätscho et al., 2010).

EXPRESSION

GCAP1 and GCAP2 are expressed in the same concentration of 3 μM in the native bovine ROS (Hwang et al., 2003). Their quantitative, relative, and cellular concentrations in the rods and cones of any other species are not known. Immunocytochemical studies show, however, that both GCAPs are present in the outer and inner segments of rods and cones (Gorczyca et al., 1995; Frins et al., 1996). Importantly, their presence in cone synaptic pedicles can be clearly defined (Venkataraman et al., 2003).

Scattered reports based on immunohistochemical studies show varying results in the same or different species. Examples are: the expression of GCAP1 is minimal in the ROS of human, monkey, and bovine retina but is maximal in the cone OS of these species (Kachi et al., 1999); GCAP2 is expressed in both outer and inner segments of the bovine rods and cones (Dizhoor et al., 1995); monkey retinas express minimal level of GCAP2 in OS of the rods and cones and in the rod inner segments (Otto-Bruc et al., 1997). These variations might be resolved on the basis of species-specifications (Cuenca et al., 1998), yet it appears that, in general, the rods and cones of all mammals express both GCAPs.

Curiously, in some species, like human and zebrafish (but not mice), GCAP3 appears as a cone-specific isoform of GCAP (Imanishi et al., 2002). And the zebrafish isoforms GCAP4, GCAP5, and GCAP7 also exhibit cone-specific expression patterns (Imanishi et al., 2004).

BIOCHEMICAL FEATURES

Ca^{2+} binding

Like most other members of the NCS-protein family, GCAPs harbor four EF-hand Ca^{2+}-binding motifs, of which three are functional (reviewed in Koch et al., 2010). These EF-hands have a nanomolar affinity for Ca^{2+} and they are the Ca^{2+}-sensor elements linked with photo-transduction.

In a recent proposal for GCAP1, the transition from the DARK State to the Illuminated State of the photoreceptors occurs by the substitution of bound Ca^{2+} with the bound Mg^{2+} to ROS-GC1 (Peshenko and Dizhoor, 2006, 2007). Ca^{2+} associates with GCAP1 with a rate of $\sim 2 \times 10^8$ M^{-1} s^{-1} (k_{on}) which is close to the diffusion limit (Sokal et al., 1999). The apparent dissociation constants of each EF-hand for Ca^{2+} are between 0.08 and 0.9 μM and between 0.1 and 1.6 μM in the absence and presence of 2 mM Mg^{2+}, respectively (Lim et al., 2009). Thus, these nanomolar affinities result in fast dissociation rates (for example, $k_{off} = k_{on} \times K_D = 2 \times 10^8$ M^{-1} s^{-1} $\times$ 0.2×10^{-6} M) = 40 s^{-1}; $1/k_{off} =$ 25 ms), consistent with the kinetics of the vertebrate photoresponse.

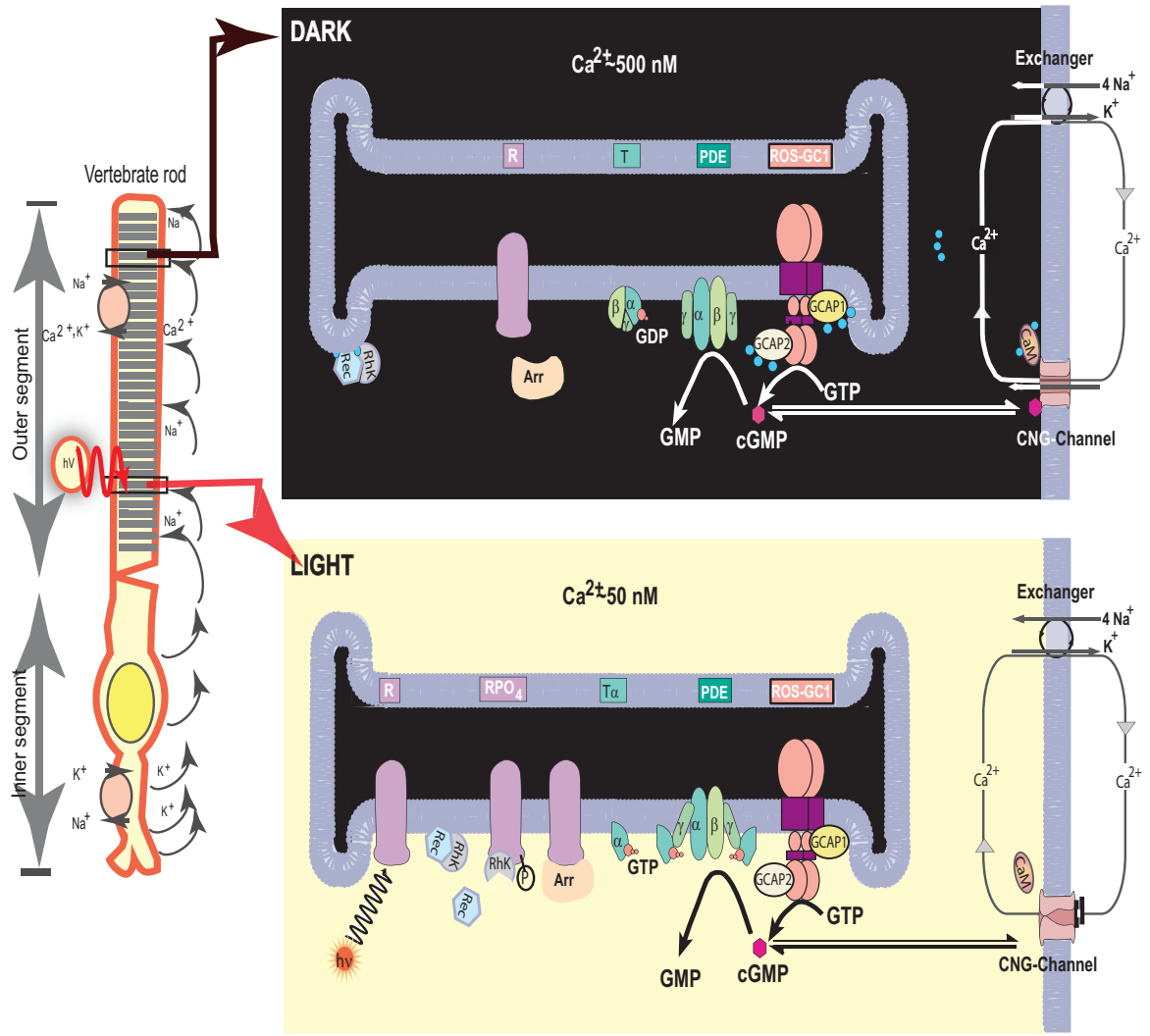

FIGURE 1 | Photo-transduction model. Left panel. An illustration of a typical vertebrate rod. In the dark a circulating current (arrows) is present, which is outward in the inner segment and carried primarily by K^+; in the outer segment the net charge flow is inward, with about 90% of the inward flow carried by Na^+ and 10% by Ca^{2+} ions. Na^+/K^+ exchange pumps in the inner segment membrane and Na^+/K^+-Ca^{2+} exchangers in the outer segment membrane (see also right panels) maintain the overall ionic gradients against the dark flows. The capture of a photon ($h\nu$) by a rhodopsin molecule in one of the disc membranes of the outer segment initiates the photo-transduction cascade. **Right upper panel.** The components of the photo-transduction cascade are shown in the dark/resting steady-state. A high concentration of cytoplasmic cGMP keeps a fraction of CNG-channels in the plasma membrane open. Ca^{2+}-ions enter the cell via the CNG-channel and are extruded via the Na^+/K^+, Ca^{2+}-exchanger. Synthesis and hydrolysis of cGMP by ROS-GC and PDE occur at a low rate. The heterotrimeric G protein transducin (T) is in its GDP-bound state and is inactive. The Ca^{2+}-binding proteins calmodulin (CaM) recoverin (Rec), and GCAPs bind to their target proteins, the CNG-channel, rhodopsin kinase (RhK) and ROS-GC, respectively. **Right lower panel.** Absorption of light by the visual pigment rhodopsin leads to the activation of the transduction cascade: the GTP-bound α-subunit of transducin activates PDE that rapidly hydrolyzes cGMP. Subsequently the CNG-channels close and the Ca^{2+}-concentration decreases. The change in cytoplasmic [Ca^{2+}] is sensed by Ca^{2+}-binding proteins: CaM dissociates from the CNG-channel which leads to an increase in cGMP sensitivity of the channel, inhibition of rhodopsin kinase by recoverin is terminated and rhodopsin can be phosphorylated. GCAPs activate ROS-GC and synthesis of cGMP increases. Arrestin (Arr) binds to phosphorylated rhodopsin and interferes with the binding and further activation of transducin. Enhancement of cGMP synthesis and termination of the cascade leads to reopening of CNG-channels. [composed from Figure 1 Pugh et al. (1997) and Figure 1 Koch et al. (2002), and reprinted with the permission from those references].

GCAP2 is similar, yet not identical, in its Ca^{2+}-binding properties. The second, third, and fourth EF-hands are functional. They display an apparent K_D of 300 nM (Ames et al., 1999), but no specific assignment for the affinity of each EF-hand has been made so far. It appears, however, that EF-hands two and four influence Ca^{2+} sensitivity of GCAP2 more than EF-hand three (Dizhoor and Hurley, 1996). Cysteine accessibility study with GCAP2 mutants shows its restricted reactivity toward Cys^{111} at sub-micromolar Ca^{2+}-concentrations, indicating that within the Ca^{2+} concentration range where ROS-GCs are regulated, Ca^{2+}-induces conformational changes in GCAP2 (Helten et al., 2007). Thus, these are the fluctuations in the free Ca^{2+} concentrations

of the rods and cones that control and signal GCAPs to transmit their messages to the bound ROS-GC and be transduced in the generation of cyclic GMP, the second messenger of photo-transduction.

Myristoylation

Given the facts that GCAPs are the members of the NCS protein family and its member recoverin, also expressed in photoreceptor cells, is acylated at its N-terminus and is embodied with a striking regulatory switch termed "Ca^{2+}-myristoyl switch" (Zozulya and Stryer, 1992), these recoverin's features were investigated for GCAPS. The findings showed that the GCAPs are, indeed, heterogeneously acylated at their N-termini; myristoyl group being of the prominent form (Palczewski et al., 1994; Olshevskaya et al., 1997). However, GCAPs do not undergo a classical calcium-myristoyl switch (Olshevskaya et al., 1997; Hwang and Koch, 2002a,b). They do not bury the myristoyl group in a hydrophobic pocket in the Ca^{2+}-free form and expose it when in Ca^{2+}-bound form (Zozulya and Stryer, 1992). This conclusion was validated by the crystallographic study of GCAP1 which showed that the group is always buried (Stephen et al., 2007).

Additional investigations demonstrated that the myristoyl group has a strong impact on the regulatory properties of GCAPs (Hwang and Koch, 2002a,b; Hwang et al., 2003): (1) It influences the Ca^{2+} sensitivity of GCAP1, but not of GCAP2, shifting its IC_{50} value for Ca^{2+} in the regulation of ROS-GC1. (2) It increases by sevenfold the affinity of GCAP1 for ROS-GC1. On the other hand, it has no effect on GCAP2. (3) It differentially regulates the catalytic efficiency, k_{cat}/V_{max}, of ROS-GC1 regulation by GCAP1 and GCAP2; the influence of the myristoyl group on catalytic efficiency is larger for GCAP1 than for GCAP2.

ROS-GC MODULATION

In preceding, and then parallel, studies to those that led to the conclusion that GCAPs are differential Ca^{2+} sensors, a similar conclusion was arrived at. These studies involved comprehensive technology of soluble constructs of ROS-GC1, direct binding measurements by surface plasmon resonance (SPR) spectroscopy, co-immunoprecipitation and functional reconstitution utilizing progressive deletion constructs and peptide competition. The first study *via* the application of ROS-GC1 deletion and ANF-RGC/ROS-GC1 hybrid mutants which retained only the catalytic domain of ROS-GC1 established that the GCAP1- and GCAP2-modulated domains in ROS-GC1 are separate and that they reside on the opposite ends of the catalytic domain (Krishnan et al., 1998). The study also showed that GCAP2 signals ROS-GC1 activation under the physiological conditions of Ca^{2+} with a $K_{1/2}$ of 10 nM, inhibits its activity with an IC_{50} value of 140 nM; and, importantly, it concluded that the intracellular region of ROS-GC1 "is composed of multiple modules, each designed to mediate a particular calcium-specific signaling pathway." It will become clear from the discussion below that the architecture of the intracellular domain of ROS-GC1 is, indeed, multi-modular and each module is pre-visioned to control the intensity and shape of each type of Ca^{2+} signal into the given production of cyclic GMP.

The mapped region of GCAP1 constitutes two domains of ROS-GC1: transduction, M^{445}-L^{456} and binding, L^{503}-I^{522} (Lange et al., 1999), and the GCAP2-modulated binding and the transduction site reside in the Y^{965}-N^{981} region of ROS-GC1 (Duda et al., 2005).

A comment is in order for the role of GCAP2 in Ca^{2+} signaling. In contrast to GCAP1, GCAP2 is the specific physiological Ca^{2+} sensor component of ROS-GC2 (Goraczniak et al., 1998; Haeseleer et al., 1999). Its IC_{50} value for Ca^{2+} is 150 nM; compared to GCAP1 for ROS-GC1, its EC_{50} value for ROS-GC2 activation is about one order of magnitude lower: compare 1 μM with 8 μM (Goraczniak et al., 1998). This feature of GCAP2 has been substantiated by the recent studies, yet they show that GCAP1 with less specificity is also the stimulant of ROS-GC2 (Helten and Koch, 2007; Peshenko et al., 2011). Importantly, the study with ROS-GC2 deletion and ANF-RGC/ROS-GC2 hybrid mutant, which retained only the catalytic domain of ROS-GC2, demonstrated that the GCAP2-modulated domain in ROS-GC2 resides at its C-terminus region of the catalytic domain. The site has not been precisely mapped, yet almost certainly it is very similar or almost identical to the corresponding ROS-GC1 site for GCAP2. Thus, it clearly indicated that the Ca^{2+} signal transduction mechanisms of two ROS-GCs in photo-transduction are very different.

Additional analysis indicated that GCAP1 and GCAP2 have different ranges of $[Ca^{2+}]$ in which they operate. Activation of ROS-GC1 by GCAP1 is half-maximal at 707 nM and that by GCAP2 at 100 nM (Hwang et al., 2003). In addition to Ca^{2+}, Mg^{2+} is essential for GCAP function. It is an essential cofactor for the ROS-GC cyclization reaction. Decreasing $[Mg^{2+}]$ from 5 to 0.5 mM lowers, by almost one order of magnitude, the $[Ca^{2+}]$ IC_{50} values of both GCAPs (Peshenko and Dizhoor, 2004). Thus, fluctuations of $[Mg^{2+}]$ in a photoreceptor cell also influence the dynamic range of cyclase regulation. However, free $[Mg^{2+}]$ apparently does not change significantly during illumination (Chen et al., 2003).

CA^{2+}-RELAY MODEL

Integration of the differential Ca^{2+} sensing properties of the GCAPs with the facts that their targeted sites in ROS-GC1 are also different have resulted in the current "Ca^{2+}-relay model" of photoreceptor guanylate cyclase activation (Koch, 2006; Koch et al., 2010). The key component of this model is that there is a switch which converts GCAP1 mode to a GCAP2 mode of the ROS-GC operation during the light-induced fall in cytoplasmic $[Ca^{2+}]$ (Hwang et al., 2003; Koch, 2006; Burgoyne, 2007). Both GCAP1 and GCAP2 are present in almost equal concentrations and their combined concentration is equal to the concentration of a ROS-GC1 dimer (Hwang et al., 2003), "both GCAPs bind to a ROS-GC1 dimer in the dark state of the cell. In this state the ROS-GC1 activity is very low, just sufficient to maintain the cytoplasmic dark concentration of cyclic GMP by keeping a balance with the low dark-state activity of the cyclic GMP hydrolyzing enzyme, phosphodiesterase. Illumination of rod or cone cells leads to a decrease in cyclic GMP and consequently to fall in $[Ca^{2+}]_i$. Depending on the light conditions and on the bleaching protocol $[Ca^{2+}]_i$ reaches an intermediate level, at which only GCAP1 becomes an activator of ROSGC1. Further decrease of $[Ca^{2+}]_i$ (by stronger illumination for example) would

also transform GCAP2 into an activator. This differential activating modus is in accordance with the observed differences in Ca^{2+}-sensitivity and shows that ROS-GC1 is regulated by GCAP1 and GCAP2, exhibiting differences in Ca^{2+}-sensitivity. Thus, the illumination-intensity-dependent regulation of ROS-GC1 is switched from a "GCAP1 mode" to a "GCAP2 mode" or vice versa (Hwang et al., 2003). Under constant background light the $[Ca^{2+}]_i$ reaches a new steady state value. In this manner, these two modes operate at different light intensities depending on the free $[Ca^{2+}]_i$ level" (Koch et al., 2010).

This model (Sharma, 2010), depicting the illumination intensity-dependent modulation of GCAPs in the Ca^{2+} signaling of ROS-GC1 is presented in **Figure 2**.

The "Ca^{2+}-relay model" explains the findings on a transgenic GCAP null mice study where the role of GCAP2 could not be concluded (Howes et al., 2002). In these mice, flash responses from rods differ from the wild-type responses in two aspects. (1) The fast recovery shortly after the maximum response amplitude is missing; (2) In some cases, the flash ends in a prominent undershoot. According to the model (Hwang et al., 2003), in case 1, because GCAP1 is missing, there is no fast recovery to the single flash. In case 2, the exogenous addition of GCAP2 causes a delayed activation of ROS-GC at lower $[Ca^{2+}]_i$ than GCAP1.

In a striking contrast to the secondary structural differences between the GCAPS *modus operandi,* the indication is that the Ca^{2+} signaling of GCAP2 causes its reversible dimerization and it is a necessary requisite to activate ROS-GCs (Olshevskaya et al., 1999). In contrast, the dimeric form of GCAP1 is inactive and does not result in activation of the ROS-GC (Hwang et al., 2004).

The knowledge gained through these studies (*vide supra*) has now begun to make inroads into defining the molecular events that result in migration of the Ca^{2+} signals to ROS-GC1 catalytic domain. Recall, the targeted domains of two GCAPs are far apart, on the opposite sides of the catalytic domain of ROS-GC1, and they perform non-overlapping tasks. The natural wisdom would be that the signaling pathways of these two GCAPs would be through distinct mechanisms.

In the first study to address this issue, the role of ^{657}WTAPELL^{663} motif of ROS-GC1 in signal migration of the two GCAPs has been analyzed. The reason behind choosing this

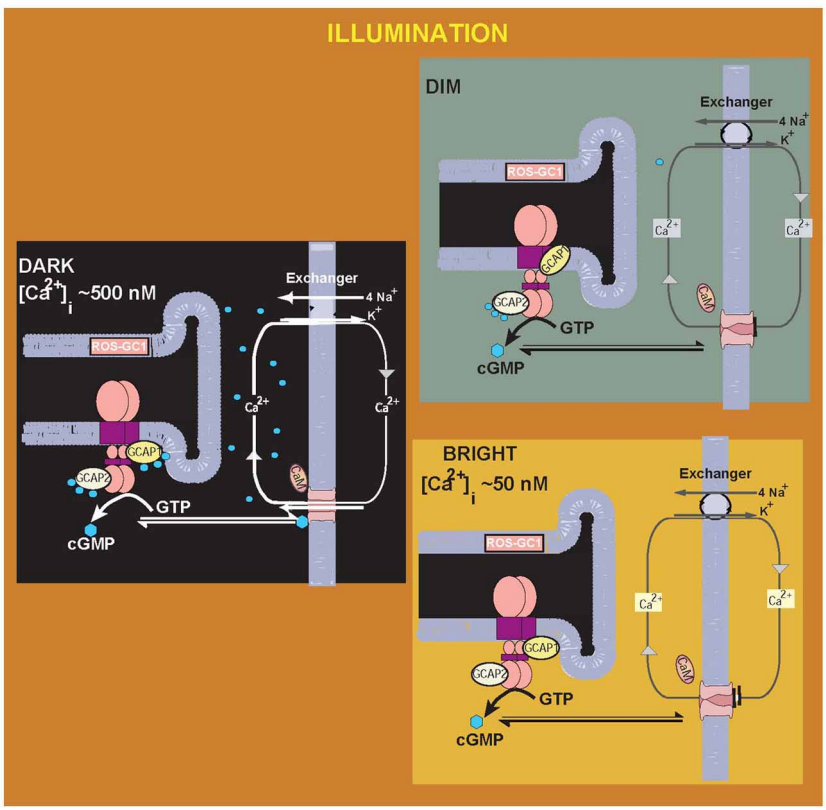

FIGURE 2 | Illumination intensity-dependent modulation of GCAPs in the $[Ca^{2+}]_i$ signaling of ROS-GC1: a Model. In the "DARK," $[Ca^{2+}]_i$ concentration is high, the Ca^{2+}-bound sensors GCAP1 and GCAP2 are bound to ROS-GC1, ROS-GC1 activity is basal, generating ground-level cytoplasmic cyclic GMP. The cyclic GMP keeps a fraction of CNG-channels in the plasma membrane open. Ca^{2+} ions enter the cell via the CNG channel and are extruded via the Na^+/K^+, Ca^{2+} exchanger. The outer segments of the rods and cones are in the depolarized state. DARK to the "DIM" or intermediate LIGHT state. The initial fall of $[Ca^{2+}]_i$ is selectively detected by GCAP1, in its Ca^{2+}-free state GCAP1 attains the activated mode. Transition to the "Bright" LIGHT state, the CNG channels are totally closed, both GCAP1 and GCAP2 are Ca^{2+}-free and are in the activated mode, ROS-GC1 activation is full and membranes of the rod and cone outer segments are in the hyperpolarized state. [adapted and reprinted from Figure 2: with permission from Sharma (2010)].

motif was that it is conserved in all members of the membrane guanylate cyclase family; and based on the ANF-RGC signaling template, it is critical for its regulatory catalytic activity (Duda et al., 2009). The question was: would this motif be also critical in ROS-GC1 signaling.

The following parameters of the motif were analyzed (Duda et al., 2011). (1) Is the motif critical for the ROS-GC1 catalytic activity? The comparative studies with a ROS-GC1 mutant in which the ^{657}WTAPELL^{663} motif was deleted (Δ^{657}WTAPELL^{663} mutant) demonstrated that the motif has no role on the structural integrity of the guanylate cyclase. It is, however, critical for the Ca^{2+} signal transduction activities of both GCAPs. Thus, it controls the total Ca^{2+} signaling activity of ROS-GC1. (2) Is the motif involved in the GCAPs binding to their target sites of ROS-GC1? This problem was analyzed *in vivo* by monitoring the interaction of GCAPs with ROS-GC1 and the deletion mutant in co-transfected cells through immnunofluorecence and *in vitro* by co-immunoprecipitation. The findings were that both GCAPs in their isolated forms are cytosolic proteins; yet when co-expressed with ROS-GC1 or its deletion-mutant, they are membrane bound with the respective cyclases. These results demonstrated that WTAPELL motif does not control the binding characteristics of any GCAP to its ROS-GC1 domain. This conclusion was validated by the co-immunoprecipitation experiments conducted with the COS cell membranes expressing wt-ROS-GC1 or the Δ^{657}WTAPELL^{663} mutant. Both, the wt and the mutant precipitated with GCAP1 and GCAP2. (3) Which residues in the motif are critical in ROS-GC1 signaling? This question was resolved by scanning one by one the residues of the motif. W^{657} was found to be the most critical residue. It controlled 73% of the GCAP1 and 70% of the GCAP2 activity. The other three residues—T^{658}, P^{660}, and E^{661}—individually controlled about 40% of the GCAP1 or GCAP2 signaling activity of ROS-GC1. Thus, all the four residues, marked in bold, of the ^{657}**WTAPE**LL^{663} motif are important for the Ca^{2+}-modulated signaling activities of the GCAPs, yet the most critical is W^{657} residue, accounting for about 70% of the total signaling activity.

INROADS INTO THE GENE-LINKED RETINAL DISEASES

For a recent comprehensive review on this topic the reader is referred to (Hunt et al., 2010; earlier findings up to the year 2002 are covered in Duda and Koch, 2002). What follows is a brief narration of the ROS-GC gene linked diseases that marked the early entry from basic to clinical medicine (reviewed in Sharma, 2010).

With the knowledge of the complete structural identity and organization of the ROS-GC1 gene (Duda et al., 1998) and of the mechanism by which its coded enzyme modulates the Ca^{2+} signal transduction it was now possible to investigate the human retinal diseases at the genetic levels and explain them in biochemical terms. In the first study, GCAP1 regulatory regions identified in the original study (Lange et al., 1999) gave a hint toward explaining one of the molecular causes of the rod dystrophy Leber's congenital amaurosis type 1 (LCA1), where the patients are born blind or become blind soon after birth. In these patients there is a point mutation ($F^{514}S$, numbering for the bovine gene; in humans $F^{565}S$) in the ROS-GC1 gene within the region L^{503}-I^{522} (Perrault et al., 1996).

Biochemical studies with the heterologously expressed ROS-GC1 mutants demonstrated that this LCA mutant has almost completely (84%) lost its basal activity and sensitivity to modulation by GCAP1 (Duda et al., 1999). These studies proved therefore, that a region in proximate distance to the transmembrane region is critical for interaction and/or regulation by GCAP1 (*vide supra*). And this region is incapacitated in the diseased state.

A similar approach was used to investigate the second type of retinal disease that correlates with mutations of the ROS-GC1 gene, named cone-rod dystrophy type 6 (CORD 6). Patients who suffer from this disease carry one or several point mutations in the dimerization domain of ROS-GC1 (Kelsell et al., 1998). One form of the mutation is ROS-GC1-E^{786}D,R^{787}C,T^{788}M. The dimer formation in this mutant is disturbed. This results in a reduced basal guanylate cyclase activity (Duda et al., 1999, 2000; Tucker et al., 1999). However, sensitivity of this mutant to GCAP1 and GCAP2 is increased. Physiological consequences of these mutations are a change in the trigger of the Ca^{2+}-feedback and thereby causing a shift in the response-intensity curve to lower light intensities. These effects explain the photophobia often reported by CORD 6 patients and the accumulating light damage of the retina leading to loss of cone and rod vision over a time period of decades. Full accounts of the biochemical and physiological aspects of LCA1 and CORD 6 associated retinal diseases have been covered in reference (Duda and Koch, 2002).

Several point mutations in the GCAP1 gene are linked with inherited progressive cone-rod dystrophies (reviewed in: Behnen et al., 2010). These are: P^{50}L, E^{89}K, Y^{99}C, D^{100}E, N^{104}K, I^{143}N/T, L^{151}F, E^{155}G, and G^{159}V. While the P^{50}L mutation does not change the activating properties of GCAP1 (Newbold et al., 2001), the other mutations significantly alter the activation profile of GCAP1 (Dizhoor et al., 1998; Sokal et al., 1998; Wilkie et al., 2001; Kitiratschky et al., 2009). The Y^{99}C mutant is constitutively active and has almost completely lost any Ca^{2+} sensitivity, i.e., it activates ROS-GC1 at low and higher $[Ca^{2+}]$ to a similar extent. P^{50}L mutant exhibits less Ca^{2+}-binding capacity (Newbold et al., 2001).

GCAP1-MODULATED ROS-GC1 TRANSDUCTION SYSTEM BEYOND ROS, CONE PHOTORECEPTOR SYNAPSE

Inherited with its novel composition and its Ca^{2+}-regulated feature, the perception in the membrane guanylate cyclase field arose that the GCAP-modulated ROS-GC transduction system is unique, linked solely to the photo-transduction machinery. If it were true, it must only reside in the OS of the rods and cones.

This question was first addressed by two groups (Liu et al., 1994; Cooper et al., 1995). Both, through immunocytochemistry, demonstrated the presence of a ROS-GC in the synaptic layers, outer plexiform layer (OPL) and inner plexiform layer (IPL) of the retina. These studies, however, made no differentiation between whether the detected cyclase was ROS-GC1 or ROS-GC2, and the presence of the GCAP component of the transduction system was not determined. Nonetheless, these studies suggested that the ROS-GC transduction system exists beyond ROS and possibly in other retinal neurons.

The presence of the GCAP1-modulated/ROS-GC1 transduction system was tested and found in the OPL through these

independent extensive means: (1) functional, (2) biochemical, (3) peptide competition, (4) crosslinking, and (5) reconstitution. The tests demonstrated that the OPL contained ROS-GC1 transduction system, which in all respects was identical to the one present in native ROS (Venkataraman et al., 2003). Immunocytochemical analysis of the retina showed that ROS-GC1 and GCAP1 were co-expressed together in the cone synaptic pedicles, which reside in the presynaptic region of the bipolar neurons (Venkataraman et al., 2003). These results demonstrated that at the biochemical level the two GCAP1-modulated Ca^{2+} signaling ROS-GC1 transduction systems, present in ROS and OPL, are identical. This linked the GCAP1/ROS-GC1 transduction system with the pre-synaptic activity of the photoreceptor-bipolar neurons.

Its physiological relevance remains untested. It is conceivable, however, that the system is the regulator of a hypothetical CNG channel in the termini of cones. In this possibility, activation of the channel triggers release of glutamate from the termini. The GCAP1/ROS-GC1 system provides a Ca^{2+}-dependent negative feedback control of the CNG channel. When the Ca^{2+} influx via voltage-dependent Ca^{2+} channels stops, for example, during hyperpolarization, the free Ca^{2+} concentration synaptic termini transiently declines. And the decline, in turn, activates the GCAP1/ROS-GC1 system. Consistent with this speculation are the findings, showing that Ca^{2+} levels fluctuate over a 10-fold range in photoreceptor synapses, reaching as low as 50 nM (reviewed in Krizaj and Copenhagen, 2002), the concentration at which GCAP1/ROS-GC1 transduction machinery is most accelerated, and the production of cyclic GMP is at its peak. Cyclic GMP will open the CNG channel; this would cause an influx of Ca^{2+}, resulting in inactivation of the GCAP1/ROS-GC1 system.

The presence of the GCAP2-modulated ROS-GC Ca^{2+} signaling transduction system in the presynaptic region of the photoreceptor-bipolar neurons has not been yet tested. Yet GCAP2 is present in the region, it interacts with the synaptic ribbon protein, RIBEYE, and the authors speculate that it may participate in the post-NADH-modulated process (Venkatesan et al., 2010).

GCAP1-MODULATED ROS-GC1 TRANSDUCTON SYSTEM NOT UNIQUE TO SOLE OPERATIONS OF VISUAL TRANSDUCTION

With revelations on existence of the GCAP1-modulated Ca^{2+} signal transduction system within and outside of the sensory transduction neurons linked with vision, the next question was: does this transduction system exist outside the domain of vision-linked neurons?

The first studies addressing this issue were conducted in the pineolocytes. They showed that it does (Venkataraman et al., 1998, 2000; reviewed in Sharma, 2010).

Briefly, with a programmed protocol in the first task through an array of functional, biochemical, molecular, and histochemical tools the ROS-GC1 present in the bovine pinealocyte membranes was characterized. Then, it was shown that it is present with and is modulated by GCAP1 in a manner identical to the photoreceptor ROS-GC1. Importantly, the transduction system was not present in the surrounding glial cells. It was concluded that operation of the ROS-GC1 transduction machinery in the pinealocytes mimics the photo-transduction machinery.

These studies made two additional significant observations, reflecting the molecular differences between the photoreceptor and the pinealocyte photo-transduction machineries. (1) the pinealocyte's were devoid of the Ca^{2+}-modulated GCAP2 arm of photoreceptor ROS-GC1; (2) They also did not contain the photoreceptor ROS-GC2 transduction system.

In a broadened search, the GCAP1-modulated ROS-GC1 Ca^{2+} signal transduction system has been characterized at the molecular, biochemical, and functional levels in the anterior region of the gustatory epithelium of the tongue, the site of gustatory transduction, linking it with the sense of taste. This finding has not been followed at the physiological level (Duda et al., 2004; reviewed in Sharma, 2010).

Being present in the sensory and sensory-linked neurons with vision and gustation transduction processes and in the pinealocytes, the subsequent question was: is the GCAP1-modulated ROS-GC1 transduction system also linked with the transduction events of the odorant?

The study focused first on the rat olfactory bulb (Duda et al., 2001). The bulb is the recipient of the odorant signal generated at the ciliated apical border. It receives the signal information in the form of action potentials. The incoming axons from the olfactory receptor cells join together and form presynaptic nets [**Figure 3** in (Duda et al., 2007)]. These nets together with the dendrites of mitral and tufted cells are termed glomeruli (Shepherd and Greer, 1998). Mitral and tufted cells constitute the second-order neurons in the olfactory system (Pinching and Powell, 1971). The information received by their dendrites is processed in the soma, and transmitted, eventually, via the olfactory tract to the five specified areas of the olfactory cortex: anterior olfactory nucleus, olfactory tubercle, pyriform cortex, amygdaloidal complex, and entorhinal complex [**Figure 3** in (Duda et al., 2007)]. These areas decode the sensory input and translate the original odorant signal into the perception of smell at the olfactory cortical centers.

Comprehensive biochemical, functional, immunohistochemical, and molecular analysis of the olfactory bulb revealed that, like the photo-transduction machinery in ROS, the bulb contains the GCAP1-modulated Ca^{2+} signaling ROS-GC1 transduction machinery (Duda et al., 2001). This machinery is present in the mitral cells where it is also manufactured (Duda et al., 2001). Thus, the mitral cell neurons house full genetic machinery for the production and expression of this entire transduction system in the olfactory neurons.

This study established the presence of the GCAP1/ROSGC1 signal transduction system in mitral cells of the olfactory bulb (Duda et al., 2001) and demonstrated that this transduction system is not restricted to the photic modulation; it is also present in the neurons linked with olfaction. Thus, the transduction system had the makings of being omnipresent in the neurons linked with the sensory perceptions.

GCAP1-MODULATED ROS-GC1 TRANSDUCTON SYSTEM IS ALSO PRESENT OUTSIDE OF THE NEURONAL CELLS

In a remarkable finding, presence of the GCAP1-modulated Ca^{2+} signal transduction system has been demonstrated at

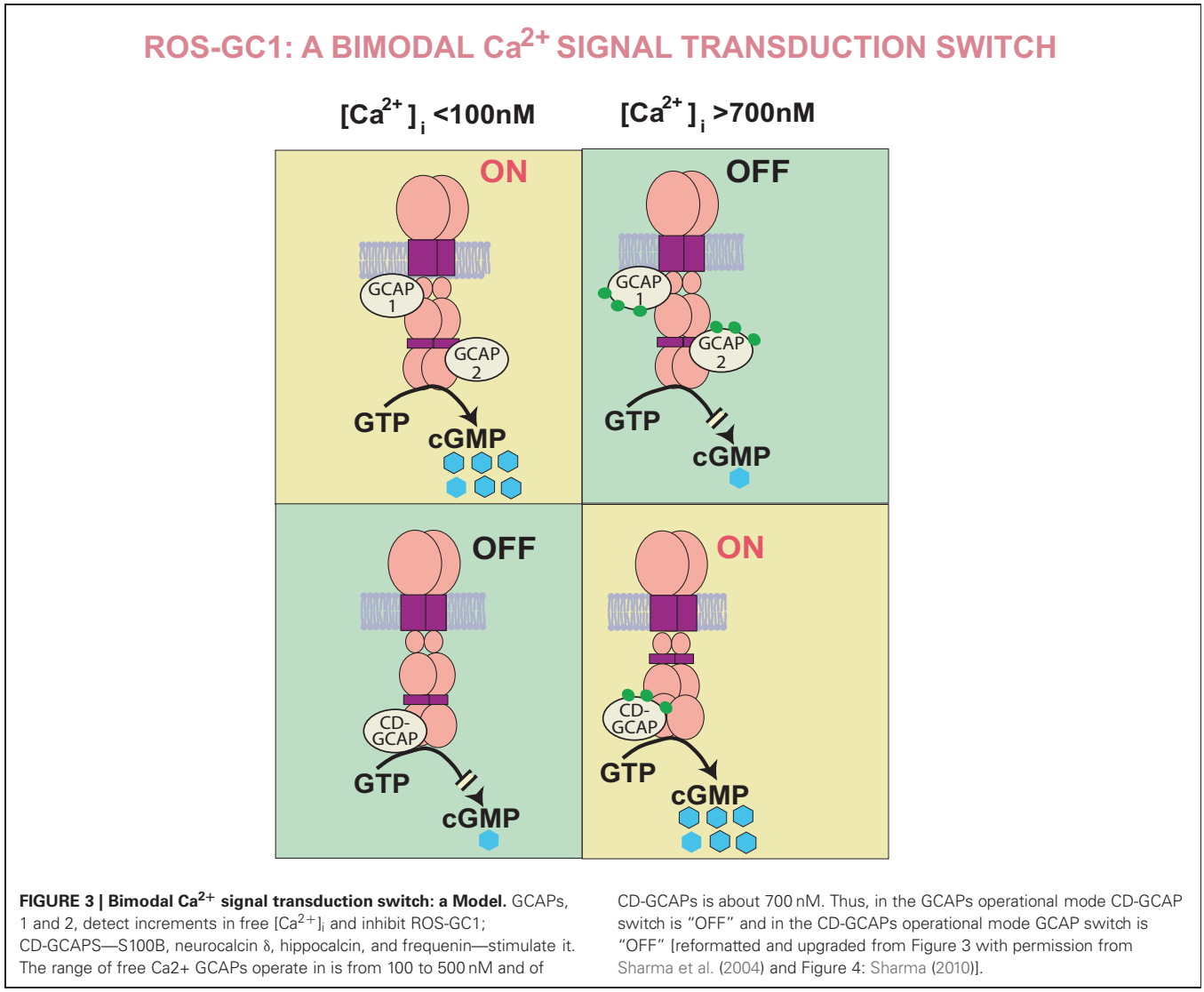

FIGURE 3 | Bimodal Ca^{2+} signal transduction switch: a Model. GCAPs, 1 and 2, detect increments in free $[Ca^{2+}]_i$ and inhibit ROS-GC1; CD-GCAPS—S100B, neurocalcin δ, hippocalcin, and frequenin—stimulate it. The range of free Ca2+ GCAPs operate in is from 100 to 500 nM and of CD-GCAPs is about 700 nM. Thus, in the GCAPs operational mode CD-GCAP switch is "OFF" and in the CD-GCAPs operational mode GCAP switch is "OFF" [reformatted and upgraded from Figure 3 with permission from Sharma et al. (2004) and Figure 4: Sharma (2010)].

the molecular, protein and functional levels in the rat testes (Jankowska et al., 2007, 2010; reviewed in Jankowska and Warchol, 2010), and at the biochemical and functional levels in the human and bovine spermatozoa as well (Jankowska et al., 2010). Histochemical studies show that the transduction system is localized in a small population of spermatocytes (Jankowska et al., 2007). Physiology of the system has not been determined. Because the system is also present in the acrosomal cap, the authors have suggested that it may have a role in regulation of the acrosomal reaction (Jankowska et al., 2010). Importantly, GCAP2 was screened for its molecular presence in the rat testes but was not found, indicating absence of the GCAP2-modulated ROS-GC1 transduction in the testes.

In summary, the following conclusions are arrived at in reference to the GCAP-modulated ROS-GC transductions system:

1. It is vital to the operation of the photo-transduction process.
2. Only Ca^{2+}-modulated GCAP2 and ROS-GC2 appear to be its unique photo-transduction components.
3. GCAPs, 1 and 2, through diverse modes regulate ROS-GC1 activity.
4. The system is present in the inner retinal neurons, yet its physiology is not determined.
5. Beyond photic transmissions, its presence in the pinealocytes, olfactory bulb, and gustatory epithelium indicate that it plays a wider role in the sensory transduction processes.
6. In the purest terms its presence in the spermatozoa questions the classification of GCAP1 as solely being a NCS family member.

DISCOVERY OF A CD-GCAP, S100B, DEFINED ROS-GC AS A CALCIUM BIMODAL TRANSDUCTION SWITCH

The feature that the increments of $[Ca^{2+}]_i$ progressively inhibit ROS-GC1 activity was intellectually challenging because it had never been observed before for any member of the membrane guanylate cyclase family. All members so far were stimulated by its effector ligands. Serendipitous studies *(vide infra)* widened its property in disclosing its remarkable nature. The ROS-GC was

both an inhibitor and stimulator of $[Ca^{2+}]_i$ signals, briefly narrated below (reviewed in: Sharma et al., 2004; Sharma and Duda, 2006; Sharma, 2010).

In a joint study, two groups reported that a retinal post-mitochondrial 100,000g supernatant fraction stimulates photoreceptor ROS-GC in a Ca^{2+}-dependent fashion (Pozdnyakov et al., 1995). The stimulatory factor was purified as a 6–7 kDa subunit protein. It oligomerized to a functional 40 kDa and stimulated the native and the cloned form of ROSGC1 with a $[Ca^{2+}]_i$ $K_{1/2}$ of 2 μM. To distinguish it from the co-temporarily discovered GCAP that inhibited ROS-GC in a Ca^{2+}-dependent fashion, the factor was named Ca^{2+}-dependent guanylate cyclase activator protein (CD-GCAP) (Pozdnyakov et al., 1995). And, importantly, it was postulated that CD-GCAP may be a positive Ca^{2+} modulator of the yet unidentified ROS-GC type guanylate cyclase present in the synaptic layers of the bovine retina (Pozdnyakov et al., 1995), a prediction proven true by the later studies (discussed below).

The factor was cloned, sequenced both in its cloned and the native forms, and reconstituted to show that it was S100B protein (Cooper et al., 1995; Duda et al., 1996; Margulis et al., 1996; Pozdnyakov et al., 1997). And, in a remarkable discovery it was established that the ROS-GC is a Ca^{2+}-bimodal switch. Its inhibitory mode operates through GCAP and the stimulatory through S100B. The switching modes are controlled by nanomolar to the micromolar range of $[Ca^{2+}]_i$.

Additional studies demonstrated that the GCAP1 and S100B-modulated domains in ROS-GC1 are far apart. They flank the catalytic domain; at its N-terminal aa503–786 segment resides the GCAP1 domain and at the C-terminal aa731–1054 segment, the CD-GCAP domain (Duda et al., 1996). The CD-GCAP and the S100B arms of the switch constitute its separate elements and they operate ROS-GC through different modes. These modes were diagrammatically depicted in a model "ROS-GC1 is a Bimodal Signal Transduction Switch" (Sharma et al., 2004). This model is reproduced in **Figure 3**.

There were two powerful impacts of these findings. (1) CORE, they demonstrated, for the first time, that the $[Ca^{2+}]_i$ signals can originate downstream of the catalytic site and then be processed upstream at the catalytic site for the generation of cyclic GMP. (2) They provided a theoretical background of a general concept where via a nearby cyclic GMP-gated channel the ROS-GC transduction system could create hyper- or de-polarization in the membranes of the sensory neurons. The ensuing voltage potentials could then become the means of transmission for sensory transduction events (Sharma, 2010).

S100B IS THE CA^{2+}-MODULATOR OF THE PHOTORECEPTOR-BIPOLAR SYNAPSE ROS-GC

To test the prediction that the S100B Ca^{2+} signaling arm of the ROS-GC1 is present in the photoreceptor-bipolar synapse region (Pozdnyakov et al., 1995), the bovine OPL was investigated (Duda et al., 2002). Serialized functional, biochemical, and immunolocalization followed by a combination of peptide competition, SPR binding, and deletion mutation studies demonstrated that upon Ca^{2+} binding S100B targets two sites in ROSGC1. One site comprises aa G^{962}-N^{981}, the other, aa I^{1030}-Q^{1041}. The former represents the binding site and later the transduction site. The K_d value for the binding site ranges from 198 to 395 nM.

These results confirmed that, indeed, the Ca^{2+} bimodal modes of the ROS-GC regulation exist in the retinal neurons and the modes define a new paradigm of Ca^{2+} signaling in the vertebrate neurons (Duda et al., 2002). In contrast to what happens in ROS, where increments in free Ca^{2+} inhibit ROS-GC1 activity, in the synapse region they stimulate ROS-GC1. The reversal in cyclase operation is caused by the substitution of GCAP in ROS with S100B in the photoreceptor-bipolar synapse. And, importantly, GCAP inhibition of ROS-GC1 occurs with Ca^{2+} $K_{1/2}$ of about 100 nM and S100 B stimulation with a $K_{1/2}$ of 850 nM. This experimentally validated the previously proposed theoretical model of S100B-modulated Ca^{2+} signaling of ROS-GC1 (**Figure 3**). It also demonstrated that S100B in the visual transduction system acts as a Ca^{2+} sensor protein.

DISCOVERY OF THE SECOND CD-GCAP, NEUROCALCIN δ, WIDENED THE CA^{2+} SIGNAL TRANSDUCTION MODES OF ROS-GC1

Besides S100 B, is there any other member of CD-GCAP linked with ROS-GC1 transduction system in the retinal neurons?

The answer is yes. First, in a heterologous system of COS cells where the sole interacting components were recombinant ROS-GC1 and recombinant bovine brain neurocalcin δ, it was demonstrated that the neurocalcin stimulated ROS-GC1 in a Ca^{2+}-dependent manner with a $K_{1/2}$ of 0.8 μM (Krishnan et al., 2004). The stimulation was specific because it did not stimulate ROS-GC2 and ANF-RGC. Also, the mechanism of stimulation was different from the prototype CD-GCAP, S100B, because the neurocalcin–modulated domain in ROS-GC1 was different from that of S100B. The common stimulatory theme of the two CD-GCAPs was explained through the comparison of their Ca^{2+}-bound crystal structures. In 3-D terms the four helix-packing arrangements of their Ca^{2+}-binding EF hands are very similar (Kumar et al., 1999; Sharma et al., 2004; Duda et al., 2006). Thus, spatially neurocalcin δ and S100B are structural and functional analogs.

These studies demonstrated that CD-GCAP is more than a one-member family and it is linked with the ROS-GC1 transduction system. This knowledge seeded in the evolution of a powerful theoretical concept where a single transducer ROS-GC1 component is designed to sense the multiple spatial forms of Ca^{2+} signals through its GCAP and CD-GCAP components and translate them into the production of a single second messenger, cyclic GMP.

NEUROCALCIN δ IS THE CA^{2+}-MODULATOR OF THE IPL ROS-GC1

Neurocalcin δ was purified and sequenced from the IPL of the retina (Krishnan et al., 2004). Its N-terminus is blocked and is acylated, predominantly in the myristoylated form. Accordingly, the cloned protein at its N-terminus contains a myristoylation site motif, MGXXXS, conserved in all other members of the NCS-protein family, with the only exception for the Kv-channel interacting protein subfamily; whose members, KChIP2, KChIP3, and KChIP4 are not myristoylated (Braunewell and Gundelfinger, 1999; Burgoyne and Weiss, 2001).

The IPL neurocalcin δ is a 20 kDa monomer protein. Like other Ca^{2+} sensor proteins (Ladant, 1995; Frins et al., 1996),

it exhibits a Ca^{2+}-dependent mobility shift. In its native form it exists as a dimer (Venkataraman et al., 2008). It has four Ca^{2+}-binding EF-hand motifs; only three—EF2, EF3, EF4—are predicted to be functional (Okazaki et al., 1992; Terasawa et al., 1992; Vijay-Kumar and kumar, 1999).

It contains an active Ca^{2+} myristoyl switch (Krishnan et al., 2004) but its small fraction is always bound with the native membranes. This intrinsic binding feature has important Ca^{2+}-dependent physiological implications. Therefore, it was studied further and validated through the analysis of the recombinant reconstituted system with the conclusions that (1) a resting cellular concentration of 100–200 nM, $[Ca^{2+}]_i$ is able to keep neurocalcin δ membrane bound. (2) In this membrane bound state, it has a stronger affinity for ROS-GC1. (3) Once the neurocalcin δ and ROS-GC1 complex is formed, existence of this complex is independent of the Ca^{2+} concentration. Any one or all three of these possibilities suggested that the membrane bound neurocalcin δ can participate in the Ca^{2+}-dependent events, occurring at millisecond time intervals, the intervals required in the visual transduction events.

In accordance with this concept, natural interaction of neurocalcin δ with ROS-GC1 was envisioned, tested and found in the IPL (Krishnan et al., 2004). Neurocalcin δ and ROS-GC1 were present together and the added presence of $[Ca^{2+}]_i$ stimulated native ROS-GC1 activity. The results also showed that the nanomolar (resting) concentration range of Ca^{2+} keeps neurocalcin δ membrane bound and creates the physical and functional interaction between neurocalcin δ and ROS-GC1. Importantly, the myristoyl group of neurocalcin causes a 2-fold amplification of the saturation activity of ROS-GC1.

Kinetic parameters of the Ca^{2+}-dependent neurocalcin δ interaction with ROS-GC1 were analyzed (Krishnan et al., 2004). Without Ca^{2+}, neurocalcin δ had no affinity for ROS-GC1. In the presence of Ca^{2+}, it bound ROS-GC1 with K_A of 2.3×10^6 M^{-1} and a K_D of 4.6×10^{-7} M.

These analyses demonstrated that the steps of neurocalcin δ binding to and dissociation from ROS-GC1 are Ca^{2+}-dependent, they occur within the physiological levels of Ca^{2+}, they are direct and of high affinity; and they occur within nano seconds, in accordance with the time span of the vision transduction steps (Krishnan et al., 2004).

That the neurocalcin δ regulation of ROS-GC1 is, indeed, unique to itself was also demonstrated with the disclosure of its target site in ROS-GC1, residing within its aa732–962 segment. It does not overlap with the GCAP1-, GCAP2-, and S100B-modulated domains of ROS-GC1 (Krishnan et al., 2004).

NEUROCALCIN δ MODULATION OF ROS-GC1 REPRESENTS A NEW MODEL OF CA^{2+} SIGNALING

Fine analysis of the aa732–962 segment pinpointed the neurocalcin δ-modulated site between aaV^{837}-L^{858} of ROS-GC1. This recognition was surprising because the site resided within the core catalytic domain. This had never been observed before for any ligand of the guanylate cyclase family members.

The nature of the site was probed by direct studies with the isolated core catalytic module of ROS-GC1 (Venkataraman et al., 2008). They yielded unforeseen results, contrary to at the time held views. (1) The neurocalcin δ directly interacts with the site; (2) it does not require the adjacent N-terminally located α-helical dimerization domain structural element (aa767–811) for its interaction; (3) The core catalytic module, housing the site, is intrinsically active, i.e., it has basic guanylate cyclase activity; (4) The core module by itself is dimeric in nature, it does not require the dimerization domain structural element for being so; and (5) the core dimeric form of the catalytic module is directly regulated by the Ca^{2+}-bound neurocalcin δ; Ca^{2+}-unbound neurocalcin δ was ineffective.

Incorporating these features, a fold recognition based model of the core catalytic domain was built and neurocalcin δ docking simulations were carried out to define the three-dimensional features of the interacting domains of the two molecules (Venkataraman et al., 2008). This model is presented in **Figure 4**.

The model displayed the following features in 3-D terms.

1. The two chains of the catalytic module are antiparallel. In each chain, the neurocalcin δ-binding-transduction motifs is located toward the N-terminal region of the chain. In these configurations, the two neurocalcin binding-transduction sites are distal to each other. The notable characteristics of these sites are that they are composed of helix-loop-helix structure.
2. The core catalytic domain V^{837}-L^{858} is the interaction site with the neurocalcin.
3. The residues in and around the EF1 hand of the neurocalcin are the primary interaction sites with its target catalytic domain.
4. The contact points between the catalytic domain and neurocalcin δ are designed to form a perfect fit. The neurocalcin-binding transduction motif of the catalytic domain consists of a helix-loop-helix structure. This structure is accessible to the solvent and comfortably fits in the V-shaped crevice of the neurocalcin δ. This crevice is formed by the defined EF-1 hand residues (**Figure 4C**). These residues form a special hydrophobic–hydrophilic patch, which may be distinctive feature of the Ca^{2+}-dependent signaling property of neurocalcin δ.

Signal transduction model

The experimentally validated facts provided by this study and these aided by the computational modeling, allowed the proposal of a stepwise neurocalcin δ signal transduction model. Step 1, the post-phototransduction signal in the IPL neurons generates a rise of free $[Ca^{2+}]_i$ in the lower micromolar range. Step 2, $[Ca^{2+}]$ binds neurocalcin δ. Step 3, neurocalcin δ undergoes Ca^{2+}-dependent configurational change. Step 4, with an EC_{50} of 0.5 μM, its defined domain in EF1-hand binds its V^{837}-L^{858} modulated region of the catalytic domain in ROS-GC1; catalytic domain in its native form exists as a dimer. Step 5, with k_{on} of 7×10^4 M^{-1} s^{-1}, catalytic domain is activated and generates cyclic GMP. Step 6, with k_{off} of 4.2×10^{-2} s^{-1}, the neurocalcin δ is dissociated and the process reverts back to the Step 1 state of the neuron. These findings defined a new transduction model for the Ca^{2+} signaling of ROS-GC1.

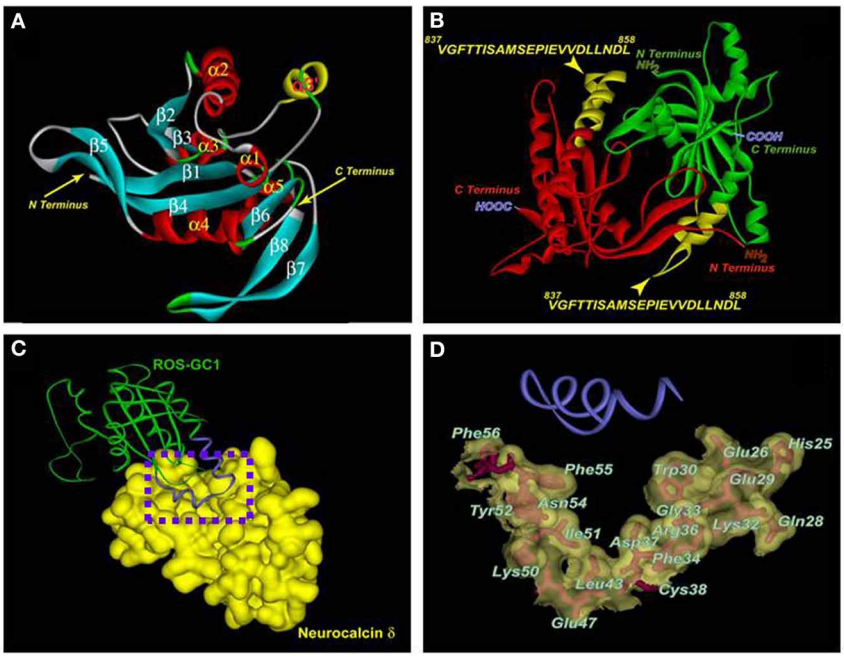

FIGURE 4 | Three-dimensional model of the ROS-GC1 catalytic domain and molecular docking of neurocalcin δ. (A) Ribbon diagram of the ROS-GC1 catalytic domain monomer. The α helices are shown in red and the β strands in cyan. Numbering is according to the protein data base file 1AZS template. The N- and C-termini are indicated by arrows. **(B)** The solvent-accessible V^{837}-L^{858} domain of ROS-GC1 catalytic domain. The two monomeric ROS-GC1 catalytic domains are indicated in red and green respectively. Within each monomer, the region corresponding to V^{837}-L^{858} is indicated in yellow and labeled. The N- and C-termini are labeled. **(C)** The ROS-GC1 catalytic domain/neurocalcin δ complex. Monomers of ROS-GC1 catalytic domain and of neurocalcin δ are depicted for clarity. ROS-GC1 catalytic domain is depicted as a green ribbon and its helix-loop-helix V^{837}-L^{858} region is in blue; the solvent accessible surface of neurocalcin δ is depicted in gold. A dotted box is drawn around the region of docking. **(D)** Residues on neurocalcin δ within 4.5 Å sphere from the interacting ROS-GC1 catalytic domain region. The docking region [dotted box in **(C)**] is expanded. The ROS-GC1 helix-loop-helix region (V^{837}-L^{858}) is depicted as a blue ribbon. The neurocalcin δ residues located within 4.5 Å sphere from the V^{837}-L^{858} region are depicted as stick models in red, embedded within the solvent surface (transparent gold). The amino acid residues are labeled. Reproduced with permission from reference Venkataraman et al. (2008).

CA^{2+}-MODULATED ODORANT-RECEPTOR ONE-GC IS A VARIANT FORM OF ROS-GC TRANSDUCTION SYTEM

The recognition that ROS-GC is a Ca^{2+} bimodal signal transduction switch offered the theoretical possibility of its universal linkage with the sensory transduction processes (*via supra*). In this pursuit, its linkage with the sense of SMELL was anticipated (reviewed in: Sharma et al., 2004; Duda et al., 2007; Sharma, 2010; Zufall and Munger, 2010). What follows is a brief recapitulation and a brief presentation of the current status of the field.

History

Ca^{2+}-modulated ROS-GC transduction system in the olfactory transduction was first discovered in the rat olfactory bulb (*vide supra*) (Duda et al., 2001). After the odorant transduction step in the olfactory cilia, the bulb receives the information in the form of action potentials. The incoming axons from the olfactory receptor cells join together and form presynaptic nets. These nets are termed glomeruli (Shepherd and Greer, 1998). They are the "microprocessor units" of the olfactory bulb. Each glomerulus consists of about 20,000–25,000 axons of the olfactory receptor cells. The glomeruli synapse with the dendrites of mitral and tufted cells, constituting the second order neurons in the olfactory bulb (Pinching and Powell, 1971). The information received by the dendrites is processed in the soma, and transmitted via the olfactory tract to the five specified areas of the olfactory cortex: anterior olfactory nucleus, olfactory tubercle, pyriform cortex, amygdaloidal complex, and entorhinal complex (**Figure 1** of reference Sharma, 2010). These areas decode the sensory input and translate the original odorant signal into the perception of SMELL at the olfactory cortical centers.

Programmed dissection of the bulb via the techniques of biochemistry, functional reconstitution, immunohistochemistry, and molecular constructs revealed that, like the rod and cone OS the bulb mitral cells contain and synthesize the elements of the GCAP1-modulated Ca^{2+}-signaling ROS-GC1 transduction system (Duda et al., 2001). Importantly, the GCAP2-modulated ROS-GC signaling system is absent. Thus, these neurons have the full information both at the gene and the protein level for the production, expression, and operation of the entire transduction machinery. Intriguingly, the machinery operates with almost the same principles as established for the photo-transduction operation. These operational principles of the mitral cell have not been evaluated at the physiological level. Nonetheless, conceptually, it is possible that via a proximal hypothetical cyclic GMP-gated channel, the increments of $[Ca^{2+}]_i$, will decrease the production of cyclic GMP and hyperpolarize membranes of the mitral cells.

This will then become the means of transmitting the original odorant signal information to the olfactory cortical centers.

DISCOVERY OF THE CA^{2+}-MODULATED ONE-GC, A VARIANT FORM OF ROS-GC, IN THE CILIA OF THE OLFACTORY EPITHELIUM DIRECTED ITS LINKAGE WITH THE ODORANT TRANSDUCTION

The finding of the Ca^{2+} signaling ROS-GC1 transduction system in the olfactory bulb provided the incentive to analyze the presence of this signaling system in the olfactory epithelium for its linkage with the process of odorant transduction. This analysis (Duda et al., 2001, 2004; reviewed in Duda et al., 2007) was aided by the prior observations with the photo-transduction machinery. Certain parallels and opposite phenotypes of the two neuronal cell systems were noted. The cilia are the counter part of the OS of rods and cones photoreceptors. OS are the sites of photo-transduction, the cilia, of the odorant transduction. Like OS, the cilia continuously shed from the olfactory receptor neurons (ORN) and undergo replacement. The OS contain the entire components of the photo-transduction system and the cilia of the odorant-transduction, a biochemical process by which an odorant signal generates electrical signal. However, it was also realized that the physiological consequences of the LIGHT signal and the ODORANT signal in their respective photo-transduction and odorant-transduction machineries are opposite; illumination results in hyperpolarization of the photoreceptor membrane, whereas odorant results in depolarization of the ORN membrane. With these considerations, intuitively, the odorant transduction-linked hypothetical ROS-GC-transduction system should be in the stimulatory mode in the semi-micromolar $[Ca^{2+}]_i$ range in the cilia, a situation opposite to that in OS. Thus, the odorant-linked ROS-GC's sensor partner should be a CD-GCAP, instead of a GCAP in OS.

At the time this hypothesis was envisioned, the consensus was that the odorant signal transduction occurs solely through the cyclic AMP signaling pathway (reviewed in Buck, 1995; Belluscio et al., 1998; Breer, 2003; Lai et al., 2005). However, there was evidence for the presence of a membrane guanylate cyclase [GC-D] in the rat ORNs (Fülle et al., 1995). GC-D had been cloned from the total rat olfactory cDNA library. Because, no regulatory ligand for GC-D was found, it was classified as an "ORPHAN" receptor guanylate cyclase. *In situ hybridization* (Fülle et al., 1995) and then immunocytochemical techniques indicated that GC-D coexisted with its cyclic GMP-PDE partner (PDE2) and, importantly, these two partners were segregated from the components of the cyclic AMP signaling pathway (Juilfs et al., 1997). Furthermore, they were present in a small subpopulation of the neuroepithelium neurons (Juilfs et al., 1997). Additional immunocytochemical studies demonstrated that this subpopulation of neurons also expresses a subunit of the cyclic GMP-selective CNG channel (Meyer et al., 2000). Thus, these neurons were not a part of the cyclic AMP signaling cascade system, instead, they were possibly wired with the cyclic GMP-selective transduction system (Juilfs et al., 1997; Meyer et al., 2000). Initial speculation was that these odorant neurons, termed necklace for their appearance, were a part of the odorant transduction system, however, this speculation was later revised to that "the function of this group of neurons may be in behavioral responses induced by hormones or pheromones, possibly related to reproduction, rather than a response to specific odorants" (Juilfs et al., 1997; Meyer et al., 2000).

To assess the possibility that a ROS-GC-like Ca^{2+}-modulated signaling system exists in the minority subgroup of the odorant neurons and is a part of the odorant transduction system, the present authors' group in their first two studies targeted two systems: isolated rat olfactory neuroepithelium and the isolated cilia, which are the sites of odorant transduction (Duda et al., 2001, 2004). Five criteria were set forth for the ROS-GC transduction machinery to qualify as a genuine transducer of the odorant signal. (1) In its native state, it must be odorant responsive; (2) the response should be rapid; (3) it must reside in the membrane portion of the cilia, the site of odorant transduction; (4) the physiological levels of $[Ca^{2+}]_i$ should mimic the odorant's response; and finally (5) with the defined components of the machinery, it should be possible to reconstitute the Ca^{2+} dependency of the machinery.

All these five criteria were met by the Ca^{2+}-modulated myr-neurocalcin δ-ONE-GC guanylate cyclase transduction system present in the cilia (Duda et al., 2004; Sharma and Duda, 2006; Duda et al., 2007): In its native state, the machinery is odorant-responsive; its response is fast, within seconds; it resides within the membrane portion of the cilia; is modulated by the physiological concentrations of free Ca^{2+} with a $K_{1/2}$ of 700 nM; and it can be reconstituted in a Ca^{2+}-dependent manner by using the sole recombinant molecules of myr-neurocalcin δ and ONE-GC. These studies established the constitution and the operational principles of the odorant-linked ONE-GC transduction machinery. ONE-GC cloned from the rat olfactory neuroepithelium (Duda et al., 2001) library was found to be identical in structure to GC-D (Fülle et al., 1995). Instead of GC-D, the authors preferred the name ONE-GC because it associated with its residence in olfactory neuroepithelium (Duda et al., 2001).

Constitution and operation

The transducer component is ONE-GC and its Ca^{2+} sensor component is neurocalcin δ. ONE-GC is a variant form of the ROSGC subfamily because it is not inhibited by the $[Ca^{2+}]_i$ signals; instead, it is only stimulated. ROS-GC1 and ROSGC2, the Ca^{2+} signal transduction components of the photo-transduction machinery, are not present in the cilia. In the resting state of the cilia, with a concentration range of 60–100 nM free Ca^{2+}, ONE-GC transduction system is partially active and is ever ready to receive and transduce the odorant signals into the production of cyclic GMP. The neurocalcin senses Ca^{2+} in 300–800 nM range, undergoes conformational change, strengthens its bondage with the ONE-GC segment, a 836–1028, and turns "on" the transduction machinery. The binding of neurocalcin δ is of high affinity with a K_D of 2.8×10^{-7} M, is rapid with fast association (k_{on} of 5.7×10^3 M^{-1} s^{-1}) and dissociation (k_{off} of 1.56×10^{-3} s^{-1}) constants. In this manner, the machinery is finely tuned to respond rapidly to the intensity-dependent fluctuations of the Ca^{2+} waves in the apical regions of the ciliary neurons (Duda et al., 2004).

It is noted that although neurocalcin δ contains an active Ca^{2+}myristoyl switch, a fraction of it is always ONE-GC bound

in its native state (Duda et al., 2001, 2004). It is the bound form that directly modulates the Ca^{2+} signals and causes activation of ONE-GC.

In this manner it was envisioned that the ONE-GC neurons via the neurocalcin-modulated Ca^{2+} signaling ONE-GC transduction system are linked with the odorant transduction, and one such recognized odorant was green pepper (Duda et al., 2004).

CA^{2+} SENSOR GCAP1 IN THE PHOTOTRANSDUCTION SYSTEM FUNCTIONS AS A CD-GCAP IN THE ODORANT ONE-GC TRANSDUCTION SYSTEM

A subsequent study demonstrated the identity of another Ca^{2+} sensor component of ONE-GC (Duda et al., 2006). It was GCAP1 but surprisingly it functioned as a CD-GCAP in the native ONE-GC neurons. There, it was bound to ONE-GC segment, aa M^{836}-C^{1110} and with a Ca^{2+} $K_{1/2}$ of 900 μM stimulated it. It was the first example and remains to be the sole example of a Ca^{2+} sensor that could function in an antithetical fashion, inhibiting one, ROS-GC, transduction system and stimulating the other, ONE-GC system.

ONE-GC IS THE ODORANT UROGUANYLIN RECEPTOR

An important gap related to the concept of the linkage of Ca^{2+}-modulated ONE-GC with the odorant transduction was that (1) how it receives the odorant signal at its extracellular domain; (2) and the signal links with its Ca^{2+}-modulated intracellular steps; and finally (3) how it is translated at its catalytic domain in the generation of cyclic GMP, the proposed second messenger of the odorant signal?

These questions began to unfold by two milestone reports (Leinders-Zufall et al., 2007; Duda and Sharma, 2008). The first, through gene-deleted mouse models, ONE-$GC^{-/-}$ and $CNGA3^{-/-}$, and patch clamp techniques demonstrated that the wild-type mice respond to the urine odor in generating the "excitatory cyclic GMP-dependent signaling action potential firing." The urine constituents responsible for creating these patterns of physiological behavior are uroguanylin and guanylin. It was thereby proven that the previously recognized necklace olfactory neurons were the ONE-GC neurons and they were wired with the cyclic GMP signaling pathway for the transduction of the two odorants, uroguanylin and guanylin.

This study also discounted the original proposal (Juilfs et al., 1997) and the impression it left that the ONE-GC signaling pathway is meant to signal the hypothetical pheromone activity which regulates the sexual behavior of the animals (Meyer et al., 2000), because ONE-GC gene null mice showed no abnormality in the mating and suckling behaviors (Leinders-Zufall et al., 2007).

The second report (Duda and Sharma, 2008) through *in vivo* cell reconstitution studies using deleted constructs of ONE-GC demonstrated that the extracellular domain of ONE-GC is the target site of the odorant uroguanylin; and the other urine odorant guanylin does not signal ONE-GC activation. Uroguanylin activates ONE-GC with an EC_{50} of 20 pM and saturates it at 500 pM. It was thereby established that ONE-GC is the sole uroguanylin odorant receptor.

These findings marked the solidification of the original BIMODAL concept that the Ca^{2+}-modulated ROS-GC subfamily occurs in many forms. Through these forms, it has the potential of being a universal signal transducer of the sensory and sensory-linked neurons. ONE-GC represents a third subfamily of membrane guanylate cyclases, differing from the ROS-GC subfamily of being a direct ligand of a natriuretic peptide at its extracellular domain. Finally, contrary to the previous proposal (Fülle et al., 1995), ONE-GC is not the orphan receptor guanylate cyclase.

The other part of the report (Duda and Sharma, 2008) constituted on the mechanism by which $[Ca^{2+}]_i$ through its sensor neurocalcin δ signals the activation of ONE-GC. Its striking feature was the disclosure of its target site, which resided directly on the ONE-GC catalytic module, aaM^{880}-L^{921}. There, it directly signaled its activation. The surprising aspect of this feature was that the isolated catalytic module by itself existed in the dimeric form. It did not require the co-presence of its putative dimerization domain component, revising the previous held views on the general mechanisms of membrane guanylate cyclase signaling (Garbers, 1992; Wilson and Chinkers, 1995; Ramamurthy et al., 2001).

Kinetics of the Ca^{2+}-bound neurocalcin δ binding to the ONE-GC target site assessed by the SPR spectroscopy were: $K_D = 2.8 \times 10^{-7}$ M; $k_{on} = 5.7 \times 10^3$ $M^{-1}s^{-1}$; $k_{off} = 1.56 \times 10^{-3}$ s^{-1}.

The study established that ONE-GC has trimodal regulation; two occur intracellularly, GCAP1- and the neurocalcin d-modulated, and one extracellularly, guanylin-modulated.

GENE KNOCKOUT STUDIES DEMONSTRATED THAT HIPPOCALCIN IS AN ADDITIONAL CA^{2+} SENSOR COMPONENT OF THE ODORANT RECEPTOR ONE-GC TRANSDUCTION PATHWAY

The hippocalcin gene deleted mouse model studies demonstrated that the hippocalcin-modulated ONE-GC transduction system also exists in the olfactory neuroepithelium and it controls ∼38% of the ONE-GC catalytic activity, ∼35% is controlled by GCAP1 and 27% by the neurocalcin (Krishnan et al., 2009). In its native state in the neuroepithelium, (1) it is bound to ONE-GC; (2) it activates ONE-GC with Ca^{2+} $K_{1/2}$ of 0.5–0.7 μM; and (3) Its EC_{50} value for the activation is 0.7 μM.

THE ODORANT, UROGUANYLIN, SIGNAL TRANSDUCTION MODEL

Given these facts that the odorant uroguanylin signals through its ONE-GC surface receptor, that the signal is amplified through its intracellular domain, that the domain is pre-bound with three of its Ca^{2+} sensors—the neurocalcin, GCAP1 and hippocalcin—a general odorant signal transduction model has been proposed (**Figure 5**). For simplicity, the model regulation is depicted for only neurocalcin, yet it is applicable to all three of its Ca^{2+} sensors. The specificity of each sensor resides for its target site in ONE-GC.

A small population of the ORNs contains a cyclic GMP signal transduction pathway. This pathway resides at the apical region of the cilia. Present in the region is ONE-GC membrane guanylate cyclase. Its outer domain is the uroguanylin receptor. In its inner domain, at the C-terminus, resides the catalytic domain. The M^{880}-L^{921} segment of this domain is bound to Ca^{2+} sensor component neurocalcin δ. In resting state, the olfactory receptor

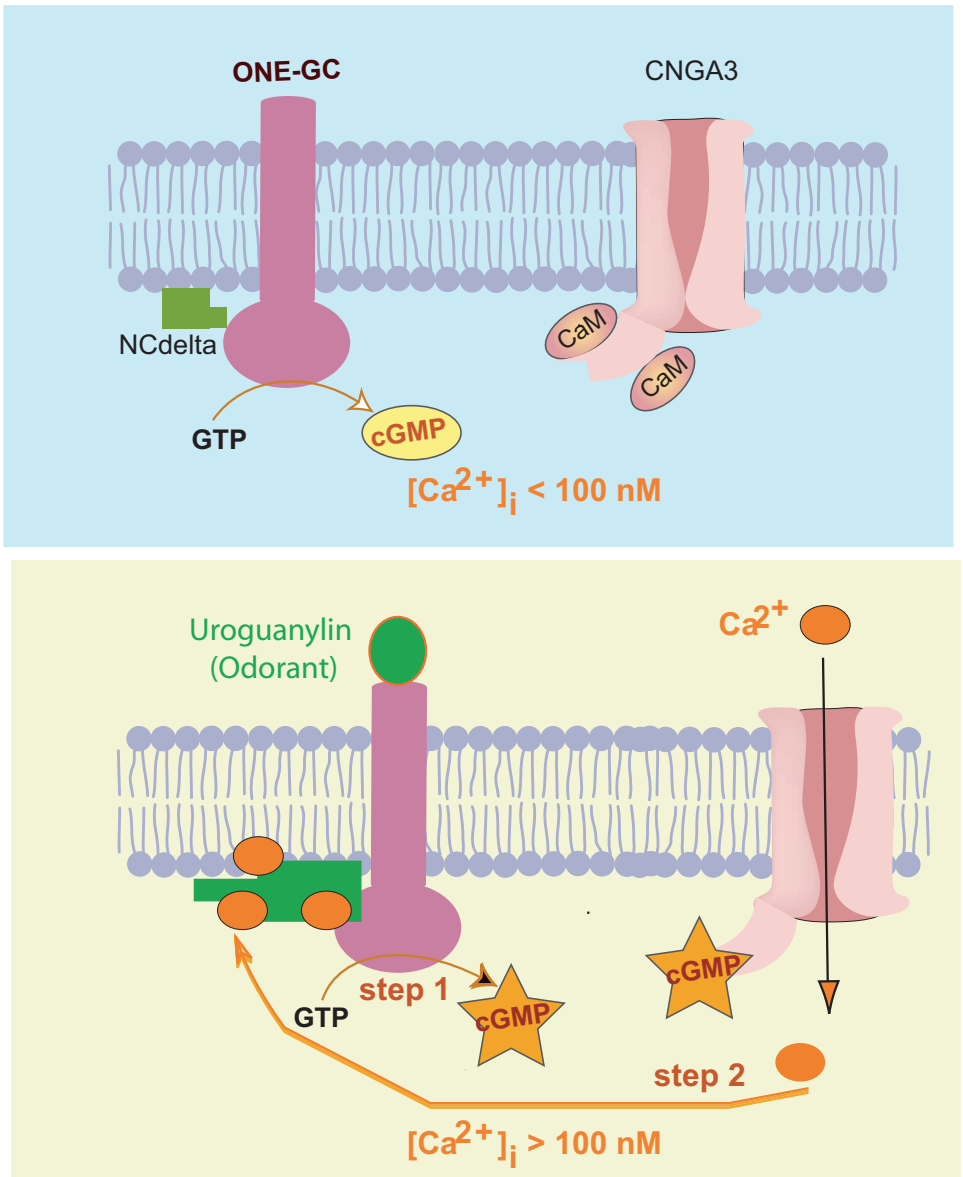

FIGURE 5 | Two-step uroguanylin-neurocalcin δ signal transduction model. Upper panel: Resting state (free $[Ca^{2+}]_i$ < 100 nM). ONE-GC is in its basal state, is bound to Ca^{2+}-free neurocalcin δ (NCdelta) with low affinity, and maintains the steady-state cyclic GMP concentration. Calmodulin (CaM)-bound cyclic GMP-gated Ca^{2+} channel (CNGA3) is closed. **Lower panel**: "Step 1," uroguanylin interacts with the receptor domain of ONE-GC causing its activation and primes ONE-GC. Cyclic GMP formed opens some of the CNGA3 channels increasing $[Ca^{2+}]_i$ to semi-micromolar range. "Step 2", Ca^{2+}-bound neurocalcin δ fully interacts with uroguanylin-primed ONEGC, causing its full activation. [reproduced and reprinted with permission from: Duda and Sharma (2009)].

neuron is in a 60–100 nM range of $[Ca^{2+}]_i$ and ONE-GC is in its basal state.

The odorant, uroguanylin, signal starts by its interaction with the receptor domain of ONE-GC. It is processed through two sequential steps. In step one, ONE-GC is primed and activated minimally. In step 2, $[Ca^{2+}]_i$ rises. With a $K_{1/2}$ of 0.3–0.8 μM, Ca^{2+} binds to the neurocalcin δ, facilitating its interaction with the ONE-GC's segment M^{880}-L^{921}, signals full activation of ONE-GC and production of the odorant second messenger cyclic GMP.

It is envisioned that the operation of step 2 starts with the generation of a small amount of cyclic GMP in step 1. This pool of cyclic GMP opens a limited number of the cyclic GMP-gated channels causing influx of $[Ca^{2+}]_i$ in the ORN. Ca^{2+} binds to the neurocalcin, which, then fully activates ONE-GC. It is noted that the ONE-GC downstream components, cyclic GMP-gated channel (CNGA3) and Ca^{2+} are physiologically linked.

The model is unique because it is fundamentally different from the photo-transduction and the peptide hormone receptor signal transduction models.

CA^{2+}-INDEPENDENT, CO_2 ODORANT ONE-GC SIGNAL TRANSDUCTION MODEL

ONE-GC in addition to being a direct odorant receptor and transducer of uroguanylin possesses an additional intriguing feature. Indirectly, through carbonic anhydrase enzyme it senses atmospheric CO_2 and gets accelerated in its production of cyclic GMP (Hu et al., 2007; Sun et al., 2009).

The study to decipher the biochemical and molecular differences of these two odorant signaling mechanisms demonstrated that (1) in contrast to uroguanylin, CO_2 transduction mechanism is Ca^{2+}-independent. (2) CO_2 transduction site, like that of uroguanylin and neurocalcin δ, resides in the core catalytic domain, aa880–1028, of ONE-GC. (3) The site, however, does not overlap the signature neurocalcin δ domain, ^{908}LSEPIE^{913}. These results demonstrated an additional new transduction mechanism of the membrane guanylate cyclases, which is different from all the previously recognized modes of the membrane guanylate cyclase family.

SUMMATION

This review has briefly chronicled the events that have resulted in the step-by-step development of the field of sensory perceptions linked with the different branches of the Ca^{2+}-modulated ROS-GC transduction systems. Its foundation rests on the initial seminal findings made about five decades ago that cyclic GMP exists in rat urine and is synthesized through the membrane guanylate cyclase enzyme (review: Sharma, 2010). For about a decade, the field passed from the initial euphoria to a complete chaos, when, barring very few, most of the laboratories denied existence of the membrane guanylate cyclase enzyme. The field was kept alive with the efforts of those few. And was ever rekindled with the first purification of a membrane guanylate cyclase, termed ANF-RGC, which, surprisingly, was also a hormone receptor. This resulted in the belief that the membrane guanylate cyclase family is solely comprised of surface receptor guanylate cyclase. The ROS-GC discovery negated that belief and dawned a new era where its new sensory perception-linked transduction mechanisms began to be unfolded. It does so with its remarkable feature of being a two-component transduction system: Ca^{2+} sensor, GCAP or CD-GCAP and the transducer ROS-GC. There are numerous GCAPs and CD-GCAPs; and ROS-GCs. This architecture enables flexibility, yet specificity, for the transduction system to respond to the multitude of Ca^{2+} signals and generate its second messenger cyclic GMP in the sensory neurons. In this "universal Ca^{2+} signal transduction" concept (**Figure 3**) the operation of ROS-GC transduction is delicately controlled by the Ca^{2+} waves generated inside the neurons. It senses intensity of the waves and through its bimodal switch turns itself "on" or "off." Through these and intermediate operations, it precisely controls the production of cyclic GMP, which, in turn, via a nearby CNG channel regulates the hyper- or depolarized state of the neuron membrane. The generated electric potential in this manner becomes a means of transmission of the sensory signals to the brain cortical centers for their perceptions.

ACKNOWLEDGMENTS

The author (Rameshwar K. Sharma) gratefully acknowledges the continuous support for the last four decades by the numerous USPHS awards from the National Institutes of Health, the beginning awards from the National Science Foundation and the Damon Runyon Walter Winchell Cancer fund. The present research is being supported by HL 084584 and HL084584S (Teresa Duda).

REFERENCES

Ames, J. B., Dizhoor, A. M., Ikura, M., Palczewski, K., and Stryer, L. (1999). Three-dimensional structure of guanylyl cyclase activating protein-2, a calcium-sensitive modulator of photoreceptor guanylyl cyclases. *J. Biol. Chem.* 274, 19329–19337.

Behnen, P., Dell'Orco, D., and Koch, K. W. (2010). Involvement of the calcium sensor GCAP1 in hereditary cone dystrophies. *Biol. Chem.* 391, 631–637.

Belluscio, L., Gold, G. H., Nemes, A., and Axel, R. (1998). Mice deficient in G(olf) are anosmic. *Neuron* 20, 69–81.

Braunewell, K. H., and Gundelfinger, E. D. (1999). Intracellular neuronal calcium sensor proteins: a family of EF-hand calcium-binding proteins in search of a function. *Cell Tissue Res.* 295, 1–12.

Breer, H. (2003). Olfactory receptors: molecular basis for recognition and discrimination of odors. *Anal. Bioanal. Chem.* 377, 427–433.

Buck, L. B. (1995). Unraveling chemosensory diversity. *Cell* 83, 349–352.

Burgoyne, R. D. (2007). Neuronal calcium sensor proteins: generating diversity in neuronal Ca2+ signalling. *Nat. Rev. Neurosci.* 8, 182–193.

Burgoyne, R. D., and Weiss, J. L. (2001). The neuronal calcium sensor family of Ca2+-binding proteins. *Biochem. J.* 353, 1–12. Erratum in: *Biochem. J.* 2001, 354, 727.

Burns, M. E., and Baylor, D. A. (2001). Activation, deactivation, and adaptation in vertebrate photoreceptor cells. *Annu. Rev. Neurosci.* 24, 779–805.

Chen, C., Nakatani, K., and Koutalos, Y. (2003). Free magnesium concentration in salamander photoreceptor outer segments. *J. Physiol.* 553, 125–135.

Cooper, N., Liu, L., Yoshida, A., Pozdnyakov, N., Margulis, A., and Sitaramayya, A. (1995). The bovine rod outer segment guanylate cyclase, ROS-GC, is present in both outer segment and synaptic layers of the retina. *J. Mol. Neurosci.* 6, 211–222.

Cuenca, N., Lopez, S., Howes, K., and Kolb, H. (1998). The localization of guanylyl cyclase-activating proteins in the mammalian retina. *Invest. Ophthalmol. Vis. Sci.* 39, 1243–1250.

Dizhoor, A. M., and Hurley, J. B. (1996). Inactivation of EF-hands makes GCAP-2 (p24) a constitutive activator of photoreceptor guanylyl cyclase by preventing a Ca2+-induced "activator-to-inhibitor" transition. *J. Biol. Chem.* 271, 19346–19350.

Dizhoor, A. M., Boikov, S. G., and Olshevskaya, E. V. (1998). Constitutive activation of photoreceptor guanylate cyclase by Y99C mutant of GCAP-1. Possible role in causing human autosomal dominant cone degeneration. *J. Biol. Chem.* 273, 17311–17314.

Dizhoor, A. M., Lowe, D. G., Olshevskaya, E. V., Laura, R. P., and Hurley, J. B. (1994). The human photoreceptor membrane guanylyl cyclase, RetGC, is present in outer segments and is regulated by calcium and a soluble activator. *Neuron* 12, 1345–1352.

Dizhoor, A. M., Olshevskaya, E. V., Henzel, W. J., Wong, S. C., Stults, J. T., Ankoudinova, I., and Hurley, J. B. (1995). Cloning, sequencing, and expression of a 24-kDa Ca(2+)-binding protein activating photoreceptor guanylyl cyclase. *J. Biol. Chem.* 270, 25200–25206.

Dizhoor, A. M., Ray, S., Kumar, S., Niemi, G., Spencer, M., Brolley, D., Walsh, K. A., Philipov, P. P., Hurley, J. B., and Stryer, L. (1991). Recoverin: a calcium sensitive activator of retinal rod guanylate cyclase. *Science* 251, 915–918.

Duda, T., Bharill, S., Wojtas, I., Yadav, P., Gryczynski, I., Gryczynski, Z., and Sharma, R. K. (2009). A trial natriuretic factor receptor guanylate cyclase signaling: new ATP-regulated transduction motif. *Mol. Cell. Biochem.* 324, 39–53.

Duda, T., Fik-Rymarkiewicz, E., Venkataraman, V., Krishnan, A., and Sharma, R. K. (2004). Calcium-modulated ciliary membrane guanylate cyclase transduction machinery: constitution and operational principles. *Mol. Cell. Biochem.* 267, 107–122.

Duda, T., Fik-Rymarkiewicz, E., Venkataraman, V., Krishnan, R., Koch, K. W., and Sharma, R. K. (2005). The calcium-sensor guanylate cyclase activating protein type 2 specific site in rod outer segment membrane guanylate cyclase type 1. *Biochemistry* 44, 7336–7345.

Duda, T., Goraczniak, R., Surgucheva, I., Rudnicka-Nawrot, M., Gorczyca, W. A., Palczewski, K., Sitaramayya, A., Baehr, W., and Sharma, R. K. (1996). Calcium modulation of bovine photoreceptor guanylate cyclase. *Biochemistry* 35, 8478–8482.

Duda, T., Goraczniak, R. M., and Sharma, R. K. (1996). Molecular characterization of S100A1-S100B protein in retina and its activation mechanism of bovine photoreceptor guanylate cyclase. *Biochemistry* 35, 6263–6266.

Duda, T., Goraczniak, R. M., Sitaramayya, A., and Sharma, R. K. (1993). Cloning and expression of an ATP-regulated human retina C-type natriuretic factor receptor guanylate cyclase. *Biochemistry* 32, 1391–1395.

Duda, T., Jankowska, A., Venkataraman, V., Nagele, R. G., and Sharma, R. K. (2001). A novel calcium-regulated membrane guanylate cyclase transduction system in the olfactory neuroepithelium. *Biochemistry* 40, 12067–12077.

Duda, T., and Koch, K. W. (2002). Retinal diseases linked with photoreceptor guanylate cyclase. *Mol. Cell. Biochem.* 230, 129–138.

Duda, T., Koch, K. W., Venkataraman, V., Lange, C., Beyermann, M., and Sharma, R. K. (2002). Ca(2+) sensor S100beta-modulated sites of membrane guanylate cyclase in the photoreceptor-bipolar synapse. *EMBO J.* 21, 2547–2556.

Duda, T., Krishnan, R., and Sharma, R. K. (2006). GCAP1: antithetical calcium sensor of ROS-GC transduction machinery. *Calcium Bind. Proteins* 1, 102–107.

Duda, T., Krishnan, A., Venkataraman, V., Lange, C., Koch, K. W., and Sharma, R. K. (1999). Mutations in the rod outer segment membrane guanylate cyclase in a cone-rod dystrophy cause defects in calcium signaling. *Biochemistry* 38, 13912–13919.

Duda, T., Pertzev, A., and Sharma, R. K. (2011). 657WTAPELL663 motif of the photoreceptor ROS-GC1: a general phototransduction switch. *Biochem. Biophys. Res. Commun.* 408, 236–241.

Duda, T., and Sharma, R. K. (2004). S100B-modulated Ca2+-dependent ROS-GC1 transduction machinery in the gustatory epithelium: a new mechanism in gustatory transduction. *FEBS Lett.* 577, 393–398.

Duda, T., and Sharma, R. K. (2008). ONE-GC membrane guanylate cyclase, a trimodal odorant signal transducer. *Biochem. Biophys. Res. Commun.* 367, 440–445.

Duda, T., and Sharma, R. K. (2009). Ca2+-modulated ONE-GC odorant signal transduction. *FEBS Lett.* 583, 1327–1330.

Duda, T., Venkataraman, V., Goraczniak, R., Lange, C., Koch, K. W., and Sharma, R. K. (1999). Functional consequences of a rod outer segment membrane guanylate cyclase (ROS-GC1) gene mutation linked with Leber's congenital amaurosis. *Biochemistry* 38, 509–515.

Duda, T., Venkataraman, V., Jankowska, A., Lange, C., Koch, K. W., and Sharma, R. K. (2000). Impairment of the rod outer segment membrane guanylate cyclase dimerization in a cone-rod dystrophy results in defective calcium signaling. *Biochemistry* 39, 12522–12533.

Duda, T., Venkataraman, V., Krishnan, A., and Sharma, R. K. (1998). Rod outer segment membrane guanylate cyclase type 1 (ROS-GC1) gene: structure, organization and regulation by phorbol ester, a protein kinase C activator. *Mol. Cell. Biochem.* 189, 63–70.

Duda, T., Venkataraman, V., Krishnan, A., Nagele, R. G., and Sharma, R. K. (2001). Negatively calcium-modulated membrane guanylate cyclase signaling system in the rat olfactory bulb. *Biochemistry* 40, 4654–4662.

Duda, T., Venkataraman, V., and Sharma, R. K. (2007). "Constitution and operational principles of the retinal and odorant-linked neurocalcin δ-dependent Ca2+ modulated ROS-GC transduction machinery," in *Neuronal Calcium Sensor Proteins*. eds P. Philipov and K. W. Koch (New York, NY: Nova Science Publishers, Inc), 91–113.

Frins, S., Bönigk, W., Müller, F., Kellner, R., and Koch, K. W. (1996). Functional characterization of a guanylyl cyclase-activating protein from vertebrate rods. Cloning, heterologous expression, and localization. *J. Biol. Chem.* 271, 8022–8027.

Fülle, H. J., Vassar, R., Foster, D. C., Yang, R. B., Axel, R., and Garbers, D. L. (1995). A receptor guanylyl cyclase expressed specifically in olfactory sensory neurons. *Proc. Natl. Acad. Sci. U.S.A.* 92, 3571–3575.

Garbers, D. L. (1992). Guanylyl cyclase receptors and their endocrine, paracrine, and autocrine ligands. *Cell* 71, 1–4.

Goraczniak, R., Duda, T., and Sharma, R. K. (1997). Structural and functional characterization of a second subfamily member of the calcium-modulated bovine rod outer segment membrane guanylate cyclase, ROS-GC2. *Biochem. Biophys. Res. Commun.* 234, 666–670.

Goraczniak, R. M., Duda, T., and Sharma, R. K. (1998). Calcium modulated signaling site in type 2 rod outer segment membrane guanylate cyclase (ROS-GC2). *Biochem. Biophys. Res. Commun.* 245, 447–453.

Goraczniak, R. M., Duda, T., Sitaramayya, A., and Sharma, R. K. (1994). Structural and functional characterization of the rod outer segment membrane guanylate cyclase. *Biochem. J.* 302, 455–461.

Gorczyca, W. A., Polans, A. S., Surgucheva, I. G., Subbaraya, I., Baehr, W., and Palczewski, K. (1995). Guanylyl cyclase activating protein. A calcium-sensitive regulator of phototransduction. *J. Biol. Chem.* 270, 22029–22036.

Haeseleer, F., Sokal, I., Li, N., Pettenati, M., Rao, N., Bronson, D., Wechter, R., Baehr, W., and Palczewski, K. (1999). Molecular characterization of a third member of the guanylyl cyclase-activating protein subfamily. *J. Biol. Chem.* 274, 6526–6535.

Hayashi, F., and Yamazaki, A. (1991). Polymorphism in purified guanylate cyclase from vertebrate rod photoreceptors. *Proc. Natl. Acad. Sci. U.S.A.* 88, 4746–4750.

Helten, A., and Koch, K. W. (2007). Calcium-dependent conformational changes in guanylate cyclase-activating protein 2 monitored by cysteine accessibility. *Biochem. Biophys. Res. Commun.* 356, 687–692.

Helten, A., Säftel, W., and Koch, K. W. (2007). Expression level and activity profile of membrane bound guanylate cyclase type 2 in rod outer segments. *J. Neurochem.* 103, 1439–1446.

Horio, Y., and Murad, F. (1991a). Solubilization of guanylyl cyclase from bovine rod outer segments and effects of lowering Ca2+ and nitro compounds. *J. Biol. Chem.* 266, 3411–3415.

Horio, Y., and Murad, F. (1991b). Purification of guanylyl cyclase from rod outer segments. *Biochim. Biophys. Acta* 1133, 81–88.

Howes, K. A., Pennesi, M. E., Sokal, I., Church-Kopish, J., Schmidt, B., Margolis, D., Frederick, J. M., Rieke, F., Palczewski, K., Wu, S. M., Detwiler, P. B., and Baehr, W. (2002). GCAP1 rescues rod photoreceptor response in GCAP1/GCAP2 knockout mice. *EMBO J.* 21, 1545–1554.

Hu, J., Zhong, C., Ding, C., Chi, Q., Walz, A., Mombaerts, P., Matsunami, H., and Luo, M. (2007). Detection of near-atmospheric concentrations of CO2 by an olfactory subsystem in the mouse. *Science* 317, 953–957.

Hunt, D. M., Buch, P., and Michaelides, M. (2010). Guanylate cyclases and associated activator proteins in retinal disease. *Mol. Cell. Biochem.* 334, 157–168.

Hurley, J. B., Dizhoor, A. M., Ray, S., and Stryer, L. (1993). Recoverin's role: conclusion withdrawn. *Science* 260, 740.

Hwang, J. Y., and Koch, K. W. (2002a). Calcium- and myristoyl-dependent properties of guanylate cyclase-activating protein-1 and protein-2. *Biochemistry* 41, 13021–13028.

Hwang, J. Y., and Koch, K. W. (2002b). The myristoylation of the neuronal Ca2+-sensors guanylate cyclase-activating protein 1 and 2. *Biochim. Biophys. Acta* 1600, 111–117.

Hwang, J. Y., Lange, C., Helten, A., Höppner-Heitmann, D., Duda, T., Sharma, R. K., and Koch, K. W. (2003). Regulatory modes of rod outer segment membrane guanylate cyclase differ in catalytic efficiency and Ca(2+)-sensitivity. *Eur. J. Biochem.* 270, 3814–3821.

Hwang, J. Y., Schlesinger, R., and Koch, K. W. (2004). Irregular dimerization of guanylate cyclase-activating protein 1 mutants causes loss of target activation. *Eur. J. Biochem.* 271, 3785–3793.

Imanishi, Y., Li, N., Sokal, I., Sowa, M. E., Lichtarge, O., Wensel, T. G., Saperstein, D. A., Baehr, W., and Palczewski, K. (2002).

Characterization of retinal guanylate cyclase-activating protein 3 (GCAP3) from zebrafish to man. *Eur. J. Neurosci.* 15, 63–78.

Imanishi, Y., Yang, L., Sokal, I., Filipek, S., Palczewski, K., and Baehr, W. (2004). Diversity of guanylate cyclase-activating proteins (GCAPs) in teleost fish: characterization of three novel GCAPs (GCAP4, GCAP5, GCAP7) from zebrafish (*Danio rerio*) and prediction of eight GCAPs (GCAP1-8) in pufferfish (*Fugu rubripes*). *J. Mol. Evol.* 59, 204–217.

Jankowska, A., Burczyńska, B., Duda, T., and Warchol, J. B. (2010). Rod outer segment membrane guanylate cyclase type 1 (ROS-GC1) calcium-modulated transduction system in the sperm. *Fertil. Steril.* 93, 904–912.

Jankowska, A., Burczynska, B., Duda, T., Warchol, J. B., and Sharma, R. K. (2007). Calcium-modulated rod outer segment membrane guanylate cyclase type 1 transduction machinery in the testes. *J. Androl.* 28, 50–58.

Jankowska, A., and Warchol, J. B. (2010). Ca(2+)-modulated membrane guanylate cyclase in the testes. *Mol. Cell. Biochem.* 334, 169–179.

Juilfs, D. M., Fülle, H. J., Zhao, A. Z., Houslay, M. D., Garbers, D. L., and Beavo, J. A. (1997). A subset of olfactory neurons that selectively express cGMP-stimulated phosphodiesterase (PDE2) and guanylyl cyclase-D define a unique olfactory signal transduction pathway. *Proc. Natl. Acad. Sci. U.S.A.* 94, 3388–3395.

Kachi, S., Nishizawa, Y., Olshevskaya, E., Yamazaki, A., Miyake, Y., Wakabayashi, T., Dizhoor, A., and Usukura, J. (1999). Detailed localization of photoreceptor guanylate cyclase activating protein-1 and -2 in mammalian retinas using light and electron microscopy. *Exp. Eye Res.* 68, 465–473.

Kelsell, R. E., Gregory-Evans, K., Payne, A. M., Perrault, I., Kaplan, J., Yang, R. B., Garbers, D. L., Bird, A. C., Moore, A. T., and Hunt, D. M. (1998). Mutations in the retinal guanylate cyclase (RETGC-1) gene in dominant cone-rod dystrophy. *Hum. Mol. Genet.* 7, 1179–1184.

Kitiratschky, V. B., Behnen, P., Kellner, U., Heckenlively, J. R., Zrenner, E., Jägle, H., Kohl, S., Wissinger, B., and Koch, K. W. (2009). Mutations in the GUCA1A gene involved in hereditary cone dystrophies impair calcium-mediated regulation of guanylate cyclase. *Hum. Mutat.* 30, 782–796.

Koch, K. W. (1991). Purification and identification of photoreceptor guanylate cyclase. *J. Biol. Chem.* 266, 8634–8637.

Koch, K. W. (2006). GCAPs, the classical neuronal calcium sensors in the retina : a Ca2+ relay model of guanylate cyclase activation. *Calcium Bind. Proteins* 1, 3–6.

Koch, K. W., and Stryer, L. (1988). Highly cooperative feedback control of retinal rod guanylate cyclase by calcium ions. *Nature* 334, 64–66.

Koch, K. W., Duda, T., and Sharma, R. K. (2002). Photoreceptor specific guanylate cyclases in vertebrate phototransduction. *Mol. Cell. Biochem.* 230, 97–106.

Koch, K. W., Duda, T., and Sharma, R. K. (2010). Ca(2+)-modulated vision-linked ROS-GC guanylate cyclase transduction machinery. *Mol. Cell. Biochem.* 334, 105–115.

Koutalos, Y., Nakatani, K., Tamura, T., and Yau, K. W. (1995). Characterization of guanylate cyclase activity in single retinal rod outer segments. *J. Gen. Physiol.* 106, 863–890.

Krishnan, A., Duda, T., Pertzev, A., Kobayashi, M., Takamatsu, K., and Sharma, R. K. (2009). Hippocalcin, new Ca(2+) sensor of a ROS-GC subfamily member, ONE-GC, membrane guanylate cyclase transduction system. *Mol. Cell. Biochem.* 325, 1–14.

Krishnan, A., Goraczniak, R. M., Duda, T., and Sharma, R. K. (1998). Third calcium-modulated rod outer segment membrane guanylate cyclase transduction mechanism. *Mol. Cell. Biochem.* 178, 251–259.

Krishnan, A., Venkataraman, V., Fik-Rymarkiewicz, E., Duda, T., and Sharma, R. K. (2004). Structural, biochemical, and functional characterization of the calcium sensor neurocalcin delta in the inner retinal neurons and its linkage with the rod outer segment membrane guanylate cyclase transduction system. *Biochemistry* 43, 2708–2723.

Krizaj, D., and Copenhagen, D. R. (2002). Calcium regulation in photoreceptors. *Front. Biosci.* 7, d2023–d2044.

Kumar, V. D., Vijay-Kumar, S., Krishnan, A., Duda, T., and Sharma, R. K. (1999). A second calcium regulator of rod outer segment membrane guanylate cyclase, ROS-GC1: neurocalcin. *Biochemistry* 38, 12614–12620.

Kutty, R. K., Fletcher, R. T., Chader, G. J., and Krishna, G. (1992). Expression of guanylate cyclase-A mRNA in the rat retina: detection using polymerase chain reaction. *Biochem. Biophys. Res. Commun.* 182, 851–857.

Ladant, D. (1995). Calcium and membrane binding properties of bovine neurocalcin delta expressed in Escherichia coli. *J. Biol. Chem.* 270, 3179–3185.

Lai, P. C., Singer, M. S., and Crasto, C. J. (2005). Structural activation pathways from dynamic olfactory receptor-odorant interactions. *Chem. Senses.* 30, 781–792.

Lange, C., Duda, T., Beyermann, M., Sharma, R. K., and Koch, K. W. (1999). Regions in vertebrate photoreceptor guanylyl cyclase ROS-GC1 involved in Ca(2+)-dependent regulation by guanylyl cyclase-activating protein GCAP-1. *FEBS Lett.* 460, 27–31.

Leinders-Zufall, T., Cockerham, R. E., Michalakis, S., Biel, M., Garbers, D. L., Reed, R. R., Zufall, F., and Munger, S. D. (2007). Contribution of the receptor guanylyl cyclase GC-D to chemosensory function in the olfactory epithelium. *Proc. Natl. Acad. Sci. U.S.A.* 104, 14507–14512.

Lim, S., Peshenko, I., Dizhoor, A., and Ames, J. B. (2009). Effects of Ca2+, Mg2+, and myristoylation on guanylyl cyclase activating protein 1 structure and stability. *Biochemistry* 48, 850–862.

Liu, X., Seno, K., Nishizawa, Y., Hayashi, F., Yamazaki, A., Matsumoto, H., Wakabayashi, T., and Usukura, J. (1994). Ultrastructural localization of retinal guanylate cyclase in human and monkey retinas. *Exp. Eye Res.* 59, 761–768.

Lowe, D. G., Dizhoor, A. M., Liu, K., Gu, Q., Spencer, M., Laura, R., Lu, L., and Hurley, J. B. (1995). Cloning and expression of a second photoreceptor-specific membrane retina guanylyl cyclase (RetGC), RetGC-2. *Proc. Natl. Acad. Sci. U.S.A.* 92, 5535–5539.

Luo, D. G., Xue, T., and Yau, K. W. (2008). How vision begins: an odyssey. *Proc. Natl. Acad. Sci. U.S.A.* 105, 9855–9862.

Makino, C. L., Dodd, R. L., Chen, J., Burns, M. E., Roca, A., Simon, M. I., and Baylor, D. A. (2004). Recoverin regulates light-dependent phosphodiesterase activity in retinal rods. *J. Gen. Physiol.* 123, 729–741. Erratum in: *J. Gen. Physiol.* 2005, 126, 81.

Margulis, A., Goraczniak, R. M., Duda, T., Sharma, R. K., and Sitaramayya, A. (1993). Structural and biochemical identity of retinal rod outer segment membrane guanylate cyclase. *Biochem. Biophys. Res. Commun.* 194, 855–861.

Margulis, A., Pozdnyakov, N., and Sitaramayya, A. (1996). Activation of bovine photoreceptor guanylate cyclase by S100 proteins. *Biochem. Biophys. Res. Commun.* 218, 243–247.

McCue, H. V., Haynes, L. P., and Burgoyne, R. D. (2010). The diversity of calcium sensor proteins in the regulation of neuronal function. *Cold Spring Harb. Perspect. Biol.* 2, a004085.

Meyer, M. R., Angele, A., Kremmer, E., Kaupp, U. B., and Muller, F. (2000). A cGMP-signaling pathway in a subset of olfactory sensory neurons. *Proc. Natl. Acad. Sci. U.S.A.* 97, 10595–10600.

Nef, P. (1996). "Guidebook to the calcium-binding proteins," in *Guidebook to Calcium Sensor Proteins*, ed M. R. Celio (Oxford: Oxford University Press), 94.

Newbold, R. J., Deery, E. C., Walker, C. E., Wilkie, S. E., Srinivasan, N., Hunt, D. M., Bhattacharya, S. S., and Warren, M. J. (2001). The destabilization of human GCAP1 by a proline to leucine mutation might cause cone-rod dystrophy. *Hum. Mol. Genet.* 10, 47–54.

Okazaki, K., Watanabe, M., Ando, Y., Hagiwara, M., Terasawa, M., and Hidaka, H. (1992). Full sequence of neurocalcin, a novel calcium-binding protein abundant in central nervous system. *Biochem. Biophys. Res. Commun.* 185, 147–153.

Olshevskaya, E. V., Ermilov, A. N., and Dizhoor, A. M. (1999). Dimerization of guanylyl cyclase-activating protein and a mechanism of photoreceptor guanylyl cyclase activation. *J. Biol. Chem.* 274, 25583–25587.

Olshevskaya, E. V., Hughes, R. E., Hurley, J. B., and Dizhoor, A. M. (1997). Calcium binding, but not a calcium-myristoyl switch, controls the ability of guanylyl cyclase-activating protein GCAP-2 to regulate photoreceptor guanylyl cyclase. *J. Biol. Chem.* 272, 14327–14333.

Otto-Bruc, A., Fariss, R. N., Haeseleer, F., Huang, J., Buczylko, J., Surgucheva, I., Baehr, W., Milam, A. H., and Palczewski, K. (1997). Localization of guanylate cyclase-activating protein 2 in mammalian

retinas. *Proc. Natl. Acad. Sci. U.S.A.* 94, 4727–4732.

Palczewski, K., Subbaraya, I., Gorczyca, W. A., Helekar, B. S., Ruiz, C. C., Ohguro, H., Huang, J., Zhao, X., Crabb, J. W., Johnson, R. S., and Baehr, W. (1994). Molecular cloning and characterization of retinal photoreceptor guanylyl cyclase-activating protein. *Neuron* 13, 395–404.

Perrault, I., Rozet, J. M., Calvas, P., Gerber, S., Camuzat, A., Dollfus, H., Châtelin, S., Souied, E., Ghazi, I., Leowski, C., Bonnemaison, M., Le Paslier, D., Frézal, J., Dufier, J. L., Pittler, S., Munnich, A., and Kaplan, J. (1996). Retinal-specific guanylate cyclase gene mutations in Leber's congenital amaurosis. *Nat. Genet.* 14, 461–464.

Peshenko, I. V., and Dizhoor, A. M. (2004). Guanylyl cyclase-activating proteins (GCAPs) are Ca^{2+}/Mg^{2+} sensors: implications for photoreceptor guanylyl cyclase (RetGC) regulation in mammalian photoreceptors. *J. Biol. Chem.* 279, 16903–16906.

Peshenko, I. V., and Dizhoor, A. M. (2006). Ca^{2+} and Mg2+ binding properties of GCAP-1. Evidence that Mg2+-bound form is the physiological activator of photoreceptor guanylyl cyclase. *J. Biol. Chem.* 281, 23830–23841.

Peshenko, I. V., and Dizhoor, A. M. (2007). Activation and inhibition of photoreceptor guanylyl cyclase by guanylyl cyclase activating protein 1 (GCAP-1): the functional role of Mg2+/Ca2+ exchange in EF-hand domains. *J. Biol. Chem.* 282, 21645–21652.

Peshenko, I. V., Olshevskaya, E. V., Savchenko, A. B., Karan, S., Palczewski, K., Baehr, W., and Dizhoor, A. M. (2011). Enzymatic properties and regulation of the native isozymes of retinal membrane guanylyl cyclase (RetGC) from mouse photoreceptors. *Biochemistry* 50, 5590–5600.

Philippov, P. P., Senin, I. I., and Koch, K. W. (2007). "Recoverin: a calcium-dependent regulator of the visual transduction," in *Neuronal Calcium Sensor Proteins*, eds P. Philipov and K. W. Koch (New York, NY: Nova Science Publishers, Inc), 139–151.

Pinching, A. J., and Powell, T. P. (1971). The neuropil of the periglomerular region of the olfactory bulb. *J. Cell. Sci.* 9, 379–409.

Pittler, S., Munnich, A., and Kaplan, J. (1996). Retinal-specific guanylate cyclase gene mutations in Leber's congenital amaurosis. *Nat. Genet.* 14, 461–464.

Pozdnyakov, N., Goraczniak, R., Margulis, A., Duda, T., Sharma, R. K., Yoshida, A., and Sitaramayya, A. (1997). Structural and functional characterization of retinal calcium-dependent guanylate cyclase activator protein (CD-GCAP): identity with S100beta protein. *Biochemistry* 36, 14159–14166.

Pozdnyakov, N., Yoshida, A., Cooper, N. G., Margulis, A., Duda, T., Sharma, R. K., and Sitaramayya, A. (1995). A novel calcium-dependent activator of retinal rod outer segment membrane guanylate cyclase. *Biochemistry* 34, 14279–14283.

Pugh, E. N. Jr., and Cobbs, W. H. (1986). Visual transduction in vertebrate rods and cones: a tale of two transmitters, calcium and cyclic GMP. *Vision Res.* 26, 1613–1643.

Pugh, E. N. Jr., Duda, T., Sitaramayya, A., and Sharma, R. K. (1997). Photoreceptor guanylate cyclases: a review. *Biosci. Rep.* 17, 429–473.

Pugh, E. N. Jr., Nikonov, S., and Lamb, T. D. (1999). Molecular mechanisms of vertebrate photoreceptor light adaptation. *Curr. Opin. Neurobiol.* 9, 410–418.

Ramamurthy, V., Tucker, C., Wilkie, S. E., Daggett, V., Hunt, D. M., and Hurley, J. B. (2001). Interactions within the coiled-coil domain of RetGC-1 guanylyl cyclase are optimized for regulation rather than for high affinity. *J. Biol. Chem.* 276, 26218–26229.

Rätscho, N., Scholten, A., and Koch, K. W. (2010). Diversity of sensory guanylate cyclases in teleost fishes. *Mol. Cell. Biochem.* 334, 207–214.

Sharma, R. K. (2002). Evolution of the membrane guanylate cyclase transduction system. *Mol. Cell. Biochem.* 230, 3–30.

Sharma, R. K. (2010). Membrane guanylate cyclase is a beautiful signal transduction machine: overview. *Mol. Cell. Biochem.* 334, 3–36.

Sharma, R. K., and Duda, T. (2006). Calcium sensor neurocalcin d-modulated ROS-GCtransduction machinery in the retinal and olfactory neurons. *Calcium Bind. Proteins* 1, 7–11.

Sharma, R. K., and Duda, T. (2010). ROS-GC subfamily membrane guanylate cyclase-linked transduction systems: taste, pineal gland and hippocampus. *Mol. Cell. Biochem.* 334, 199–206.

Sharma, R. K., Duda, T., Venkataraman, V., and Koch, K. W. (2004). Calcium modulated mammalian membrane guanylate cyclase ROS-GC transduction machinery in sensory neurons. *Curr. Topics Biochem. Res.* 322, 111–144.

Shepherd, G. M., and Greer, C. A. (1998). "Olfactory bulb," in *The Synaptic Organization Of The Brain,* ed G. M. Shepherd (New York, NY: Oxford University Press), 159–203.

Shyjan, A. W., de Sauvage, F. J., Gillett, N. A., Goeddel, D. V., and Lowe, D. G. (1992). Molecular cloning of a retina-specific membrane guanylyl cyclase. *Neuron* 9, 727–737.

Sokal, I., Li, N., Surgucheva, I., Warren, M. J., Payne, A. M., Bhattacharya, S. S., Baehr, W., and Palczewski, K. (1998). GCAP1 (Y99C) mutant is constitutively active in autosomal dominant cone dystrophy. *Mol. Cell.* 2, 129–133.

Sokal, I., Otto-Bruc, A. E., Surgucheva, I., Verlinde, C. L., Wang, C. K., Baehr, W., and Palczewski, K. (1999). Conformational changes in guanylyl cyclase-activating protein 1 (GCAP1) and its tryptophan mutants as a function of calcium concentration. *J. Biol. Chem.* 274, 19829–19837.

Stephen, R., Bereta, G., Golczak, M., Palczewski, K., and Sousa, M. C. (2007). Stabilizing function for myristoyl group revealed by the crystal structure of a neuronal calcium sensor, guanylate cyclase-activating protein 1. *Structure* 15, 1392–1402.

Stephen, R., Filipek, S., Palczewski, K., and Sousa, M. C. (2008). Ca2+-dependent regulation of phototransduction. *Photochem. Photobiol.* 84, 903–910.

Stryer, L. (1986). Cyclic GMP cascade of vision. *Annu. Rev. Neurosci.* 9, 87–119.

Stryer, L. (1991). Visual excitation and recovery. *J. Biol. Chem.* 266, 10711–10714.

Subbaraya, I., Ruiz, C. C., Helekar, B. S., Zhao, X., Gorczyca, W. A., Pettenati, M. J., Rao, P. N., Palczewski, K., and Baehr, W. (1994). Molecular characterization of human and mouse photoreceptor guanylate cyclase-activating protein (GCAP) and chromosomal localization of the human gene. *J. Biol. Chem.* 269, 31080–31089.

Sun, L., Wang, H., Hu, J., Han, J., Matsunami, H., and Luo, M. (2009). Guanylyl cyclase-D in the olfactory CO2 neurons is activated by bicarbonate. *Proc. Natl. Acad. Sci. U.S.A.* 106, 2041–2046.

Terasawa, M., Nakano, A., Kobayashi, R., and Hidaka, H. (1992). Neurocalcin: a novel calcium-binding protein from bovine brain. *J. Biol. Chem.* 267, 19596–19599.

Tucker, C. L., Woodcock, S. C., Kelsell, R. E., Ramamurthy, V., Hunt, D. M., and Hurley, J. B. (1999). Biochemical analysis of a dimerization domain mutation in RetGC-1 associated with dominant cone-rod dystrophy. *Proc. Natl. Acad. Sci. U.S.A.* 96, 9039–9044.

Venkataraman, V., Duda, T., Ravichandran, S., and Sharma, R. K. (2008). Neurocalcin delta modulation of ROS-GC1, a new model of Ca(2+) signaling. *Biochemistry* 47, 6590–6601.

Venkataraman, V., Duda, T., and Sharma, R. K. (1998). The alpha(2D/A)-adrenergic receptor-linked membrane guanylate cyclase: a new signal transduction system in the pineal gland. *FEBS Lett.* 427, 69–73.

Venkataraman, V., Duda, T., Vardi, N., Koch, K. W., and Sharma, R. K. (2003). Calcium-modulated guanylate cyclase transduction machinery in the photoreceptor–bipolar synaptic region. *Biochemistry* 42, 5640–5648.

Venkataraman, V., Nagele, R., Duda, T., and Sharma, R. K. (2000). Rod outer segment membrane guanylate cyclase type 1-linked stimulatory and inhibitory calcium signaling systems in the pineal gland: biochemical, molecular, and immunohistochemical evidence. *Biochemistry* 39, 6042–6052.

Venkatesan, J. K., Natarajan, S., Schwarz, K., Mayer, S. I., Alpadi, K., Magupalli, V. G., Sung, C. H., and Schmitz, F. (2010). Nicotinamide adenine dinucleotide-dependent binding of the neuronal Ca2+ sensor protein GCAP2 to photoreceptor synaptic ribbons. *J. Neurosci.* 30, 6559–6576.

Vijay-Kumar, S., and Kumar, V. D. (1999). Crystal structure of recombinant bovine neurocalcin. *Nat. Struct. Biol.* 6, 80–88.

Wensel, T. G. (2008). Signal transducing membrane complexes of photoreceptor outer segments. *Vis. Res.* 48, 2052–2061.

Wilkie, S. E., Li, Y., Deery, E. C., Newbold, R. J., Garibaldi, D., Bateman, J. B., Zhang, H., Lin, W., Zack, D. J., Bhattacharya, S. S., Warren, M. J., Hunt, D. M., and Zhang, K. (2001). Identification and functional consequences of a new mutation (E155G) in the gene for GCAP1 that causes autosomal

dominant cone dystrophy. *Am. J. Hum. Genet.* 69, 471–480.

Wilson, E. M., and Chinkers, M. (1995). Identification of sequences mediating guanylyl cyclase dimerization. *Biochemistry* 34, 4696–4701.

Zozulya, S., and Stryer, L. (1992). Calcium-myristoyl protein switch. *Proc. Natl. Acad. Sci. U.S.A.* 89, 11569–11573.

Zufall, F., and Munger, S. D. (2010). Receptor guanylyl cyclases in mammalian olfactory function. *Mol. Cell. Biochem.* 33, 191–197.

Conflict of Interest Statement: The authors declare that the research was conducted in the absence of any commercial or financial relationships that could be construed as a potential conflict of interest.

Received: 08 February 2012; accepted: 20 March 2012; published online: 09 April 2012.

*Citation: Sharma RK and Duda T (2012) Ca^{2+}-sensors and ROS-GC: interlocked sensory transduction elements: a review. Front. Mol. Neurosci. **5**:42. doi: 10.3389/fnmol.2012.00042*

frontiers in
MOLECULAR NEUROSCIENCE

REVIEW ARTICLE
published: 29 February 2012
doi: 10.3389/fnmol.2012.00026

EF hand-mediated Ca^{2+}- and cGMP-signaling in photoreceptor synaptic terminals

Frank Schmitz*, Sivaraman Natarajan, Jagadeesh K. Venkatesan†, Silke Wahl, Karin Schwarz and Chad P. Grabner*

Department of Neuroanatomy, Medical School Homburg/Saar, Institute for Anatomy and Cell Biology, Saarland University, Saarland, Germany

Edited by:
Karl-Wilhelm Koch, Carl von Ossietzky University Oldenburg, Germany

Reviewed by:
Karl-Wilhelm Koch, Carl von Ossietzky University Oldenburg, Germany
Florentina Soto, Washington University in St. Louis, USA

****Correspondence:***
Frank Schmitz and Chad P. Grabner, Department of Neuroanatomy, Medical School Homburg/Saar, Institute for Anatomy and Cell Biology, Saarland University, Kirrbergerstrasse, University Campus, 66421 Homburg/Saar, Germany.
e-mail: frank.schmitz@uks.eu; chadgrabner@gmail.com

†Present Address:
Department of Experimental Orthopedics, Saarland University, University Hospital of Orthopedics, Homburg/Saar, Germany.

Photoreceptors, the light-sensitive receptor neurons of the retina, receive and transmit a plethora of visual informations from the surrounding world. Photoreceptors capture light and convert this energy into electrical signals that are conveyed to the inner retina. For synaptic communication with the inner retina, photoreceptors make large active zones that are marked by synaptic ribbons. These unique synapses support continuous vesicle exocytosis that is modulated by light-induced, graded changes of membrane potential. Synaptic transmission can be adjusted in an activity-dependent manner, and at the synaptic ribbons, Ca^{2+}- and cGMP-dependent processes appear to play a central role. EF-hand-containing proteins mediate many of these Ca^{2+}- and cGMP-dependent functions. Since continuous signaling of photoreceptors appears to be prone to malfunction, disturbances of Ca^{2+}- and cGMP-mediated signaling in photoreceptors can lead to visual defects, retinal degeneration (rd), and even blindness. This review summarizes aspects of signal transmission at the photoreceptor presynaptic terminals that involve EF-hand-containing Ca^{2+}-binding proteins.

Keywords: photoreceptor, ribbon synapse, synaptic ribbon, GCAP, RIBEYE, CaBP4, $Ca_V1.4$ calcium channel, EF-hands

INTRODUCTION

Vision belongs to the most important senses of the human body. The light-sensitive retina within our eyes screens the optical world around us and transmits this information to the brain. At the beginning of the complex task of visual perception, photoreceptors physically detect light energy and transmit the information to the inner retina where further processing takes place. The retina employs two different classes of photoreceptors, rod and cones, to begin sorting out different components of light. Rod photoreceptors are specialized to operate at the lowest level of light, single photon detection, and are thus saturated in daylight (Pahlberg and Sampath, 2011). Cone photoreceptors mediate color vision and operate at higher light intensities. In primates, e.g., humans, three different types of cones with long (L)-, medium (M)-, and short (S)- wavelength sensitivities provide color vision; simpler, non-primate mammals, e.g., mice, are dichromatic and possess only two types of cones (L-S-cones, for review, see Abramov and Gordon, 1994).

Mammalian photoreceptors in general are slender, highly polarized neurons with a bipolar morphology (**Figure 1**). The outer segment (OS) is the distal process that contacts the pigment epithelium and this is where phototransduction takes place. At the molecular level, phototransduction principally occurs via a light-induced transduction cascade that finally leads to closure of cGMP-gated cation channels (CNG-channels; cyclic nucleotide-gated (CNG) channels) which causes the cell to hyperpolarize from about −35 mV to −40 mV in the dark to about −70 mV in very bright light (for review, see Burns and Baylor, 2001; Chen, 2005). At the "opposite" (vitread) end of the photoreceptor, the presynaptic terminal transmits the light information to dendrites of secondary neurons, bipolar, and horizontal cells (**Figures 1A,B**). The vast array of light information detected by the photoreceptor OS must be transmitted at the first synapse

Abbreviations: NCS, neuronal Ca^{2+}-sensor proteins; ROS-GC rod outer segment guanylate cyclase; GC, guanylate cyclase; OS, outer segments; IS, inner segments; OPL, outer plexiform layer (containing photoreceptor ribbon synapses); PDE6, cGMP phosphodiesterase 6; CNG, cyclic nucleotide-gated; CNG channel, cyclic nucleotide-gated channel; HCN channel, hyperpolarization-activated, cyclic nucleotide-gated channel; LTCC, L-type calcium channels; VGCC, voltage-gated calcium channels; CSNB, congenital stationary night blindness; GCAP, guanylate cyclase-activating protein; $[Ca^{2+}]_i$ cytoplasmic concentration of free Ca^{2+}; ER, endoplasmic reticulum; CDI, calcium-dependent inactivation; VDI, voltage-dependent inactivation; KHD, kinase homology domain; CTR, carboxy-terminal region; LCA, Leber congenital amaurosis; CORD, cone-rod dystrophy; ON-bipolar cells, bipolar cells that depolarize in response to illumination; OFF-bipolar cells, bipolar cells that hyperpolarize in response to illumination; ERG, electroretinogram; KO, knockout; SIM, structured illumination microscopy.

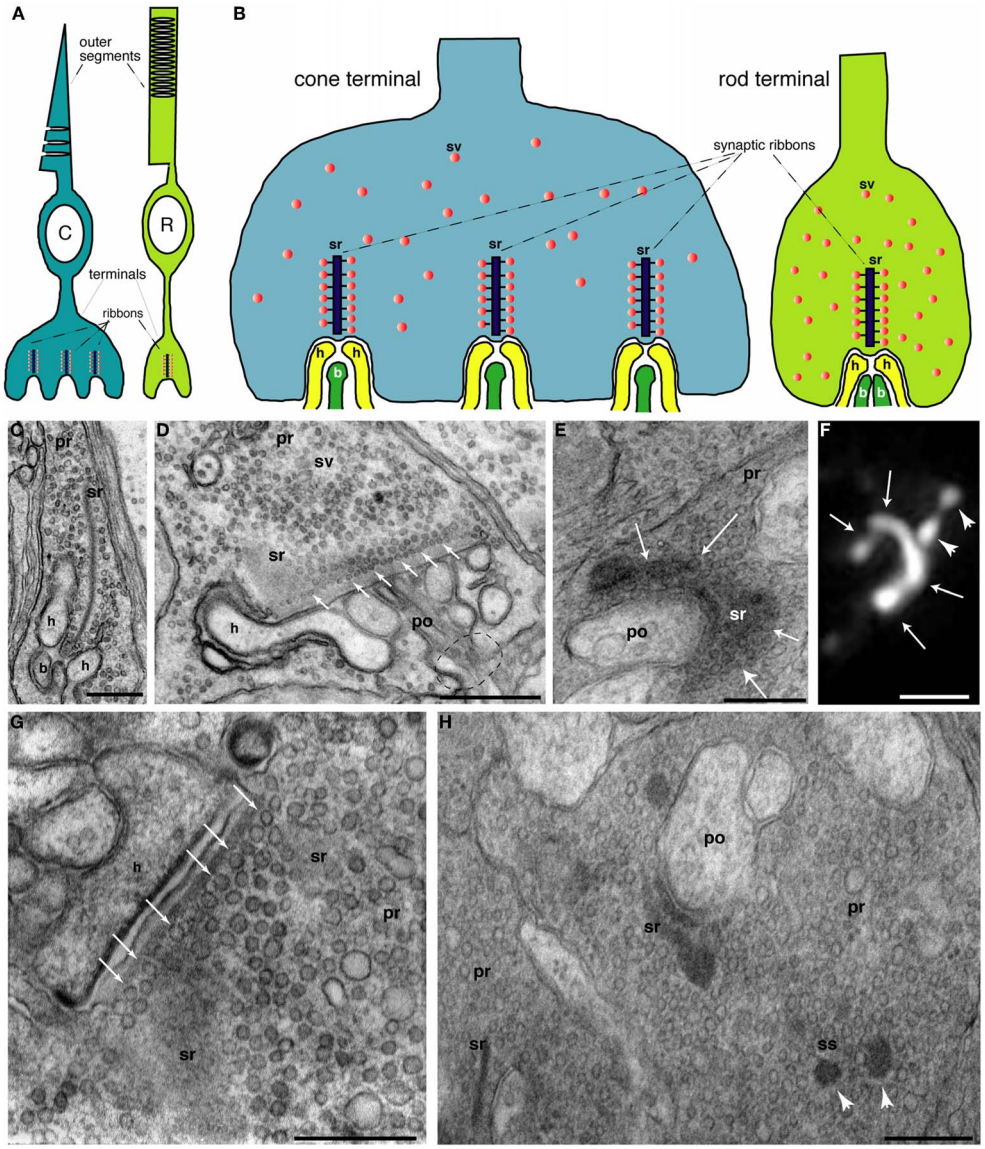

FIGURE 1 | (A) Schematic, simplified drawing of rod (R) and cone (C) photoreceptors. Outer segments (OS) in which phototransduction occurs are depicted as well as the presynaptic terminal where light information is passed from photoreceptors to the secondary neurons, bipolar, and horizontal cells (depicted in yellow and dark green colors in **Figure 1B**). Subcellular details of photoreceptors including the inner segments were omitted for sake of clarity. **(B)** Schematic, simplified drawing of rod and cone photoreceptor presynaptic terminals. Rod synapses possess only a single, large active zone with a single synaptic ribbon (sr) whereas cones possess multiple active zones (20–50). Only invaginating ribbon synapses are depicted. Non-invaginating, non-ribbon type synapses (Regus-Leidig and Brandstätter, 2011) are not shown. **(C–E, G–H)** Electron micrographs of photoreceptor terminals. **(C)** Shows a cross-sectioned ribbon (sr) with its typical bar-shaped appearance in a rod terminal. The synaptic ribbon is associated with large numbers of synaptic vesicles (sv) **(D)**. The rod photoreceptor in **(D)** is largely sectioned parallel to the plate-like synaptic ribbon. In the left part, the section passes through the synaptic ribbon (sr); more to the right, the plane of section is parallel, but close to the plate-like synaptic ribbon. Many docked synaptic vesicles can be observed at the base of the synaptic ribbon (small white arrows). The dashed circle indicates the site where the postsynaptic dendrites enter the postsynaptic cavity formed by the invagination of the presynaptic photoreceptor terminal. **(E)** Also shows a tangential view of the synaptic ribbon. The plate-like character of the ribbon is visible. White arrows denote the ribbon plate which is bended along the presynaptic plasma membrane in a horseshoe-like manner. The horseshoe-shaped appearance of the synaptic ribbon can be also visualized by immunolabeling with anti-RIBEYE antibodies and super-resolution, structured illumination microscopy (SIM) (white arrows in **F**). White arrowheads in **(F)** show spherical synaptic spheres (ss), intermediate structures in the assembly and disassembly of plate-shaped synaptic ribbons [see also below; in **(H)**; for review, see Schmitz (2009)]. Figure **(G)** demonstrates many docked synaptic vesicles at the base of the synaptic ribbon (white arrows) which are probably readily releasable. **(H)** Electron micrograph of an immature, developing terminal from the early, postnatal mouse retina (postnatal day 6). The ribbon complex is not yet fully assembled. Besides bar-shaped ribbons (sr), spherical precursors of synaptic ribbons, the synaptic spheres (ss), are also present in the presynaptic terminal. Abbreviations: C, cone photoreceptor; R, rod photoreceptor; sr, synaptic ribbon; ss, synaptic spheres; sv, synaptic vesicle; pr, presynaptic terminal; po, postsynaptic dendrite; h, horizontal cell postsynaptic dendrite; b, bipolar cell postsynaptic dendrite. Scale bars: 400 nm **(C)**; 800 nm **(D)**; 320 nm **(E)**; 1 μm **(F)**, 400 nm **(G)**, 500 nm **(H)**.

of the visual system, the photoreceptor synapse (for review, see Wässle, 2004; Heidelberger et al., 2005; Schmitz, 2009; Matthews and Fuchs, 2010; Regus-Leidig and Brandstätter, 2011).

STRUCTURAL AND FUNCTIONAL SPECIALIZATIONS OF PHOTORECEPTOR RIBBON SYNAPSES: A SYNAPSE TUNED FOR PHASIC AND CONTINUOUS RELEASE

Both types of photoreceptors, rods, and cones, form ribbon synapses to communicate with their secondary neurons, i.e., bipolar and horizontal cells in the outer plexiform layer of the retina. In mammals, ribbon synapses are also made by retinal bipolar cells, photoreceptor-like neurons in the pineal gland as well as auditory and vestibular hair cells (Schmitz, 2009; Matthews and Fuchs, 2010; Regus-Leidig and Brandstätter, 2011). Ribbon synapses are characterized by large, electron-dense structures, the synaptic ribbons (**Figure 1**; for review, see Schmitz, 2009). Synaptic ribbons in photoreceptor synapses are plate-like structures which appear bar-shaped in electron micrographs if cross-sectioned (**Figure 1**; Schmitz, 2009). In rod synapses, typically one synaptic ribbon is contained at a single active zone; in cone synapses 20–50 active zones are present with each usually containing one synaptic ribbon (Wässle, 2004; Regus-Leidig and Brandstätter, 2011). In hair cell ribbon synapses, most synaptic ribbons are spherical in shape (for review, see Matthews and Fuchs, 2010). The synaptic ribbon is associated along its entire surface area with a large number of synaptic vesicles that are filled with the neurotransmitter glutamate. It is anchored at the active zone of the presynaptic plasma membrane; in photoreceptors via the electron-dense arciform density (for review, see Schmitz, 2009; Matthews and Fuchs, 2010; Regus-Leidig and Brandstätter, 2011). RIBEYE is the major component of synaptic ribbons (Schmitz et al., 2000; Magupalli et al., 2008; Schmitz, 2009; Uthaiah and Hudspeth, 2010). It consists of a large and unique aminoterminal A-domain, and a carboxyterminal B-domain which is largely identical with the nuclear co-repressor C-terminal-binding protein 2 (CtBP2). The B-domain/CtBP2 and a related protein, CtBP1, have developed from a family of dehydrogenases and both specifically bind NAD(H) (for review, see Schmitz, 2009).

Typically, ribbon synapses do not respond to bursts of action potentials but are specialized to transmit a large bandwidth of stimulus intensities via fine, graded changes in membrane potential. To report even small changes of receptor potential in response to differing light stimuli, ribbon synapses modulate the rate of tonic vesicle exocytosis (for review, see Heidelberger et al., 2005; Matthews and Fuchs, 2010; Wan and Heidelberger, 2011). Photoreceptor terminals may contain up to several hundred thousands of highly motile synaptic vesicles depending upon the species and type of synapse (for review, see Schmitz, 2009; Matthews and Fuchs, 2010), which support the high basal synaptic vesicle turnover driven by the synaptic ribbon (**Figure 1**). Various studies, mostly done with fish retinal bipolar cells, indicated that ribbon-associated vesicles are primed and readily-releasable (for review, see Heidelberger et al., 2005; Matthews and Fuchs, 2010; Wan and Heidelberger, 2011). Synaptic ribbons were proposed to capture and prime synaptic vesicles for immediate release. By this way of thinking, the synaptic ribbons would provide a battery of ready-to-go vesicles that could support continuous release for extended periods of time (Jackman et al., 2009). Synaptic ribbons are hot spots of exocytosis as visualized with TIRF-microscopy (Zenisek et al., 2000), and more recently by the analyses of terminals with photodamaged synaptic ribbons that showed strongly depressed release (Snellman et al., 2011). At the base of the synaptic ribbons, voltage-gated L-type calcium channels are highly enriched (tom Dieck et al., 2005). These channels allow voltage-dependent Ca^{2+}-influx at the ribbon synapse which triggers synaptic vesicle release (for review, see Heidelberger et al., 2005; Schmitz, 2009; Striessnig et al., 2010). L-type calcium channels are considered ideally suited to serve the continuously active ribbon synapses (see below). Submicromolar (average) concentrations of Ca^{2+} are capable of supporting tonic exocytosis in photoreceptors (for review, see Heidelberger et al., 2005). Specific signaling properties of ribbon synapses could require higher Ca^{2+}-concentrations that might be achieved at the base of the synaptic ribbons (Beutner et al., 2001; Choi et al., 2008; Jackman et al., 2009; Jarsky et al., 2010; Graydon et al., 2011). A recent study predicted concentrations up to 100 μM around the presynaptic Ca^{2+}-channels (Graydon et al., 2011), which could support coordinated multivesicular release (Singer et al., 2004; Khimich et al., 2005; Jarsky et al., 2010; Graydon et al., 2011). RIBEYE is involved in the clustering of Ca^{2+}-channels in inner ear hair cells (Sheets et al., 2011), and in agreement with this, several studies found a correlation between the ribbon size and the dimension of Ca^{2+}-microdomains (Johnson et al., 2008; Frank et al., 2009, 2010).

The size and number of synaptic ribbons can vary considerably (Hull et al., 2006; Johnson et al., 2008; Frank et al., 2009, 2010; Regus-Leidig et al., 2010; Liberman et al., 2011; for review, see Vollrath and Spiwoks-Becker, 1996; Schmitz, 2009; Regus-Leidig and Brandstätter, 2011). The plate-shaped synaptic ribbons in photoreceptors appear to assemble and disassemble via spherical intermediates, the synaptic spheres (for review, see Schmitz, 2009; Mercer and Thoreson, 2011b). In the mouse retina, structural changes of synaptic ribbons are activity- (illumination-) dependent; structural changes of fish synaptic ribbons are also strongly influenced by circadian signals (Emran et al., 2010; for review, see Vollrath and Spiwoks-Becker, 1996; Regus-Leidig and Brandstätter, 2011). The activity-dependent plasticity of the synaptic ribbon complex is related to the performance of the visual system also at the systems level (Balkema et al., 2001). At photoreceptor ribbon synapses, postsynaptic dendrites of bipolar and horizontal cells contact the presynaptic release sites in an invagination of the presynaptic terminal (**Figure 1**). At this site, the released glutamate is detected by the metabotropic glutamate receptor 6 (mGluR6) on the tips of ON-bipolar cells; horizontal cells as well as OFF-bipolar cells employ ionotropic glutamate receptors (Wässle, 2004; DeVries et al., 2006; Morgans et al., 2010).

Recent data revealed that EF-hand-containing proteins play an important role in the activity-dependent adaptational processes at the photoreceptor synapse. These findings suggest that the photoreceptor synaptic apparatus is adjusted during changes in illumination, thus allowing synaptic communication to continue in a

senseful manner if background illumination changes over a broad range. The processes in the presynaptic photoreceptor terminals that involve EF-hand-containing proteins, including distinct neuronal Ca^{2+}-sensor (NCS) - proteins and Ca^{2+}-binding proteins (CaBPs), will be summarized in the present review. Postsynaptic activity-dependent signaling is covered by other recent reviews (Burgoyne, 2007; Koike et al., 2010; Morgans et al., 2010).

Ca^{2+}-IONS AND EF-HAND-CONTAINING Ca^{2+}-BINDING PROTEINS: OUTLINE

Ca^{2+}-ions are crucial intracellular messengers that have central roles in synaptic transmission ranging from triggering of synaptic vesicle exocytosis, vesicle recruitment, and recovery as well as different aspects of synaptic plasticity (for review, Neher and Sakaba, 2008). Ca^{2+}-binding EF-hand-containing proteins are perfect candidates for participating in photoreceptor signaling. These proteins are characterized by high-affinity Ca^{2+}-binding motifs and consist of a helix-loop-helix motif (Burgoyne, 2007). The loop region, typically 12 residues long, is rich in acidic amino acids that chelate the Ca^{2+} (as well as Mg^{2+}). The founder molecule is calmodulin, and related to calmodulin are two classes of EF-hand-containing proteins (**Figures 2** and **3**): (1) the family of neuronal calcium sensor (NCS) proteins that include the guanylate cyclase activating proteins (GCAPs) and (2) the family of calcium-binding proteins (CaBPs) that include calcium-binding protein 4 (CaBP4) (for review, see Haeseleer et al., 2002; Burgoyne, 2007). Furthermore, individual proteins contain EF-hand motifs as important functional parts of their primary structure, e.g., the α1-subunit of L-type voltage-gated Ca^{2+}-channels (VGCCs).

$[Ca^{2+}]_i$ IN PRESYNAPTIC PHOTORECEPTOR TERMINALS

EF-hand-containing proteins typically bind Ca^{2+} in the submicromolar range and are regulated by $[Ca^{2+}]_i$. In photoreceptor terminals, presynaptic $[Ca^{2+}]_i$ is controlled by various mechanisms. These include $[Ca^{2+}]_i$- influx through calcium-permeable channels in the presynaptic plasma membrane (VGCCs, probably also CNG- and hyperpolarization-activated, cyclic nucleotide-gated (HCN)-channels), Ca^{2+}-buffering systems in the presynaptic terminals, Ca^{2+}-release from the ER (e.g., Ca^{2+}-induced Ca^{2+}-release) as well as extrusion from the cytosol into the ER and the extracellular space (e.g., via plasma membrane Ca^{2+}-ATPase; Na^+/Ca^{2+}, K^+-exchanger) (Rieke and Schwartz, 1994; Savchenko et al., 1997; Krizaj and Copenhagen, 2002; Suryanarayanan and Slaughter, 2006; Johnson et al., 2007; Knop et al., 2008; Szikra et al., 2008, 2009; Babai et al., 2010; Seeliger et al., 2011). Importantly, Ca^{2+}-concentrations in the presynaptic terminals of photoreceptors have been imaged *in-situ* using two-photon-microscopy (Choi et al., 2008; Jackman et al., 2009). In the anole lizard (*Anolis segrei*), 360–600 nm global (average) Ca^{2+} were measured in cone terminals of dark-adapted retinas; 190–250 nm of global average Ca^{2+} after bright illumination at physiological extracellular Ca^{2+}-concentrations. At the base of the synaptic ribbon, $[Ca^{2+}]_i$ could be much higher than these average values (>4 μM) (Choi et al., 2008; Jackman et al., 2009).

These $[Ca^{2+}]_i$ values in the presynaptic terminal differ from $[Ca^{2+}]_i$ values in the OS. In the OS of mouse retinas, dark values of 250 nm were measured; down to 23 nm $[Ca^{2+}]_i$ were measured in the OS of mice at saturating illumination (Olshevskaya et al., 2002; Woodruff et al., 2002; Koch, 2006; Baehr and Palczewski, 2009). Species-dependent differences in OS $[Ca^{2+}]_i$ values have been observed: dark values of ≈700 nm $[Ca^{2+}]_i$ were measured in salamander rod OS; many species have dark $[Ca^{2+}]_i$ values of ≈500 nm (Olshevskaya et al., 2002; Woodruff et al., 2002; Koch, 2006; Karan et al., 2010). Differences of $[Ca^{2+}]_i$ between presynaptic terminals and outer/inner segments could result from the elongated, slender shape of photoreceptors and various Ca^{2+}-extrusion mechanisms between OSs and presynaptic terminals (Krizaj and Copenhagen, 2002). Additionally, signals in the presynaptic terminals are shaped by feedback responses from secondary neurons (Jackman et al., 2010; Regus-Leidig and Brandstätter, 2011).

L-TYPE VOLTAGE-GATED CALCIUM CHANNELS IN PHOTORECEPTOR PRESYNAPTIC TERMINALS

The rate of synaptic vesicle exocytosis at ribbon synapses is highly dependent on changes in membrane potential, and the role of voltage-gated calcium channels in this process has been intensively investigated. Synaptic vesicle exocytosis in rod and cone photoreceptor synapses is triggered via Ca^{2+}-influx through L-type voltage-gated calcium channels (LTCCs) at the active zones (for review, see Morgans et al., 2005; Striessnig et al., 2010; Catterall, 2011). The α1-subunit is the largest subunit of LTCCs. $Ca_V1.4$ (often also denoted as α1F-subunit (Cacna1f); Catterall et al., 2005) is believed to represent the main pore forming α1-subunit of LTCCs involved in neurotransmitter release at photoreceptor synapses. This assumption is based on several findings: (1) immunocytochemical analyses (Nachman-Clewner et al., 1999; Morgans, 2001; for review, see Morgans et al., 2005); (2) analyses of spontaneous and engineered $Ca_V1.4$ mouse knockouts (for review, see Doering et al., 2007; Striessnig et al., 2010). (3) human patients suffering from congenital stationary night blindness (CSNB) show mutations in the $Ca_V1.4$ gene (for review, see Doering et al., 2007; Striessnig et al., 2010). Some studies also observed expression of $Ca_V1.3$ (also denoted as α1D-subunit (Cacna1d); Catterall et al., 2005) in photoreceptor synapses (Xiao et al., 2007; Kersten et al., 2010). Inner ear hair cell ribbon synapses employ $Ca_V1.3$ as pore-forming Ca^{2+}-channel α1-subunit (for review, see Striessnig et al., 2010). But while hearing is severely impaired, vision appears to be normal in $Ca_V1.3$ knockout mice (for review, see Striessnig et al., 2010).

$Ca_V1.4$ (α1F) is ≈2000 amino acids long and organized into four homologous domains (domain I–IV) (Catterall et al., 2005; Catterall, 2011). Both N- and C-terminus reside in the cytoplasm (**Figure 2**). The C-terminus (CTR) of $Ca_V1.4$ possesses important regulatory functions and consists of a Ca^{2+}-binding EF-hand domain, a pre-IQ and IQ-domain as well as an important regulatory region at the very carboxyterminus, the so-called CTM (C-terminal modulator) or ICDI (inhibitor of CDI) (Singh et al., 2006; Wahl-Schott et al., 2006; Striessnig et al., 2010). The CTM performs functionally important intramolecular interactions with the carboxyterminus of $Ca_V1.4$ (see below). The α1-subunit associates with cytoplasmic β-subunits, predominantly at the loop region between domain I and II of $Ca_V1.4$ (Dolphin,

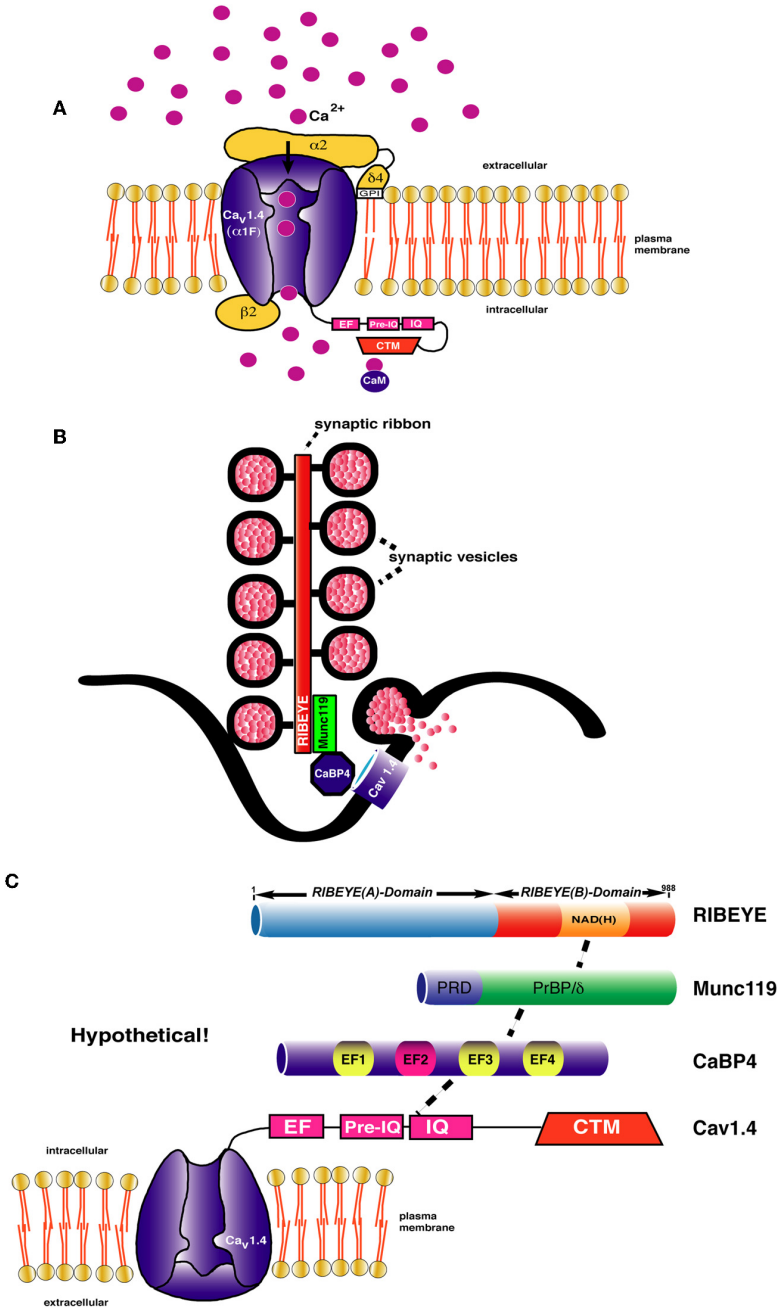

FIGURE 2 | (A) Schematic representation of L-type Ca^{2+}-channel composition of rod photoreceptor synapses [drawn modified based on Lacinova (2005)]. The channels are immobilized at the active zone close to the base of the synaptic ribbon. The α1F-subunit is considered the pore-forming subunit that supports voltage-dependent entry of Ca^{2+}. Ca^{2+} ions are depicted as pink spheres. The cytoplasmic C-terminus of $Ca_V1.4$ α 1-subunit contains an EF-hand, Pre-IQ-, and IQ-domain. In other Ca_V1 channels, e.g., $Ca_V1.2$, these carboxyterminal domains mediate Ca^{2+} -dependent inactivation [for review, see Striessnig et al. (2010)]. In $Ca_V1.4$, CDI is prevented by the additional CTM region that forms an intramolecular interaction with the above mentioned domains [Singh et al. (2006); Wahl-Schott et al. (2006)]. The β2-subunit interacts with the α1-subunit at the cytoplasmic loop connecting domain I with domain II [Catterall (2011)]. The alpha2-delta4 (α2δ4)-subunit, linked to each other with disulfide-bridges (not shown), complements the channel composition [Wycisk et al. (2006); Mercer et al. (2011a)]. The δ-subunit possesses a single transmembrane segment which is post-translationally cleaved off and replaced by a GPI anchor [Davies et al. (2010)] **(B,C)** Schematic depiction of the synaptic ribbon. Protein-protein interaction cascades are shown that could link RIBEYE to presynaptic calcium channels. Although all individual interactions (e.g., RIBEYE-Munc119; Munc119-CaBP4; CaBP4-$Ca_V1.4$) have been demonstrated [Alpadi et al. (2008); Haeseleer et al. (2004, 2008)], it is not clear whether all shown interactions can occur at the same time. Other interactions that might link the ribbons to presynaptic calcium channels, e.g., via association with RIM-proteins are not shown. Domain structures of the interacting proteins are only schematically depicted. CaBP4 contains 4 EF-hands from which EF2 (depicted in red) is non-functional. EF1, EF3, and EF4 are functional EF-hands (depicted in yellow). Abbreviations: CaM, calmodulin; PrBP/δ, prenyl-binding protein delta homology domain; PRD, proline-rich domain; IQ, IQ-domain; NAD(H), nicotine amide dinucleotide; CTM, C-terminal modulator.

2003; Buraei and Yang, 2010). The β2-protein appears to be the main β-channel subunit in photoreceptor LTCCs (Ball et al., 2002, 2011). β-subunits are important for the trafficking of the α1-subunit and for the kinetics of channel opening (Dolphin, 2003; Buraei and Yang, 2010). The $Ca_V1.4$ channel is complemented by an α 2δ-subunit, which is the α 2δ 4 protein in photoreceptor synapses (Wycisk et al., 2006; Mercer et al., 2011a).

The properties of $Ca_V1.4$ and $Ca_V1.3$ can be modulated over a wide range (for review, see Striessnig et al., 2010). In some contexts, $Ca_V1.4$ and $Ca_V1.3$ open at relatively negative membrane potentials (below –40 mV) which is an important requirement for photoreceptors that vary their membrane potential between –35 and –40 mV (in the dark) to less than –55 mV in the light (see above). Furthermore, for the tonically active photoreceptor synapses it is important that a sufficient Ca^{2+}-concentration is maintained that allows sustained, continuous exocytosis. This could be well accomplished by a calcium channel that does not inactivate or inactivates only very slowly. $Ca_V1.4$ shows no Ca^{2+}-dependent inactivation (CDI) and very slow voltage-dependent inactivation (VDI) (Singh et al., 2006; Wahl-Schott et al., 2006; Striessnig et al., 2010). This low degree or lack of inactivation could very well support continuous Ca^{2+}-influx and subsequently tonic exocytosis. Further supplies of Ca^{2+} that may help maintain sustained release could come from Ca^{2+}-induced Ca^{2+} release or store-operated Ca^{2+}-entry (Suryanarayanan and Slaughter, 2006; Szikra et al., 2008, 2009; Babai et al., 2010).

The biological purpose of CDI (and VDI), in general, is to provide neurons with a negative feedback mechanism that can protect from Ca^{2+}-overflow and subsequent cell death. CDI is mediated by the EF-hand, the pre-IQ-domain, and the IQ-domain in the CTR of $Ca_V1.4$ to which Ca^{2+}/calmodulin can bind (for review, see Doering et al., 2007; Striessnig et al., 2010). In $Ca_V1.4$, CDI is absent because of a modulatory domain in the CTR of $Ca_V1.4$ that prevents binding of Ca^{2+}-calmodulin to the pre-IQ/IQ-domain. CDI would probably not be compatible with the need of continuous, tonic exocytosis at photoreceptor synapses that also requires tonic Ca^{2+}-influx to drive exocytosis. Mutations in the $Ca_V1.4$ gene are associated with incomplete stationary night blindness (CSNB2) (for review, see Striessnig et al., 2010). Inhibition of CDI in inner ear hair cells is mediated by the binding of CaBP4 to the CTR of $Ca_V1.3$ (Yang et al., 2006). CaBP4 is an EF-hand-containing protein of the CaBP-family (Haeseleer et al., 2004; Haeseleer, 2008).

In photoreceptor synapses, CaBP4 could have an additional function. Binding of CaBP4 to the IQ-domain of $Ca_V1.4$ shifts the activation curve of the channel to more negative values (Haeseleer et al., 2004), thereby extending the operational range of the channel. At –40 mV, the membrane potential in the dark, the depolarized condition, the channel is at the very beginning of its activation curve (for review, see Striessnig et al., 2010). At –50 mV, a membrane potential which is easily achieved during illumination, the $Ca_V1.4$ channel would be closed. A CaBP4-induced hyperpolarizing shift of the $Ca_V1.4$ activation curve (shift of approximate 10–15 mV) would allow the channel to operate at more negative membrane potentials. It should be kept in mind that many of the biophysical characterizations were obtained from powerful, but simplified, model systems, e.g., transfected HEK cells. Channel regulation in the synapse could be more complex.

Mutations in the CaBP4 gene lead to autosomal recessive CSNB and Leber's congenital amaurosis (LCA)-like phenotype in humans (Zeitz et al., 2006; Aldahmesh et al., 2010); CaBP4 knockout mice have severe disturbances in synaptic transmission emphasizing the physiological importance of this protein. Interestingly, RIBEYE, the main component of synaptic ribbons binds to Munc119 (Alpadi et al., 2008), a protein which has been linked with a cone-rod dystrophy (CORD) (Kobayashi et al., 2000). Munc119, on the other hand, interacts with CaBP4 (Haeseleer, 2008; Alpadi and Schmitz, unpublished data). This multicomponent molecular connection could influence the gating of Ca^{2+}-channels at the active zone of photoreceptors (**Figure 2**).

The β-subunit of LTCC—together with other channel subunits (i.e., α2δ4; **Figure 2**) and further channel-associated proteins—plays an important role in the regulation of the kinetics of Ca^{2+}-channel opening, intracellular channel trafficking, and density at the plasma membrane (Dolphin, 2003; Davies et al., 2007; Buraei and Yang, 2010; Striessnig et al., 2010). Deletion of β2-subunit cause similar phenotypes as in CSNB2 patients with $Ca_V1.4$ mutations (Ball et al., 2002). β-subunit might be involved in the positional priming of calcium channels and the exocytotic machinery. β-subunits of LTCC bind to the RIM family of active zone proteins (Kiyonaka et al., 2007; Miki et al., 2007; Gebhart et al., 2010) via a carboxyterminal region that includes the C2B-domain of RIMs. RIM proteins are important for vesicle exocytosis, various steps of presynaptic plasticitiy and for the immobilization of Ca^{2+}-channels as shown mostly for conventional synapses (Han et al., 2011; Kaeser et al., 2011). RIMs are also components of the active zone complex of photoreceptors including the synaptic ribbons (Wang et al., 1997). Via the proline-rich region, RIM proteins bind to the RIM-binding proteins (RBPs) which associate with the β-subunit of L-type Ca^{2+}-channels (Hibino et al., 2002). Most interestingly, RIM knockouts lead to loss of Ca^{2+}-channel immobilization in conventional synapses (Han et al., 2011; Kaeser et al., 2011, for review, see Kaeser, 2011). RIM proteins are also important in modulating voltage-gated Ca^{2+}-channels as judged by a mutation in the C2A-domain of RIM1 that causes cone-rod dystrophy (CORD7) (Miki et al., 2007).

In conclusion, modulation of L-type Ca^{2+}-channel properties appears to have a powerful influence on synaptic transmission at the photoreceptor synapse (Striessnig et al., 2010). The plasticity is mediated by the EF-hand/Pre-IQ/IQ-domain-containing carboxyterminal region of the α-channel subunits. Tuning of the Ca^{2+}-channels could be involved in the adjustment of synaptic transmission during different levels of illumination and/or for slower, adaptation of the exocytotic machinery for overall changes of light- and dark-adaptation during day- and night time. Interestingly, L-type calcium channel expression in photoreceptors is likely under circadian control (Ko et al., 2007).

EF-HAND PROTEINS AND Ca^{2+}-/cGMP-DEPENDENT PLASTICITY AT THE SYNAPTIC RIBBON

As described above, EF-hand motif-containing proteins are important Ca^{2+}-dependent modulators of presynaptic

voltage-gated Ca^{2+}-channel functions. Also the synaptic ribbons are subject to Ca^{2+}-dependent dynamic changes which in turn could feedback on presynaptic Ca^{2+}-levels. Presynaptic Ca^{2+}-channels are anchored at the active zone of photoreceptor synapses by the synaptic ribbons. RIBEYE appears to have a central role in the clustering of Ca^{2+}-channels in inner ear hair cells (Sheets et al., 2011). Ribbon-associated proteins, e.g., the above mentioned RIM proteins or the protein bassoon, could potentially also play an important role (Wang et al., 1997; tom Dieck et al., 2005; Frank et al., 2010; Han et al., 2011; Kaeser et al., 2011). The ribbon-associated protein bassoon anchors synaptic ribbons to the active zone probably via its interaction with RIBEYE (tom Dieck et al., 2005). Bassoon is important for ribbon synapse development and maintaining the stability of the synaptic ribbon complex (Dick et al., 2003; tom Dieck et al., 2005; Regus-Leidig et al., 2010).

Recent studies suggested that activity-dependent structural changes of photoreceptor synaptic ribbons, i.e., assembly and disassembly of synaptic ribbons, are mediated by GCAP2, the guanylate cyclase-activating protein 2 (Venkatesan et al., 2010). GCAP2 belongs to a family of small Ca^{2+}-regulated, EF-hand-containing proteins of the NCS protein family (Koch, 2006; Burgoyne, 2007; Koch et al., 2010; Sharma, 2010). GCAPs are well known to regulate guanylate cyclase (GC) activity in photoreceptor OSs in a Ca^{2+}-dependent manner. How GCAPs could work in the presynaptic photoreceptor terminals to regulate synaptic plasticity is unclear. Current knowledge and ideas about GCAP/GC/cGMP-mediated signaling events in the presynaptic terminals will be summarized in the present review. To elucidate possible similarities between regulatory mechanisms in the OS and synaptic terminals, some key events of OS phototransduction will be also included.

GUANYLATE CYCLASE-ACTIVATING PROTEINS (GCAPs) IN PHOTORECEPTORS

Guanalyte cyclase-activating proteins (GCAPs) are small, EF-hand-containing Ca^{2+}-binding proteins of ≈24 kDa (**Figure 3**). GCAPs belong to the subfamily of NCS proteins (Koch, 2006; Burgoyne, 2007). They contain four EF-hands, and the first EF-hand in GCAPs is non-functional due to exchanges of critical amino acids in the Ca^{2+}-binding loop (**Figure 3**). Instead, EF1 provides a binding interface for the membrane-bound photoreceptor guanylate cyclases (ROS-GCs; Ermilov et al., 2001; see below). EF2–4 are functionally active and bind Ca^{2+} (as well as Mg^{2+}). In the OSs, the free intracellular Mg^{2+}-concentration is largely constant (at ≈1 mM) and not affected by changes in illumination (Chen, 2005; Peshenko et al., 2011a). In contrast, free intracellular Ca^{2+} levels change strongly upon illumination as described above. If Ca^{2+} (and cGMP) is high (in the dark), Ca^{2+} will replace the bound Mg^{2+} at the EF-hands of GCAPs (Stephen et al., 2008; Dizhoor et al., 2010; Peshenko et al., 2011a). The replacement of Mg^{2+} by Ca^{2+} at the EF-hands of GCAPs is functionally important because this changes the character of interaction with important effector proteins, the guanylate cyclases (GC, see below). GCAP proteins are myristoylated at their N-terminus (for review, see Palczewski et al., 2004; Koch, 2006; Baehr and Palczewski, 2007, 2009). In contrast to the recoverin-like NCS proteins, GCAPs do not perform a Ca^{2+}-dependent myristoyl-switch (Stephen et al., 2007; Ames and Lim, 2011). Irrespective whether Ca^{2+} is bound or not, the myristoyl chain remains buried inside the molecule and is not involved in Ca^{2+}-dependent membrane anchoring (**Figure 3**). Instead, the myristoyl residue has been suggested to stabilize the conformation of the protein (Stephen et al., 2007).

Three GCAP isoforms (GCAP1, GCAP2, and GCAP3) are expressed in mammalian retinas with species-dependent differences (Palczewski et al., 2004; Koch, 2006; Baehr and Palczewski, 2007, 2009; Dizhoor et al., 2010). In rod photoreceptors of mouse retinas, both GCAP1 and GCAP2 are expressed. GCAP1 appears to be the predominant isoform in cones (Palczewski et al., 2004; Koch, 2006; Baehr and Palczewski, 2007, 2009). Consistently, mutations of the GCAP1 gene lead to cone-dominated dystrophies in the human retina as well as in the respective mouse models (Jiang et al., 2005; Buch et al., 2011). GCAP3 expression is restricted to cone photoreceptors in the human retina; in the mouse retina GCAP3 is not expressed arguing that GCAP3 is probably dispensable for vision in mice (for review, see Baehr and Palczewski, 2007, 2009). Despite strong sequence similarities, biophysical and biochemical properties of GCAP proteins differ (e.g., Ca^{2+}-affinities, dimerization properties, and activation of GCs; Ermilov et al., 2001; Olshevskaya et al., 2002; Koch et al., 2010). In photoreceptor outer segments (OS), GCAPs constitutively associate with membranes via interaction with ROS-GCs (Olshevskaya et al., 2002; Stephen et al., 2007; Ames and Lim, 2011). Mice with a deletion of GCAP1 and GCAP2 genes showed increased amplitudes of single photon responses and a delayed recovery phase (for review, see Palczewski et al., 2004; Baehr and Palczewski, 2007, 2009).

GCAP EFFECTOR PROTEINS IN PHOTORECEPTOR OUTER SEGMENTS

In photoreceptor OSs, GCAP effector proteins have been extensively characterized (Karan et al., 2010; Hunt et al., 2010; Koch et al., 2010). Main effectors of GCAP proteins are the ≈115 kDa membrane-bound rod outer segment-guanylate cyclases (ROS-GCs). Two ROS-GCs are found in mammalian photoreceptors: ROS-GC1 (retGC1, GC-E) and ROS-GC2 (retGC2, GCF) (for review, see Olshevskaya et al., 2002; Potter, 2011). ROS-GCs are large, type 1 transmembrane proteins (≈1100 aa; **Figure 4**) with an extracellular domain, a transmembrane domain, and a cytoplasmic domain that consists of a short juxtamembrane domain (JMD), a kinase homology domain (KHD), a dimerization domain (DD), a catalytic domain (CCD) that converts GTP into cGMP and C-terminal extension (CTE). Both ROS-GC1 and ROS-GC2 are expressed in rods; ROS-GC2 appears to be absent from mouse cone photoreceptors (Haire et al., 2006; Karan et al., 2010). ROS-GCs play a crucial role in photoreceptor OS phototransduction. A light-induced conformational change of rhodopsin leads to a transducin-mediated activation of phosphodiesterase 6 (PDE6) and subsequently reduced levels of cGMP (Burns and Baylor, 2001). Thus, light generates a drop in cGMP levels in the OSs and subsequent closure of cGMP-gated CNG-channels (Biel and Michalakis, 2009). As a result of light-induced closure of CNG channels intracellular Ca^{2+} levels drop in the OS from about 250nM (dark) to less than <50 nM

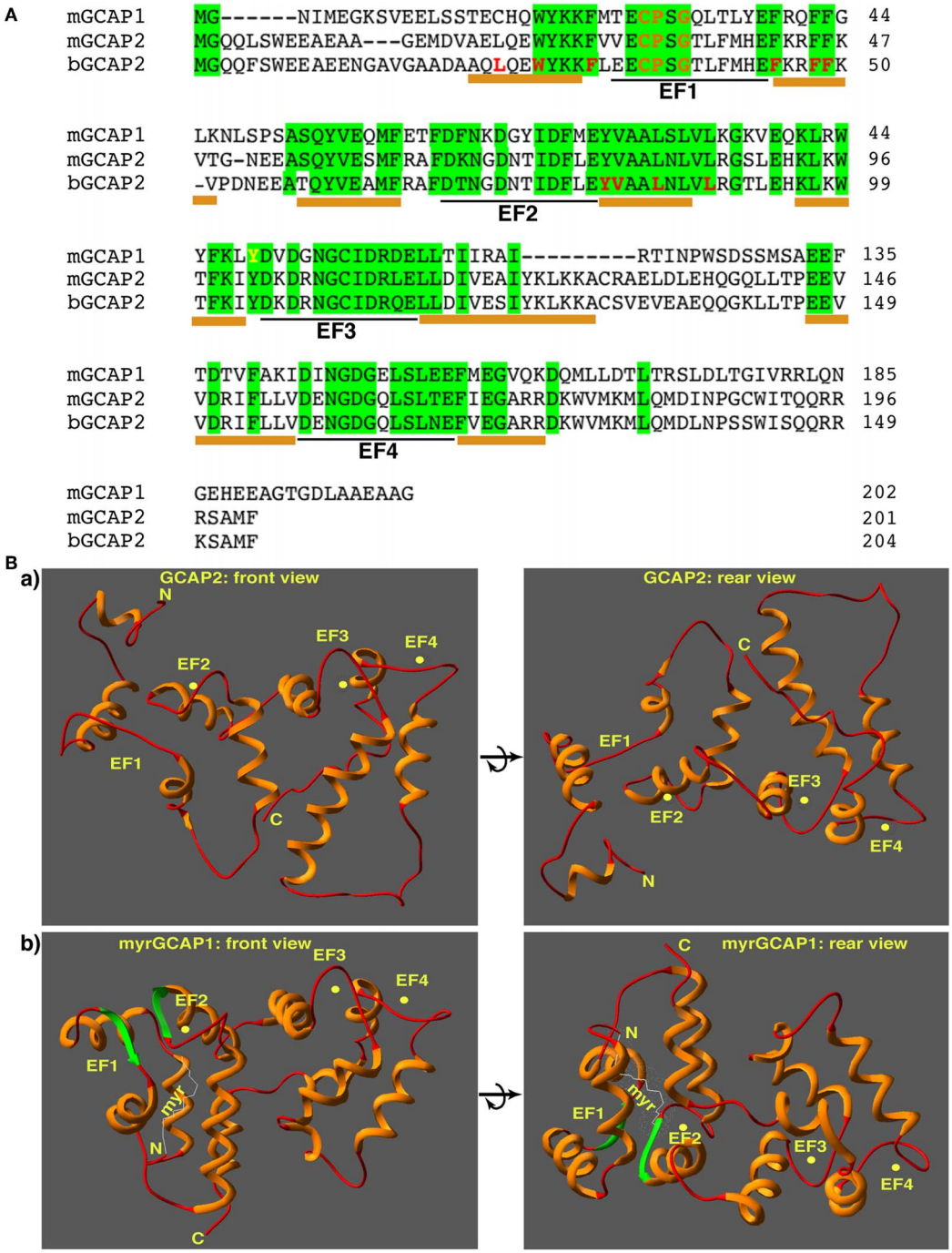

FIGURE 3 | (A) Sequence alignment of GCAP1 and GCAP2 from the indicated species (mGCAP1: NP032215, GI: 40254633; mGCAP2: NP_666191, GI: 22122571; bGCAP2: NP_777211, GI: 27807519). Amino acid residues identical in all three indicated GCAP proteins are highlighted in green. Underlined below the aligned amino acid sequences is the Ca^{2+}-/Mg^{2+}-chelating loop region located between the E- and F- helices of the respective EF-hands. It is flanked on both sides by an α-helix (underlined in amber). The amino acid sequences of the EF-hands of GCAP1 and GCAP2 are highly homologous. Amino acids identical in mGCAP1, mGCAP2, and bGCAP2 are highlighted in green. EF-hands are highly conserved; the C-terminus of GCAP1 of GCAP2 is divergent. The CTR of GCAP2, but not of GCAP1, binds to the NADH-binding sub-domain of RIBEYE(B) [Venkatesan et al. (2010)]. Amino acids in GCAP2 highlighted in red appear to be involved in the interaction with ROS-GCs [Ames et al. (1999)]. Residues in the loop region of EF1 that are incompatible with Ca^{2+}-chelation and also involved in ROS-GC target interaction are shown in orange [Ames et al. (1999); Hwang et al. (2004)]. Abbreviations: mGCAP1, mouse GCAP1; mGCAP2, mouse GCAP2, bGCAP2, bovine GCAP2. **(B)** Structure of unmyristoylated GCAP2 (a) [Ames et al. (1999); pdb-file: 1jba] and myristoylated GCAP1 (b) [Stephen et al. (2007); pdb-file: 2R2I]. The structure is shown from the front (left) with the Ca^{2+}-chelating loops on top as well as from the back (right) to document the location of the CTR region that binds to RIBEYE(B) in the case of GCAP2 [Venkatesan et al. (2010)]. Ca^{2+} ions are schematically depicted as yellow spheres.

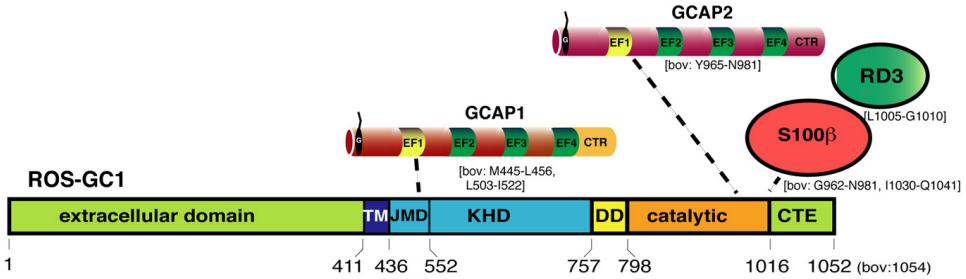

FIGURE 4 | Schematic representation of ROS-GC1 and ROS-GC1-interaction partners in photoreceptors. ROS-GC1 contains an aminoterminal extracellular domain, transmembrane domain (TM), kinase homology domain (KHD), dimerization domain (DD), and the catalytic domain that converts GTP into cGMP. The aminoterminal portion of the KHD is also referred to as juxtamembrane domain (JMD) [Lange et al. (1999)]. The borders of the respective domains are schematically depicted in the amino acid sequence of human ROS-GC1 (NP_000171, GI: 4504217). Numbers indicated correspond to the mature ROS-GC1 protein (without leader sequence). The borders of the individual domains were determined by the analyses of various ROS-GC1 constructs; the precise structure of photoreceptor ROS-GC1 (e.g., X-ray-structure) is not yet available. At the intracellular domains of ROS-GC1, different NCS proteins bind at different locations. GCAP1 binds to the JMD, the aminoterminal portion of the kinase homology domain of ROS-GC1 probably via its aminoterminal EF1 hand. In contrast, S100β and GCAP2 bind close to each other to the catalytic domain. The binding of GCAPs appears to compete with the binding of the retinal degeneration protein 3 (RD3). While GCAPs inhibit mostly ROS-GC1 activity at high Ca^{2+} -concentrations, S100β stimulates ROS-GC1 activity at high Ca^{2+}. The Ca^{2+}-concentrations needed by S100β to stimulate ROS-GC1 activity is high but could be achieved at the active zone of photoreceptors close to presynaptic Ca^{2+}-channels. The numbers below the schematic depiction of ROS-GC1 domains depict the respective borders in human ROS-GC1 sequence. Most of the mapping of the ROS-GC1 interacting proteins has been done with bovine ROS-GC1 reviewed in Sharma (2010). For some interactions (e.g., GCAP1), multiple interaction sites were reported. GCAP1 was also reported to bind to the catalytic domain though with lower affinity than at the KHD [for review, Sharma (2002, 2010)]. The respective amino acid regions of bovine ROS-GC1 involved in the interaction with the indicated proteins are indicated in square brackets. Non-photoreceptor-interacting proteins of ROS-GC1 [Sharma, (2010)] are not depicted. Abbreviations: TM, transmembrane domain; JMD, juxtamembrane domain; DD, dimerization domain; CTE, carboxyterminal extension; RD3, retinal degeneration 3. Proteins and protein domains are only schematically depicted and not drawn in scale.

(light) in the mouse retina. Light-induced decreased levels of cGMP need to be replenished in order to be able to detect the next flash of light. Recovery of cGMP levels is accomplished by a Ca^{2+}-dependent feedback mechanism mediated by GCAP proteins. After illumination (at low Ca^{2+}), GCAPs are in the Mg^{2+}-bound state and stimulate GC activity. In contrast, in the Ca^{2+}-bound state (at high Ca^{2+} in the dark) GCAPs inhibit GC activity (Koch, 2006; Sharma, 2010; Sakurai et al., 2011). Thus, GCAPs work as bimodal regulators of GCs: as an inhibitor of GC activity function (if Ca^{2+} is bound) and as an activator of GC function (and cGMP synthesis) if Mg^{2+} is bound. At low Ca^{2+} levels (light), GCAPs activate GCs and thus raise cGMP levels to restore pre-flash cGMP levels. These fundamental properties of GCAP proteins are crucial for the Ca^{2+}-dependent feedback of the phototransduction cascade. This is necessary to make the OS responsive to new flashes of light and to reset the sensitivity of the phototransduction cascade to different levels of illumination. Particularly EF-hand 3 (EF3) emerged as key region that determines whether GCAPs act as an activator or inhibitor of GCs (Olshevskaya et al., 2002; Baehr and Palczewski, 2007, 2009).

GCAP1 binds to the juxtamembrane KHD of ROS-GCs (for review, see Koch et al., 2010). GCAP2 binds directly to the catalytic domain of ROS-GCs. Despite high sequence similarities, GCAPs are not functionally equivalent; many regulatory properties differ (for review, see Koch, 2006; Dizhoor et al., 2010; Koch et al., 2010). GCAP2 has a higher affinity for Ca^{2+} than GCAP1 (for review, see Koch, 2006; Dizhoor et al., 2010). Different Ca^{2+}-affinities of GCAPs could enhance the operational range of Ca^{2+}-regulation of GCs and give rise to the Ca^{2+}-relay model of GC activation/inhibition in the OS (for review, see Koch, 2006; Burgoyne, 2007). At intermediate levels, Ca^{2+} is still bound to GCAP2 whereas GCAP1 is already Ca^{2+}-free (Mg^{2+}-bound version). As a consequence, GCAP1 would stimulate GC activity at these intermediate concentrations, whereas GCAP2 would still be inhibitory. Recently, it was found that the RD3 protein, which is associated with LCA, also binds to the carboxyterminal of ROS-GC and inhibits GC activity by an allosteric mechanism (Azadi et al., 2010; Peshenko et al., 2011b). RD3 binding to ROS-GCs promotes dissociation of GCAPs from the ROS-GC complex.

GCAPS IN PHOTORECEPTOR PRESYNAPTIC TERMINALS AND THEIR INVOLVEMENT IN ACTIVITY-DEPENDENT CHANGES OF SYNAPTIC RIBBONS

Various studies demonstrated the presence of GCAP proteins in photoreceptor presynaptic terminals (Otto-Bruc et al., 1997; Kachi et al., 1999; Cuenca et al., 1998; Pennesi et al., 2003; Makino et al., 2008; Venkatesan et al., 2010). But the significance of GCAP proteins in the presynaptic terminals is not well understood. One function of GCAP-mediated signaling appears to mediate the Ca^{2+}-dependent regulation of synaptic ribbon plasticity (Venkatesan et al., 2010). Synaptic ribbons are dynamic structures (for review, see Vollrath and Spiwoks-Becker, 1996; Schmitz, 2009). The synaptic ribbon undergoes activity- (illumination-) dependent changes. Illumination leads to smaller and less numerable synaptic ribbons in the mouse retina (Spiwoks-Becker et al., 2004). The dynamics of these structures is known to be dependent upon Ca^{2+} and cGMP (Vollrath and Spiwoks-Becker, 1996). Chelating intracellular Ca^{2+} leads to a disassembly of synaptic

ribbons at the electron microscopic level (Spiwoks-Becker et al., 2004; Regus-Leidig et al., 2010). Immunocytochemical analyses of these effects revealed a sequential process (Regus-Leidig et al., 2010). First, synaptic ribbon components, such as RIBEYE, piccolo and RIM1, were removed, in parallel to the disassembly of synaptic ribbons at the ultrastructural level. In a second step, bassoon, an important mediator of synaptic ribbon stability and organizer of the active zone (Dick et al., 2003; for review, see Joselevitch and Zenisek, 2010; Regus-Leidig and Brandstätter, 2011), is removed from the active zone (Regus-Leidig et al., 2010). Venkatesan et al. (2010) demonstrated that RIBEYE, the main component of synaptic ribbons, binds to the carboxyterminal region of GCAP2 in a NAD(H)-dependent manner (**Figure 5**). Overexpression of GCAP2 in the presynaptic terminals of photoreceptors leads to disassembly of synaptic ribbons and a reduction in their number (Venkatesan et al., 2010). Therefore, one function of GCAP2 could be to regulate the assembly and disassembly of synaptic ribbons. The molecular mechanisms, how this could be achieved are currently unknown.

Which GCAP effectors in the synapse might execute its synaptic functions? ROS-GC1, the GCAP effector in the OS, has been localized to the photoreceptor synapses by immunoperoxidase methods and other sensitive techniques (Liu et al., 1994; Cooper et al., 1995; Duda et al., 2002). Conventional immunofluorescence microscopic analyses using mouse retina failed to detect ROS-GC1 in photoreceptor synapses (Azadi et al., 2010; Karan et al., 2010). This might be attributed to the lower sensitivity of immunofluorescence microscopy in comparison to immunoperoxidase techniques. Possibly, ROS-GC1 might be masked in the presynaptic matrix, not accessible to antibodies or the amount is close to the detection limits. Different antibodies with different affinities or species differences might also contribute to the different levels of immunoreactivities of ROS-GC1 in synaptic terminals. In the bovine retina, a strong ROS-GC1 was observed in photoreceptor terminals (Venkataraman et al., 2003). GC activity was demonstrated also histochemically in photoreceptor terminals (Rambotti et al., 2002). Biochemical data supported the presence of ROS-GC1 in photoreceptor synapses (Duda et al., 2002; Venkataraman et al., 2003). In contrast to the photoreceptor OS, ROS-GC1 in photoreceptor synaptic terminals is stimulated, not inhibited, by the presence of high concentrations of intracellular Ca^{2+} (Duda et al., 2002; Venkataraman et al., 2003; for review, see Sharma, 2002, 2010; Koch, 2006). The Ca^{2+}-stimulated ROS-GC1 activity is mediated by the EF-hand protein S100β (previously also called CD-GCAP) that has been localized to the presynaptic photoreceptor terminal (Duda et al., 2002;

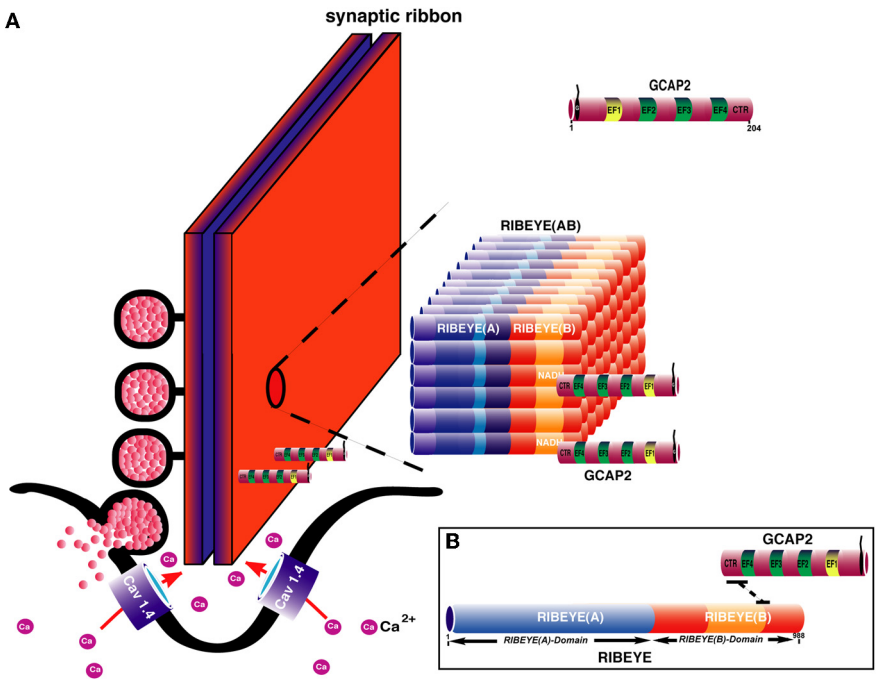

FIGURE 5 | (A) Hypothetical model for the assembly of the synaptic ribbon: the scaffold of the synaptic ribbon is built by RIBEYE proteins, the major, and unique component of synaptic ribbons via multiple RIBEYE-RIBEYE interactions [Magupalli et al. (2008); Schmitz (2009)]. In this model, the A-domain is located in the center of the ribbon to build the core of the synaptic ribbon. The B-domain faces the cytoplasmic side of the synaptic ribbon where it interacts with various proteins, e.g., Munc119 (see also **Figure 2**) and with the GCAP2. Interaction with GCAP2 could regulate assembly and disassembly of synaptic ribbons which is known to be Ca^{2+}-dependent [Vollrath and Spiwoks-Becker (1996); Schmitz (2009)]. Overexpression of GCAP2 leads to ribbon disassembly. The recruitment of GCAP2 by RIBEYE could influence Ca^{2+}-buffering at the synaptic ribbon thus also influencing synaptic signaling. The differently colored portions in RIBEYE(A)-domain represent RIBEYE-RIBEYE interaction sites [Magupalli et al. (2008)]. How GCAP2 regulates ribbon assembly and disassembly is unknown but could involve GCAP effectors, e.g., ROS-GCs (**Figure 4**) which were reported to be present in the presynaptic terminals. (**B**) Molecular dissection of RIBEYE-GCAP2 interaction: the carboxyterminal region (CTR) of GCAP2 interacts with the hinge 2 region of RIBEYE(B) [Venkatesan et al. (2010)].

Venkataraman et al., 2003; Sharma, 2010). S100β binds to the catalytic domain of ROS-GC and subsequently enhances ROS-GC1 activity at high Ca^{2+}-concentrations. These Ca^{2+}-concentrations could be achieved close to the synaptic ribbon (Choi et al., 2008; Jackman et al., 2009; Graydon et al., 2011). Thus, S100β binds to ROS-GC1 at the catalytic domain, similar to GCAP2 (Duda et al., 2002, 2005; Sharma, 2002, 2010). It is possible that S100β competes with GCAP2 for binding to ROS-GC1.

The regulation of cGMP levels could be the key in the regulation of activity-dependent synaptic ribbon plasticity. cGMP was reported to stabilize synaptic ribbons in the pineal gland (Seidel et al., 1990; Spessert et al., 1992). cGMP-dependent protein kinases could be effectors that might mediate the stabilizing effect of cGMP on synaptic ribbons. cGMP-dependent kinases have been localized to photoreceptor synapses (Feil et al., 2005). But the involvement of these kinases in ribbon dynamics has not yet been elucidated. Interestingly, the RD3 protein, which blocks binding of GCAP2 to ROS-GC1, is present in the presynaptic terminals (Azadi et al., 2010; Peshenko et al., 2011b). Thus, a complex interplay of several proteins that compete for binding to ROS-GCs modulates cGMP-dependent signaling in the photoreceptor synapse in a complex manner. The recruitment of GCAP2 to synaptic ribbons and the subsequent disassembly of synaptic ribbons could be due to changes in cGMP levels that induce further downstream effects or due to increased GCAP2-mediated Ca^{2+}-buffering. Future investigations have to discriminate between these possibilities. The importance of cGMP and cGMP-dependent protein kinases for synaptic ribbon dynamics is supported by a recent study that showed a synaptic ribbon-protective effect of cGMP in an inner ear trauma model (Jaumann et al., 2012). In this study, the authors demonstrated that inhibition of cGMP-hydrolyzing PDE5 leads to stabilization of synaptic ribbons in a cGMP-regulated protein kinase 1-dependent manner in inner hair cells. Analyses of GCAP1/2 double knockout mice also pointed to a synaptic function of GCAPs proteins at the photoreceptor synapse (Okawa et al., 2010). GCAP1/2 knockout mice show disturbed signal processing at the synapse: although the single-photon-responses in OS of GCAP knockout mice were much larger than in wildtype mice, the synaptic processing of this information, as measured by recordings from postsynaptic bipolar cells, was more inefficient. A main synaptic function of GCAPs appears to improve the signal-to-noise ratio of synaptic transmission (Okawa et al., 2010). The underlying molecular mechanisms are still unknown but could involve structural changes of the synapse.

cGMP IS AN IMPORTANT MODULATOR OF SYNAPTIC PLASTICITY IN PHOTORECEPTOR TERMINALS

Various other aspects of plasticity in photoreceptor presynaptic terminals are mediated by cGMP (Rieke and Schwartz, 1994; Vollrath and Spiwoks-Becker, 1996; Savchenko et al., 1997; Zhang and Townes-Anderson, 2002; Zhang et al., 2005). The group of Townes-Anderson showed that outgrowth of neurites in rods and cones photoreceptor depends upon influx of Ca^{2+} (for review, see Townes-Anderson and Zhang, 2006). In cones, Ca^{2+} enters the presynaptic terminal through cGMP-gated Ca^{2+}-channels to mediate this type of synaptic plasticity. Hyperpolarization-activated, cyclic nucleotide-gated (HCN) channels could be further effectors of presynaptic cGMP. HCN1 channels have been demonstrated in presynaptic photoreceptor terminals (Müller et al., 2003; Knop et al., 2008; Seeliger et al., 2011; Tanimoto et al., 2012). cGMP-regulated channels could extend the range of synaptic transmission e.g., at very negative membrane potentials at which L-type calcium channels might already be closed (Rieke and Schwartz, 1994; Savchenko et al., 1997). Soluble GCs could also contribute to the generation of cGMP. Several studies suggest that this source of cGMP production could play a role in neurotransmitter release and structural plasticity in photoreceptor terminals (Savchenko et al., 1997; Kourennyi et al., 2004; Zhang et al., 2005; Blom et al., 2009; Sato et al., 2011).

IMBALANCE OF cGMP AND Ca^{2+}-HOMEOSTASIS IN PHOTORECEPTORS LEADS TO DISEASE

As described above, cGMP and Ca^{2+} homeostasis are intimately related and possess a central role for phototransduction and light-adaptation. Tight control of cGMP and Ca^{2+}-levels are of central importance for the survival of photoreceptors (Hunt et al., 2010). Various severe neurodegenerative diseases of the retina are associated with disturbances of the cGMP/Ca^{2+}-homeostasis (Fain, 2006; Barabas et al., 2010; Paquet-Durand et al., 2011). These include Retinitis pigmentosa (RP), LCA, and distinct forms of cone and rod dystrophies (Baehr and Palczewski, 2009; Jiang and Baehr, 2010; Paquet-Durand et al., 2011). Mutations in the ROS-GC1 gene can lead to LCA, a devastating degeneration leading to childhood blindness, or a cone-rod-dystrophy (CORD 6) (for review, see Hunt et al., 2010). Diseases associated with ROS-GC2 are not known. The gene for GCAP1 has been associated with a form of cone-rod dystrophy, CORD3 (for review, see Jiang and Baehr, 2010). Missense mutations in GCAP1 cause loss of photoreceptors, particularly cones. Many of the disease-causing mutations are located in EF3 and EF4 or indirectly affect the structure of these EF-hands. The disease mutants lead to a decrease in Ca^{2+}-sensitivity thus making these mutants to constitutive, Ca^{2+}-insensitive activators of GCs. As a result, cGMP and Ca^{2+} levels are pathologically increased leading to photoreceptor cell death (Baehr and Palczewski, 2009; Jiang and Baehr, 2010; Paquet-Durand et al., 2011). The retinal degeneration 1 (rd1) mouse is characterized by a loss-of-function mutation in the gene encoding for the β-subunit of the photoreceptor-specific PDE6 (for a recent review, see Barabas et al., 2010). Consequently, rd1 mice have low PDE6 activity and high levels of cGMP which lead to photoreceptor cell death, predominantly in rods. Also the proteins discussed above, i.e., $Ca_V1.4$, Munc119, RIM, and CaBP4, have high clinical relevance; mutations in the respective genes cause various severe degenerative diseases of the retina, as described above.

OPEN QUESTIONS/PERSPECTIVES

Activity-dependent, adaptative signaling in photoreceptor presynaptic terminals is just at the beginning of being understood. Currently, knowledge about these processes in the synapse lags behind to what is known about dynamic processes in the OS. Ca^{2+}, cGMP, and EF-hand-containing proteins likely play

numerous roles in signaling at the photoreceptor synapse and activity-dependent synaptic changes. Dynamics of synaptic ribbons at a molecular level may involve control of RIBEYE-RIBEYE interactions. How these interactions are controlled at a molecular level is currently not known. The involved effector molecules and molecular pathways need to be elucidated. Differences between rod and cone dynamic signaling need to be worked out since the purpose of synaptic transmission at these two different types of photoreceptor synapses is different (although related). Are there differences in adaptative signaling in cone and rod synapses and eventually also between the different active zones present in cone synapses? Recent Ca^{2+}-imaging analyses strongly argue that this is the case (Johnson et al., 2007; Sheng et al., 2007). Most of our current knowledge about the physiology of retinal ribbon synapses was obtained from goldfish bipolar cells and salamander photoreceptors. The mouse retina with its powerful genetic possibilities just entered the stage. Mouse knockout models as well as the possibility of manipulating the mouse retina with recombinant viruses can be expected to provide further important insights into signal processing at the photoreceptor synapse.

ACKNOWLEDGMENTS

Work by the authors is supported by the German Research Community (DFG) SFB894 TPA7, GRK1326 and the Human Frontiers Science Organization HFSP. Thanks to Dr. Jutta Schmitz-Kraemer for critically reading the manuscript. The authors apologize that not all relevant original papers could be mentioned due to limitations in space.

REFERENCES

Abramov, I., and Gordon, J. (1994). Color appearance: on seeing red- or yellow, or green, or blue. *Ann. Rev. Psychol.* 45, 451–485.

Aldahmesh, M. A., Al-Owain, M., Alqahtani, F., Hazzaa, S., and Alkurya, F. S. (2010). A null mutation in CaBP4 causes Leber's congenital amaurosis-like phenotype. *Mol. Vis.* 16, 207–212.

Alpadi, K., Magupalli, V. G., Käppel, S., Köblitz, L., Schwarz, K., Seigel, G. M., Sung, C. H., and Schmitz, F. (2008). RIBEYE recruits Munc119, the mammalian ortholog of the *Caenorhabditis elegans* protein unc119 to synaptic ribbons of photoreceptor synapses. *J. Biol. Chem.* 283, 26461–26467.

Ames, J. B., Dizhoor, A. M., Ikura, M., Palczewski, K., and Stryer, L. (1999). Three-dimensional structure of guanylyl cyclase activating protein-2, a calcium-sensitive modulator of photoreceptor guanylyl cyclases. *J. Biol. Chem.* 274, 19329–19337.

Ames, J. B., and Lim, S. (2011). Molecular structure and target recognition of neuronal calcium sensor proteins *Biochim. Biophys. Acta* [Epub ahead of print].

Azadi, S., Molday, L. L., and Molday, R. S. (2010). RD3, the protein associated with Leber congenital amaurosis type 12, is required for guanylate cyclase trafficking in photoreceptor cells. *Proc. Natl. Acad. Sci. U.S.A.* 107, 21158–21163.

Babai, N., Morgans, C. W., and Thoreson, W. B. (2010). Calcium-induced calcium release contributes to synaptic release from mouse rod photoreceptors. *Neuroscience* 165, 1447–1456.

Baehr, W., and Palczewski, K. (2007). Guanylate-cyclase-activating proteins and retina disease. *Subcell. Biochem.* 45, 71–91.

Baehr, W., and Palczewski, K. (2009). Focus on molecules: guanylate cyclase-activating proteins (GCAPs). *Exp. Eye Res.* 89, 2–3.

Balkema, G. W., Cusick, K., and Nguyen, T. H. (2001). Diurnal variation in synaptic ribbon length and visual threshold. *Vis. Neurosci.* 18, 789–792.

Ball, S. L., McEnery, M. W., Yunker, A. M., Shin, H. S., and Gregg, R. G. (2011). Distribution of voltage gated calcium channel β subunits in the mouse retina. *Brain Res.* 1412, 1–8.

Ball, S. L., Powers, P. A., Shin, H. S., Morgans, C. W., Peachey, N. S., and Gregg, R. G. (2002). Role of the β2 subunit of voltage-dependent Ca2+ channels in the retinal outer plexiform layer. *Invest. Ophthalmol. Vis. Sci.* 43, 1595–1603.

Barabas, P., Peck, C. C., and Krizaj, D. (2010). Do calcium channel blockers rescue dying photoreceptors in the Pde6brd1 mouse? *Adv. Exp. Med. Biol.* 664, 491–499.

Beutner, D., Voets, T., Neher, E., and Moser, T. (2001). Calcium dependence of exocytosis and endocytosis at the cochlear inner hair cell afferent synapse. *Neuron* 29, 681–690.

Biel, M., and Michalakis, S. (2009). Cyclic nucleotide-gated channels. *Handb. Exp. Pharamacol.* 191, 111–136.

Blom, J. J., Blute, T. A., and Eldred, W. D. (2009). Functional localization of the nitric oxide/cGMP pathway in the salamander retina. *Vis. Neurosci.* 26, 275–286.

Buch, P. K., Mihelec, M., Cottrill, P., Wilkie, S. E., Pearson, R. A., Duran, Y., West, E. L., Michaelides, M., and Hunt, D. M. (2011). Dominant cone-rod dystrophy: a mouse model generated by gene targeting of the GCAP1/Guca1a gene. *Plos One* 3, 18089. doi: 10.1371/journal.pone.0018089

Buraei, Z., and Yang, Y. (2010). The β-subunit of Ca2+ channels. *Physiol. Rev.* 90, 1461–1506.

Burgoyne, R. D. (2007). Neuronal calcium sensor proteins: generating diversity in neuronal Ca2+-signalling. *Nat. Rev. Neurosci.* 8, 182–193.

Burns, M. E., and Baylor, D. A. (2001). Activation, deactivation, and adaptation in vertebrate photoreceptor cells. *Ann. Rev. Neurosci.* 24, 779–805.

Catterall, W. A., Perez-Reyes, E., Snutch, T. P., and Striessnig, J. (2005). International union of pharmacology. XLVIII. Nomenclature and structure-function relationships of voltage-gated calcium channels. *Pharmacol. Rev.* 57, 411–425.

Catterall, W. A. (2011). Voltage-gated calcium channels. *Cold Spring Harb. Persp. Biol.* 3, a003947.

Chen, K. (2005). The vertebrate phototransduction cascade: amplification and termination mechanisms. *Rev. Physiol. Biochem. Pharmacol.* 154, 101–121.

Choi, S. Y., Jackman, S., Thoreson, W. B., and Kramer, R. H. (2008). Light regulation of Ca2+ in the cone photoreceptor synaptic terminal. *Vis. Neurosci.* 25, 693–700.

Cooper, N., Liu, N., Yoshida, A., Pozdnyakov, N., Margulies, A., and Sitaramayya, A. (1995). The bovine rod outer segment guanylate cyclase, ROS-GC, is present in both outer segment and synaptic layers of the retina. *J. Mol. Neurosci.* 6, 211–222.

Cuenca, N., Lopez, S., Howes, K., and Kolb, H. (1998). The localization of guanylyl cyclase-activating proteins in the mammalian retina. *Invest. Ophthalmol. Vis. Sci.* 39, 1249–1250.

Davies, A., Hendrich, J., Van Minh, A. T., Wratten, J., Douglas, L., and Dolphin, A. C. (2007). Functional biology of the alpha(2)delta subunits of voltage-gated calcium channels. *Trends Pharmacol. Sci.* 28, 220–228.

Davies, A., Kadurin, I., Alvarez-Laviada, A., Douglas, L., Nieto-Rostro, M., Bauer, C. S., Pratt, W. S., and Dolphin, A. C. (2010). The α2δ subunits of voltage-gated calcium channels form GPI-anchored proteins, a posttranslational modification essential for function. *Proc. Natl. Acad. Sci. U.S.A.* 107, 1654–1659.

DeVries, S. H., Li, W., and Saszik, S. (2006). Parallel processing in two transmitter microenvironments at the cone photoreceptor synapse. *Neuron* 50, 735–748.

Dick, O., tom Dieck, S., Altrock, W. D., Ammermüller, J., Weiler, R., Garner, C. C., Gundelfinger, E. D., and Brandstätter, J. H. (2003). The presynaptic active zone protein bassoon is essential for photoreceptor ribbon synapse formation in the retina. *Neuron* 37, 775–786.

Dizhoor, A. M., Olshevskaya, E. V., and Peshenko, I. V. (2010). Mg2+/Ca2+ cation binding cycle of guanylyl cyclase activating proteins (GCAPs): role in the regulation of photoreceptor guanylyl cyclase. *Mol. Cell. Biochem.* 334, 117–124.

Doering, C. J., Peloquin, J. B., and McRory, J. E. (2007). The CaV1.4 channel. *Channels* 1, 3–10.

Dolphin, A. C. (2003). β subunits of voltage-gated calcium channels. *J. Bioenerg. Biomembr.* 35, 599–620.

Duda, T., Fik-Rymarkiewicz, E., Venkataraman, V., Krishnan, R., Koch, K. W., and Sharma, R. K. (2005). The calcium-sensor guanylate cyclase activating protein type 2 specific site in rod outer segment membrane guanylate cyclase type 1. *Biochemistry* 44, 7336–7345.

Duda, T., Koch, K. W., Venkataraman, V., Lange, C., Beyermann, M.,

and Sharma, R. K. (2002). Ca2+-sensor S100β-modulated sites of membrane guanylate cyclase in the photoreceptor-bopolar synapse. *EMBO J.* 21, 2547–2556.

Emran, F., Rihel, J., Adolph, A. R., and Dowling, J. E. (2010). Zebrafish larvae lose vision at night. *Proc. Natl. Acad. Sci. U.S.A.* 107, 6034–6039.

Ermilov, A. N., Olshevskaya, E. V., and Dizhoor, A. M. (2001). Instead of binding calcium, one of the EF-hand structures in guanylyl cyclase activating protein 2 is required for targeting photoreceptor guanylyl cyclase. *J. Biol. Chem.* 51, 48143–48148.

Fain, G. L. (2006). Why photoreceptors die and why they don't. *Bioessays* 28, 344–354.

Feil, S., Zimmermann, A., Knorn, A., Brummer, S., Schlossmann, J., Hofmann, F., and Feil, R. (2005). Distribution of cGMP-dependent protein kinase type I and its isoform in the mouse brain and retina. *Neuroscience* 135, 863–868.

Frank, T., Khimich, D., Neef, A., and Moser, T. (2009). Mechanisms contributing to synaptic Ca2+ signals and their heterogeneity in hair cells. *Proc. Natl. Acad. Sci. U.S.A.* 106, 4483–4488.

Frank, T., Rutherford, M. A., Strenzke, N., Neef, A., Pangrsic, T., Khimich, D., Fejtova, D., Gundelfinger, E. D., Liberman, M. C., Harke, B., Bryan, K. E., Lee, A., Egner, A., Riedel, D., and Moser, T. (2010). Bassoon and the synaptic ribbon organize Ca2+-channels and vesicles to add release sites and promote refilling. *Neuron* 68, 724–738.

Gebhart, M., Juhasz-Vedres, G., Zuccotti, A., Brandt, N., Engel, J., Trockenbacher, A., Kaur, G., Obermair, G. J., Knipper, M., Koschak, A., and Striessnig, J. (2010). Modulation of CaV1.3 channel gating by Rab3 interacting molecule. *Mol. Cell. Neurosci.* 44, 246–259.

Graydon, C. W., Cho, S., Li, G. L., Kachar, B., and von Gersdorff, H. (2011). Sharp Ca2+ nanodomains beneath the ribbon promote highly synchrous multivesicular release at hair cell synapses. *J. Neurosci.* 31, 16637–16650.

Haeseleer, F., Imanishi, Y., Maeda, T., Possin, D. E., Maeda, A., Lee, A., Rieke, F., and Palczewski, K. (2004). Essential role of Ca2+-binding protein 4, a CaV1.4 channel regulator, in photoreceptor synaptic function. *Nat. Neurosci.* 7, 1079–1087.

Haeseleer, F., Imanishi, Y., Sokal, I., Filipek, S., and Palzewski, K. (2002). Calcium-binding proteins: intracellular sensors from the calmodulin superfamily. *Biochem. Biophys. Res. Commun.* 290, 615–623.

Haeseleer, F. (2008). Interaction and colocalization of CaBP4 and unc119 (MRG4) in photoreceptors. *Invest. Ophthalmol. Vis. Sci.* 49, 2366–2375.

Haire, S. E., Pang, J., Boye, S. L., Sokal, I., Craft, C. M., Palczewski, K., Hauswirth, M. M., and Semple-Rowland, S. L. (2006). Light-driven cone arrestin translocation in cones of postnatal guanylate cyclase-1 knockout mouse retina treated with AAV-GC1. *Invest. Ophthalmol. Vis. Sci.* 47, 3745–3753.

Han, Y., Kaeser, P. S., Südhof, T. C., and Schneggenburger, R. (2011). RIM determines Ca2+ channel density and vesicle docking at the presynaptic active zone. *Neuron* 69, 304–316.

Heidelberger, R., Thoreson, W. B., and Witkovsky, P. (2005). Synaptic transmission at retinal ribbon synapses. *Prog. Retin. Eye Res.* 24, 682–720.

Hibino, H., Pironkova, R., Onwumere, O., Vologodskaia, M., Hudspeth, A. J., and Lesage, F. (2002). RIM binding proteins (RBPs) couple Rab3-interacting molecules (RIMs) to voltage-gated Ca2+-channels. *Neuron* 34, 411–423.

Hull, C., Studholme, K., Yazulla, S., and von Gersdorff, H. (2006). Diurnal changes in exocytosis and the number of synaptic ribbons at active zones of an ON-type bipolar cell terminal. *J. Neurophysiol.* 96, 2025–2033.

Hunt, D. M., Buch, P., and Michaelidis, M. (2010). Guanylate cyclases and associated activator proteins in retinal disease. *Mol. Cell. Biochem.* 334, 157–168.

Hwang, J.-Y., Schlesinger, R., and Koch, K. W. (2004). Irregular dimerization of guanylate cyclase-activating protein 1 mutants causes loss of target activation. *Eur. J. Biochem.* 271, 3785–3793.

Jackman, S. L., Babai, N., Chambers, J. J., Thoreson, W. B., and Kramer, R. H. (2010). A positive feedback synapse from horizontal cells to cone photoreceptors. *Plos Biol.* 9, e1001057. doi: 10.1371/journal.pbio.1001057

Jackman, S. L., Choi, S. Y., Thoreson, W. B., Rabl, K., Bartoletti, T. M., and Kramer, R. H. (2009). Role of the synaptic ribbon in transmitting the cone light response. *Nat. Neurosci.* 12, 303–310.

Jarsky, T., Tian, M., and Singer, J. H. (2010). Nanodomain control of exocytosis is responsible for the signalling capability of a retinal ribbon synapse. *J. Neurosci.* 30, 11885–11895.

Jaumann, M., Dettling, J., Gubelt, M., Zimmermann, U., Gerling, A., Paquet-Durand, F., Feil, S., Wolpert, S., Franz, C., Varakina, K., Xiong, H., Brandt, N., Kuhn, S., Geisler, H. S., Rohbock, K., Ruth, P., Schlossmann, J., Hütter, J., Sandner, P., Feil, R., Engel, J., Knipper, M., and Rüttiger, L. (2012). cGMP-Prgk1 signaling and Pde5 inhibition shelter cochlear hair cells and hearing function. *Nat. Med.* 18, 252–259.

Jiang, L., and Baehr, W. (2010). GCAP1 mutations associated with autosomal dominant cone dystrophy. *Adv. Exp. Med. Biol.* 664, 273–282.

Jiang, L., Katz, B. J., Yang, Z., Zhao, Y., Faulkner, N., Hu, J., Baird, J., Baehr, W., Creel, D. J., and Zhang, K. (2005). Autosomal dominant cone dystrophy caused by a novel mutation in the GCAP1 gene (Guca1A). *Mol. Vis.* 11, 143–151.

Johnson, J. E. Jr., Perkins, G. A., Anand Giddabasappa, C. S., Chaney, S., Xiao, W., White, A. D., Brown, J. M., Waggoner, J., Ellisman, M. H., and Fox, D. A. (2007). Spatiotemporal regulation of ATP and Ca2+ dynamics in vertebrate rod and cone ribbon synapses. *Mol. Vis.* 13, 887–919.

Johnson, S. L., Forge, A., Knipper, M., Münkner, S., and Marcotti, W. (2008). Tonotopic variation in the calcium dependence of neurotransmitter release and vesicle pool replenishment at mammalian auditory ribbon synapses. *J. Neurosci.* 28, 7670–7678.

Joselevitch, C., and Zenisek, D. (2010). The cytomatrix protein bassoon contributes to fast transmission at conventional and ribbon synapses. *Neuron* 68, 604–606.

Kachi, S., Nishizawa, Y., Olshevskaya, E., Yamazaki, A., Miyake, Y., Wakabashi, T., Dizhoor, A. M., and Usukura, J. (1999). Detailed localization of photoreceptor guanylate cyclase activating protein-1 and -2 in mammalian retinas using light and electron microscopy. *Exp. Eye Res.* 68, 465–473.

Kaeser, P. (2011). Pushing vesicles over the RIM. *Cell. Logist.* 1, 106–110.

Kaeser, P. S., Deng, L., Wang, Y., Dulubova, I., Liu, X., Rizo, J., and Südhof, T. C. (2011). RIM tethers Ca2+ channels to presynaptic active zones via a direct PDZ-domain interaction. *Cell* 144, 282–295.

Karan, S., Frederick, J. M., and Baehr, W. (2010). Novel functions of photoreceptor guanylate cyclases revealed by targeted deletion. *Mol. Cell. Biochem.* 334, 141–155.

Kersten, F. J. K., van Wijk, E., van Reenwijk, J., van der Zwaag, B., Märker, T., Peters, T. A., Katsanis, N., Wolfrum, U., Keunen, J. E. E., Roepman, R., and Kremer, H. (2010). Association of whirlin with CaV1.3(α1D) channels in photoreceptors, defining a novel member of the Usher protein network. *Invest. Ophthalmol. Vis. Sci.* 51, 2338–2346.

Khimich, D., Nouvian, R., Pujol, R., tom Dieck, S., Egner, A., Gundelfinger, E. D., and Moser, T. (2005). Hair cell synaptic ribbons are essential for synchronous auditory signalling. *Nature* 434, 889–894.

Kiyonaka, S., Wakamori, M., Miki, T., Uriu, Y., Nonaka, M., Bito, H., Beedle, A. M., Mori, E., Hara, Y., De Waard, M., Kanagawa, M., Itakura, M., Takahashi, M., Campbell, K. P., and Mori, Y. (2007). RIM1 confers sustained activity and neurotransmitter vesicle anchoring to presynaptic Ca2+-channels. *Nat. Neurosci.* 10, 691–701.

Knop, G. C., Seeliger, M. W., Thiel, F., Mataruga, A., Kaupp, U. B., Friedburg, C., Tanimoto, N., and Kaupp, U. B. (2008). Light responses in the mouse retina are prolonged upon targeted deletion of the HCN1 channel gene. *Eur. J. Neurosci.* 28, 2221–2230.

Ko, M. L., Liu, Y., Dryer, S. E., and Ko, G. Y. (2007). The expression of L-type voltage-gated calcium channels in retinal photoreceptors is under circadian control. *J. Neurochem.* 103, 784–792.

Kobayashi, A., Higashide, T., Hamasaki, D., Kubota, S., Sakuma, A., An, W., Fujimaki, T., McLaren, M. J., Weleber, R. G., and Inana, G. (2000). HRG4 (UNC119) mutation found in cone-rod dystrophy causes retinal degeneration in a transgenic model. *Invest. Ophthalmol. Vis. Sci.* 41, 3268–3277.

Koch, K. W. (2006). GCAPs, the classical neuronal calcium sensors in the retina. In: Calcium binding proteins. *Landes Biosci.* 1, 3–6.

Koch, K. W., Duda, T., and Sharma, R. K. (2010). Ca2+-modulated vision-linked ROS-GC guanylate cyclase transduction machinery. *Mol. Cell. Biochem.* 334, 105–115.

Koike, C., Numata, T., Ueda, H., Mori, Y., and Furukawa, T. (2010), TRPM1: a vertebrate TRP channel responsible for retinal ON bipolar function. *Cell Calcium* 48, 95–101.

Kourennyi, D. E., Liu, X. D., Hart, J., Mahmud, F., Baldridge, W. H., and Barnes, S. (2004). Reciprocal modulation of calcium dynamics at rod and cone photoreceptor synapses

by nitric oxide. *J. Neurophysiol.* 92, 477–483.

Krizaj, D., and Copenhagen, D. R. (2002). Calcium regulation in photoreceptors. *Front. Biosci.* 7, 2023–2044.

Lacinova, L. (2005). Voltage-dependent calcium channels. *Gen. Physiol. Biophys.* 24(S1), 1–78.

Lange, C., Duda, T., Beyermann, M., Sharma, R. K., and Koch, K.-W. (1999). Regions in vertebrate photoreceptor guanylyl cyclase ROS-GC1 involved in Ca2+-dependent regulation by guanylyl cyclase-activating protein GCAP-1. *FEBS Lett.* 460, 27–31.

Liberman, L. D., Wang, H., and Liberman, M. C. (2011). Opposing gradients of ribbon size and AMPA receptor expression underlie sensitivity differences among cochlear-nerve/hair-cell synapses. *J. Neurosci.* 31, 801–808.

Liu, X., Seno, K., Nishizawa, Y., Hayashi, F., Yamazaki, A., Matsumoto, H., Wakabayashi, T., and Usukura, J. (1994). Ultrastructural localization of retinal guanylate cyclase in human and monkey retina. *Exp. Eye Res.* 59, 761–768.

Magupalli, V. G., Schwarz, K., Alpadi, K., Natarajan, S., Seigel, G. M., and Schmitz, F. (2008). Multiple RIBEYE – RIBEYE interactions create a dynamic scaffold for the formation of synaptic ribbons. *J. Neurosci.* 28, 7954–7967.

Makino, C. L., Peshenko, I. V., Wen, X. H., Olshevskaya, E. V., Barrett, R., and Dizhoor, A. M. (2008). A role for GCAP2 in regulating the photoreceptor response: guanylyl cyclase activation and rod physiology in GUCA1B knockout mice. *J. Biol. Chem.* 283, 29135–29143.

Matthews, G., and Fuchs, P. (2010). The diverse roles of ribbon synapses in sensory neurotransmission. *Nat. Rev. Neurosci.* 11, 812–822.

Mercer, A. J., Chen, M., and Thoreson, W. B. (2011a). Lateral mobility of presynaptic L-type calcium channels at photoreceptor ribbon synapses. *J. Neurosci.* 31, 4397–4406.

Mercer, A. J., and Thoreson, W. B. (2011b). The dynamic architecture of photoreceptor ribbon synapses: cytoskeletal, extracellular matrix, and intramembrane proteins. *Vis. Neurosci.* 28, 453–471.

Miki, T., Kiyonaka, S., Uriu, Y., deWaard, M., Wakamori, M., Beedle, A. M., Campbell, K., and Mori, Y. (2007). Mutation associated with an autosomal dominant cone-rod dystrophy CORD7 modifies RIM1-mediated modulation of voltage-gated Ca2+-channels. *Channels* 1, 144–147.

Morgans, C. W. (2001). Localization of the α1F calcium channel subunit in the rat retina. *Invest. Ophthalmol. Vis. Sci.* 42, 2414–2418.

Morgans, C. W., Bayley, P. R., Oesch, N., Ren, G., Akileswaran, L., and Taylor, W. R. (2005). Photoreceptor calcium channels: insight from night blindness. *Vis. Neurosci.* 22, 561–568.

Morgans, C. W., Brown, R. L., and Duvoisin, R. M. (2010). TRPM1: an endpoint of the mGluR6 signal transduction cascade in retinal ON-bipolar cells. *Bioesssays* 32, 609–614.

Müller, F., Scholten, A., Ivanova, E., Haverkamp, S., Kremmer, E., and Kaupp, U. B. (2003). HCN channels are expressed differentially in retinal bipolar cells and concentrated at synaptic terminals. *Eur. J. Cell Biol.* 17, 2084–2096.

Nachman-Clewner, M., St Jules, R., and Townes-Anderson, E. (1999). L-type calcium channels in the photoreceptor synapse: localization and role in synaptic plasticity. *J. Comp. Neurol.* 415, 1–16.

Neher, E., and Sakaba, T. (2008). Multiple roles of calcium ions in the regulation of neurotransmitter release. *Neuron* 59, 861–872.

Okawa, H., Miyagishima, J., Arman, A. C., Hurley, J. B., Field, G. F., and Sampath, A. P. (2010). Optimal processing of photoreceptor signals is required to maximize behavioural sensitivity. *J. Physiol.* 588, 1947–1960.

Olshevskaya, E. V., Ermilov, A. N., and Dizhoor, A. M. (2002). Factors that affect regulation of cGMP synthesis in vertebrate photoreceptors and their genetic link to human retinal degeneration. *Mol. Cell. Biochem.* 230, 139–147.

Otto-Bruc, A., Fariss, R. N., Haeseleer, F., Huang, J., Buczylko, J., Surgocheva, I., Baehr, W., Milam, A. H., and Palczewski, K. (1997). Localization of guanylate cyclase-activating protein 2 in mammalian retina. *Proc. Natl. Acad. Sci. U.S.A.* 94, 4727–4732.

Pahlberg, J., and Sampath, A. P. (2011). Visual thresholds is set by linear and nonlinear mechanisms: how neural circuits in the retina improve the signal-to-noise ratio of the single photon response. *Bioessays* 33, 438–447.

Paquet-Durand, F., Beck, S., Michalakis, S., Goldmann, T., Huber, S., Mühlfriedel, R., Trifunovic, D., Fischer, M. D., Fahl, E., Duetsch, G., Becirovic, E., Wolfrum, U., van Veen, T., Biel, M., Tanimoto, N., and Seeliger, M. W. (2011). A key role for cyclic nucleotide gated (CNG) channels in cGMP related retinitis pigmentosa. *Hum. Mol. Genet.* 20, 941–947.

Palczewski, K., Sokal, I., and Baehr, W. (2004). Guanylate cyclase-activating proteins: structure, function and diversity. *Biochem. Biophys. Res. Comm.* 322, 1123–1130.

Pennesi, M. E., Howes, K. A., Baehr, W., and Wu, S. M. (2003). Guanylate cyclase activating protein (GCAP1) 1 rescues cone recovery kinetics in GCAP1/GCAP2 knockout mice. *Proc. Natl. Acad. Sci. U.S.A.* 100, 6783–6788.

Peshenko, I. V., Olshevskaya, E. V., Savchenko, A. B., Karan, S., Palczewski, K., Baehr, W., and Dizhoor, A. M. (2011a). Enzymatic properties and regulation of the native isozymes of retinal membrane guanylyl cyclase (RetGC) from mouse photoreceptors. *Biochemistry* 50, 5590–5600.

Peshenko, I. V., Olshevskaya, E. V., Azadi, S., Molday, L. L., Molday, R. S., and Dizhoor, A. M. (2011b). Retinal degeneration 3 (RD3) protein inhibits catalytic activity of retinal membrane guanylyl cyclase (RetGC) and its stimulation by activating proteins. *Biochemistry* 50, 9511–9519.

Potter, L. R. (2011). Guanylyl cyclase structure, function and regulation. *Cell Signal.* 23, 1921–1926.

Rambotti, M. G., Spreca, A., Giambanco, I., Sorci, G., and Donato, R. (2002). Ultracytochemistry as a tool for the study of the cellular and subcellular localization of membrane-bound guanylate cyclases (GC) activity. Applicability to both receptor-activated and receptor-independent GC activity. *Mol. Cell. Biochem.* 230, 85–96.

Regus-Leidig, H., and Brandstätter, J. H. (2011). Structure and function of a complex sensory synapse. *Acta Physiol. (Oxf)* [Epub ahead of print].

Regus-Leidig, H., Specht, D., tom Dieck, S., and Brandstätter, J. H. (2010). Stability of active zone components at the photoreceptor ribbon complex. *Mol. Vis.* 16, 2690–2770.

Rieke, F., and Schwartz, E. A. (1994). A cGMP-gated current can control exocytosis at cone synapses. *Neuron* 13, 863–873.

Sakurai, K., Chen, J., and Kefalov, V. J. (2011). Role of guanylyl cyclase modulation in mouse cone phototransduction. *J. Neurosci.* 22, 7991–8000.

Sato, M., Ohtsuka, T., and Stell, W. K. (2011). Endogenous nitric oxide enhances the light-response of cones during light-adaptation in the rat retina. *Vis. Res.* 51, 131–137.

Savchenko, A., Barnes, S., and Kramer, R. H. (1997). Cyclic-nucleotide-gated channels mediate synaptic feedback by nitric oxide. *Nature* 390, 694–698.

Schmitz, F. (2009). The making of synaptic ribbons: how they are built and what they do. *Neuroscientist* 15, 611–624.

Schmitz, F., Königstorfer, A., and Südhof, T. C. (2000). RIBEYE, a component of synaptic ribbons: a protein's journey through evolution provides insights into synaptic ribbon function. *Neuron* 28, 857–872.

Seeliger, M. W., Brombas, A., Weiler, R., Humphries, P., Knop, G., Tanimoto, N., and Müller, F. (2011). Modulation of rod photoreceptor output by HCN1 channels is essential for regular mesopic cone vision. *Nat. Commun.* 2, 532.

Seidel, A., Kantarjian, A., and Vollrath, L. (1990). A possible role for cyclic guanosine monophosphate in the rat pineal gland. *Neurosci. Lett.* 110, 227–231.

Sharma, R. K. (2002). Evolution of the membrane guanylate cyclase transduction system. *Mol. Cell. Biochem.* 230, 3–30.

Sharma, R. K. (2010). Membrane guanylate cyclase is a beautiful signal transduction machinery. *Mol. Cell. Biochem.* 334, 3–36.

Sheets, L., Trapani, J. G., Mo, W., Obholzer, N., and Nicolson, T. (2011). RIBEYE is required for presynaptic Ca(V)1.3 channel localization and afferent innervation of sensory hair cells. *Development* 138, 1309–1319.

Sheng, Z., Choi, S. Y., Dharia, A., Li, J., Sterling, P., and Kramer, R. H. (2007). Synaptic Ca2+ in darkness is lower in rods than in cones, causing slower tonic release of vesicles. *J. Neurosci.* 27, 5033–5042.

Singer, J. H., Lassová, L., Vardi, N., and Singer, J. S. (2004). Coordinated multivesicular release at a mammalian ribbon synapse. *Nat. Neurosci.* 7, 826–833.

Singh, A., Hamedinger, D., Hoda, J. C., Gebhart, M., Koschak, A., Romanin, C., and Striessnig, J. (2006). C-terminal modulator controls Ca2+-dependent gating of Ca(v)1.4 L-type Ca2+ channels. *Nat. Neurosci.* 9, 1108–1116.

Snellman, J., Mehta, B., Babai, N., Bartoletti, T. M., Akmentin, W., Francis, A., Matthews, G., Thoreson, W. B., and Zenisek, D. (2011). Acute destruction of the synaptic ribbon reveals a role for the ribbon in vesicle priming. *Nat. Neurosci.* 14, 1135–1141.

Spessert, R., Gupta, B. B. P., Seidel, A., Maitra, S. K., and Vollrath, L. (1992). Involvement of cyclic guanosine monophosphate (cGMP) and cytosolic guanylate cyclase in the regulation of synaptic ribbon numbers in the rat pineal gland. *Brain Res.* 570, 231–236.

Spiwoks-Becker, I., Glas, M., Lasarzik, I., and Vollrath, L. (2004). Synaptic ribbons lose and regain material in response to illumination changes. *Eur. J. Neurosci.* 19, 1559–1571.

Stephen, R., Bereta, G., Golczak, M., Palczewski, K., and Souza, M. C. (2007). Stabilizing function for myristoyl group revealed by the crystal structure of a neuronal calcium sensor, guanylate cyclase-activating protein 1. *Structure* 15, 1392–1402.

Stephen, R., Filipek, S., Palczewski, K., and Souza, M. C. (2008). Ca2+-dependent regulation of phototransduction. *Photochem. Photobiol.* 84, 903–910.

Striessnig, J., Bolz, H. J., and Koschak, A. (2010). Channelopathies in CaV 1.1, CaV1.3, and CaV1.4 voltage-gated L-type Ca2+-channels. *Pflugers Arch.* 460, 361–374.

Suryanarayanan, A., and Slaughter, M. M. (2006). Synaptic transmission mediated by internal calcium stores in rod photoreceptors. *J. Neurosci.* 26, 1759–1766.

Szikra, T., Barabas, P., Bartoletti, T. M., Huang, W., Akopian, A., Thoreson, W. B., and Krizaj, D. (2009). Calcium homeostasis and cone signalling are regulated by interactions between calcium stores and plasma membrane ion channels. *Plos One* 4, e6723. doi: 10.1371/journal.pone.0006723

Szikra, T., Cusato, K., Thoreson, W. B., Barabas, P., Bartoletti, T. M., and Krizaj, D. (2008). Depletion of calcium stores regulates calcium influx and signal transmission in rod photoreceptors. *J. Physiol.* 586, 4859–4875.

Tanimoto, N., Brombas, A., Müller, F., and Seeliger, M. W. (2012). HCN1 channels significantly shape retinal photoresponses. *Adv. Exp. Med. Biol.* 723, 807–812.

tom Dieck, S., Altrock, W. D., Kessels, M. M., Qualmann, B., Regus, H., Brauner, D., Fejtova, A., Bracko, O., Gundelfinger, E. D., and Brandstätter, J. H. (2005). Molecular dissection of the photoreceptor ribbon synapse: physical interaction of bassoon and Ribeye is essential for the assembly of the ribbon complex. *J. Cell Biol.* 168, 825–836.

Townes-Anderson, E., and Zhang, N. (2006). "Synaptic plasticity and structural remodelling of rod and cone cells," in *Plasticity of the Visual System: From Genes to Circuits*, eds R. Pinaud, L. A. Tremere, and P. DeWeerds, (Berlin, Heidelberg, NY: Springer Science), 13–31.

Uthaiah, R. C., and Hudspeth, A. J. (2010). Molecular anatomy of the hair cell's ribbon synapse. *J. Neurosci.* 30, 12387–12399.

Venkataraman, V., Duda, T., Vardi, N., Koch, K. W., and Sharma, R. K. (2003). Calcium-modulated guanylate cyclase transduction machinery in the photoreceptor-bipolar synaptic region. *Biochemistry* 42, 5640–5648.

Venkatesan, J. K., Natarajan, S., Schwarz, K., Mayer, S. I., Alpadi, K., Magupalli, V. G., Sung, C. H., and Schmitz, F. (2010). Nicotinamide adenine dinucleotide-dependent binding of the neuronal Ca2+ sensor protein GCAP2 to photoreceptor synaptic ribbons. *J. Neurosci.* 30, 6559–6567.

Vollrath, L., and Spiwoks-Becker, I. (1996). Plasticity of retinal ribbon synapses. *Microsc. Res. Tech.* 35, 472–487.

Wahl-Schott, C., Baumann, L., Cuny, H., Eckert, C., Griessmaier, K., and Biel, M. (2006). Switching off calcium-dependent inactivation in L-type calcium channels by an autoinhibitory domain. *Proc. Natl. Acad. Sci. U.S.A.* 103, 15657–15662.

Wan, Q. F., and Heidelberger, R. (2011). Synaptic release at mammalian bipolar cell terminals. *Vis. Neurosci.* 28, 109–119.

Wang, Y., Okamoto, M., Schmitz, F., Hofmann, K., and Südhof, T. C. (1997). RIM is a putative effector in regulating synaptic-vesicle fusion. *Nature* 388, 593–598.

Wässle, H. (2004). Parallel processing in the mammalian retina. *Nat. Rev. Neurosci.* 5, 1–12.

Woodruff, M. L., Sampath, A. P., Matthews, H. R., Krasnoperova, N. V., Lem, J., and Fain, G. L. (2002). Measurement of cytoplasmic calcium concentration in the rods of wild-type and transducin knockout mice. *J. Physiol.* 542, 843–854.

Wycisk, K. A., Budde, B., Feil, S., Skosyrski, S., Buzzi, F., Neidhardt, J., Glaus, E., Nürnberg, P., Rüther, K., and Berger, W. (2006). Structural and functional abnormalities of retinal ribbon synapses due to Cacna2d4 mutation. *Invest. Ophthalmol. Vis. Sci.* 47, 3523–3530.

Xiao, H., Chen, X., and Steele, Jr. E. C. (2007). Abundant L-type calcium channel CaV1.3 (alpha1D) subunit mRNA is detected in rod photoreceptors of the mouse retina via in-situ hybridization. *Mol. Vis.* 13, 764–771.

Yang, P. S., Alseikhan, B. A., Hiel, H., Grant, L., Mori, M. X., Yang, W., Fuchs, P. A., and Yue, D. T. (2006). Switching of the Ca2+-dependent inactivation of CaV1.3-channels by calcium binding proteins of auditory hair cells. *J. Neurosci.* 26, 10677–10689.

Zeitz, C., Kloeckener-Gruissem, B., Forster, U., Kohl, S., Magyar, I., Wissinger, B., Mátyás, G., Borruat, F. X., Schorderet, D. F., Zrenner, E., Munier, F. L., and Berger, W. (2006). Mutations in CABP4, the gene encoding the Ca2+-binding protein 4, cause autosomal recessive night blindness. *Am. J. Hum. Genet.* 79, 657–667.

Zenisek, D., Steyer, J. A., and Almers, W. (2000). Transport, capture and exocytosis of synaptic vesicles at active zones. *Nature* 406, 849–854.

Zhang, N., and Townes-Anderson, E. (2002). Regulation of structural plasticity by different channel types in rod and cone photoreceptors. *J. Neurosci.* 22, 7065–7079.

Zhang, N., Beuve, A., and Townes-Anderson, E. (2005). The nitric-cGMP signalling pathway differentially regulates presynaptic structural plasticity in cone and rod cells. *J. Neurosci.* 25, 2761–2770.

Conflict of Interest Statement: The authors declare that the research was conducted in the absence of any commercial or financial relationships that could be construed as a potential conflict of interest.

Received: 09 January 2012; paper pending published: 25 January 2012; accepted: 15 February 2012; published online: 29 February 2012.

Citation: Schmitz F, Natarajan S, Venkatesan JK, Wahl S, Schwarz K and Grabner CP (2012) EF hand-mediated Ca^{2+}- and cGMP-signaling in photoreceptor synaptic terminals. Front. Mol. Neurosci. 5:26. doi: 10.3389/fnmol.2012.00026

frontiers in
MOLECULAR NEUROSCIENCE

ORIGINAL RESEARCH ARTICLE
published: 22 February 2012
doi: 10.3389/fnmol.2012.00019

Interaction of GCAP1 with retinal guanylyl cyclase and calcium: sensitivity to fatty acylation

Igor V. Peshenko, Elena V. Olshevskaya and Alexander M. Dizhoor*

Department of Basic Science and Pennsylvania College of Optometry, Salus University, Elkins Park, PA, USA

Edited by:
Michael R. Kreutz, Leibniz-Institute for Neurobiology, Germany

Reviewed by:
Carlo Sala, CNR Institute of Neuroscience, Italy
Karl-Wilhelm Koch, Carl von Ossietzky University Oldenburg, Germany

****Correspondence:***
Alexander M. Dizhoor, Department of Basic Science and Pennsylvania College of Optometry, Salus University, 8360 Old York Road, Elkins Park, PA 19027, USA.
e-mail: adizhoor@salus.edu

Guanylyl cyclase activating proteins (GCAPs) are calcium/magnesium binding proteins within neuronal calcium sensor proteins group (NCS) of the EF-hand proteins superfamily. GCAPs activate retinal guanylyl cyclase (RetGC) in vertebrate photoreceptors in response to light-dependent fall of the intracellular free Ca^{2+} concentrations. GCAPs consist of four EF-hand domains and contain N-terminal fatty acylated glycine, which in GCAP1 is required for the normal activation of RetGC. We analyzed the effects of a substitution prohibiting N-myristoylation (Gly2 → Ala) on the ability of the recombinant GCAP1 to co-localize with its target enzyme when heterologously expressed in HEK293 cells. We also compared Ca^{2+} binding and RetGC-activating properties of the purified non-acylated G2A mutant and C14:0 acylated GCAP1 *in vitro*. The G2A GCAP1 expressed with a C-terminal GFP tag was able to co-localize with the cyclase, albeit less efficiently than the wild type, but much less effectively stimulated cyclase activity *in vitro*. Ca^{2+} binding isotherm of the G2A GCAP1 was slightly shifted toward higher free Ca^{2+} concentrations and so was Ca^{2+} sensitivity of RetGC reconstituted with the G2A mutant. At the same time, myristoylation had little effect on the high-affinity Ca^{2+}-binding in the EF-hand proximal to the myristoyl residue in three-dimensional GCAP1 structure. These data indicate that the N-terminal fatty acyl group may alter the activity of EF-hands in the distal portion of the GCAP1 molecule via presently unknown intramolecular mechanism.

Keywords: photoreceptors, calcium, guanylyl cyclase, myristoylation

INTRODUCTION

Retinal guanylyl cyclase activating proteins (GCAPs) form a subfamily within the neuronal calcium sensor (NCS) proteins group of the EF-hand superfamily (reviewed in: Burgoyne, 2007). The GCAPs are closely related to neurocalcin, hippocalcin, recoverin, and other NCS proteins and share a number of typical features for the group: they consist of two pairs of calmodulin-type EF-hands (Ames et al., 1999; Stephen et al., 2006, 2007), of which the N-terminal EF-hand 1 does not bind divalent cation, and are modified at the N-terminus by fatty acyl group (**Figure 1A**). The modification is commonly referred to as myristoylation, although in mammalian retinal proteins, the N-terminal Gly group can be fatty acylated by one of four different C14 and C12 derivatives (Dizhoor et al., 1992; Johnson et al., 1994), all of which can be found in GCAP (Palczewski et al., 1994).

Among the NCS proteins, GCAPs arguably have the most clearly understood physiological function. The GCAPs regulate activity of retinal membrane guanylyl cyclase (RetGC) in photoreceptors in a Ca^{2+}-sensitive manner (Koch and Stryer, 1988; Dizhoor et al., 1994, 1995; Gorczyca et al., 1994) and thus critically expedite recovery and light adaptation of rods and cones (Mendez et al., 2001; Burns et al., 2002; Sakurai et al., 2011). Rods and cones maintain partially depolarized state in the dark by opening a fraction of cGMP-gated channels in the outer segment, thus allowing influx of Na^+ and Ca^{2+}. In the light, when bleached photopigment activates phototransduction cascade, cGMP becomes rapidly depleted by light-activated phosphodiesterase and the cGMP-gated channels become closed, thus causing hyperpolarization of the membrane—the first cellular step in visual signal detection (reviewed in: Fu and Yau, 2007). Photoreceptors can quickly recover from excitation and adapt to background illumination by re-opening cGMP-gated channels, and GCAPs control one of the key biochemical pathways expediting the recovery and light adaptation. In response to illumination, GCAPs activate cGMP re-synthesis via negative calcium feedback mechanism that trails the excitation state of the photoreceptor (reviewed in: Pugh et al., 1997, 1999). Ca^{2+} is constantly extruded from the outer segment via Na/Ca, K-exchanger, in the dark, when several percent of the cGMP-gated channels are open at any given time, Ca^{2+} can re-enter the outer segment through the open channels and accumulates in the cytoplasm at submicromolar concentrations. In mouse rods, the measured steady-state concentrations in the dark approach 250 nm (as high as 410–560 nm free Ca^{2+} were reported in lower vertebrates) and rapidly fall nearly 10-fold in the light, when the cGMP-gated channels are shut down (Gray-Keller and Detwiler, 1994; Sampath et al., 1999; Woodruff et al., 2002). Therefore, GCAPs bind Ca^{2+} and maintain their inhibitory conformation that

Abbreviations: EGTA, ethylene glycol-bis(2-aminoethylether)-N,N,N′,N′-tetraacetic acid; GCAP, guanylyl cyclase activating protein; RetGC, retinal membrane guanylyl cyclase; GFP, green fluorescent protein; NCS proteins, neuronal calcium binding proteins.

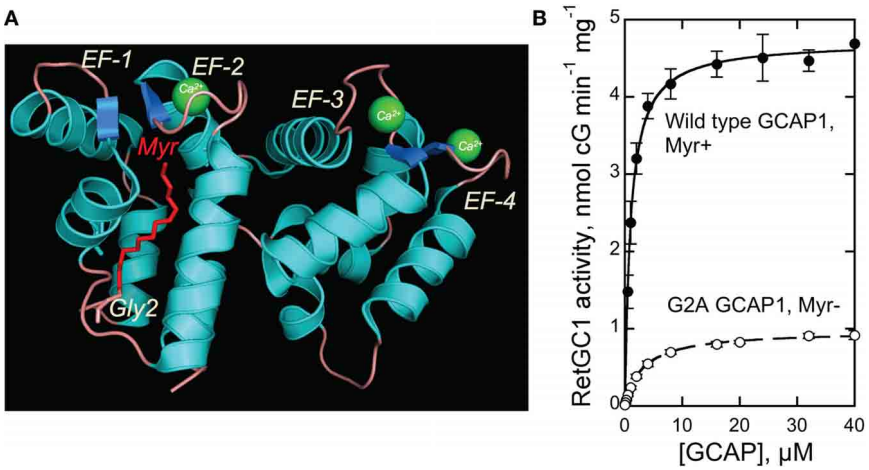

FIGURE 1 | (A) Structure of myristoylated GCAP1 [Stephen et al. (2007)]. Myristoyl residue buried inside the EF-1/EF-2 pair of EF-hands is shown in *red*. **(B)** Dose-dependence of recombinant RetGC1 activation by myristoylated and G2A GCAP1 (mean ± SD). For details of the assay—see Materials and Methods.

decelerates RetGC in the dark (Dizhoor and Hurley, 1996; Dizhoor et al., 1998). Mg^{2+} can actively compete with Ca^{2+} binding in EF-hand domains of GCAPs (Peshenko and Dizhoor, 2004), and at the low free Ca^{2+} levels in the light it converts GCAPs into Mg^{2+}-bound, RetGC activator state. This stimulates cGMP synthesis and, therefore, allows the rod to timely re-open the cGMP-gated channels and recover from the hyperpolarization state. Following the completion of recovery, Ca^{2+} returned through the re-opened cGMP-gated channels converts GCAPs back to their Ca^{2+}-bound inhibitory form, thus completing the light-driven functional cycle of GCAP (reviewed in: Dizhoor et al., 2010).

GCAPs exist in several isoforms (Imanishi et al., 2004), of which GCAP1 (Gorczyca et al., 1994; Palczewski et al., 1994) and GCAP2 (Dizhoor et al., 1994, 1995) are ubiquitous among all tested vertebrate species. They regulate RetGC with distinctly different sensitivities to Ca^{2+} (Hwang and Koch, 2002; Hwang et al., 2003; Peshenko et al., 2004, 2011) and, therefore, sequentially activate RetGC at different phases of rod photoresponse (Makino et al., 2008). The two GCAPs also differ in their requirement of the N-fatty acylation for their function. While N-myristoylation has relatively modest impact on the regulatory activity of GCAP2 *in vitro* (Olshevskaya et al., 1997), it is much more critically needed for the activity of GCAP1 (Otto-Bruc et al., 1997; Hwang and Koch, 2002). The best-known Ca^{2+}-dependent conformational change described for NCS proteins is a "calcium-myristoyl switch"—Ca^{2+}-dependent release of the myristoylated N-terminus from the cavity created by alpha-helical structures of EF-hands 1 and 2 (Zozulya and Stryer, 1992; Dizhoor et al., 1993; Ames et al., 1995, 1997; Lim et al., 2011). In contrast, NMR data argue that myristoyl chain does not undergo Ca^{2+}-myristoyl switch in GCAP1 and GCAP2 (Hughes et al., 1998; Lim et al., 2009), and it remains buried inside the protein in the X-ray crystal structure of GCAP1 (Stephen et al., 2007) (**Figure 1A**). In this study, we addressed functional effects of N-fatty acylation in bovine GCAP1 on its interaction with the target enzyme and the ability to "sense" Ca^{2+}.

MATERIALS AND METHODS

MUTAGENESIS

Mutations were introduced in bovine GCAP1 cDNA by "splicing by overlap extension" technique using PCR reactions catalyzed by high-fidelity Phusion Flash polymerase (Finnzymes). The resultant products were ligated into the NcoI/BamHI sites of pET11d (Novagene) vector, sequenced, and transformed into expressing cell lines as described previously in detail (Peshenko and Dizhoor, 2006). RetGC1 tagged by mOrange was constructed by inserting mOrange (Clontech) cDNA into a modified human RetGC1 cDNA-harboring pRCCMV plasmid (Laura et al., 1996) as follows. The XhoI-XhoI fragment of the vector was excised by XhoI digest and self-ligation, then the coding region for the extracellular domain of RetGC1 was modified by ligating a linker fragment into the HindIII/BsteII sites to introduce two new restriction sites, NheI and AgeI beginning after 33 base pairs downstream from the leader peptide-coding fragment. The mOrange cDNA, PCR-amplified with the NheI and AgeI sites at the 5′- and 3′-end, respectively, was ligated into the corresponding restriction sites of the modified pRetGC1-RCCMV plasmid. The resultant construct encoded 238 a.a. mOrange protein sequence downstream from the 51 a.a. leader peptide, replacing a short fragment, Ala63–Phe68, of the RetGC1 extracellular domain.

GCAP1 PURIFICATION

Myristoylated bovine D6S GCAP1 was produced in BLR(DE3) *E. coli* strains harboring yeast N-myristoyl transferase (NMT), extracted from inclusion bodies and purified to ∼95% electrophoretic purity using Ca^{2+} precipitation, butyl-Sepharose chromatography, and high-resolution gel-filtration as previously described in detail (Peshenko and Dizhoor, 2006). The expressing strain for non-myristoylated G2A GCAP1 lacked the NMT plasmid.

Ca^{2+}/EGTA BUFFERS

Ca^{2+}/EGTA mixtures were prepared according to Tsien and Pozzan (1989), protocol and verified with Ca^{2+} fluorescent

indicator dyes as described previously (Peshenko and Dizhoor, 2006). The free metal concentrations in assays containg 2 mM Ca^{2+}/EGTA buffer were calculated using Bound and Determined and MaxChelator software with proper corrections for pH, salt and nucleotide concentrations, and temperature.

Ca^{2+} BINDING ASSAY

Ca^{2+} binding isotherms were obtained using previously described modification of a fluorescent indicator dye titration approach (Peshenko and Dizhoor, 2006). Briefly, each GCAP1 was diluted from 300–350 μm stock solution to 20–40 μm final concentration in 0.6 ml of 100 mm MOPS/KOH (pH 7.2), 40 mM KCl, 1 mM dithiothreitol, and 0.5 μM BAPTA 2 (Molecular Probes/Invitrogen). The mixture assembled in a plastic cuvette was titrated at 23°C with addition of 3 μl aliquots of calibrated $CaCl_2$ solution.

GUANYLYL CYLASE ASSAYS

RetGC activity was assayed as described previously (Peshenko and Dizhoor, 2007; Peshenko et al., 2011). Briefly, the assay mixture (25 μl) incubated at 30°C contained 30 mM MOPS–KOH (pH 7.2), 60 mM KCl, 4 mM NaCl, 1mM DTT, 2 mM Ca^{2+}/EGTA buffer, 1 mM free Mg^{2+}, 0.3 mM ATP, 4 mM cGMP, 10 mM creatine phosphate, 0.5 unit of creatine phosphokinase, 1 mM GTP, 1 μCi of [α-^{32}P]GTP, 0.1 μCi of [8–^{3}H]cGMP (Perkin Elmer), PDE6 inhibitors zaprinast, and dipyridamole. The resultant [^{32}P]cGMP product and the [^{3}H]cGMP internal standard was analyzed by TLC using fluorescently backed polyethyleneimine cellulose plates (Merck) developed in 0.2 M LiCl.

EXPRESSION OF RetGC1 IN HEK293 CELLS

HEK293 cells grown at 37°C, 5% CO_2, in high-glucose Dulbecco's modified Eagle medium (DMEM, Invitrogen) supplemented with 10% fetal bovine serum (Invitrogen) were transfected using the Ca^{2+}-phosphate method (a Promega Profection protocol) with 40 μg per 100 μm culture dish of pRCCMV plasmid coding for human RetGC1, and the membranes containing recombinant RetGC1 were isolated as previously described in detail (Peshenko et al., 2004).

CO-EXPRESSION OF RetGC1 AND GCAP1 IN HEK 293 CELLS AND CONFOCAL LASER SCANNING MICROSCOPY

Fluorescently tagged GCAP1 was co-expressed in HEK293 cells with human RetGC1 as previously described (Peshenko et al., 2008, 2010). Cells grown in 2 cm^2 cover slip chambers were typically transfected with a mixture of 3 μg pRCCMV plasmid harboring RetGC1 cDNA and 0.02 μg of the GCAP1-GFP pQBI25fN3 plasmid. In 24 h the cells were either viewed directly or fixed with freshly prepared 4% paraformaldehyde at room temperature for subsequent immunostaining. The images were collected using FV1000 Spectral laser confocal system and analyzed using Olympus FluoView FV10-ASW software as previously described (Peshenko et al., 2008).

RESULTS AND DISCUSSION

We tested the RetGC1—stimulating activity of a non-myristoylated recombinant bovine G2A GCAP1 produced in *E. coli* in comparison with the myristoylated GCAP1 (**Figure 1B**). Both myristoylated and non-myristoylated protein were produced using D6S variant of GCAP1, required for high-efficiency myristoylation in BLR(DE3) *E. coli* strain harboring yeast myristoyl transferase (Dizhoor et al., 1998; Krylov et al., 1999). To ensure the complete lack of myristoylation, the N-terminal Gly2 (**Figure 1A**) replaced with Ala prevents recognition of GCAP1 by NMT (Otto-Bruc et al., 1997). Molecular masses of the purified non-myristoylated G2A GCAP1 and myristoylated GCAP1 verified by ESI-QTOF mass-spectrometry matched, within one mass unit accuracy, their predicted molecular masses (23,365 and 23,561, respectively). Consistently with the previously reported observations using native photoreceptor membranes (Otto-Bruc et al., 1997; Hwang and Koch, 2002), the G2A GCAP1 stimulated the activity of the recombinant RetGC1 expressed in HEK293 cells much less efficiently (**Figure 1B**).

The dose-dependence of the RetGC activation suggests that the binding of the G2A GCAP1 to its target enzyme is impeded. It needs to be emphasized that GCAP binding to RetGC cannot be measured directly, because detergents required for extraction of RetGC from the membranes inactivate GCAP/RetGC interaction (Koch, 1991; Lambrecht and Koch, 1992). We, therefore, tested GCAP/RetGC complex formation using previously described semi-quantitative analysis of GCAP1-GFP co-localization with RetGC in HEK293 cells (Peshenko et al., 2008) (**Figure 2**). GCAP1-GFP expressed in the absence of the target enzyme (**Figure 2A**) distributes in a diffuse pattern throughout the cell, with similar intensity of the fluorescence in the cytoplasm and the nucleus (with the exception of the nucleoli and vacuoles) (Peshenko et al., 2008). The first EF-hand in GCAP1 and GCAP2 does not bind Ca^{2+}, but has been implicated in target recognition/binding instead (Ermilov et al., 2001; Hwang et al., 2004). Therefore, a mutation replacing the conserved CysPro in the EF-hand 1 loop with Gly prevents RetGC stimulation (Hwang et al., 2004). This mutation results in a diffuse pattern of GCAP1-GFP, even when it is co-expressed with RetGC1 (**Figure 2B**). In a sharp contrast, wild type GCAP1-GFP is co-localizes to the membranes containing co-expressed RetGC1 (**Figure 2C**), thus producing a "tennis racquet" membrane localization pattern specific for GCAP1/RetGC1 binding, as was previously demonstrated (Peshenko et al., 2008, 2011). The G2A GCAP1-GFP co-localization with RetGC1 was generally similar to that of wild type GCAP1, although not as sharply defined as for the wild type (**Figure 2D**). This indicates that the lack of myristoylation *per se* does not block RetGC/GCAP interaction, consistently with the activity assay in **Figure 1** and the earlier observations by Hwang and Koch (2002) and Dell'Orco et al. (2010). However, a semi-quantitative analysis performed on a large number of cells reveals that the efficiency of the complex formation has been reduced (**Figures 2E,F**). The quantification analysis is based on the decrease of the fluorescence intensity in the nucleus relative to the cell membranes, caused by absorption of the tagged GCAP1 by RetGC1 expressed in the membranes (Peshenko et al., 2008, 2011). In the absence of RetGC, the ratio of the GCAP1-GFP compartmentalization between the cytoplasm and the nucleus (excluding nucleoli) for average cell is close to 1, but in the presence of RetGC1 it drastically, almost 14-fold (**Figure 2**), increases

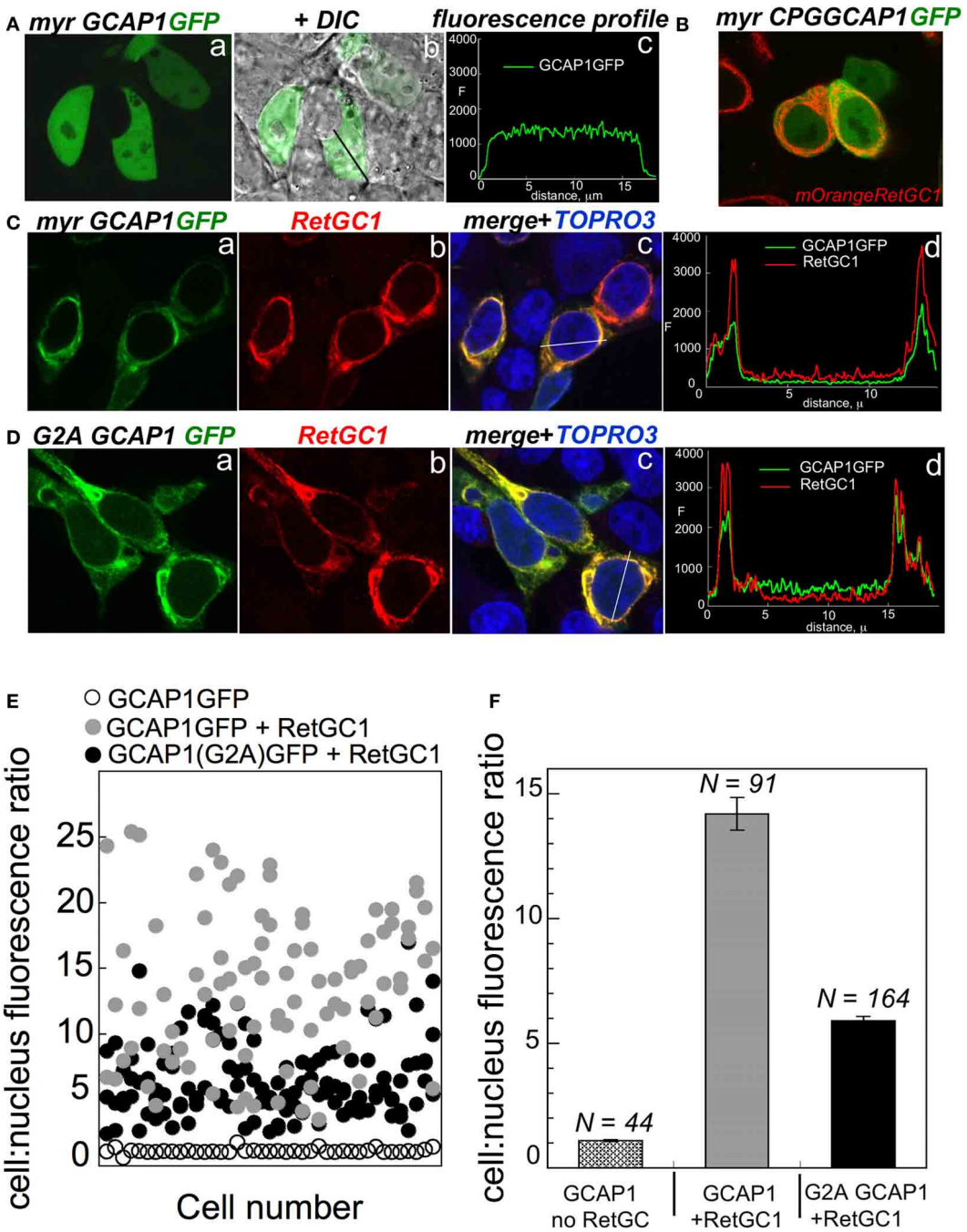

FIGURE 2 | The effect of myristoylation on co-localization of GCAP1 with RetGC in HEK293 cells. (A) GCAP1-GFP expressed in HEK293 cells without RetGC1 produces diffuse pattern spreading over the cytoplasm and the nucleus (Peshenko et al., 2008); *a*—fluorescence of GCAP1-GFP, *b*—same, but superimposed on DIC image of the cells, *c*—GCAP1 GFP fluorescence profile recorded across the cell along the black line in "*b*." **(B)** GCAP1 GFP mutant, in which a conserved CysPro pair in EF-hand 1 loop required for interaction with RetGC is replaced by Gly (Hwang et al., 2004), was co-expressed with RetGC1 tagged at the N-terminus with mOrange variant of red fluorescent protein using protocol described in (Peshenko et al., 2008, 2011); notice that the diffuse pattern of GCAP1-GFP persists despite the presence of RetGC1. **(C)** Membrane localization of wild type GCAP1-GFP (*green*) co-expressed with RetGC1 (*red*); *a*—fluorescence of GCAP1-GFP, *b*—anti-RetGC1 immunofluorescence of AlexaFluor 568, *c*—GCAP1 GFP (*green*) and anti-RetGC1 (*red*) fluorescence profile recorded across the cell along the white line shown in "*b*"; the nuclei in "*c*" were counterstained with TO-PRO3 (*pseudo-blue*). **(D)** Same as **C**, but using G2A GCAP1-GFP mutant. **(E)** Distribution of GCAP1-GFP fluorescence between the membranes and the nucleus quantified as described in (Peshenko et al., 2008); each data point corresponds to an individual cell; ○—GCAP1-GFP expressed alone, ●—GCAP1-GFP co-expressed with RetGC1, ●—G2A GCAP1-GFP co-expressed with RetGC1. **(F)** The GCAP1-GFP fluorescence distribution ratio (mean ± SEM) averaged from panel *E* demonstrates that the G2A GCAP1 mutant compartmentalizes with the RetGC1, although less efficiently than the wild type.

in favor of the membrane localization (Peshenko et al., 2008). Same analysis for the G2A GCAP1 yields more modest average value of 6-fold. Therefore, although myristoylation is not essential for the RetGC/GCAP binding, it evidently improves the efficiency of the complex formation. At the same time, the lower level of activation of the cyclase in **Figure 1B** as compared with the less prominently decreased co-localization efficiency in **Figure 2F** implies that there is additional effect of myristoylation—it has to be involved in the creation of the conformation required for the optimal cyclase stimulation within the GCAP/RetGC complex. It also needs to be noted that the attachment of the C-terminal GFP tag *per se* does not affect the regulatory properties of GCAP1 as the Ca^{2+} sensor of guanylyl cyclase (Peshenko et al., 2008).

The effect of N-myristoylation in GCAP1 on the cyclase binding and activation could *a priori* result from stabilizing effect of the fatty chain buried inside the protein structure (Stephen et al., 2007), such that in the absence of myristoylation GCAP1 becomes more easily misfolded. Previous analysis of the non-acylated GCAP1 by circular dichroism spectra (Dell'Orco et al., 2010) argues that the metal-bound non-myristoylated protein is fairly stable, at least at the level of the secondary structure. On the other hand, the Ca^{2+} binding isotherms (Dell'Orco et al., 2010) also suggested that at least one of the EF-hands in non-myristoylated GCAP1 became unable to bind Ca^{2+} within submicromolar Ca^{2+} range. Hence, one could not rule out the possibility of partial misfolding of GCAP1 three-dimensional structure. However, the data in **Figure 3** argue that under the conditions of our experiments the G2A GCAP1 is affected in a very subtle manner that merely results in a slight change of its Ca^{2+} sensitivity, rather than critical loss of Ca^{2+} binding affinity in any of the three metal-binding EF-hands. The fluorescent indicator dye titration analysis (Peshenko and Dizhoor, 2006) shows that the G2A GCAP1 has a normal stoichiometry of Ca^{2+} binding—three per molecule, saturating at low micromolar range of free Ca^{2+} (**Figure 3B**).

The overall apparent affinity of the G2A GCAP1 for Ca^{2+} in our experiments (**Figure 3B**) was markedly better than we could expect for the non-myristoylated GCAP1 based on previous reports. The respective macroscopic equilibrium constants, K_1, K_2, and K_3, derived from the three-center binding model (**Figure 3B**) were 2.0×10^7, 1.7×10^7, and $3.2 \times 10^6\ M^{-1}$ for the myristoylated and 1.5×10^7, 1.0×10^7, and $2.2 \times 10^6\ M^{-1}$ for the non-acylated G2A GCAP1. These values substantially deviate from those observed by Dell'Orco et al. (2010)—2.5×10^8, 3.2×10^7, and $7.9 \times 10^7\ M^{-1}$ for myristoylated *versus* 6.3×10^7, 5.0×10^6, and $2.0 \times 10^3\ M^{-1}$ for non-myristoylated GCAP1. The binding isotherm in our study (*solid line*) looks substantially different from the isotherm "reconstituted" using the previously reported (Dell'Orco et al., 2010) constants (*dashed line*)—both reach the same binding stoichiometry, but in very different free Ca^{2+} range. Based on our results, we can positively state that not only the stoichiometry of Ca^{2+} binding does not change in the non-myristoylated GCAP1, but it also reaches saturation within nearly the same low micromolar range as myristoylated protein, with only a slight right-shift of the binding curve (**Figures 3A,B**). It needs to be mentioned that indirect evaluation of Ca^{2+} binding affinities was also performed previously using a complex microcalorimetric pattern of heat release by GCAP1 in response to Ca2+ binding (Lim et al., 2009). However, using the Ca^{2+} binding isotherm (such as in Peshenko and Dizhoor (2006) and this study) is a more reliable approach to determine the actual binding constants, because, unlike microcalorimetry, it is not affected by a complex relationship between heat release and absorption resulting from Ca^{2+} binding and conformational changes in the GCAP1 molecule (Lim et al., 2009).

To verify that our analysis did not simply fail to reveal a major difference between the two forms of GCAP1 due to an insufficient resolution of the Ca^{2+} binding assay, we also tested Ca^{2+} binding by non-acylated GCAP1 mutants in which we inactivated one (EF-4) or two (EF-3 and EF-4) EF-hands using the D144N/D148G ($EF4^-$) and the D100N/D102G/D144N/D148G ($EF3,4^-$) substitutions, respectively, (Peshenko and Dizhoor, 2006). In both cases, we clearly observed the corresponding decrease of Ca^{2+} binding by one (**Figure 3C**) or two (**Figure 3D**) mol Ca^{2+} per mol GCAP1, respectively. So we find no indications that any of the three metal binding EF-hands in the non-acylated GCAP1 undergo possible misfolding severely affecting binding of Ca^{2+}. Therefore, the general fold of GCAP1 is highly unlikely to be critically compromised by the absence of the myristoyl group. It is much more likely that the fatty acyl group changes GCAP1 structure in a fairly subtle manner, only slightly affecting Ca^{2+} binding within the physiological free Ca^{2+} range.

The reason for the difference in the Ca^{2+} binding affinities in our study and that by Dell'Orco et al. (2010) is not immediately apparent. The trace amount of EDTA (~1:20 molar ratio to GCAP1, or 1:60 per mol of Ca^{2+} binding sites) was negligible in our assays and could not skew the results by more than few percent [which also would be toward lower, contrary to the higher than in Dell'Orco et al. (2010), average affinity in our experiments (**Figure 3B**)]. In the method we use (Peshenko and Dizhoor, 2006), the fluorescent chelator indicator was also present at a very low (~1:60–1:40) molar ratio to GCAP1 (as low as 1:180–1:120 per mol of Ca^{2+} binding sites), quite negligible in comparison with the calcium buffer capacity of GCAP1 itself and ~40–60 times lower than in the method used by Dell'Orco et al. (2010). This may have prevented some potential effect of the chelator dye itself on the non-myristoylated protein. Alternatively, the difference could be related to the use of the protein purification protocol that more efficiently removes poorly folded fraction of low-affinity GCAP1 in our study.

Despite the substantial quantitative difference, we would nonetheless emphasize that we have a qualitative agreement with the findings by Dell'Orco et al. (2010)—Ca^{2+}-sensitivity of the G2A GCAP1 is reduced compared to the myristoylated form (**Figure 3A**). Even though the binding ratio at saturation remained three Ca^{2+} ions per GCAP1, there was a slight shift of the curve toward higher micromolar free Ca^{2+} range for the non-myristoylated GCAP1. Evidently, it is the lack of myristoylation what alters the properties of GCAP1, not the G2A mutation *per se* (**Figure 3A**).

From the overall shift in Ca^{2+} binding affinity in non-acylated GCAP1 (**Figure 3A**), the result shown in **Figure 3D** appears most intriguing. The affinity of EF-hand 2, the only metal-binding site left in the non-acylated D100N/D102G/D144N/D148G GCAP1

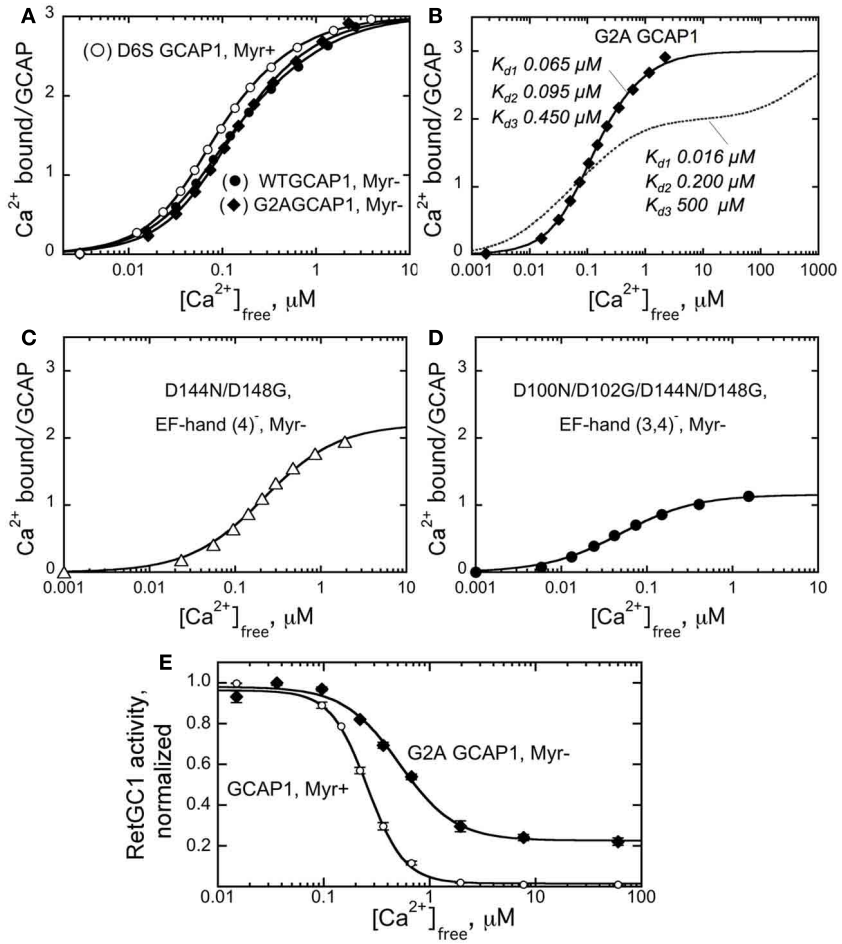

FIGURE 3 | Ca^{2+} sensitivity of GCAP1 is affected by myristoylation. **(A–D)**, Ca^{2+} binding isotherms obtained using fluorescent indicator dye BAPTA-2 titration protocol (Peshenko and Dizhoor, 2006). **(A)** Ca^{2+} binding by myristoylated D6S GCAP1 (○), non-myristoylated WT GCAP1 (●), and non-myristoylated G2A GCAP1 (◆). **(B)** Comparison of the experimental data for Ca^{2+} binding by G2A GCAP1 (◆) with the theoretical curve for three-center binding model calculated using previously reported macroscopic association constants, 6.3×10^7, 5.0×10^6, and 2.0×10^3 M^{-1} (Dell'Orco et al., 2010) (- - -); the corresponding dissociation constants are shown next to each trace. **(C,D)** Change of the binding stoichiometry in non-myristoylated GCAP1 with one (D144N/D148G, **C**) or two (D100N/D102G/D144N/D148G, **D**) EF-hands inactivated. The data were fitted using two different models: panels **(A,B)**—by three-center binding model, $Ca_{bound}/GCAP = (K_1Ca_f + 2K_1K_2Ca_f^2 + 3K_1K_2K_3Ca_f^3)/(1 + K_1Ca_f + K_1K_2Ca_f^2 + K_1K_2K_3Ca_f^3)$, where K_1, K_2, and K_3 are macroscopic equilibrium constants; panels **(C,D)**—by simplified hyperbolic saturation function, $(Ca_{bound}/GCAP) = B_{max} \times Ca_{free}/(Ca_{free} + K_d)$, where Ca_{bound} is the concentration of Ca^{2+} bound to GCAP1, calculated as $Ca_{bound} = Ca_{total} - Ca_{free}$, B_{max} is mol of Ca^{2+} bound per mol of GCAP1 at saturation, K_d is the apparent dissociation constant. The data shown are representative from 3 to 5 independent experiments producing virtually identical results. **(E)** Normalized activity of the recombinant RetGC1 expressed in HEK293 cells reconstituted with 10 μM purified myristoylated GCAP1 (○) or G2A GCAP1 (●) at different free Ca^{2+} concentrations and 1 mm free Mg^{2+}. The activities in each series were normalized by the maximal activity in the corresponding series. The data were fitted by the equation, $A = A_{max} + (A_{max} - A_{min})/(1 + (Ca_{free}/Ca_{1/2})^n)$, where A is RetGC activity, $Ca_{1/2}$ is the free Ca^{2+} concentration producing 50% effect and n is the Hill coefficient. For other conditions of the assay see Materials and Methods.

mutant (**Figure 3D**), remains high ($K_d \sim 0.04\,\mu m \pm 0.01$), virtually the same as in the myristoylated D100N/D102G/D144N/D148G mutant [$0.03 \pm 0.01\,\mu m$, Peshenko and Dizhoor (2006)]. In other words, myristoylation appears to have a surprisingly little effect on the high-affinity Ca^{2+} binding in the EF-hand 2 proximal to the fatty acyl group in the three-dimensional structure of GCAP1 (**Figure 1**). Instead of affecting metal binding in the neighboring EF-hand 2, the myristoyl moiety, in a rather paradoxical manner, seemingly influences the efficiency of Ca^{2+} binding in a more distal portion of the molecule (EF-hand 3 or 4).

In our previous studies (Peshenko and Dizhoor, 2007; Peshenko et al., 2008), we identified the EF-hand 3/EF-hand 4 portion of the molecule as critical for the Ca^{2+}-dependent activator-to-inhibitor transition of GCAP1. In a good qualitative agreement with the earlier observations of Hwang and Koch (2002) and the shift in the Ca^{2+}-binding isotherm to the higher Ca^{2+} range (**Figure 3A**), the G2A GCAP1 regulated recombinant RetGC1 with a noticeably lower sensitivity to Ca^{2+} [$(Ca)_{1/2}$ increased from 260 nM in wild type to 520 nM in the G2A mutant (**Figure 3E**)]. Since the high-affinity binding in EF-hand 2 does

not seem to be critically affected by myristoylation (**Figure 3D**), the observed changes in Ca^{2+} sensitivity of RetGC1 (**Figure 3E**) are, again, likely attributable to the change in the function of EF-hand 3 and/or 4. It also needs to be pointed that even though the decrease in Ca^{2+} sensitivity of RetGC regulation by GCAP1 is relatively modest, ∼2-fold, a shift like this can be large enough to adversely affect the levels of free cGMP and Ca^{2+} in the dark and provoke photoreceptor death in transgenic mice (Olshevskaya et al., 2004; Woodruff et al., 2007). Therefore, the role of myristoylation in maintaining normal Ca^{2+} sensitivity of GCAP1 as a Ca^{2+} sensor should be rather important for its normal physiological function.

Our results indicate that myristoyl residue inside the GCAP1 molecule affects proximal structural element(s) involved in the target enzyme recognition, such as EF-1 (see Ermilov et al., 2001; Hwang et al., 2004), but also influences Ca^{2+} binding efficacy in a more distal part of the molecule through a presently unknown and somewhat paradoxical mechanism. The possibility that the intramolecular interactions exist between the myristoyl moiety and the remote portions of the GCAP1 structure also suggests that such interaction can be affected by the environment of the myristoyl group and deserves closer in-depth study. This study is currently in progress and could provide a new insight into the structure-function relationships underlying the Ca^{2+} sensor action of GCAP1 as a member of the NCS protein group.

ACKNOWLEDGMENTS

This work was supported by the NIH grant EY11522 from NEI. Alexander M. Dizhoor is the Martin and Florence Hafter Chair Professor of Pharmacology.

REFERENCES

Ames, J. B., Dizhoor, A. M., Ikura, M., Palczewski, K., and Stryer, L. (1999). Three-dimensional structure of guanylyl cyclase activating protein-2, a calcium-sensitive modulator of photoreceptor guanylyl cyclases. *J. Biol. Chem.* 274, 19329–19337.

Ames, J. B., Ishimam, R., Tanaka, T., Gordon, J. I., Stryer, L., and Ikura, M. (1997). Molecular mechanics of calcium-myristoyl switches. *Nature* 389, 198–202.

Ames, J. B., Tanaka, T., Ikura, M., and Stryer, L. (1995). Nuclear magnetic resonance evidence for Ca(2+)-induced extrusion of the myristoyl group of recoverin. *J. Biol. Chem.* 270, 30909–30913.

Burgoyne, R. D. (2007). Neuronal calcium sensor proteins, generating diversity in neuronal Ca2+ signalling. *Nat. Rev. Neurosci.* 8, 182–193.

Burns, M. E., Mendez, A., Chen, J., and Baylor, D. A. (2002). Dynamics of cyclic GMP synthesis in retinal rods. *Neuron* 36, 81–91.

Dell'Orco, D., Behnen, P., Linse, S., and Koch, K. W. (2010). Calcium binding, structural stability and guanylate cyclase activation in GCAP1 variants associated with human cone dystrophy. *Cell. Mol. Life Sci.* 67, 973–984.

Dizhoor, A. M., Boikov, S. G., and Olshevskaya, E. V. (1998). Constitutive activation of photoreceptor guanylate cyclase by Y99C mutant of GCAP-1. Possible role in causing human autosomal dominant cone degeneration. *J. Biol. Chem.* 273, 17311–17314.

Dizhoor, A. M., Chen, C. K., Olshevskaya, E. V., Sinelnikova, V., Phillipov, P., and Hurley, J. B. (1993). Role of the acylated amino terminus of recoverin in Ca(2+)-dependent membrane interaction. *Science* 259, 829–832.

Dizhoor, A. M., Ericsson, L. H., Johnson, R. S., Kumar, S., Olshevskaya, E. V., Zozulya, S., Neubert, T. A., Stryer, L., Hurley, J. B., and Walsh, K. A. (1992). The NH2 terminus of retinal recoverin is acylated by a small family of fatty acids. *J. Biol. Chem.* 267, 16033–16036.

Dizhoor, A. M., and Hurley, J. B. (1996). Inactivation of EF-hands makes GCAP-2 (p24) a constitutive activator of photoreceptor guanylyl cyclase by preventing a Ca2+-induced "activator-to-inhibitor" transition. *J. Biol. Chem.* 271, 19346–19350.

Dizhoor, A. M., Lowe, D. G., Olshevskaya, E. V., Laura, R. P., and Hurley, J. B. (1994). The human photoreceptor membrane guanylyl cyclase, RetGC, is present in outer segments and is regulated by calcium and a soluble activator. *Neuron* 12, 1345–1352.

Dizhoor, A. M., Olshevskaya, E. V., Henzel, W. J., Wong, S. C., Stults, J. T., Ankoudinova, I., and Hurley, J. B. (1995). Cloning, sequencing, and expression of a 24-kDa Ca(2+)-binding protein activating photoreceptor guanylyl cyclase. *J. Biol. Chem.* 270, 25200–25206.

Dizhoor, A. M., Olshevskaya, E. V., and Peshenko, I. V. (2010). Mg2+/Ca2+ cation binding cycle of guanylyl cyclase activating proteins (GCAPs), role in regulation of photoreceptor guanylyl cyclase. *Mol. Cell. Biochem.* 334, 117–124.

Ermilov, A. N., Olshevskaya, E. V., and Dizhoor, A. M. (2001). Instead of binding calcium, one of the EF-hand structures in guanylyl cyclase activating protein-2 is required for targeting photoreceptor guanylyl cyclase. *J. Biol. Chem.* 276, 48143–48148.

Fu, Y., and Yau, K. W. (2007). Phototransduction in mouse rods and cones. *Pflugers Arch.* 454, 805–819.

Gorczyca, W. A., Gray-Keller, M. P., Detwiler, P. B., and Palczewski, K. (1994). Purification and physiological evaluation of a guanylate cyclase activating protein from retinal rods. *Proc. Natl. Acad. Sci. U.S.A.* 91, 4014–4018.

Gray-Keller, M. P., and Detwiler, P. B. (1994). The calcium feedback signal in the phototransduction cascade of vertebrate rods. *Neuron* 13, 849–861.

Hughes, R. E., Brzovic, P. S., Dizhoor, A. M., Klevit, R. E., and Hurley, J. B. (1998). Ca2+-dependent conformational changes in bovine GCAP-2. *Protein Sci.* 7, 2675–2680.

Hwang, J. Y., and Koch, K. W. (2002). Calcium- and myristoyl-dependent properties of guanylate cyclase-activating protein-1 and protein-2. *Biochemistry* 41, 13021–13028.

Hwang, J. Y., Lange, C., Helten, A., Hoppner-Heitmann, D., Duda, T., Sharma, R. K., and Koch, K. W. (2003). Regulatory modes of rod outer segment membrane guanylate cyclase differ in catalytic efficiency and Ca2+-sensitivity. *Eur. J. Biochem.* 270, 3814–3821.

Hwang, J. Y., Schlesinger, R., and Koch, K. W. (2004). Irregular dimerization of guanylate cyclase-activating protein 1 mutants causes loss of target activation. *Eur. J. Biochem.* 271, 3785–3793.

Imanishi, Y., Yang, L., Sokal, I., Filipek, S., Palczewski, K., and Baehr, W. (2004). Diversity of guanylate cyclase-activating proteins (GCAPs) in teleost fish, characterization of three novel GCAPs (GCAP4, GCAP5, GCAP7) from zebrafish (*Danio rerio*) and prediction of eight GCAPs (GCAP1–8) in pufferfish (*Fugu rubripes*). *J. Mol. Evol.* 59, 204–217.

Johnson, R. S., Ohguro, H., Palczewski, K., Hurley, J. B., Walsh, K. A., and Neubert, T. A. (1994). Heterogeneous N-acylation is a tissue- and species-specific post-translational modification. *J. Biol. Chem.* 269, 21067–21071.

Koch, K. W. (1991). Purification and identification of photoreceptor guanylate cyclase. *J. Biol. Chem.* 266, 8634–8637.

Koch, K. W., and Stryer, L. (1988). Highly cooperative feedback control of retinal rod guanylate cyclase by calcium ions. *Nature* 334, 64–66.

Krylov, D. M., Niemi, G. A., Dizhoor, A. M., and Hurley, J. B. (1999). Mapping sites in guanylyl cyclase activating protein-1 required for regulation of photoreceptor membrane guanylyl cyclases. *J. Biol. Chem.* 274, 10833–10839.

Laura, R. P., Dizhoor, A. M., and Hurley, J. B. (1996). The membrane guanylyl cyclase, retinal guanylyl cyclase-1, is activated through its intracellular domain. *J. Biol. Chem.* 271, 11646–11651.

Lim, S., Peshenko, I., Dizhoor, A., and Ames, J. B. (2009). Effects of Ca2+, Mg2+, and myristoylation on guanylyl cyclase activating protein 1 structure and stability. *Biochemistry* 48, 850–862.

Lim, S., Strahl, T., Thorner, J., and Ames, J. B. (2011). Structure of a Ca2+-myristoyl switch protein that controls activation of a phosphatidylinositol 4-kinase in fission yeast. *J. Biol. Chem.* 286, 12565–12577.

Lambrecht, H. G., and Koch, K. W. (1992). Recoverin, a novel calcium-binding protein from vertebrate photoreceptors. *Biochim. Biophys. Acta* 1160, 63–66.

Makino, C. L., Peshenko, I. V., Wen, X.-H., Elena, V., Olshevskaya, E. V., Barrett, R., and Dizhoor, A. M. (2008). A role for GCAP2 in regulating the photoresponse: guanylyl cyclase activation and rod electrophysiology in GUCA1B knockout mice. *J. Biol. Chem.* 283, 29135–29143.

Mendez, A., Burns, M. E., Sokal, I., Dizhoor, A. M., Baehr, W., Palczewski, K., Baylor, D. A., and Chen, J. (2001). Role of guanylate cyclase-activating proteins (GCAPs) in setting the flash sensitivity of rod photoreceptors. *Proc. Natl. Acad. Sci. U.S.A.* 98, 9948–9953.

Olshevskaya, E. V., Calvert, P. D., Woodruff, M. L., Peshenko, I. V., Savchenko, A. B., Makino, C. L., Ho, Y. S., Fain, G. L., and Dizhoor, A. M. (2004). The Y99C mutation in guanylyl cyclase-activating protein 1 increases intracellular Ca2+ and causes photoreceptor degeneration in transgenic mice. *J. Neurosci.* 24, 6078–6085.

Olshevskaya, E. V., Hughes, R. E., Hurley, J. B., and Dizhoor, A. M. (1997). Calcium binding, but not a calcium-myristoyl switch, controls the ability of guanylyl cyclase-activating protein GCAP-2 to regulate photoreceptor guanylyl cyclase. *J. Biol. Chem.* 272, 14327–14333.

Otto-Bruc, A., Buczylko, J., Surgucheva, I., Subbaraya, I., Rudnicka-Nawrot, M., Crabb, J. W., Arendt, A., Hargrave, P. A., Baehr, W., and Palczewski, K. (1997). Functional reconstitution of photoreceptor guanylate cyclase with native and mutant forms of guanylate cyclase-activating protein 1. *Biochemistry* 36, 4295–4302.

Palczewski, K., Subbaraya, I., Gorczyca, W. A., Helekar, B. S., Ruiz, C. C., Ohguro, H., Huang, J., Zhao, X., Crabb, J. W., Johnson, R. S., Walsh, K. A., Gray-Keller, M. P., Detwiller, P. B., and Baehr, W. (1994). Molecular cloning and characterization of retinal photoreceptor guanylyl cyclase-activating protein. *Neuron* 13, 395–404.

Peshenko, I. V., and Dizhoor, A. M. (2004). Guanylyl cyclase-activating proteins (GCAPs) are Ca2+/Mg2+ sensors: implications for photoreceptor guanylyl cyclase (RetGC) regulation in mammalian photoreceptors. *J. Biol. Chem.* 279, 16903–16906.

Peshenko, I. V., and Dizhoor, A. M. (2006). Ca2+ and Mg2+ binding properties of GCAP-1. Evidence that Mg2+-bound form is the physiological activator of photoreceptor guanylyl cyclase. *J. Biol. Chem.* 281, 23830–23841.

Peshenko, I. V., and Dizhoor, A. M. (2007). Activation and inhibition of photoreceptor guanylyl cyclase by guanylyl cyclase activating protein 1 (GCAP-1): the functional role of Mg2+/Ca2+ exchange in EF-hand domains. *J. Biol. Chem.* 282, 21645–21652. Epub 22007 Jun 21641.

Peshenko, I. V., Moiseyev, G. P., Olshevskaya, E. V., and Dizhoor, A. M. (2004). Factors that determine Ca2+ sensitivity of photoreceptor guanylyl cyclase. Kinetic analysis of the interaction between the Ca2+-bound and the Ca2+-free guanylyl cyclase activating proteins (GCAPs) and recombinant photoreceptor guanylyl cyclase 1 (RetGC-1). *Biochemistry* 43, 13796–13804.

Peshenko, I. V., Olshevskaya, E. V., and Dizhoor, A. M. (2008). Binding of guanylyl cyclase activating protein 1 (GCAP1) to retinal guanylyl cyclase (RetGC1). The role of individual EF-hands. *J. Biol. Chem.* 283, 21747–21757.

Peshenko, I. V., Olshevskaya, E. V., Savchenko, A. B., Karan, S., Palczewski, K., Baehr, W., and Dizhoor, A. M. (2011). Enzymatic properties and regulation of the native isozymes of retinal membrane guanylyl cyclase (RetGC) from mouse photoreceptors. *Biochemistry* 50, 5590–5600.

Peshenko, I. V., Olshevskaya, E. V., Yao, S., Ezzeldin, H. H., Pittler, S. J., and Dizhoor, A. M. (2010). Activation of retinal guanylyl cyclase RetGC1 by GCAP1: stoichiometry of binding and effect of new LCA-related mutations. *Biochemistry* 49, 709–717.

Pugh, E. N. Jr., Duda, T., Sitaramayya, A., and Sharma, R. K. (1997). Photoreceptor guanylate cyclases: a review. *Biosci. Rep.* 17, 429–473.

Pugh, E. N. Jr., Nikonov, S., and Lamb, T. D. (1999). Molecular mechanisms of vertebrate photoreceptor light adaptation. *Curr. Opin. Neurobiol.* 9, 410–418.

Sakurai, K., Chen, J., and Kefalov, V. J. (2011). Role of guanylyl cyclase modulation in mouse cone phototransduction. *J. Neurosci.* 31, 7991–8000.

Sampath, A. P., Matthews, H. R., Cornwall, M. C., Bandarchi, J., and Fain, G. L. (1999). Light-dependent changes in outer segment free-Ca2+ concentration in salamander cone photoreceptors. *J. Gen. Physiol.* 113, 267–277.

Stephen, R., Bereta, G., Golczak, M., Palczewski, K., and Sousa, M. C. (2007). Stabilizing function for myristoyl group revealed by the crystal structure of a neuronal calcium sensor, guanylate cyclase-activating protein 1. *Structure* 15, 1392–1402.

Stephen, R., Palczewski, K., and Sousa, M. C. (2006). The crystal structure of GCAP3 suggests molecular mechanism of GCAP-linked cone dystrophies. *J. Mol. Biol.* 359, 266–275.

Tsien, R., and Pozzan, T. (1989). Measurement of cytosolic free Ca2+ with quin2. *Methods Enzymol.* 172, 230–262.

Woodruff, M. L., Olshevskaya, E. V., Savchenko, A. B., Peshenko, I. V., Barrett, R., Bush, R. A., Sieving, P. A., Fain, G. L., and Dizhoor, A. M. (2007). Constitutive excitation by Gly90Asp rhodopsin rescues rods from degeneration caused by elevated production of cGMP in the dark. *J. Neurosci.* 27, 8805–8815.

Woodruff, M. L., Sampath, A. P., Matthews, H. R., Krasnoperova, N. V., Lem, J., and Fain, G. L. (2002). Measurement of cytoplasmic calcium concentration in the rods of wild-type and transducin knockout mice. *J. Physiol.* 542, 843–854.

Zozulya, S., and Stryer, L. (1992). Calcium-myristoyl protein switch. *Proc. Natl. Acad. Sci. U.S.A.* 89, 11569–11573.

Conflict of Interest Statement: The authors declare that the research was conducted in the absence of any commercial or financial relationships that could be construed as a potential conflict of interest.

Received: 09 January 2012; accepted: 09 February 2012; published online: 22 February 2012.

Citation: Peshenko IV, Olshevskaya EV and Dizhoor AM (2012) Interaction of GCAP1 with retinal guanylyl cyclase and calcium: sensitivity to fatty acylation. Front. Mol. Neurosci. 5:19. doi: 10.3389/fnmol.2012.00019

frontiers in
MOLECULAR NEUROSCIENCE

ORIGINAL RESEARCH ARTICLE
published: 0θ April 2012
doi: 10.3389/fnmol.2012.00044

Antithetical modes of and the Ca^{2+} sensors targeting in ANF-RGC and ROS-GC1 membrane guanylate cyclases

Teresa Duda[1]*, Alexandre Pertzev[1], Karl-W. Koch[2] and Rameshwar K. Sharma[1]

[1] *Research Divisions of Biochemistry and Molecular Biology, The Unit of Regulatory and Molecular Biology, Salus University, Elkins Park, PA, USA*
[2] *Department of Biology and Environmental Sciences, Biochemistry Group, University of Oldenburg, Oldenburg, Germany*

Edited by:
Michael R. Kreutz, Leibniz-Institute for Neurobiology, Germany

Reviewed by:
Frank Schmitz, Saarland University, Germany
Lee Haynes, The University of Liverpool, UK

****Correspondence:***
Teresa Duda, Research Divisions of Biochemistry and Molecular Biology, The Unit of Regulatory and Molecular Biology, Salus University, 8360 Old York Road, Elkins Park, PA 19027, USA.
e-mail: tduda@salus.edu

The membrane guanylate cyclase family has been branched into three subfamilies: natriuretic peptide hormone surface receptors, Ca^{2+}-modulated neuronal ROS-GC, and Ca^{2+}-modulated odorant surface receptor ONE-GC. The first subfamily is solely modulated by the extracellularly generated hormonal signals; the second, by the intracellularly generated sensory and sensory-linked signals; and the third, by combination of these two. The present study defines a new paradigm and a new mechanism of Ca^{2+} signaling. (1) It demonstrates for the first time that ANF-RGC, the prototype member of the surface receptor subfamily, is stimulated by free $[Ca^{2+}]_i$. The stimulation occurs *via* myristoylated form of neurocalcin *δ*, and both the guanylate cyclase and the calcium sensor neurocalcin δ are present in the glomerulosa region of the adrenal gland. (2) The EF-2, EF-3 and EF-4 hands of GCAP1 sense the progressive increment of $[Ca^{2+}]_i$ and with a $K_{1/2}$ of 100 nM turn ROS-GC1 "OFF." In total reversal, the same EF hands upon sensing the progressive increment of $[Ca^{2+}]_i$ with $K_{1/2}$ turn ONE-GC "ON." The findings suggest a universal Ca^{2+}-modulated signal transduction theme of the membrane guanylate cyclase family; demonstrate that signaling of ANF-RGC occurs by the peptide hormones and also by $[Ca^{2+}]_i$ signals; that for the Ca^{2+} signal transduction, ANF-RGC functions as a two-component transduction system consisting of the Ca^{2+} sensor neurocalcin δ and the transducer ANF-RGC; and that the neurocalcin δ in this case expands beyond its NCS family. Furthermore, the study shows a novel mechanism of the $[Ca^{2+}]_i$ sensor GCAP1 where it acts as an antithetical NCS for the signaling mechanisms of ROS-GC1 and ONE-GC.

Keywords: calcium, GCAP1, neurocalcin δ, neuronal calcium sensors, membrane guanylate cyclase, cyclic GMP, atrial natriuretic factor receptor membrane guanylate cyclase, olfactory neuroepithelium membrane guanylate cyclase

INTRODUCTION

Ca^{2+} sensor proteins form a group of Ca^{2+} binding proteins that, in defined concentrations of free intracellular Ca^{2+}, function as modulators of the activities of specific target proteins. They acquire these modulatory abilities by binding Ca^{2+} through specific helix-loop-helix structural motifs called EF hands. Binding of Ca^{2+} to the EF hand motif triggers conformational changes in the respective Ca^{2+} sensor protein that enable it to perform Ca^{2+}-dependent functions ranging from regulation of ion channels permeability to gene expression, cellular survival and apoptosis (reviewed in Bhattacharya et al., 2004; Braunewell, 2005). Neuronal Ca^{2+} sensor (NCS) proteins constitute a subfamily of Ca^{2+} sensor proteins and were initially considered to be expressed exclusively in neurons, but now are found in other tissues as well. NCS proteins are subclassified into five groups based on their sequence similarities. In mammals, 14 conserved NCS proteins exist (reviewed in Burgoyne, 2007) and all of them have 4 EF hand Ca^{2+} binding motifs but inactivating amino acid substitutions make the first EF hand non-functional for Ca^{2+} binding. In addition to the first inactive EF hand, recoverin and K^+-channel interacting protein type1 (KChIP1) harbor another non-functional EF hand. Except for KChIP2, 3 and 4 all mammalian NCS proteins contain a consensus sequence for N-terminal myristoylation (reviewed in Burgoyne and Weiss, 2001; Burgoyne et al., 2004). Some isoforms of KChIP2 and 3 are possibly palmitoylated (Takimoto et al., 2002). Both myristoylation and palmitoylation of NCS proteins allows for some of them membrane association, either permanently or transiently in response to changes in the intracellular Ca^{2+} concentration. For GCAP1 and NCS-1, however, Ca^{2+} plays no role in membrane attachment of the protein (Hwang and Koch, 2002; O'Callaghan et al., 2002; Orban et al., 2010).

Neurocalcin δ together with visinin-like proteins (VILIPs) and hippocalcin form a distinct subfamily of NCS proteins. It is acylated at the N-terminus by myristic acid and undergoes a classical calcium-myristoyl switch (Ladant, 1995) e.g. it buries the myristoyl group in a hydrophobic pocket in a Ca^{2+}-free form and expose it in Ca^{2+}-bound form as it is observed for recoverin (Zozulya and Stryer, 1992). However, once it binds in a Ca^{2+}-dependent fashion to the membrane phospholipids part of it remains membrane bound even after removing Ca^{2+} by the addition of EGTA (Krishnan et al., 2004). Although the highest level of neurocalcin δ has been detected in neuronal tissues, its expression level in peripheral tissues is also significant. Functionally,

neurocalcin δ has been linked to receptor endocytosis through interaction with α- and β-clathrin and β-adaptin (Ivings et al., 2002), trafficking and membrane delivery of glutamate receptors of the kainate type (Coussen and Mulle, 2006), and due to its Ca^{2+}-dependent affinity for S100B protein and tubulin β-chain (Okazaki et al., 1995), with microtubule assembly (Iino et al., 1995). In the sensory and sensory-linked neurons, the presence of neurocalcin δ has been found in the inner plexiform layer of the retina, *e.g.* in the amacrine and ganglion cells (Krishnan et al., 2004), olfactory sensory neurons (Duda et al., 2001, 2004) and very recently, it has been identified in type II cells of mouse circumvallate taste papillae, indicating its possible role in the gustatory transduction (Rebello et al., 2011).

Further, neurocalcin δ can act as Ca^{2+}-dependent modulator of membrane guanylate cyclase ROS-GC1 in the retina and ONE-GC, in the olfactory neuroepithelium. There, it co-localizes with its respective target guanylate cyclases (Duda et al., 2001, 2004; Krishnan et al., 2004). The exact physiological significance of the ROS-GC1-neurocalcin δ signaling system in the retinal neurons is not known yet, it has, however, been proposed that the system may be involved in synaptic processes (Krishnan et al., 2004). In the olfactory neuroepithelium neurocalcin δ serves as a Ca^{2+} sensor component of the two-step odorant uroguanylin signaling machinery (Duda and Sharma, 2009).

Guanylate cyclase activating protein type 1 (GCAP1) is a well characterized member of the NCS proteins subfamily (reviewed in Palczewski et al., 2004; Sharma et al., 2004; Behnen et al., 2010; Koch et al., 2010). Like other homologs and orthologs of the subfamily, it harbors four EF hand Ca^{2+} binding motifs, of which the first one is inactive. GCAP1 is acylated at the N-terminus by myristic acid that is buried in a hydrophobic pocket (Stephen et al., 2007) and changing Ca^{2+} concentrations do not trigger exposure of the myristoyl group (Orban et al., 2010). Instead the myristoyl group remains buried in a hydrophobic cavity. Thus, GCAP1 does not interact with the membranes in a Ca^{2+}-dependent fashion (Hwang and Koch, 2002; Haynes and Burgoyne, 2008) and does not undergo a classical calcium myristoyl switch. Identified first in the retinal photoreceptors (Gorczyca et al., 1994; Frins et al., 1996), GCAP1 transmits Ca^{2+} signals to and controls the activity of rod outer segment guanylate cyclase, ROS-GC. It activates ROS-GC in the absence of Ca^{2+}, when immediately after illumination the cytoplasmic Ca^{2+} drops in a photoreceptor cell. GCAPs are thought to switch to a Ca^{2+}-free but Mg^{2+}-bound state, which represents the activating form (Peshenko and Dizhoor, 2006). Increasing concentrations of free Ca^{2+} diminish the activation process leading even to an inhibition below the basal cyclase activity level (Duda et al., 1996). This regulatory process of ROS-GC is essential for the photoresponse recovery of visual cells (Mendez et al., 2001; Howes et al., 2002).

Here, new observations on Ca^{2+}-dependent modes of neurocalcin δ and GCAP1 in modulating membrane guanylate cyclase signaling are presented. The results disclose a new model of Ca^{2+}-neurocalcin δ signaling of ANF-RGC and a new signaling mechanism of GCAP1 in which it serves as an antithetical Ca^{2+} sensor in the phototransduction and the olfactory sensory neurons. Thus, they indicate an increasing complexity in the regulatory modes of membrane guanylate cyclases and this enables them to perform multiple cellular functions.

MATERIALS AND METHODS

Mutagenesis. Point mutations in ONE-GC and GCAP1 cDNA were introduced using Quick Change mutagenesis kit (Stratagene) and appropriate mutagenic primers. ONE-GC $F^{585}S$ mutation-Forward primer 5′-TGGCTGAAGAAGTCTGAGGCAGGC ACG-3′; Reverse primer 5′-CGTGCCTGCCTCAGACTTCTTCAG CCA-3′ (the mutated sequence is underlined). Construction of the GCAP1($D^{100}E$) mutant is described in detail in (Kitiratschky et al., 2009). The mutants were verified by sequencing. To construct the ANF-RGC Ext^{-} mutant two Hpa1 restriction sites were introduced at nucleotide positions 437–442 (Forward primer 5′-GTGGTGCTGCCGCTG GTAAACAACACCTCGTACCCG-3′, Reverse primer 5′-CGG GTACGAGGTGTTTACCAGCGGCAGCACCAC-3′; Hpa1 recognition sequence is underlined) and at nucleotide positions 1697–1702 (Forward primer 5′-AATGAGGACCCAG CCGTAAACCAAGACCACTTT-3′; Reverse primer 5′-AAAGTG GTCTTGGTTTACGGCTGGGTCCTCATT-3′; Hpa1 recognition sequence is underlined). The 1242 bp fragment was excised and the remaining part was religated.

Expression in COS cells. COS7 cells (simian virus 40-transformed African green monkey kidney cells) were maintained in DMEM medium supplemented with 10% fetal bovine serum and penicillin, streptomycin antibiotics on 10 cm diameter cell culture dishes in humidified atmosphere of 95% O_2/5% CO_2. At approximately 65% confluency the cells were transfected with 25 μg of appropriate plasmid cDNA using calcium phosphate co-precipitation technique (Sambrook et al., 1989). In control experiments the cells were transfected with 25 μg of empty expression vector. 64 h after transfection cells were washed with 50 mM Tris-HCl pH 7.4/10 mM Mg^{2+} buffer, homogenized and the particulate fraction pelleted by centrifugation.

Guanylate cyclase activity assay. The membranes were incubated on ice-bath with or without GCAP1 or neurocalcin δ in the assay system containing 10 mM theophylline, 15 mM phosphocreatine, 20 μg creatine kinase and 50 mM Tris-HCl, pH 7.5. Appropriate Ca^{2+} concentrations were adjusted with pre-calibrated Ca^{2+}/EGTA solutions (Molecular Probes). The total assay volume was 25 μl. The reaction was initiated by addition of the substrate solution (4 mM $MgCl_2$ and 1 mM GTP, final concentration) and maintained by incubation at 37°C for 10 min. The reaction was terminated by the addition of 225 μl of 50 mM sodium acetate buffer, pH 6.2 followed by heating on a boiling water bath for 3 min. The amount of cyclic GMP formed was determined by radioimmunoassay (Nambi et al., 1982).

Expression and purification of GCAP1, GCAP1($D^{100}E$) and neurocalcin δ. GCAP1 was expressed and purified as in (Duda et al., 1999), GCAP1($D^{100}E$) as in (Kitiratschky et al., 2009), and neurocalcin δ as in (Duda et al., 2004).

Antibodies. The specificity of antibody against neurocalcin δ has been described previously (Duda et al., 2004). Antibody against ANF-RGC was raised against the kinase homology domain in rabbits. Specificity of the antibody was tested through Western blot using membranes of COS cells expressing all three

receptor guanylate cyclases, ANF-RGC, CNP-receptor guanylate cyclase (CNP-RGC) and enterotoxin receptor guanylate cyclase (STa-RGC). The antibody recognized only ANF-RGC (data not shown). The antibodies were affinity purified. Secondary antibodies conjugated to a fluorescent dye (DyLight 488 and DyLight 549) were purchased from Jackson ImmunoResearch Laboratories, Inc., West Grove, PA.

Immunohistochemistry. Mice were sacrificed by lethal injection of ketamine/xylazine (the protocol approved by the Salus University IUCAC) and perfused through the heart, first with a standard Tris-buffered saline (TBS) and then with freshly prepared 4% paraformaldehyde in TBS. The adrenal glands were removed and fixed for 1–4 h in 4% paraformaldehyde with TBS at 4°C, cryoprotected in 30% sucrose overnight at 4°C and cut into 20 μm sections using Hacker-Bright OTF5000 microtome cryostat (HACKER Instruments and Industries Inc., Winnsboro, SC). The sections were washed with TBS, blocked in 10% normal serum in TBS/0.5% Triton X-100 (TTBS) for 1 h at room temperature, washed with TTBS, incubated with respective antibody in blocking solution overnight at 4°C, washed with TTBS for and then incubated with DyLight conjugated donkey anti-rabbit antibody (200:1) for 1 h, washed with TTBS. Images were acquired using an inverted Olympus IX81 microscope/FV1000 Spectral laser confocal system, and analyzed using Olympus FluoView FV10-ASW software. Digital images were processed using Adobe Photoshop software.

Western blot. After boiling in a gel-loading buffer [62.5 mM Tris-HCl, (pH 7.5), 2% SDS, 5% glycerol, 1 mM β-mercaptoethanol (βME), and 0.005% bromophenol blue] the proteins (membranes of transfected COS cells or mouse adrenal gland homogenate) were subjected to SDS-polyacrylamide gel electrophoresis in a buffer (pH 8.3) containing 0.025 M Tris, 0.192 M glycine, and 0.1% SDS. The proteins were transferred to immobilon membranes (Millipore) in the same buffer but containing 5% methanol. The blot was incubated in (TBS pH 7.5) containing 100 mM Tris-HCl, 0.9% NaCl, and 0.05% Tween-20 (TBS-T) with 5% powdered non-fat Carnation milk (blocking buffer) overnight at 4°C and rinsed with TBS-T. The antibodies were added to the solution and the incubation continued for 1 h at room temperature. After the blot was rinsed with with TBS-T, the incubation was continued with the secondary antibody conjugated to horseradish peroxidase in blocking buffer for another hour. Finally, the blot was treated with SuperSignal^{R} West Pico chemiluminescent substrate (Thermo Scienitifc; according to the manufacturer's protocol). The immunoreactive band was visualized by exposing the blot to Kodak X-ray film.

RESULTS AND DISCUSSION

ANF RECEPTOR GUANYLATE CYCLASE, ANF-RGC, IS MODULATED BY Ca^{2+} SIGNALS

Neurocalcin δ transmits Ca^{2+} signal to ANF-RGC

Based on almost three decades of research the family of mammalian membrane guanylate cyclases has been firmly divided into two subfamilies, receptor guanylate cyclases and intracellular Ca^{2+} regulated guanylate cyclases. The first group included the receptor for natriuretic factor type A (ANF) and type B (BNP) guanylate cyclase ANF-RGC, the receptor for type C natriuretic peptide guanylate cyclase CNP-RGC, and heat-stable enterotoxin (and also guanylin and uroguanylin) receptor guanylate cyclase STa-RGC; the second group is comprised of the photoreceptor guanylate cyclases ROS-GC1 and ROS-GC2 and the olfactory neuroepithelium guanylate cyclase ONE-GC.

To determine whether a receptor guanylate cyclase could also respond to Ca^{2+} signals transmitted to it through a calcium sensor protein, the prototype receptor cyclase ANF-RGC and NCS protein neurocalcin δ were chosen. A clue for selecting neurocalcin δ was the observation that it targets the conserved membrane guanylate cyclase catalytic domain of ROS-GC1.

Membranes of COS cells expressing recombinant ANF-RGC were incubated with series of increasing concentrations of purified myristoylated neurocalcin δ at a fixed 10 μM Ca^{2+}. No extracellular ligand of ANF-RGC, ANF or BNP, was added to the reaction mixture. ANF-RGC activity was stimulated in the neurocalcin δ concentration-dependent manner; half-maximal activation of the cyclase occurred at ∼0.5 μM and the maximal activation of 4.8-fold above the basal value was observed at 2 μM myristoylated neurocalcin δ (**Figure 1**: closed circles). The calculated Hill's coefficient for the stimulatory effect was 2.1 ± 0.5. In the membranes of cells transfected with the vector alone the cyclase activity was negligible, 0.2 pmol cyclic GMP $min^{-1}(mg\ protein)^{-1}$ (**Figure 1**: closed diamonds) and was unaffected by neurocalcin δ in the presence of Ca^{2+}. To verify that the observed effect of Ca^{2+}-neurocalcin δ is specific the cyclase activity was measured in the presence of neurocalcin δ but in the absence of Ca^{2+} (1 mM EGTA was added to the reaction mixture). The absence of Ca^{2+} did not affect the basal ANF-RGC activity; it was 12 ± 2 pmol cyclic GMP $min^{-1}(mg\ protein)^{-1}$

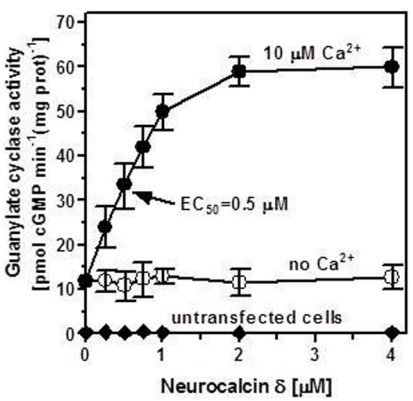

FIGURE 1 | Ca^{2+}-bound neurocalcin δ stimulates ANF-RGC activity. COS cells were transfected with ANF-RGC cDNA and their membrane fraction was analyzed for neurocalcin δ-dependent cyclase activity in the absence (open circles) and presence of 10 μM Ca^{2+} (closed circles). COS cells transfected with an empty vector were analyzed identically (closed diamonds). The extracellular hormone ligand of ANF-RGC, the atrial natriuretic factor (ANF) was absent from the reaction mixture. The experiment was done in triplicate and repeated four times. The results shown are average ± SD from these experiments. The EC_{50} value was determined graphically. Neurocalcin δ used was myristoylated. The myristoylated form of neurocalcin δ was expressed and purified as described in Krishnan et al. (2004).

in the presence of 10 μM Ca^{2+} and 11.9 ± 1.8 pmol cyclic GMP min^{-1}(mg protein)$^{-1}$ in the presence of 1 mM EGTA. In the absence of Ca^{2+} neurocalcin δ, however, did not stimulate ANF-RGC activity (**Figure 1**: open circles). Thus, ANF-RGC activity is not only regulated by ANF or BNP; *in vitro* it is also regulated by myristoylated neurocalcin δ in the presence of Ca^{2+}.

Neurocalcin δ targets the intracellular domain of ANF-RGC

It is well established that ANF and BNP, the hormone-ligands of ANF-RGC, signal through the cyclase's extracellular domain (Duda et al., 1991; Ogawa et al., 2004; reviewed in Sharma, 2002, 2010). Neurocalcin δ, on the other hand, is an intracellular protein, therefore the respective target sites of these two types of ligand, ANF/BNP and neurocalcin δ, reside on the opposite sites of the transmembrane domain of ANF-RGC. To determine the biochemical requirements for neurocalcin δ effect on ANF-RGC activity namely, whether the isolated intracellular portion of ANF-RGC is sufficient for neurocalcin δ to exhibit its stimulatory effect or whether the intact ANF-RGC protein is necessary, an ANF-RGC deletion mutant was prepared in which the extracellular receptor domain (aa 12–433) was deleted. The mutant, however, had retained the leader sequence to ensure its proper membrane targeting. This mutant was transiently expressed in COS cells and their membranes were appropriately treated with ANF or myristoylated neurocalcin δ and 10 μM Ca^{2+}. Both proteins had comparable basal guanylate cyclase activities, 13 and 12.2 pmol cyclic GMP min^{-1}(mg protein)$^{-1}$ for the full-length ANF-RGC and the deletion mutant, respectively. As expected, the mutant was unresponsive to ANF (**Figure 2**: open circles), however, neurocalcin δ stimulated its activity in a dose-dependent fashion (**Figure 2**: closed diamonds). The stimulatory profile was indistinguishable from that of the full-length ANF-RGC (**Figure 2**: closed circles). Also the Hill's coefficients for the neurocalcin δ effect on both cyclases were identical 2.1 ± 0.5 and 2.05 ± 0.4 for the full-length ANF-RGC and for the deletion mutant, respectively. It is, therefore, concluded that the extracellular domain has no structural role in ANF-RGC ability to respond to and be stimulated by myristoylated neurocalcin δ.

ANF-RGC and neurocalcin δ co-exist in the glomerulosa cells of the adrenal gland

Are these *in vitro* biochemical findings on ANF-RGC activity modulation by Ca^{2+} *via* neurocalcin δ of physiological relevance? A first hint could be the co-expression of both proteins in the same tissue, organ or cell type. Guided by intuition the mouse adrenal gland was analyzed for the presence of ANF-RGC and neurocalcin δ, first by Western blot and then through immunocytochemistry.

The gland was homogenized and the homogenate after SDS-polyacrylamide gel electrophoresis was analyzed for the presence of ANF-RGC or neurocalcin δ by Western blot. As shown in **Figure 3**, with antibody against ANF-RGC as a probe (panel "ANF-RGC") an intense immunoreactive band was observed at expected molecular weight of ∼130 kDa. With neurocalcin δ antibody as a probe (**Figure 3**: panel "NCδ") the presence of an immunoreactive protein with mobility of ∼23 kDa corresponding to the molecular weight of neurocalcin δ was observed. These results show that both ANF-RGC and neurocalcin δ are expressed in the mouse adrenal, they, however, do not provide information whether these proteins are expressed in the same type of adrenal gland cells. To determine whether these proteins co-localize in the

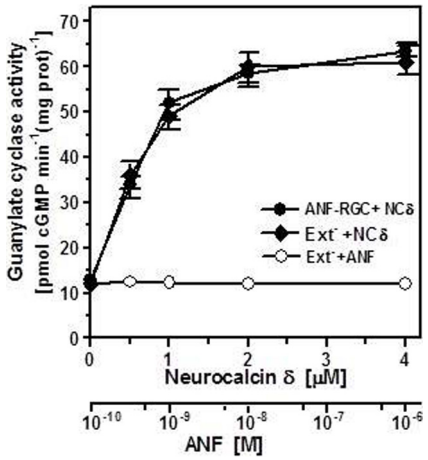

FIGURE 2 | The intracellular portion of ANF-RGC is sufficient for neurocalcin δ and Ca^{2+} to stimulate ANF-RGC activity. The ANF-RGC deletion mutant lacking the extracellular receptor domain aa12–433, was constructed and expressed in COS cells. The particulate fraction of these cells was assayed for guanylate cyclase activity in the presence of increasing concentrations of myristoylated neurocalcin δ and 10 μM Ca^{2+} or 0.5 mM ATP and increasing concentrations of ANF. Membranes of COS cells expressing full-length ANF-RGC were processed in parallel as positive control. The experiment was performed in triplicate and repeated two times. The results shown are mean ± SD from these experiments.

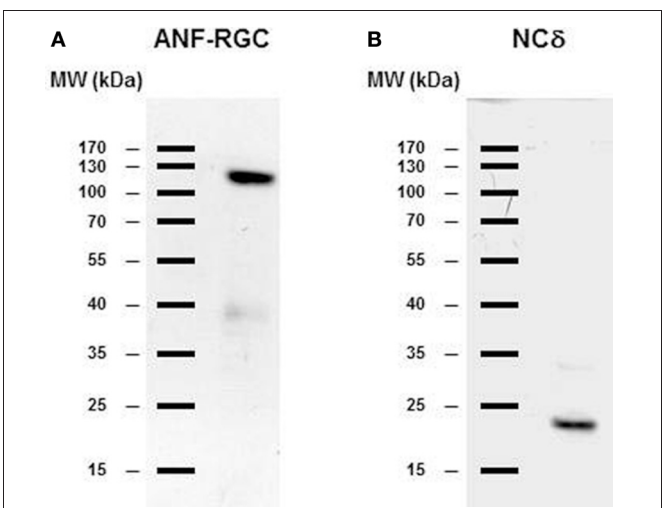

FIGURE 3 | ANF-RGC and neurocalcin δ are expressed in the mouse adrenal gland. Mouse adrenal gland was homogenized in 50 mM Tri-HCl/10 mM $MgCl_2$ buffer (pH 7.5) containing protease inhibitor cocktail (Sigma). The proteins (∼40 μg/lane) were subject to SDS-polyacrylamide gel electrophoresis and analyzed by Western blot using antibody against ANF-RGC or neurocalcin δ as described in the "Materials and Methods" section. **(A)** immunoreactivity with ANF-RGC antibody. **(B)** immunoreactivity with neurocalcin δ antibody.

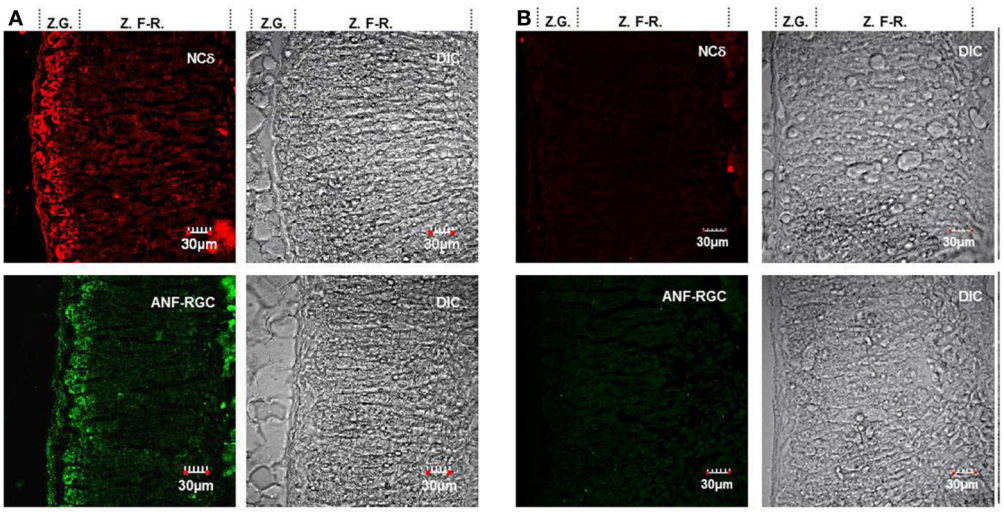

FIGURE 4 | ANF-RGC and neurocalcin δ are co-expressed in the glomerulosa cells of mouse adrenal gland. (A) Serial cryosections of the mouse adrenal gland were immunostained with neurocalcin δ (panel "NCδ") or ANF-RGC (panel "ANF-RGC") antibodies. The DIC image showing the integrity of the adrenal gland sections are presented at the left ("DIC"). "Z.G." and "Z.F-R." denote zona glomerulosa and zona fasciculata-reticularis, respectively. Intense staining with either antibody was observed in the zona glomerulosa. **(B)** The immunostaining with the primary antibodies is specific. The mouse adrenal gland cryosections were processed identically as in **(A)** except that the primary antibody for ANF-RGC or neurocalcin δ was omitted in the respective incubation mixture but incubation with fluorescently labeled secondary antibody was carried out as in **(A)**. The DIC image showing the integrity of the sections are presented ("DIC").

adrenal gland immunocytochemical analyzes were carried out. Sections of the adrenal gland were immunostained with specific antibodies against ANF-RGC and neurocalcin δ. Because both antibodies used were raised in rabbits, co-immunostaining was not feasible, therefore, staining of consecutive sections was performed. The results are shown in **Figure 4A**. Intense staining with anti neurocalcin δ antibody was observed in the adrenal zona glomerulosa (**Figure 4A**: panel "NCδ" Z.G.). Also, strong immunoreactivity with ANF-RGC antibodies was observed in zona glomerulosa (**Figure 4A**: panel "ANF-RGC" Z.G.). This localization of ANF-RGC within the mouse adrenal gland is consistent with the protein's localization in the bovine adrenal gland (Meloche et al., 1988). To verify the specificity of the staining, in control reactions the primary antibodies were omitted but secondary antibody was added. Without the primary antibodies there was no specific staining in the sections analyzed (**Figure 4B**: control). It was therefore concluded that both ANF-RGC and neurocalcin δ co-exist in the adrenal glomerulosa cells. Although some faint staining in both sections was observed for the fasciculate-reticularis cells (Z.F-R. region in both "NCδ" and "ANF-RGC" panels), without detailed co-localization experiments it is not possible to conclude on ANF-RGC and neurocalcin δ co-existence there.

The second question asked was: are ANF-RGC and neurocalcin δ co-existing in the adrenal gland functionally linked? Mouse adrenal gland was homogenized in the presence of 1 mM EGTA or 10 μM Ca^{2+}, the particulate fraction was prepared and analyzed for guanylate cyclase activity. In the absence of Ca^{2+} the activity was 70 ± 9 pmol cyclic GMP min^{-1} (mg protein)$^{-1}$ and in the presence of Ca^{2+}, 245 ± 28 pmol cyclic GMP min^{-1}(mg protein)$^{-1}$ (**Figure 5**). At this stage it is not possible to conclude with certainty, however, if native neurocalcin δ in the adrenal gland is pre-bound to ANF-RGC or if it is undergoing a Ca^{2+} mirystoyl switch and interacts with ANF-RGC in a reversible manner, the guanylate cyclase activity measured at 10 μM Ca^{2+} reflects the neurocalcin δ-stimulated ANF-RGC activity.

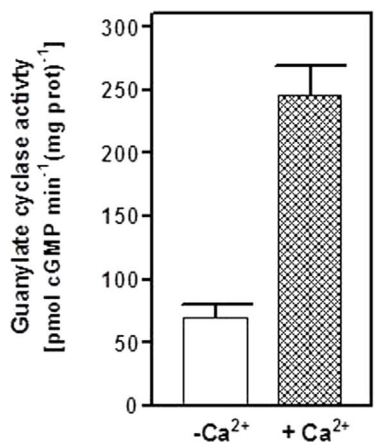

FIGURE 5 | Neurocalcin δ stimulates ANF-RGC in membranes of mouse adrenal gland. Mouse adrenal gland was homogenized in Tris-Mg^{2+} buffer pH 7.4 with or without 10 μM Ca^{2+}. The particulate fractions were prepared from each homogenate and assayed for guanylate cyclase activity. The experiment was done in triplicate and repeated two times. The results shown are average ± SD from these experiments.

What is the physiological significance of neurocalcin δ modulation of ANF-RGC activity in the adrenal zona glomerulosa? At this moment there is no definite answer to this question. A clue, however, may be provided by the facts that the adrenal glomerulosa cells are the site of aldosterone synthesis, that aldosterone synthesis is triggered by the increase in cytosolic Ca^{2+} concentration, and that the ANF-RGC activity offsets the renin-angiotensin-aldosterone system and inhibits aldosterone synthesis (Burnett et al., 1984; Brenner et al., 1990; Aoki et al., 2000; Shi et al., 2001). Because a measurable time is necessary for hormonal (ANF) turning "ON" the ANF-RGC signal transduction system resulting in the inhibition of aldosterone synthesis, it is tempting to hypothesize that before the hormonal ANF signal is activated, Ca^{2+}-bound neurocalcin δ stimulates ANF-RGC. In this situation ANF-RGC response will be very rapid and the cyclic GMP produced will start to inhibit aldosterone synthesis almost immediately. Cyclic GMP synthesized by ANF-RGC affects number of effectors of aldosterone synthesis. They include cyclic GMP-gated channels, cyclic GMP-dependent protein kinases, and cyclic GMP-regulated phosphodiesterases (reviewed in Lohmann et al., 1997; Pfeifer et al., 1999). Several reports indicate that cyclic GMP-driven inhibition of aldosterone synthesis is, at least in part, mediated by cyclic GMP-stimulated phosphodiesterase (PDE 2) that is expressed at high levels in adrenal glomerulosa cells (MacFarland et al., 1991; Côté et al., 1999). This hypothesis needs now experimental validation.

GCAP1 - ANTITHETICAL CALCIUM SENSOR

Since its discovery, GCAP1 has been exclusively regarded as the component of the phototransduction machinery sensing the fall in Ca^{2+} concentration after illumination, transmitting this information to photoreceptor guanylate cyclase ROS-GC and stimulating it to synthesize cyclic GMP at a faster rate (reviewed in Pugh et al., 1997; Koch et al., 2010). With the ensuing raise of Ca^{2+} concentration, Ca^{2+}-bound GCAP1 inhibits ROS-GC activity bringing it to the basal level. This activator/inhibitor mode of GCAP1 operation is well established both *in vivo* and *in vitro*.

Recent work, however, indicated that GCAP1 could target to another sensory membrane guanylate cyclase, an odorant receptor ONE-GC [alternatively termed GC-D (Fülle et al., 1995)] expressed in a subpopulation of olfactory sensory neurons (Duda et al., 2006; Pertzev et al., 2010).

GCAP1 transmits the Ca^{2+}-stimulatory signal to the odorant receptor guanylate cyclase, ONE-GC

Recombinant ONE-GC expressed in COS cell was exposed to increasing Ca^{2+} concentrations and constant, 4 μM, GCAP1 concentration. As a positive control, recombinant ROS-GC1 was treated identically. Both cyclases were expressed in COS to approximately the same level as verified by Western blot (**Figure 6** inset). As expected, based on previous reports (Duda et al., 1996), at or below 10 nM Ca^{2+}, GCAP1 maximally stimulated ROS-GC1 (**Figure 6**: closed circles). The stimulation decreased with increasing free Ca^{2+} concentration and the half-maximal inhibition was at about 100 nM Ca^{2+}. Contrary to that, at about 100 nM Ca^{2+} there was practically no effect on GCAP1-dependent ONE-GC activity (**Figure 6**: open circles). However, with the Ca^{2+} concentrations increasing beyond 100 nM there was a dose-dependent increase in ONE-GC activity. The half-maximal activation of the cyclase occurred at 0.7 μM Ca^{2+} and the maximal activation at about 2.5 μM. At Ca^{2+} concentrations above 2.5 μM there was no statistically significant increase in the cyclase activity. The expression levels of ROS-GC1 and ONE-GC in COS cells was comparable (**Figure 6**: inset). These results essentially confirm the previous published in Duda et al. (2006). The main conclusion is that GCAP1 can function as calcium-dependent regulator of guanylate cyclase activity, but depending on the target it can activate the cyclase in a Ca^{2+}-dependent manner with reverse premise making it an antithetical modulator.

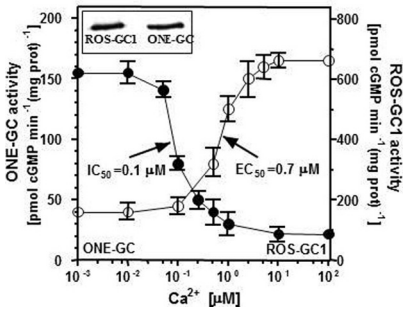

FIGURE 6 | Antithetical Ca^{2+} modulated GCAP1 effect on ONE-GC and ROS-GC1 activities. Membranes of COS cells expressing ONE-GC or ROS-GC1 (control) were individually assayed for guanylate cyclase activity in the presence of 4 μM GCAP1 and indicated concentrations of Ca^{2+}. The experiment was carried out in triplicate and repeated three times. The results shown are shown are average ± SD from these experiments. The IC_{50} and EC_{50} values were determined graphically. **Inset:** Expression levels of ROS-GC1 and ONE-GC in COS cells were monitored by Western blot using antibodies against ROS-GC1 or ONE-GC.

How can GCAP1 exhibit these opposite modulatory effects? To answer this question GCAP1 and ONE-GC mutants were employed.

Several mutations in the GCAP1 gene have been found in patients suffering from autosomal dominant cone-rod dystrophies (Behnen et al., 2010). All these mutations except one are located within the regions coding for EF hands 3 and 4. The $D^{100}E$ mutation is within EF hand 3; it causes perturbation in Ca^{2+} coordination, and leads to a dramatic decrease in affinity for Ca^{2+}. As a consequence, the $D^{100}E$ mutant remains in an active conformation at 10 μM Ca^{2+}. The activation is half-maximal at 20 μM Ca^{2+} and the cyclase activity returns to the basal level only at approx. 60 μM free Ca^{2+} (Behnen et al., 2010; Dell'Orco et al., 2010). This mutant was tested for its effect on ONE-GC activity in the presence of two Ca^{2+} concentrations, 10 nM and 10 μM. For comparison, in parallel experiment, the effect of the $D^{100}E$ mutant on ROS-GC1 activity at the same Ca^{2+} concentrations was determined. The results are shown in **Figure 7**. The mutant stimulated ROS-GC1 activity at both tested Ca^{2+} concentrations. It, however, had no effect on ONE-GC activity at 10 nM Ca^{2+} but stimulated its activity at 10 μM Ca^{2+}. Thus, dysfunctional EF hand 3 does not have any effect on Ca^{2+}-dependent GCAP1 stimulation of ONE-GC. Because the third EF hand has the highest

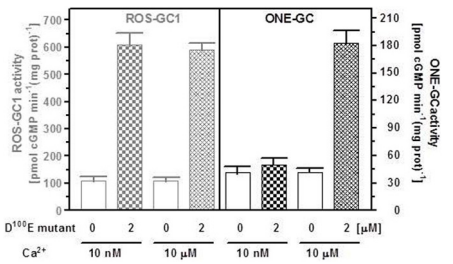

FIGURE 7 | The $D^{100}E$ GCAP1 mutant stimulates both ONE-GC and ROS-GC1 at high Ca^{2+} concentration but only ROS-GC1 in the absence of Ca^{2+}. The membrane fraction of COS cells expressing ONE-GC or ROS-GC1 (control) were assayed for guanylate cyclase activity in the presence (2 μM) or absence of $D^{100}E$ GCAP1 mutant and 1 mM EGTA (10 μM Ca^{2+}) or 10 μM Ca^{2+}. The experiment was done in triplicate and repeated two times for reproducibility. The results shown are average ± SD from these experiments.

affinity for Ca^{2+} (Lim et al., 2009) these results indicated that low affinity Ca^{2+} binding to GCAP1 is sufficient for ONE-GC stimulation. These results further showed that the $D^{100}E$ mutation in GCAP1 leads to a protein conformation that can act as a constitutive activator with Ca^{2+}-sensing properties that are significantly shifted to higher free Ca^{2+}. One can deduce from these results that the interaction sites of GCAP1 in ROS-GC1 and ONE-GC are different, i.e., are not located in corresponding homologous regions. This hypothesis was tested by creating a mutant of ONE-GC with a point mutation in a region that is conserved among sensory guanylate cyclases and that is critical for GCAP1-dependent regulation of ROS-GC1.

GCAP1 signaling modes in its Ca^{2+}-free and Ca^{2+}-bound states are different

The first ROS-GC1 gene mutation linked with visual disorder was the $F^{514}S$ mutation identified in cases of Leber's congenital amaurosis type 1 (LCA1) (Perrault et al., 1996). Studies aimed at explaining the molecular basis of LCA1 demonstrated that this mutation totally disables GCAP1 modulation of ROS-GC1 activity (Duda et al., 1999). Because phenylalanine in this position is conserved in all membrane guanylate cyclases, the obvious question to ask was: would a similar mutation in ONE-GC disable GCAP1-mediated Ca^{2+} signaling of its activity? ONE-GC $F^{585}S$ mutant (corresponding to the $F^{514}S$ in ROS-GC1) was constructed and its activity was determined in the presence of 10 μM Ca^{2+} and increasing concentrations of GCAP1 (**Figure 8A**: closed circles). The results show that contrary to ROS-GC1 and its $F^{514}S$ mutant (**Figure 8A**: open and closed triangles, respectively; the activity was measured in the absence of Ca^{2+}), the F→S mutation in ONE-GC does not affect the Ca^{2+}-GCAP1-dependent activation of the cyclase (**Figure 8A**: compare the profiles with closed and open circles). The Hill's coefficients calculated for the GCAP1 stimulation of wt ONE-GC and of its $F^{585}S$ mutant were virtually identical, 1.83 ± 0.3. The mutation also does not affect the Ca^{2+} sensitivity of the mutant (**Figure 8B**: compare the closed and

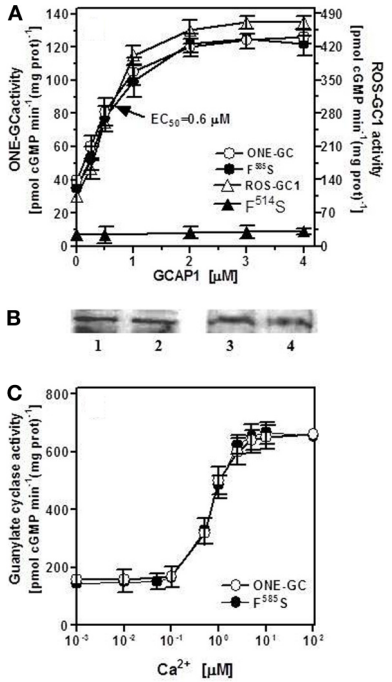

FIGURE 8 | $F^{585}S$ mutation does not affect Ca^{2+}-GCAP1 signaling of ONE-GC activity. (A) Membranes of COS cells expressing ONE-GC or its $F^{585}S$ mutant were assayed for guanylate cyclase activity in the presence of increasing concentrations of GCAP1 and constant 10 μM Ca^{2+}; Membranes of COS cells expressing ROS-GC1 or its $F^{514}S$ mutant were analyzed for GCAP1 effect in the absence of Ca^{2+} (1 mM EGTA was present in the assay mixture). **(B)** Membranes of COS cells expressing ONE-GC and its $F^{585}S$ mutant or ROS-GC1 and its $F^{514}S$ mutant were analyzed by Western blot using antibodies against ROS-GC1 and ONE-GC. Approx 20 μg of membrane protein was applied on each lane of the gel. Lane 1, ONE-GC; Lane 2, ONE-GC $F^{585}S$; Lane 3, ROS-GC1; Lane 4, ROS-GC1 $F^{514}S$. **(C)** Membranes of COS cells expressing ONE-GC or its $F^{585}S$ mutant were assayed for guanylate cyclase activity in the presence of increasing concentrations of Ca^{2+} and constant, 4 μM GCAP1. The experiments were done in triplicate and repeated for reproducibility with different preparations of transfected COS cells. The results presented (mean ± SD) are from one representative experiment.

open circles). It is, therefore, concluded that Ca^{2+}-free and Ca^{2+}-bound GCAP1 exert different signals for activation of membrane guanylate cyclase. They probably do so by acting on different target regions, since the mutation $F^{514}S$ is located in a previously identified interaction and/or regulatory region of ROS-GC1 (Lange et al., 1999). Finally, while the $F^{514}S$ mutation in ROS-GC1 results in blindness at birth or soon thereafter (Perrault et al., 1996), the corresponding $F^{585}S$ mutation in ONE-GC would not result in anosmia.

ACKNOWLEDGMENTS

This study was supported by the National Heart Blood and Lung Institute: HL084584 and S82701 and by the Pennsylvania Lions Sight Conservation and Eye Research Foundation (Teresa Duda) and by the Deutsche Forschungsgemeinschaft (KO948/10-1) (Karl.-W. Koch).

REFERENCES

Aoki, H., Richmond, M., Izumo, S., and Sadoshima, J. (2000). Specific role of the extracellular signal-regulated kinase pathway in angiotensin II-induced cardiac hypertrophy *in vitro*. *Biochem. J.* 347, 275–284.

Behnen, P., Dell'Orco, D., and Koch, K. W. (2010). Involvement of the calcium sensor GCAP1 in hereditary cone dystrophies. *Biol. Chem.* 391, 631–637.

Bhattacharya, S., Bunick, C. G., and Chazin, W. J. (2004). Target selectivity in EF-hand calcium binding proteins. *Biochim. Biophys. Acta* 1742, 69–79.

Braunewell, K. H. (2005). The darker side of Ca^{2+} signaling by neuronal Ca^{2+}-sensor proteins: from Alzheimer's disease to cancer. *Trends Pharmacol. Sci.* 26, 345–351.

Brenner, B. M., Ballermann, B. J., Gunning, M. E., and Zeidel, M. L. (1990). Diverse biological actions of atrial natriuretic peptide. *Physiol. Rev.* 70, 665–699.

Burgoyne, R. D. (2007). Neuronal calcium sensor proteins: generating diversity in neuronal Ca^{2+} signalling. *Nat. Rev. Neurosci.* 8, 182–193.

Burgoyne, R. D., O'Callaghan, D. W., Hasdemir, B., Haynes, L. P., and Tepikin, A. V. (2004). Neuronal Ca^{2+}-sensor proteins: multitalented regulators of neuronal function. *Trends Neurosci.* 27, 203–209.

Burgoyne, R. D., and Weiss, J. L. (2001). The neuronal calcium sensor family of Ca^{2+}-binding proteins. *Biochem. J.* 353, 1–12.

Burnett, J. C. Jr., Granger, J. P., and Opgenorth, T. J. (1984). Effect of synthetic atrial natriuretic factor on renal function and rennin release. *Am. J. Physiol.* 247, F863–F866.

Côté, M., Payet, M. D., Rousseau, E., Guillon, G., and Gallo-Payet, N. (1999). Comparative involvement of cyclic nucleotide phosphodiesterases and adenylyl cyclase on adrenocorticotropin-induced increase of cyclic adenosine monophosphate in rat and human glomerulosa cells. *Endocrinology* 140, 3594–3601.

Coussen, F., and Mulle, C. (2006). Kainate receptor-interacting proteins and membrane trafficking. *Biochem. Soc. Trans.* 34, 927–930.

Dell'Orco, D., Behnen, P., Linse, S., and Koch, K. W. (2010). Calcium binding, structural stability and guanylate cyclase activation in GCAP1 variants associated with human cone dystrophy. *Cell. Mol. Life Sci.* 67, 973–984.

Duda, T., Fik-Rymarkiewicz, E., Venkataraman, V., Krishnan, A., and Sharma, R. K. (2004). Calcium-modulated ciliary membrane guanylate cyclase transduction machinery: constitution and operational principles. *Mol. Cell. Biochem.* 267, 107–122.

Duda, T., Goraczniak, R., Surgucheva, I., Rudnicka-Nawrot, M., Gorczyca, W. A., Palczewski, K., Sitaramayya, A., Baehr, W., and Sharma, R. K. (1996). Calcium modulation of bovine photoreceptor guanylate cyclase. *Biochemistry* 35, 8478–8482.

Duda, T., Goraczniak, R. M., and Sharma, R. K. (1991). Site-directed mutational analysis of a membrane guanylate cyclase cDNA reveals the atrial natriuretic factor signaling site. *Proc. Natl. Acad. Sci. U.S.A.* 88, 7882–7886.

Duda, T., Jankowska, A., Venkataraman, V., Nagele, R. G., and Sharma, R. K. (2001). A novel calcium-regulated membrane guanylate cyclase transduction system in the olfactory neuroepithelium. *Biochemistry* 40, 12067–12077.

Duda, T., Krishnan, R., and Sharma, R. K. (2006). GCAP1-Antithetical calcium sensor of ROS-GC transduction machinery. *Calcium Bind. Proteins* 1, 102–107.

Duda, T., and Sharma, R. K. (2009). Ca^{2+}-modulated ONE-GC odorant signal transduction. *FEBS Lett.* 583, 1327–1330.

Duda, T., Venkataraman, V., Goraczniak, R., Lange, C., Koch, K. W., and Sharma, R. K. (1999). Functional consequences of a rod outer segment membrane guanylate cyclase (ROS-GC1) gene mutation linked with Leber's congenital amaurosis. *Biochemistry* 38, 509–515.

Frins, S., Bönigk, W., Müller, F., Kellner, R., and Koch, K. W. (1996). Functional characterization of a guanylyl cyclase-activating protein from vertebrate rods. Cloning, heterologous expression, and localization. *J. Biol. Chem.* 271, 8022–8027.

Fülle, H. J., Vassar, R., Foster, D. C., Yang, R. B., Axel, R., and Garbers, D. L. (1995). A receptor guanylyl cyclase expressed specifically in olfactory sensory neurons. *Proc. Natl. Acad. Sci. U.S.A.* 92, 3571–3575.

Gorczyca, W. A., Gray-Keller, M. P., Detwiler, P. B., and Palczewski, K. (1994). Purification and physiological evaluation of a guanylate cyclase activating protein from retinal rods. *Proc. Natl. Acad. Sci. U.S.A.* 91, 4014–4018.

Haynes, L. P., and Burgoyne, R. D. (2008). Unexpected tails of a Ca^{2+} sensor. *Nat. Chem. Biol.* 4, 90–91.

Howes, K. A., Pennesi, M. E., Sokal, I., Church-Kopish, J., Schmidt, B., Margolis, D., Frederick, J. M., Rieke, F., Palczewski, K., Wu, S. M., Detwiler, P. B., and Baehr, W. (2002). GCAP1 rescues rod photoreceptor response in GCAP1/GCAP2 knockout mice. *EMBO J.* 21, 1545–1554.

Hwang, J. Y., and Koch, K. W. (2002). Calcium- and myristoyl-dependent properties of guanylate cyclase-activating protein-1 and protein-2. *Biochemistry* 41, 13021–13028.

Iino, S., Kobayashi, S., Okazaki, K., and Hidaka, H. (1995). Immunohistochemical localization of neurocalcin in the rat inner ear. *Brain Res.* 680, 128–134.

Ivings, L., Pennington, S. R., Jenkins, R., Weiss, J. L., and Burgoyne, R. D. (2002). Identification of Ca^{2+}-dependent binding partners for the neuronal calcium sensor protein neurocalcin delta: interaction with actin, clathrin and tubulin. *Biochem. J.* 363, 599–608.

Kitiratschky, V. B., Behnen, P., Kellner, U., Heckenlively, J. R., Zrenner, E., Jägle, H., Kohl, S., Wissinger, B., and Koch, K. W. (2009). Mutations in the GUCA1A gene involved in hereditary cone dystrophies impair calcium-mediated regulation of guanylate cyclase. *Hum. Mutat.* 30, E782–E796.

Koch, K. W., Duda, T., and Sharma, R. K. (2010). $Ca^{(2+)}$-modulated vision-linked ROS-GC guanylate cyclase transduction machinery. *Mol. Cell. Biochem.* 334, 105–115.

Krishnan, A., Venkataraman, V., Fik-Rymarkiewicz, E., Duda, T., and Sharma, R. K. (2004). Structural, biochemical, and functional characterization of the calcium sensor neurocalcin delta in the inner retinal neurons and its linkage with the rod outer segment membrane guanylate cyclase transduction system. *Biochemistry* 43, 2708–2723.

Ladant, D. (1995). Calcium and membrane binding properties of bovine neurocalcin delta expressed in Escherichia coli. *J. Biol. Chem.* 270, 3179–3185.

Lange, C., Duda, T., Beyermann, M., Sharma, R. K., and Koch, K. W. (1999). Regions in vertebrate photoreceptor guanylyl cyclase ROS-GC1 involved in $Ca^{(2+)}$-dependent regulation by guanylyl cyclase-activating protein GCAP-1. *FEBS Lett.* 460, 27–31.

Lim, S., Peshenko, I., Dizhoor, A., and Ames, J. B. (2009). Effects of Ca^{2+}, Mg^{2+}, and myristoylation on guanylyl cyclase activating protein 1 structure and stability. *Biochemistry* 48, 850–862.

Lohmann, S. M., Vaandrager, A. B., Smolenski, A., Walter, U., and de Jonge, H. R. (1997). Distinct and specific functions of cGMP-dependent protein kinases. *Trends Biochem. Sci.* 22, 307–312.

MacFarland, R. T., Zelus, B. D., and Beavo, J. A. (1991). High concentrations of a cGMP-stimulated phosphodiesterase mediate ANP-induced decreases in cAMP and steroidogenesis in adrenal glomerulosa cells. *J. Biol. Chem.* 266, 136–142.

Meloche, S., McNicoll, N., Liu, B., Ong, H., and de Léan, A. (1988). Atrial natriuretic factor R1 receptor from bovine adrenal zona glomerulosa: purification, characterization, and modulation by amiloride. *Biochemistry* 27, 8151–8158.

Mendez, A., Burns, M. E., Sokal, I., Dizhoor, A. M., Baehr, W., Palczewski, K., Baylor, D. A., and Chen, J. (2001). Role of guanylate cyclase-activating proteins (GCAPs) in setting the flash sensitivity of rod photoreceptors. *Proc. Natl. Acad. Sci. U.S.A.* 98, 9948–9953.

Nambi, P., Aiyar, N. V., and Sharma, R. K. (1982). Adrenocorticotropin-dependent particulate guanylate cyclase in rat adrenal and adrenocortical carcinoma: comparison of its properties with soluble guanylate cyclase and its relationship with ACTH-induced steroidogenesis. *Arch. Biochem. Biophys.* 217, 638–646.

O'Callaghan, D. W., Ivings, L., Weiss, J. L., Ashby, M. C., Tepikin, A. V., and Burgoyne, R. D. (2002). Differential use of myristoyl groups on neuronal calcium sensor proteins as a determinant of spatio-temporal aspects of Ca^{2+} signal transduction. *J. Biol. Chem.* 277, 14227–14237.

Ogawa, H., Qiu, Y., Ogata, C. M., and Misono, K. S. (2004). Crystal structure of hormone-bound atrial natriuretic peptide receptor extracellular domain: rotation mechanism for transmembrane signal transduction. *J. Biol. Chem.* 279, 28625–28631.

Okazaki, K., Obata, N. H., Inoue, S., and Hidaka, H. (1995). S100 beta is a target protein of neurocalcin delta, an abundant isoform in glial cells. *Biochem. J.* 306, 551–555.

Orban, T., Bereta, G., Miyagi, M., Wang, B., Chance, M. R., Sousa, M. C., and Palczewski, K. (2010).

Conformational changes in guanylate cyclase-activating protein 1 induced by Ca^{2+} and N-terminal fatty acid acylation. *Structure* 18, 116–126.

Palczewski, K., Sokal, I., and Baehr, W. (2004). Guanylate cyclase-activating proteins: structure, function, and diversity. *Biochem. Biophys. Res. Commun.* 322, 1123–1130.

Perrault, I., Rozet, J. M., Calvas, P., Gerber, S., Camuzat, A., Dollfus, H., Châtelin, S., Souied, E., Ghazi, I., Leowski, C., Bonnemaison, M., Le Paslier, D., Frézal, J., Dufier, J. L., Pittler, S., Munnich, A., and Kaplan, J. (1996). Retinal-specific guanylate cyclase gene mutations in Leber's congenital amaurosis. *Nat. Genet.* 14, 461–464.

Pertzev, A., Duda, T., and Sharma, R. K. (2010). $Ca^{(2+)}$ sensor GCAP1: a constitutive element of the ONE-GC-modulated odorant signal transduction pathway. *Biochemistry* 49, 7303–7313.

Peshenko, I. V., and Dizhoor, A. M. (2006). Ca^{2+} and Mg^{2+} binding properties of GCAP-1. Evidence that Mg^{2+}-bound form is the physiological activator of photoreceptor guanylyl cyclase. *J. Biol. Chem.* 281, 23830–23841.

Pfeifer, A., Ruth, P., Dostmann, W., Sausbier, M., Klatt, P., and Hofmann, F. (1999). Structure and function of cGMP-dependent protein kinases. *Rev. Physiol. Biochem. Pharmacol.*135, 105–149.

Pugh, E. N. Jr, Duda, T., Sitaramayya, A., and Sharma, R. K. (1997). Photoreceptor guanylate cyclases: a review. *Biosci. Rep.* 17, 429–473.

Rebello, M. R., Atkas, A., and Medle, K. F. (2011). Expression of calcium binding proteins in mouse type II taste cells. *J. Histochem. Cytochem.* 59, 530–539.

Sambrook, M. J., Fritsch, E. F., and Maniatis, T. (1989). *Molecular Cloning: A Laboratory Manual*, 2nd Edn. Cold Spring Harbor, NY: Cold Spring Harbor Laboratory.

Sharma, R. K. (2002). Evolution of the membrane guanylate cyclase transduction system. *Mol. Cell. Biochem.* 230, 3–30.

Sharma, R. K. (2010). Membrane guanylate cyclase is a beautiful signal transduction machine: overview. *Mol. Cell. Biochem.* 334, 3–36.

Sharma, R. K., Duda, T., Venkataraman, V., and Koch, K. W. (2004). Calcium modulated mammalian membrane guanylate cyclase ROS-GC transduction machinery in sensory neurons. *Curr. Top. Biochem. Res.* 322, 111–144.

Shi, S.-J., Nguyen, H. T., Sharma, G. D., Navar, G., and Pandey, K. N. (2001). Genetic disruption of atrial natriuretic peptide receptor-a alters rennin and angiotensinII levels. *Am. J. Physiol. Renal Physiol.* 281, F665–F673.

Stephen, R., Bereta, G., Golczak, M., Palczewski, K., and Sousa, M. C. (2007). Stabilizing function for myristoyl group revealed by the crystal structure of a neuronal calcium sensor, guanylate cyclase-activating protein 1. *Structure* 15, 1392–1402.

Takimoto, K., Yang, E. K., and Conforti, L. (2002). Palmitoylation of KChIP splicing variants is required for efficient cell surface expression of Kv4.3 channels. *J. Biol. Chem.* 277, 26904–26911.

Zozulya, S., and Stryer, L. (1992). Calcium-myristoyl protein switch. *Proc. Natl. Acad. Sci. U.S.A.* 89, 11569–11573.

Conflict of Interest Statement: The authors declare that the research was conducted in the absence of any commercial or financial relationships that could be construed as a potential conflict of interest.

Received: 07 March 2012; accepted: 21 March 2012; published online: 09 April 2012.

Citation: Duda T, Pertzev A, Koch K-W and Sharma RK (2012) Antithetical modes of and the Ca^{2+} sensors targeting in ANF-RGC and ROS-GC1 membrane guanylate cyclases. Front. Mol. Neurosci. 5:44. doi: 10.3389/fnmol.2012.00044

frontiers in
MOLECULAR NEUROSCIENCE

ORIGINAL RESEARCH ARTICLE
published: 08 March 2012
doi: 10.3389/fnmol.2012.00028

Synergetic effect of recoverin and calmodulin on regulation of rhodopsin kinase

Ilya I. Grigoriev[1], Ivan I. Senin[1]*, Natalya K. Tikhomirova[1], Konstantin E. Komolov[1,2†], Sergei E. Permyakov[3], Evgeni Yu. Zernii[1]*, Karl-Wilhelm Koch[2] and Pavel P. Philippov[1]

[1] *Department of Cell Signaling, A.N. Belozersky Institute of Physico-Chemical Biology, Lomonosov Moscow State University, Moscow, Russia*
[2] *Biochemistry Group, Department of Biology and Environmental Sciences, University of Oldenburg, Oldenburg, Germany*
[3] *Institute for Biological Instrumentation of the Russian Academy of Sciences, Pushchino, Moscow Region, Russia*

Edited by:
Michael R. Kreutz, Leibniz-Institute for Neurobiology, Germany

Reviewed by:
Karl Heinz Braunewell, Southern Research Institute, USA
Jacques Haiech, University of Strasbourg, France

****Correspondence:***
Ivan I. Senin and Evgeni Yu. Zernii, Department of Cell Signaling, A.N. Belozersky Institute of Physico-Chemical Biology, Lomonosov Moscow State University, Leninskie Gory 1, Building 40, Moscow 119992, Russia.
e-mail: senin@belozersky.msu.ru; zerni@belozersky.msu.ru

†Present address:
Konstantin E. Komolov, Department of Biochemistry and Molecular Biology, Thomas Jefferson University, Philadelphia, PA 19107, USA.

Phosphorylation of photoactivated rhodopsin by rhodopsin kinase (RK or GRK1), a first step of the phototransduction cascade turnoff, is under the control of Ca^{2+}/recoverin. Here, we demonstrate that calmodulin, a ubiquitous Ca^{2+}-sensor, can inhibit RK, though less effectively than recoverin does. We have utilized the surface plasmon resonance technology to map the calmodulin binding site in the RK molecule. Calmodulin does not interact with the recoverin-binding site within amino acid residues M1-S25 of the enzyme. Instead, the high affinity calmodulin binding site is localized within a stretch of amino acid residues V150-K175 in the N-terminal regulatory region of RK. Moreover, the inhibitory effect of calmodulin and recoverin on RK activity is synergetic, which is in agreement with the existence of separate binding sites for each Ca^{2+}-sensing protein. The synergetic inhibition of RK by both Ca^{2+}-sensors occurs over a broader range of Ca^{2+}-concentration than by recoverin alone, indicating increased Ca^{2+}-sensitivity of RK regulation in the presence of both Ca^{2+}-sensors. Taken together, our data suggest that RK regulation by calmodulin in photoreceptor cells could complement the well-known inhibitory effect of recoverin on RK.

Keywords: rhodopsin kinase, calmodulin, recoverin, phosphorylation, surface plasmon resonance

INTRODUCTION

Key aspects of the neuronal activity from neurotransmission to gene expression are regulated by changes in the intracellular free calcium concentration. Effects of calcium on various processes in the cell are mediated by Ca^{2+} sensor proteins. The important property of these proteins is the ability to change their conformation upon Ca^{2+}-binding, thereby transmitting the signal to the effector enzymes. The effects of calcium in different cells of the most tissues are mediated primarily by ubiquitous calcium sensor calmodulin (Hoeflich and Ikura, 2002), belonging to the large group of EF-hand calcium-binding proteins. In addition to calmodulin, the other EF-hand calcium-sensitive proteins of the neuronal calcium sensor (NCS) and caldendrin/calneuron families are expressed in neurons (McCue et al., 2010). These proteins regulate different aspects of neuronal function including neurotransmitter release, channel and receptor regulation, control of gene transcription, neuronal growth, and survival. NCS proteins provide a fine-tuning of regulatory mechanisms triggered by changes in calcium level in neurons while calmodulin operates more as an universal sensor of calcium signals. Some of the protein targets are common for both calmodulin and NCS proteins and in a number of cases they were shown to compete for the same binding sites in target molecules (Schaad et al., 1996; Haynes et al., 2006; Few et al., 2011).

The concentration of calmodulin in neurons (including rod outer segments, ROS) is normally 10–25 μM (Liebman, 1972; Kohnken et al., 1981; Kakiuchi et al., 1982) and is comparable to the level of NCS family proteins (maximum intracellular concentration of 30–40 μM was observed in the case of hippocalcin in hippocampal neurons and recoverin in photoreceptors; Klenchin et al., 1995; McCue et al., 2010; Mikhaylova et al., 2011). In this case, one of the possible mechanisms underlying the effective functioning of the NCSs is based on the different affinities of NCSs and calmodulin to calcium. This is for example realized when calmodulin and NCS proteins regulate a specific target protein in different ranges of cytoplasmic calcium (for review, see Burgoyne, 2007; McCue et al., 2010).

In addition to competitive regulation based on the variable Ca^{2+}-sensitivity, the effective functioning of NCSs, and calmodulin can be implemented through their interaction with target proteins using separate binding sites. The examples of simultaneous regulation of the effector enzymes by several Ca^{2+}-binding proteins are quite common. In photoreceptor cells, retinal guanylyl cyclase 1 contains independent binding sites for four Ca^{2+}-binding proteins: guanylyl cyclase activating protein 1 (GCAP1; Lange et al., 1999), GCAP2 (Duda et al., 2005), S100B (Duda et al., 2002), and neurocalcin (Venkataraman et al., 2008).

Four Ca^{2+} binding EF-hand proteins are involved in regulation of sodium/proton exchanger 1 (NHE) via different sites on either juxtamembrane region of NHE1 (calcineurin homologous proteins 1, 2, and tescalcin) or C-terminal regulatory domain (calmodulin; Köster et al., 2011). Another example includes Ca^{2+}-dependent regulation of chimeric calmodulin-dependent protein kinase from plants (Sathyanarayanan et al., 2000). This enzyme contains visinin-like domain, which serves as an intramolecular NCS-like regulator. Such a structure allows the enzyme to complement the external regulation of its activity by calmodulin with intramolecular regulation utilizing the visinin-like domain.

Recoverin is an NCS protein that is primarily expressed in the photoreceptor cells, where it plays a key role in the recovery phase of phototransduction by regulating the activity of rhodopsin kinase (RK; Gorodovikova and Philippov, 1993; Kawamura, 1993; Gorodovikova et al., 1994a,b; Chen et al., 1995; Klenchin et al., 1995; Senin et al., 1995; Makino et al., 2004). Recoverin consists of two domains each containing a pair (functional and non-functional) of EF-hand-type Ca^{2+}-binding sites (Flaherty et al., 1993). The N-terminus of the protein is acylated with myristic acid (Dizhoor et al., 1992). Upon binding of two calcium ions, recoverin undergoes a series of conformational changes allowing the exposure of the amino acid residues of its hydrophobic pocket intended for interaction with RK (Tanaka et al., 1995; Ames et al., 1997, 2006; Komolov et al., 2005). In parallel, the myristoyl group of recoverin becomes exposed imparting the interaction with photoreceptor membranes (so-called Ca^{2+}/myristoyl switch mechanism; Zozulya and Stryer, 1992; Dizhoor et al., 1993). In the photoreceptor cells, recoverin inhibits RK in the dark while this inhibition is relieved upon illumination and the subsequent drop of the intracellular calcium level (Senin et al., 2002b). It allows RK to phosphorylate bleached receptor, rhodopsin, which is the first step to its desensitization (Wilden et al., 1986).

RK (or GRK1) is a member of the G protein-coupled receptor-kinase (GRK) family that specifically phosphorylate agonist-occupied G protein-coupled receptors (GPCRs) and initiate the recruitment of arrestins that induces further receptor desensitization and internalization (Pronin et al., 2002). The common feature of GRKs is the central catalytic domain flanked by two sections of the regulatory RH-domain [from regulator of G protein signaling (RGS) homology] (Singh et al., 2008; Boguth et al., 2010). A C-terminal cysteine residue in RK is modified by a farnesyl group which is involved both in the binding of the enzyme to membranes and in the interaction with its substrate rhodopsin (Inglese et al., 1992; McCarthy and Akhtar, 2000). The recoverin-binding site in RK is localized in the N-terminal portion of the molecule upstream of the RH-domain and consists of the first 25 amino acid residues of the enzyme (Ames et al., 2006; Higgins et al., 2006). Binding of recoverin to this site does not prevent receptor-kinase interaction and thus formation of a transient ternary complex between the kinase, recoverin, and the receptor. Instead, recoverin affects a conformational transition in the RK molecule that is necessary for the phosphorylation of the receptor (Komolov et al., 2009). Previous work has provided some quantitative characteristics of RK regulation by recoverin. The equilibrium dissociation constant (K_D) of recoverin–RK complex is about 6 μM (Satpaev et al., 1998). The half-maximal inhibition of rhodopsin phosphorylation occurs at 3–6 μM recoverin and at 1.5–3 μM $[Ca^{2+}]_{free}$ (Klenchin et al., 1995; Senin et al., 1997; Weiergräber et al., 2006; Zernii et al., 2011).

While retina-specific GRK1 (RK) and GRK7 are regulated by Ca^{2+}/recoverin, other GRKs (GRK2-6) are found to be inhibited by the universal mediator of Ca^{2+} signaling calmodulin (Chuang et al., 1996; Pronin et al., 1997). It was shown that calmodulin binding sites in GRK2 and GRK5 are located at both the N- and C-terminal regions of their RH domains and seem to be independent (Levay et al., 1998). Another report suggests that the activity of RK can be regulated not only by recoverin, but also by some additional NCSs as well as by the other Ca^{2+}-binding proteins presented in the photoreceptor cell (De Castro et al., 1995). Among the latter is calmodulin (Kohnken et al., 1981) which in surface plasmon resonance (SPR) studies binds to RK in a Ca^{2+}-dependent manner. The apparent K_D of that complex was 0.1 μM and the half-maximal binding was observed at 3 μM Ca^{2+} (Levay et al., 1998). Since calmodulin and recoverin are colocalized with RK in photoreceptor cells (Kohnken et al., 1981; Dizhoor et al., 1991; Palczewski et al., 1993; Eckmiller, 2002), the actual process of the Ca^{2+}-dependent regulation of rhodopsin phosphorylation by the enzyme could involve both Ca^{2+}-sensors. In the present study, we demonstrate that a Ca^{2+}-dependent regulation of the RK activity is indeed jointly mediated by recoverin and calmodulin. In particular, we show the synergetic inhibition of the enzyme activity by these Ca^{2+}-sensitive regulators. Additionally, we study the structural basis of this process by mapping the calmodulin binding site in the RK molecule.

MATERIALS AND METHODS

PURIFICATION OF RECOVERIN AND CALMODULIN

Heterologous expression and purification of myristoylated wild-type recoverin has been described in detail in a previous study (Senin et al., 2002a). Calmodulin was purified from bovine brain according to Gopalakrishna and Anderson (1982) with some modifications. Briefly, 100 g of brain tissue was extracted with 200 ml of 50 mM Tris–HCl pH 7.5, 1 mM EDTA, 1 mM 2-mercaptoethanol, 0.5 mM phenylmethylsulfonyl fluoride (PMSF). The extract was subjected to isoelectric precipitation at pH 4.3 followed by heat denaturation of the dissolved pellet at 100°C. Further, renaturated calmodulin was loaded onto a phenyl-Sepharose 6B column (GE Healthcare) equilibrated with 50 mM Tris–HCl pH 7.5, 1 mM 2-mercaptoethanol, 0.1 mM $CaCl_2$. The column was washed with the same buffer containing 0.5 M NaCl, and calmodulin fractions were eluted with 1 mM EGTA. The resulted fractions were pooled and loaded onto a 5-ml HiTrap DEAE FF anion exchange chromatography column (GE Healthcare) pre-equilibrated with 50 mM Tris–HCl pH 7.5, 1 mM 2-mercaptoethanol at 1 ml/min. After washing the column with the same buffer (∼10 column volumes), calmodulin was eluted by 30 ml of a linear ionic strength gradient (0–500 mM NaCl) at 0.5 ml/min. Calmodulin containing fractions as revealed by SDS-PAGE were pooled, dialyzed overnight versus 20 mM Tris–HCl pH 8.0, concentrated, and stored at −80°C.

PREPARATION OF ROD OUTER SEGMENTS AND UREA-WASHED ROS MEMBRANES

Bovine ROS were prepared from frozen retinae according to a well-established procedure (Papermaster and Dreyer, 1974) with some modifications. All procedures were performed under dim red light. 200 frozen retinae were thawed in 200 ml of buffer A [20 mM Tris–HCl pH 8.0, 0.1 mM EDTA, 1 mM dithiothreitol (DTT)] containing 45% (w/v) sucrose and the resulted mixture was vigorously shaken for 10 min. The suspension was then centrifuged (3,000 *g*, 4˚C) for 20 min and the pellet was discarded. The ROS containing supernatant was diluted twice with buffer A and centrifuged (8,600 *g*, 4˚C) for 30 min. The supernatant was discarded and the pellet containing crude ROS was resuspended in minimal volume of buffer A with addition of 34% (w/v) sucrose, layered over a freshly prepared 34–36% sucrose density step gradient and centrifuged (72,000 *g*, 4˚C) for 2 h. The centrifugation resulted in formation of the compact band containing ROS fraction, which was carefully removed, diluted twice with buffer A and centrifuged for 15 min at 27,200 *g*, 4˚C. The resulting intact ROS pellet was stored at −80˚C. Urea-washed ROS membranes were prepared by homogenizing ROS in 5 M urea followed by five-times washing with buffer A as previously described (Senin et al., 2002a).

PREPARATION OF RK CONSTRUCTS AND NATIVE RK

Standard cloning techniques were applied to generate seven RK constructs from a full-length RK cDNA template in a pT7-7 plasmid. DNA fragments corresponding to the RK amino terminal region (N-RK: M1-G183), RK carboxy terminal region (C-RK: I455-S561) as well as to RK amino terminal region stretches M1-S25, M1-L102, L102-G183, D100-V150, and F125-K175 were PCR-amplified and inserted into the pGEX-5x-1 vector to achieve expression as glutathione *S*-transferase (GST) fusion proteins. Procedures for heterologous expression and affinity chromatography purification of GST–RK constructs were the same as previously described (Komolov et al., 2009). Native RK was purified from ROS as described in detail elsewhere (Senin et al., 2011).

PHOSPHORYLATION ASSAY

RK activity was measured using an *in vitro* rhodopsin phosphorylation assay essentially as described (Weiergräber et al., 2006). Briefly, the assay was performed in 50 μl reaction mixture containing 10 μM rhodopsin (urea-washed ROS membranes), 20 mM Tris–HCl pH 7.5, 2 mM $MgCl_2$, 1 mM γ-^{32}P-ATP (30–100 dpm/pmol), 1 mM DTT, 1 mM PMSF, and 0.3–0.5 units of rhodopsin kinase with addition of either 200 μM $CaCl_2$ or 1 mM EGTA. Recoverin and/or calmodulin at concentrations indicated in the figure legends was added, as appropriate. 1,2-bis (*o*-amino-5-bromophenoxy) ethane-*N*,*N*,*N*′,*N*′-tetraacetic acid tetrapotassium salt (5,5′-dibromo-BAPTA) was used as a Ca^{2+}-buffer in Ca^{2+}-titration experiments according to our previous work (Senin et al., 2002a). The reaction was initiated by addition of ATP and samples were incubated under continuous light for 30 min at 37˚C. Incubation was terminated by adding 1 ml of 10% (w/v) trichloroacetic acid. The resulting precipitate was collected by centrifugation and washed three times with 1 ml of 10% trichloroacetic acid; the final pellet was used for Cherenkov counting. The data were analyzed in SigmaPlot 11 (Systat Software) by plotting relative RK activity [assuming 100% activity at no inhibitor(-s) added] versus Ca^{2+}-sensing protein(-s) or free Ca^{2+} concentration and by fitting the plot to four parameter Hill sigmoidal (Eq. 1):

$$y = y_0 + \frac{ax^b}{c^b + x^b} \tag{1}$$

where y is the relative RK activity and x is the recoverin and/or calmodulin or free calcium concentration. The resulting values b (Hill coefficient, n) and c (half-maximal inhibition, IC_{50}) were expressed as best-fit value ± SE of the fit.

SURFACE PLASMON RESONANCE

Surface plasmon resonance measurements were performed on a BIACORE 2000 instrument (GE Healthcare) at 25˚C. Details of the operation principle, the immobilization procedures and of the evaluation of sensorgrams had been described before (Koch, 2000; Komolov et al., 2006). The analysis of how various GST–RK constructs interact with calmodulin was performed as described recently for recoverin (Komolov et al., 2009) with some modifications. GST–RK fusion proteins were captured on the surface of a CM5 sensor chip (GE Healthcare) with pre-immobilized goat anti-GST antibodies (GE Healthcare) resulting in a surface density of approximately 1 ng/mm^2. Calmodulin was applied in the mobile phase in running buffer (20 mM Tris–HCl pH 7.5, 100 mM NaCl, 2 mM $CaCl_2$, 1 mM $MgCl_2$, 0.005% Tween 20) at 10 μl/min flow rate. Calmodulin concentration in steady-state affinity analysis was varied from 10 to 150 μM. Each calmodulin response was double-referenced by subtracting a blank (buffer) and control (injection over GST-coated surface lacking the RK fragments) response (Myszka, 1999). The sensorgrams were also normalized to the amount of immobilized GST–RK. The apparent K_Ds for calmodulin–RK peptide complexes were determined by equilibrium analysis as follows: the SPR amplitudes recorded at steady-state of the association phase of each calmodulin injection versus calmodulin concentrations in the mobile phase were plotted using SigmaPlot 11 software and the plots were fitted to the one site saturation ligand-binding model (Eq. 2):

$$y = \frac{B_{max}x}{K_D + x} \tag{2}$$

where K_D is the apparent equilibrium dissociation constant and B_{max} is a maximal SPR signal. The resulting K_D values were expressed as best-fit value ± SE of the fit.

ANALYTICAL PROCEDURES

Rhodopsin content in urea-washed ROS membranes was determined as described previously (Senin et al., 1995). Concentrations of purified recoverin and calmodulin were determined spectrophotometrically assuming ε_{280} of 27,500 and 3,030 M^{-1} cm^{-1}, respectively (Wallace et al., 1983; Johnson et al., 1997). Concentrations of GST–RK constructs were measured using Bradford protein assay (Bio-Rad Laboratories) calibrated with bovine serum albumin. The purity of all the proteins obtained was assessed by SDS-PAGE with Coomassie Brilliant Blue R250 staining.

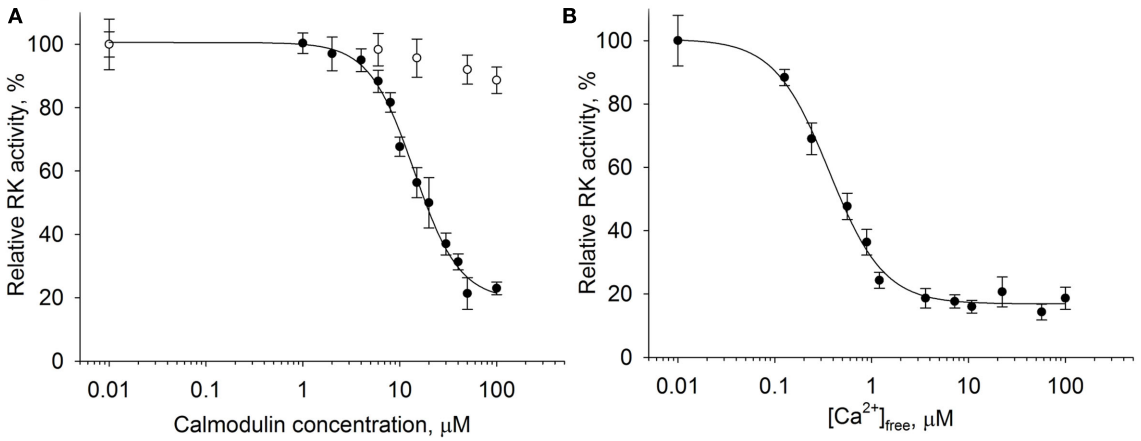

FIGURE 1 | Ca^{2+}-dependent inhibition of rhodopsin kinase by calmodulin. Rhodopsin kinase activity was measured as a function of either calmodulin or free Ca^{2+} concentrations by *in vitro* phosphorylation assay. **(A)** Inhibition of RK activity by increasing calmodulin concentrations at saturating Ca^{2+} concentration (200 μM, ●) or at 1 mM EGTA (○). Fitting of the data as described in Section "Materials and Methods" yielded $IC_{50} = 14.1 \pm 0.9$ μM and $n = 1.85 \pm 0.18$. **(B)** Inhibition of RK activity by 30 μM calmodulin at different concentrations of free Ca^{2+}. Half-maximal inhibition was observed at $[Ca^{2+}]_{free}$ of 0.36 ± 0.03 μM with a Hill coefficient of 1.53 ± 0.13. Data points represent mean ± SE of the mean from three independent experiments.

RESULTS

Ca^{2+}-DEPENDENT INHIBITION OF RHODOPSIN KINASE BY CALMODULIN

It is well-known that recoverin inhibits RK *in vitro* in the micromolar range of free Ca^{2+} concentrations ($[Ca^{2+}]_{free}$). Taking into account previous data (Pronin et al., 1997; Levay et al., 1998) it can be supposed that the RK activity can be additionally regulated by calmodulin. We performed a detailed investigation of the ability of calmodulin to affect rhodopsin phosphorylation by RK in a Ca^{2+}-dependent manner. For this purpose we applied the *in vitro* phosphorylation assay in the reconstituted system consisting of 0.3–0.5 units of RK purified from ROS, 10 μM dark-adapted rhodopsin in the content of urea-washed ROS membranes, and various concentrations of calmodulin ranging from 0.01 to 100 μM (**Figure 1A**). The experiment was conducted at high (200 μM $[Ca^{2+}]_{free}$) or low (1 mM EGTA) Ca^{2+} levels.

According to our data, calmodulin inhibited RK in the presence of Ca^{2+}; the inhibition was half-maximal at 14 μM protein concentration. In the absence of Ca^{2+}, calmodulin was ineffective. We further examined rhodopsin phosphorylation by RK as a function of free Ca^{2+} concentration in the presence of saturating concentration (30 μM) of calmodulin (**Figure 1B**). Inhibition reached half maximum at 0.36 μM $[Ca^{2+}]_{free}$ with a Hill coefficient of 1.53. In summary, these findings indicate the ability of calmodulin to operate *in vitro* as a Ca^{2+}-dependent inhibitor of RK.

MAPPING OF THE CALMODULIN BINDING SITE IN RHODOPSIN KINASE

The observed ability of calmodulin to inhibit RK in a Ca^{2+}-dependent manner poses a question whether it binds to the same site in the RK molecule as recoverin does or whether these two Ca^{2+}-sensors interact with separate specific sites in the enzyme. We employed a biosensor-based technique, the SPR spectroscopy, to study the interaction of recoverin and calmodulin with GST-fused N-terminal RK peptide M1-S25 containing the recoverin-binding site (Higgins et al., 2006; here and below, see **Figure 2A** for a schematic representation of RK fusions constructed and tested). The RK peptide was captured on the anti-GST antibody-coated sensor chip and the binding of Ca^{2+}-loaded forms of calmodulin and recoverin (both at concentration of 40 μM) to the immobilized RK fragment was monitored in real-time resulting in sensorgrams shown at **Figure 2B**.

As expected, recoverin interacted with the RK fragment containing the first 25 amino acids of the enzyme (**Figure 2B**). The apparent K_D of recoverin for M1-S25 fragment was about 17 μM, as determined in titration series (data not shown). The interaction of calmodulin with the same RK peptide was negligible (**Figure 2B**). These results suggest the existence of separate binding sites for calmodulin and recoverin. To identify calmodulin binding site(s), we constructed two recombinant GST fusion fragments that encompass amino terminal (N-RK: M1-G183) and carboxy terminal (C-RK: I455-S561) regulatory regions of RK. Only the N-RK fragment readily captured supplied calmodulin (**Figure 3A**), while the calmodulin binding to C-RK fragment was almost absent. To further localize the calmodulin binding site within N-RK, we tested the ability of calmodulin to interact with N-RK fragments of smaller size: M1-L102 and L102-G183. The interaction occurred in both cases but the response was much more pronounced for M102-G183 (**Figure 3B**). Moreover, we showed that within the RK sequence L102-G183 the calmodulin binding site is presumably localized within a short stretch of 25 amino acids present in positions 150–175 since the N-RK fragment F125-K175 bound calmodulin, but the fragment D100-V150 did not (**Figure 3C**). The additional low affinity site for calmodulin is localized within the RK sequence S26-L102 since the interaction of RK fragment M1-S25 with calmodulin was negligible (**Figures 2B** and **3B**). To evaluate the quantitative characteristics of the effects observed, we carried out steady-state affinity analysis of calmodulin interaction to those GST–RK constructs, which displayed a significant binding to the Ca^{2+}-sensor. The analysis was performed by recording series of sensorgrams at different calmodulin concentrations (in the range of 10–150 μM) and measuring SPR signal amplitudes at steady-state (**Figure 3D**). The apparent

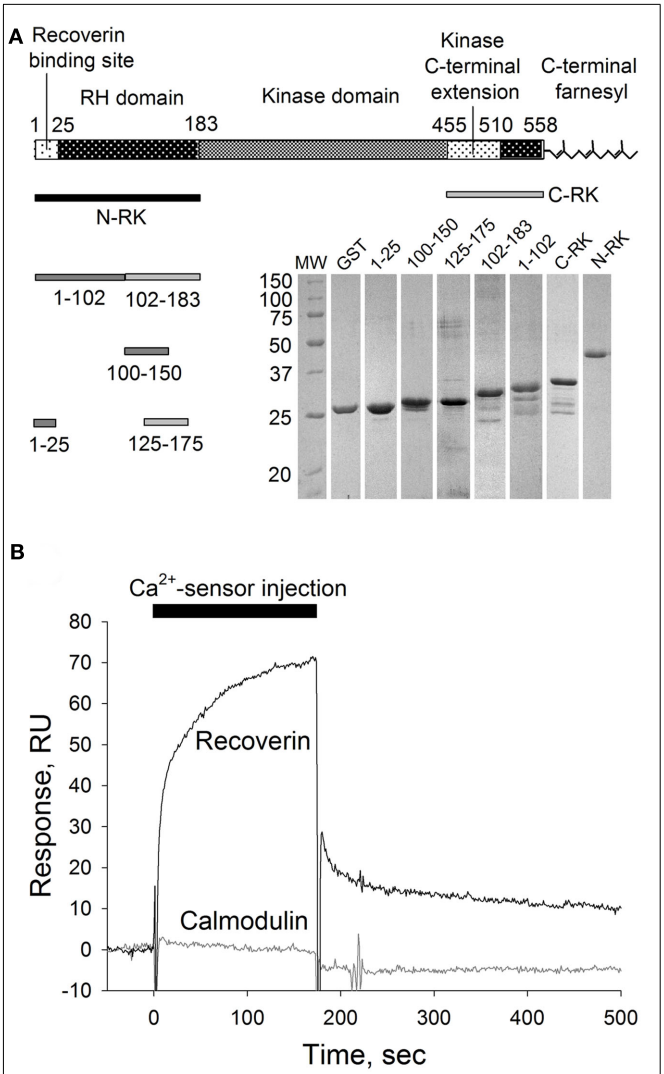

FIGURE 2 | SPR analysis of calmodulin interaction with recoverin-binding site in RK. (A) Schematic representation of RK polypeptide according to Singh et al. (2008) and corresponding GST–RK fusion proteins used in this study. Inset: Coomassie-stained SDS-PAGE of the GST–RK fusion proteins obtained. **(B)** Overlay of sensorgrams recorded during consecutive injections of Ca^{2+}-loaded recoverin or calmodulin at 40 μM concentration over the sensor chip surface with immobilized RK fragment corresponding to the residues M1-S25 fused with GST. The reference signal recorded from the surface with immobilized GST was subtracted.

equilibrium dissociation constants were determined as concentrations required for half-maximal saturation of the binding signal. The obtained K_D values were 63 μM for the full-length N-RK, 54 μM for the M1-L102 fragment, 23 μM for the L102-G183 fragment, and 17 μM for the F125-K175 fragment.

Thus, both high and low affinity calmodulin binding sites are localized within the N-terminal regulatory part of RK, and they are separated from the recoverin-binding site consisting of M1-S25 sequence of the enzyme. Together, our findings indicate that both Ca^{2+}-sensors, recoverin, and calmodulin, are able to bind RK using separate specific sites, suggesting the possibility of their simultaneous binding to and inhibition of RK.

SYNERGETIC INHIBITION OF RHODOPSIN KINASE BY CALMODULIN AND RECOVERIN

We have found that calmodulin displays an inhibitory effect on RK at free Ca^{2+} concentrations ranging from 0.01 to 1 μM (**Figure 1B**). The range overlaps with the physiological changes of Ca^{2+} concentrations found in the photoreceptor cell (Gray-Keller and Detwiler, 1994). Moreover, the revealed inhibitory action of calmodulin was observed at Ca^{2+}concentrations even below the Ca^{2+}-sensitivity of recoverin, the well-established RK regulator. Since both proteins colocalize in photoreceptor cells with RK, we asked whether these two Ca^{2+}-sensors could have a joint effect on RK activity. Thus we utilized the *in vitro* phosphorylation assay examining the ability of calmodulin and recoverin to simultaneously regulate the activity of RK. Urea-washed ROS membranes containing 10 μM rhodopsin were incubated with 0.3–0.5 units of RK in the presence of increasing concentrations of either calmodulin, recoverin, or their 1:1 mixture at the saturating free Ca^{2+} concentration (200 μM).

Remarkably, calmodulin and recoverin were able to synergistically inhibit the RK activity (**Figure 4A**). While the IC_{50} for calmodulin or recoverin alone were 14.1 and 5.8 μM, respectively, their joint action resulted in half-maximal RK inhibition at 4.6 μM of the total Ca^{2+}-sensing protein concentration in the mixture. Approximation of the experimental data was performed with the Hill equation and revealed that the interaction between RK and recoverin was cooperative with Hill coefficient of 1.6. A good curve fit was also possible when approximating the same data with one site (Langmuir) ligand-binding model (data not shown). Collectively, these results point out that the inhibition of RK by recoverin occurs at equimolar stoichiometric ratio of the proteins. In contrast, the inhibition of RK by calmodulin alone as well as the synergetic inhibition by both Ca^{2+} sensors had Hill indexes of about 2. The latter fact evidences for the cooperative binding of two molecules of Ca^{2+}-sensor per one RK molecule. The inhibitory effect of calmodulin on RK was found to occur at lower free Ca^{2+} concentrations than the effect of recoverin. Calmodulin inhibited RK at a half-maximal free Ca^{2+} concentration of 0.36 μM while the inhibitory effect of recoverin was at 1.36 μM Ca^{2+} (**Figure 4B**). The synergetic inhibition of RK by the 30-μM calmodulin/recoverin mixture was observed at a half-maximal free Ca^{2+} concentration of 1.07 μM. Apparently, the synergetic action of both Ca^{2+}-sensors caused a shift in the affinity of the target–effector interaction and at the same time an extension of the operating Ca^{2+}-range. In Ca^{2+}-titration experiments where the RK inhibition by calmodulin or recoverin was studied, the Hill coefficients were within the range of 1.53–1.66, indicating similar cooperative action of the cation in the case of both Ca^{2+}-sensors. Thus, our data indicate that calmodulin complements the inhibitory action of recoverin on RK and increases the sensitivity of RK inhibition to Ca^{2+}.

MODELING OF EQUILIBRIUM BETWEEN RK, RECOVERIN, CALMODULIN, AND CALCIUM IONS

We further used the parameters obtained to create a model of the synergetic inhibition of RK by calmodulin and recoverin. Since the combined use of both Ca^{2+}-sensors increases efficiency of RK inhibition (**Figure 4A**), the fully competitive scheme of RK

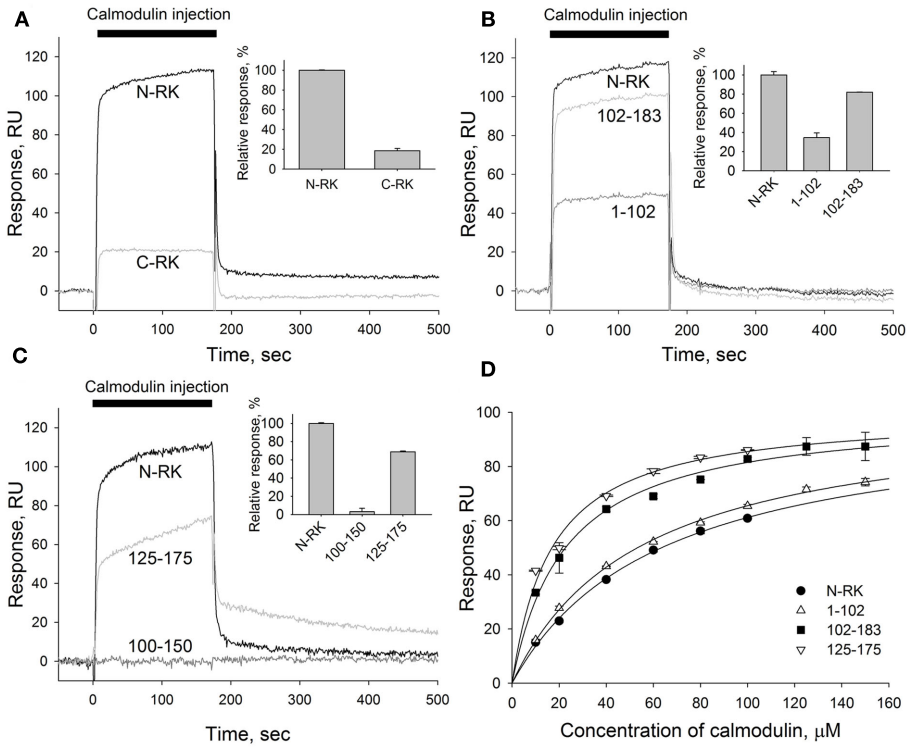

FIGURE 3 | Mapping of the calmodulin binding site in the N-terminal region of RK. (A–C) A representative overlay of SPR sensorgrams showing real-time binding of calmodulin to RK fragments anchored on the sensorchip surface via GST tags using anti-GST antibodies covalently coupled to the dextran matrix. Sixty micromolar calmodulin in running buffer containing 2 mM Ca^{2+} was injected over the surfaces with immobilized N-terminal or C-terminal regions of RK (termed N-RK and C-RK, respectively) **(A)**, N-RK and its fragments corresponding to the residues M1-L102 and L102-G183 **(B)**, or N-RK and its fragments corresponding to the residues D100-V150 and F125-K175 **(C)**. The sensorgrams were normalized to the amounts of immobilized fragments, and the reference signal from a control surface with immobilized GST was subtracted. *Insets* show relative responses at the end of the injection observed for each GST–RK fragment indicating the amount of calmodulin bound. **(D)** Steady-state affinity analysis of calmodulin binding to the full-length N-RK or its fragments M1-L102, L102-G183, or F125-K175. Binding of calmodulin was recorded at concentrations ranging from 10 to 150 μM. The amplitudes of binding signals at equilibrium were determined, normalized, and are shown as a function of calmodulin concentration. Apparent K_Ds were determined as half-maximal calmodulin concentrations required for saturation of SPR amplitudes as described under Section "Materials and Methods." The obtained values for N-RK, M1-L102, L102-G183, and F125-K175 are 63 ± 3, 54 ± 2, 23 ± 2, and 17.0 ± 1.5 μM, respectively. Data points represent mean ± SE of the mean from two independent experiments. The calculated K_Ds are expressed as best-fit value ± SE of the fit.

regulation was excluded. The SPR experiments strongly evidence for the presence of separate recoverin- and calmodulin binding sites. The simplified scheme of chemical equilibria describing this case looks as follows (the rationale behind the use of this scheme is explained in the Modeling of Equilibrium Between RK, Recoverin, Calmodulin, and Calcium Ions in Appendix):

$$\begin{array}{ccccccc} & & & & K_R & & \\ & RK & + & n\cdot R & \leftrightarrow & RK\cdot R_n & \\ & + & & & & + & \\ & m\cdot C & & & & m\cdot C & \\ K_C & \updownarrow & & & & \updownarrow & K_{CR} \\ & C_m\cdot RK & + & n\cdot R & \leftrightarrow & C_m\cdot RK\cdot R_n & \\ & & & & K_{RC} & & \end{array} \quad [1]$$

$$\begin{array}{ccccc} & & & K_{MR} & \\ R_0 & + & v\cdot M & \leftrightarrow & R \\ & & & K_{MC} & \\ C_0 & + & w\cdot M & \leftrightarrow & C \end{array} \quad [2]$$

Here, M denotes calcium ion, R and C denote Ca^{2+}-bound states of recoverin and calmodulin, respectively, while R_0 and C_0 denote their Ca^{2+}-free states. Each of the equilibria is characterized by its own association constant (see Modeling of Equilibrium Between RK, Recoverin, Calmodulin, and Calcium Ions in Appendix; **Table 1**). Fitting of the experimental data shown in **Figure 4** to the Hill equation gives estimates of the most of the constants and binding stoichiometries of Schemes [1] and [2]. Notably, these values implicitly take into account the presence of membranes, which are known to increase the affinity of recoverin to Ca^{2+} (Zozulya and Stryer, 1992) and to affect the distribution of RK between soluble and membrane-bound forms (Sanada et al., 1996). Therefore, these values should be considered as effective. The analysis of the experimental data shown in **Figure 4A** (see Modeling of Equilibrium Between RK, Recoverin, Calmodulin, and Calcium Ions in Appendix) enabled us to estimate all parameters of the Scheme [1] (**Table 1**). According to our analysis, the binding of Ca^{2+}-loaded recoverin molecules to RK facilitates its further association with Ca^{2+}-bound calmodulin, as manifested by 1.55-fold increase in

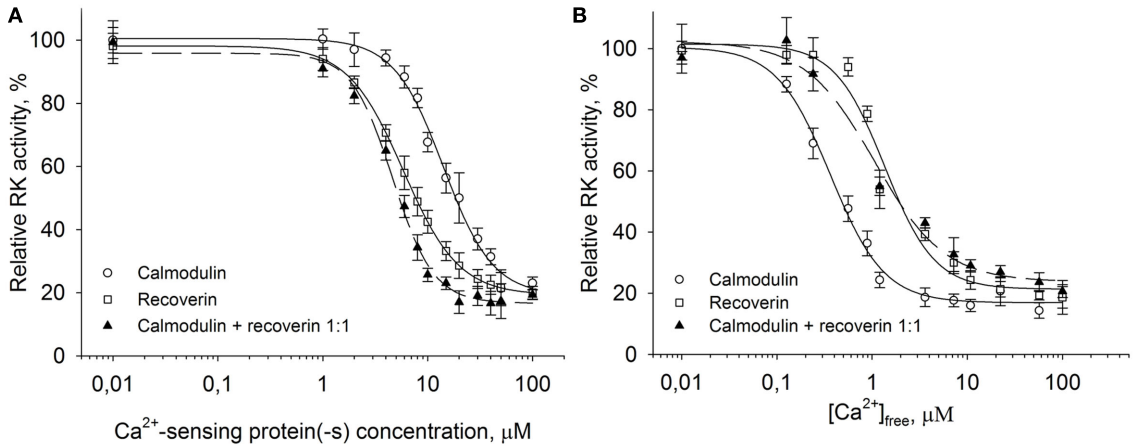

FIGURE 4 | Synergetic inhibition of rhodopsin kinase by recoverin and calmodulin. Rhodopsin kinase activity was measured as a function of Ca^{2+}-sensor protein or free Ca^{2+} concentration by *in vitro* phosphorylation assay. **(A)** Inhibition of RK by increasing concentrations of either calmodulin (○), recoverin (□), or their mixture in the 1:1 ratio (▲) at saturating free Ca^{2+} concentration (200 μM). Fitting the data to the Hill equation as described in Section "Materials and Methods" resulted in $IC_{50} = 14.1 \pm 0.9$ μM, $n = 1.8 \pm 0.2$ for calmodulin, $IC_{50} = 5.8 \pm 0.7$ μM, $n = 1.6 \pm 0.3$ for recoverin, and $IC_{50} = 4.6 \pm 0.2$ μM, $n = 2.2 \pm 0.2$ for calmodulin/recoverin 1:1 mixture. **(B)** Inhibition of RK activity by either calmodulin (○), recoverin (□), or their 1:1 mixture (▲) at different free Ca^{2+} concentrations. Concentration of each Ca^{2+}-sensing protein including their mixture was 30 μM. Fitting the data to the Hill equation as described under Section "Materials and Methods" resulted in values of $IC_{50} = 0.36 \pm 0.03$ μM, $n = 1.53 \pm 0.13$ for calmodulin, $IC_{50} = 1.36 \pm 0.13$ μM, $n = 1.66 \pm 0.23$ for recoverin, and $IC_{50} = 1.07 \pm 0.15$ μM, $n = 1.2 \pm 0.1$ for their 1:1 mixture. The fitted curves are drawn *solid* for calmodulin or recoverin data sets, and *dashed* for their mixture. Data points represent mean ± SE of the mean from three independent experiments.

Table 1 | The parameters of the equilibrium between RK, recoverin, calmodulin, and calcium ions.

Equilibrium association constant	Value, M^{-1}	Hill coefficient	Value
K_R	1.7e5	n	1.6
K_C	7.1e4	m	1.8
K_{RC}	2.7e5	–	–
K_{CR}	1.1e5	–	–
K_{MR}	7.4e5	v	1.66
K_{MC}	2.8e6	w	1.53

The parameters of Schemes [1] and [2] are derived from fitting of the experimental data shown in ***Figure 4*** *to the Hill equation, except for the K_{RC} and K_{CR} values, which were estimated from analysis of the data shown in* ***Figure 4A*** *using Eqs A11 and A12 in Appendix (see Modeling of Equilibrium Between RK, Recoverin, Calmodulin, and Calcium Ions in Appendix), respectively.*

the constant of calmodulin binding to RK. Similarly, association of calmodulin with RK increases its recoverin-binding constant 1.59-fold (**Table 1**). Thus, the modeling results suggest that recoverin and calmodulin could act in a concerted manner, mutually facilitating inhibition of RK.

The changes in RK-inhibiting activity shown in **Figure 4B** reflect association of the Ca^{2+}-sensing proteins with calcium ions. These processes can be approximated by the Hill equation based model (Scheme [2]), which is widely used for simplified description of such complex processes. Alternatively, the Ca^{2+}-dependence of interaction between calmodulin and its target could be described by the model of sequential filling of EF-hands (Dagher et al., 2011). However, this approach requires the introduction into the Scheme [2] of additional chemical equilibria, which would drastically complicate modeling of the system. According to our analysis based on Scheme [2] (see Modeling of Equilibrium Between RK, Recoverin, Calmodulin, and Calcium Ions in Appendix), the half-maximal synergetic inhibition of RK by calmodulin and recoverin occurs at free Ca^{2+} concentration of 0.71 μM. This value is between the respective values obtained for calmodulin (0.36 μM) and recoverin (1.36 μM). The corresponding experimental value equals to 1.07 μM (**Figure 4B**) which is close to the theoretical estimate.

DISCUSSION

In the present work we have demonstrated that the ubiquitous Ca^{2+}-sensor calmodulin is able to function as an inhibitor of RK. Moreover, we found that the inhibition of RK by calmodulin can complement the inhibitory action of the well-known RK regulator recoverin. Previous attempts to study the ability of calmodulin to regulate GRKs, including GRK1 (RK), were performed using relatively low concentrations of calmodulin (not exceeding 10 μM; Chuang et al., 1996; Pronin et al., 1997) at which its inhibitory effect could not be seen to the full extent. According to our data, the inhibition of RK by calmodulin at saturating Ca^{2+} concentrations was observed in the range of calmodulin concentration from 2 to 30 μM and was half-maximal at 14 μM of the Ca^{2+}-sensor, whereas recoverin was a more effective inhibitor, as it showed a half-maximal inhibitory effect on the RK activity at 5.8 μM. The calcium range of RK inhibition by calmodulin (0.05–1 μM of $[Ca^{2+}]_{free}$) overlapped with the physiological range of the cation concentration (0.05–0.55 μM of $[Ca^{2+}]_{free}$) in ROS (Gray-Keller and Detwiler, 1994). The synergetic action of calmodulin and recoverin on the RK activity was within 0.05–1 μM of $[Ca^{2+}]_{free}$.

These values are slightly above the physiological range of Ca^{2+} concentration in ROS. However, the recoverin affinity for Ca^{2+} is significantly increased in the presence of RK and ROS membranes (Zozulya and Stryer, 1992; Ames et al., 1995; Senin et al., 1995, 2004). Similarly, the affinity of calmodulin for Ca^{2+} increases upon binding to target enzymes (Shifman et al., 2006). Therefore, extrapolation to the *in vivo* conditions (including high membrane content and presence of target proteins) indicates that the apparent Ca^{2+}-dependence of the synergetic action of calmodulin and recoverin on RK activity could reach the physiological (i.e., submicromolar) range of the calcium concentration. Our experimental results were supplemented with theoretical validation of the ability of calmodulin and recoverin to synergistically bind RK. Different approaches could be applied to modeling of equilibria between RK, recoverin, calmodulin, and calcium ions. Full description of the system would require characterization of each step of the calcium-binding to the calcium-sensing proteins (Dagher et al., 2011), as well as characterization of all protein–protein interactions in the system. Considering that membranes are known to affect the distribution of RK and recoverin between soluble and membrane-bound fractions, as well as to modulate calcium affinity of recoverin (Zozulya and Stryer, 1992; Senin et al., 1995; Sanada et al., 1996), it can be concluded that the total number of chemical equilibria is significantly higher (see Modeling of Equilibrium Between RK, Recoverin, Calmodulin, and Calcium Ions in Appendix). This objective difficulty can be compensated via usage of the Hill model-based representation of the system, which describes the multiple processes of ligand-binding as a single event. Despite being phenomenological, this approach enabled us to estimate the synergy of binding of calmodulin and recoverin to RK. According to our analysis (see Modeling of Equilibrium Between RK, Recoverin, Calmodulin, and Calcium Ions), binding of either calcium sensor to RK results in 1.5-fold increase of the affinity of the complex to another Ca^{2+}-sensing protein. The analysis also showed that the half-maximal synergetic inhibition of RK by calmodulin and recoverin occurs at free Ca^{2+} concentration of 0.71 μM, which is close to the corresponding experimental value of 1.07 μM.

The structural aspects underlying the synergetic regulation of RK by calmodulin and recoverin can be identified from the experiments on mapping of the calmodulin binding site in RK using a biosensor-based approach (SPR spectroscopy). Our findings indicate that the interaction of calmodulin and recoverin with RK occurs by means of separate binding sites in the N-terminal region of the enzyme, which makes the co-inhibitory action of the two Ca^{2+}-sensors possible. The recoverin-binding site is known to be located in the first 25 amino acid residues of RK (Ames et al., 2006; Higgins et al., 2006). According to our data, RK contains two calmodulin binding sites. The first, low affinity site is located within the sequence S26-L102 of N-terminal regulatory region of RK, which is in agreement with a previous report (Levay et al., 1998). The second high affinity site was identified within the residues V150-K175 of the same RK region. In other studies this fragment was not tested for the ability to bind calmodulin. The C-terminal regulatory region of RK (I455-S561) did not interact with calmodulin both in the current and in the earlier studies. In addition, the report by Levay et al. (1998) suggested another calmodulin binding site within the residues A341-E400. This site is located in the large lobe of the catalytic domain of the enzyme (Singh et al., 2008). However, calmodulin apparently has no effect on the catalytic activity of RK since in our experiments it did not affect the ability of the enzyme to phosphorylate the C-terminal peptide of rhodopsin containing phosphorylation sites (data not shown). Thus, the suggested interaction of calmodulin with A341-E400 site seems to be out of the physiological relevance. Moreover, it was shown that the recombinant fragment corresponding to the full-length catalytic domain of RK (E184-D454) is not able to interact with rhodopsin (Komolov et al., 2009), although the domain function should include this interaction. The latter suggests that this fragment does not fully acquire its native structure. These observations led us not to consider parts of the catalytic domain in the context of Ca^{2+}-dependent regulation of RK by calmodulin.

It should be mentioned that the affinities of calmodulin and recoverin to the RK peptides determined in our SPR experiments were lower than in the previous work (Levay et al., 1998). The possible reason of this discrepancy can be the different strategies applied for the immobilization of the interaction partners on the sensor chip. Levay et al. (1998) immobilized calmodulin and recoverin on the chip via cysteine residues. Calmodulin was biotinylated via the cysteine residue and further captured on the streptavidin-coated surface while recoverin was directly attached to the sensor chip surface via thiol coupling with its cysteine residue. These cysteine residues were shown to play a critical role in the Ca^{2+}-dependent operating of both proteins (Lukas et al., 1984; Permyakov et al., 2007, 2012). Thus, the functional state of calmodulin and recoverin on the sensor chip could be significantly affected upon the immobilization procedure. We used an experimental configuration opposite to their approach with RK fragments being retained on the sensor chip surface and recoverin/calmodulin being supplied in the mobile phase. RK fragments in this case were captured on the surface under mild conditions using antigen–antibody interaction. This strategy might better preserve the protein integrity in BIACORE experiments and therefore affinity constants determined by SPR for calmodulin interaction with its binding site (17 μM) correlate better with the IC_{50} for calmodulin-mediated RK inhibition (14 μM).

Based on the location of the recoverin and calmodulin binding sites in RK one may suggest the putative mechanisms underlying the intrinsic inhibition activity in the case of each Ca^{2+}-sensor. As it was previously mentioned, recoverin inhibits RK by affecting the conformational transitions of the enzyme required for the formation of the efficient enzyme-substrate complex between RK and rhodopsin C-terminus. Such a mechanism is due to the ability of recoverin to bind to the N-terminal site M1-S25 of RK that is critical for the function of the enzyme (Higgins et al., 2006; Huang et al., 2009; Komolov et al., 2009; Zernii et al., 2011). It is likely that the mechanism of RK inhibition by calmodulin involves a Ca^{2+}-dependent interference with the interaction between RK and photoexcited rhodopsin. This is possible, if the calmodulin binding site in RK overlaps with the receptor docking site. The sequence F150-K175 in RK identified in our work as the high affinity calmodulin binding site contains amino acid residues Y167, Q173, W174, L177 which could be involved in rhodopsin recognition since the corresponding residues in the GRKs 5 and 6 were recently

found to be critical for the phosphorylation of the activated receptors (Baameur et al., 2010). Thus, calmodulin may be suggested to inhibit RK by blocking sterically the association of the enzyme with the responsive sites in its receptor substrate rhodopsin. Preliminary observations made by us further support this conclusion, namely that the fragment F150-K175 of RK is indeed capable of direct binding to rhodopsin in a light-dependent manner. Such a mechanism does not contradict the current hypothesis of the formation of the heteromeric complex between RK, rhodopsin, and Ca^{2+}-sensor(s) (Komolov et al., 2009), since it is known that the receptor binding involves not only the N-terminal regulatory region of RK containing the above mentioned fragment but also the C-terminal farnesyl modification of the enzyme (McCarthy and Akhtar, 2000).

Considering the above speculations the question arises what could be the mechanism underlying the synergetic inhibition of RK by both Ca^{2+}-sensors. The SPR experiments strongly evidence that the recoverin- and calmodulin binding sites in RK are separate. Since combined action of recoverin and calmodulin increases efficiency of RK inhibition, the competitive scheme of the enzyme regulation by two Ca^{2+}-sensors is unlikely. The modeling of equilibrium between RK, recoverin, calmodulin, and calcium ions revealed that the binding of Ca^{2+}/recoverin to RK results in 1.5-fold facilitation of binding of the enzyme to Ca^{2+}/calmodulin, and *vice versa*. Taking into account the higher affinity of recoverin to RK and its higher intracellular concentration as compared to calmodulin it can be suggested that the binding of Ca^{2+}/recoverin to the enzyme precedes that of Ca^{2+}/calmodulin. Presumably, the binding of recoverin to the first 25 amino acid residues of RK allosterically increases the availability of the high affinity calmodulin binding site V150-K175 for the interaction with calmodulin. This is consistent with the fact that the presence of recoverin shifts the binding of calmodulin to RK (and consequent inhibition of the enzyme) to the lower calmodulin concentration. The suggested sequential filling of Ca^{2+}-sensor binding sites in RK, namely recoverin followed by calmodulin, is in agreement with the fact that the Ca^{2+}-dependence of the synergetic inhibition effect is close to the recoverin Ca^{2+}-dependent inhibition profile. Thus, the following consecutive mechanism of RK regulation by recoverin and calmodulin in photoreceptors can be suggested. At high calcium concentration (0.5–0.6 μM of $[Ca^{2+}]_{free}$) present in dark-adapted photoreceptors, RK is strongly inhibited by the synergetic action of both Ca^{2+}-sensors. Shortly after the light absorption, when the Ca^{2+}-concentration has not yet decreased, recoverin still allosterically inhibits phosphorylation of rhodopsin by RK however not affecting the interaction between the enzyme and the cytoplasmic loops of the receptor. In the same time calmodulin prevents this interaction thus allowing the receptor to effectively activate transducin. This is important for the ability of rod photoreceptors to respond to even low illumination levels. During the lowering of the intracellular Ca^{2+} concentration associated with phototransduction, recoverin dissociates from the complex with RK, which decreases the affinity of the enzyme to calmodulin. In these conditions calmodulin alone can still inhibit the enzyme though less effectively than it does in combination with recoverin. Further light-induced decrease in free Ca^{2+} concentration down to 0.025–0.05 μM triggers the dissociation of calmodulin from RK switching the enzyme to the full active form, which causes desensitization of the receptor.

In summary, our study suggested a novel mechanism of regulation of rhodopsin desensitization by rhodopsin kinase involving Ca^{2+}-sensor proteins. Further studies are required for firm establishment of the physiological role of this phenomenon and unraveling the molecular details of the proposed mechanism.

ACKNOWLEDGMENTS

We thank Dr. Daniele Dell'Orco for the assistance with the BIACORE measurements. This work was supported by the grants from the Russian Foundation for Basic Research ## 09-04-01778-a (to Ivan I. Senin), 09-04-00666-a (to Evgeni Yu. Zernii), 09-04-00395, and ofi-m-11-04-12108 (to Pavel P. Philippov); the President of Russia # MD-4423.2010.4 (to Ivan I. Senin); the Deutsche Forschungsgemeinschaft ## KO948/7-1, KO948/7-2 (to Karl-Wilhelm Koch); the Program of the Russian Academy of Sciences «Molecular and Cellular Biology»(to Sergei E. Permyakov).

REFERENCES

Ames, J. B., Ishima, R., Tanaka, T., Gordon, J. I., Stryer, L., and Ikura, M. (1997). Molecular mechanics of calcium-myristoyl switches. *Nature* 389, 198–202.

Ames, J. B., Levay, K., Wingard, J. N., Lusin, J. D., and Slepak, V. Z. (2006). Structural basis for calcium-induced inhibition of rhodopsin kinase by recoverin. *J. Biol. Chem.* 281, 37237–37245.

Ames, J. B., Porumb, T., Tanaka, T., Ikura, M., and Stryer, L. (1995). Amino-terminal myristoylation induces cooperative calcium binding to recoverin. *J. Biol. Chem.* 270, 4526–4533.

Baameur, F., Morgan, D. H., Yao, H., Tran, T. M., Hammitt, R. A., Sabui, S., McMurray, J. S., Lichtarge, O., and Clark, R. B. (2010). Role for the regulator of G-protein signaling homology domain of G protein-coupled receptor kinases 5 and 6 in beta 2-adrenergic receptor and rhodopsin phosphorylation. *Mol. Pharmacol.* 77, 405–415.

Boguth, C. A., Singh, P., Huang, C. C., and Tesmer, J. J. (2010). Molecular basis for activation of G protein-coupled receptor kinases. *EMBO J.* 29, 3249–3259.

Burgoyne, R. D. (2007). Neuronal calcium sensor proteins: generating diversity in neuronal Ca2+ signalling. *Nat. Rev. Neurosci.* 8, 182–193.

Chen, C. K., Inglese, J., Lefkowitz, R. J., and Hurley, J. B. (1995). Ca(2+)-dependent interaction of recoverin with rhodopsin kinase. *J. Biol. Chem.* 270, 18060–18066.

Chuang, T. T., Paolucci, L., and De Blasi, A. (1996). Inhibition of G protein-coupled receptor kinase subtypes by Ca^{2+}/calmodulin. *J. Biol. Chem.* 271, 28691–28696.

Dagher, R., Peng, S., Gioria, S., Fève, M., Zeniou, M., Zimmermann, M., Pigault, C., Haiech, J., and Kilhoffer, M. C. (2011). A general strategy to characterize calmodulin-calcium complexes involved in CaM-target recognition: DAPK and EGFR calmodulin binding domains interact with different calmodulin-calcium complexes. *Biochim. Biophys. Acta* 1813, 1059–1067.

De Castro, E., Nef, S., Fiumelli, H., Lenz, S. E., Kawamura, S., and Nef, P. (1995). Regulation of rhodopsin phosphorylation by a family of neuronal calcium sensors. *Biochem. Biophys. Res. Commun.* 216, 133–140.

Dizhoor, A. M., Chen, C. K., Olshevskaya, E., Sinelnikova, V. V., Phillipov, P., and Hurley, J. B. (1993). Role of the acylated amino terminus of recoverin in Ca(2+)-dependent membrane interaction. *Science* 259, 829–832.

Dizhoor, A. M., Ericsson, L. H., Johnson, R. S., Kumar, S., Olshevskaya, E., Zozulya, S., Neubert, T. A., Stryer, L., Hurley, J. B., and Walsh, K. A. (1992). The NH2 terminus of retinal recoverin is acylated by a small family of fatty acids. *J. Biol. Chem.* 267, 16033–16036.

Dizhoor, A. M., Ray, S., Kumar, S., Niemi, G., Spencer, M., Brolley, D.,

Walsh, K. A., Philipov, P. P., Hurley, J. B., and Stryer, L. (1991). Recoverin: a calcium sensitive activator of retinal rod guanylate cyclase. *Science* 251, 915–918.

Duda, T., Fik-Rymarkiewicz, E., Venkataraman, V., Krishnan, R., Koch, K. W., and Sharma, R. K. (2005). The calcium-sensor guanylate cyclase activating protein type 2 specific site in rod outer segment membrane guanylate cyclase type 1. *Biochemistry* 44, 7336–7345.

Duda, T., Koch, K. W., Venkataraman, V., Lange, C., Beyermann, M., and Sharma, R. K. (2002). Ca(2+) sensor S100beta-modulated sites of membrane guanylate cyclase in the photoreceptor-bipolar synapse. *EMBO J.* 21, 2547–2556.

Eckmiller, M. S. (2002). Calmodulin immunolocalization in outer segments of *Xenopus laevis* photoreceptors. *Cell Tissue Res.* 308, 439–442.

Few, A. P., Nanou, E., Scheuer, T., and Catterall, W. A. (2011). Molecular determinants of CaV2.1 channel regulation by calcium binding protein-1. *J. Biol. Chem.* 286, 41917–41923.

Flaherty, K. M., Zozulya, S., Stryer, L., and McKay, D. B. (1993). Three-dimensional structure of recoverin, a calcium sensor in vision. *Cell* 75, 709–716.

Gopalakrishna, R., and Anderson, W. B. (1982). Ca^{2+}-induced hydrophobic site on calmodulin: application for purification of calmodulin by phenyl-Sepharose affinity chromatography. *Biochem. Biophys. Res. Commun.* 104, 830–836.

Gorodovikova, E. N., Gimelbrant, A. A., Senin, I. I., and Philippov, P. P. (1994a). Recoverin mediates the calcium effect upon rhodopsin phosphorylation and cGMP hydrolysis in bovine retina rod cells. *FEBS Lett.* 349, 187–190.

Gorodovikova, E. N., Senin, I. I., and Philippov, P. P. (1994b). Calcium-sensitive control of rhodopsin phosphorylation in the reconstituted system consisting of photoreceptor membranes, rhodopsin kinase and recoverin. *FEBS Lett.* 353, 171–172.

Gorodovikova, E. N., and Philippov, P. P. (1993). The presence of a calcium-sensitive p26-containing complex in bovine retina rod cells. *FEBS Lett.* 335, 277–279.

Gray-Keller, M. P., and Detwiler, P. B. (1994). The calcium feedback signal in the phototransduction cascade of vertebrate rods. *Neuron* 13, 849–861.

Haynes, L. P., Fitzgerald, D. J., Wareing, B., O'Callaghan, D. W., Morgan, A., and Burgoyne, R. D. (2006). Analysis of the interacting partners of the neuronal calcium-binding proteins L-CaBP1, hippocalcin, NCS-1 and neurocalcin delta. *Proteomics* 6, 1822–1832.

Higgins, M. K., Oprian, D. D., and Schertler, G. F. (2006). Recoverin binds exclusively to an amphipathic peptide at the N terminus of rhodopsin kinase, inhibiting rhodopsin phosphorylation without affecting catalytic activity of the kinase. *J. Biol. Chem.* 281, 19426–19432.

Hoeflich, K. P., and Ikura, M. (2002). Calmodulin in action: diversity in target recognition and activation mechanisms. *Cell* 108, 739–742.

Huang, C. C., Yoshino-Koh, K., and Tesmer, J. J. (2009). A surface of the kinase domain critical for the allosteric activation of G protein-coupled receptor kinases. *J. Biol. Chem.* 284, 17206–17215.

Inglese, J., Glickman, J. F., Lorenz, W., Caron, M. G., and Lefkowitz, R. J. (1992). Isoprenylation of a protein kinase. Requirement of farnesylation/alpha-carboxyl methylation for full enzymatic activity of rhodopsin kinase. *J. Biol. Chem.* 267, 1422–1425.

Johnson, W. C. Jr., Palczewski, K., Gorczyca, W. A., Riazance-Lawrence, J. H., Witkowska, D., and Polans, A. S. (1997). Calcium binding to recoverin: implications for secondary structure and membrane association. *Biochim. Biophys. Acta* 1342, 164–174.

Kakiuchi, S., Yasuda, S., Yamazaki, R., Teshima, Y., Kanda, K., Kakiuchi, R., and Sobue, K. (1982). Quantitative determinations of calmodulin in the supernatant and particulate fractions of mammalian tissues. *J. Biochem.* 92, 1041–1048.

Kawamura, S. (1993). Rhodopsin phosphorylation as a mechanism of cyclic GMP phosphodiesterase regulation by S-modulin. *Nature* 362, 855–857.

Klenchin, V. A., Calvert, P. D., and Bownds, M. D. (1995). Inhibition of rhodopsin kinase by recoverin. Further evidence for a negative feedback system in phototransduction. *J. Biol. Chem.* 270, 16147–16152.

Koch, K. W. (2000). Identification and characterization of calmodulin binding sites in cGMP-gated channel using surface plasmon resonance spectroscopy. *Meth. Enzymol.* 315, 785–797.

Kohnken, R. E., Chafouleas, J. G., Eadie, D. M., Means, A. R., and McConnell, D. G. (1981). Calmodulin in bovine rod outer segments. *J. Biol. Chem.* 256, 12517–12522.

Komolov, K. E., Senin, I. I., Kovaleva, N. A., Christoph, M. P., Churumova, V. A., Grigoriev, I. I., Akhtar, M., Philippov, P. P., and Koch, K. W. (2009). Mechanism of rhodopsin kinase regulation by recoverin. *J. Neurochem.* 110, 72–79.

Komolov, K. E., Senin, I. I., Philippov, P. P., and Koch, K. W. (2006). Surface plasmon resonance study of G protein/receptor coupling in a lipid bilayer-free system. *Anal. Chem.* 78, 1228–1234.

Komolov, K. E., Zinchenko, D. V., Churumova, V. A., Vaganova, S. A., Weiergräber, O. H., Senin, I. I., Philippov, P. P., and Koch, K. W. (2005). One of the Ca2+ binding sites of recoverin exclusively controls interaction with rhodopsin kinase. *Biol. Chem.* 386, 285–289.

Köster, S., Pavkov-Keller, T., Kühlbrandt, W., and Yildiz, O. (2011). Structure of human Na+/H+ exchanger NHE1 regulatory region in complex with calmodulin and Ca^{2+}. *J. Biol. Chem.* 286, 40954–40961.

Lange, C., Duda, T., Beyermann, M., Sharma, R. K., and Koch, K. W. (1999). Regions in vertebrate photoreceptor guanylyl cyclase ROS-GC1 involved in Ca(2+)-dependent regulation by guanylyl cyclase-activating protein GCAP-1. *FEBS Lett.* 460, 27–31.

Levay, K., Satpaev, D. K., Pronin, A. N., Benovic, J. L., and Slepak, V. Z. (1998). Localization of the sites for Ca^{2+}-binding proteins on G protein-coupled receptor kinases. *Biochemistry* 37, 13650–13659.

Liebman, P. A. (1972). "Microspectrophotometry of photoreceptors," in *Handbook of Sensory Physiology*, ed. H. J. A. Dartnall (New York: Springer-Verlag), 7, 481–528.

Lukas, T. J., Iverson, D. B., Schleicher, M., and Watterson, D. M. (1984). Structural characterization of a higher plant calmodulin: *Spinacia oleracea*. *Plant Physiol.* 75, 788–795.

Makino, C. L., Dodd, R. L., Chen, J., Burns, M. E., Roca, A., Simon, M. I., and Baylor, D. A. (2004). Recoverin regulates light-dependent phosphodiesterase activity in retinal rods. *J. Gen. Physiol.* 123, 729–741.

McCarthy, N. E., and Akhtar, M. (2000). Function of the farnesyl moiety in visual signalling. *Biochem. J.* 347, 163–171.

McCue, H. V., Haynes, L. P., and Burgoyne, R. D. (2010). The diversity of calcium sensor proteins in the regulation of neuronal function. *Cold Spring Harb. Perspect. Biol.* 2, a004085.

Mikhaylova, M., Hradsky, J., and Kreutz, M. R. (2011). Between promiscuity and specificity: novel roles of EF-hand calcium sensors in neuronal Ca^{2+} signalling. *J. Neurochem.* 118, 695–713.

Myszka, D. G. (1999). Improving biosensor analysis. *J. Mol. Recognit.* 12, 279–284.

Palczewski, K., Buczylko, J., Lebioda, L., Crabb, J. W., and Polans, A. S. (1993). Identification of the N-terminal region in rhodopsin kinase involved in its interaction with rhodopsin. *J. Biol. Chem.* 268, 6004–6013.

Papermaster, D. S., and Dreyer, W. J. (1974). Rhodopsin content in the outer segment membranes of bovine and frog retinal rods. *Biochemistry* 13, 2438–2444.

Permyakov, S. E., Nazipova, A. A., Denesyuk, A. I., Bakunts, A. G., Zinchenko, D. V., Lipkin, V. M., Uversky, V. N., and Permyakov, E. A. (2007). Recoverin as a redox-sensitive protein. *J. Proteome Res.* 6, 1855–1863.

Permyakov, S. E., Zernii, E. Y., Knyazeva, E. L., Denesyuk, A. I., Nazipova, A. A., Kolpakova, T. V., Zinchenko, D. V., Philippov, P. P., Permyakov, E. A., and Senin, I. I. (2012). Oxidation mimicking substitution of conservative cysteine in recoverin suppresses its membrane association. *Amino Acids* 42. doi: 10.1007/s00726-011-0843-0

Pronin, A. N., Loudon, R. P., and Benovic, J. L. (2002). Characterization of G protein-coupled receptor kinases. *Meth. Enzymol.* 343, 547–559.

Pronin, A. N., Satpaev, D. K., Slepak, V. Z., and Benovic, J. L. (1997). Regulation of G protein-coupled receptor kinases by calmodulin and localization of the calmodulin binding domain. *J. Biol. Chem.* 272, 18273–18280.

Sanada, K., Shimizu, F., Kameyama, K., Haga, K., Haga, T., and Fukada, Y. (1996). Calcium-bound recoverin targets rhodopsin kinase to membranes to inhibit rhodopsin phosphorylation. *FEBS Lett.* 384, 227–230.

Sathyanarayanan, P. V., Cremo, C. R., and Poovaiah, B. W. (2000). Plant chimeric Ca^{2+}/calmodulin-dependent protein kinase. Role of the neural visinin-like domain in regulating autophosphorylation and calmodulin affinity. *J. Biol. Chem.* 275, 30417–30422.

Satpaev, D. K., Chen, C. K., Scotti, A., Simon, M. I., Hurley, J. B., and Slepak, V. Z. (1998). Autophosphorylation and ADP regulate the Ca^{2+}-dependent interaction of recoverin

with rhodopsin kinase. *Biochemistry* 37, 10256–10262.

Schaad, N. C., De Castro, E., Nef, S., Hegi, S., Hinrichsen, R., Martone, M. E., Ellisman, M. H., Sikkink, R., Rusnak, F., Sygush, J., and Nef, P. (1996). Direct modulation of calmodulin targets by the neuronal calcium sensor NCS-1. *Proc. Natl. Acad. Sci. U.S. A.* 93, 9253–9258.

Senin, I. I., Dean, K. R., Zargarov, A. A., Akhtar, M., and Philippov, P. P. (1997). Recoverin inhibits the phosphorylation of dark-adapted rhodopsin more than it does that of bleached rhodopsin: a possible mechanism through which rhodopsin kinase is prevented from participation in a side reaction. *Biochem. J.* 321(Pt 2), 551–555.

Senin, I. I., Fischer, T., Komolov, K. E., Zinchenko, D. V., Philippov, P. P., and Koch, K. W. (2002a). Ca^{2+}-myristoyl switch in the neuronal calcium sensor recoverin requires different functions of Ca^{2+}-binding sites. *J. Biol. Chem.* 277, 50365–50372.

Senin, I. I., Koch, K. W., Akhtar, M., and Philippov, P. P. (2002b). Ca^{2+}-dependent control of rhodopsin phosphorylation: recoverin and rhodopsin kinase. *Adv. Exp. Med. Biol.* 514, 69–99.

Senin, I. I., Höppner-Heitmann, D., Polkovnikova, O. O., Churumova, V. A., Tikhomirova, N. K., Philippov, P. P., and Koch, K. W. (2004). Recoverin and rhodopsin kinase activity in detergent-resistant membrane rafts from rod outer segments. *J. Biol. Chem.* 279, 48647–48653.

Senin, I. I., Tikhomirova, N. K., Churumova, V. A., Grigoriev, I. I., Kolpakova, T. A., Zinchenko, D. V., Philippov, P. P., and Zernii, E. Y. (2011). Amino acid sequences of two immune-dominant epitopes of recoverin are involved in Ca^{2+}/recoverin-dependent inhibition of phosphorylation of rhodopsin. *Biochemistry Mosc.* 76, 332–338.

Senin, I. I., Zargarov, A. A., Alekseev, A. M., Gorodovikova, E. N., Lipkin, V. M., and Philippov, P. P. (1995). N-myristoylation of recoverin enhances its efficiency as an inhibitor of rhodopsin kinase. *FEBS Lett.* 376, 87–90.

Shifman, J. M., Choi, M. H., Mihalas, S., Mayo, S. L., and Kennedy, M. B. (2006). Ca^{2+}/calmodulin-dependent protein kinase II (CaMKII) is activated by calmodulin with two bound calciums. *Proc. Natl. Acad. Sci. U.S.A.* 103, 13968–13973.

Singh, P., Wang, B., Maeda, T., Palczewski, K., and Tesmer, J. J. (2008). Structures of rhodopsin kinase in different ligand states reveal key elements involved in G protein-coupled receptor kinase activation. *J. Biol. Chem.* 283, 14053–14062.

Tanaka, T., Ames, J. B., Harvey, T. S., Stryer, L., and Ikura, M. (1995). Sequestration of the membrane-targeting myristoyl group of recoverin in the calcium-free state. *Nature* 376, 444–447.

Venkataraman, V., Duda, T., Ravichandran, S., and Sharma, R. K. (2008). Neurocalcin delta modulation of ROS-GC1, a new model of Ca(2+) signaling. *Biochemistry* 47, 6590–6601.

Wallace, R. W., Tallant, E. A., and Cheung, W. Y. (1983). Assay of calmodulin by Ca^{2+}-dependent phosphodiesterase. *Meth. Enzymol.* 102, 39–47.

Weiergräber, O. H., Senin, I. I., Zernii, E. Y., Churumova, V. A., Kovaleva, N. A., Nazipova, A. A., Permyakov, S. E., Permyakov, E. A., Philippov, P. P., Granzin, J., and Koch, K. W. (2006). Tuning of a neuronal calcium sensor. *J. Biol. Chem.* 281, 37594–37602.

Wilden, U., Hall, S. W., and Kühn, H. (1986). Phosphodiesterase activation by photoexcited rhodopsin is quenched when rhodopsin is phosphorylated and binds the intrinsic 48-kDa protein of rod outer segments. *Proc. Natl. Acad. Sci. U.S.A.* 83, 1174–1178.

Zernii, E. Y., Komolov, K. E., Permyakov, S. E., Kolpakova, T., Dell'Orco, D., Poetzsch, A., Knyazeva, E. L., Grigoriev, I. I., Permyakov, E. A., Senin, I. I., Philippov, P. P., and Koch, K. W. (2011). Involvement of the recoverin C-terminal segment in recognition of the target enzyme rhodopsin kinase. *Biochem. J.* 435, 441–450.

Zozulya, S., and Stryer, L. (1992). Calcium-myristoyl protein switch. *Proc. Natl. Acad. Sci. U.S.A.* 89, 11569–11573.

Conflict of Interest Statement: The authors declare that the research was conducted in the absence of any commercial or financial relationships that could be construed as a potential conflict of interest.

Received: 05 January 2012; accepted: 17 February 2012; published online: 08 March 2012.

Citation: Grigoriev II, Senin II, Tikhomirova NK, Komolov KE, Permyakov SE, Zernii EY, Koch K-W and Philippov PP (2012) Synergetic effect of recoverin and calmodulin on regulation of rhodopsin kinase. Front. Mol. Neurosci. ***5****:28. doi: 10.3389/fnmol.2012.00028*

APPENDIX

MODELING OF EQUILIBRIUM BETWEEN RK, RECOVERIN, CALMODULIN, AND CALCIUM IONS

In the simplest case the process of binding of two ligand (L) molecules by a protein (P) is described with the "four-states" scheme:

$$\begin{array}{ccccc} \mathrm{P} & + & \mathrm{L} & \leftrightarrow & \mathrm{PL} \\ + & & & & + \\ \mathrm{L} & & & & \mathrm{L} \\ \updownarrow & & & & \updownarrow \\ \mathrm{LP} & + & \mathrm{L} & \leftrightarrow & \mathrm{LPL} \end{array}$$

This scheme may be approximated by the scheme of sequential filling of the ligand-binding sites of the protein upon certain ratio of the equilibrium binding constants, describing the scheme. In the case of equilibrium between RK, recoverin, calmodulin, and calcium ions the following equilibria should be taken into account: (1) two four-states schemes, describing the calmodulin–calcium and RK–calmodulin interactions (overall, eight equilibria); (2) one sequential binding scheme, describing the recoverin–calcium interaction (two equilibria); (3) one equilibrium between RK and recoverin; (4) additional equilibria related to the presence of mixed RK forms with simultaneously bound calmodulin and recoverin molecule(s). Overall, the number of chemical equilibria describing this system exceeds 11. Furthermore, the experiments were performed in the presence of membranes, which affect the distribution of recoverin and RK between soluble and membrane-bound forms (Zozulya and Stryer, 1992; Sanada et al., 1996). Hence, the number of equilibria describing this system is actually much higher. The complexity of this system prevents from usage of microscopic constants for its description. The alternative approach is the use of effective equilibrium constants, describing separate stages of the process. Although this approach is phenomenological, it greatly facilitates description of the system and enables to establish the synergy between calmodulin- and recoverin-binding sites of RK.

The following simplified scheme of chemical equilibria describing the interactions between RK, recoverin, calmodulin, and calcium ions can be suggested:

$$\begin{array}{ccccccc} & & & & K_R & & \\ & \mathrm{RK} & + & \mathrm{n}\cdot\mathrm{R} & \leftrightarrow & \mathrm{RK}\cdot\mathrm{R_n} & \\ & + & & & & + & \\ & \mathrm{m}\cdot\mathrm{C} & & & & \mathrm{m}\cdot\mathrm{C} & \\ K_C & \updownarrow & & & & \updownarrow & K_{CR} \\ & \mathrm{C_m}\cdot\mathrm{RK} & + & \mathrm{n}\cdot\mathrm{R} & \leftrightarrow & \mathrm{C_m}\cdot\mathrm{RK}\cdot\mathrm{R_n} & \\ & & & & K_{RC} & & \end{array} \qquad [A1]$$

$$\begin{array}{ccccc} & & K_{\mathrm{MR}} & & \\ \mathrm{R_0} & + & \mathrm{v}\cdot\mathrm{M} & \leftrightarrow & \mathrm{R} \\ & & K_{\mathrm{MC}} & & \\ \mathrm{C_0} & + & \mathrm{w}\cdot\mathrm{M} & \leftrightarrow & \mathrm{C} \end{array} \qquad [A2]$$

Here, M denotes calcium ion, R and C denote Ca^{2+}-bound states of recoverin and calmodulin, respectively, while R_0 and C_0 denote their Ca^{2+}-free states. Each of the equilibria is characterized by its own effective association constant:

$$K_{\mathrm{R}}^{\mathrm{n}} = [\mathrm{RK}\cdot\mathrm{R_n}]/([\mathrm{RK}]\cdot[\mathrm{R}]^{\mathrm{n}}) \quad (A1)$$

$$K_{\mathrm{C}}^{\mathrm{m}} = [\mathrm{C_m}\cdot\mathrm{RK}]/([\mathrm{RK}]\cdot[\mathrm{C}]^{\mathrm{m}}) \quad (A2)$$

$$K_{\mathrm{RC}}^{\mathrm{n}} = [\mathrm{C_m}\cdot\mathrm{RK}\cdot\mathrm{R_n}]/([\mathrm{C_m}\cdot\mathrm{RK}]\cdot[\mathrm{R}]^{\mathrm{n}}) \quad (A3)$$

$$K_{\mathrm{CR}}^{\mathrm{m}} = [\mathrm{C_m}\cdot\mathrm{RK}\cdot\mathrm{R_n}]/([\mathrm{RK}\cdot\mathrm{R_n}]\cdot[\mathrm{C}]^{\mathrm{m}}) \quad (A4)$$

$$K_{\mathrm{MR}}^{\mathrm{v}} = [\mathrm{R}]/([\mathrm{R_0}]\cdot[\mathrm{M}]^{\mathrm{v}}) \quad (A5)$$

$$K_{\mathrm{MC}}^{\mathrm{w}} = [\mathrm{C}]/([\mathrm{C_0}]\cdot[\mathrm{M}]^{\mathrm{w}}) \quad (A6)$$

Combining the Eqs A1–A4, the following relationship between the parameters of the Scheme [A1] can be derived:

$$K_{\mathrm{RC}}^{\mathrm{n}}/K_{\mathrm{CR}}^{\mathrm{m}} = K_{\mathrm{R}}^{\mathrm{n}}/K_{\mathrm{C}}^{\mathrm{m}} \quad (A7)$$

The changes in RK-inhibiting activity (see **Figure 4A**) reflect association of the Ca^{2+}-sensing proteins with RK under saturating Ca^{2+} level, so at the middle of the transition the following condition takes place:

$$[\mathrm{RK}\cdot\mathrm{R_n}] + [\mathrm{C_m}\cdot\mathrm{RK}] + [\mathrm{C_m}\cdot\mathrm{RK}\cdot\mathrm{R_n}] = [\mathrm{RK}] \quad (A8)$$

Using Eqs A1–A3, the latter equation can be rewritten:

$$K_{\mathrm{R}}^{\mathrm{n}}\cdot[\mathrm{R}]^{\mathrm{n}} + K_{\mathrm{C}}^{\mathrm{m}}\cdot[\mathrm{C}]^{\mathrm{m}}\cdot\left(1 + K_{\mathrm{RC}}^{\mathrm{n}}\cdot[\mathrm{R}]^{\mathrm{n}}\right) = 1 \quad (A9)$$

Assuming that the synergetic inhibition of RK by recoverin/calmodulin mixture occurs at $[\mathrm{C}] = [\mathrm{R}] = 4.6\,\mu\mathrm{M}$ (see **Figure 4A**; other numerical values are taken from **Table 1**),

$$K_{\mathrm{R}}^{\mathrm{n}} + K_{\mathrm{C}}^{\mathrm{m}}\cdot[\mathrm{R}]^{\mathrm{m-n}}\cdot\left(1 + K_{\mathrm{RC}}^{\mathrm{n}}\cdot[\mathrm{R}]^{\mathrm{n}}\right) = [\mathrm{R}]^{-\mathrm{n}} \quad (A10)$$

$$K_{\mathrm{RC}}^{\mathrm{n}} = [\mathrm{R}]^{-\mathrm{n}}\cdot\left[\left([\mathrm{R}]^{-\mathrm{n}} - K_{\mathrm{R}}^{\mathrm{n}}\right)\cdot[\mathrm{R}]^{\mathrm{n-m}}/K_{\mathrm{C}}^{\mathrm{m}} - 1\right] \quad (A11)$$

$$K_{\mathrm{RC}} = 2.7\mathrm{e}5\ \mathrm{M}^{-1}$$

Hence, from Eq. 7,

$$K_{\mathrm{CR}} = K_{\mathrm{C}}\cdot\left(K_{\mathrm{RC}}/K_{\mathrm{R}}\right)^{\mathrm{n/m}} = 1.1\mathrm{e}5\ \mathrm{M}^{-1} \quad (A12)$$

The Ca^{2+}-dependence of RK-inhibiting activity of recoverin and calmodulin (see **Figure 4B**) reflects association of the Ca^{2+}-sensing proteins with calcium ions, so at the middle of the transition the following equation takes place:

$$[\mathrm{R}] + [\mathrm{C}] + \mathrm{n}\cdot[\mathrm{RK}\cdot\mathrm{R_n}] + \mathrm{m}\cdot[\mathrm{C_m}\cdot\mathrm{RK}] + (\mathrm{m}+\mathrm{n}) \cdot[\mathrm{C_m}\cdot\mathrm{RK}\cdot\mathrm{R_n}] = [\mathrm{R_0}] + [\mathrm{C_0}] \quad (A13)$$

Since total concentration of RK was about 20 nM, the concentrations of all RK states may be neglected in comparison with concentrations of the RK-free forms of recoverin and calmodulin:

$$[\mathrm{R}] + [\mathrm{C}] = [\mathrm{R_0}] + [\mathrm{C_0}] \quad (A14)$$

Considering the material balance in the system,

$$[\mathrm{R}] + [\mathrm{R_0}] = \mathrm{R_0} \quad (A15)$$

$$[\mathrm{C}] + [\mathrm{C_0}] = \mathrm{C_0} \quad (A16)$$

where R_0 and C_0 are total concentrations of recoverin and calmodulin, respectively.

The system of Eqs A14–A16 and A5–A6 can be solved with respect to [M].

Substituting Eqs A5–A6 into Eqs A14–A16,

$$K_{MR}^{v} \cdot [R_0] \cdot [M]^{v} + K_{MC}^{w} \cdot [C_0] \cdot [M]^{w} = [R_0] + [C_0] \quad (A17)$$

$$K_{MR}^{v} \cdot [R_0] \cdot [M]^{v} + [R_0] = [R_0] \quad (A18)$$

$$K_{MC}^{w} \cdot [C_0] \cdot [M]^{w} + [C_0] = [C_0] \quad (A19)$$

From Eqs A17–A19:

$$[R_0] \cdot \left(K_{MR}^{v} \cdot [M]^{v} - 1\right) + [C_0] \cdot \left(K_{MC}^{w} \cdot [M]^{w} - 1\right) = 0 \quad (A20)$$

$$[R_0] = R_0 \big/ \left(1 + K_{MR}^{v} \cdot [M]^{v}\right) \quad (A21)$$

$$[C_0] = C_0 \big/ \left(1 + K_{MC}^{w} \cdot [M]^{w}\right) \quad (A22)$$

Substituting Eqs A21–A22 into Eq. 20, and considering that $R_0 = C_0$:

$$\left(K_{MR}^{v} \cdot [M]^{v} - 1\right) \big/ \left(1 + K_{MR}^{v} \cdot [M]^{v}\right) + \left(K_{MC}^{w} \cdot [M]^{w} - 1\right) \big/ \left(1 + K_{MC}^{w} \cdot [M]^{w}\right) = 0 \quad (A23)$$

$$K_{MR}^{v} \cdot [M]^{v} - 1 + K_{MR}^{v} \cdot K_{MC}^{w} \cdot [M]^{v+w} - K_{MC}^{w} \cdot [M]^{w} + K_{MC}^{w} \cdot [M]^{w} - 1 + K_{MR}^{v} \cdot K_{MC}^{w} \cdot [M]^{v+w} - K_{MR}^{v} \cdot [M]^{v} = 0 \quad (A24)$$

$$K_{MR}^{v} \cdot K_{MC}^{w} \cdot [M]^{v+w} = 1 \quad (A25)$$

$$[M] = \left(K_{MR}^{-v} \cdot K_{MC}^{-w}\right)^{1/(v+w)} = 0.71\ \mu M \quad (A26)$$

frontiers in
MOLECULAR NEUROSCIENCE

ORIGINAL RESEARCH ARTICLE
published: 12 April 2012
doi: 10.3389/fnmol.2012.00038

Structural basis for the regulation of L-type voltage-gated calcium channels: interactions between the N-terminal cytoplasmic domain and Ca^{2+}-calmodulin

Zhihong Liu and Hans J. Vogel*

Department of Biological Sciences, University of Calgary, Calgary, AB, Canada

Edited by:
Michael R. Kreutz, Leibniz-Institute for Neurobiology, Germany

Reviewed by:
Karl-Wilhelm Koch, Carl von Ossietzky University Oldenburg, Germany
Yogendra Sharma, Centre for Cellular and Molecular Biology, India

***Correspondence:**
Hans J. Vogel, Biochemistry Research Group, Department of Biological Sciences, University of Calgary, 2500 University Drive N.W., Calgary, AB T2N 1N4, Canada.
e-mail: vogel@ucalgary.ca

It is well-known that the opening of L-type voltage-gated calcium channels can be regulated by calmodulin (CaM). One of the main regulatory mechanisms is calcium-dependent inactivation (CDI), where binding of apo-CaM to the cytoplasmic C-terminal domain of the channel can effectively sense an increase in the local calcium ion concentration. Calcium-bound CaM can bind to the IQ-motif region of the C-terminal region and block the calcium channel, thereby providing a negative feedback mechanism that prevents the rise of cellular calcium concentrations over physiological limits. Recently, an additional Ca^{2+}/CaM-binding motif (NSCaTE, N-terminal spatial Ca^{2+} transforming element) was identified in the amino terminal cytoplasmic region of $Ca_v1.2$ and $Ca_v1.3$. This motif exists only in $Ca_v1.2$ and $Ca_v1.3$ channels, and a pronounced N-lobe (Ca^{2+}/CaM) CDI effect was found for $Ca_v1.3$. To understand the molecular basis of this interaction, the complexes of Ca^{2+}/CaM with the biosynthetically produced N-terminal region (residues 1–68) and NSCaTE peptide (residues 48–68) were investigated. We discovered that the NSCaTE motif in the N-terminal cytoplasmic region adopts an α-helical conformation, most likely due to its high alanine content. Additionally, the complex exhibits an unusual 1:2 protein:peptide stoichiometry when bound to Ca^{2+}-CaM, and the N-lobe of CaM has a much stronger affinity for the peptide than the C-lobe. The complex structures of the isolated N- and C-lobe of Ca^{2+}/CaM and the NSCaTE peptide were determined by nuclear magnetic resonance spectroscopy and data-driven protein-docking methods. Moreover, we also demonstrated that calcium binding protein 1, which competes with CaM for binding to the C-terminal cytoplasmic domain, binds only weakly to the NSCaTE region. The structures provide insights into the possible roles of this motif in the calcium regulatory network. Our study provides structural evidence for the CaM-bridge model proposed in previous studies.

Keywords: calmodulin, NSCaTE, L-type voltage-gated calcium channel, calcium-dependent inactivation, NMR

It has long been known that calmodulin (CaM) can regulate the activity of the voltage-gated calcium channels (VGCCs) (Qin et al., 1999; Zuhlke et al., 1999, 2000; Kim et al., 2004). The interactions between CaM and the IQ-motif in the C-terminal cytoplasmic tail of VGCC occupy the central position in the calcium-dependent feedback regulation loop (Fallon et al., 2005; Van Petegem et al., 2005; Dunlap, 2007). CaM seems to be mainly involved in two opposing mechanisms to control the calcium influx: calcium-dependent inactivation (CDI) and calcium-dependent facilitation (CDF). Depending on the type of channel, CaM can bind to the IQ-motif with either a parallel (L-type) or an anti-parallel (P/Q type) orientation (Fallon et al., 2005; Van Petegem et al., 2005; Kim et al., 2008; Mori et al., 2008). Apo- and Ca^{2+}-CaM both have a flexible dumbbell structure in solution (Yamniuk and Vogel, 2004; Ishida and Vogel, 2006). The N- and C-lobe of CaM play different roles in CDI and CDF (Zuhlke and Reuter, 1998; Peterson et al., 1999; Zuhlke et al., 1999, 2000; DeMaria et al., 2001; Pitt et al., 2001; Dick et al., 2008). Recently, complexes of Ca^{2+}-CaM with the IQ-motifs from both L-type and P/Q-type channels have been crystallized. These high-resolution structures have resolved many ambiguities from previous studies but have also raised some new questions (Fallon et al., 2005; Van Petegem et al., 2005; Houdusse et al., 2006; Mori et al., 2008).

In addition to CaM, the main channel-pore forming α_{1c} subunit of the channel is also regulated by $Ca_v\beta$ subunits, CaMKII and the CaBP-family proteins (Yuan and Bers, 1994; Hudmon

Abbreviations: CaM, calmodulin; CaBP1, calcium binding protein 1; NSCaTE, N-terminal spatial Ca^{2+} transforming element; VGCCs, voltage-gated calcium channels; SCaM4, soybean calmodulin isoform 4; SCaM4-CT, the C-lobe of soybean calmodulin isoform 4; MAPK, mitogen-activated protein kinase; NtMKP1, *N. tabacum* MAPK phosphatase; GAD, plant glutamate decarboxylase; SUMO, small ubiquitin-like modifier protein; RMSD, root mean-square deviation; ITC, isothermal titration calorimetry; NMR, nuclear magnetic resonance; CD, dircular dichroism; CDI, calcium-dependent inactivation; CDF, calcium-dependent facilitation; VDI, voltage-dependent inactivation; HADDOCK, high ambiguity-driven biomolecular docking.

et al., 2005; Grueter et al., 2006; Buraei and Yang, 2010). Recently, it has been found that a sequence of ∼10 amino acid residues in the N-terminal cytoplasmic domains of $Ca_v1.2$ and $Ca_v1.3$, known as the N-terminal spatial Ca^{2+} transforming element (NSCaTE) motif (Dick et al., 2008), is also involved in CDI regulation. The functional significance of this particular region has been clearly demonstrated for $Ca_v1.2$ and $Ca_v1.3$ *in vivo* (Dick et al., 2008). Interestingly, P/Q-type VGCCs lack this motif in their N-terminal region. However, upon the artificial introduction of this motif into the $Ca_v2.2$ N-terminus, local calcium selectivity could also be demonstrated. The results of these experiments illustrate an important function for the NSCaTE region in the regulation of specific L-type VGCCs.

To better understand the function of this motif at the molecular level, the complex of Ca^{2+}/CaM and the NSCaTE peptide was investigated in this work. First, two constructs [long (1–68) and short (48–68)] of the $Ca_v1.2$ N-terminus, both including the NSCaTE sequence, were made biosynthetically. The interactions between these peptides and CaM were characterized by isothermal titration calorimetry (ITC), steady state fluorescence and nuclear magnetic resonance (NMR) spectroscopy. Although the majority of the N-terminal domain is unstructured, surprisingly, a helical conformation was found for the NSCaTE Ca^{2+}/CaM-binding motif even in aqueous solution. Moreover, an unusual 1:2 stoichiometry of CaM to peptide binding was observed. It was also found that the N-lobe of CaM could bind to $Ca_v1.2$NT more tightly than the C-lobe. We also demonstrate that the NSCaTE region binds poorly to the related calcium binding protein 1 (CaBP1) protein (Oz et al., 2011). The relatively low affinity between CaM and the NSCaTE peptide prevented the determination of a complex structure of the intact protein by NMR spectroscopy. Instead, the structure of each lobe of CaM in complex with the NSCaTE was determined separately, making use of the fact that the two isolated lobes of CaM are known to retain their native structure (Thulin et al., 1984). The N-lobe Ca^{2+}-CaM/NSCaTE complex was solved by routine NMR methods, and a comparison between the NMR determined complex structure and a high ambiguity-driven biomolecular docking (HADDOCK)-generated complex structure was made (Dominguez et al., 2003). The C-lobe Ca^{2+}-CaM/NSCaTE complex structure was generated by a combined NMR and data-driven docking strategy. In this paper, we present a model for this complicated regulatory network. The cytoplasmic N- and C-termini of the calcium channel, CaM and CaBP1 are all involved in this network, and the possible roles for these interacting partners are discussed below.

MATERIALS AND METHODS

CaBP1, CaM, AND ITS N/C-LOBE CONSTRUCTS

Both CaM (and its N- and C-lobes) and CaBP1 were expressed using the pET30b vector (Novagen). The N-lobe of CaM contains residues 1–77, and the C-lobe contains residues 78–148. The gene for human CaBP1 was synthesized by BlueHeron, Ltd. (Rockville, MD, USA) and was optimized for *Escheichia coli* expression. Compared with the wild-type S-CaBP1, the first 15 AAs of this CaBP1 variant are missing, similar to the CaBP1(Δ2–15) construct used in the recent CaBP1 structure determined by X-ray crystallography (Findeisen and Minor, 2010). The calmodulin protein and its isolated lobes were purified using a phenyl-Sepharose hydrophobic column (Pharmacia). A previously described protocol for the purification of most CaBPs was used with minor modifications (Queiroz et al., 2001). The frozen pellet was resuspended in 50 mM Tris-HCl, 2 mM ethylenedimainetetraacetic acid (EDTA), 1 mM DTT, 150 mM KCl, 1.5 mg/ml phenylmethanesulfonylfluoride (PMSF), pH 7.5. The sample was always incubated on ice, and all operations were performed in the cold room (∼4°C). The sample was homogenized, and a French press was used to lyse the cells. The soluble protein and debris were separated by centrifugation at 18,000 rpm for 1 h. The supernatant was loaded slowly onto the first hydrophobic column, which had been pre-equilibrated with 50 mM Tris-HCl, 2 mM EDTA, 1 mM DTT, 150 mM KCl, pH 7.5 (buffer A). A total of 200–250 mL of the flow-through solution was collected. $CaCl_2$ and $MgCl_2$ were then added to give final concentrations of 10 mM Ca^{2+} and 5 mM Mg^{2+} prior to loading onto the second column, which was pre-equilibrated with 50 mM Tris-HCl, 1 mM $CaCl_2$, 1 mM $MgCl_2$, 1 mM DTT, 100 mM KCl, pH 7.5 (buffer B). After loading, the column was washed with approximately 100 mL of buffer B, after which the proteins were immediately eluted with buffer C (50 mM Tris-HCl, 50 mM KCl, 2 mM EDTA, and 1 mM DTT; pH 7.5) because of the relatively low affinity of the N- and C-lobes of CaM and CaBP1 for the hydrophobic column. The fractions were then pooled together and were further purified using anion exchange. An AKTA purifier system with a Resource Q anion-exchange column (GE Healthcare) was used. Following the anion-exchange purification, all fractions containing the desired protein were collected and dialyzed against 1 g/L ammonium bicarbonate. After five or six buffer exchanges, the sample was flash frozen and lyophilized. The protein powder was stored at −20°C for further studies.

SHORT AND LONG CONSTRUCTS OF $Ca_V1.2$NT

The DNA sequence of the full-length (124 AAs) N-terminal cytoplasmic domain of $Ca_v1.2_\alpha$ was ordered from GENEART, Life Technologies. The codons of this construct were optimized for expression in *E. coli*. The expression constructs were made in a modified pET15b vector that included a 6× His tag and a small ubiquitin-like modifier protein (SUMO) tag before a tobacco etch virus (TEV) protease-cleavage site (Panavas et al., 2009). Two DNA sequences were successfully cloned between the KpnI and BamHI sites. In initial expression experiments, multiple bands were observed for the 1–124 construct; we, therefore, analyzed shorter constructs and found that a 1–68 construct gave rise to one band. A shorter construct (residues 48–68), which is slightly longer than the NSCaTE motif (residues 52–60) was also made. The longer construct started at the N-terminal end of $Ca_v1.2_\alpha$ and ended in the same region as the short peptide (residues 1–68). The proteins were purified on a Ni-NTA column. After the cleavage of the SUMO tag with TEV protease, the cleaved protein was reloaded onto the Ni column. The flow-through solution containing the peptides was concentrated, and the concentration was determined by OD_{280} using extinction coefficients obtained from ProtParam (ExPASy), 8480 M^{-1} cm^{-1} for the long peptide and 5500 M^{-1} cm^{-1} for the short peptide. Since the peptides contain

Trp residues, their concentration can be accurately determined. Also the concentration of Ca^{2+}-CaM can be readily determined from the absorbance spectra of the two Tyr residues. The peptide purity was verified by SDS-PAGE and mass spectrometry.

Circular dichroism (cd) spectroscopy

Circular dichroism (CD) spectra were recorded on a Jasco J-810 spectrometer (Jasco, Inc., Easton, MD, USA). Samples were prepared in 10 mM Tris (pH 7.0) with a concentration of 20 uM. Trifluoroethanol (TFE) was added as a co-solvent in solution. A 1 mm pathlength cuvette was used for all spectra.

ISOTHERMAL TITRATION CALORIMETRY

All ITC experiments were performed on a Microcal VP-ITC instrument. The ITC buffer consisted of 20 mM HEPES, 100 mM KCl, and 5 mM $CaCl_2$, pH 7.0. For experiments with apo-CaM, 5 mM EDTA was used instead of 1 mM $CaCl_2$. The ITC cell was filled with 50 μM intact CaM, N- or C-lobe CaM, or CaBP1. A highly concentrated solution of the NSCaTE peptide was then injected (5 μL each) into the cell. The concentration of the C-lobe of CaM was determined by the absorbance at OD_{280}. However, the N-lobe of CaM has no Trp or Tyr residues. The N-lobe concentration, therefore, was estimated by weight and verified by the Bio-Rad protein assay. The concentration of CaBP1 was measured by OD_{280} with an extinction coefficient of 2980 M^{-1} cm^{-1}. All experiments were run at 25°C. The data were fit to either a one-site binding model (N-/C-lobe of CaM and CaBP1) or a two-site binding model (intact CaM). Control experiments were performed to adjust the baseline of each experiment.

FLUORESCENCE SPECTROSCOPY

All experiments were performed on a Varian Cary Eclipse spectrofluorimeter. The NSCaTE peptide contains one Trp residue and was selectively excited at 295 nm with a 5 nm excitation slit width. The emission spectra were recorded from 300 to 450 nm with a 10 nm emission slit width. All samples were dissolved in a solution of 20 mM HEPES and 100 mM KCl at pH 7.0. A 50 μM peptide concentration was used in the cell. Concentrated CaM or N-/C-lobe CaM (0.7–1.0 mM) was titrated into 1 mL of the peptide in 5 μL aliquots. The changes in the fluorescence intensity for each titration at Δ_{max} were recorded and used to calculate the binding constant, K_a:

$$[P \cdot L] = \frac{\sqrt{C} \pm \sqrt{D}}{2}$$

$$C = ([P]_T + [L]_T + K_d)^2$$

$$D = C - 4[P]_T[L]_T$$

where $[P]_T$ and $[L]_T$ are the total concentrations of the protein and the peptide. The Caligator 1.05 software, developed by the group of S. Linse, was used to calculate the K_a (Andre and Linse, 2002).

NMR EXPERIMENTS

All NMR samples were prepared in buffer containing 20 mM Bis-Tris, 100 mM KCl, pH 7.0. For all complexes, the saturation of the labeled component was monitored with ^1H–^{15}N HSQC experiments. The titrations were complete when no further peak shifts were observed.

All ^1H–^{15}N HSQC experiments were performed at 25°C on 500 MHz and 700 MHz NMR instruments. For the ^1H(F2) and ^{15}N(F1) dimensions, 1024 × 256 real data points were used.

The backbone assignments were completed for the following peptides/proteins in the free or bound state: the $^{13}C/^{15}N$-labeled free-state long NSCaTE peptide, the $^{13}C/^{15}N$-labeled short NSCaTE peptide saturated with the unlabeled N-/C-lobe CaM and the $^{13}C/^{15}N$-labeled CaM N-/C-lobe bound to the unlabeled short NSCaTE peptide. Routine 3D NMR backbone assignment experiments (CBCACONH, HNCACB, HNCO, and HNCACO) were used. The side chain assignments were made using CCCONH, HCCCONH, and HCCH-TOCSY experiments. All of these experiments are the same as those used in the structure determination of the soybean calmodulin isoform 4 (SCaM4)/MAPK-phosphatase peptide complex (Ishida et al., 2009).

A sample containing the $^{13}C/^{15}N$-labeled Ca^{2+}/CaM N-lobe saturated with the unlabeled NSCaTE peptide was used to acquire the $^{13}C/^{15}N$ double-filtered 2D-NOESY spectrum, and the intramolecular NOEs between the CaM N-lobe and peptide were determined. To obtain the structures of the short peptide in complex with the N-lobe of CaM, another sample containing the $^{13}C/^{15}N$-labeled NSCaTE peptide saturated with the deuterated Ca^{2+}/CaM N-lobe was examined. The side chain and the ^{15}N-edited 3D-NOESY experiments were performed to obtain unambiguous chemical shift assignments for the NSCaTE peptide and intrapeptide NOEs.

Heteronuclear ^1H–^{15}N NOE experiments were performed for the long $Ca_v1.2$NT peptide. A 5 sec pre-saturation time was used. The experiment was performed on a 500 MHz NMR instrument.

The structures of the complex of the Ca^{2+}/CaM-NT with the NSCaTE peptide and of Ca^{2+}/CaM-CT saturated with the NSCaTE peptide were determined using the NOE-based proton–proton distances derived from the ^{15}N-edited 3D-NOESY. The dihedral angles along the sequence of each protein were calculated by TALOS (Cornilescu et al., 1999). These restraints were used in the calculation of the final structure by CYANA 2.0 (Guntert, 2004).

RESULTS

THE NSCaTE REGION ADOPTS A HELICAL CONFORMATION IN AQUEOUS SOLUTION

The NSCaTE motif only exists in the $Ca_v1.2$ and $Ca_v1.3$ L-type calcium channels (**Figure 1**). This sequence does not conform to any other known CaM-binding motif. Most linear peptides do not adopt stable secondary structures in aqueous solution. However, our experimental results show that part of the long NSCaTE (1–68) peptide can adopt a relatively stable helical conformation in aqueous solution from residue S51 to residue A62. The ^1H–^{15}N HSQC peak dispersion of the isotope-labeled peptide is only around approximately 1 ppm (7.7–8.7 ppm; see **Figure 2A**), which is normal for a peptide in a random coil conformation. However, the NSCaTE region, which extends from S51 to A62, is helical according to the secondary structure prediction based on the chemical shift index (CSI) of the backbone heavy atoms

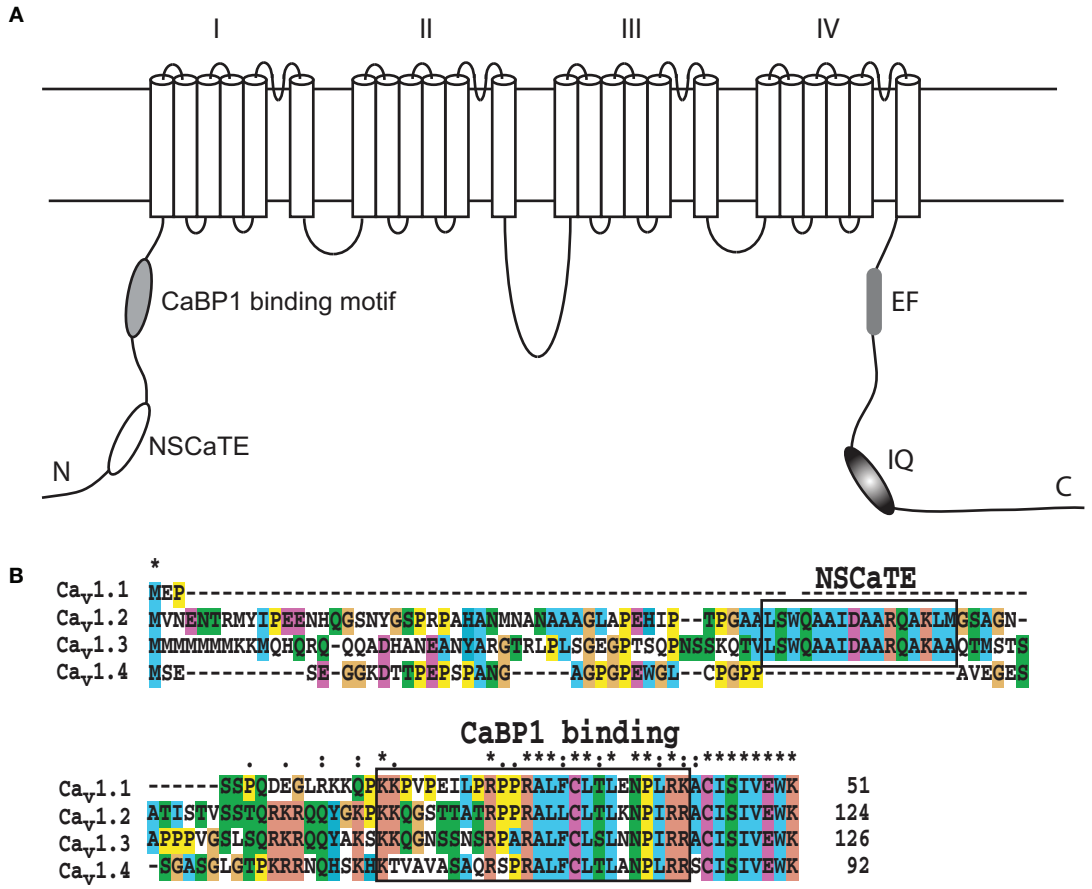

FIGURE 1 | (A) Schematic of the pore-forming α-subunit of the L-type voltage-gated calcium channels Cav1.2 and Cav1.3 indicating the position of the various regulatory elements. **(B).** Sequence alignment of the N-terminal sequences of the human L-type voltage-gated calcium channels. The alignment was performed with ClustalW, and the default color settings were used. The Ca^{2+}/CaM and CaBP1 binding motifs are highlighted with *black boxes*.

(**Figure 2B**). The remainder of the N-terminal domain of the channel is unstructured, which is consistent with the outcome of protein disorder predictions (see Appendix **Figure A1**) NMR relaxation experiments were also performed with the long peptide (**Figure 2C**). The $\{^1H\}$–^{15}N NOE experiments only showed positive values for the structured helix portion, while all other residues had negative values. The average NOE values for the structured region were also quite small (0.251 ± 0.033), indicating the relative flexibility of this region. The CD spectrum of this peptide indicated the presence of a mixture of random coil and helical conformations. We also showed that the percentage of the helical conformation with increasing amounts of TFE as a co-solvent in solution (see Appendix **Figure A2**). As expected, the TFE cosolvent appeared to further stabilize the small helix (Zhang et al., 1993). The intensities of the ^1H–^{15}N HSQC peaks were not evenly distributed along the sequence; the peaks for the helical portion had the strongest intensity. The backbone sequence assignment could be completed for almost the entire peptide sequence. We noticed that the NSCaTE region had a high percentage of alanine (4/11, residues L50–R60). Of all amino acids, alanine has the highest helix-forming propensity (Pace and Scholtz, 1998), which could be a likely reason for the spontaneous helix formation in this region. However, the severe overlap of the alanine signals hindered a complete backbone assignment. Several small, unassigned peaks in the spectrum may have arisen from a minor conformation of the peptide, possibly arising from a *cis-trans* conformational exchange from several proline residues in the random coil region.

THE NSCaTE PEPTIDE BINDS TO Ca^{2+}/CaM WITH A 2:1 STOICHIOMETRY

The ITC experiments demonstrated that the binding of the NSCaTE peptide to wild-type CaM is exothermic (**Figures 3A,B**). An unusual 2:1 stoichiometry (peptide:protein) was observed, which is similar to the binding between the GAD peptide and CaM (Yuan and Vogel, 1998) and the binding of MAPK-phosphatase to CaM (Rainaldi et al., 2007). The NMR titration experiments also confirmed this result, as the HSQC peaks only ceased to shift after more than two equivalents of peptide were added (data not shown). It should be noted that this stoichiometry is different from the 1:1 binding reported by Benmocha et al. (2009). The two-site binding model showed that the two sites

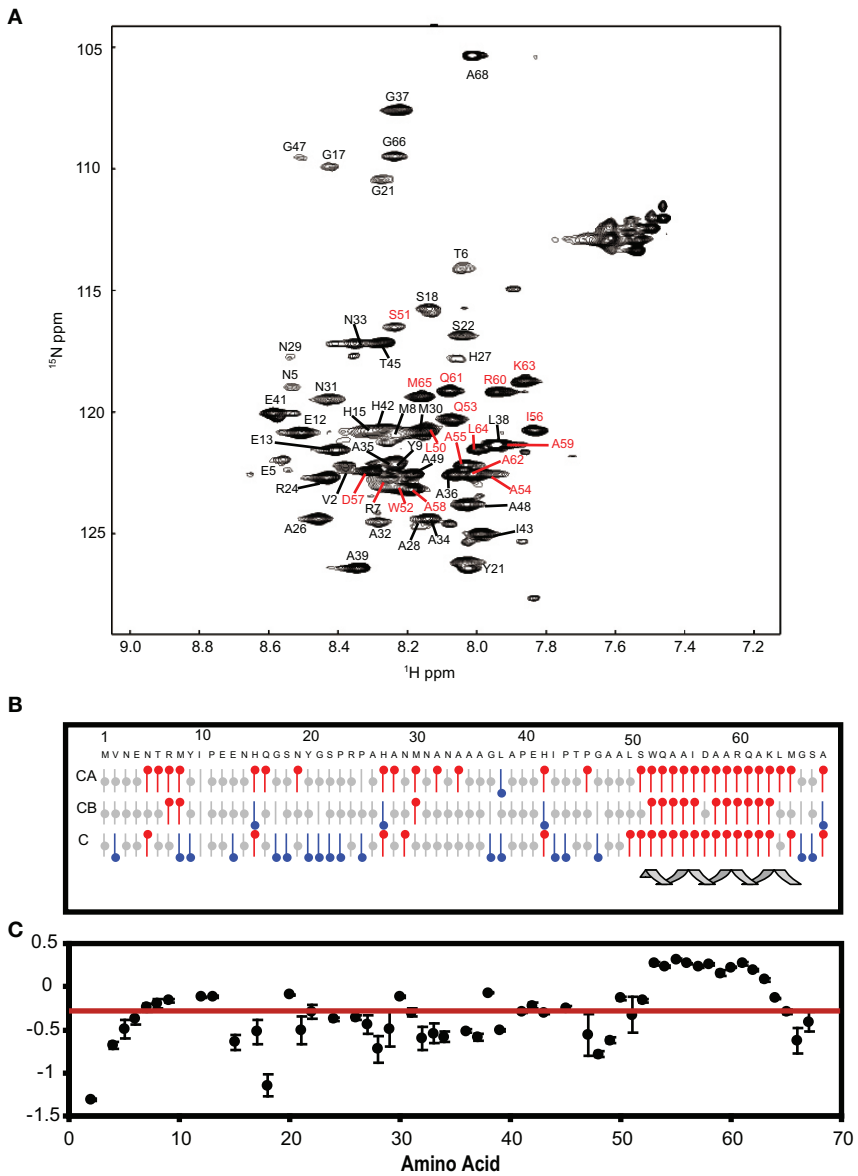

FIGURE 2 | (A) ^{1}H–^{15}N HSQC spectrum of the long NSCaTE (AA 1–68) peptide. (B) Secondary structure prediction based on the ^{13}C chemical shifts of the long NSCaTE construct ($Ca_v1.2NT_{1-68}$). **(C)** Heteronuclear {^{1}H}–^{15}N NOE data for the long NSCaTE construct ($Ca_v1.2NT_{1-68}$).

had different binding affinities, which was confirmed by studying the binding of each isolated lobe to the peptide (**Figures 3C,D**). This sequential mode of binding resembles that reported for the MAPK-phosphatase, where both lobes of CaM can bind with different affinities (Rainaldi et al., 2007). A 1:1 stoichiometry was found for each lobe, and the N-lobe had a stronger affinity than the C-lobe (**Table 1**). However, the binding affinities of the NSCaTE peptide ($K_d \sim \mu M$) to both domains were relatively weaker than other CaM-binding peptides, such as the IQ peptide from the C-terminal tail of the same channel ($K_d \sim nM$) (Van Petegem et al., 2005). Compared with the IQ peptide, which has a total of 21 AAs (K1617–E1637) involved in binding with residue Ile1624 in the middle, the effective binding region of the NSCaTE peptide was much shorter (10 AAs, S51–R60). This short region could not span both lobes of Ca^{2+}/CaM in the classical 1:1 mode. The same was observed for the MAPK-phosphatase/Ca^{2+}-CaM interaction, where the CaM-binding domain is also only 10 residues long (Ishida et al., 2009).

From previous *in vivo* studies, we know that three residues (W52, I56, and R60) are critical for the binding of Ca^{2+}/CaM to the NSCaTE peptide in causing the CDI effect (Dick et al., 2008). W52 is especially important, as the W52A mutation completely abolishes the NSCaTE CDI function *in vivo*. Using site-directed mutagenesis, we also made W52A and I56A mutations in our long construct as well as an L64A mutation. Whereas the L64A mutation had no effect on the binding to CaM (as determined

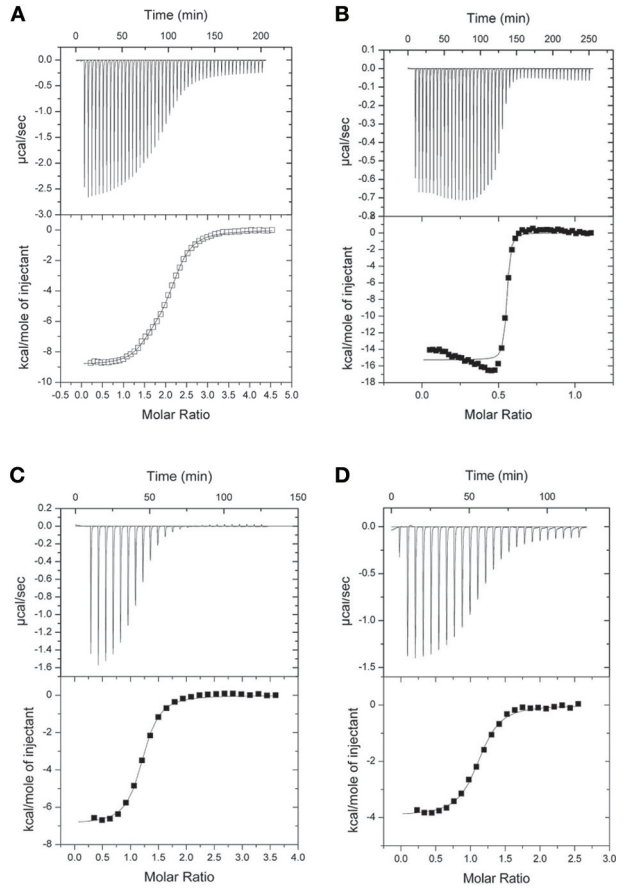

FIGURE 3 | ITC characterization of the interactions of Ca^{2+}/CaM with the long NSCaTE peptide. (A) NSCaTE peptide titrated into Ca^{2+}/CaM. **(B)** Ca^{2+}/CaM titrated into NSCaTE peptide. **(C)** NSCaTE peptide titrated into Ca^{2+}/CaM-NT. **(D)** NSCaTE peptide titrated into Ca^{2+}/CaM-CT.

by ITC), the W52A mutation completely abolished and the I56A mutation decreased the Ca^{2+}-CaM affinity (data not shown), thereby confirming the importance of these two residues for productive binding. As CaM has no Trp residues, the chemical environment of the indole-ring of the W52 residue of the NSCaTE peptide in the complex could be directly investigated by steady state fluorescence spectroscopy (**Figure A3**). Similar to other unstructured CaM-binding peptides containing tryptophan residues, the highest intensity of the broad fluorescence emission of the long peptide in aqueous solution occurred at approximately 355 nm, indicating a fully solvent-exposed Trp. As the peptide was saturated with the intact CaM or with the separate N- and C-lobes of CaM, a blue shift was observed for the highest emission peak at approximately 325 nm with an increase in the fluorescence intensity. This result is similar to those obtained upon the binding of CaM-binding domain peptides from MLCK, CaMKI, and CaMKII (Van Lierop et al., 2002; Yamniuk and Vogel, 2004). The 1:2 stoichiometry was also confirmed by fluorescence spectroscopy titration experiments. The maximum fluorescence emission intensity did not increase after one peptide was saturated with the N-lobe of CaM. However, the intensity slowly increased even after a 2.5-fold excess of C-lobe CaM bound to the peptide. The binding constants determined by this method were $1.39 \times 10^6\ M^{-1}$ for the N-lobe and $2.32 \times 10^5\ M^{-1}$ for the C-lobe, which were similar to the values determined by the ITC experiments.

STRUCTURE DETERMINATION

Severe peak broadening in the NMR spectra prevented us from determination of the structure of the complex formed between the intact CaM and the NSCaTE peptide. We investigated different strategies in an attempt to overcome this problem. First, we tried to use the fast structure determination method that relies on the use of CaM's methionine-methyl NOEs (Gifford et al., 2011). However, because of the intermediate binding affinity, the methionine-CH_3 group peaks involved in the binding interface was too broad to be confidently assigned. A similar situation has been encountered for the CaM-binding peptide of the N-terminal β-subunit of the olfactory rod CNG channel (Orsale et al., 2003). Because each lobe of CaM can bind one peptide, we superimposed the ^1H–^{15}N HSQC from the N- and C-lobe complexes onto the intact CaM complex (**Figure 4B**). The high degree of overlap indicated that the truncation induced only minor perturbations in the complex structure of each lobe. We first determined the solution structures of the protein lobes in the complex using regular NMR methods. To obtain unambiguous chemical shifts of the peptide in each lobe complex, the backbone and side-chain experiments were also run for the

Table 1 | Isothermal titration calorimetry data[a].

	Fitting mode[b]	*N*	K_d (uM)	ΔH (kcal mol^{-1})	ΔS (cal mol^{-1} K^{-1})
Ca^{2+}-CaM[c]	One	2.04 ± 0.01	2.90 ± 0.11	−9.22 ± 0.04	−5.59
	Two	1.43 ± 0.04	0.16 ± 0.03	−8.84 ± 0.04	1.44
		0.79 ± 0.03	3.80 ± 0.18	−6.39 ± 0.28	3.36
Ca^{2+}-CaM NT[c]	One	1.16 ± 0.01	0.65 ± 0.06	−6.91 ± 0.07	5.13
Ca^{2+}-CaM CT[c]	One	1.12 ± 0.02	1.33 ± 0.30	−3.86 ± 0.09	13.9
Ca^{2+}-CaBP1[d]	One	0.80 ± 0.01	25.8 ± 4.81	3.98 ± 0.29	34.3

[a] *All data obtained at 25° C.*

[b] *Data fitting with one or two binding sites.*

[c] *Data obtained with Ca^{2+}-CaM is endothermic.*

[d] *Data obtained with Ca^{2+}-CaBP1 is exothermic.*

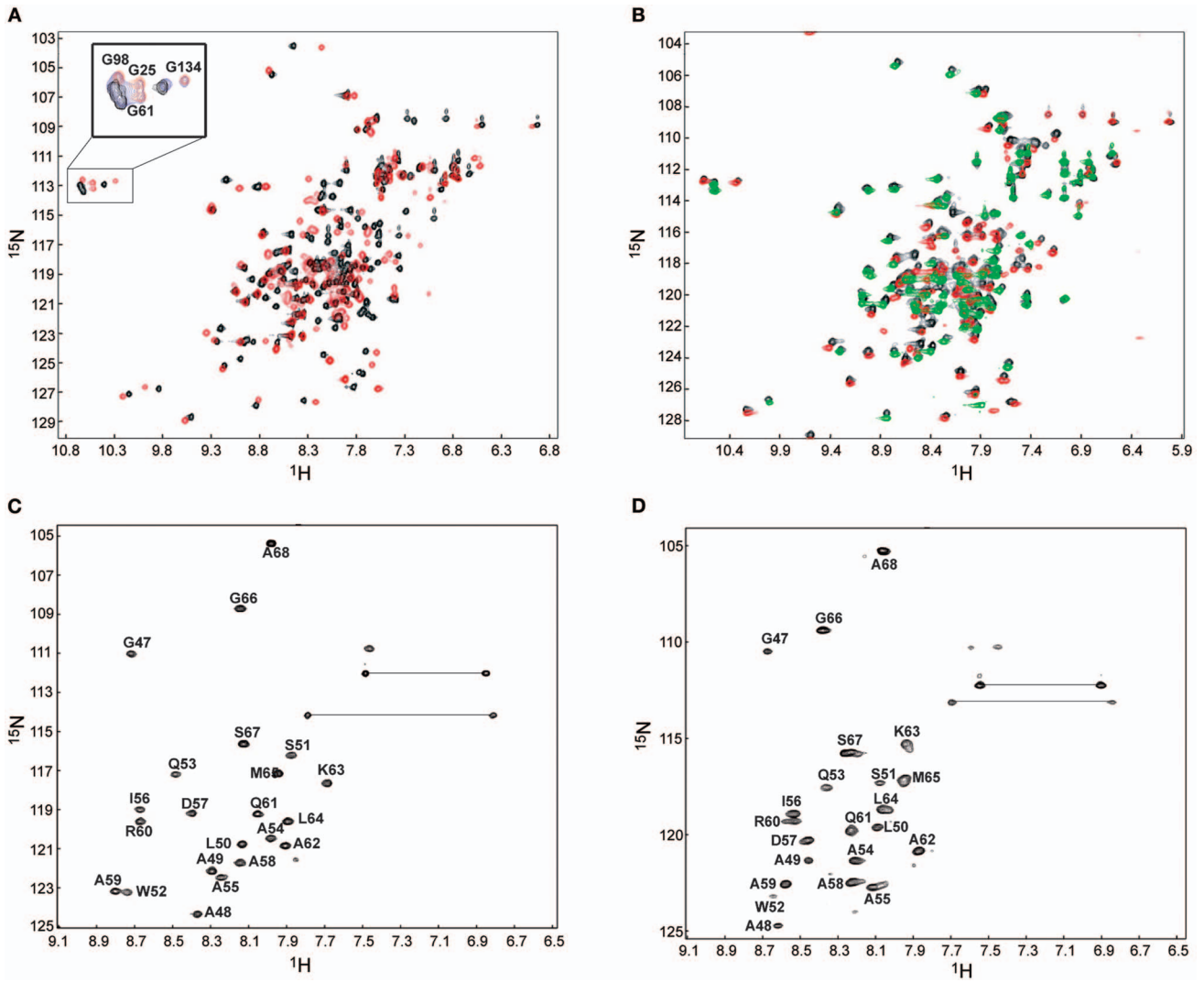

FIGURE 4 | ^{1}H–^{15}N HSQC for the binding of Ca^{2+}/CaM to the short NSCaTE peptide. (A) Ca^{2+}/CaM is shown in *black*, and fully peptide saturated Ca^{2+}/CaM is *red*. The conformational change as indicated by the peaks shifts of the four EF-hand Gly residue is highlighted in the *top left corner*. **(B)** Superposed HSQC spectra of intact Ca^{2+}/CaM, Ca^{2+}/CaM-NT (*red*) and Ca^{2+}/CaM-CT (*green*) in the complex with the peptide. **(C)** ^{1}H–^{15}N HSQC spectrum of the ^{13}C/^{15}N-labeled NSCaTE peptide saturated with Ca^{2+}/CaM-NT. **(D)** ^{1}H–^{15}N HSQC spectrum of the ^{13}C/^{15}N-labeled NSCaTE peptide saturated with Ca^{2+}/CaM-CT.

^{13}C/^{15}N-labeled peptides in the complex. Compared with the peptide in aqueous solution (**Figure 2A**), the bound peptides had better dispersed peaks (**Figures 4C,D**). Secondary structure predictions were performed based on the CSI, and the helical conformation we observed for the unbound state of NSCaTE was maintained in both peptides in the complex. The peaks from the C-lobe CaM-bound peptide were broader than those for the N-lobe, which is consistent with the lower affinity of the C-lobe complex. The ^{13}C/F$_3$-filtered and ^{13}C/F$_1$-edited NOESY–HSQC exhibited only a few intermolecular NOEs for the C-lobe complex, much fewer than those obtained for the N-lobe complex. These differences prevented the direct determination of the C-lobe complex structure based on isotope-filtered NMR methods. On the other hand, the N-lobe complex could be defined in this fashion.

We also made several comparisons between the isolated lobe and the intact CaM protein-peptide complex. From the backbone assignments for the intact Ca^{2+}-CaM/NSCaTE complex, we calculated the weighted average secondary shifts (WASS) along the sequence (**Figure A4A**). Combined with the heteronuclear ^{1}H–^{15}N NOE data (**Figure A4B**), we confirmed through the WASS, as expected from the isolated structures, that the regular secondary structures of Ca^{2+}/CaM are maintained in this complex, including the flexible N-/C-termini and the central linker. The residues of the loop region between the two EF-hands for each lobe also had lower NOE values, which indicated their higher flexibility. In the sequence, eight continuous segments had positive WASS values. These segments corresponded to the eight helices of the four EF-hands that are normally observed in CaM complexes.

The Ca^{2+}/CaM N-lobe complex structure was determined with a routine NMR method. The backbone and side chain chemical shifts of both the CaM N-lobe and the NSCaTE peptide were assigned with various triple-resonance NMR experiments, and the intermolecular NOEs were acquired from the half-filtered NOESY–HSQC experiments. In total, more than 95% of the backbone and side chain heavy atoms and protons were assigned. Many of the intermolecular NOEs came from the N-lobe methionine-methyl or aromatic ring protons to the peptide protons. About half of the intermolecular NOEs in the half-filtered spectrum were confirmed and used in the final complex structure determination. To validate our structure calculation, we also generated a complex model with the protein–protein docking program HADDOCK 2.0. The structures determined for the Ca^{2+}/CaM N-lobe and the peptide in the complex were used as the initial models. The hydrophobic pocket of the N-lobe (A15, L18, F19, L32, V35, M36, L39, M51, V55, F65, M71, and M72) was used as the N-lobe binding interface. The three residues of the peptide (W52, I56, and R60) that have been confirmed to be critical for CaM-binding were defined as the active peptide residues, and the remainder of the peptide residues was defined as passive residues. All of the residues involved in the binding surface were semi-flexible, which allows for the rotation of the side chain atoms. In total, 1000 structures were calculated with the HADDOCK web server (http://haddock.chem.uu.nl) (Dominguez et al., 2003), and the first 20 structures in the cluster with the lowest Haddock score were chosen as the representative complex ensemble. Because the intermolecular NOEs were not available for the C-lobe complex, this data-driven docking method was the only way to generate the complex structure. The Ca^{2+}/CaM-CT structure in this complex was calculated first, and the hydrophobic surface was defined as the following residues: A88, V91, F92, L105, V108, M109, L112, M124, A128, F141, M144, and M145. The peptide structure from the N-lobe complex was used as the initial peptide structure, and the same three residues (W52, I56, and R60) were used as the active residues for the HADDOCK calculation. Both Ca^{2+}-CaM NT/CT in the complex were further refined with the addition of backbone H–N RDC restraints [XPLOR-NIH, version 2.21 (Schwieters et al., 2003)].

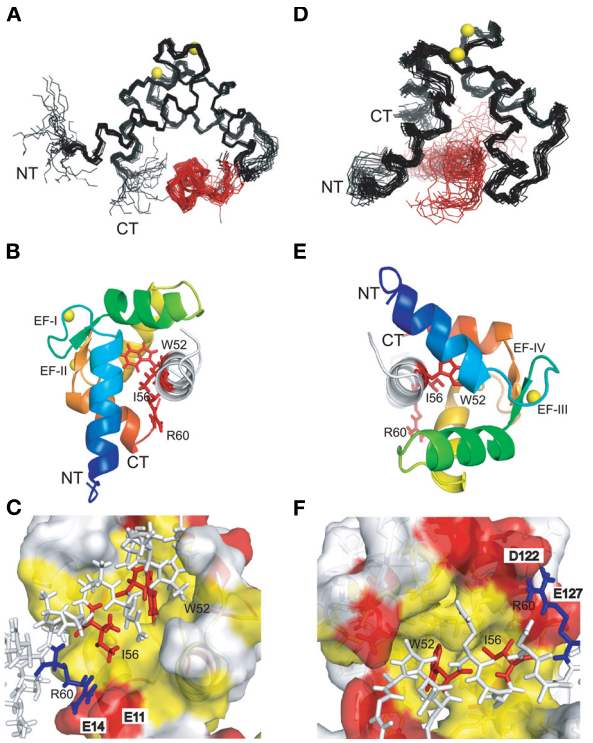

FIGURE 5 | NMR solution structures of the complexes of the N-lobe (A, B, C) and the C-lobe (D, E, F) of Ca^{2+}-CaM with the short NSCaTE peptide. (A, D) Backbone representation of the ensemble of the 20 lowest energy structures of the Ca^{2+}/CaM-NT-NSCaTE complex (**A**, calculated by CYANA2.1) or the Ca^{2+}/CaM-CT-NSCaTE complex (**D**, generated by HADDOCK). The CaM lobes are shown in *black*, and the peptide bundles are *red*. The calcium ions in the EF-hand loop are *yellow*. The peptide is shown in *white*, and the three critical residues (W52, I56, and R60) are highlighted in *red*. **(B, E)** Ribbon representations of the lowest energy structures for the Ca^{2+}/CaM NT **(B)** and CT **(E)** complexes. The four helices in each lobe follow the default PyMOL rainbow color setting (blue–green–yellow–orange) from the N-terminus to the C-terminus. **(C, F)** Binding surface representations of the Ca^{2+}/CaM NT **(C)** and CT **(F)** complexes. The binding pocket of each lobe is highlighted in *yellow* (hydrophobic residues) and *red* (negatively charged residues). The NSCaTE peptide is shown in a stick representation (*white*), and the two critical hydrophobic residues (W52 and I56, red) and the positively charged residue (R60, blue) are highlighted.

STRUCTURE OF Ca^{2+}/CaM N-/C-LOBE BOUND TO THE NSCaTE PEPTIDE

Both complexes of the separate N- and C-lobes of CaM bound to the NSCaTE peptide are shown in **Figure 5**. For the N-lobe complex, the 20 lowest energy solution structures based on the NMR restraints are shown as an ensemble on the top left (**Figure 5A**). The backbone root mean-square deviation (RMSD) was 0.54 Å (For a summary of the NMR data see **Table 2**). As indicated in the ^{1}H–^{15}N heteronuclear NOE experiment, the loop region connecting the two EF-hands had a larger RMSD. Similar to most Ca^{2+}/CaM-target peptide complexes, the N-lobe of CaM is composed of two EF-hands. Each EF-hand contains two helices connected by a calcium binding loop, and the two EF-hands were bridged by a short pair of anti-parallel β-strands from the two calcium binding loops (Gifford et al., 2007). The two helices in each EF-hand were perpendicular to each other and exposed hydrophobic residues, forming a continuous hydrophobic surface which can interact with the NSCaTE peptide. As shown using site-directed mutagenesis and fluorescence spectroscopy, W52 of the peptide is the most important residue for CaM binding. In **Figure 6**, we list the contact residues that are within 4 Å for the side chains of CaM and the peptide. As expected, W52 contacted the most residues of CaM. The total W52 side chain contact surface was 208.5 Å^2, which was much larger than the 95.4 Å^2 side chain contact surface of the other hydrophobic residue, I56. The total interacting interface between the NSCaTE peptide and CaM was 1520.7 Å^2. The peptide and CaM-NT adopted more of an anti-parallel orientation in which the N-terminus of the peptide was close to the C-terminus of CaM-NT. As not all intermolecular NOEs could be confidently assigned (shown in

Table 2 | Statistics for the Ca^{2+}-CaM/Ca_v1.2NT NSCaTE peptide structural ensemble[a].

	CaM_{NT}/ peptide complex	CaM_{CT}[b]
DISTANCE RESTRAINTS		
Total	1345	886
Sequential	733	503
Medium range	358	188
Long range	254	195
Intermolecular	37	N/A
Residual dipolar coupling restraints	70	69
Dihedral angle restraints	140	128
Hydrogen bonds	84	46
COORDINATE PRECISION (Å)		
Backbone	0.47 ± 0.10	0.45 ± 0.08
All heavy atoms	0.90 ± 0.12	0.98 ± 0.06
RMS DEVIATIONS FROM EXPERIMENTAL DATA		
Average distance restraint violation (Å)	0.0169 ± 0.0011	0.0101 ± 0.0009
Average dihedral angle restraint violation (degree)	0.7595 ± 0.0714	0.5460 ± 0.1449
RAMACHANDRAN STATISTICS (%)		
Most favored	90.0	90.9
Additionally allowed	9.9	9.1
Generously allowed	0.1	0.0
Disallowed	0.0	0.0

[a] *PDB ID: NT, 2LQC; CT, 2LQP. BMRB access code: NT, 18302; CT, 18323.*

[b] *In the presence of the NSCaTE peptide.*

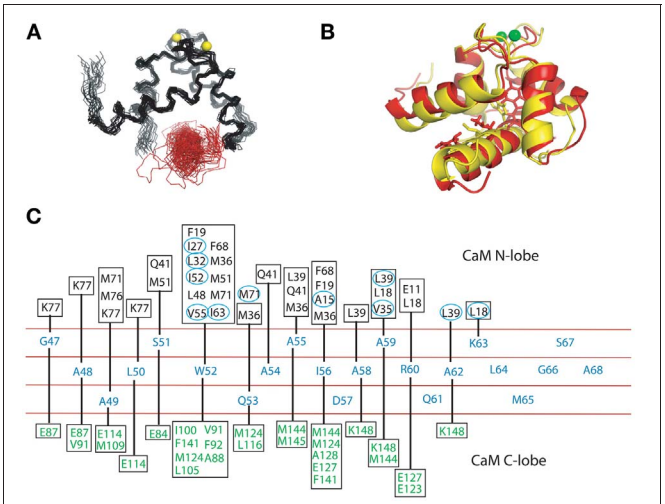

FIGURE 6 | (A). Structure ensemble of the complex of the Ca^{2+}/CaM NT and the NSCaTE motif (generated by HADDOCK 2.0). The colors used here are similar to those in **Figure 4A**. **(B)** Ribbon representation of the overlap of the calculated (*red*) and HADDOCK-generated (*yellow*) structures. **(C)** Contact residues between the CaM lobe (NT, calculated by CYANA 2.1, or CT, generated by HADDOCK 2.0) and the NSCaTE peptide (<4 Å). The peptide is shown in the middle, and each residue is listed along the sequence. The contact residues from the N-lobe of CaM are listed above the peptide diagram. The residues with the actual NOE restraints used in the calculations are highlighted with *blue circles*. The contact residues from the C-lobe of CaM are listed below the peptide diagram.

Figure 6C), we compared the HADDOCK-generated structures to the NOE-based complex structures. When we overlaid the CaM region of the 20 Haddock complex structures, the peptide backbone structures were not as convergent (RMSD = 2.34 ± 1.08 Å) as we found for the NOE-based structure due to the relatively wide hydrophobic interacting interface on Ca^{2+}-CaM N-lobe. Additionally, in the ribbon representation (**Figure 6B**), we observed a different arrangement of the W52 aromatic ring. However, the overall orientation of the peptide backbone relative to CaM-NT was not significantly different in the two methods. This consistency validated the NOE-based structure. Interestingly, the peptide complexed with the C-lobe adopted a parallel orientation. Compared with the CaM/GAD complex, which also exhibits 2:1 stoichiometry, the orientation between the C-lobe of CaM and the peptide was reversed. This difference may be a result of the position of the tryptophan residue in the peptide sequence.

The structure of the C-lobe complex structure generated by HADDOCK had a much higher peptide backbone RMSD (**Figure 5D**) than the N-lobe structure (**Figure 5A**). While the backbone of the Ca^{2+}-CaM C-lobe in the complex is well defined, the position of the peptide is not well defined, which gives rise to the relatively high numbers. In addition, the area near the anchoring residue W52 had low RMSDs, while the C-terminal part of the peptide had diverse orientations. This finding was consistent with the lower peptide affinity observed for the CaM C-lobe. To better understand the preferential peptide binding of the CaM NT, we compared the two complex structures. The average total binding interface area for the C-lobe complex was 1440.0 Å, which is smaller than the interface area we found for the N-lobe. The buried surface for W52 in this complex was 194.4 Å, which was also somewhat smaller than the corresponding value in the N-lobe. However, the contribution from the sidechain of the I56 residue was similar to that in the N-lobe. In both complexes, the tip of the sidechain of the R60 was in close proximity to negatively charged residues (E11 of the N-lobe and E123/127 of the C-lobe). Possible salt bridges between these residues could provide extra anchoring contacts.

It is always interesting to compare different CaM-binding peptides, as many different complex structures have been found (Ishida and Vogel, 2006). The NSCaTE is the first peptide known to bind preferentially to the Ca^{2+}/CaM N-lobe. The *Nicotiana tabacum* MAPK phosphatase (NtMKP1) peptide from *N. tabacum* MAPK-phosphatase is one of the few naturally occurring CaM-binding peptides that can bind only to the Ca^{2+}/CaM C-lobe (Ishida et al., 2009). However, although both the NSCaTE and NtMKP1 peptides could bind to the CaM C-lobe, the NtMKP1 peptide bound much more tightly and in an opposite orientation than the NSCaTE peptide (**Figure 7E**). By comparing the sequences of both peptides, we detected many more positively charged residues at the N-terminus of the NtMKP1 peptide, along with two hydrophobic "double-anchoring" residues (W3620 and L3623) (Ishida et al., 2009). There were no positive charges close

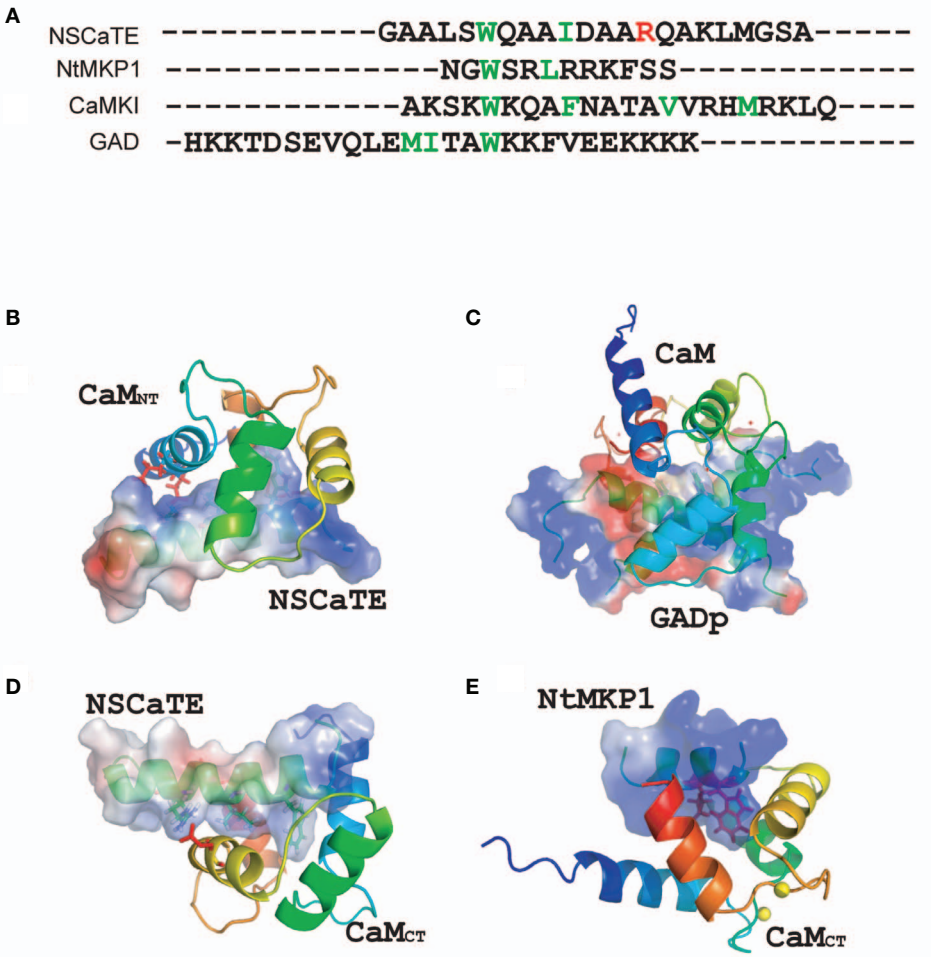

FIGURE 7 | (A) Sequence comparisons of different calmodulin-binding motifs (NSCaTE, NtMKP1, CaMKI, and GAD). **(B)** Complex structure representations of the NSCaTE peptide and Ca^{2+}-CaM NT. **(C)** Complex structure representations of the NSCaTE peptide and Ca^{2+}-CaM CT. **(D)** Complex structure representations of the GAD peptide and Ca^{2+}-CaM (PDB ID: 1NWD). **(E)** Complex structure representations of the NtMKP1 peptide and Ca^{2+}-CaM CT (PDB ID: 2KN2).

to the main anchoring residue, W52, of the NSCaTE peptide. The positively charged residue R60 of NSCaTE was close to the negatively charged residue E123 on the third helix of the CaM C-lobe (**Figure 7C**). Similar to the 2:1 stoichiometry of the NSCaTE peptide to Ca^{2+}/CaM that we found in this study, two carboxy-terminal peptides of plant glutamate decarboxylase (GAD) could interact with the two lobes of Ca^{2+}/CaM simultaneously (Yap et al., 2003). These two GAD peptides were anti-parallel to each other and formed an X shape in the complex, which could not be identified in our complex. As noted in the paper by Yap et al., the high percentage of negative charges in the GAD peptide could pair with the basic residues, and the electrostatic interactions between charged residues were critical for creating the dimer interface. This result was confirmed by examining the potential surface of the GAD peptide dimer in the complex (**Figure 7D**). The N/C terminal positively charged residues of one peptide could approach the C/N terminal negatively charged residues of the second GAD peptide in the bound butterfly-shaped peptide dimer. A continuous positively charged patch was formed on each side of the peptide dimer and facilitated the binding with each CaM lobe. However, we found only one positively charged residue (R60) and one negatively charged residue (D57) in the NSCaTE peptide, which would not provide enough electrostatic interactions for a peptide dimer similar to GAD in the complex of CaM with NSCaTE. The lack of multiple anchoring hydrophobic and positively charged residues combined with the short length is the main reasons for the unique binding character of the NSCaTE peptide.

DISCUSSION

As one of the main sources for calcium influx in a cell, voltage-gated calcium channels play a variety of important roles in neuron transduction, in smooth and cardiac muscle contraction and in gene transcription. Each type of calcium channel has its own build-in control mechanisms, depending on the presence of various additional channel subunits ($Ca_V\beta$) (McGee et al., 2004; Takahashi et al., 2005; Grueter et al., 2006), regulatory calcium binding proteins and other molecules (Peterson et al., 1999;

DeMaria et al., 2001; Fallon et al., 2005). Among the four types of voltage-gated calcium channel (L-, P/Q-, N-, and R-types), the NSCaTE motif was found only in two subtypes ($Ca_v1.2$ and $Ca_v1.3$) of the L-type VGCCs, which is clearly evident from the alignment of the N-terminal sequences of the four L-type channels (**Figure 1B**). The C-terminal portion of the N-terminal cytoplasmic domains of the L-type channels has nearly identical sequences, but their N-terminal ends are very different. Each of these four types of channels has a unique and preferred expression pattern. $Ca_v1.1$ is mainly expressed in skeletal muscle, and its full function relies on ryanodine receptors. $Ca_v1.4$ is mainly located in neurons, especially in the retina. Both $Ca_v1.1$ and 1.4 have a relatively weak CDI and play important functions in the dark-adapted light sense (Zhou et al., 2004). Compared with $Ca_v1.1/1.4$, $Ca_v1.2$ and 1.3 exhibit much stronger CDI, consistent with their functions in cardiac muscle-related EC coupling, which requires rapid and regular muscle contraction and relaxation. Recently, the importance of Ca_v1 L-type channels in the nervous system has been summarized by Calin-Jageman and Lee (2008). Ca_v1 channels are widely expressed in pre- and postsynaptic region of neuron in the cerebral cortex, hippocampus and retina. Through the regulation of the neuronal Ca^{2+} signal, Ca_v1 channels can trigger electrical and signaling cascades of various activities, such as synaptic plasticity, gene expression, and long-term memory. CDI and CDF are the main mechanisms of the VGCCs-related regulation. It has been shown that the binding of the C-terminal IQ-motif to CaM provides the main basis for the self-control of the VGCC through the mechanisms of CDI and CDF. The CDI and CDF effects, however, do not only depend on the sequences and CaM-binding patterns of the IQ-motif in the C-terminal cytoplasmic region of the channels. These processes are also finely tuned by other interaction partners, including the amino terminal cytoplasmic region of the channel. The whole N-terminal sequence was re-examined by the Lee group (Oz et al., 2011), and they found that the initial sequence is critical for the voltage-dependent inactivation (VDI) kinetics of both long and short isoforms. Interestingly, they also identified a new motif at the C-terminal end of N-terminal cytoplasmic domain of the channel. This new motif cannot bind CaM, but it can bind to CaBP1 in either the calcium- or apo-form *in vivo*. Considering the high conservation of this motif in L-type channels, a consistent function for this region can be expected.

In our *in vitro* experiments with NSCaTE, a 1:2 stoichiometric ratio was identified with various techniques. However, CaM is considered as an associated channel subunit currently in most research, with a stoichiometry of 1:1. Although channel dimerization has also been observed, more evidence is still needed to support such a model. If the model presented in this study is correct, this unique 1:2 CaM to NSCaTE peptide ratio could affect channel dimerization in the presence of exogenousCaM. In addition, we found that the NSCaTE motif spontaneously adopted a helical conformation in aqueous solution, which was observed by both NMR and CD spectroscopy. This conformation is different from the conformation observed in most CaM-binding domain peptides, where a transition from the random coil of the unbound state to the helical conformation of the bound state is required for most peptides. The high alanine content of NSCaTE is a likely reason for the naturally occurring helical conformation. Considering the relative weak-binding affinity of this motif toCaM, the presence of the preformed helical conformation is consistent with its role as a minor CDI regulator in special channels, as smaller entropy–enthalpy changes would occur due to the lack of a drastic conformational change.

Another interesting property of the NSCaTE motif is that the motif bound more tightly to the Ca^{2+}-CaM N-lobe than to the C-terminal lobe of Ca^{2+}-CaM. This binding preference is different from that of most CaM-binding peptides, especially when compared with the IQ-motif from the C-terminal cytoplasmic domain of the same calcium channel. From the crystal structure of the CaM/$Ca_v1.2$ IQ-motif complex (Fallon et al., 2005; Van Petegem et al., 2005), we already have a deeper understanding of the fundamental channel self-control mechanism in L-type channels, as apo-CaM can also bind to the IQ region, and thereby it can provide a quick response to the elevation of the local calcium ion concentrations close to the channel pore. Once bound to calcium, CaM binds to the IQ-motif in an unique parallel mode due to the higher positive charge in the C-terminal half of the IQ-peptide. This special binding mode allows the Ca^{2+}-CaM C-lobe to dominate the regulation of CDI. A single mutation (IQ/AQ) or double mutation (IQ/AA) will abolish CDI and alleviate an apparent CDF that is severely blocked in the wild-type protein. Van Petegem et al. (2005) proposed a possible *in vivo* model where the Ca^{2+}-CaM C-lobe is anchored to the C-terminal IQ-motif, but other regions of the channel can compete for the N-lobe of Ca^{2+}-CaM and finely tune the CDI dominated by the C-terminal IQ-motif. This model provides a reasonable explanation for the real function of NSCaTE. Although a trial pull-down assay failed to provide *in vitro* evidence for this model, *in vivo* FRET experiments revealed a FRET ratio (FR) larger than one and a meaningful dissociation constant of approximately 20–30 uM in both chimeric and wild-type constructs (Dick et al., 2008). The removal of the critical tryptophan residues of NSCaTE will

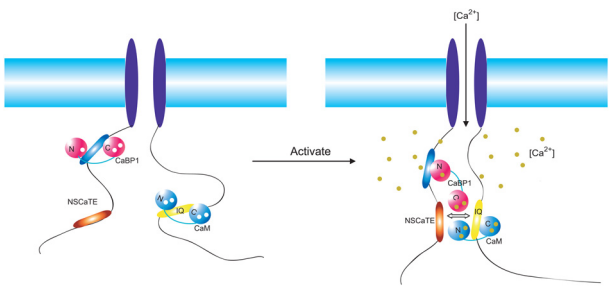

FIGURE 8 | Overview of the regulatory network of the $Ca_v1.2$ (α_{1c}). Two motifs (NSCaTE, Ca^{2+}/CaM specific, *red*; CaBP1 binding motif, *blue*) in the N-terminus and the IQ motif (*yellow*) in the C-terminus are represented by *oval bars*. The regulatory calcium binding proteins CaBP1 and CaM are shown in *red and blue*, respectively. These proteins are bound to the N-terminus of the channel and the IQ motif in the resting state. Upon membrane depolarization and channel opening, both CaM and CaBP1 bind calcium ions and interact with different motifs. The cross-interference among these binding partners is critical for the distinct regulatory functions of each type of channel.

abolish any interactions between the N-/C-terminal regions bridged by CaM and the corresponding CDI. The mutations of the other two important residues within the motif (Ile and Arg) did modulate its regulatory action by weaker binding and attenuated CDI. The correlation between the NSCaTE motif affinity to CaM and the CDI effect has been systematically investigated by alanine scanning along the motif sequence, and the concept of the local Ca^{2+} selectivity for this motif has been strengthened in the work done by Tadross et al. (2008).

Other calcium binding proteins, known as CaBPs, are often coexpressed with VGCCs in addition to CaM in neurons, especially those in the presynaptic density. One isoform, CaBP1, can alleviate the CDI caused by CaM and induce CDF. Zhou et al. demonstrated that the N-terminus of $Ca_v1.2$ is critical for CaBP1 function and that the removal of the N-terminus will completely abolish the effect of CaBP1 (Zhou et al., 2004, 2005). In addition, another sequence, which does not overlap with the N-terminus of α_{1c}, has been identified as a CaBP1-specific binding motif. However, this identification cannot completely exclude the possibility of an interaction between CaBP1 and the NSCaTE region, due to the high amino acid sequence similarity between CaM and the C-terminal lobe of CaBP1. We, therefore, also investigated the binding of CaBP1 to the NSCaTE region (See **Figure A5**). Our data indicate that the calcium-bound CaBP1 interacts only very weakly with the NSCaTE motif through its C-lobe. A recently solved CaBP1 X-ray structure (Findeisen and Minor, 2010) can help us understand the possible role of NSCaTE in the complicated CDI regulatory network involving CaM, CaBP1, IQ, and the N-terminus (containing NTI, NSCaTE, and the CaBP1 binding motif) of $Ca_v1.2$ and $Ca_v1.3$. Extensive mutation and domain swap studies have shown that the N-lobe and residue E94 in the central linker are critical for CaBP1-inhibited CDI and induced CDF. However, we also notice that Ca^{2+}-CaBP1 can bind to the IQ-motif, and unlike CaM, the binding site is the same for the N- and C-lobes of CaBP1. In addition, the C-lobe of Ca^{2+}-CaBP1 cannot compete with the C-lobe of Ca^{2+}-CaM for the IQ motif binding, and mutating either or both EF-hands of C-lobe CaBP1 will partially recover inhibited CDI (Findeisen and Minor, 2010).

In conclusion, although the interactions between the IQ-motif in the C-terminal cytoplasmic region of the channels and CaM seem to dominate the regulation of the voltage-gated calcium channel, other parts of the channels and channel-binding proteins can further fine tune each channel, to allow them to carry out their unique function in various cells and tissues. A simplified model is presented in **Figure 8** to describe this complicated regulatory network for $Ca_v1.2$ and $Ca_v1.3$ at different calcium binding stages. In the resting state, apo-CaM is bound near the IQ-motif region, and apo-CaBP1 interacts with its N-terminal binding motif. Once the channel opens due to a change in the membrane potential, the calcium flows into the cytoplasm and initially saturates CaM and CaBP1 that are located near the channel pore. Ca^{2+}-CaM then binds to the IQ-motif with a parallel domain arrangement and induces CDI/CDF. The N-lobe of Ca^{2+}-CaM can also bind to the NSCaTE motif and accelerate the closing of the channel. In doing so, Ca^{2+}-CaM acts almost like an "adaptor" protein bridging between the two cytoplasmic domains of the channel [for discussions see Yamniuk et al. (2007)]. Simultaneously, the N-lobe of CaBP1 continues to interact with its motif in the N-terminal, while its C-lobe adopts an open conformation. The C-lobe of Ca^{2+}-CaBP1 can also interact with NSCaTE and compete weakly with the N-lobe of Ca^{2+}-CaM, which in turn may inhibit the acceleration of CDI. However, this simplified model does not include other regulatory partners, such as the I–II loop of the α_{1c} subunit of the channel, the $Ca_v\beta$-subunit and regulation through CaMKII. More binding studies and structural details, therefore, are needed to deconstruct this complicated regulatory network.

ACKNOWLEDGMENTS

This project was funded by an operating grant from the Canadian Institutes of Health Research. Hans J. Vogel is the holder of a Scientist award from the Alberta Heritage Foundation for Medical Research.

REFERENCES

Andre, I., and Linse, S. (2002). Measurement of Ca^{2+}-binding constants of proteins and presentation of the Ca Ligator software. *Anal. Biochem.* 305, 195–205.

Benmocha, A., Almagor, L., Oz, S., Hirsch, J. A., and Dascal, N. (2009). Characterization of the calmodulin-binding site in the N terminus of $Ca_v1.2$. *Channels (Austin)* 3, 337–342.

Buraei, Z., and Yang, J. (2010). The β subunit of voltage-gated Ca^{2+} channels. *Physiol. Rev.* 90, 1461–1506.

Calin-Jageman, I., and Lee, A. (2008). Ca_v1 L-type Ca^{2+}channel signaling complexes in neurons. *J. Neurochem.* 105, 573–583.

Cornilescu, G., Delaglio, F., and Bax, A. (1999). Protein backbone angle restraints from searching a database for chemical shift and sequence homology. *J. Biomol. NMR* 13, 289–302.

DeMaria, C. D., Soong, T. W., Alseikhan, B. A., Alvania, R. S., and Yue, D. T. (2001). Calmodulin bifurcates the local Ca^{2+} signal that modulates P/Q-type Ca^{2+} channels. *Nature* 411, 484–489.

Dick, I. E., Tadross, M. R., Liang, H., Tay, L. H., Yang, W., and Yue, D. T. (2008). A modular switch for spatial Ca^{2+} selectivity in the calmodulin regulation of Ca_v channels. *Nature* 451, 830–834.

Dominguez, C., Boelens, R., and Bonvin, A. M. J. J. (2003). HADDOCK: a protein-protein docking approach based on biochemical or biophysical information. *J. Am. Chem. Soc.* 125, 1731–1737.

Dunlap, K. (2007). Calcium channels are models of self-control. *J. Gen. Physiol.* 129, 379–383.

Fallon, J. L., Halling, D. B., Hamilton, S. L., and Quiocho, F. A. (2005). Structure of calmodulin bound to the hydrophobic IQ domain of the cardiac $Ca_v1.2$ calcium channel. *Structure* 13, 1881–1886.

Findeisen, F., and Minor, D. L. Jr. (2010). Structural basis for the differential effects of CaBP1 and calmodulin on $Ca_v1.2$ calcium-dependent inactivation. *Structure* 18, 1617–1631.

Gifford, J. L., Ishida, H., and Vogel, H. J. (2011). Fast methionine-based solution structure determination of calcium calmodulin complexes. *J. Biomol. NMR* 50, 71–81.

Gifford, J. L., Walsh, M. P., and Vogel, H. J. (2007). Structures and metal-ion-binding properties of the Ca^{2+}-binding helix-loop-helix EF-hand motifs. *Biochem. J.* 405, 199–221.

Grueter, C. E., Abiria, S. A., Dzhura, I., Wu, Y., Ham, A. J., Mohler, P. J., Anderson, M. E., and Colbran, R. J. (2006). L-type Ca^{2+} channel facilitation mediated by phosphorylation of the beta subunit by CaMKII. *Mol. Cell* 23, 641–650.

Guntert, P. (2004). Automated NMR structure calculation with CYANA. *Methods Mol. Biol.* 278, 353–378.

Houdusse, A., Gaucher, J. F., Krementsova, E., Mui, S., Trybus, K. M., and Cohen, C. (2006). Crystal structure of apo-calmodulin bound

to the first two IQ motifs of myosin V reveals essential recognition features. *Proc. Natl. Acad. Sci. U.S.A.* 103, 19326–19331.

Hudmon, A., Schulman, H., Kim, J., Maltez, J. M., Tsien, R.W., and Pitt, G. S. (2005). CaMKII tethers to L-type Ca^{2+} channels, establishing a local and dedicated integrator of Ca^{2+} signals for facilitation. *J. Cell Biol.* 171, 537–547.

Ishida, H., Rainaldi, M., and Vogel, H. J. (2009). Structural studies of soybean calmodulin isoform 4 bound to the calmodulin-binding domain of tobacco mitogen-activated protein kinase phosphatase-1 provide insights into a sequential target binding mode. *J. Biol. Chem.* 284, 28292–28305.

Ishida, H., and Vogel, H. J. (2006). Protein-peptide interaction studies demonstrate the versatility of calmodulin target protein binding. *Protein Pept. Lett.* 13, 455–465.

Kim, E. Y., Rumpf, C. H., Fujiwara, Y., Cooley, E. S., Van Petegem, F., and Minor, D. L. Jr. (2008). Structures of Ca_v2 Ca^{2+}/CaM-IQ domain complexes reveal binding modes that underlie calcium-dependent inactivation and facilitation. *Structure* 16, 1455–1467.

Kim, J., Ghosh, S., Nunziato, D. A., and Pitt, G. S. (2004). Identification of the components controlling inactivation of voltage-gated Ca^{2+} channels. *Neuron* 41, 745–754.

McGee, A. W., Nunziato, D. A., Maltez, J. M., Prehoda, K. E., Pitt, G. S., and Bredt, D. S. (2004). Calcium channel function regulated by the SH3-GK module in beta subunits. *Neuron* 42, 89–99.

Mori, M. X., Vander Kooi, C. W., Leahy, D. J., and Yue, D. T. (2008). Crystal structure of the Ca_v2 IQ domain in complex with Ca^{2+}/calmodulin: high-resolution mechanistic implications for channel regulation by Ca^{2+}. *Structure* 16, 607–620.

Orsale, M., Melino, S., Contessa, G. M., Torre, V., Andreotti, G., Motta, A., Paci, M., Desideri, A., and Cicero, D. O. (2003). Two distinct calcium-calmodulin interactions with N-terminal regions of the olfactory and rod cyclic nucleotide-gated channels characterized by NMR spectroscopy. *FEBS Lett.* 548, 11–16.

Oz, S., Tsemakhovich, V., Christel, C. J., Lee, A., and Dascal, N. (2011). CaBP1 regulates voltage-dependent inactivation and activation of $Ca_v1.2$ (L-type) calcium channels. *J. Biol. Chem.* 286, 13945–13953.

Pace, C. N., and Scholtz, J. M. (1998). A helix propensity scale based on experimental studies of peptides and proteins. *Biophys. J.* 75, 422–427.

Panavas, T., Sanders, C., and Butt, T. R. (2009). SUMO fusion technology for enhanced protein production in prokaryotic and eukaryotic expression systems. *Methods Mol. Biol.* 497, 303–317.

Peterson, B. Z., DeMaria, C. D., Adelman, J. P., and Yue, D. T. (1999). Calmodulin is the Ca^{2+} sensor for Ca^{2+}-dependent inactivation of L-type calcium channels. *Neuron* 22, 549–558.

Pitt, G. S., Zuhlke, R. D., Hudmon, A., Schulman, H., Reuter, H., and Tsien, R. W. (2001). Molecular basis of calmodulin tethering and Ca^{2+}-dependent inactivation of L-type Ca^{2+} channels. *J. Biol. Chem.* 276, 30794–30802.

Qin, N., Olcese, R., Bransby, M., Lin, T., and Birnbaumer, L. (1999). Ca^{2+}-induced inhibition of the cardiac Ca^{2+} channel depends on calmodulin. *Proc. Natl. Acad. Sci. U.S.A.* 96, 2435–2438.

Queiroz, J. A., Tomaz, C. T., and Cabral, J. M. (2001). Hydrophobic interaction chromatography of proteins. *J. Biotechnol.* 87, 143–159.

Rainaldi, M., Yamniuk, A. P., Murase, T., and Vogel, H. J. (2007). Calcium-dependent and -independent binding of soybean calmodulin isoforms to the calmodulin binding domain of tobacco MAPK phosphatase-1. *J. Biol. Chem.* 282, 6031–6042.

Schwieters, C. D., Kuszewski, J. J., Tjandra, N., and Clore, G. M. (2003). The Xplor-NIH NMR molecular structure determination package. *J. Magn. Reson.* 160, 65–73.

Tadross, M. R., Dick, I. E., and Yue, D. T. (2008). Mechanism of local and global Ca^{2+} sensing by calmodulin in complex with a Ca^{2+} channel. *Cell* 133, 1228–1240.

Takahashi, S. X., Miriyala, J., Tay, L. H., Yue, D. T., and Colecraft, H. M. (2005). A $Ca_v\beta$ SH_3/guanylate kinase domain interaction regulates multiple properties of voltage-gated Ca^{2+} channels. *J. Gen. Physiol.* 126, 365–377.

Thulin, E., Andersson, A., Drakenberg, T., Forsen, S., and Vogel, H. J. (1984). Metal ion and drug binding to proteolytic fragments of calmodulin: proteolytic, cadmium-113, and proton nuclear magnetic resonance studies. *Biochemistry* 23, 1862–1870.

Van Lierop, J. E., Wilson, D. P., Davis, J. P., Tikunova, S., Sutherland, C., Walsh, M. P., and Johnson, J. D. (2002). Activation of smooth muscle myosin light chain kinase by calmodulin. Role of LYS^{30} and GLY^{40}. *J. Biol. Chem.* 277, 6550–6558.

Van Petegem, F., Chatelain, F. C., and Minor, D. L. Jr. (2005). Insights into voltage-gated calcium channel regulation from the structure of the $Ca_v1.2$ IQ domain-Ca^{2+}/calmodulin complex. *Nat. Struct. Mol. Biol.* 12, 1108–1115.

Yamniuk, A. P., Rainaldi, M., and Vogel, H. J. (2007). Calmodulin has the potential to function as a Ca-dependent adaptor protein. *Plant Signal. Behav.* 2, 354–357.

Yamniuk, A. P., and Vogel, H. J. (2004). Calmodulin's flexibility allows for promiscuity in its interactions with target proteins and peptides. *Mol. Biotechnol.* 27, 33–57.

Yap, K. L., Yuan, T., Mal, T. K., Vogel, H. J., and Ikura, M. (2003). Structural basis for simultaneous binding of two carboxy-terminal peptides of plant glutamate decarboxylase to calmodulin. *J. Mol. Biol.* 328, 193–204.

Yuan, W., and Bers, D. M. (1994). Ca-dependent facilitation of cardiac Ca current is due to Ca-calmodulin-dependent protein kinase. *Am. J. Physiol.* 267, H982–H993.

Yuan, T., and Vogel, H. J. (1998). Calcium-calmodulin-induced dimerization of the carboxyl-terminal domain from petunia glutamate decarboxylase: a novel calmodulin-peptide interaction motif. *J. Biol. Chem.* 273, 30328–30335.

Zhang, M., Yuan, T., and Vogel, H. J. (1993). A peptide analog of the calmodulin-binding domain of myosin light chain kinase adopts an α-helical structure in aqueous trifluoroethanol. *Protein Sci.* 2, 1931–1937.

Zhou, H., Kim, S. A., Kirk, E. A., Tippens, A. L., Sun, H., Haeseleer, F., and Lee, A. (2004). Ca^{2+}-binding protein-1 facilitates and forms a postsynaptic complex with $Ca_v1.2$ (L-type) Ca^{2+} channels. *J. Neurosci.* 24, 4698–4708.

Zhou, H., Yu, K., McCoy, K. L., and Lee, A. (2005). Molecular mechanism for divergent regulation of $Ca_v1.2$ Ca^{2+} channels by calmodulin and Ca^{2+}-binding protein-1. *J. Biol. Chem.* 280, 29612–29619.

Zuhlke, R. D., Pitt, G. S., Deisseroth, K., Tsien, R. W., and Reuter, H. (1999). Calmodulin supports both inactivation and facilitation of L-type calcium channels. *Nature* 399, 159–162.

Zuhlke, R. D., Pitt, G. S., Tsien, R. W., and Reuter, H. (2000). Ca^{2+}-sensitive inactivation and facilitation of L-type Ca^{2+} channels both depend on specific amino acid residues in a consensus calmodulin-binding motif in the α_{1c} subunit. *J. Biol. Chem.* 275, 21121–21129.

Zuhlke, R. D., and Reuter, H. (1998). Ca^{2+}-sensitive inactivation of L-type Ca^{2+} channels depends on multiple cytoplasmic amino acid sequences of the α_{1c} subunit. *Proc. Natl. Acad. Sci. U.S.A.* 95, 3287–3294.

Conflict of Interest Statement: The authors declare that the research was conducted in the absence of any commercial or financial relationships that could be construed as a potential conflict of interest.

Received: 01 February 2012; paper pending published: 19 February 2012; accepted: 13 March 2012; published online: 12 April 2012.

Citation: Liu Z and Vogel HJ (2012) Structural basis for the regulation of L-type voltage-gated calcium channels: interactions between the N-terminal cytoplasmic domain and Ca^{2+}-calmodulin. Front. Mol. Neurosci. 5:38. doi: 10.3389/fnmol.2012.00038

APPENDIX

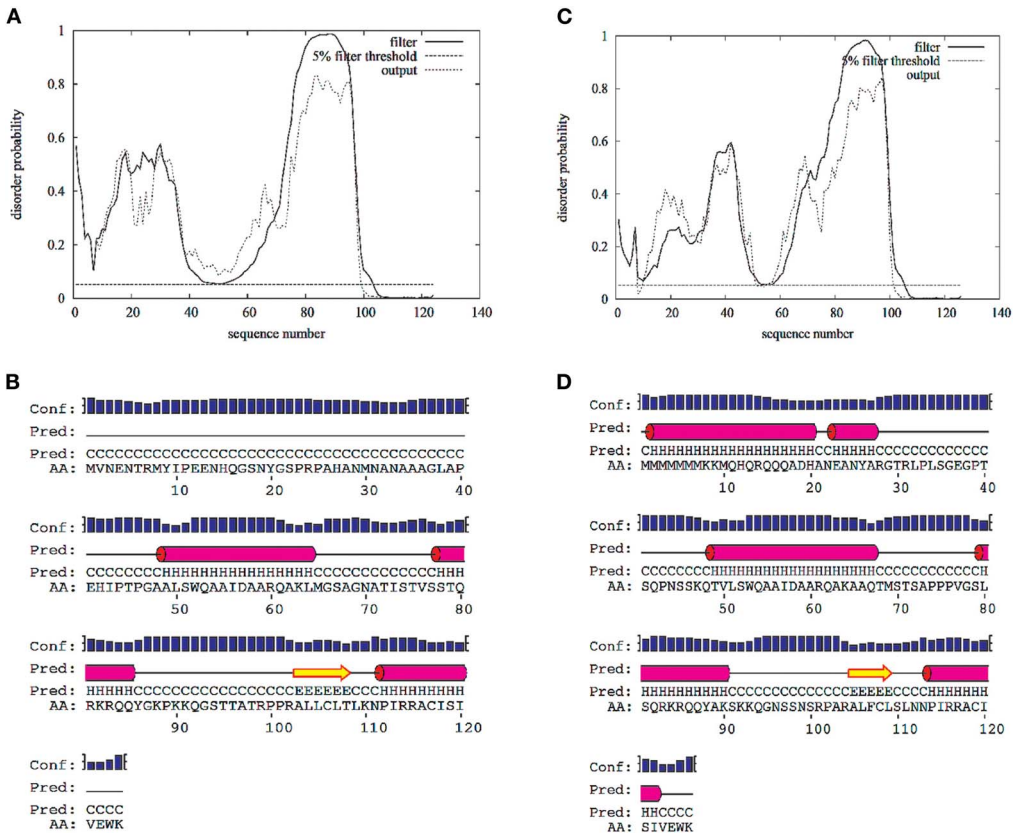

FIGURE A1 | Disorder and secondary structure predictions for the N-terminal cytoplasmic domain of the L-type voltage-gated calcium channel $Ca_v1.2$ (1–124 AAs)(A,B) and $Ca_v1.3$ (1–126) (C,D). Predictions were calculated with the web-server DISOPRED2 (http://bioinf.cs.ucl.ac.uk/disopred/) and PSIPRED (http://bioinf.cs.ucl.ac.uk/psipred).

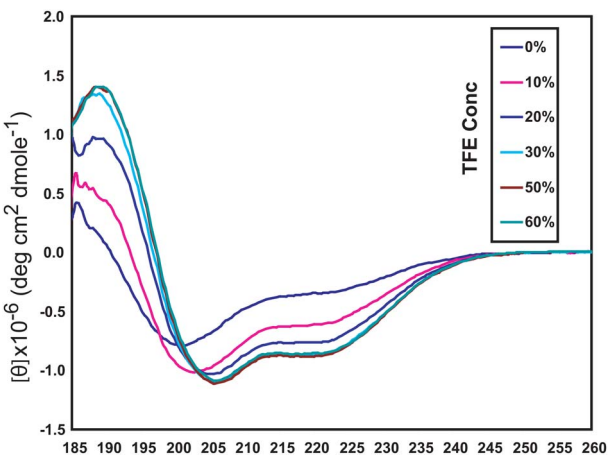

FIGURE A2 | Circular dichroism (CD) spectroscopy of the long NSCaTE motif in aqueous solution with various concentrations of TFE (trifluoroethanol).

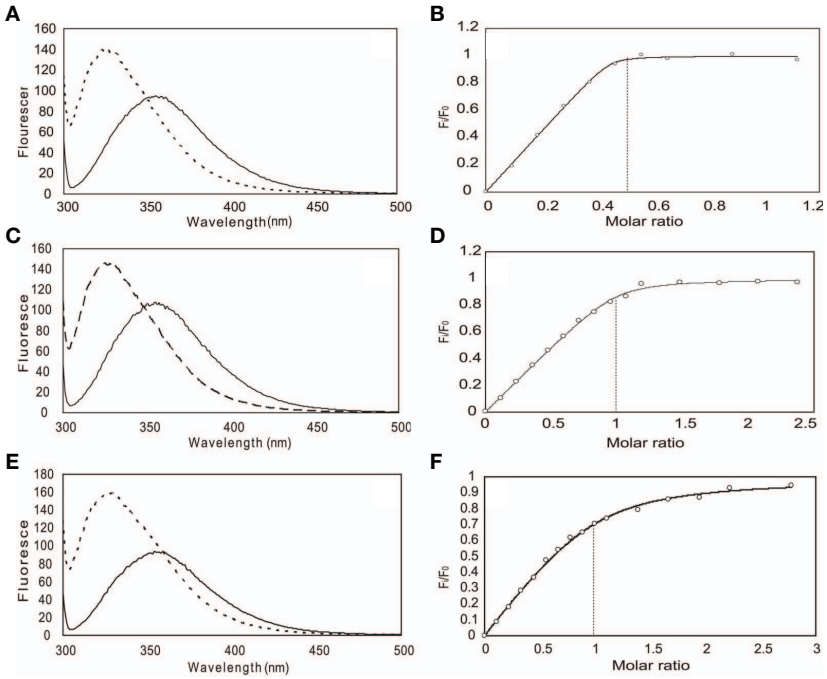

FIGURE A3 | Steady-state fluorescence spectroscopy (left) and binding curves (right) obtained for the long NSCaTE peptide with CaM. (In panels A, C and E, the solid line is recorded without protein and the dotted line is after addition of protein). (A, B) Intact CaM, **(C, D)** N-lobe of CaM, **(E, F)** C-lobe of CaM.

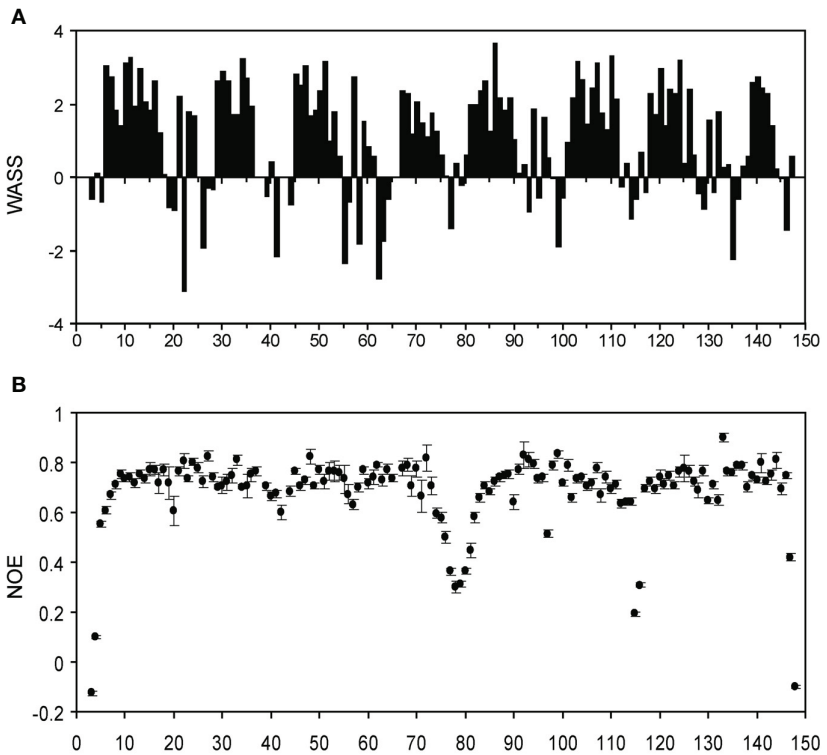

FIGURE A4 | (A) Weighted average secondary shifts (WASS) for the short NSCaTE bound state of intact Ca^{2+}/CaM. A total of 2.5 equivalents of unlabeled peptide was added to saturate the protein. **(B)** $\{^1H\}$-^{15}N NOE data for the short NSCaTE bound state of Ca^{2+}/CaM.

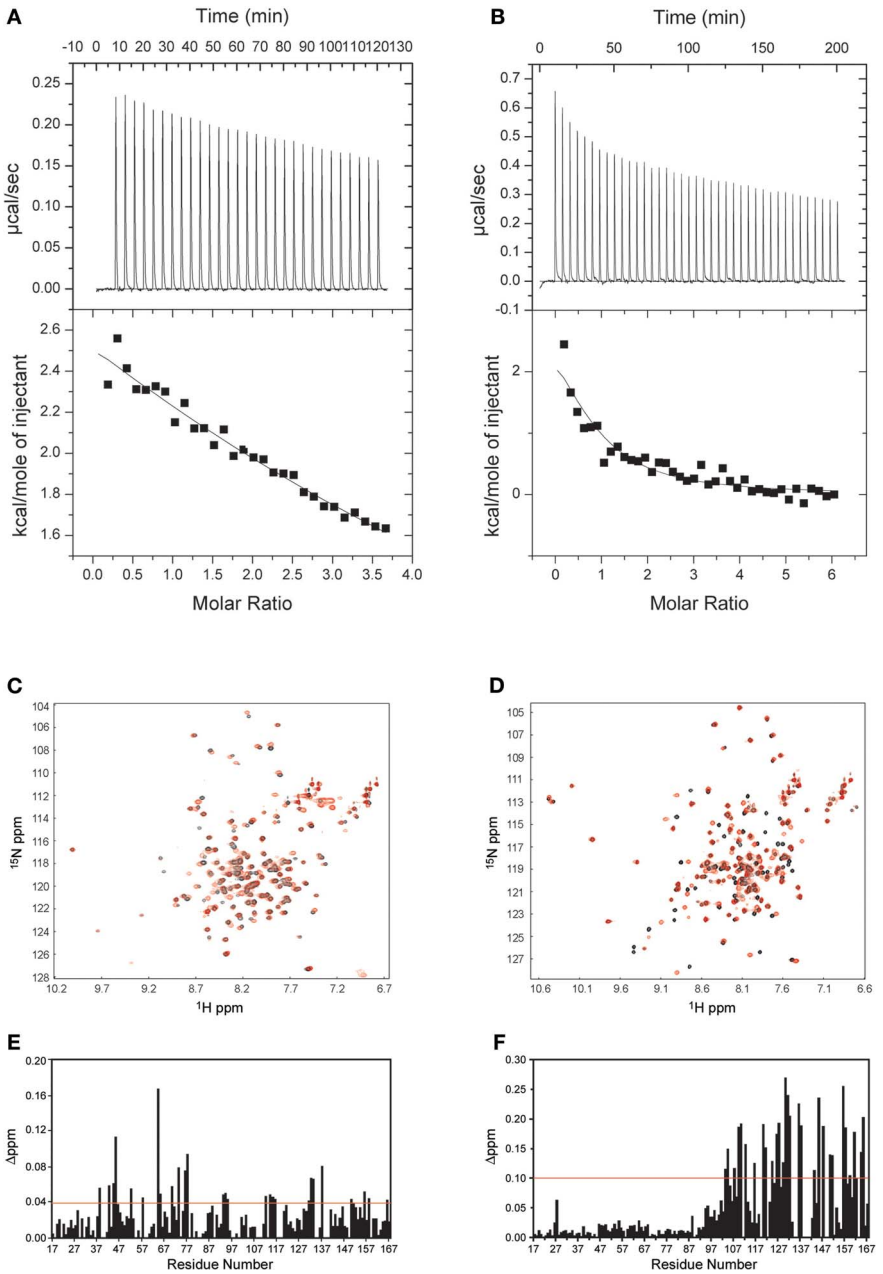

FIGURE A5 | Interactions between CaBP1 and the long NSCaTE motif. **(A,C,E)** Apo-CaBP1 with NSCaTE peptide: ITC **(A)**, ^{1}H–^{15}N HSQC **(C)** and chemical shift perturbation (E). **(B,D,F)** Ca^{2+}/CaBP1 with NSCaTE peptide: ITC **(B)**, ^{1}H–^{15}N HSQC **(D)** and chemical shift perturbation **(F)**. Please note that compared to Ca^{2+}-CaBP1, the binding of NSCaTE to apo-CaBP1 was extremely weak as indicated by the ITC and NMR data. The ITC data show that both binding events are exothermic.

frontiers in
MOLECULAR NEUROSCIENCE

ORIGINAL RESEARCH ARTICLE
published: 18 April 2012
doi: 10.3389/fnmol.2012.00053

NCS-1 associates with adenosine A_{2A} receptors and modulates receptor function

Gemma Navarro[1], Johannes Hradsky[2], Carmen Lluís[1], Vicent Casadó[1], Peter J. McCormick[1], Michael R. Kreutz[2] and Marina Mikhaylova[2]*

[1] Faculty of Biology, Centro de Investigación Biomédica en Red Sobre Enfermedades Neurodegenerativas and Department of Biochemistry and Molecular Biology, University of Barcelona, Barcelona, Spain
[2] Research Group "Neuroplasticity", Leibniz-Institute for Neurobiology, Magdeburg, Germany

Edited by:
Jose R. Naranjo, Centro Nacional de Biotecnologia/Consejo Superior de Investigaciones Cientificas, Spain

Reviewed by:
Joël Bockaert, Inserm, France
Karl H. Braunewell, Southern Research Institute, USA

***Correspondence:**
Marina Mikhaylova, Research Group "Neuroplasticity", Leibniz Institute for Neurobiology, Brenneckestr. 6, 39118 Magdeburg, Germany.
e-mail: mikhaylova@lin-magdeburg.de

Modulation of G protein-coupled receptor (GPCR) signaling by local changes in intracellular calcium concentration is an established function of Calmodulin (CaM) which is known to interact with many GPCRs. Less is known about the functional role of the closely related neuronal EF-hand Ca^{2+}-sensor proteins that frequently associate with CaM targets with different functional outcome. In the present study we aimed to investigate if a target of CaM—the A_{2A} adenosine receptor is able to associate with two other neuronal calcium binding proteins (nCaBPs), namely NCS-1 and caldendrin. Using bioluminescence resonance energy transfer (BRET) and co-immunoprecipitation experiments we show the existence of A_{2A}—NCS-1 complexes in living cells whereas caldendrin did not associate with A_{2A} receptors under the conditions tested. Interestingly, NCS-1 binding modulated downstream A_{2A} receptor intracellular signaling in a Ca^{2+}-dependent manner. Taken together this study provides further evidence that neuronal Ca^{2+}-sensor proteins play an important role in modulation of GPCR signaling.

Keywords: adenosine A_{2A} receptor, GPCRs, NCS-1, caldendrin, calmodulin, calcium signaling, BRET

INTRODUCTION

Adenosine receptors belong to the GPCR family and have been classified on the basis of their molecular, biochemical, and pharmacological properties in four subtypes that are broadly distributed among different tissues including brain. The adenosine A_{2A} receptor is a G_s coupled receptor (Kull et al., 2000; Vu, 2005) that modulates cAMP production mediated by adenylyl cyclase activation upon ligand binding. A_{2A} receptors are particularly abundant in the basal ganglia and exhibit a somato-dendritic localization in GABAergic enkephalinergic neurons of the striatum (Schiffmann et al., 2007). However, they can also be found in several other brain regions including the olfactory bulb and hippocampus (Sebastião and Ribeiro, 2009). The current understanding of the role of A_{2A} receptors in the brain emphasizes their ability to interact with GPCRs of other neuromodulatory or neurotransmitter systems, and to provide a fine tuning of neuronal activity (Sebastião and Ribeiro, 2009). A_{2A} receptors mostly exist as either homodimers or heteromers (Canals et al., 2004; Sebastião and Ribeiro, 2009). A_{2A} receptor activation facilitates opioid and CB_1 receptor signaling in the striatum (Carriba et al., 2007; Sebastião and Ribeiro, 2009) and heterodimerization with the metabotropic glutamate receptor mGluR5 has a synergistic effect at the level of adenylate cyclase and MAPK activation upon A_{2A} and mGluR5 receptor co-stimulation (Ferré et al., 2002; Nishi et al., 2005). The most studied receptor heteromer, however, is the heteromer of adenosine A_{2A} and dopamine D_2 receptor, where A_{2A} receptors counteract D_2 receptor activation (Ferré et al., 2008; Navarro et al., 2009).

We have previously reported the Ca^{2+}-mediated modulation of the quaternary structure and function of A_{2A}-D_2 receptor heteromers (Navarro et al., 2009). Calmodulin (CaM) transduces a local change in Ca^{2+} concentrations to the receptor heteromer function via direct binding to the carboxy terminus of the A_{2A} receptor in a A_{2A}-D_2 receptor heteromer, modulating thereby MAPK signaling upon agonist stimulation in a Ca^{2+}-dependent manner (Navarro et al., 2009). The fine-tuning of other GPCRs via Ca^{2+}/CaM interaction has been studied already in some detail (for review see Ferré et al., 2010; Mikhaylova et al., 2011). Interestingly, the third intracellular loop of many GPCRs is not only participating in binding of G proteins but also represents a motif that is predicted to bind CaM. Indeed CaM can interact in a Ca^{2+}-sensitive manner with dopamine D_2, μ opioid, muscarinergic, and other receptors (Ritter and Hall, 2009; Ferré et al., 2010). The functional consequences of the CaM interaction with GPCRs frequently include an attenuation of G protein coupling (Nickols et al., 2004; Ritter and Hall, 2009). Interaction of CaM with the carboxy-terminus has been demonstrated not only for the adenosine A_{2A} receptor but for metabotropic glutamate receptors (mGluR5 and mGluR7) as well (Minakami et al., 1997; Nakajima et al., 1999; Ferré et al., 2010). However, interaction and modulation of GPCRs signaling is not an exclusive feature of CaM. Other calcium binding proteins from the CaM superfamily have been shown to interact with GPCRs directly or can attenuate receptor desensitization via association with the particular G protein-coupled receptor kinases (GRKs/Kabbani et al., 2002; Komolov et al., 2009). One of the

classical examples is the interaction between the dopamine D_2 receptor and NCS-1 where binding of NCS-1 to the cytoplasmic tail of the D_2 receptor inhibits its phosphorylation and subsequent internalization after ligand binding (Kabbani et al., 2002). Therefore, it is conceivable that other calcium binding proteins from the CaM superfamily could also specifically interact with certain GPCRs. Evolutionary and historically the neuronal members of the CaM superfamily are divided into two large groups named neuronal calcium sensor proteins (NCS) and neuronal Calcium Binding proteins (nCaBPs/Mikhaylova et al., 2011). Both groups resemble the structure of their common ancestor (CaM) with four EF-hand Ca^{2+}-binding motifs. However, not all EF-hands are able to bind Ca^{2+} ions although they still might be involved in protein-protein interactions. In the current study we aimed to investigate whether one of the most abundant and widely distributed members of the NCS group—NCS-1 (Burgoyne, 2007; Mikhaylova et al., 2011) and the founding member of the nCaBP group—caldendrin (Seidenbecher et al., 1998) are able to associate with the adenosine A_{2A} receptor. All three proteins have overlap in their expression profiles and can be found in the same brain regions and the same type of neurons (Sebastião and Ribeiro, 1996; Martone et al., 1999; Laube et al., 2002; Bernstein et al., 2003; Rosin et al., 2003). To address this issue we implemented bioluminescence resonance energy transfer (BRET) and co-immunoprecipitation approaches and checked the functional role of the interaction by A_{2A} receptor agonist induced MAPK and AKT signaling in co-transfected HEK293 cells.

MATERIALS AND METHODS

cDNA CONSTRUCTS AND ANTIBODIES

cDNA constructs encoding human adenosine A_{2A} receptor (A_{2A} in pEYFP-N1, A_{2A} in pRluc-N1, and A_{2A} in pGFP-2-N1 vectors) or human dopamine D_2 receptor and CaM in pEYFP-N1 vector, were previously described (Navarro et al., 2009). NCS-1 in pEYFP-N1 vector was published previously (Zhao et al., 2001). NCS-1 in pTagRFP-N or pEGFP-N1 vectors was subcloned from the pNCS-1-YFP-N1 plasmid using XhoI and BamHI restriction sites. Caldendrin was subcloned from a caldendrin-EGFP-N1 plasmid (Dieterich et al., 2008) into a pEYFP-N1 vector using EcoRI and BamHI restriction sites. The identity of the newly cloned construct was confirmed by sequencing analysis. pEGFP-N1 (Clontech), pTagRFP-N (Evrogen, Moscow, Russia), and pcDNA3.1 (Invitrogen, Darmstadt, Germany) were used as a corresponding negative controls for co-immunoprecipitation experiments and in surface biotinylation studies.

The following primary antibodies were used: Anti-NCS-1 rabbit (Santa Cruz Biotechnology, Heidelberg, Germany), anti-GFP mouse (MMS-118R, HiSS Diagnostics, Freiburg, Germany), anti-Renilla Luciferase mouse (Millipore, Schwalbach, Germany), anti-phospho-ERK1/2 mouse (Sigma-Aldrich, Madrid, Spain), anti-ERK1/2 rabbit (Sigma-Aldrich, Madrid, Spain), and anti-phospho-AKT rabbit (SAB Signalway antibody, Madrid, Spain). The secondary antibodies were: goat anti-mouse immunoglobulins HRP conjugated (P0447, Dako, Hamburg, Germany), goat anti-rabbit IgG HRP conjugated (#7074, Cell Signaling, Frankfurt am Main, Germany), peroxidase-AffiniPure goat anti-mouse IgG, light chain* specific antibody (Jackson ImmunoResearch) and Alexa Fluor 568 goat anti-rabbit IgG (A11031, A11036, Invitrogen, Darmstadt, Germany).

CELL CULTURE AND TRANSIENT TRANSFECTION

HEK293, HEK-293T cells, and COS-7 cells were grown in Dulbecco's modified Eagle's medium (DMEM) supplemented with 2 mM L-glutamine, 100 U/ml penicillin/streptomycin, and 5% (v/v) heat inactivated Fetal Bovine Serum (FBS) (Invitrogen, Paisley, Scotland, UK). For immunocytochemistry experiments HEK-293 and COS-7 cells were plated on 18 mm coverslips, grown for 24 h and then transfected with Lipofectamine 2000 (Invitrogen, Karlsruhe, Germany) according to the manufacturer's protocol. Twenty-four hours after transfection the cells were fixed with 4% paraformaldehyde (PFA) and processed for immunostaining as described below. For surface biotinylation experiments HEK293T cells were grown in 75 cm^2 culture flasks and transfected with Polyfect (Qiagen) according to the manufacturer's protocol. HEK-293T cells for BRET experiments were transfected with the plasmids encoding CaM, NCS-1, caldendrin, and adenosine A_{2A} receptor fusion proteins by PEI (PolyEthylenImine, Sigma, Steinheim, Germany) as previously described (Carriba et al., 2008).

IMMUNOCYTOCHEMISTRY, LASER SCANNING MICROSCOPY, AND IMAGE ANALYSIS

Coverslips with transfected HEK-293 and COS-7 were fixed with 4% PFA for 10 min at 37°C, extensively washed with PBS and immunostained for endogenous NCS-1 as described before (Mikhaylova et al., 2009) with anti-NCS-1 rabbit antibody in a dilution of 1:300. COS-7 cells transfected with A_{2A}-Rluc construct were stained with anti-Renilla Luciferase mouse antibody in dilution 1:500. F-actin was stained with Alexa Fluor 568 phalloidin (Molecular probes, Life Technologies, Darmstadt, Germany) diluted in 1:1000 in PBS and incubated for 10 min at room temperature. Fluorescence images were obtained on a TCS SP5 II confocal laser scanning microscope (Leica, Germany) using a 63× oil objective and zoom factors in the range of 1–4×. A 405 laser line was used for visualizing DAPI staining, 488 for GFP/YFP, 568 for the Alexa 568, and TagRFP. Images were acquired as *z*-stacks with 0.3 µm *z*-step. Maximum projections of *z*-stack were created in the ImageJ program (ImageJ, NIH).

BRET ASSAYS

HEK-293T cells were grown in six-well plates till about 60% confluence and then were transiently co-transfected with a constant amount of cDNA encoding for Rluc fusion protein and with increasing amounts of cDNA, corresponding to the protein fused to YFP. Two hours before quantifying fluorescence intensity, the supplemented medium (DMEM) was replaced by HBSS in the presence (1.26 mM) or in the absence of Ca^{2+}. Cells supplemented with Ca^{2+} were treated with 1 µm of ionomycin 10 min prior to the fluorescence measurements. To quantify protein-YFP expression, cells (20 µg protein) were distributed in 96-well microplates (black plates with a transparent bottom), and fluorescence was read in a Mithras LB 940 using an excitation filter at 400 nm. Protein-fluorescence expression was

determined as fluorescence of the sample minus the fluorescence of cells expressing the BRET donor alone. For BRET measurements, cell suspensions (20 μg protein) were distributed in 96-well microplates (Corning 3600, white plates; Sigma) and 5 μM coelenterazine H (Molecular Probes, Eugene, OR) was added. After 1 min, the readings were collected using a Mithras LB 940 that allows the integration of the signals detected in the short-wavelength filter at 485 nm (440–500 nm) and the long-wavelength filter at 530 nm (510–590 nm). To quantify protein-Rluc luminescence readings were also collected after 10 min of adding coelenterazine H. The net BRET is defined as [(long-wavelength emission)/(short-wavelength emission)]-Cf where Cf corresponds to [(long-wavelength emission)/(short-wavelength emission)] for the donor construct expressed alone in the same experiment. BRET is expressed as mili BRET units (mBU) determined as net BRET × 1000. A hyperbolic saturation curve showing an increase in BRET signal as a function of the acceptor fusion protein expression (acceptor protein expression relative to the donor protein expression, YFP/Rluc) is indicative of a specific interaction between the receptor-Rluc and Ca^{2+} sensor-YFP fusion constructs (Ayoub and Pfleger, 2010). BRET curves were fitted by using a non-linear regression equation, assuming a single phase with GraphPad Prism software (San Diego, CA, USA) to obtain the $BRET_{max}$ and $BRET_{50}$ values. The $BRET_{50}$ parameter represents the acceptor/donor ratio giving 50% of the $BRET_{max}$ and was used to estimate the relative affinity of the interaction. BRET data are expressed as means ± S.E.M. of 4–6 different experiments grouped as a function of the amount of BRET acceptor. Statistical differences in BRET parameters were analyzed with bifactorial ANOVA followed by *post-hoc* Bonferroni's tests ($p = 0.05$).

CO-IMMUNOPRECIPITATION ASSAY (CO-IP) AND IMMUNOBLOTTING

Heterologous Co-IP was performed with extracts from HEK293T cells transiently expressing A_{2A}-YFP, D_2-YFP, GFP, and NCS-1-tagRFP. Endogenous NCS-1 was co-immunoprecipitated from HEK293T cells transfected only with A_{2A} -YFP or GFP plasmids. YFP-tagged receptors and GFP control were immunoprecipitated for 12 h at 4°C with anti-GFP mouse antibody coupled to magnetic beads. Purification of antibody bound complexes was done using the μMACS™ GFP Isolation Kit (Miltenyi Biotec GmbH, Germany) according to the protocols supplied by manufactures, except that six washing steps were introduced to remove the unspecific binding to the beads. Another set of experiments was performed for A_{2A}-YFP and GFP with overexpressed NCS-1-TagRFP. Extraction of proteins from HEK293T cells was done as described previously (Hradsky et al., 2011). NCS-1 was immunoprecipitated with anti-NCS-1 rabbit antibody coupled to Protein G sepharose (GE Healthcare) or corresponding rabbit IgG controls overnight at 4°C. In both cases, high Ca^{2+} and Ca^{2+}-free conditions were achieved by addition of 0.5 mM of Ca^{2+} and 1 mM of Mg^{2+} or 2 mM EGTA and 1 mM Mg^{2+}, respectively, to the cell extracts during immunoprecipitation as well as into the washing buffers. Beads with precipitated protein complexes were washed three times with corresponding extraction buffers and eluted with 2× SDS sample buffer. Eluted samples were checked on SDS-PAGE/WB using anti-NCS-1 and anti-GFP antibody. To measure the effect of Ca^{2+} on the efficiency of co-immunoprecipitation, the total amount of A_{2A} receptor co-purified at different conditions was quantified using the "Gel Analyzer" plug-in provided in the ImageJ software (NIH, USA). The maximal binding observed with anti-NCS-1 antibody in the presence of Ca^{2+} was taken as 100% for each experiment individually and % deviations from this condition were measured for the other groups. Confidence interval was calculated and data were represented as averages of 4–5 independent experiments ± standard error mean (S.E.M).

SURFACE BIOTINYLATION ASSAY

HEK293T cells overexpressing A_{2A} -YFP alone or together with NCS-1-TagRFP and GFP control co-transfected with NCS-1-TagRFP were grown for 48 h in supplemented DMEM. Then growth medium was removed, cells were washed twice with HBSS and serum-free DMEM was added for another 2 h. Cells were labeled with Sulfo-NHS-SS-Biotin (Pierce) for 15 min at 4°C according to the manufacturers manual. Unbound biotin was sequestered and cells were harvested by scrapping, proteins were extracted with 1× TBS containing 1% Triton-X-100 over 1 h at 4°C. Equal amounts of extract were bound to Streptavidin beads (Life Technologies) and biotinylated proteins were eluted with 2× SDS and subjected to SDS-PAGE. A_{2A} -YFP protein bands were detected with anti-GFP mouse antibody. NCS-1-TagRFP was visualized with anti-NCS-1 rabbit antibody on the same membrane. The efficiency of surface biotinylation for A_{2A}–YFP in the presence or absence of NCS-1-TagRFP ($n = 4$) was quantified by measuring the optical densities of GFP signal as described above. Obtained values were compared between groups with and without overexpressed NCS-1 (the later one is taken as 100%). Statistical comparison was done with bifactorial ANOVA followed by *post-hoc* Bonferroni's tests.

MAPK AND AKT PHOSPHORYLATION ASSAYS

A detailed protocol for activation of adenosine A_{2A} receptors in HEK293T cells by addition of the A_{2A} receptor agonist CGS21680 (100 nM) has been described previously (Navarro et al., 2009). Briefly, HEK293T cells expressing A_{2A} and NCS-1 or the corresponding controls were grown in 25 cm^2 flasks to 50% confluence and cultured in serum-free medium overnight before the experiment. Two hours before the experiment, the cells medium was changed to HBSS buffer containing 1.26 mM Ca^{2+} and cells were treated or not with 1 μM ionomycin for 5 min before the addition of CGS21680. After cell lysis and estimation of protein concentration equal amounts of each sample (10 μg) were subjected to SDS-PAGE. To determine the level of ERK1/2 and pAKT phosphorylation, the membranes were then probed with a mouse anti-phospho-ERK1/2 antibody or phospho-AKT antibody. Total-ERK1/2 antibody was used as a loading control. The levels of phosphorylated ERK1/2 and phosphorylated AKT were normalized for differences in loading using the total ERK1/2 protein bands. Quantitative analysis of detected bands was performed by Odyssey V3.0 software. Statistical comparison was done with bifactorial ANOVA followed by *post-hoc* Bonferroni's tests ($^*p = 0.05$).

RESULTS

MOLECULAR INTERACTIONS BETWEEN ADENOSINE A_{2A} RECEPTOR AND CALCIUM SENSOR PROTEINS IN LIVING CELLS

The BRET technique can be successfully used as a method to test a protein—protein interaction in living cells (De and Gambhir, 2005; Carriba et al., 2008). Particularly, previously reported direct binding between the carboxy terminus of the A_{2A} receptor and CaM (Woods et al., 2008) was verified and extensively characterized using BRET (Navarro et al., 2009). This method is based on the fact that a luminescent donor (Rluc) oxidates the substrate coelenterazine H emitting bioluminescence that can be transferred to a fluorescent acceptor (YFP) when the distance between the donor and the acceptor is about 4.4 nm, (Dacres et al., 2010)—a typical distance between proteins interacting in a macro complex. The advantage of the BRET technique over classical techniques like co-immunoprecipitation is that it is performed in living cells and the protein concentrations of each protein can be carefully controlled with the interaction monitored over a range of protein concentrations and ratios. We have chosen BRET to test if the A_{2A} receptor is capable of forming a complex with other members of the CaM superfamily, namely NCS-1 and caldendrin. We compared the BRET efficiency between HEK293T cells co-expressing A_{2A} fused to *Renilla luciferase* (Rluc) and CaM, NCS-1 or caldendrin fused to YFP (**Figures 1A–C**). In agreement with our previous findings, the saturation curve obtained upon increasing CaM-YFP expression, indicated a specific interaction between CaM and A_{2A} ($BRET_{max}$ 60 ± 7 mBU and $BRET_{50}$ 41 ± 6). BRET occurred already at resting conditions but $BRET_{max}$ was increased ($p = 0.05$) after 10 min of stimulation with 1 μM of ionomycin ($BRET_{max}$ 78 ± 7 and $BRET_{50}$ 48 ± 8/**Figure 1A**). Interestingly, a clear and saturable BRET signal was also observed when increasing amounts of NCS-1-YFP were co-expressed with a constant amount of A_{2A}-Rluc ($BRET_{max}$ 43 ± 4 mBU and $BRET_{50}$ 11 ± 5, **Figure 1B**) again demonstrating a specific interaction. Elevation of intracellular Ca^{2+} concentration by preincubation of HEK293T cells with ionomycin (1 μM) for 10 min, increased ($p = 0.05$) both $BRET_{max}$ (57 ± 6 mBU) and $BRET_{50}$ (33 ± 9/**Figure 1B**). These results can be interpreted in two ways, neither of which is exclusive of the other. In one, Ca^{2+} led to conformational changes in the A_{2A}-NCS-1 complex that reduces the distance between Rluc and YFP fused to the C-terminal domain of the two interacting fusion proteins. In the other, Ca^{2+} increases complex formation by increasing the affinity between the two proteins.

Next we investigated if A_{2A} and caldendrin can form heteromers. A non-specific (linear) and low BRET signal was obtained in this case, a result consistent with two proteins not interacting (**Figure 1C**). An increase in intracellular Ca^{2+} levels had no effect on BRET efficiency either. Taken together these results suggest that caldendrin might not be an interaction partner of the A_{2A} receptor and that not all EF-hand proteins produce a BRET signal indicative of an interaction.

To get more insight in this, we performed co-immunoprecipitation experiments with transfected HEK293T cells. Interestingly, we found that NCS-1 is expressed endogenously in this cell line (**Figures 2A,B**). Immunostaining with anti-NCS-1 antibody showed an extranuclear punctate pattern as expected for a N-terminal myristoylated protein that exhibits membrane

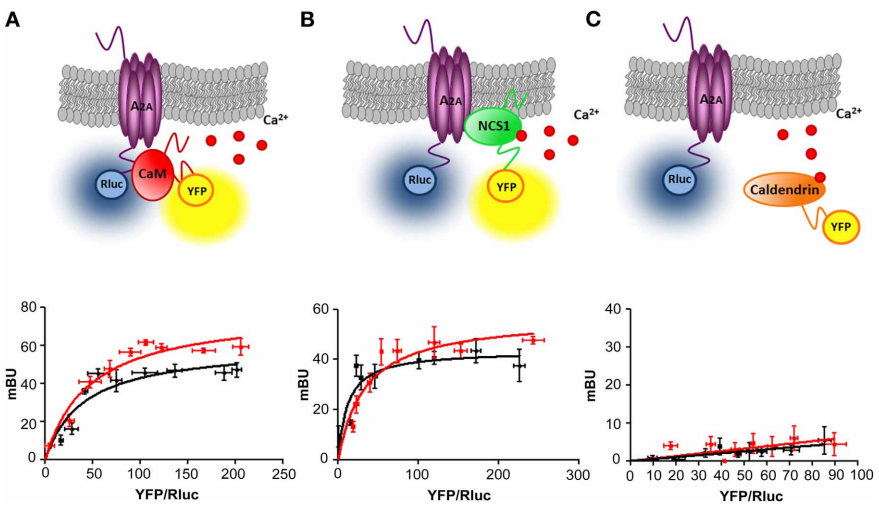

FIGURE 1 | Adenosine A_{2A} receptors interact with calmodulin and NCS-1 but not with caldendrin. BRET measurements were performed in HEK-293T cells co-transfected with 0.2 μg cDNA corresponding to the donor A_{2A}-Rluc and increasing amounts of the cDNA (0.1–2 μg) corresponding to CaM-YFP **(A)**, NCS-1-YFP **(B)** or caldendrin-YFP **(C)**. In **A** and **B** a clear BRET saturation curves were seen. Both interactions occur at basal Ca^{2+} levels (black curve) but can be facilitated in the presence of Ca^{2+}/ionomycin (red curve). No positive BRET interaction was seen for A_{2A}-Rluc and caldendrin-YFP at either Ca^{2+} concentrations **(C)**. Both fluorescence and luminescence of each sample were measured before every experiment to confirm similar donor expression (approximately 100,000 bioluminescence units) while monitoring the increase in acceptor expression (1000–35,000 fluorescence units). The relative amount of BRET is given as a function of 100× the ratio between the fluorescence of the acceptor (YFP) and the luciferase activity of the donor (Rluc). Average of 5–6 independent experiments measured in triplicates are plotted as mean value ± S.E.M. At the top images a schematic representation of BRET is given.

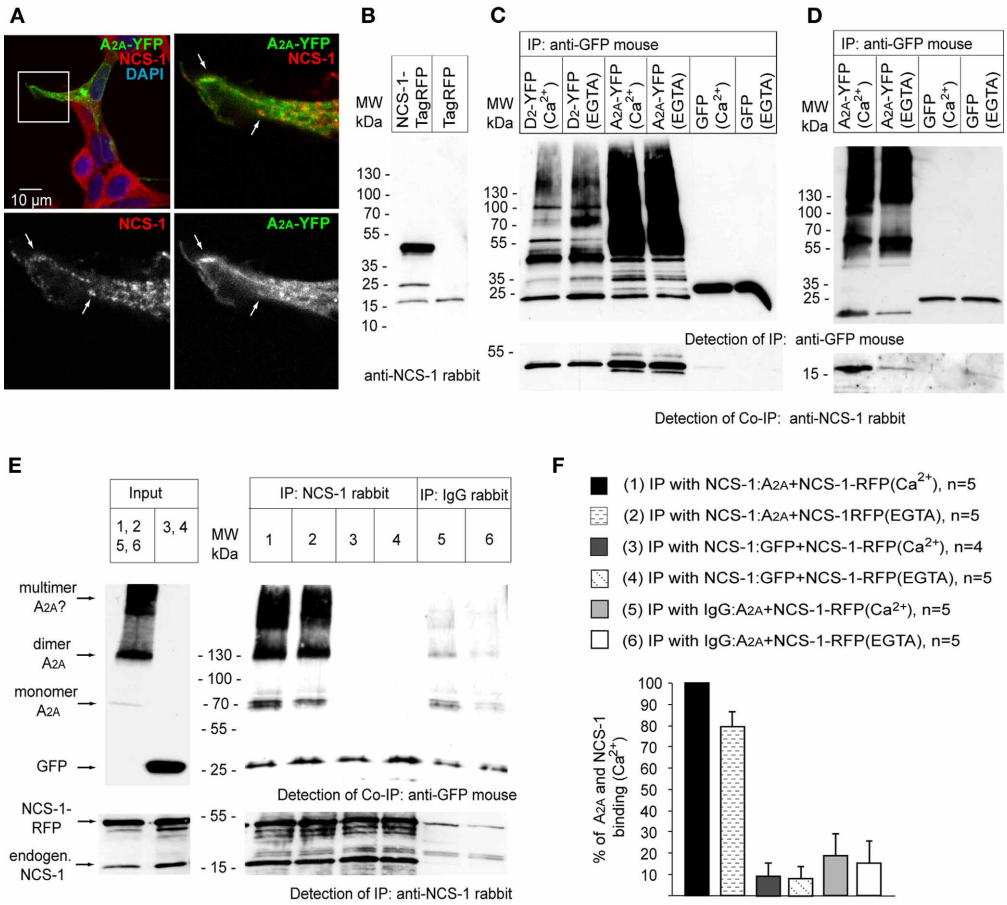

FIGURE 2 | Adenosine A_{2A} receptors form a complex with endogenous and the overexpressed NCS-1 in co-immunoprecipitation experiments. HEK293 cells express endogenous NCS-1 **(A)** that shows partial co-localization with overexpressed adenosine A_{2A} receptor at the plasma membrane of transfected cells (low panel, white arrows indicate the co-localizing spots). **(B)** HEK293T cell transfected with NCS-1-TagRFP or Tag-RFP probed with anti-NCS-1 rabbit antibody. NCS-1-TagRFP band can bee seen in the range of 45 kDa. Note a weak 18 kDa band of endogenous NCS-1 present in both samples. Additional band about 25 kDa in the first lane could be a degradation product of NCS-1-TagRFP. **(C)** Overexpressed A_{2A}-YFP and NCS-1-TagRFP can be co-immunoprecipitated from HEK293T cell extract. Dopamine D_2 receptor with YFP-tag is included as a positive control. YFP-fused receptors or GFP control were detected with anti-GFP mouse antibody, detection of NCS-1-TagRFP was done with anti-NCS-1 rabbit antibody. **(D)** Endogenous NCS-1 is co-immunoprecipitated with A_{2A}-YFP from HEK293T cell extract. **(E)** Immunoprecipitation (IP) is performed with anti-NCS-1 rabbit antibody. Anti-NCS-1 antibody show positive immunoprecipitation of the antigene (low panel). Note, that there is endogenous NCS-1 expressed in HEK293 cells but at much lower levels then overexpressed NCS-1. Mostly a homomeric form of A_{2A}-YFP is detected with anti-GFP mouse antibody (upper panel). **(F)** The binding of A_{2A} receptor to NCS-1 is enhanced in the presence of Ca^{2+}. Quantification of immunoprecipitated A2A-YFP. Data represented as average of 4–5 independent experiments ± SEM.

localization. The co-localization between endogenous NCS-1 and overexpressed A_{2A}-YFP was mostly restricted to the cell periphery (**Figure 2A**). We then performed co-immunoprecipitation experiments with HEK293T cells co-transfected with A_{2A}-YFP and NCS-1-TagRFP or the corresponding control contructs (**Figure 2C**). Dopamine D_2 receptor (D_2-YFP) was included as a positive control since its interaction with NCS-1 is well established (Kabbani et al., 2002; Lian et al., 2011). The mouse anti-GFP antibody led to immunoprecipitation of receptor-YFP in complex with overexpressed (**Figure 2C**) or endogenous (**Figure 2D**) NCS-1. In the case of overexpression, the binding of NCS-1 to D_2 and A_{2A} receptors already occurred in the presence of EGTA (**Figure 2C**). Immunoprecipitation of overexpressed and endogenous NCS-1 with rabbit anti-NCS-1 bound to Protein G sepharose have shown that A_{2A}-YFP was efficiently co-purified with NCS-1-TagRFP (**Figure 2E**). The corresponding controls with unspecific rabbit IgG showed again some unspecific binding of N-myristoylated NCS-1 to the beads but it was significantly lower as compared to immunoprecipitations done with the anti-NCS-1 antibody (**Figures 2E,F**). Interestingly, analogous to the BRET experiments the presence Ca^{2+} had a positive effect on the interaction (**Figures 2D,E** and **F**) and mostly a homomeric A_{2A}-YFP receptor formed a complex with NCS-1 (**Figure 2E**).

OVEREXPRESSION OF NCS-1 HAS NO IMPACT ON SURFACE EXPRESSION OF THE A_{2A} RECEPTOR IN NON-STIMULATED CELLS

NCS-1 is involved in regulation of vesicular trafficking from the trans-Golgi network (TGN) to the plasma membrane and

associates with the Golgi membranes via its N-terminal myristoyl tail where it regulates activity of phosphatidylinositol 4-kinase IIIβ (PI-4KIIIβ), thus providing a Ca^{2+}-dependent control for the regulated local synthesis of phosphatidylinositol 4-phosphate (PI(4)P) and for the exit of vesicles from TGN (Zhao et al., 2001; Haynes et al., 2005; Mikhaylova et al., 2009). At the plasma membrane NCS-1 is involved in transduction of Ca^{2+} signaling and regulating the activity of different kinases and surface receptors (for review see Mikhaylova et al., 2011). A_{2A} receptor traverses the secretory trafficking pathway from the ER to the Golgi complex on the way to the plasma membrane. Therefore, we next asked how the presence of NCS-1 would affect the expression of A_{2A} receptor at the plasma membrane and where in the cell the complex of A_{2A} receptor and NCS-1 might occur. To address the first question, we performed a quantitative surface biotinylation assay to compare the surface expression of A_{2A} receptor with and without co-transfection of NCS-1. Two major bands corresponding to the monomer and the dimer of A_{2A} receptor were biotinylated and purified with streptavidin beads (**Figure 3A**). Additional bands appearing in streptavidin-bound fraction but not in whole-cell extract might represent a differentially modified (for example glycosilated, phosphorylated, etc.) plasma membrane receptor fraction. Although there we observed a slight increase in immunoreactivity of biotinylated A_{2A} when co-expressed with NCS-1, we have not found any significant effect on surface receptor expression in non-stimulated HEK293T cells (**Figure 3B**). Next, for the co-localization study we have chosen COS-7 cells because they are significantly larger than HEK293T cells. After 24 h of overexpression, significant amounts of A_{2A}-YFP fluorescence was still associated with the ER and the Golgi membranes. Considerable overlap of A_{2A} -YFP and NCS-1-TagRFP fluorescence, however, was mostly seen close to the plasma membrane compartment (**Figure 3C**). Therefore, in another set of experiments we included phalloidin-568 staining to visualize a dense cortical actin cytoskeleton along the cell membranes. Additionally, since the excitation/emission spectrum of TagRFP is largely overlapping with Alexa Fluor 568, we replaced the fusion constructs by NCS-1-YFP and A_{2A}-Rluc (**Figure 3D**). Again we could see a co-localization of A_{2A} and NCS-1 fluorescence overlapping with F-actin at the edges of the cell membrane

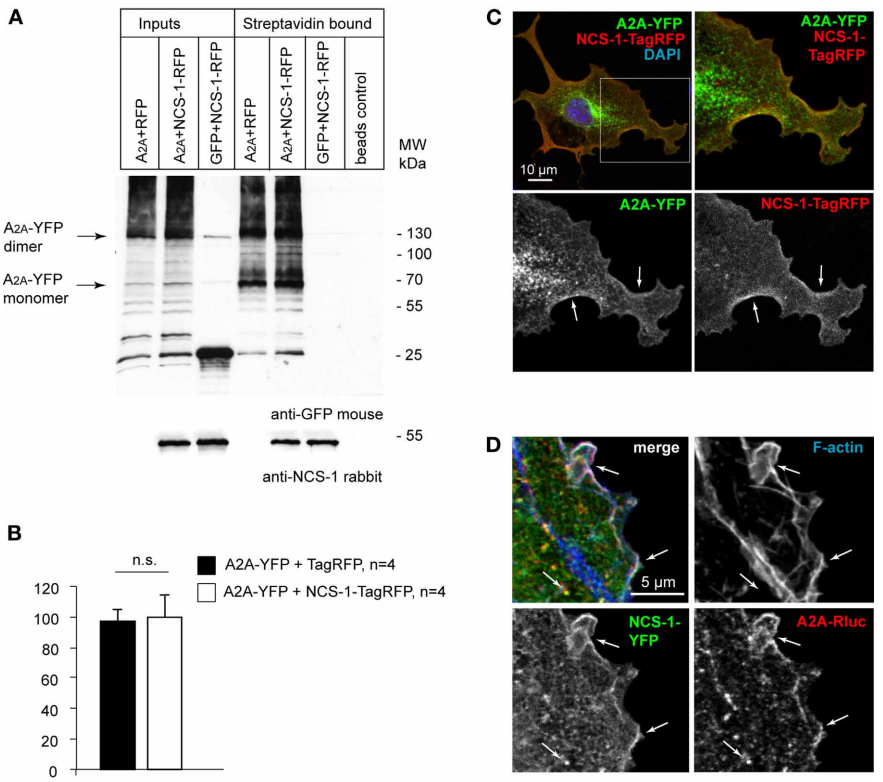

FIGURE 3 | NCS-1 does not interfere with the trafficking and surface expression of adenosine A_{2A} receptors in the basal conditions (no agonist stimulation). (A) HEK293T cells overexpressing A_{2A}-YFP alone or together with NCS-1-TagRFP and GFP control co-transfected with NCS-1-TagRFP were labeled with Sulfo-NHS-SS-Biotin for 15 min at 4°C and biotinylated proteins were purified with Streptavidin beads. Detection was done with anti-GFP and anti-NCS-1 antibody. Note the SDS-resistant dimer of A_{2A}-YFP. NCS-1-TagRFP is also co-purified with surface biotinylated proteins suggesting that there might be another binding partner of NCS-1 endogenously expressing in HEK293T cells. **(B)** Although there are slight differences in amount of surface labeled A_{2A}-YFP between TagRFP and NCS-1-TagRFP expressing cells, no clear effect of NCS-1 overexpression can be seen. **(C)** Confocal image of a COS-7 cell co-expressing with A_{2A}-YFP and NCS-1-TagRFP for 24 h shows co-localization of both proteins at the cell periphery (white arrows indicate co-localization). **(D)** A2A-Rluc co-localizes with NCS-1-YFP and cortical F-actin along the plasma membrane of transfected COS-7 cells. Note the intracellular vesicular structures showing overlapping fluorescence of A2A and NCS-1.

as well as in small clusters in the cytosol (**Figure 3D**). These clusters could represent post-Golgi transport carriers, endosomes or some other vesicular compartments.

BINDING OF NCS-1 TO THE A_{2A} RECEPTOR DIMER HAS A DIFFERENTIAL EFFECT ON AGONIST-INDUCED INTRACELLULAR SIGNALING

Homodimers of adenosine A_{2A} receptor are the predominant form of the receptor at the cell membrane (Canals et al., 2004). Moreover, based on the co-immunprecipitation data, where mostly the homomeric form of A_{2A} was co-purified with NCS-1, we questioned if NCS-1 could interact with the A_{2A} homodimer. We performed BRET saturation curves in HEK293T cells expressing an A_{2A}- Rluc and increasing amounts of A_{2A}-YFP in the presence or absence of NCS-1 (**Figure 4A**). The presence of NCS-1 modified the $BRET_{max}$ ($p = 0.01$) and $BRET_{50}$ ($p = 0.05$) corresponding to the formation of a A_{2A} homodimer ($BRET_{max}$ 196 ± 10 mBU and $BRET_{50}$ 63 ± 7 in the absence of NCS-1; $BRET_{max}$ 131 ± 9 mBU and $BRET_{50}$ 90 ± 10 in the presence of NCS-1). This result demonstrates that NCS-1 interacts with A_{2A} receptor homodimers and induces changes in their quaternary structure in a manner that suggests a greater distance between donor and acceptor, a change in orientation, and/or a diminished number of heteromers. Another possibility that we cannot exclude would be

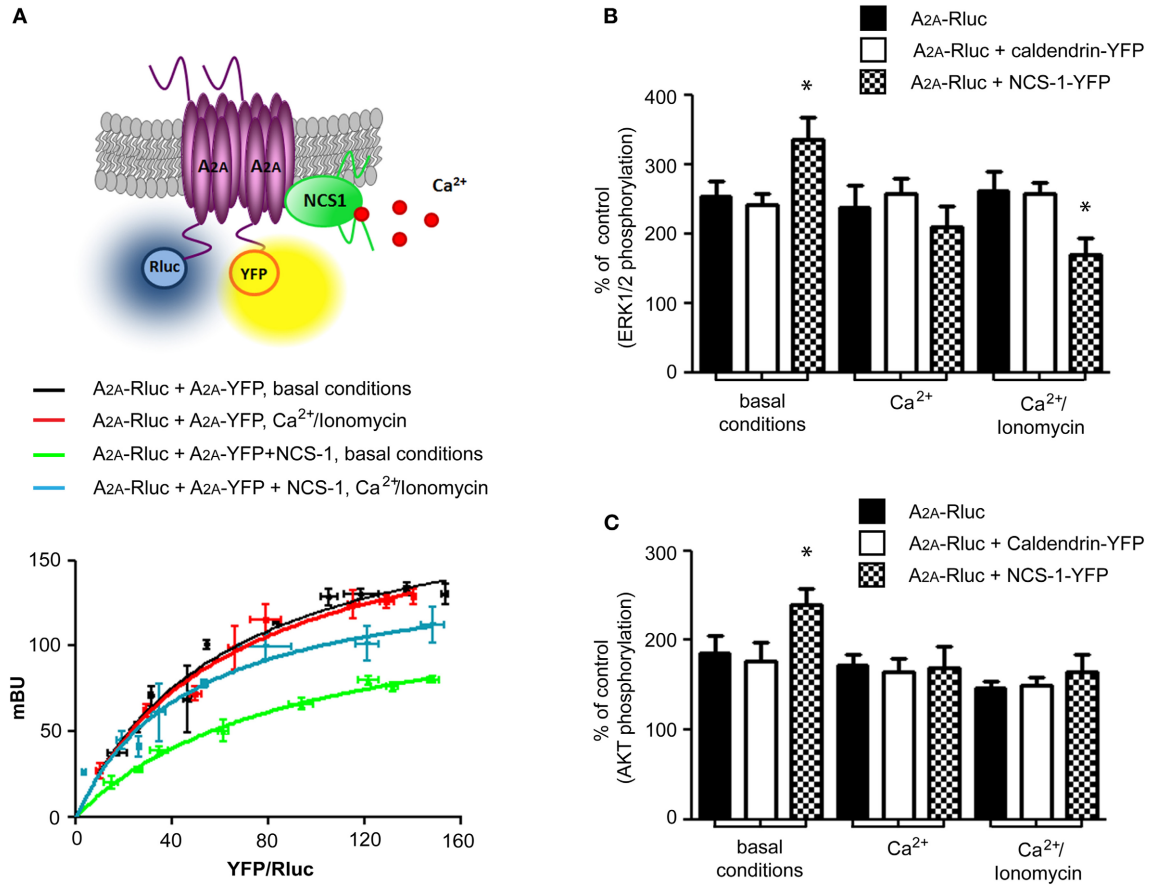

FIGURE 4 | NCS-1 associates with a A_{2A}–A_{2A} homodimer and modulates the adenosine A_{2A} receptor signaling in a Ca^{2+} dependent manner. **(A)** BRET saturation curves were obtained from HEK-293T cells co-transfected with 0.2 μg cDNA corresponding to A_{2A}-Rluc fusion protein and increasing amounts of cDNA (0.05–1 μg) corresponding to A_{2A}-YFP fusion protein without (black and red curves) or with 0.5 μg of the cDNA corresponding to NCS-1 (green and blue curves). Measurements were done either at basal conditions (black and green curves) or after treatment of cells with 1 μM of ionomycin for 10 min (red and blue curves). Ca^{2+} has no effect on A_{2A} receptor homodimerization itself (red curve compared to the black one) but modifies A_{2A}-A_{2A}-NCS-1 heteromeric complex structure (blue curve compared to the green one). Both fluorescence and luminescence of each sample were measured before every experiment to confirm similar donor expression (approximately 100,000 bioluminescence units) while monitoring the increase in acceptor expression (1000–27,000 fluorescence units). The relative amount of BRET is given as a function of 100× the ratio between the fluorescence of the acceptor (YFP) and the luciferase activity of the donor (Rluc). Average of 5–6 independent experiments measured in triplicates are plotted as mean value ± S.E.M. A schematic representation of BRET is given at the top. In **(B)** and **(C)** HEK-293T cells transfected with 0.5 μg cDNA corresponding to adenosine A_{2A} receptor alone or with cDNA corresponding to caldendrin-YFP (0.8 μg) or NCS-1-YFP (0.6 μg) were stimulated with 100 nM of CGS 2168 at the basal condition, in the presence of 1.26 mM of Ca^{2+} in HBSS buffer or in the presence of both 1.26 mM of Ca^{2+} and 1 μM of Ca^{2+} ionophore ionomycin. Equal amount of protein were analyzed by SDS-PAGE using phospho-ERK1/2 **(B)** or phospho-AKT **(C)** and total-ERK1/2 antibodies. Quantification of eight independent experiments indicates stimulatory effect on NCS-1 on MAPK signaling **(B)** or pAKT levels **(C)** at the basal Ca^{2+} conditions. $^*p = 0.05$.

a change in the density of adenosine A_{2A} receptors at the plasma membrane upon overexpression of NCS-1. However, we have not found significant increases in the amount of A_{2A} receptor associated with the plasma membrane using surface biotinylation assay (**Figure 3A**). BRET experiments were always carried out at constant amounts of receptors between compared groups. Since we performed our study in intact HEK293T cells, a small change in plasma membrane density of A_{2A} receptors would presumably be compensated for by a change in density in other intracellular membranes. Thus, the changes measured in the BRET assay are most likely due to differences in receptor-receptor interaction. An elevation in Ca^{2+} levels by treating cells with ionomycin (1 μM) did not modify A_{2A}–A_{2A} homomerization but modified the $BRET_{50}$ ($p = 0.05$) in the presence of NCS-1 ($BRET_{max}$ 148 ± 10 mBU and $BRET_{50}$ 48 ± 7), indicating a change in the receptor association between NCS-1 and the A_{2A} heteromer in the presence of Ca^{2+} (**Figure 4A**).

The adenosine A_{2A} receptor is a G_s coupled receptor that regulates cAMP production. The activation of the A_{2A} receptor regulates a number of protein and lipid kinases, including MAPK 1-3 (ERK1/2) phosphorylation and activity (Wyatt et al., 2002; Navarro et al., 2009) and V-akt murine thymoma viral oncogene homolog 1 (AKT, also called PKB/Mori et al., 2004). To test the effect of NCS-1 overexpression on A_{2A} receptor function we analyzed MAPK and AKT signaling pathways. 2-[p-(2-carboxyethyl)phenylethylamino]-50 ethylcarboxamidoadenosine (CGS 21680) is a selective agonist of A_{2A} type of adenosine receptors. CGS21680-induced ERK1/2 and AKT phosphorylation was assessed in transiently transfected HEK293T cells at basal conditions or at elevated calcium levels. Agonist stimulation of A_{2A} in NCS-1-YFP transfected cells induced a significant increase in ERK1/2 phosphorylation at basal conditions and this effect was reversed when cells were pre-treated with Ca^{2+}/Ionomycin (**Figure 4B**). As a negative control, overexpression of caldendrin-YFP, that showed no interaction with A_{2A} receptors, had no effect on ERK1/2 activity at any condition tested, demonstrating further the specificity of the NCS-1-induced effects (**Figure 4B**). Finally, NCS-1 promoted the CGS21680-induced AKT phosphorylation at resting Ca^{2+} levels and again this effect was blocked when intracellular Ca^{2+} concentrations were increased with ionomycin (**Figure 4C**).

DISCUSSION

Adenosine receptors cross talk has been established with other GPCRs, ionotropic receptors, and receptor kinases to regulate their function with most of the characterized interactions occur via the A_{2A} receptor type (Sebastião and Ribeiro, 2009). Most important, the role of A_{2A} receptors in the brain is related to their ability to interact with other receptor systems (Sebastião and Ribeiro, 2009). Indeed, cross talk between the A_{2A} receptor and D_2 type dopamine receptor, metabotropic glutamate receptor mGluR5 or endocanabinoid receptor CB_1 in striatum modulates the signaling induced by these receptors and has important clinical implications for the treatment of Parkinson disease, schizophrenia, addiction, and potentially other brain disorders (Ferré et al., 2002; Carriba et al., 2007; Ferré et al., 2008).

Another level of complexity to the regulation of GPCRs signaling is added by cross talk between GPCRs system and intracellular Ca^{2+} signaling via CaM. Among a number of other GPCRs, CaM has been shown to bind to the carboxy-terminus adenosine A_{2A} receptors in a A_{2A}-D_2 receptor heteromer. Elevation of intracellular Ca^{2+} levels then triggers conformational changes in this complex via CaM providing a selective modulation of A_{2A}-D_2 receptor heteromer-mediated activation of the MAPK pathway (Navarro et al., 2009). Evolutionary and based on the history of their discovery, calcium sensors from the CaM superfamily that are particularly abundant in brain are divided into two larger groups named NCS and nCaBPs (Mikhaylova et al., 2011). Although CaM is ubiquitously expressed in all eukaryotic cells, emerging evidence supports a role for NCS and nCaBPs other than CaM in the regulation of a number of effectors. For example, there are interactions that are specific for particular calcium sensors (hippocalcin—PSD95; caldendrin—LC3/Seidenbecher et al., 2004; Dieterich et al., 2008; Jo et al., 2010) and that cannot be competed by CaM. Moreover, many CaM targets can interact with more than one NCS or nCaBPs. Voltage-gated Ca^{2+} channels (Ca_V) (P/Q-, N-, and L-type), TRPC1/5 channels, GPCRs, IP3R, and PI-4KIIIβ are among them (for review see Mikhaylova et al., 2011). We have chosen two representative candidate proteins from each group of CaM-like calcium sensors. NCS-1 (also known as frequinin) is one of the first discovered and well-characterized NCS proteins. NCS-1, like other members of this family of proteins, has a widespread distribution in the brain and spinal cord (Martone et al., 1999). In terms of its structural organization, NCS-1 can associate with intracellular membranes via a N-terminal myristoyl tail and like CaM it has four EF-hand motifs where the first EF-hand is cryptic and does not coordinate Ca^{2+}. Differently from CaM that displays a dumbbell conformation of the two EF-hand domains, NCS-1 exhibits a globular fold and NCS-1 can bind Ca^{2+} with higher affinity than CaM (in the range of 0.5–0.8 μM in Mg^{2+} bound form/Aravind et al., 2008; Mikhaylova et al., 2009). Ca^{2+} binding induces conformational changes and the exposure of hydrophobic surfaces for the interaction with the target protein or membrane. Caldendrin is the founding member of the nCaBP group of Ca^{2+} sensors (Seidenbecher et al., 1998). Most important, based on alignments of its carboxy terminal half that resembles the organization of CaM, caldendrin is the closest homolog of CaM in brain (Seidenbecher et al., 1998; Mikhaylova et al., 2006, 2011; McCue et al., 2010).

To test if NCS-1 and caldendrin are able to interact with A_{2A} receptor in living cells we measured BRET between A_{2A}—Rluc as the donor and calcium sensor—YFP as the acceptor. We observed a positive saturable signal only between A_{2A} and NCS-1 but not caldendrin. This result was surprising, as caldendrin is more closely related to CaM than NCS-1. Like CaM, binding of NCS-1 occurred already under basal Ca^{2+}-conditions and was further facilitated by increased intracellular Ca^{2+} levels. We were able to confirm these data by heterologous co-immunoprecipitations from HEK293T cells transiently expressing A_{2A} or D_2 receptors and NCS-1. These data suggest that NCS-1 is a novel interaction partner of A_{2A} receptor. Both proteins associate with membranes and can be found along the secretory trafficking pathway but

mainly co-localize at the post-Golgi trafficking compartments including the cell membrane. Although there was a slight increase in the amount of surface receptor when cells were overexpressing NCS-1, this might be due to the stimulatory effect of NCS-1 on the activity of the Golgi localized enzyme PI-4KIIIβ but not likely due to trafficking of A_{2A} itself. Activation of PI-4KIIIβ leads to the increase in production of PI(4)P—rate limiting phosphoinositide in the TGN-to-plasma membrane trafficking (Zhao et al., 2001; Haynes et al., 2005; Mikhaylova et al., 2009) and would in general enhance the surface delivery of transmembrane proteins.

Using BRET we have found that NCS-1 is associated with a A_{2A} homodimer. More than 90% of A_{2A} overexpressed in HEK293T cells is functional only in dimeric form (Canals et al., 2004) and this indicates that NCS-1 associates with a functional A_{2A} receptor. Interestingly, in a recent paper of Lian and colleagues (2011) the NMR structure of Ca^{2+}-bound NCS-1 and the dopamine D_2 receptor binding peptide have indicated that monomeric NCS-1 can simultaneously bind two D_2 receptors. Similarly, Ca^{2+} stabilizes a A_{2A}-A_{2A}-NCS-1 heteromeric complex. It is tempting to speculate, that this might relate to conformational changes in monomeric NCS-1 which induces conformational changes in the heteromer which then has differential consequences in terms of agonist-induced intracellular signaling. At basal conditions, stimulation with the A_{2A} receptor agonist CGS21680 had a positive effect on phosphorylation of ERK1/2 and AKT. In contrast, preincubation of cells with Ca^{2+}/ionomycin reduced the agonist-induced ERK1/2 phosphorylation. Most important, this effect is specific for NCS-1 since overexpression of CaM had no effect on A_{2A} receptor homomer signaling but instead was important for A_{2A}—D_2 induced ERK1/2 phosphorylation (Navarro et al., 2009). The contribution of endogenous NCS-1 from HEK293 cells is probably very minor since the expression levels are quite low and we have not seen any change induced by elevated Ca^{2+} in the cells overexpressing only A_{2A} receptor alone.

In summary, in this study we provide the first evidence for a novel interaction between the adenosine A_{2A} receptor and NCS-1. We demonstrate that Ca^{2+} modulates both the association and the intracellular signaling in living cells and that this effect is specific for NCS-1 in the sense that caldendrin does not bind and that the association of CaM has different functional consequences. Understanding the role of NCS-1 in heteromerization of GPCRs will provide further insights on the function of GPCRs and might have potential clinical applications.

ACKNOWLEDGMENTS

We are grateful to C. Borutzki, M. Marunde, and S. Hochmuth for the professional technical assistance. This work was supported by research grants from the DFG (SFB 779 TPB8, SFB 854 TP7, Kr 1879/3-1), the DZNE Magdeburg and by SAF2010-18472 and SAF2011-23813 from Spanish Government.

REFERENCES

Aravind, P., Chandra, K., Reddy, P. P., Jeromin, A., Chary, K. V., and Sharma, Y. (2008). Regulatory and structural EF-hand motifs of neuronal calcium sensor-1, Mg^{2+} modulates Ca^{2+} binding, Ca^{2+} -induced conformational changes, and equilibrium unfolding transitions. *J. Mol. Biol.* 376, 1100–1115.

Ayoub, M. A., and Pfleger, K. D. (2010). Recent advances in bioluminescence resonance energy transfer technologies to study GPCR heteromerization. *Curr. Opin. Pharmacol.* 10, 44–52.

Bernstein, H. G., Seidenbecher, C. I., Smalla, K. H., Gundelfinger, E. D., Bogerts, B., and Kreutz, M. R. (2003). Distribution and cellular localization of caldendrin immunoreactivity in adult human forebrain. *J. Histochem. Cytochem.* 51, 1109–1112.

Burgoyne, R. D. (2007). Neuronal calcium sensor proteins: generating diversity in neuronal Ca^{2+} signalling. *Nat. Rev. Neurosci.* 8, 182–193.

Canals, M., Burgueño, J., Marcellino, D., Cabello, N., Canela, E. I., Mallol, J., Agnati, L., Ferré, S., Bouvier, M., Fuxe, K., Ciruela, F., Lluis, C., and Franco, R. (2004). Homodimerization of adenosine A_{2A} receptors: qualitative and quantitative assessment by fluorescence and bioluminescence energy transfer. *J. Neurochem.* 88, 726–734.

Carriba, P., Navarro, G., Ciruela, F., Ferré, S., Casadó, V., Agnati, L., Cortés, A., Mallol, J., Fuxe, K., Canela, E. I., Lluís, C., and Franco, R. (2008). Detection of heteromerization of more than two proteins by sequential BRET-FRET. *Nat. Methods* 5, 727–733.

Carriba, P., Ortiz, O., Patkar, K., Justinova, Z., Stroik, J., Themann, A., Müller, C., Woods, A. S., Hope, B. T., Ciruela, F., Casadó, V., Canela, E. I., Lluis, C., Goldberg, S. R., Moratalla, R., Franco, R., and Ferré, S. (2007). Striatal adenosine A2A and cannabinoid CB1 receptors form functional heteromeric complexes that mediate the motor effects of cannabinoids. *Neuropsychopharmacology* 32, 2249–2259.

Dacres, H., Wang, J., Dumancic, M. M., and Trowell, S. C. (2010). Experimental determination of the Förster distance for two commonly used bioluminescent resonance energy transfer pairs. *Anal. Chem.* 82, 432–435.

De, A., and Gambhir, S. S. (2005). Noninvasive imaging of protein-protein interactions from live cells and living subjects using bioluminescence resonance energy transfer. *FASEB J.* 19, 2017–2019.

Dieterich, D. C., Karpova, A., Mikhaylova, M., Zdobnova, I., König, I., Landwehr, M., Kreutz, M., Smalla, K. H., Richter, K., Landgraf, P., Reissner, C., Boeckers, T. M., Zuschratter, W., Spilker, C., Seidenbecher, C. I., Garner, C. C., Gundelfinger, E. D., and Kreutz, M. R. (2008). Caldendrin-Jacob: a protein liaison that couples NMDA receptor signalling to the nucleus. *PLoS Biol.* 6:e34. doi: 10.1371/journal.pbio.0060034

Ferré, S., Karcz-Kubicha, M., Hope, B. T., Popoli, P., Burgueño, J., Gutiérrez, M. A., Casadó, V., Fuxe, K., Goldberg, S. R., Lluis, C., Franco, R., and Ciruela, F. (2002). Synergistic interaction between adenosine A2A and glutamate mGlu5 receptors: implications for striatal neuronal function. *Proc. Natl. Acad. Sci. U.S.A.* 99, 11940–11945.

Ferré, S., Quiroz, C., Woods, A. S., Cunha, R., Popoli, P., Ciruela, F., Lluis, C., Franco, R., Azdad, K., and Schiffmann, S. N. (2008). An update on adenosine A2A-dopamine D2 receptor interactions: implications for the function of G protein-coupled receptors. *Curr. Pharm. Des.* 14, 1468–1474.

Ferré, S., Woods, A. S., Navarro, G., Aymerich, M., Lluís, C., and Franco, R. (2010). Calcium-mediated modulation of the quaternary structure and function of adenosine A_{2A}-dopamine D2 receptor heteromers. *Curr. Opin. Pharmacol.* 10, 67–72.

Haynes, L. P., Thomas, G. M., and Burgoyne, R. D. (2005). Interaction of neuronal calcium sensor-1 and ADP-ribosylation factor 1 allows bidirectional control of phosphatidylinositol 4-kinase beta and trans-Golgi network-plasma membrane traffic. *J. Biol. Chem.* 280, 6047–6054.

Hradsky, J., Raghuram, V., Reddy, P. P., Navarro, G., Hupe, M., Casado, V., McCormick, P. J., Sharma, Y., Kreutz, M. R., and Mikhaylova, M. (2011). Post-translational membrane insertion of tail-anchored transmembrane EF-hand Ca^{2+} sensor calneurons requires the TRC40/Asna1 protein chaperone. *J. Biol. Chem.* 286, 36762–36776.

Jo, J., Son, G. H., Winters, B. L., Kim, M. J., Whitcomb, D. J., Dickinson, B. A., Lee, Y. B., Futai, K., Amici, M., Sheng, M., Collingridge, G. L., and Cho, K. (2010). Muscarinic receptors induce LTD of NMDAR EPSCs via a mechanism involving hippocalcin, AP2 and PSD-95. *Nat. Neurosci.* 13, 1216–1224.

Kabbani, N., Negyessy, L., Lin, R., Goldman-Rakic, P., and Levenson, R. (2002). Interaction with neuronal calcium sensor NCS-1 mediates desensitization of the D2 dopamine receptor. *J. Neurosci.* 22, 8476–8486.

Komolov, K. E., Senin, I. I., Kovaleva, N. A., Christoph, M. P., Churumova, V. A., Grigoriev, I. I., Akhtar, M., Philippov, P. P., and Koch, K. W. (2009). Mechanism of rhodopsin kinase regulation by recoverin. *J. Neurochem.* 110, 72–79.

Kull, B., Svenningsson, P., and Fredholm, B. B. (2000). Adenosine A(2A) receptors are colocalized with and activate g(olf) in rat striatum. *Mol. Pharmacol.* 58, 771–777.

Laube, G., Seidenbecher, C. I., Richter, K., Dieterich, D. C., Hoffmann, B., Landwehr, M., Smalla, K. H., Winter, C., Böckers, T. M., Wolf, G., Gundelfinger, E. D., and Kreutz, M. R. (2002). The neuron-specific Ca^{2+}-binding protein caldendrin: gene structure, splice isoforms, and expression in the rat central nervous system. *Mol. Cell. Neurosci.* 19, 459–475.

Lian, L. Y., Pandalaneni, S. R., Patel, P., McCue, H. V., Haynes, L. P., and Burgoyne, R. D. (2011). Characterisation of the interaction of the C-terminus of the dopamine D2 receptor with neuronal calcium sensor-1. *PLoS One* 6:e27779. doi: 10.1371/journal.pone.0027779

Martone, M. E., Edelmann, V. M., Ellisman, M. H., and Nef, P. (1999). Cellular and subcellular distribution of the calcium-binding protein NCS-1 in the central nervous system of the rat. *Cell Tissue Res.* 295, 395–407.

McCue, H. V., Haynes, L. P., and Burgoyne, R. D. (2010). Bioinformatic analysis of CaBP/calneuron proteins reveals a family of highly conserved vertebrate Ca^{2+}-binding proteins. *BMC Res. Notes* 3, 118.

Mikhaylova, M., Hradsky, J., and Kreutz, M. R. (2011). Between promiscuity and specificity: novel roles of EF-hand calcium sensors in neuronal Ca^{2+} signalling. *J. Neurochem.* 118, 695–713.

Mikhaylova, M., Reddy, P. P., Munsch, T., Landgraf, P., Suman, S. K., Smalla, K. H., Gundelfinger, E. D., Sharma, Y., and Kreutz, M. R. (2009). Calneurons provide a calcium threshold for trans-Golgi network to plasma membrane trafficking. *Proc. Natl. Acad. Sci. U.S.A.* 106, 9093–9098.

Mikhaylova, M., Sharma, Y., Reissner, C., Nagel, F., Aravind, P., Rajini, B., Smalla, K. H., Gundelfinger, E. D., and Kreutz, M. R. (2006). Neuronal Ca^{2+} signaling via caldendrin and calneurons. *Biochim. Biophys. Acta* 1763, 1229–1237.

Minakami, R., Jinnai, N., and Sugiyama, H. (1997). Phosphorylation and calmodulin binding of the metabotropic glutamate receptor subtype 5 (mGluR5) are antagonistic *in vitro*. *J. Biol. Chem.* 272, 20291–20298.

Mori, Y., Higuchi, M., Masuyama, N., and Gotoh, Y. (2004). Adenosine A2A receptor facilitates calcium-dependent protein secretion through the activation of protein kinase A and phosphatidylinositol-3 kinase in PC12 cells. *Cell Struct. Funct.* 29, 101–110.

Nakajima, Y., Yamamoto, T., Nakayama, T., and Nakanishi, S. (1999). A relationship between protein kinase C phosphorylation and calmodulin binding to the metabotropic glutamate receptor subtype 7. *J. Biol. Chem.* 274, 27573–27577.

Navarro, G., Aymerich, M. S., Marcellino, D., Cortés, A., Casadó, V., Mallol, J., Canela, E. I., Agnati, L., Woods, A. S., Fuxe, K., Lluís, C., Lanciego, J. L., Ferré, S., and Franco, R. (2009). Interactions between calmodulin, adenosine A_{2A}, and dopamine D2 receptors. *J. Biol. Chem.* 284, 28058–28068.

Nickols, H. H., Shah, V. N., Chazin, W. J., and Limbird, L. E. (2004). Calmodulin interacts with the V2 vasopressin receptor: elimination of binding to the C terminus also eliminates arginine vasopressin-stimulated elevation of intracellular calcium. *J. Biol. Chem.* 279, 46969–46980.

Nishi, A., Watanabe, Y., Higashi, H., Tanaka, M., Nairn, A. C., and Greengard, P. (2005). Glutamate regulation of DARPP-32 phosphorylation in neostriatal neurons involves activation of multiple signaling cascades. *Proc. Natl. Acad. Sci. U.S.A.* 102, 1199–1204.

Ritter, S. L., and Hall, R. A. (2009). Fine-tuning of GPCR activity by receptor-interacting proteins. *Nat. Rev. Mol. Cell Biol.* 10, 819–830.

Rosin, D. L., Hettinger, B. D., Lee, A., and Linden, J. (2003). Anatomy of adenosine A_{2A} receptors in brain: morphological substrates for integration of striatal function. *Neurology* 61, S12–S18.

Schiffmann, S. N., Fisone, G., Moresco, R., Cunha, R. A., and Ferré, S. (2007). Adenosine A_{2A} receptors and basal ganglia physiology. *Prog. Neurobiol.* 83, 277–292.

Sebastião, A. M., and Ribeiro, J. A. (1996). Adenosine A2 receptor-mediated excitatory actions on the nervous system. *Prog. Neurobiol.* 48, 167–189.

Sebastião, A. M., and Ribeiro, J. A. (2009). Tuning and fine-tuning of synapses with adenosine. *Curr. Neuropharmacol.* 7, 180–194.

Seidenbecher, C. I., Landwehr, M., Smalla, K. H., Kreutz, M., Dieterich, D. C., Zuschratter, W., Reissner, C., Hammarback, J. A., Böckers, T. M., Gundelfinger, E. D., and Kreutz, M. R. (2004). Caldendrin but not calmodulin binds to light chain 3 of MAP1A/B: an association with the microtubule cytoskeleton highlighting exclusive binding partners for neuronal Ca(2+)-sensor proteins. *J. Mol. Biol.* 336, 957–970.

Seidenbecher, C. I., Langnaese, K., Sanmartí-Vila, L., Boeckers, T. M., Smalla, K. H., Sabel, B. A., Garner, C. C., Gundelfinger, E. D., and Kreutz, M. R. (1998). Caldendrin, a novel neuronal calcium-binding protein confined to the somatodendritic compartment. *J. Biol. Chem.* 273, 21324–21331.

Vu, C. B. (2005). Recent advances in the design and optimization of adenosine A_{2A} receptor antagonists. *Curr. Opin. Drug Discov. Devel.* 8, 458–468.

Woods, A. S., Marcellino, D., Jackson, S. N., Franco, R., Ferré, S., Agnati, L. F., and Fuxe, K. (2008). How calmodulin interacts with the adenosine A(2A) and the dopamine D(2) receptors. *J. Proteome Res.* 7, 3428–3434.

Wyatt, A. W., Steinert, J. R., Wheeler-Jones, C. P., Morgan, A. J., Sugden, D., Pearson, J. D., Sobrevia, L., and Mann, G. E. (2002). Early activation of the p42/p44MAPK pathway mediates adenosine-induced nitric oxide production in human endothelial cells: a novel calcium-insensitive mechanism. *FASEB J.* 16, 1584–1594.

Zhao, X., Várnai, P., Tuymetova, G., Balla, A., Tóth, Z. E., Oker-Blom, C., Roder, J., Jeromin, A., and Balla, T. (2001). Interaction of neuronal calcium sensor-1 (NCS-1) with phosphatidylinositol 4-kinase beta stimulates lipid kinase activity and affects membrane trafficking in COS-7 cells. *J. Biol. Chem.* 276, 40183–40189.

Conflict of Interest Statement: The authors declare that the research was conducted in the absence of any commercial or financial relationships that could be construed as a potential conflict of interest.

Received: 13 January 2012; paper pending published: 25 January 2012; accepted: 02 April 2012; published online: 18 April 2012.

Citation: Navarro G, Hradsky J, Lluís C, Casado V, McCormick PJ, Kreutz MR and Mikhaylova M (2012) NCS-1 associates with adenosine A_{2A} receptors and modulates receptor function. Front. Mol. Neurosci. 5:53. doi: 10.3389/fnmol.2012.00053

frontiers in
MOLECULAR NEUROSCIENCE

REVIEW ARTICLE
published: 23 February 2012
doi: 10.3389/fnmol.2012.00020

The visinin-like proteins VILIP-1 and VILIP-3 in Alzheimer's disease—old wine in new bottles

Karl H. Braunewell [1,2]*

[1] *Molecular and Cellular Neuroscience Laboratory, Department Biochemistry and Molecular Biology, Southern Research Institute, Birmingham, AL, USA*
[2] *Guest group In vitro-Electrophysiology, Department of Neurophysiology, Medical Faculty, Ruhr-University Bochum, Bochum, Germany*

Edited by:
Jose R. Naranjo, Centro Nacional de Biotecnología, Spain

Reviewed by:
Laura Mateos, Karolinska Institutet, Sweden
Robert Burgoyne, University of Liverpool, UK

***Correspondence:**
Karl H. Braunewell, Molecular and Cellular Neuroscience Laboratory, Department Biochemistry and Molecular Biology, Southern, Research Institute, 2000 Ninth Avenue South, Birmingham, AL 35205, USA.
e-mail: braunewell@sri.org

The neuronal Ca^{2+}-sensor (NCS) proteins VILIP-1 and VILIP-3 have been implicated in the etiology of Alzheimer's disease (AD). Genome-wide association studies (GWAS) show association of genetic variants of VILIP-1 (*VSNL1)* and VILIP-3 (*HPCAL1)* with AD+P (+psychosis) and late onset AD (LOAD), respectively. In AD brains the expression of VILIP-1 and VILIP-3 protein and mRNA is down-regulated in cortical and limbic areas. In the hippocampus, for instance, reduced VILIP-1 mRNA levels correlate with the content of neurofibrillary tangles (NFT) and amyloid plaques, the pathological characteristics of AD, and with the mini mental state exam (MMSE), a test for cognitive impairment. More recently, VILIP-1 was evaluated as a cerebrospinal fluid (CSF) biomarker and a prognostic marker for cognitive decline in AD. In CSF increased VILIP-1 levels correlate with levels of Aβ, tau, ApoE4, and reduced MMSE scores. These findings tie in with previous results showing that VILIP-1 is involved in pathological mechanisms of altered Ca^{2+}-homeostasis leading to neuronal loss. In PC12 cells, depending on co-expression with the neuroprotective Ca^{2+}-buffer calbindin D28K, VILIP-1 enhanced tau phosphorylation and cell death. On the other hand, VILIP-1 affects processes, such as cyclic nucleotide signaling and dendritic growth, as well as nicotinergic modulation of neuronal network activity, both of which regulate synaptic plasticity and cognition. Similar to VILIP-1, its interaction partner α4β2 nicotinic acetylcholine receptor (nAChR) is severely reduced in AD, causing severe cognitive deficits. Comparatively little is known about VILIP-3, but its interaction with cytochrome b5, which is part of an antioxidative system impaired in AD, hint toward a role in neuroprotection. A current hypothesis is that the reduced expression of visinin-like protein (VSNLs) in AD is caused by selective vulnerability of subpopulations of neurons, leading to the death of these VILIP-1-expressing neurons, explaining its increased CSF levels. While the Ca^{2+}-sensor appears to be a good biomarker for the detrimental effects of Aβ in AD, its early, possibly Aβ-induced, down-regulation of expression may additionally attenuate neuronal signal pathways regulating the functions of dendrites and neuroplasticity, and as a consequence, this may contribute to cognitive decline in early AD.

Keywords: cAMP/cGMP signaling, cognition, MAPK pathways, neurite outgrowth, neuroprotection, neuronal Ca^{2+}-sensors, nicotinic acetylcholine receptors, plasma membrane redox system

INTRODUCTION

In the old scriptures it is said: neither do men put new wine into old bottles, else the bottles break, and the wine runneth out, and the bottles perish, but they put new wine into new bottles, and both are preserved (Matthew 9:17). In science the phrase "To put old wine in new bottles" is often used when we aim to put old knowledge in the context of new findings, in the hope to create a good tasting wine. Recent findings on the implication of neuronal Ca^{2+}-sensor (NCS) proteins in the etiology of Alzheimer's disease (AD), particularly the role of VILIP-1 as cerebrospinal fluid (CSF) biomarker for AD, its correlation with MMSE scores and predictive value for cognitive decline in healthy individuals (Lee et al., 2008; Craig-Schapiro et al., 2009; Tarawneh et al., 2011), provoke new questions about what role these Ca^{2+}-sensors play in early cognitive impairment in AD. Some of our previous knowledge about these proteins may help to find answers for these questions. Thus, in this review I will focus on two members of the visinin-like protein (VSNL)-subfamily of NCS proteins, VILIP-1 and VILIP-3, reiterate some of the background information about these Ca^{2+}-signaling proteins, and summarize the current knowledge about their effects on neuronal signaling, which may be of potential relevance for the understanding of their link to disease severity and early cognitive decline in AD.

THE VISININ-LIKE PROTEINS

Multiple Ca^{2+}-sensing proteins have been identified in the central nervous system (CNS) over the last decades, reflecting the importance of the fine-tuning of the regulative function of

Ca^{2+} in neurons. Several of these proteins have been grouped together and termed NCS proteins (Nef, 1996; Braunewell and Gundelfinger, 1999; Burgoyne and Weiss, 2001; Burgoyne, 2007). Fourteen NCS protein genes related to the ubiquitous Ca^{2+}-sensor protein calmodulin exist in various species, and have been subdivided into five subfamilies. VILIP-1 (visinin-like protein 1, gene name *VSNL*1), VILIP-2 (visinin-like protein 2, gene name *hippocalcin-like 4, HPCAL4*), VILIP-3 (visinin-like protein 3, gene name *HPCAL1*), hippocalcin (gene name *HPCA*) and neurocalcin δ (gene name: *NCALD)* show amino acid identities between 67% and 94%, and form the subfamily of VSNLs (Braunewell and Gundelfinger, 1999; Burgoyne and Weiss, 2001; Spilker et al., 2002a; Burgoyne et al., 2004; Braunewell and Klein-Szanto, 2009). Branch 1 of the VSNL subfamily consists of VILIP-1 and VILIP-2, which are 89% homologous, and branch 2 consists of hippocalcin and VILIP-3, which share 94% identity, and both are 91% identical to neurocalcin δ (Spilker et al., 2002a). VILIP-1 was first cloned as visinin-like protein in chicken (Lenz et al., 1992), as neural visinin-like protein 1 in rat (NVP-1) (Kuno et al., 1992), as neurocalcin α from cow (Kato et al., 1998) and as VSNL1 in man (Polymeropoulos et al., 1995). VILIP-3 orthologs are rem-1 from chicken (Kraut et al., 1995), NVP-3 from rat (Kajimoto et al., 1993) and hHLP2 from man (Kobayashi et al., 1994). The protein sequences of VILIP-1 and VILIP-3 show 100% evolutionary conservation from chicken to man, indicating an important functional role of these Ca^{2+}-sensors in the CNS of various species.

THE DISTRIBUTION OF VILIP-1 AND VILIP-3 IN THE CNS

VSNLs show a distinct but widespread expression pattern with high expression levels in nerve cells (Braunewell and Gundelfinger, 1999), but see Gierke et al. (2004) for an overview on peripheral distribution of the proteins at lower levels. In the periphery VILIP-1 has been implicated in cell migration and is a putative tumor migration suppressor gene in several forms of cancer (for review see Braunewell and Klein-Szanto, 2009). A comprehensive mRNA expression study of the VSNL subfamily describes the expression of VILIP-1, VILIP-2, VILIP-3 and hippocalcin in the rat brain (Paterlini et al., 2000). VILIP-1 mRNA shows a widespread distribution in most brain areas except the caudate-putamen. VILIP-3 exhibits strong expression in the cerebellum where it localizes to Purkinje and granule cells, and additional expression in the forebrain including neocortex, hippocampus and caudate-putamen (Paterlini et al., 2000). Comparative expression studies have been performed at the protein level, including studies of VILIP-1 and VILIP-3 in the rat cerebellum and hippocampus (Spilker et al., 2000), of neurocalcin isoforms α (VILIP-1) and δ in the rat cerebellum (Kato et al., 1998), and of VILIP-1 and VILIP-3 in the human brain (Bernstein et al., 1999). Immunohistochemical studies with VILIP-1-specific antibodies show expression in principal and non-principal neurons. Particularly strong expression levels are found in subpopulations of calbindin-D28K and calretinin-positive GABAergic interneurons in all hippocampal regions in the rat brain (Zhao and Braunewell, 2008). In hippocampal interneurons VILIP-1 co-localizes mainly with the so-called Ca^{2+}-buffer proteins calbindin-D28K and calretinin (60–70%), but much less pronounced with parvalbumin (<10%) (Bernstein et al., 1999; Zhao and Braunewell, 2008). The rat expression profile differs from the profile in the human hippocampus. VILIP-1 immunoreactive neurons were found in the hippocampal CA1, CA4 and hilus regions, but were weak in the CA2 and CA3 areas in the human brain (Bernstein et al., 1999). Strong VILIP-3 protein and mRNA expression has been localized in the cerebellum, but expression in other brain regions including cortex and hippocampus has been observed (Spilker et al., 2000; Hamashima et al., 2001; Spilker and Braunewell, 2003). High expression levels of VILIP-3 exist in the dentate gyrus at the mRNA level (Spilker et al., 2000). VILIP-1 and VILIP-3 co-localize in hippocampal neurons in culture, showing a strong expression for VILIP-1 in many neurons and weaker expression of VILIP-3 in a subset of neurons (Spilker and Braunewell, 2003). To further understand the roles of these proteins in AD pathology, cellular and subcellular co-localization studies of VSNLs with their interaction partners need to be performed in AD brains and in AD animal models in the future.

THE CA^{2+}-MYRISTOYL SWITCH, TARGET INTERACTION, AND NEURONAL CA^{2+}-SIGNALING

VSNLs consist of 191–193 amino acid residues and harbor EF-hands as Ca^{2+}-binding motif. EF-hands consist of several core amino acids involved in the coordinative binding of Ca^{2+} (D-X-D/N-X-D/N-X-Y-$(X)_4$-E). All VSNLs possess 4 EF-hands, however, EF-hand 1 is dysfunctional due to changes in the core amino acid sequence (Braunewell, 2009; Braunewell and Klein-Szanto, 2009). At their N-terminus VSNLs bear a consensus sequence (M-G-$(X)_3$-S) for N-terminal myristoylation, which leads to the co-translational attachment of a C14 myristic fatty acid. This modification enables all VSNLs to translocate to subcellular membrane compartments (Kobayashi et al., 1993; Ladant, 1995; Lenz et al., 1996; Spilker et al., 2002b) by a molecular mechanism termed Ca^{2+}-myristoyl switch (Zozulya and Stryer, 1992). The molecular mechanism of the switch has been first analyzed in detail from tertiary structure data for the NCS protein recoverin. Binding of Ca^{2+} to recoverin induces a conformational change leading to surface exposure of hydrophobic protein parts and exposure of the myristoyl side chain, thereby making these structures available for interaction with cellular membranes and/or target proteins (Tanaka et al., 1995; Ames et al., 1996, 1997). In living cells, after increasing the intracellular Ca^{2+}-concentration, VSNLs can translocate to subcellular membrane compartments (Ivings et al., 2002; Spilker et al., 2002b; O'Callaghan et al., 2002, 2003; Spilker and Braunewell, 2003). However, the Ca^{2+}-dependent subcellular membrane localization of endogenously expressed VILIP-1 and VILIP-3 differed substantially in the same hippocampal neuron. VILIP-1 shows cell surface membrane association, including membranes of axons and dendrites, which is in line with the described function of VILIP-1 as modulator of cell surface associated proteins (Braunewell et al., 1997, 2001b; Lin et al., 2002a,b; Chaumont et al., 2008; Richler et al., 2011). In addition, VILIP-1 only affiliates with trans-Golgi membranes following a Ca^{2+}-stimulus in hippocampal neurons (Spilker and Braunewell, 2003), while VILIP-3 showed a weak Ca^{2+}-independent Golgi localization that was only gradually enhanced following stimulation

of hippocampal neurons (Spilker et al., 2002b). Furthermore, VILIP-3 interacts with intracellular juxtanuclear membranes and granular structures in the whole cytosol (Spilker and Braunewell, 2003), which fits to a possible function as a modulator of MAP kinases (Spilker et al., 2002a), and the ER-localized plasma membrane redox system (PMRS) (Oikawa et al., 2004). Interestingly in this context, under conditions of disturbed Ca^{2+}-homeostasis in AD an enhanced juxtanuclear membrane localization of VSNLs exists (Braunewell et al., 2001a; Blandini et al., 2004). We will need additional studies using markers for cellular organelles to understand their distinct subcellular distribution pattern and the re-distribution mechanisms following normal and pathological Ca^{2+}-signals.

The reversible localization of Ca^{2+}-sensors to distinct membrane compartments and signaling scaffolds in living neurons has been postulated to be a signal transduction mechanism for the selective activation of downstream signaling cascades, such as receptors, receptor signaling complexes and signal effector molecules (Spilker et al., 2002b; Spilker and Braunewell, 2003). Besides EF-hand 1 as a putative functional domain for VILIP-1 and VILIP-3, basic amino acids in the N-terminus have been postulated to be involved in interaction with phospholipids, particularly with their phosphatidylinositol phosphate (PIP) headgroups. Unmyristoylated VILIP-1 can bind to artificial phospholipid bilayers in the absence of Ca^{2+}, and monolayer adsorption measurements showed a preference of binding to $PI(4,5)P_2$ over $PI(3,4,5)P_3$ (Braunewell et al., 2010; Wang et al., 2011). Furthermore, VILIP-1 and hippocalcin have been shown to interact with $PI(4,5)P_2$ at the cell surface membrane in hippocampal neurons (O'Callaghan et al., 2005; Braunewell et al., 2010). The functional implications of the additional phospholipid interaction are not yet understood. EF-hand 1 forms the most variable part in the sequence of NCS proteins and, therefore, comprises a possible interaction site with target proteins (Lian et al., 2011). NCSs, such as VSNLs, serve as effectors to transduce cellular Ca^{2+}-signals. Similar to the prototypical Ca^{2+}-sensor calmodulin, the VSNLs appear to be modulators of multiple intracellular targets showing a "pleiotropy" of actions. VILIP-1 affects cAMP- and cGMP signaling and downstream signaling pathways including the rhoA/ROCK signaling pathway (Braunewell et al., 1997, 2001a; Mahloogi et al., 2003; Brackmann et al., 2005; Jheng et al., 2006; Chen et al., 2009). It interacts with several ligand-gated ion channels, such as glutamate receptors of the kainate subtype GluR6 (Coussen et al., 2005), the P2X2 ATP receptor (Chaumont et al., 2008), and the α4β2 nicotinic acetylcholine receptor (nAChR) (Lin et al., 2002a). Interestingly, VILIP-1 forms dimers, which appears to be important for the interaction with receptor dimers/multimers, such as α4β2 nAChR and the natriuretic peptide B receptor (NPR2, NPR-B) (Li et al., 2011; Wang et al., 2011). Functionally, VILIP-1 enhances surface expression of NPR-B, P2X2 ATP receptor and α4β2 nAChR (Brackmann et al., 2005; Chaumont et al., 2008; Gierke et al., 2008). In contrast to VILIP-1, comparatively little is known about signaling activities of VILIP-3. Although it forms dimers with VILIP-1 (Jheng et al., 2006), VILIP-3 does not affect the VILIP-1 target NPR-B (Spilker and Braunewell, 2003; Chen et al., 2009). In contrast, VILIP-3 directly or indirectly enhances activity of ERK1 and ERK2 (extracellular signal-regulated kinase 1 and 2) MAPK (mitogen-activated protein kinase) signaling (Spilker et al., 2002a), and interacts with cytochrome b5, with unknown functional impact (Oikawa et al., 2004).

NEURONAL CA^{2+}-SIGNALING AND AD

According to the amyloid β (Aβ) hypothesis, excessive accumulation of Aβ assemblies in the brain is involved in the etiology of AD (**Figure 1**). Gradual accumulation of aggregated Aβ initiates a complex, multistep cascade that includes inflammatory changes, gliosis, neuritic/synaptic changes, transmitter loss, and formation of neurofibrillary tangles (NFT), leading to cognitive impairments and ultimately to extensive cell death in both sporadic (late-onset AD, LOAD: ApoE4 and other risk factors) and familial or genetically linked AD (FAD with the

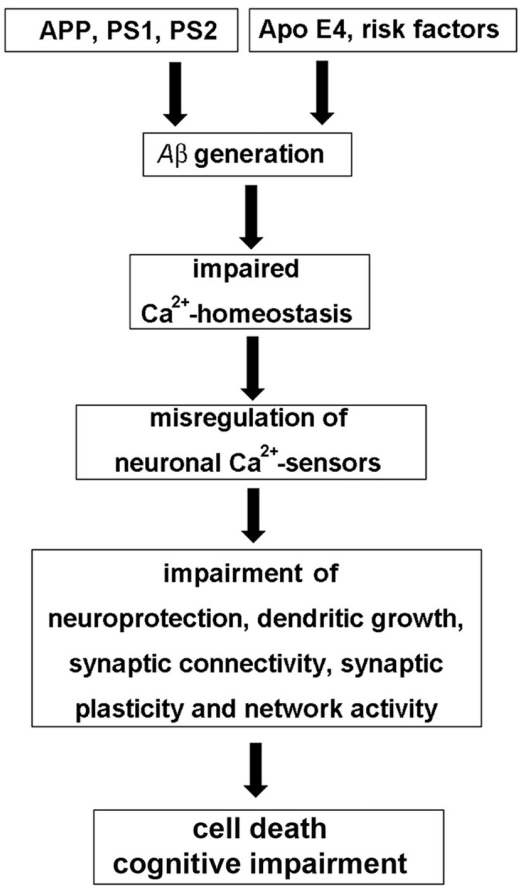

FIGURE 1 | The "neuronal Ca^{2+}-sensor hypothesis" of Alzheimer's disease. In the Aβ hypothesis of AD genetic risk factors, such as mutations in the amyloid precursor protein (APP) and the presenilins PS1 and PS2, but also risks factors such as the apolipoprotein gene ApoeE4, age, nutrition or exercise in sporadic AD lead to the excessive generation of toxic forms of the Aβ peptide, which is derived from APP. Aβ then causes an impairment of neuronal Ca^{2+}-homeostasis resulting in the misregulation of neuronal Ca^{2+}-sensor (NCS) proteins. Pathological expression and function of NCS proteins affects various neuronal signaling pathways involved in neuroprotection, neuronal connectivity, and synaptic plasticity, which, among other mechanisms, contribute to cognitive impairment and cell death observed in AD.

genetic risk factors APP—amyloid precursor protein, PS1 and PS2—presenilins 1 and 2) (Hardy and Selkoe, 2002; Holtzman et al., 2011). The molecular mechanisms involved are not completely understood. However, any AD hypothesis is challenged to explain that the changes in synaptic physiology and the onset of cognitive impairments long precede the massive cell death that characterizes the later stages of AD. An extension of the Aβ hypothesis to account for this fact, is the Ca^{2+}-hypothesis of AD. The hypothesis aims to explain how abnormal Aβ metabolism induces a change in Ca^{2+}-homeostasis, which then initiates both, the early decline in memory and the later, more massive changes in Ca^{2+}-levels and the following increase in neuronal cell death (for review see Foster, 2007; Bezprozvanny and Mattson, 2008; Berridge, 2010; Supnet and Bezprozvanny, 2010; Chakroborty and Stutzmann, 2011). Aβ induces a massive disturbance of Ca^{2+}-homeostasis by enhancing both, the entry of external Ca^{2+} as well as the sensitivity of the InsP3 and ryanodine receptors, that release Ca^{2+} from internal stores. Aβ oligomers have been reported to increase Ca^{2+}-influx by forming Ca^{2+}-pores in the plasma membrane and by regulating existing plasma membrane Ca^{2+}-channels. However, increased intracellular Ca^{2+}-levels are not only functionally linked to Aβ, but also to presenilin mutations and ApoE4 expression. The initial localized up-regulation of Ca^{2+}-levels will then lead to re-modeling of Ca^{2+}-signaling pathways, such as for instance NCS signaling (**Figure 1**), which leads to subtle effects on neurotransmission and synaptic plasticity underlying cognition (Chakroborty and Stutzmann, 2011), and later to changes affecting mitochondrial (Supnet and Bezprozvanny, 2010) and endoplasmatic reticulum Ca^{2+}-pathways (Bezprozvanny and Mattson, 2008), causing massive neuronal cell death. A current focus of the Ca^{2+}-hypothesis is to understand how the initial subtle dys-regulation of Ca^{2+}-signaling affects neuroplasticity and brings about the early loss of memory. It also has been postulated that since the defect in cognition occurs before there is any sign of massive cell death, the development of drugs to normalize the subtle changes in Ca^{2+}-signaling may arrest the slow progression of AD (Berridge, 2010).

THE ROLE OF NCS PROTEINS IN AD: NEUROPROTECTION VERSUS NEUROTOXICITY

NCS proteins have been implicated in cognitive processes and in the pathology of AD (for review see Blandini et al., 2004; Buxbaum, 2004; Braunewell, 2005; Braunewell and Bernstein, 2009; Craig-Schapiro et al., 2009). There is less protein expression of VILIP-1, and the numbers of VILIP-1- and, to a lesser degree, VILIP-3-immunoreactive neurons are reduced in the temporal cortex of AD patients, (Bernstein et al., 1999). These data point to a disease-related loss of VSNLs. In AD brains, extracellularly located VSNLs are in close association with the pathologic lesions, such as dystrophic nerve cell processes, amorphous and neuritic plaques, and extracellular NFTs, indicating that they may be involved in the pathophysiology of altered Ca^{2+}-homeostasis in AD (Braunewell et al., 2001a). In PC12 pheochromocytoma cells, VILIP-1 over-expression enhances hyper-phosphorylation of tau protein, which destabilizes microtubules, and, in transfected PC12 cells, it increases Ca^{2+}-mediated cell death (Schnurra et al., 2001). Co-expression of the Ca^{2+}-buffer protein, calbindin-D28K, which is neuroprotective and down-regulated in AD (Iacopino and Christakos, 1992; McMahon et al., 1998), attenuates the effect of VILIP-1 on cell death induced by ionomycin. In this context, VILIP-1 has a widespread distribution in the brain, including in GABAergic neurons (Bernstein et al., 1999). In addition to being expressed in most pyramidal neurons of human and rat hippocampi, it largely co-localizes with calbindin-D28K and calretinin in GABAergic interneurons (Zhao and Braunewell, 2008), but less with parvalbumin-positive interneurons. In interneurons of transgenic AD mouse models and in AD brains, the Ca^{2+}-buffer proteins, calbindin-D28K and calretinin, are down-regulated (Kaufmann et al., 1998; Palop et al., 2003, 2007; Popović et al., 2008; Baglietto-Vargas et al., 2010; Takahashi et al., 2010). These findings suggest that the ratio of expression of Ca^{2+}-sensor to Ca^{2+}-buffer proteins may define subpopulations of neurons particularly vulnerable to Aβ-induced and Ca^{2+}-mediated neurotoxicity (**Figure 2**). Since interneurons are essential for the generation of synchronous rhythmic activity in the hippocampus, which is underlying cognitive processing/memory encoding, the early alterations of hippocampal inhibitory functionality in AD may result in the cognitive impairments seen in the initial stages of the disease (Palop and Mucke, 2010). On

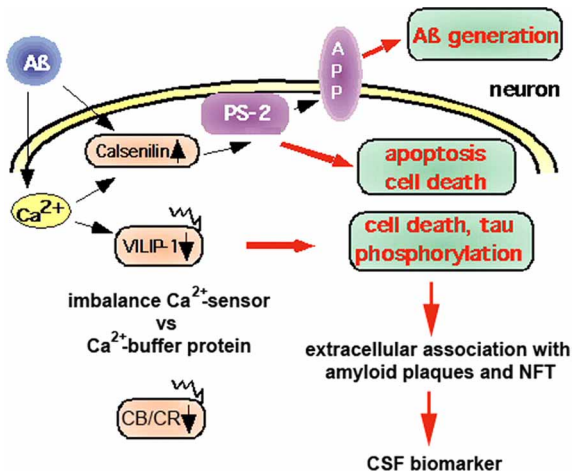

FIGURE 2 | Neuroprotective versus neurotoxic role of Ca^{2+}-binding proteins in the pathology of AD. Aβ deposition is believed to cause changes in the Ca^{2+}-homeostasis that lead to pathological expression and activation of NCS proteins, such as calsenilin and VILIP-1. Calsenilin, which is up-regulated in AD, promotes apoptotic cell death in a manner dependent on presenilin-2 (PS2), but has been found to be neuroprotective in PC12 cells. In contrast, VILIP-1 is down-regulated in AD. Over-expression of VILIP-1 leads to tau phosphorylation and cell death in PC12 neurons, which is attenuated by expression of the Ca^{2+}-buffer protein calbindin-D28K. Thus, in AD brains, an imbalance in the ratio of Ca^{2+}-sensor (Calsenilin, VILIP-1) versus Ca^{2+}-buffer proteins (CB/CR: calbindin-D28K, calretinin) in subpopulations of neurons may lead to their selective vulnerability and early loss, and, in turn, to the appearance of extracellular VSNLs, which are associated with the pathologic hallmarks amyloid plaques and neurofibrillary tangles (NFT). VILIP-1 is detected in the cerebrospinal fluid (CSF) of AD patients, and serves as a CSF biomarker. Increased levels correlate with CSF *t*-tau, *p*-tau, the ApoE ε4/ε4 genotype, and with mini mental state examination (MMSE) scores of AD patients.

the other hand, for the related VSNL hippocalcin a neuroprotective role has been postulated in age-related neurodegeneration (Masuo et al., 2007). The only other NCS protein that has been implicated in AD (**Figure 2**) and which is not belonging to the VILIP subfamily, is Calsenilin/DREAM/KChIP3. It was independently identified as a NCS protein that interacts with presenilins (PS1 and 2), serves as a transcription repressor, and binds to A-type potassium channels (Buxbaum et al., 1998; Carrión et al., 1999; An et al., 2000). Calsenilin levels are elevated in the cortex region of AD brains and in the neocortex and the hippocampus of brains of Swedish mutant beta-amyloid precursor protein (sweAPP) transgenic mice. When cultured cortical and hippocampal neurons are exposed to Aβ this induces both calsenilin protein and mRNA expression, and cell death, whereas calsenilin expression blockade protects against Aβ toxicity (Jo et al., 2004). In contrast, in Xenopus oocytes calsenilin reversed the pathogenic effects of mutant PS1 on $Ins(1,4,5)P_3$-mediated Ca^{2+}-signaling. Presenilin mutations perturb intracellular Ca^{2+}-signaling pathways contributing to the key features of AD, such as increased Aβ production, tau hyper-phosphorylation, and enhanced vulnerability to cell death. Calsenilin expression reversed the mutant PS-1-enhanced amplitudes and altered kinetics of Ca^{2+}-signals in oocytes (Leissring et al., 2000). Rivas et al. found recently, using the yeast two-hybrid assay, that DREAM interacts with peroxiredoxin 3 (Prdx3), an antioxidant enzyme found in mitochondria (Rivas et al., 2011). The peroxiredoxin system is a cellular defense system against oxidative stress, and the decreased protein levels of Prdx3 in AD has been discussed as the results of mitochondrial damage, which may reduce cellular protection against oxidative damage (Kim et al., 2001). The Prdx3-DREAM interaction modulates the DREAM redox state and in turn modulates transcriptional repression by DREAM. Since transient DREAM knockdown in PC12 cells sensitizes these cells to H(2)O(2)-induced oxidative stress, this would suggest a protective role for DREAM against oxidative damage (Rivas et al., 2011). In the future the careful re-evaluation of the potential neurotoxic versus neuroprotective roles of NCS proteins in AD-related cellular models and in AD animal models is necessary to define whether different NCS proteins show neurotoxic and/or neuroprotective properties under the specific conditions of disturbed Ca^{2+}-homeostasis in AD brains.

VSNLs AS BIOMARKERS FOR AD—OLD WINE IN NEW BOTTLES

Association of VSNLs with the pathologic hallmarks of AD have been published more than a decade ago. More recent support for a functional role of VSNLs in AD comes from genome-wide association studies (GWAS). An SNP for VILIP-1 associates (rs4038131, $p = 5.9 \times 10^{-7}$) with AD and subsequent psychosis (Hollingworth et al., 2011). For VILIP-3, there was an association of 2 SNPs (rs1019785, rs10197851, $p = 3.67 \times 10^{-6}$, $p = 7.13 \times 10^{-6}$) with LOAD; this was replicated in the NIH LOAD data set (Lee et al., 2011). VILIP-1 seems to have additional roles in the cognitive impairments associated with AD. The early findings of reduced protein expression of VSNLs (Bernstein et al., 1999; Schnurra et al., 2001) have been confirmed for brain areas other than the temporal cortex, and extended to changes in mRNA levels. For example, in postmortem brains of AD patients, there is lower expression of VILIP-1 mRNA in the amygdala, cingulate cortex, hippocampus, and cerebellum (Loring et al., 2001; Youn et al., 2007). Whole-genome expression profiling of RNA obtained from the frontal cortex identified genes associated with cognitive decline, and expression of VILIP-1 mRNA correlated with NFT content and with the MMSE scores of AD patients (Wilmot et al., 2008). Similarly, two independent re-analyses were performed on a microarray dataset corresponding to hippocampus gene expression for AD subjects with varying degrees of severity (contributed by Blalock et al., 2004), found down-regulation of VILIP-1 mRNA, association with NFT content in the hippocampus, and again an association with the MMSE score (Miller et al., 2008; Gómez Ravetti et al., 2010). These data indicate that VILIP-1 expression is lost not only due to loss of VILIP-1-expressing neurons (Bernstein et al., 1999; Schnurra et al., 2001), but also to pathological down-regulation of VILIP-1 mRNA levels. The lowered VILIP-1 mRNA expression correlated with the severity of cognitive decline, as measured by MMSE scores for AD subjects. Similarly, an observation by Lee et al., 2008 ties in with these results on VILIP-1-MMSE correlation in microarray studies (Miller et al., 2008; Gómez Ravetti et al., 2010). In this study, CSF samples were analyzed by ELISA to measure concentrations of Aβ1–42, *t*-tau, *p*-tau, and VILIP-1. However, in contrast to VILIP-1 mRNA signals, in the CSF of AD subjects, VILIP-1 protein is increased, relative to controls. There was also strong correlation of increased CSF-VILIP-1 with CSF *t*-tau, *p*-tau, the ApoE ε4/ε4 genotype, and lowered MMSE scores of AD patients (Lee et al., 2008). The new findings of the appearance of the intracellular protein VILIP-1 in the CSF is consistent with the older view that VILIP-1 is released from neurons during neurotoxic insults, and that extracellular VILIP-1 then associates with the pathologic characteristics of AD (Schnurra et al., 2001; Braunewell et al., 2001a). Thus, although VILIP-1 mRNA appears to be actively down-regulated in AD and the down-regulation correlates with reduced MMSE scores, at the same time neurons expressing VILIP-1 seem to be particularly vulnerable against Aβ-induced disturbances of Ca^{2+}-homeostasis, and these neurons appear to die early on in the disease. This would explain how the intracellular protein is released from neurons and can then be found associated with amyloid plaques and NFT, and finally makes its way into the CSF. Thus, there appears to be significant correlation of reduced VILIP-1 mRNA as well as enhanced CSF protein levels with reduced MMSE scores and early cognitive decline in AD.

VILIP-1 AND COGNITIVE IMPAIRMENT IN AD?

Since VILIP-1 concentrations in the CSF correlate with MMSE scores, CSF-VILIP-1 has been proposed as a marker for declined cognition and disease severity (Verbeek and Olde Rikkert, 2008; Craig-Schapiro et al., 2009). This assumption from the Lee et al., 2008 study prompted a larger study in 300 subjects, where VILIP-1 was confirmed as a CSF biomarker for early AD (Tarawneh et al., 2011). In this study VILIP-1 also showed elevated plasma levels. Importantly, the Holtzman group also describes a 2–3 year follow-up study in cognitively healthy control subjects, in which CSF levels of VILIP-1 in still healthy individuals had predictive

value for future cognitive decline (Tarawneh et al., 2011). Thus, the correlation of CSF VILIP-1 with MMSE scores suggests that VILIP-1 in the CSF is a valid biomarker, and is a prognostic marker for cognitive decline in early AD (Craig-Schapiro et al., 2009; Tarawneh et al., 2011). Notably, in non-AD dementias no increased VILIP-1 CSF levels were detected, pointing to the possibility that VILIP-1 may be linked to disease-specific mechanisms or alterations in signaling pathways (Tarawneh et al., 2011). These novel observations should raise a variety of new research questions. More support that VILIP-1 is directly associated with cognitive capabilities comes from a study showing that VSNL1 SNPs are associated with performance in the Wisconsin Card Sorting Test, an assessment of frontal cortical function in schizophrenia patients with cognitive impairments (Braunewell et al., 2011). These results also raise the question of whether VILIP-1, in addition to its role in Aβ-induced and Ca^{2+}-mediated neuronal death, might be involved in neuronal signaling pathways and mechanisms of impaired synaptic plasticity and cognition in AD. Other related NCS proteins, including Calsenilin/DREAM/KChIP3 and NCS-1, affect synaptic plasticity (Sippy et al., 2003; Fontán-Lozano et al., 2009; Saab et al., 2009; Wu et al., 2010). VSNLs are specialized mediators of Ca^{2+}-signals in neuronal signaling processes known to affect cognition. VILIP-2 was shown to slow inactivation of Ca(V)2.1 channels in a myristoylation dependent manner (Few et al., 2005). Ca(V)2.1 channels conduct P/Q-type Ca^{2+}-currents, and initiate synaptic transmission at most synapses in the CNS. The VILIP-2-dependent facilitation and inactivation of these channels contributes to short-term synaptic plasticity (Nanou et al., 2012). Hippocalcin acts as Ca^{2+}-sensor for hippocampal long-term depression (Palmer et al., 2005), and hippocalcin knockout animals display impaired spatial and associative memory (Kobayashi et al., 2005). Moreover, it was shown show that expression of hippocalcin, but not of a hippocalcin myristoylation mutant, leads to an enhanced slow afterhyperpolarization current I(sAHP) in cultured hippocampal neurons. A train of action potentials activates potassium channels in a Ca^{2+}-dependent manner to produce the sAHP current, which in turns dampens neuronal excitability. This was strongly reduced in hippocalcin knockout animals (Tzingounis et al., 2007). The modulation of sAHP currents is believed to regulate neuronal excitability, synaptic efficacy, and the threshold for tetanus-induced synaptic plasticity. Hippocalcin and neurocalcin δ, but not VILIP-2, can also act as a Ca^{2+}-sensor for the sAHP current in the cerebral cortex, indicating that VSNLs can gate sAHPs and thus neuronal excitability in various brain regions (Villalobos and Andrade, 2010). It is likely that VILIP-1 and -3 have similar functions in regulating neuronal excitability and synaptic plasticity, particularly since VILIP-1 up-regulation has been linked to mGluR-dependent long-term potentiation (Braunewell et al., 2003; Brackmann et al., 2004).

VILIP-1, DENDRITIC CONNECTIVITY AND COGNITIVE IMPAIRMENT IN AD

A major question is how VILIP-1 and VILIP-3 may influence cognition. One possibility for VILIP-1 is that it activates cyclic AMP- and cyclic GMP-signaling by enhancing surface expression of membrane-localized adenylyl and guanylyl cyclases (Brackmann et al., 2005; Braunewell et al., 2011). Thereby, VILIP-1 might influence cAMP and cGMP-dependent neuronal processes, including neuronal differentiation, neurite outgrowth, different forms of synaptic plasticity and learning and memory (Schuman and Madison, 1991; Telegdy, 1994; Monfort et al., 2002). The regulation of cAMP-levels by VILIP-1 has been initially detected in stably transfected rat C6 glioma cells (Braunewell et al., 1997). The myristoylation-deficient mutant of VILIP-1, which lacks the myristoylation consensus motif and, therefore, does not exhibit the Ca^{2+}-myristoyl switch, showed a dominant-negative effect on cAMP-levels in C6 cells. Already basic cAMP levels appeared to be elevated in VILIP-1-transfected C6 cells, which is the cause for induction of differentiation of those glioma cells (Braunewell and Gundelfinger, 1997). VILIP-1 appears to influence adenylyl cyclase activity in selected cell types including human embryonic kidney cells (Lin et al., 2002b), the pancreatic β cell line MIN6 (Dai et al., 2006), and various skin tumor cell lines, where it also affects rhoA signaling (Mahloogi et al., 2003; Schönrath et al., 2011). No direct interaction of VILIP-1 with adenylyl cyclase isoforms has been detected, but VILIP-1 expression was shown to enhance surface expression of different adenylyl cyclase isoforms in skin tumor cell lines leading to enhanced tumor cell migration (Schönrath et al., 2011).

VILIP-1 enhances neurite outgrowth in SH-SY5Y neuroblastoma via effects on cAMP-signaling (Braunewell et al., 2011). The cAMP signaling pathway overcomes Aβ-induced inhibition of neurite formation in SH-SY5Y neurons and in the hippocampus in transgenic APP/PS1 mice, carrying human AD mutations (Smith et al., 2009). In SH-SY5Y cells, Aβ reduces cAMP levels and increases levels of the GTP-bound (active) form of rhoA, which is eliminated by the rho-associated protein kinase (ROCK) inhibitor, Y-27632 (Petratos et al., 2008). Manipulation of the cAMP-rhoA/ROCK signaling pathway using the ROCK inhibitor leads to the extension of long neurites in SH-SY5Y cells. Consistent with the effect of VILIP-1 on cAMP signaling in SH-SY5Y neurons, the reduction of its expression through exposure of cells to siRNA results in loss of dendritic arborisation as measured as reduced number of dendrites in a Sholl analysis in hippocampal neurons. This effect is likely due to the observed reduced VILIP-1-dependent formation of cAMP in hippocampal neurons. As expected over-expression of VILIP-1 led to an increase in the number of dendrites in these neurons (Braunewell et al., 2011). It is noteworthy that calbindin-D28K, the neuroprotective Ca^{2+}-buffer protein which is down-regulated in AD and co-localizes with VILIP-1 in hippocampal interneurons (Gierke et al., 2008; Zhao and Braunewell, 2008), promotes neuronal differentiation and neurite outgrowth of hippocampal precursor cells and dopaminergic neurons (Choi et al., 2001; Kim et al., 2006). Similarly, hippocalcin enhances basic fibroblast growth factor-induced neurite outgrowth in a hippocampal cell line (Oh et al., 2008). Interestingly in another study, VILIP-1 and neurocalcin δ were found to be developmentally up-regulated in axon tracts in the olfactory system. Counter-intuitively, their overexpression led to reduced axon outgrowth, but left dendrite length unaffected in hippocampal neurons in the same study (Yamatani et al., 2010). Whereas neurocalcin δ also showed reduced branch

point and dendrite numbers, VILIP-1 appeared to only slightly increase dendrite numbers, although not significantly (Yamatani et al., 2010). It is highly likely that different VSNLs may affect different neuronal compartments, with VILIP-1 reducing axonal (Yamatani et al., 2010), but enhancing dendritic differentiation (Braunewell et al., 2011). However, comparative studies on axonal versus dendritic differentiation will have to be performed in the same experimental set up to further substantiate this hypothesis. Particularly the effect of VILIP-1 and, possibly, VILIP-3 on dendritic arborization and connectivity may underlie altered synaptic function and hippocampal network connectivity, and thus may contribute to the cognitive decline in early phases of AD. The loss of distinct Ca^{2+}-buffer and Ca^{2+}-sensor proteins in subpopulations of hippocampal interneurons, may render these neurons particularly vulnerable against Aβ-induced morphological disturbances, such as reduced dendritic spinogenesis in AD, which are significantly contributing to cognitive decline (Smith et al., 2009; Wei et al., 2010).

VILIP-1, NICOTINERGIC SIGNALING AND COGNITIVE IMPAIRMENT IN AD

One other possibility how VILIP-1 may affect cognition lies in the fact that VILIP-1 interacts with the α4β2 nAChR (Lin et al., 2002a). Reduced levels of nAChRs and cholinergic neurotransmission are involved in the etiology of AD, and acetylcholinesterase inhibitors are used for the treatment of AD (Buckingham et al., 2009). The high-affinity $\alpha_4\beta_2$ nAChR is the main nicotine binding site in the brain, and appears to mediate nicotine-dependent improvements in attention, learning, and working memory (Rezvani and Levin, 2001; Levin et al., 2006). These facts have sparked interest in the development of novel treatments for cognitive dysfunction in CNS disorders, based on modulation of nAChR activity. In clinical trials, agonists and antagonists of the major α7- and α4-containing nAChRs are beneficial (Buckingham et al., 2009; Bacher et al., 2009; Fedorov et al., 2009). Since VILIP-1 is an endogenous modulator of $\alpha_4\beta_2$ nAChR, it is conceivable that the down-regulation of VILIP-1 mRNA at early stages of AD leads to deficits in $\alpha_4\beta_2$ nAChR activity in the hippocampus. In a yeast two-hybrid screen for protein-protein interactions, VILIP-1 bound to a 30-amino acid region in the large intracellular loop of the α4 -subunit of the $\alpha_4\beta_2$ nAChR. Co-expression of VILIP-1 with recombinant $\alpha_4\beta_2$ nAChR up-regulated the surface expression levels by twofold and increased the agonist-sensitivity to acetylcholine by threefold. The VILIP-1 myristoylation mutant or mutants not able to bind Ca^{2+} are found to attenuate the modulation of $\alpha_4\beta_2$ nAChR (Lin et al., 2002a). Similarly, in hippocampal neurons, co-expression of VILIP-1 with recombinant $\alpha_4\beta_2$ nAChR up-regulated its surface expression and increased the agonist sensitivity to acetylcholine, suggesting that VILIP-1 is a modulator of α4β2 nAChR, and leading to functional up-regulation of the receptor (Zhao et al., 2009a). VILIP-1 and $\alpha_4\beta_2$ nAChR were found in a complex with the trans-Golgi SNARE syntaxin 6, involved in Golgi to surface membrane trafficking and constitutive exocytosis. Moreover, the nicotine-induced, and α7 nAChR-mediated Ca^{2+}-myristoyl switch of VILIP-1 in hippocampal neurons provides a crosstalk mechanism for the interaction of α7 with α4β2 nAChRs, in that the α7 nAChR mediated Ca^{2+}-influx in neurons can activate α4β2 nAChRs via VILIP-1 (Zhao et al., 2009b **Figure 3**). In rat and human hippocampi, VILIP-1 and α4β2 nAChR are co-localized in a subpopulation of interneurons (Gierke et al., 2008; Zhao and Braunewell, 2008). In view of the prominent expression of VILIP-1 in calbindin-positive interneurons and in disinhibitory, calretinin-positive interneurons in the hippocampal formation, which are also partly positive for α4β2 nAChR (Zhao and Braunewell, 2008), VILIP-1 is well positioned to regulate hippocampal network activity. The interaction of VILIP-1 with α4β2 nAChR enhances GABAergic signaling in interneurons, and the frequency of IPSCs (inhibitory postsynaptic currents) in pyramidal neurons (Gierke et al., 2008), thereby likely changing the activity of the hippocampal neuronal network, and thus synaptic plasticity and cognition (Rezvani and Levin, 2001; Levin et al., 2006). Interneurons are involved in the generation of synchronous rhythmic activity in the hippocampus essential for cognitive processing/memory encoding. Therefore, early alterations in hippocampal interneurons in AD may result in the cognitive impairments seen in the initial stages of the disease (Palop et al., 2003, 2007; Baglietto-Vargas et al., 2010). In AD the loss of VILIP-1 expression may thus lead to a loss of surface expression and functional activity of α4β2 nAChRs in interneurons, and in turn reduction of GABAergic interneuron activity (**Figure 3**). The effect of VILIP-1 on nicotinergic signaling, in hippocampal interneurons, for instance, may explain the correlation of CSF VILIP-1 levels and VILIP-1 mRNA levels with MMSE scores and cognition. Thus, down-regulation of VILIP-1

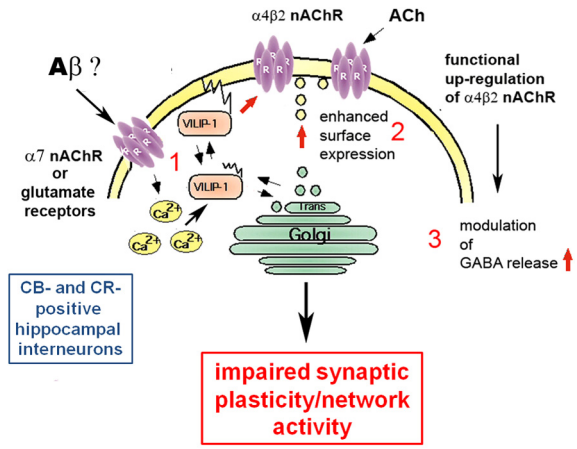

FIGURE 3 | Molecular mechanisms of the involvement of VILIP-1 in pathological network activity and cognition. (1) The amyloid β peptide binds to and activates receptors, such as the α7 nAChR and NMDA-type glutamate receptors, leading to changes in the cellular Ca^{2+}-homeostasis. The increase in Ca^{2+} concentrations shuttles VILIP-1 to the cell surface and Golgi membranes. **(2)** VILIP-1 enhances surface expression and sensitivity of α4β2 nAChRs in interneurons. **(3)** In hippocampal interneurons VILIP-1 enhances up-regulation of α4β2 nAChRs and thereby modulates GABA release. This leads to a VILIP-1-dependent enhancement of ACh-evoked IPSCs in hippocampal pyramidal cells. The pathological down-regulation of VILIP-1 in AD may thus negatively affect hippocampal network activity and synaptic plasticity, and lead to cognitive disturbances in the AD brain.

affecting α4β2 nAChR expression and activity in interneurons may contribute to cognitive impairments in AD.

VILIP-3 AND THE PLASMA MEMBRANE REDOX SYSTEM IN AD

Comparatively little is known about functional activities of VILIP-3. VILIP-3 affects ERK1/2-phosphorylation in PC12 cells (Spilker et al., 2002a), has been discussed to enhance cAMP levels in the prostatic epithelial cell line NbE-1 (Tang et al., 2012), and VILIP-3 as well as hippocalcin, interact with the microsomal enzyme cytochrome b5, which in turn interacts with cytochrome b5 reductase located in the endoplasmic reticulum-perinuclear region in microsomal membranes (Oikawa et al., 2004). Cytochrome b5 belongs to the PMRS (Hyun et al., 2006). Membrane-associated oxidative stress has been implicated in the synaptic dysfunction and neuronal degeneration that occurs in AD, but the underlying mechanisms are unknown. The PMRS provides electrons for energy metabolism and recycling of antioxidants, and is impaired in AD (Hyun et al., 2010). The activities of several PMRS enzymes are decreased in plasma membranes from the hippocampus and cerebral cortex of 3xTgAD mice, an animal model of AD. Neurons over-expressing the PMRS enzymes (NQO1 or cytochrome b5 reductase) exhibit increased resistance to Aβ (Hyun et al., 2010). Under conditions of disturbed Ca^{2+}-homeostasis in AD, there is an enhanced pathological, juxtanuclear localization of VILIP-3 (Braunewell et al., 2001a). The Ca^{2+}-dependent translocation of VILIP-3 to the endoplasmic reticulum (ER)-rich perinuclear region, may indicate that VILIP-3 impacts the microsomal monooxygenase complex composed of cytchrome b5-reductase, cytochrome P450, and other reductases of the ER. Although the functional implications of the interaction are not yet known, reduced expression of VILIP-3 may decrease PMSR activity and lead to enhanced oxidative stress. Thus, increased levels of VILIP-3 may be neuroprotective against Aβ-induced oxidative stress. In this context, hippocalcin also appears to be neuroprotective (Mercer et al., 2000; Lindholm et al., 2002). Hippocalcin−/− mice are more sensitive to thapsigargin-induced cell death and to excitotoxicity caused by kainic acid and quinolinic acid (Korhonen et al., 2005; Masuo et al., 2007). Moreover, these mice display increased caspase-12 activation and an age-dependent increase in neurodegeneration (Masuo et al., 2007). Interestingly, DREAM, which is upregulated in AD (Jo et al., 2004), was found to interact with the mitochondrial antioxidant enzyme Prdx3 (Rivas et al., 2011). Prdx3 expression protected against pesticide-induced mitochondrial damage, it improved cognition and decreased Aβ levels in APP transgenic mice (Chen et al., 2012). DREAM knockdown sensitizes H(2)O(2)-induced oxidative stress in PC12 cells, thus DREAM up-regulation has been discussed to be neuroprotective against oxidative stress (Rivas et al., 2011). It will be interesting to investigate whether there is actually co-localization of DREAM with Prdx3 in mitochondria or in the cytosol, and whether this interaction leads to neuroprotection under pathological conditions in an AD model. Taken together, these results indicate that plasma membrane, ER and mitochondrial redox systems play a crucial role in both oxidative stress-induced cell death and in cognitive impairment in AD, and it will be important to clarify whether the observed interactions of NCS proteins with different components of redox systems may affect the functionality of antioxidant systems in AD, and vice versa. These interactions may underlie some of the neurotoxic/neuroprotective and cognitive functions of NCS proteins in AD.

FUTURE PERSPECTIVES

There are many open questions concerning the role of Ca^{2+}-signaling and particularly the role of Ca^{2+}-sensors, such as Calsenilin and VSNLs, in the etiology of AD. The complex pattern of up- and down-regulation of NCSs, and of Ca^{2+}-buffers, such as calbindin-D28K and calretinin, may have multiple additive effects on neuronal pathways and systems at various levels and intensities, and thereby significantly contribute to cognitive impairments in AD and to neuronal death at the later stages of AD. In order to determine the effects of VSNLs, in conjunction with their respective interaction partners and associated signaling pathways, and to determine whether they are therapeutic targets for treatment of cognitive impairments in AD, several important questions need to be answered in the future (Working hypothesis **Figure 4**). First, (**1**) what are the mechanisms of VILIP down-regulation in AD. One possibility is a direct down-regulation by Aβ, or alternatively via Aβ-supression of neurotrophin signaling. Next, (**2**) what is the role VSNLs play in Aβ-induced Ca^{2+}-overload, leading to reduced activity of the PMRS and to impaired neuroprotection in vulnerable subpopulations of neurons. (**3**) What are the signaling pathways involved in the effect of VILIP-1 on tau-phosphorylation and (**4**) on dendritic growth and spinogenesis in neurons? Finally, whether there is changed expression of VSNLs, particularly in

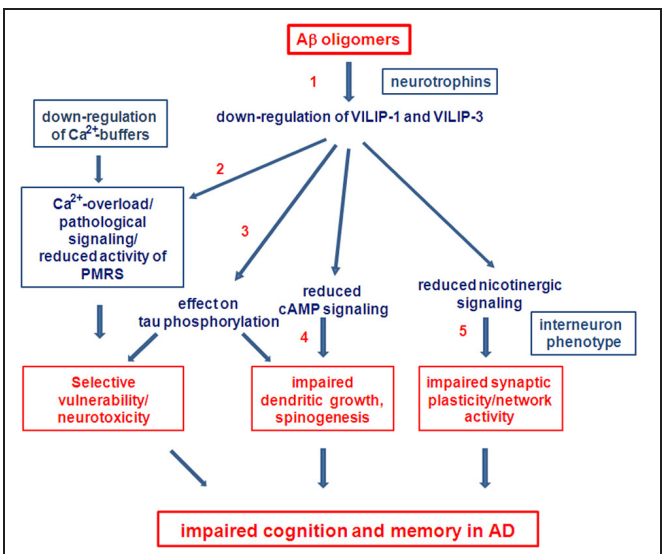

FIGURE 4 | Future perspectives. Working hypothesis and open questions on the involvement of VSNLs and associated signaling pathways as mediators of Aβ oligomer-induced cell death and detrimental effects on cognition in AD.

interneurons, that affects network activity and synaptic plasticity in transgenic AD animal models, and most importantly (**5**) whether for instance VILIP-1, via its modulatory effect on cAMP and nicotinergic signaling plays a role for impaired synaptic plasticity and cognition in animal models. Such an effect could contribute to some of the early cognitive impairments observed in AD.

ACKNOWLEDGMENTS

Work in Karl Heinz Braunewell's laboratories has been supported by grants from DFG (Br1579/8–1 and Br1579/9–1/2, Priority Program of the German Research Foundation SPP1226), Alzheimer's Drug Discovery foundation (ADDF), and Southern Research Institute (SRI) startup funding. The comprehensive and authoritative peer-review of this article is greatly appreciated.

REFERENCES

Ames, J. B., Ishima, R., Tanaka, T., Gordon, J. I., Stryer, L., and Ikura, M. (1997). Molecular mechanics of calcium-myristoyl switches. *Nature* 389, 198–202.

Ames, J. B., Tanaka, T., Stryer, L., and Ikura, M. (1996). Portrait of a myristoyl switch protein. *Curr. Opin. Struct. Biol.* 6, 432–438.

An, W. F., Bowlby, M. R., Betty, M., Cao, J., Ling, H. P., Mendoza, G., Hinson, J. W., Mattsson, K. I., Strassle, B. W., Trimmer, J. S., and Rhodes, K. J. (2000). Modulation of A-type potassium channels by a family of calcium sensors. *Nature* 403, 553–556.

Bacher, I., Wu, B., Shytle, D. R., and George, T. P. (2009). Mecamylamine-a nicotinic acetylcholine receptor antagonist with potential for the treatment of neuropsychiatric disorders. *Expert Opin. Pharmacother.* 10, 2709–2721.

Baglietto-Vargas, D., Moreno-Gonzalez, I., Sanchez-Varo, R., Jimenez, S., Trujillo-Estrada, L., Sanchez-Mejias, E., Torres, M., Romero-Acebal, M., Ruano, D., Vizuete, M., Vitorica, J., and Gutierrez, A. (2010). Calretinin interneurons are early targets of extracellular amyloid-beta pathology in PS1/AbetaPP Alzheimer mice hippocampus. *J. Alzheimers Dis.* 21, 119–132.

Bernstein, H-G., Baumann, B., Danos, P., Diekmann, S., Bogerts, B., Gundelfinger, E. D., and Braunewell, K-H. (1999). Regional and cellular distribution of neural visinin-like protein immunoreactivities (VILIP-1 and VILIP-3) in human brain. *J. Neurocytol.* 28, 655–662.

Berridge, M. J. (2010). Calcium hypothesis of Alzheimer's disease. *Pflugers Arch.* 459, 441–449.

Bezprozvanny, I., and Mattson, M. P. (2008). Neuronal calcium mishandling and the pathogenesis of Alzheimer's disease. *Trends Neurosci.* 31, 454–463.

Blalock, E. M., Geddes, J. W., Chen, K. C., Porter, N. M., Markesbery, W. R., and Landfield, P. W. (2004). Incipient Alzheimer's disease: microarray correlation analyses reveal major transcriptional and tumor suppressor responses. *Proc. Natl. Acad. Sci. U.S.A.* 101, 2173–2178.

Blandini, F., Braunewell, K-H., Manahan-Vaughan, D., Orzi, F., and Sarti, P. (2004). Neurodegeneration and energy metabolism: from chemistry and clinics. *Cell Death Differ.* 11, 479–484.

Brackmann, M., Schuchmann, S., Anand, R., and Braunewell, K-H. (2005). Neuronal Ca^{2+} sensor protein VILIP-1 affects cGMP signalling of guanylyl cyclase B by regulating clathrin-dependent receptor recycling in hippocampal neurons. *J. Cell. Sci.* 118, 2495–2505.

Brackmann, M., Zhao, C., Kuhl, D., Manahan-Vaughan, D., and Braunewell, K. H. (2004). MGluRs regulate the expression of neuronal calcium sensor proteins NCS-1 and VILIP-1 and the immediate early gene arg3.1/arc in the hippocampus *in vivo*. *Biochem. Biophys. Res. Commun.* 322, 1073–1079.

Braunewell, K. H. (2005). The dark side of Ca^{2+} signalling by neuronal Ca^{2+}- sensor proteins: from Alzheimer's disease to cancer. *Trends Pharmacol. Sci.* 26, 345–351.

Braunewell, K. H. (2009). VSNL-1. UCSD-nature molecule pages. doi: 10.1038/mp.a004095.01.

Braunewell, K. H., and Bernstein, H. G. (2009). Notes on visinin-like proteins and Alzheimer's disease. *Clin. Chem.* 55, 1041–1043.

Braunewell, K. H., Brackmann, M., and Manahan-Vaughan, D. (2003). Group I mGluRs regulate the expression of the intracellular neuronal calcium sensor protein VILIP-1 *in vitro* and *in vivo*: possible implications for mGluR-dependent hippocampal plasticity? *Neuropharmacology* 44, 707–715.

Braunewell, K. H., and Gundelfinger, E. D. (1997). Low level expression of calcium-sensor protein VILIP induces cAMP- dependent differentiation in rat C6 glioma cells. *Neurosci. Lett.* 234, 139–142.

Braunewell, K. H., and Gundelfinger, E. D. (1999). Intracellular neuronal calcium sensor proteins: a family of EF-hand calcium-binding proteins in search of a function. *Cell Tissue Res.* 299, 1–12.

Braunewell, K. H., Dwary, A. D., Richter, F., Trappe, K., Zhao, C., Giegling, I., Schönrath, K., and Rujescu, D. (2011). Association of VSNL1 with schizophrenia, frontal cortical function, and biological significance for its gene product as a modulator of cAMP levels and neuronal morphology. *Transl Psychol* 1, e22.

Braunewell, K. H., and Klein-Szanto, A. J. P. (2009). Visinin-like proteins (VSNLs): interaction partners and emerging functions in signal transduction of a subfamily of neuronal Ca^{2+}-sensor proteins. *Cell Tissue Res.* 335, 301–316.

Braunewell, K. H., Paul, B., Altarche-Xifro, W., Noack, C., Lange, K., and Hofmann, A. (2010). Interactions of visinin-like proteins with phosphoinositides. *Aust. J. Chem.* 63, 350.

Braunewell, K. H., Riederer, P., Spilker, C., Gundelfinger, E. D., Bogerts, B., and Bernstein, H. G. (2001a). Abnormal localization of two neuronal calcium sensor proteins, visinin-like proteins (VILIPs)-1 and -3, in neocortical brain areas of Alzheimer disease patients. *Dement. Geriatr. Cogn. Disord.* 2, 110–115.

Braunewell, K. H., Brackmann, M., Schaupp, M., Spilker, C., Anand, R., and Gundelfinger, E. D. (2001b). Intracellular neuronal calcium sensor (NCS) protein VILIP-1 modulates cGMP signalling pathways in transfected neural cells and cerebellar granule neurones. *J. Neurochem.* 78, 1277–1286.

Braunewell, K. H., Spilker, C., Behnisch, T., and Gundelfinger, E. D. (1997). The neuronal calcium-sensor protein VILIP modulates cyclic AMP accumulation in stably transfected C6 glioma cells: amino-terminal myristoylation determines functional activity. *J. Neurochem.* 68, 2129–2139.

Buckingham, S. D., Jones, A. K., Brown, L. A., and Sattelle, D. B. (2009). Nicotinic acetylcholine receptor signalling: roles in Alzheimer's disease and amyloid neuroprotection. *Pharmacol. Rev.* 61, 39–61.

Burgoyne, R. D. (2007). Neuronal calcium sensor proteins: generating diversity in neuronal Ca^{2+} signalling. *Nat. Rev. Neurosci.* 8, 182–193.

Burgoyne, R. D., O'Callaghan, D. W., Hasdemir, B., Haynes, L. P., and Tepikin, A. V. (2004). Neuronal Ca^{2+}-sensor proteins: multitalented regulators of neuronal function. *Trends Neurosci.* 27, 203–209.

Burgoyne, R. D., and Weiss, J. L. (2001). The neuronal calcium sensor family of Ca^{2+}-binding proteins. *Biochem. J.* 353, 1–12.

Buxbaum, J. D. (2004). A role for calsenilin and related proteins in multiple aspects of neuronal function. *Biochem. Biophys. Res. Commun.* 322, 1140–1144.

Buxbaum, J. D., Choi, E. K., Luo, Y., Lilliehook, C., Crowley, A. C., Merriam, D. E., and Wasco, W. (1998). Calsenilin: a calcium-binding protein that interacts with the presenilins and regulates the levels of a presenilin fragment. *Nat. Med.* 4, 1177–1181.

Carrión, A. M., Link, W. A., Ledo, F., Mellström, B., and Naranjo, J. R. (1999). DREAM is a Ca^{2+}-regulated transcriptional repressor. *Nature* 398, 80–84.

Chaumont, S., Compan, V., Toulme, E., Richler, E., Housley, G. D., Rassendren, F., and Khakh, B. S. (2008). Regulation of P2X2 receptors by the neuronal calcium sensor VILIP1. *Sci. Signal.* 1, ra8.

Chakroborty, S., and Stutzmann, G. E. (2011). Early calcium dysregulation in Alzheimer's disease: setting the stage for synaptic dysfunction. *Sci. China Life Sci.* 54, 752–762.

Chen, L., Yoo, S. E., Na, R., Liu, Y., and Ran, Q. (2012). Cognitive impairment and increased Aβ levels induced by paraquat exposure are attenuated by enhanced removal of mitochondrial H(2)O(2). *Neurobiol. Aging* 33, 432.e15–26.

Chen, K. C., Wang, L. K., and Chang, L. S. (2009). Regulatory elements and functional implication for the formation of dimeric visinin-like protein-1. *J. Pept. Sci.* 15, 89–94.

Choi, W. S., Chun, S. Y., Markelonis, G. J., Oh, T. H., and Oh, Y. J. (2001). Overexpression of calbindin-D28K induces neurite outgrowth in dopaminergic neuronal cells via

activation of p38 MAPK. *Biochem. Biophys. Res. Commun.* 287, 656–661.

Coussen, F., Perrais, D., Jaskolski, F., Sachidhanandam, S., Normand, E., Bockaert, J., Marin, P., and Mulle, C. (2005). Co-assembly of two GluR6 kainate receptor splice variants within a functional protein complex. *Neuron* 47, 555–566.

Craig-Schapiro, R., Fagan, A. M., and Holtzman, D. M. (2009). Biomarkers of Alzheimer's disease. *Neurobiol. Dis.* 35, 128–140.

Dai, F. F., Zhang, Y., Kang, Y., Wang, Q., Gaisano, H. Y., Braunewell, K. H., Chan, C. B., and Wheeler, M. B. (2006). The neuronal Ca^{2+} sensor protein visinin-like protein-1 is expressed in pancreatic islets and regulates insulin secretion. *J. Biol. Chem.* 281, 21942–22153.

Fedorov, N. B., Benson, L. C., Graef, J., Lippiello, P. M., and Bencherif, M. (2009). Differential pharmacologies of mecamylamine enantiomers: positive allosteric modulation and noncompetitive inhibition. *J. Pharmacol. Exp. Ther.* 328, 525–532.

Few, A. P., Lautermilch, N. J., Westenbroek, R. E., Scheuer, T., and Catterall, W. A. (2005). Differential regulation of CaV2.1 channels by calcium-binding protein 1 and visinin-like protein-2 requires N-terminal myristoylation. *J. Neurosci.* 25, 7071–7080.

Fontán-Lozano, A., Romero-Granados, R., del-Pozo-Martín, Y., Suárez-Pereira, I., Delgado-García, J. M., Penninger, J. M., and Carrión, A. M. (2009). Lack of DREAM protein enhances learning and memory and slows brain aging. *Curr. Biol.* 19, 54–60.

Foster, T. C. (2007). Calcium homeostasis and modulation of synaptic plasticity in the aged brain. *Aging Cell* 6, 319–325.

Gierke, P., Zhao, C., Bernstein, H. G., Noack, C., Anand, R., Heinemann, U., and Braunewell, K. H. (2008). Implication of neuronal Ca(2+)-sensor protein VILIP-1 in the glutamate hypothesis of schizophrenia. *Neurobiol. Dis.* 32, 162–175.

Gierke, P., Zhao, C., Brackmann, M., Linke, B., Heinemann, U., and Braunewell, K. H. (2004). Expression analysis of members of the neuronal calcium sensor protein family: combining bioinformatics and Western blot analysis. *Biochem. Biophys. Res. Commun.* 323, 38–43.

Gómez Ravetti, M., Rosso, O. A., Berretta, R., and Moscato, P. (2010). Uncovering molecular biomarkers that correlate cognitive decline with the changes of hippocampus' gene expression profiles in Alzheimer's disease. *PLoS One* 5:e10153 doi: 10.1371/journal.pone.0010153

Hamashima, H., Tamaru, T., Noguchi, H., Kobayashi, M., and Takamatsu, K. (2001). Immunochemical assessment of neural visinin-like calcium-binding protein 3 expression in rat brain. *Neurosci. Res.* 39, 133–143.

Hardy, J., and Selkoe, D. J. (2002). The amyloid hypothesis of Alzheimer's disease: progress and problems on the road to therapeutics. *Science* 297, 353–356.

Hollingworth, P., Sweet, R., Sims, R., Harold, D., Russo, G., Abraham, R., Stretton, A., Jones, N., Gerrish, A., Chapman, J., Ivanov, D., Moskvina, V., Lovestone, S., Priotsi, P., Lupton, M., Brayne, C., Gill, M., Lawlor, B., Lynch, A., Craig, D., McGuinness, B., Johnston, J., Holmes, C., Livingston, G., Bass, N. J., Gurling, H., McQuillin, A.; the GERAD Consortium; the National Institute on Aging Late-Onset Alzheimer's Disease Family Study Group, Holmans, P., Jones, L., Devlin, B., Klei, L., Barmada, M. M., Demirci, F. Y., Dekosky, S. T., Lopez, O. L., Passmore, P., Owen, M. J., O'Donovan, M. C., Mayeux, R., Kamboh, M. I., and Williams, J. (2011). Genome-wide association study of Alzheimer's disease with psychotic symptoms. *Mol. Psychiatry* [Epub ahead of print].

Holtzman, D. M., Morris, J. C., and Goate, A. M. (2011). Alzheimer's disease: the challenge of the second century. *Sci. Transl. Med.* 3, 77sr1.

Hyun, D. H., Emerson, S. S., Jo, D. G., Mattson, M. P., and de Cabo, R. (2006). Calorie restriction up-regulates the plasma membrane redox system in brain cells and suppresses oxidative stress during aging. *Proc. Natl. Acad. Sci. U.S.A.* 103, 19908–19912.

Hyun, D. H., Mughal, M. R., Yang, H., Lee, J. H., Ko, E. J., Hunt, N. D., de Cabo, R., and Mattson, M. P. (2010). The plasma membrane redox system is impaired by amyloid β-peptide and in the hippocampus and cerebral cortex of 3xTgAD mice. *Exp. Neurol.* 225, 423–429.

Iacopino, A. M., and Christakos, S. (1992). Specific reduction of calcium-binding protein (28-kilodalton calbindin-D) gene expression in aging and neurodegenerative diseases. *Proc. Natl. Acad. Sci. U.S.A.* 87, 4078–4082.

Ivings, L., Pennington, S. R., Jenkins, R., Weiss, J. L., and Burgoyne, R. D. (2002). Identification of Ca^{2+}-dependent binding partners for the neuronal calcium sensor protein neurocalcin delta: interaction with actin, clathrin and tubulin. *Biochem. J.* 363, 599–608.

Jheng, F. F., Wang, L., Lee, L., and Chang, L. S. (2006). Functional contribution of Ca^{2+} and Mg2+ to the intermolecular interaction of visinin-like proteins. *Protein J.* 25, 250–256.

Jo, D. G., Lee, J. Y., Hong, Y. M., Song, S., Mook-Jung, I., Koh, J. Y., and Jung, Y. K. (2004). Induction of pro-apoptotic calsenilin/DREAM/KChIP3 in Alzheimer's disease and cultured neurons after amyloid-beta exposure. *J. Neurochem.* 88, 604–611.

Kajimoto, Y., Shirai, Y., Mukai, H., Kuno, T., and Tanaka, C. (1993). Molecular cloning of two additional members of the neural visinin-like Ca(2+)-binding protein gene family. *J. Neurochem.* 61, 1091–1096.

Kato, M., Watanabe, Y., Iino, S., Takaoka, Y., Kobayashi, S., Haga, T., and Hidaka, H. (1998). Cloning and expression of a cDNA encoding a new neurocalcin isoform (neurocalcin alpha) from bovine brain. *Biochem. J.* 331, 871–876.

Kaufmann, W. A., Barnas, U., Humpel, C., Nowakowski, K., DeCol, C., Gurka, P., Ransmayr, G., Hinterhuber, H., Winkler, H., and Marksteiner, J. (1998). Synaptic loss reflected by secretoneurin-like immunoreactivity in the human hippocampus in Alzheimer's disease. *Eur. J. Neurosci.* 10, 1084–1094.

Kim, J. H., Lee, J. A., Song, Y. M., Park, C. H., Hwang, S. J., Kim, Y. S., Kaang, B. K., and Son, H. (2006). Overexpression of calbindin-D28K in hippocampal progenitor cells increases neuronal differentiation and neurite outgrowth. *FASEB J.* 20, 109–111.

Kim, S. H., Fountoulakis, M., Cairns, N., and Lubec, G. (2001). Protein levels of human peroxiredoxin subtypes in brains of patients with Alzheimer's disease and Down syndrome. *J. Neural Transm. Suppl.* 61, 223–235.

Kobayashi, M., Masaki, T., Hori, K., Masuo, Y., Miyamoto, M., Tsubokawa, H., Noguchi, H., Nomura, M., and Takamatsu, K. (2005). Hippocalcin-deficient mice display a defect in cAMP response element-binding protein activation associated with impaired spatial and associative memory. *Neuroscience* 133, 471–484.

Kobayashi, M., Takamatsu, K., Fujishiro, M., Saitoh, S., and Noguchi, T. (1994). Molecular cloning of a novel calcium-binding protein structurally related to hippocalcin from human brain and chromosomal mapping of its gene. *Biochim. Biophys. Acta* 1222, 515–518.

Kobayashi, M., Takamatsu, K., Saitoh, S., and Nogushi, T. (1993). Myristoylation of hippocalcin is linked to its membrane association properties. *J. Biol. Chem.* 268, 18898–18904.

Korhonen, L., Hansson, I., Kukkonen, J. P., Brännvall, K., Kobayashi, M., Takamatsu, K., and Lindholm, D. (2005). Hippocalcin protects against caspase-12-induced and age-dependent neuronal degeneration. *Mol. Cell. Neurosci.* 28, 85–95.

Kraut, N., Frampton, J., and Graf, T. (1995). Rem-1, a putative direct target gene of the Myb-Ets fusion oncoprotein in haematopoietic progenitors, is a member of the recoverin family. *Oncogene* 10, 1027–1036.

Kuno, T., Kajimoto, Y., Hashimoto, T., Mukai, H., Shirai, Y., Saheki, S., and Tanaka, C. (1992). cDNA cloning of a neural visinin-like Ca(2+)-binding protein. *Biochem. Biophys. Res. Commun.* 184, 1219–1225.

Ladant, D. (1995). Calcium and membrane binding properties of bovine neurocalcin delta expressed in Escherichia coli. *J. Biol. Chem.* 270, 3179–3185.

Lee, J. M., Blennow, K., Andreasen, N., Laterza, O., Modur, V., Olander, J., Gao, F., Ohlendorf, M., and Ladenson, J. H. (2008). The brain injury biomarker VLP-1 is increased in the cerebrospinal fluid of Alzheimer disease patients. *Clin. Chem.* 54, 1617–1623.

Lee, J. H., Cheng, R., Barral, S., Reitz, C., Medrano, M., Lantigua, R., Jiménez-Velazquez, I. Z., Rogaeva, E., StGeorge-Hyslop, P. H., and Mayeux, R. (2011). Identification of novel loci for Alzheimer disease and replication of CLU, PICALM, and BIN1 in Caribbean Hispanic individuals. *Arch. Neurol.* 68, 320–328.

Leissring, M. A., Yamasaki, T. R., Wasco, W., Buxbaum, J. D., Parker, I., and LaFerla, F. M. (2000). Calsenilin reverses presenilin-mediated enhancement of calcium signaling. *Proc. Natl. Acad. Sci. U.S.A.* 97, 8590–8593.

Lenz, S. E., Braunewell, K. H., Weise, C., Nedlina-Chittka, A., and Gundelfinger, E. D. (1996). The neuronal EF-hand Ca(2+)-binding protein VILIP: interaction with cell membrane and actin-based cytoskeleton. *Biochem. Biophys. Res. Commun.* 225, 1078–1083.

Lenz, S. E., Henschel, Y., Zopf, D., Voss, B., and Gundelfinger, E. D. (1992). VILIP, a cognate protein of the retinal calcium binding proteins visinin and recoverin, is expressed in the developing chicken brain. *Brain Res. Mol. Brain Res.* 15, 133–140.

Levin, E. D., McClernon, F. J., and Rezvani, A. H. (2006). Nicotinic effects on cognitive function: behavioral characterization, pharmacological specification, and anatomic localization. *Psychopharmacology (Berl.)* 184, 523–539.

Li, C., Pan, W., Braunewell, K. H., and Ames, J. B. (2011). Structural analysis of Mg2+ and Ca^{2+} binding, myristoylation, and dimerization of the neuronal calcium sensor and visinin-like protein 1 (VILIP-1). *J. Biol. Chem.* 286, 6354–6366.

Lian, L. Y., Pandalaneni, S. R., Patel, P., McCue, H. V., Haynes, L. P., and Burgoyne, R. D. (2011). Characterisation of the interaction of the C-terminus of the dopamine D2 receptor with neuronal calcium sensor-1. *PLoS One* 6:e27779. doi: 10.1371/journal.pone.0027779

Lin, L., Jeanclos, E. M., Treuil, M., Braunewell, K. H., Gundelfinger, E. D., and Anand, R. (2002a). The calcium sensor protein visinin-like protein-1 modulates the surface expression and agonist-sensitivity of the a4β2 nicotinic acetylcholine receptor. *J. Biol. Chem.* 277, 41872–41878.

Lin, L., Braunewell, K. H., Gundelfinger, E. D., and Anand, R. (2002b). Functional analysis of calcium-binding EF-hand motifs of visinin-like protein-1. *Biochem. Biophys. Res. Commun.* 296, 827–832.

Lindholm, D., Mercer, E. A., Yu, L. Y., Chen, Y., Kukkonen, J., Korhonen, L., and Arumäe, U. (2002). Neuronal apoptosis inhibitory protein: structural requirements for hippocalcin binding and effects on survival of NGF-dependent sympathetic neurons. *Biochim. Biophys. Acta* 1600, 138–147.

Loring, J. F., Porter, J. G., Seilhammer, J., Kaser, M. R., and Wesselschmidt, R. (2001). A gene expression profile of Alzheimer's disease. *DNA Cell Biol.* 20, 683–695.

Mahloogi, H., Gonzalez-Guerrico, A. M., De Cicco, R. L., Bassi, D. E., Goodrow, T., Braunewell, K. H., and Klein-Szanto, A. J. P. (2003). Graduate decrease of VILIP-1 Expression during mouse skin tumor progression and its role in regulating tumor cell invasive behavior. *Cancer Res.* 63, 4997–5004.

Masuo, Y., Ogura, A., Kobayashi, M., Masaki, T., Furuta, Y., Ono, T., and Takamatsu, K. (2007). Hippocalcin protects hippocampal neurons against excitotoxin damage by enhancing calcium extrusion. *Neuroscience* 145, 495–504.

McMahon, A., Wong, B. S., Iacopino, A. M., Ng, M. C., Chi, S., and German, D. C. (1998). Calbindin-D28k buffers intracellular calcium and promotes resistance to degeneration in PC12 cells. *Brain Res. Mol. Brain Res.* 54, 56–63.

Mercer, E. A., Korhonen, L., Skoglösa, Y., Olsson, P. A., Kukkonen, J. P., and Lindholm, D. (2000). NAIP interacts with hippocalcin and protects neurons against calcium-induced cell death through caspase-3-dependent and -independent pathways. *EMBO J.* 19, 3597–3607.

Miller, J. A., Oldham, M. C., and Geschwind, D. H. (2008). A systems level analysis of transcriptional changes in Alzheimer's disease and normal aging. *J. Neurosci.* 28, 1410–1420.

Monfort, P., Munoz, M. D., Kosenko, E., and Felipo, V. (2002). Long-term potentiation in hippocampus involves sequential activation of soluble guanylate cyclase, cGMP-dependent protein kinase, and cGMP-degrading phosphodiesterase. *J. Neurosci.* 22, 10116–10124.

Nanou, E., Martinez, G. Q., Scheuer, T., and Catterall, W. A. (2012). Molecular determinants of modulation of CaV2.1 channels by visinin-like protein 2. *J. Biol. Chem.* 287, 504–513.

Nef, P. (1996). "Neuron-specific calcium sensors (the NCS subfamily)," in: *Guidebook to the Calcium-Binding Proteins,* ed M. R. Celio (New York: Oxford University Press), 94–98.

O'Callaghan, D. W., Haynes, L. P., and Burgoyne, R. D. (2005). High-affinity interaction of the N-terminal myristoylation motif of the neuronal calcium sensor protein hippocalcin with phosphatidylinositol 4,5-bisphosphate. *Biochem. J.* 391, 231–238.

O'Callaghan, D. W., Ivings, L., Weiss, J. L., Ashby, M. C., Tepikin, A. V., and Burgoyne, R. D. (2002). Differential use of myristoyl groups on neuronal calcium sensor proteins as a determinant of spatio-temporal aspects of Ca^{2+} signal transduction. *J. Biol. Chem.* 277, 14227–14237.

O'Callaghan, D. W., Tepikin, A. V., and Burgoyne, R. D. (2003). Dynamics and calcium sensitivity of the Ca^{2+}-myristoyl switch protein hippocalcin in living cells. *J. Cell Biol.* 163, 715–721.

Oh, D. Y., Cho, J. H., Park, S. Y., Kim, Y. S., Yoon, Y. J., Yoon, S. H., Chung, K. C., Lee, K. S., and Han, J. S. (2008). A novel role of hippocalcin in bFGF-induced neurite outgrowth of H19–7 cells. *J. Neurosci. Res.* 86, 1557–1565.

Oikawa, K., Kimura, S., Aoki, N., Atsuta, Y., Takiyama, Y., Nagato, T., Yanai, M., Kobayashi, H., Sato, K., Sasajima, T., and Tateno, M. (2004). Neuronal calcium sensor protein visinin-like protein-3 interacts with microsomal cytochrome b5 in a Ca^{2+}-dependent manner. *J. Biol. Chem.* 279, 15142–11552.

Palmer, C. L., Lim, W., Hastie, P. G., Toward, M., Korolchuk, V. I., Burbidge, S. A., Banting, G., Collingridge, G. L., Isaac, J. T., and Henley, J. M. (2005). Hippocalcin functions as a calcium sensor in hippocampal LTD. *Neuron* 47, 487–494.

Palop, J. J., Chin, J., Roberson, E. D., Wang, J., Thwin, M. T., Bien-Ly, N., Yoo, J., Ho, K. O., Yu, G. Q., Kreitzer, A., Finkbeiner, S., Noebels, J. L., and Mucke, L. (2007). Aberrant excitatory neuronal activity and compensatory remodeling of inhibitory hippocampal circuits in mouse models of Alzheimer's disease. *Neuron* 55, 697–711.

Palop, J. J., Jones, B., Kekonius, L., Chin, J., Yu, G. Q., Raber, J., Masliah, E., and Mucke, L. (2003). Neuronal depletion of calcium-dependent proteins in the dentate gyrus is tightly linked to Alzheimer's disease-related cognitive deficits. *Proc. Natl. Acad. Sci. U.S.A.* 100, 9572–9577.

Palop, J. J., and Mucke, L. (2010). Amyloid-beta-induced neuronal dysfunction in Alzheimer's disease: from synapses toward neural networks. *Nat. Neurosci.* 13, 812–818.

Paterlini, M., Revilla, V., Grant, A. L., and Wisden, W. (2000). Expression of the neuronal calcium sensor protein family in the rat brain. *Neuroscience* 99, 205–216.

Petratos, S., Li, Q. X., George, A. J., Hou, X., Kerr, M. L., Unabia, S. E., Hatzinisiriou, I., Maksel, D., Aguilar, M. I., and Small, D. H. (2008). The beta-amyloid protein of Alzheimer's disease increases neuronal CRMP-2 phosphorylation by a Rho-GTP mechanism. *Brain* 131, 90–108.

Polymeropoulos, M. H., Ide, S., Soares, M. B., and Lennon, G. G. (1995). Sequence characterization and genetic mapping of the human VSNL1 gene, a homolo gue of the rat visinin-like peptide RNVP1. *Genomics* 29, 273–275.

Popoviæ, M., Caballero-Bleda, M., Kadish, I., and Van Groen, T. (2008). Subfield and layer-specific depletion in calbindin-D28K, calretinin and parvalbumin immunoreactivity in the dentate gyrus of amyloid precursor protein/presenilin 1 transgenic mice. *Neuroscience* 155, 182–191.

Rezvani, A. H., and Levin, E. D. (2001). Cognitive effects of nicotine. *Biol. Psychiatry* 49, 258–267.

Richler, E., Shigetomi, E., and Khakh, B. S. (2011). Neuronal P2X2 receptors are mobile ATP sensors that explore the plasma membrane when activated. *J. Neurosci.* 31, 16716–16730.

Rivas, M., Aurrekoetxea, K., Mellström, B., and Naranjo, J. R. (2011). Redox signaling regulates transcriptional activity of the Ca^{2+}-dependent repressor DREAM. *Antioxid. Redox Signal.* 14, 1237–1243.

Saab, B. J., Georgiou, J., Nath, A., Lee, F. J., Wang, M., Michalon, A., Liu, F., Mansuy, I. M., and Roder, J. C. (2009). NCS-1 in the dentate gyrus promotes exploration, synaptic plasticity, and rapid acquisition of spatial memory. *Neuron* 63, 643–656.

Schnurra, I., Riederer, P., Bernstein, H. G., and Braunewell, K. H. (2001). The neuronal calcium sensor (NCS) protein VILIP-1 is associated with amyloid plaques and extracellular tangles and promotes cell death and tau-phosphorylation *in vitro*: a link between calcium sensors and Alzheimer's disease? *Neurobiol. Dis.* 8, 900–909.

Schönrath, K., Pan, W., Klein-Szanto, A. J., and Braunewell, K. H. (2011). Involvement of VILIP-1 (visinin-like protein) and opposite roles of cyclic AMP and GMP signalling in *in vitro* cell migration of murine skin squamous cell carcinoma. *Mol. Carcinog.* 50, 319–333.

Schuman, E. M., and Madison, D. V. (1991). A requirement for the intercellular messenger nitric oxide in long-term potentiation. *Science* 254, 1503–1506.

Sippy, T., Cruz-Martín, A., Jeromin, A., and Schweizer, F. E. (2003). Acute changes in short-term plasticity at synapses with elevated levels of neuronal calcium sensor-1. *Nat. Neurosci.* 6, 1031–1038.

Smith, D. L., Pozueta, J., Gong, B., Arancio, O., and Shelanski, M. (2009). Reversal of long-term dendritic spine alterations in Alzheimer disease models. *Proc. Natl. Acad. Sci. U.S.A.* 106, 16877–16882.

Spilker, C., and Braunewell, K-H. (2003). The calcium-myristoyl switch of neuronal calcium sensor (NCS) proteins: same biochemical principle but different calcium-dependent localization of VILIP-3 and -1 in hippocampal neurons. *Mol. Cell. Neurosci.* 24, 766–778.

Spilker, C., Gundelfinger, E. D., and Braunewell, K-H. (2002a). Different properties of the intracellular neuronal Calcium sensor proteins VILIP-1 and VILIP-3: from subcellular localization to cellular function. *Biochim. Biophys. Acta - proteins and proteomics* 1600, 118–127.

Spilker, C., Dresbach, T., and Braunewell, K-H. (2002b). Reversible translocation and activity-dependent localization of the calcium-myristoyl switch protein VILIP-1 to different membrane compartments in living hippocampal neurons. *J. Neurosci.* 22, 7331–7339.

Spilker, C., Richter, K., Smalla, K-H., Manahan-Vaughan, D., Gundelfinger, E. D., and Braunewell, K-H. (2000). The neuronal EF-hand calcium-binding protein VILIP-3 is expressed in cerebellar Purkinje cells and shows a calcium-dependent membrane association. *Neuroscience* 96, 121–129.

Supnet, C., and Bezprozvanny, I. (2010). The dysregulation of intracellular calcium in Alzheimer disease. *Cell Calcium* 47, 183–189.

Takahashi, H., Brasnjevic, I., Rutten, B. P., Van Der Kolk, N., Perl, D. P., Bouras, C., Steinbusch, H. W., Schmitz, C., Hof, P. R., and Dickstein, D. L. (2010). Hippocampal interneuron loss in an APP/PS1 double mutant mouse and in Alzheimer's disease. *Brain Struct. Funct.* 214, 145–160.

Tanaka, T., Ames, J. B., Harvey, T. S., Stryer, L., and Ikura, M. (1995). Sequestration of the membrane-targeting myristoyl group of recoverin in the calcium-free state. *Nature* 376, 444–447.

Tang, W. Y., Morey, L. M., Cheung, Y. Y., Birch, L., Prins, G. S., and Ho, S. M. (2012). Neonatal exposure to estradiol/bisphenol A alters promoter methylation and expression of Nsbp1 and Hpcal1 genes and transcriptional programs of Dnmt3a/b and Mbd2/4 in the rat prostate gland throughout life. *Endocrinology* 153, 42–55.

Tarawneh, R., D'Angelo, G., Macy, E., Xiong, C., Carter, D., Cairns, N. J., Fagan, A. M., Head, D., Mintun, M. A., Ladenson, J. H., Lee, J. M., Morris, J. C., and Holtzman, D. M. (2011). Visinin-like protein-1:diagnostic and prognostic biomarker in Alzheimer disease. *Ann. Neurol.* 70, 274–285.

Telegdy, G. (1994). The action of ANP, BNP and related peptides on motivated behavior in rats. *Rev. Neurosci.* 5, 309–315.

Tzingounis, A. V., Kobayashi, M., Takamatsu, K., and Nicoll, R. A. (2007). Hippocalcin gates the calcium activation of the slow after-hyperpolarization in hippocampal pyramidal cells. *Neuron* 53, 487–493.

Verbeek, M. M., and Olde Rikkert, M. G. (2008). Cerebrospinal fluid biomarkers in the evaluation of Alzheimer disease. *Clin. Chem.* 54, 1589–1591.

Villalobos, C., and Andrade, R. (2010). Visinin-like neuronal calcium sensor proteins regulate the slow calcium-activated afterhyperpolarizing current in the rat cerebral cortex. *J. Neurosci.* 30, 14361–14365.

Wang, C. K., Simon, A., Jessen, C. M., Oliveira, C. L., Mack, L., Braunewell, K. H., Ames, J. B., Pedersen, J. S., and Hofmann, A. (2011). Divalent cations and redox conditions regulate the molecular structure and function of Visinin-like Protein-1. *PLoS One* 6:e26793. doi: 10.1371/journal.pone.0026793

Wei, W., Nguyen, L. N., Kessels, H. W., Hagiwara, H., Sisodia, S., and Malinow, R. (2010). Amyloid beta from axons and dendrites reduces local spine number and plasticity. *Nat. Neurosci.* 13, 190–196.

Wilmot, B., McWeeney, S. K., Nixon, R. R., Montine, T. J., Laut, J., Harrington, C. A., Kaye, J. A., and Kramer, P. L. (2008). Translational gene mapping of cognitive decline. *Neurobiol. Aging* 29, 524–541.

Wu, L. J., Mellström, B., Wang, H., Ren, M., Domingo, S., Kim, S. S., Li, X. Y., Chen, T., Naranjo, J. R., and Zhuo, M. (2010). DREAM (downstream regulatory element antagonist modulator) contributes to synaptic depression and contextual fear memory. *Mol. Brain* 3, 3

Yamatani, H., Kawasaki, T., Mita, S., Inagaki, N., and Hirata, T. (2010). Proteomics analysis of the temporal changes in axonal proteins during maturation. *Dev. Neurobiol.* 70, 523–537.

Youn, H., Jeoung, M., Koo, Y., Ji, H., Markesbery, W. R., Ji, I., and Ji, T. H. (2007). Kalirin is underexpressed in Alzheimer's disease hippocampus. *J. Alzheimers Dis.* 11, 385–397.

Zhao, C., and Braunewell, K-H. (2008). Expression of the neuronal calcium sensor VILIP-1 in the rat hippocampus. *Neuroscience* 153, 1202–1212.

Zhao, C. J., Noack, C., Brackmann, M., Gloveli, T., Maelicke, A., Heinemann, U., Anand, R., and Braunewell, K. H. (2009a). Neuronal Ca^{2+} sensor VILIP-1 leads to the upregulation of functional alpha4beta2 nicotinic acetylcholine receptors in hippocampal neurons. *Mol. Cell. Neurosci.* 40, 280–292.

Zhao, C., Anand, R., and Braunewell, K. H. (2009b). Nicotine-induced Ca^{2+}-myristoyl switch of neuronal Ca^{2+} sensor VILIP-1 in hippocampal neurons: a possible crosstalk mechanism for nicotinic receptors. *Cell. Mol. Neurobiol.* 29, 273–286.

Zozulya, S., and Stryer, L. (1992). Calcium-myristoyl protein switch. *Proc. Natl. Acad. Sci. U.S.A.* 89, 11569–11573.

Conflict of Interest Statement: The author declares that the research was conducted in the absence of any commercial or financial relationships that could be construed as a potential conflict of interest.

Received: 13 January 2012; paper pending published: 19 January 2012; accepted: 09 February 2012; published online: 23 February 2012.

*Citation: Braunewell KH (2012) The visinin-like proteins VILIP-1 and VILIP-3 in Alzheimer's disease—old wine in new bottles. Front. Mol. Neurosci. **5**:20. doi: 10.3389/fnmol.2012.00020*

frontiers in
MOLECULAR NEUROSCIENCE

ORIGINAL RESEARCH ARTICLE
published: 03 May 2012
doi: 10.3389/fnmol.2012.00058

Reduced Mid1 expression and delayed neuromotor development in daDREAM transgenic mice

Mara Dierssen[1]*, Laura Fedrizzi[2], Rosa Gomez-Villafuertes[3,4], María Martinez de Lagran[1], Alfonso Gutierrez-Adan[5], Ignasi Sahún[1], Belen Pintado[3], Juan C. Oliveros[3], Xose M. Dopazo[3,4], Paz Gonzalez[3,4], Marisa Brini[6], Britt Mellström[3,4], Ernesto Carafoli[7] and Jose R. Naranjo[3,4]

[1] *Genomic Regulation Center, Parc de Recerca Biomèdica de Barcelona, Centro de Investigación Biomédica en Red de Enfermedades Raras, Barcelona, Spain*
[2] *Department of Biological Chemistry, University of Padua, Padua, Italy*
[3] *National Center of Biotechnology, Consejo Superior de Investigaciones Científicas, Madrid, Spain*
[4] *Centro de Investigación Biomédica en Red, Enfermedades Neurodegenerativas, Madrid, Spain*
[5] *Department of Animal Reproduction, Instituto Nacional de Investigación y Tecnología Agraria y Alimentaria, Madrid, Spain*
[6] *Department of Comparative Biomedicine and Food Science, University of Padova, Padova, Italy*
[7] *Venetian Institute of Molecular Medicine, Padua, Italy*

Edited by:
Beat Schwaller, University of Fribourg, Switzerland

Reviewed by:
Ye He, University of California San Francisco, USA
Joachim Krebs, Max Planck Institute for Biophysical Chemistry, Germany

****Correspondence:***
Mara Dierssen, Centro de Regulación Genómica, Dr. Aiguader 88, E-08003 Barcelona, Spain.
e-mail: mara.dierssen@crg.es;
Jose R. Naranjo, Centro Nacional de Biotecnología, Consejo Superior de Investigaciones Científicas, Darwin 3, E-28049 Madrid, Spain.
e-mail: naranjo@cnb.csic.es

Downstream regulatory element antagonist modulator (DREAM) is a Ca^{2+}-binding protein that binds DNA and represses transcription in a Ca^{2+}-dependent manner. Previous work has shown a role for DREAM in cerebellar function regulating the expression of the sodium/calcium exchanger 3 (NCX3) in cerebellar granular neurons to control Ca^{2+} homeostasis and survival of these neurons. To achieve a global view of the genes regulated by DREAM in the cerebellum, we performed a genome-wide analysis in transgenic cerebellum expressing a Ca^{2+}-insensitive/CREB-independent dominant active mutant DREAM (daDREAM). Here we show that DREAM regulates the expression of the midline 1 (Mid1) gene early after birth. As a consequence, daDREAM mice exhibit a significant shortening of the rostro-caudal axis of the cerebellum and a delay in neuromotor development early after birth. Our results indicate a role for DREAM in cerebellar function.

Keywords: midline 1, cerebellar lobes, nuclear calcium, transcriptomic analysis

INTRODUCTION

Downstream regulatory element antagonist modulator (DREAM), also named calsenilin or KChIP-3, is a Ca^{2+}-binding protein of the neuronal calcium sensors family able to repress transcription of specific genes in a Ca^{2+}-dependent manner (Carrion et al., 1999), to interact with presenilins and to modify APP processing (Buxbaum et al., 1998; Lilliehook et al., 2003) and to regulate the membrane expression and gating of Kv4 potassium channels (An et al., 2000; Ruiz-Gomez et al., 2007) and of voltage-dependent calcium channels (Thomsen et al., 2009; Anderson et al., 2010). In addition, DREAM modulates downstream signaling of different membrane receptors including NMDA (Wu et al., 2010; Zhang et al., 2010) and THSR (Rivas et al., 2009).

Transcriptional activity of DREAM is triggered by its sumoylation-dependent nuclear translocation (Palczewska et al., 2011), regulated by redox state (Rivas et al., 2011), and accomplished by its Ca^{2+}-dependent specific binding to DNA and to other nucleoproteins, including CREM and CREB (Ledo et al., 2000, 2002; Rivas et al., 2004; Scsucova et al., 2005; Zaidi et al., 2006). In addition, high affinity binding of DREAM to DRE sequences in the DNA requires Ca^{2+}-dependent DREAM oligomerization (Carrion et al., 1998; Osawa et al., 2001, 2005).

Downstream regulatory element antagonist modulator is widely expressed in the central nervous system as well as in the thyroid gland, testis, and the immune system (Carrion et al., 1999). Tissue-specific target genes for DREAM regulation have been identified first *in vitro* (Carrion et al., 1999; Link et al., 2004) and more recently *in vivo*, using DREAM null mice (Cheng et al., 2002) and especially transgenic mice expressing a dominant active DREAM mutant (daDREAM; Gomez-Villafuertes et al., 2005; Savignac et al., 2005, 2010; Rivera-Arconada et al., 2010). Specifically, a significant increase in prodynorphin mRNA was found in spinal cord from DREAM null mice (Cheng et al., 2002) and a decrease in NCX3 and BDNF mRNA and protein levels were reported in hippocampus and cerebellum (Gomez-Villafuertes et al., 2005) and in spinal cord (Rivera-Arconada et al., 2010) respectively, from daDREAM mice. The regulatory effect of daDREAM on the expression of transcriptional targets was shown to be specific, since for instance no change in the expression of other members of the sodium/calcium exchanger family could be observed in hippocampus and cerebellum of daDREAM transgenic mice (Gomez-Villafuertes et al., 2005). As expected, transcriptional regulation by DREAM of various cellular targets has diverse and tissue-specific functional consequences. In the CNS, this includes changes in sensory noxious perception (Cheng et al., 2002; Rivera-Arconada et al., 2010), β-amyloid accumulation (Lilliehook et al., 2003), and learning and memory formation (Alexander et al., 2009), as well as modified T-cell proliferation and Ig production (Savignac et al., 2005, 2010) in the immune system.

Taking the cerebellum as an example, previous work using primary cultures of cerebellar granular neurons has shown the role of DREAM in the regulation of NCX3 expression, which in turn is fundamental for the maintenance of Ca^{2+} homeostasis and viability of the cerebellar granular neurons in the culture (Gomez-Villafuertes et al., 2005). In the present study, to further investigate the functional involvement of DREAM-mediated transcription in cerebellar function, we have performed a transcriptomic analysis of the cerebellum from daDREAM transgenic mice. We found that expression of the midline 1 gene (Mid 1) is repressed in daDREAM mice. Related to this, daDREAM mice exhibit a significant shortening of the rostro-caudal axis of the cerebellum and a severe delay in neuromotor development early after birth.

RESULTS

GENOME-WIDE ANALYSIS IN daDREAM CEREBELLUM

To search for DREAM transcriptional targets that could disclose a role for DREAM in cerebellar function, we performed genome-wide analysis in a line of transgenic mice previously reported to express daDREAM in the cerebellum (Gomez-Villafuertes et al., 2005). Comparison of basal gene expression in wild type and transgenic adult cerebellum, using cDNA microarrays, identified only 11 genes whose expression was significantly altered in daDREAM transgenic cerebellum (Gene Expression Omnibus accession number GSE34765; **Figure 1**). Up- and down-regulated genes are presented in **Table 1** and the bioinformatics analysis is shown in **Tables A1** and **A2** in Appendix.

Among the genes with modified expression (**Table 1**), we focused our attention on the significant down regulation of the Mid 1 gene, an ubiquitin ligase specific for the protein phosphatase 2A (PP2A; Trockenbacher et al., 2001). Loss of function mutations in the Mid1 protein cause the X-linked Opitz BBB/G syndrome, a congenital anomaly disorder characterized by developmental defects of midline structures (Opitz, 1987; Quaderi et al., 1997). Importantly, Mid1 deficient mice mimic the hypoplasia of the anterior portion of the medial cerebellum (Lancioni et al., 2010), a clinical feature present in Opitz patients, suggesting that DREAM, through the regulation of Mid1, might participate in cerebellar development. Real-time qPCR analysis confirmed the reduced level of Mid1 mRNA in the cerebellum of adult transgenic mice as well as in the hippocampus (**Figure 2A**), areas with significant expression of daDREAM (**Figure 2B**). As reported for other DREAM target genes like prodynorphin in the hippocampus (Cheng et al., 2002) or CANT1 in the cerebellum (Cali et al., 2012), probably due to functional compensation by other members of the KChIP family, no change in the expression of Mid1 was observed in cerebellum or hippocampus from DREAM knockout mice (**Figure 2C**). Western blot analysis of cerebellum and hippocampus from daDREAM mice confirmed the reduced levels of Mid1 protein with respect to wild type mice (**Figure 2D**). Taken together, these results implicate endogenous DREAM/KChIPs in the regulation of Mid1 gene expression in the brain.

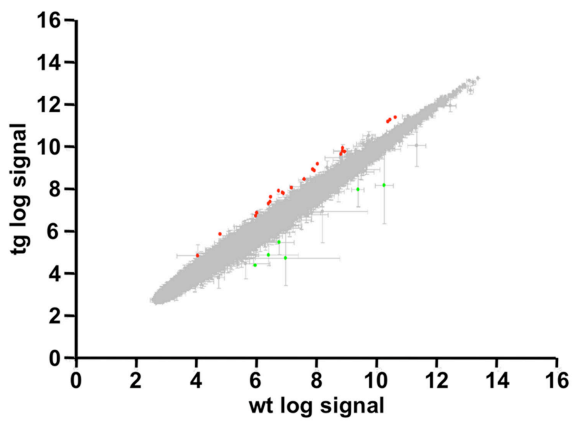

FIGURE 1 | Genome-wide analysis in daDREAM and wild type cerebellum. Statistical values and scatter plot of all probes contained in the genome-wide analysis. Spots with |Fold Change| >1.6 and FDR <0.1 are highlighted in green (repressed genes) and red (induced genes).

DREAM REGULATES EARLY POSTNATAL Mid1 EXPRESSION

Mid1 is widely expressed at early human embryonic stages, however during organogenesis the expression pattern becomes more restricted to the tissues affected in the Opitz syndrome (Pinson et al., 2004). The development of the cerebellum in mice is mostly postnatal and is complete after the second week of life (reviewed in Millen and Gleeson, 2008). To investigate a role for DREAM in the regulation of Mid1 and cerebellar development, we next analyzed the expression of the daDREAM transgene during cerebellar development and the consequences on Mid1 expression. Real-time qPCR analysis showed that the expression of daDREAM in the cerebellum was very high early after birth (P2) and got down at P7–P21 (**Figure 3A**) to values slightly higher than adult levels (see **Figure 2B**). Expression of Mid1 in wild type cerebellum was high early after birth (P2–P7) and reached adult levels at P21 (notice the different scale in **Figure 2A**). Expression of daDREAM was associated with a significant reduction of Mid1 mRNA levels in transgenic cerebellum (**Figure 3A**). Early postnatal expression of the transgene was not exclusive to the cerebellum and was observed as well in other brain areas, like the hippocampus (**Figure 3B**). Expression of daDREAM in the hippocampus was also associated with a significant reduction of Mid1 mRNA levels (**Figure 3B**).

CEREBELLAR MORPHOLOGICAL CHANGES IN daDREAM MICE

Absence of Mid1 protein in Mid1 null mice results in abnormal formation of the anterobasal cardinal lobe, which is evident already at P0–P2 (Lancioni et al., 2010). In adult Mid1 null mice, although abnormal in shape, even the anterior vermal lobes maintain the correct layer organization and thickness (Lancioni et al., 2010). According to the significant reduction in Mid1 expression, adult daDREAM mice showed a significant shortening in the antero-posterior axis but also in the left–right axis (**Figures 4A,B**). Sagittal sections from P15 wild type and daDREAM mice confirmed a correct layer organization of transgenic cerebellum and showed the shortening of the rostro-caudal axis (**Figure 4C**).

IMPAIRED MOTOR DEVELOPMENT IN daDREAM MICE

Absence of Mid1 protein in Mid1 null mice has been associated with impaired motor coordination in the adulthood. To assess possible changes during early postnatal development that could be

Table 1 | List of induced and repressed genes in daDREAM vs. wild type cerebellum.

Fold change	*P*-value x 10^{-5}	FDR	Probe ID	Transcript ID	Gene symbol	Gene description
1.70	0.922	0.023	1440557_at	Mm.186257.1	Ipw	Imprinted gene in the Prader–Willi syndrome region
1.75	1.792	0.038	1436733_at	Mm.40013.1	E130309F12Rik	RIKEN cDNA E130309F12 gene
1.86	0.914	0.026	1460049_s_at	Mm.213028.1	1500015O10Rik	RIKEN cDNA 1500015O10 gene
1.95	0.319	0.0160	1417654_at	Mm.3815.1	Sdc4	Syndecan 4
2.10	0	0	1449340_at	Mm.43375.1	Sostdc1	Sclerostin domain containing 1
−4.68	0.035	0.000	1436240_at	Mm.216255.1	B230214O09Rik	RIKEN cDNA B230214O09 gene
−4.17	0.177	0.016	1431214_at	Mm.157900.1	LOC433762	Hypothetical gene LOC433762
−2.95	0.133	0.027	1440139_at	Mm.174301.1	gb:BB729836	Moderately similar to S12207 hypothetical protein
−2.83	0.231	0.030	1438239_at	Mm.24820.1	Mid1	Midline 1
−2.60	0.408	0.037	1425545_x_at	Mm.33263.2	H2-D1	Histocompatibility 2, D region locus 1
−2.38	0.639	0.048	1419327_at	Mm.22635.1	Pdxdc1	Pyridoxal-dependent decarboxylase domain containing 1

Genes with FDR <0.05 were included in the list of induced or repressed candidates.

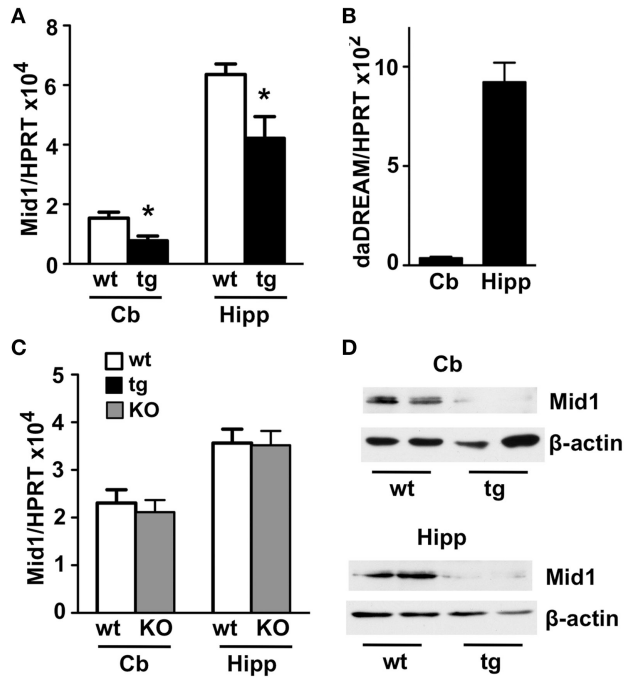

FIGURE 2 | Real-time qPCR and western blot analysis of Mid1 expression in adult brain. Levels of Mid1 **(A,C)** and daDREAM **(B)** mRNA in the cerebellum (Cb) and the hippocampus (Hipp) from wild type (wt), transgenic (tg), and DREAM$^{-/-}$ (KO) mice are shown. Values are normalized with respect to HPRT mRNA content. Results are the mean ± SEM of 14–18 mice in three independent experiments. $*P < 0.05$ (two-tailed, unpaired *t*-test) relative to wild type mice. **(D)** Immunoblot analysis of adult brain cerebellum and hippocampal lysates (50 μg) shows that the 70- to 75-kDa expected band for the Mid 1 protein is reduced in transgenic compared to wild type mice. β-Actin was used as protein loading control. The experiment, in duplicates, was repeated twice.

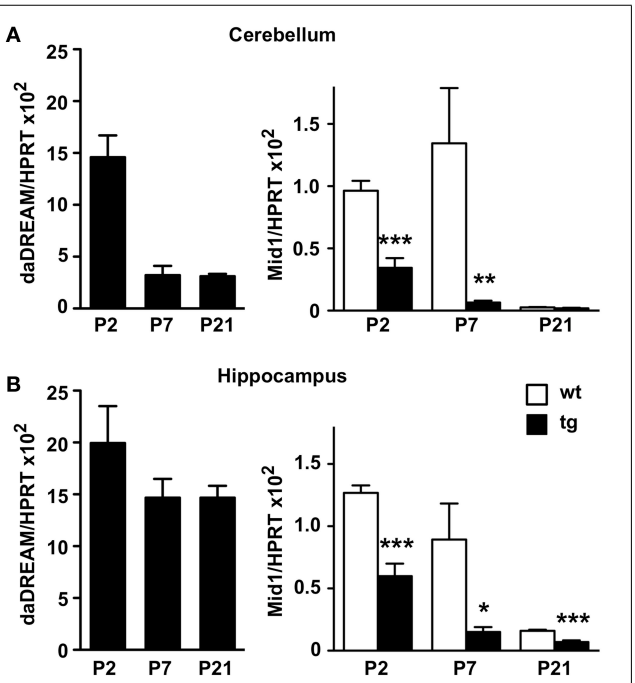

FIGURE 3 | Real-time qPCR analysis of Mid1 expression during postnatal development. Levels of daDREAM and Mid1 mRNA at the indicated postnatal day from wild type (wt) and transgenic (tg) mice in cerebellum **(A)** and hippocampus **(B)** are shown. Values are normalized with respect to HPRT mRNA content. Results are the mean ± SEM of 8–12 mice in two independent experiments. $*P < 0.05$, $**P < 0.01$, $***P < 0.001$ (two-tailed, unpaired *t*-test) relative to wild type mice.

related to Mid1 down regulation in daDREAM mice, we employed a test battery consisting of somatometric, neurologic, and sensorial and motor tests. No differences in somatometric growth, or in the appearance of developmental landmarks, i.e., eye opening, fur appearance, or incisor eruption, were detected in daDREAM mice. However, significant changes were observed in neuromotor development as assessed by the pivoting and the walking tests on postnatal days 7, 10, and 14. In the pivoting locomotion task, wild type, and daDREAM mice showed similar activity at P7. However, the normal age-dependent increase in activity, which is reflecting the adequate maturation of motor systems in wild type, was significantly reduced in daDREAM mice at P10 (**Figure 5A**).

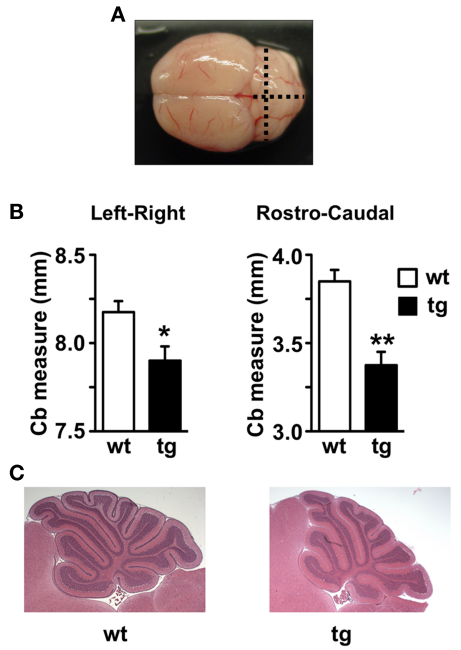

FIGURE 4 | Anatomical analysis of adult and postnatal cerebellum. **(A)** Image of whole adult mouse brain showing the left–right and rostro-caudal axis used for the measurement. **(B)** Measurement of left–right and rostro-caudal axis of the cerebellum in wild type and (wt) transgenic (tg) adult mice ($n = 6$). $^{*}P < 0.05$, $^{**}P < 0.01$ (two-tailed, unpaired *t*-test) relative to wild type mice. **(C)** For comparison, sagittal sections through the cerebellar vermis of postnatal P15 wild type (wt) and transgenic (tg) mice after staining with hematoxylin/eosin are shown.

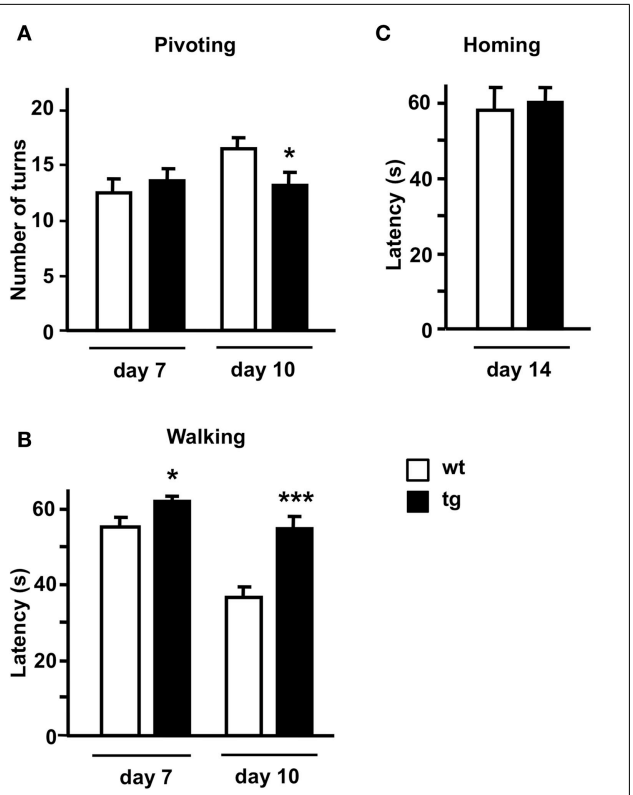

FIGURE 5 | Neuromotor development in postnatal mice. Behavioral analysis **(A)** pivoting test, **(B)** walking test, and **(C)** homing test were performed at the indicated postnatal days in wild type and (wt) transgenic (tg) mice ($n = 16$–18). $^{*}P < 0.05$, $^{***}P < 0.001$ (two-tailed, unpaired *t*-test) relative to wild type mice.

Assessment of walking activity confirmed the hypoactive phenotype in daDREAM mice and, even at P7 the latency to walk in transgenic mice was significantly longer than in wild type mice (**Figure 5B**). At P10, the reduction in walking latency observed in wild type (33.6% of reduction, P7 vs. P10) was significantly less pronounced in daDREAM mice (10.8% reduction, P7 vs. P10; **Figure 5B**). This result, along with the affected pivoting activity in daDREAM mice, could suggest a supraspinal deficiency, indicating that the postnatal development of brain structures directly implicated in the motor function might be affected in daDREAM mice. This defect is specific of motor function, since daDREAM mice showed normal latency to reach their nest in the homing test compared to wild types (**Figure 5C**). This normal latency might suggest a normal development of other functional domains such as sensory perception.

DISCUSSION

Genome-wide analysis of different tissues or brain areas from daDREAM transgenic mice has rendered discrete lists of potential DREAM regulated genes with some overlapping as well as tissue-specific targets (Savignac et al., 2010; Jose R. Naranjo, unpublished observations). In all cases, including the present data, these lists include both repressed and induced genes suggesting that besides the direct repressor action of DREAM, interactions between DREAM and other transcriptional regulators (Ledo et al., 2002; Rivas et al., 2004, 2011; Scsucova et al., 2005; Zaidi et al., 2006) or indirect/secondary transcriptional effects might contribute to gene induction in daDREAM transgenic tissues. In the case of the daDREAM cerebellum, the list of genes with modified expression is especially short. This is not related to technical problems with the hybridization of the array since the bioinformatics analysis of the hybridization signals (see **Figure 1**) shows a perfectly normal distribution. Instead, the low number of hits might reflect the limitation of the technique, showing for instance a minor and not significant down regulation (−1.15-fold; *P*-value 0.06) of the NCX3 gene (also named Slc8a3: solute carrier family 8) previously validated as a direct DREAM target and shown to be repressed by more than 50% in daDREAM cerebellum (Gomez-Villafuertes et al., 2005). Alternatively, the low number of targets may simply reflect the limited but specific functionality of DREAM in the cerebellum, a brain region where DREAM expression shows the lowest level among the different areas in the CNS (Carrion et al., 1999; Rhodes et al., 2004).

Among induced genes, syndecan 4 is a transmembrane proteoglycan for which there are no reports relating a function in brain or cerebellum. Sclerostin domain containing 1 (Sostdc1) is a secreted inhibitor of the Wnt and Bmp pathways, that antagonizes BMP signaling in the mesenchymal induction of teeth and orofacial morphogenesis, regulating also the spatial patterning of

teeth and hair. Deletion of Sostdc1 leads to the full development of single extra incisors adjacent to the main incisors (Munne et al., 2009). On the other hand, induced expression of sclerostin domain containing 1 (Sostdc1) has been reported in the brain of mice deficient in phenylalanine hydroxylase (PAH), an animal model for the autosomal recessive disorder phenylketonuria (Park et al., 2009), though the functional meaning of this increased expression is not known. In daDREAM mice, however, induced levels of Sostdc1 do not have an effect on dentation and hair appearance since both are normal.

Among repressed genes, the Mid1 protein is biochemically well characterized and a role in brain development has been reported. Thus, early studies of Mid1 function recognized its ubiquitin ligase activity and have identified its specific role in the degradation of protein phosphatase 2A by the proteosome (Trockenbacher et al., 2001). Importantly, PP2A is the major serine–threonine–tau phosphatase in the brain and dephosphorylates also other microtubule-associated proteins like 4EBP1 and p70S6K, two targets of the mTOR kinase (Nojima et al., 2003). Loss of function mutations of the Mid1 protein are associated with developmental midline malformations present in Opitz syndrome patients (Opitz, 1987; Quaderi et al., 1997). Furthermore, cells derived from Opitz syndrome patients show decreased formation of mTORC1, the complex between mTOR and its interacting proteins Raptor and mLST8, as well as S6K1 phosphorylation, cell size, and cap-dependent translation. Expression of wild type Mid1 or activated mTOR protein rescue the phenotype, suggesting that mTORC1 plays a key role in Opitz syndrome pathogenesis (Liu et al., 2011). In addition, a recent study has identified the binding of the cytoskeletal-associated Mid1/α4/PP2A complex to polyribosomes and mRNAs via a purine-rich sequence motif called MIDAS (MID1 association sequence) increasing the stability and translational efficiency of these mRNAs (Aranda-Orgilles et al., 2011). Notably, the MIDAS motif is frequent in mRNAs related to development and energy metabolism and mutated Mid1 does not interact with MIDAS-containing mRNAs suggesting that defects associated with the Opitz syndrome could be produced by altered protein translation of some of these mRNAs (Aranda-Orgilles et al., 2011). About the mechanism by which Mid1 could affect brain development it has been hypothesized that by controlling PP2A activity, Mid1 is regulating the activity of Gli3 (Krauss et al., 2008) a Wnt target gene related to the development of the hippocampus (Hasenpusch-Theil et al., 2012), which has been implicated in three human pathological conditions sharing common features with Opitz syndrome (Biesecker, 2006). Lack of the murine Mid1 gene results in motor coordination defects as well as motor, non-associative, and procedural learning impairments that may correlate with the developmental delays of Opitz syndrome patients (Lancioni et al., 2010). The behavioral analysis in this study was done in adult mice with no specific focus on postnatal development. Our data report an early down regulation of Mid1 expression in daDREAM mice and suggest a delayed neuromotor development in these mice. Down regulation of Mid1 mRNA levels is not restricted to the cerebellum and is also observed in the hippocampus, a brain area with strong expression of the daDREAM mutant. Whether hippocampal morphology is altered in daDREAM mice and to what extent the reduction in other genes like NCX3 contribute to the morphological and neuromotor phenotypes remain to be investigated.

As expected for a protein with developmental functions, expression of Mid1 in adult brain is reduced compared to postnatal levels. Interestingly, however, expression in the adult hippocampus is higher than in the adult cerebellum. This may suggest a specific function for Mid1 in adult hippocampus and the existence of strong trans-activating mechanisms to compensate a presumable stronger repression due to higher levels of DREAM protein in hippocampus compared to cerebellum.

Analysis of the post-transcriptional regulation of the Mid1 mRNA has shown that alternative use of different transcription start sites, alternative splicing, and the existence of different polyadenylation signal results in a wide variety of Mid1 isoforms (Landry and Mager, 2002; Winter et al., 2004). Less is known, however, about the transcriptional mechanisms that regulate Mid1 expression. Like in the case of the BDNF gene, another example of a gene with multiple transcription start sites, specific regulatory regions have been assigned to each transcription start site. Interestingly, *in silico* analysis of these different promoters, both in the human and the mouse genes, has identified putative DRE sites (**Table 2**), mostly located in the complementary strand, a circumstance previously reported for DRE sites in the ICER (Link et al., 2004) and the interferon γ (Savignac et al., 2005) genes. Nevertheless, *in vitro* analysis of the ability of these sites to bind recombinant DREAM and especially chromatin immunoprecipitation studies should confirm the *in silico* predictions.

In conclusion, the results from the genome-wide analysis of the cerebellum from daDREAM mice indicate that endogenous DREAM, in addition to regulate NCX3, might also contribute to cerebellar function through the regulation of Mid1 gene expression.

MATERIALS AND METHODS

TRANSGENIC MICE

A cDNA encoding human DREAM with two amino acid substitutions at EF-hands 2, 3, and 4 and at the N-terminal LCD

Table 2 | Downstream response elements, DREs, present in the 5′ untranslated region of different Mid1 isoforms.

Species	Isoform	Position in mRNA	Sequence[a,b]	Orientation
Mouse	Var 1[c]	155–164	tgatgacccc	←
	Var 2	68–78	cttgacattgt	←
	Var 2	261–270	gggtcatgga	←
Human	Var 1	317–328	gggtcatggga	→
	Var 2[d]	161–173	ctgatgacaca	←
	Var 4	158–168	taatgactcca	←
	Var 4	259–268	aatgacgtaa	←

[a] *The core sequence is underlined.*

[b] *For comparison the mouse interferon γ DRE site in the complementary strand (←) is atcggctgacctagag and the human dynorphin forward element (→) is agccggagtcaaggag.*

[c] *The same element is present in mouse variant 2 at position 316–327.*

[d] *The same element is present in variants 1, 3, 6, 7, 8, and 9.*

(daDREAM) was cloned downstream of the human CaMK-IIα promoter (Mayford et al., 1995) in a bicistronic expression vector containing an IRES and the LacZ reporter gene. DREAM transgenic mice were prepared by pronuclear microinjection of this cassette in the C57BL/6xCBA hybrid background. Transgenic progeny were identified by Southern blotting and qualitative PCR of tail DNA using specific primers; forward 5′-TTGCAGTGCACGGCAGATACACTTGCTGA-3′ and reverse 5′-CCACTGGTGTGGG CCATAATTCAATTCGC-3′. An amplified fragment of 326 bp indicated the presence of the transgene. Founder males were backcrossed to C57BL/6 females to generate lines that were maintained as heterozygous and age- and sex-matched littermates were used as controls. Of the different transgenic lines generated, in this study we used transgenic line 33 that shows expression of the transgene in different brain areas, including the cerebellum (Gomez-Villafuertes et al., 2005; Wu et al., 2010).

MICROARRAY

RNA from whole cerebellum from wild type and transgenic mice was prepared using TRIzol (Invitrogen) and the RNAeasy Mini Kit (Qiagen). RNA was quantified and the quality was assessed with a 2100 Bioanalyzer (Agilent technologies). cDNA was synthesized from 4 μg of total RNA using one-cycle target labeling and control reagents (Affymetrix) to produce biotin labeled cRNA. The cRNA preparation (15 μg) was fragmented at 94°C for 35 min into 35–200 bases in length. Labeled cRNAs were hybridized to Affymetrix chips (GeneChip Mouse Genome 430 2.0 Array). Each sample was added to a hybridization solution containing 100 mM 2-(*N*-morpholino) ethanesulfonic acid, 1 M Na^+, and 20 mM of EDTA in the presence of 0.01% of Tween-20 to a final cRNA concentration of 0.05 μg/ml. Hybridization was performed for 16 h at 45°C. Each microarray was washed and stained with streptavidin–phycoerythrin in a Fluidics station 450 (Affymetrix) and scanned at 1.56 μm resolution in a GeneChip® Scanner 3000 7G System (Affymetrix).

MICROARRAY DATA ANALYSIS

Three biological replicates were independently hybridized for each cell type. GeneChip intensities were background-corrected, normalized and summarized by the RMA method (Irizarry et al., 2003) using the "Affy" package (Gautier et al., 2004) from Bioconductor. Rank Products method (Breitling et al., 2004) was applied to identify differentially expressed genes as implemented in the "RankProd" package (Hong et al., 2006) from Bioconductor. Genes with FDR <0.05 were included in the list of induced or repressed candidates. FIESTA viewer was used to facilitate the application of these numerical filters and the selection of candidate genes (Oliveros, 2007). For the functional annotation of the results GeneCodis 3.0 was used (Nogales-Cadenas et al., 2009) applying a hypergeometric distribution and a FDR threshold of 0.05 for detecting over-represented Gene Ontology terms in candidate genes.

REAL-TIME QUANTITATIVE PCR

RNA was isolated from whole tissues using TRIzol (Invitrogen), treated with DNAse (Ambion), and reverse transcribed using hexamer primer and Moloney murine leukemia virus reverse transcriptase. To confirm the absence of genomic DNA, each sample was processed in parallel without reverse transcriptase. Real-time quantitative PCR (qPCR) for endogenous DREAM, and daDREAM was performed as described (Savignac et al., 2005). Validation of microarray up- or down-regulated genes was with specific primers and TaqMan MGB probes (Applied Biosystems). The results were normalized as indicated by parallel amplification of HPRT.

WESTERN BLOT ANALYSIS

Fifty micrograms of total protein from cerebellum or hippocampus were resolved in SDS-PAGE and transferred to PVDF membranes (Millipore). Antibodies against Mid1 (Ab 70770, Abcam) and β-actin (Sigma) were used.

ANATOMICAL ANALYSIS

For observation of adult cerebellum, 2-months-old wild type and transgenic mice were anesthetized and whole brains were carefully removed from the skull. Coronal and sagittal sections were taken and measurements of left–right and rostro-caudal axis were performed. For histological analysis, brains from 15-days-old pups (P15) were harvested and fixed in 4% paraformaldehyde for 48 h at 4°C. Brains were processed for paraffin embedding and microtome sectioning. Brain sagittal sections of 10 μm were stained with hematoxylin/eosin using standard procedures.

BEHAVIORAL ANALYSIS

Experiments were performed in newborn mice homozygous for the transgene and wild type littermates. Mice were initially housed in a temperature (21 ± 1°C) and humidity (65 ± 10%) controlled room with a 12/12-h light/dark cycle (lights on from 0800 to 2000 hours) with *ad libitum* food and water. Breeding pairs were formed and females visibly close to parturition were isolated. To avoid the effects of parity on behavioral ontogeny (Crusio and Schmitt, 1996) the first litter not used for the experiments. Testing involved approximately equal amounts of males and females. Experiments were carried out during the dark phase of the light–dark cycle. Behavioral tests and animal care were conducted according the EU and local ethical guidelines (EU directive 86/609 and Appendix A of the Council of Europe Convention ETS123, EU decree 2001-486 Decree 214/97 and Spanish law 32/2007) and approved by the local ethical committee (CEEA-PRBB). All behavioral experiments were carried out with the experimenter blind to the genotype. Developmental landmarks analyzed include: (i) assessment of body growth and body length were recorded from P1, the day of birth; (ii) fur appearance: beginning on P2 appearance of immature fur was observed and fur was defined as the mature hair being raised; (iii) incisor eruption: beginning on P7 pups were inspected daily for the emergence of both lower and upper incisor from the gingival; and (iv) eye opening, beginning on P9 pups were inspected daily for the complete opening of both eyelids. Neuromotor development was assessed on P7 and P10 by means of the pivoting and walking tests and general psychomotor development on P14 by means of the homing test.

In the pivoting locomotion test, the total number of degrees turned by the pup during a 60-s period was recorded. The test was performed on a flat surface covered with a paper on which lines

had been drawn to delineate four 90° quadrants. The number of degrees was scored only in completed 90° segments.

In the walking test, the latency for a mouse to lift up on all four legs and walk a distance exceeding its body length was measured on a flat surface covered with a green paper.

For the homing test, individual pups on postnatal day 14 were transferred to a cage containing new sawdust in 3/4 and 1/4 of sawdust of the home litter ("goal arena"). The pups were placed in the opposite side of the goal arena, near to the wall. The time taken to reach the home litter sawdust was recorded. A cut-off time of 180 s was applied.

Significance of the effects was assessed by two-tailed, unpaired Student's *t*-test was used for comparisons between groups. Analysis was processed using the SPSS program.

AUTHOR CONTRIBUTIONS

Conceived and designed the experiments: Mara Dierssen, Britt Mellström, Marisa Brini, Ernesto Carafoli, and Jose R. Naranjo. Performed the experiments: Laura Fedrizzi, Rosa Gomez-Villafuertes, María Martinez de Lagran, Alfonso Gutierrez-Adan, Ignasi Sahún, Belen Pintado, Xose M. Dopazo, and Paz Gonzalez. Analyzed the data: Britt Mellström, Juan C. Oliveros, Mara Dierssen, and Jose R. Naranjo. Wrote the paper: Mara Dierssen, Britt Mellström, and Jose R. Naranjo.

ACKNOWLEDGMENTS

Work was supported by grants from DGICYT (SAF2005-04682; SAF2007: /-62449/-64062/-31093E/-60827; SAF2008-03469; SAF2010-16427; SAF2010-21784), Spanish Ministry of Health (PI 082038), DURSI (2009SGR1313), Fundación Reina Sofía (PI 006/09), La Marató (2007-062231), La Caixa (BM04-167-0), and Areces, EU sixth Framework Program (PROMEMORIA; PHECOMP_037669; LSH-037627; NeuroNE, LSHG-CT-2006-037627; PS09/02673; and CureFXS, ERA-NET E-Rare, EU/FIS PS09102673).

REFERENCES

Alexander, J. C., Mcdermott, C. M., Tunur, T., Rands, V., Stelly, C., Karhson, D., Bowlby, M. R., An, W. F., Sweatt, J. D., and Schrader, L. A. (2009). The role of calsenilin/DREAM/KChIP3 in contextual fear conditioning. *Learn. Mem.* 16, 167–177.

An, W. F., Bowlby, M. R., Betty, M., Cao, J., Ling, H. P., Mendoza, G., Hinson, J. W., Mattsson, K. I., Strassle, B. W., Trimmer, J. S., and Rhodes, K. J. (2000). Modulation of A-type potassium channels by a family of calcium sensors. *Nature* 403, 553–556.

Anderson, D., Mehaffey, W. H., Iftinca, M., Rehak, R., Engbers, J. D., Hameed, S., Zamponi, G. W., and Turner, R. W. (2010). Regulation of neuronal activity by Cav3-Kv4 channel signaling complexes. *Nat. Neurosci.* 13, 333–337.

Aranda-Orgilles, B., Rutschow, D., Zeller, R., Karagiannidis, A. I., Kohler, A., Chen, C., Wilson, T., Krause, S., Roepcke, S., Lilley, D., Schneider, R., and Schweiger, S. (2011). Protein phosphatase 2A (PP2A)-specific ubiquitin ligase MID1 is a sequence-dependent regulator of translation efficiency controlling 3-phosphoinositide-dependent protein kinase-1 (PDPK-1). *J. Biol. Chem.* 286, 39945–39957.

Biesecker, L. G. (2006). What you can learn from one gene: GLI3. *J. Med. Genet.* 43, 465–469.

Breitling, R., Armengaud, P., Amtmann, A., and Herzyk, P. (2004). Rank products: a simple, yet powerful, new method to detect differentially regulated genes in replicated microarray experiments. *FEBS Lett.* 573, 83–92.

Buxbaum, J. D., Choi, E. K., Luo, Y., Lilliehook, C., Crowley, A. C., Merriam, D. E., and Wasco, W. (1998). Calsenilin: a calcium-binding protein that interacts with the presenilins and regulates the levels of a presenilin fragment. *Nat. Med.* 4, 1177–1181.

Cali, T., Fedrizzi, L., Ottolini, D., Gomez-Villafuertes, R., Mellstrom, B., Naranjo, J. R., Carafoli, E., and Brini, M. (2012). Ca2+ -activated nucleotidase 1, a novel target gene for the transcriptional repressor DREAM (downstream regulatory element antagonist modulator), is involved in protein folding and degradation. *J. Biol. Chem.* PMID: 22451650. [Epub ahead of print].

Carrion, A. M., Link, W. A., Ledo, F., Mellstrom, B., and Naranjo, J. R. (1999). DREAM is a Ca2+ -regulated transcriptional repressor. *Nature* 398, 80–84.

Carrion, A. M., Mellstrom, B., and Naranjo, J. R. (1998). Protein kinase A-dependent derepression of the human prodynorphin gene via differential binding to an intragenic silencer element. *Mol. Cell. Biol.* 18, 6921–6929.

Cheng, H. Y., Pitcher, G. M., Laviolette, S. R., Whishaw, I. Q., Tong, K. I., Kockeritz, L. K., Wada, T., Joza, N. A., Crackower, M., Goncalves, J., Sarosi, I., Woodgett, J. R., Oliveira-Dos-Santos, A. J., Ikura, M., Van Der Kooy, D., Salter, M. W., and Penninger, J. M. (2002). DREAM is a critical transcriptional repressor for pain modulation. *Cell* 108, 31–43.

Crusio, W. E., and Schmitt, A. (1996). Prenatal effects of parity on behavioral ontogeny in mice. *Physiol. Behav.* 59, 1171–1174.

Gautier, L., Cope, L., Bolstad, B. M., and Irizarry, R. A. (2004). Affy – analysis of Affymetrix GeneChip data at the probe level. *Bioinformatics* 20, 307–315.

Gomez-Villafuertes, R., Torres, B., Barrio, J., Savignac, M., Gabellini, N., Rizzato, F., Pintado, B., Gutierrez-Adan, A., Mellstrom, B., Carafoli, E., and Naranjo, J. R. (2005). Downstream regulatory element antagonist modulator regulates Ca2+ homeostasis and viability in cerebellar neurons. *J. Neurosci.* 25, 10822–10830.

Hasenpusch-Theil, K., Magnani, D., Amaniti, E. M., Han, L., Armstrong, D., and Theil, T. (2012). Transcriptional analysis of Gli3 mutants identifies Wnt target genes in the developing hippocampus. *Cereb. Cortex* PMID: 22235033. [Epub ahead of print].

Hong, F., Breitling, R., Mcentee, C. W., Wittner, B. S., Nemhauser, J. L., and Chory, J. (2006). RankProd: a bioconductor package for detecting differentially expressed genes in meta-analysis. *Bioinformatics* 22, 2825–2827.

Irizarry, R. A., Hobbs, B., Collin, F., Beazer-Barclay, Y. D., Antonellis, K. J., Scherf, U., and Speed, T. P. (2003). Exploration, normalization, and summaries of high density oligonucleotide array probe level data. *Biostatistics* 4, 249–264.

Krauss, S., Foerster, J., Schneider, R., and Schweiger, S. (2008). Protein phosphatase 2A and rapamycin regulate the nuclear localization and activity of the transcription factor GLI3. *Cancer Res.* 68, 4658–4665.

Lancioni, A., Pizzo, M., Fontanella, B., Ferrentino, R., Napolitano, L. M., De Leonibus, E., and Meroni, G. (2010). Lack of Mid1, the mouse ortholog of the Opitz syndrome gene, causes abnormal development of the anterior cerebellar vermis. *J. Neurosci.* 30, 2880–2887.

Landry, J. R., and Mager, D. L. (2002). Widely spaced alternative promoters, conserved between human and rodent, control expression of the Opitz syndrome gene MID1. *Genomics* 80, 499–508.

Ledo, F., Kremer, L., Mellstrom, B., and Naranjo, J. R. (2002). Ca2+ -dependent block of CREB-CBP transcription by repressor DREAM. *EMBO J.* 21, 4583–4592.

Ledo, F., Link, W. A., Carrion, A. M., Echeverria, V., Mellstrom, B., and Naranjo, J. R. (2000). The DREAM-DRE interaction: key nucleotides and dominant negative mutants. *Biochim. Biophys. Acta* 1498, 162–168.

Lilliehook, C., Bozdagi, O., Yao, J., Gomez-Ramirez, M., Zaidi, N. F., Wasco, W., Gandy, S., Santucci, A. C., Haroutunian, V., Huntley, G. W., and Buxbaum, J. D. (2003). Altered Abeta formation and long-term potentiation in a calsenilin knock-out. *J. Neurosci.* 23, 9097–9106.

Link, W. A., Ledo, F., Torres, B., Palczewska, M., Madsen, T. M., Savignac, M., Albar, J. P., Mellstrom, B., and Naranjo, J. R. (2004). Day-night changes in downstream regulatory element antagonist modulator/potassium channel interacting protein activity contribute to circadian gene expression in pineal gland. *J. Neurosci.* 24, 5346–5355.

Liu, E., Knutzen, C. A., Krauss, S., Schweiger, S., and Chiang, G. G. (2011). Control of mTORC1 signaling by the Opitz syndrome protein MID1. *Proc. Natl. Acad. Sci. U.S.A.* 108, 8680–8685.

Mayford, M., Wang, J., Kandel, E. R., and O'Dell, T. J. (1995). CaMKII regulates the frequency-response function of hippocampal synapses for the production of both LTD and LTP. *Cell* 81, 891–904.

Millen, K. J., and Gleeson, J. G. (2008). Cerebellar development and disease. *Curr. Opin. Neurobiol.* 18, 12–19.

Munne, P. M., Tummers, M., Jarvinen, E., Thesleff, I., and Jernvall, J. (2009). Tinkering with the inductive mesenchyme: Sostdc1 uncovers the role of dental mesenchyme in limiting tooth induction. *Development* 136, 393–402.

Nogales-Cadenas, R., Carmona-Saez, P., Vazquez, M., Vicente, C., Yang, X., Tirado, F., Carazo, J. M., and Pascual-Montano, A. (2009). GeneCodis: interpreting gene lists through enrichment analysis and integration of diverse biological information. *Nucleic Acids Res.* 37, W317–W322.

Nojima, H., Tokunaga, C., Eguchi, S., Oshiro, N., Hidayat, S., Yoshino, K., Hara, K., Tanaka, N., Avruch, J., and Yonezawa, K. (2003). The mammalian target of rapamycin (mTOR) partner, raptor, binds the mTOR substrates p70 S6 kinase and 4E-BP1 through their TOR signaling (TOS) motif. *J. Biol. Chem.* 278, 15461–15464.

Oliveros, J. C. (2007). "FIESTA at BioinfoGP" in *An Interactive Server for Analyzing DNA Microarray Experiments with Replicates.* Available at: http://bioinfogp.cnb.csic.es/tools/FIESTA

Opitz, J. M. (1987). G syndrome (hypertelorism with esophageal abnormality and hypospadias, or hypospadias-dysphagia, or "Opitz-Frias" or "Opitz-G" syndrome) – perspective in 1987 and bibliography. *Am. J. Med. Genet.* 28, 275–285.

Osawa, M., Dace, A., Tong, K. I., Valiveti, A., Ikura, M., and Ames, J. B. (2005). Mg2+ and Ca2+ differentially regulate DNA binding and dimerization of DREAM. *J. Biol. Chem.* 280, 18008–18014.

Osawa, M., Tong, K. I., Lilliehook, C., Wasco, W., Buxbaum, J. D., Cheng, H. Y., Penninger, J. M., Ikura, M., and Ames, J. B. (2001). Calcium-regulated DNA binding and oligomerization of the neuronal calcium-sensing protein, calsenilin/DREAM/KChIP3. *J. Biol. Chem.* 276, 41005–41013.

Palczewska, M., Casafont, I., Ghimire, K., Rojas, A. M., Valencia, A., Lafarga, M., Mellstrom, B., and Naranjo, J. R. (2011). Sumoylation regulates nuclear localization of repressor DREAM. *Biochim. Biophys. Acta* 1813, 1050–1058.

Park, J. W., Park, E. S., Choi, E. N., Park, H. Y., and Jung, S. C. (2009). Altered brain gene expression profiles associated with the pathogenesis of phenylketonuria in a mouse model. *Clin. Chim. Acta* 401, 90–99.

Pinson, L., Auge, J., Audollent, S., Mattei, G., Etchevers, H., Gigarel, N., Razavi, F., Lacombe, D., Odent, S., Le Merrer, M., Amiel, J., Munnich, A., Meroni, G., Lyonnet, S., Vekemans, M., and Attie-Bitach, T. (2004). Embryonic expression of the human MID1 gene and its mutations in Opitz syndrome. *J. Med. Genet.* 41, 381–386.

Quaderi, N. A., Schweiger, S., Gaudenz, K., Franco, B., Rugarli, E. I., Berger, W., Feldman, G. J., Volta, M., Andolfi, G., Gilgenkrantz, S., Marion, R. W., Hennekam, R. C., Opitz, J. M., Muenke, M., Ropers, H. H., and Ballabio, A. (1997). Opitz G/BBB syndrome, a defect of midline development, is due to mutations in a new RING finger gene on Xp22. *Nat. Genet.* 17, 285–291.

Rhodes, K. J., Carroll, K. I., Sung, M. A., Doliveira, L. C., Monaghan, M. M., Burke, S. L., Strassle, B. W., Buchwalder, L., Menegola, M., Cao, J., An, W. F., and Trimmer, J. S. (2004). KChIPs and Kv4 alpha subunits as integral components of A-type potassium channels in mammalian brain. *J. Neurosci.* 24, 7903–7915.

Rivas, M., Aurrekoetxea, K., Mellstrom, B., and Naranjo, J. R. (2011). Redox signaling regulates transcriptional activity of the Ca(2+)-dependent repressor DREAM. *Antioxid. Redox Signal.* 14, 1237–1243.

Rivas, M., Mellstrom, B., Naranjo, J. R., and Santisteban, P. (2004). Transcriptional repressor DREAM interacts with thyroid transcription factor-1 and regulates thyroglobulin gene expression. *J. Biol. Chem.* 279, 33114–33122.

Rivas, M., Mellstrom, B., Torres, B., Cali, G., Ferrara, A. M., Terracciano, D., Zannini, M., Morreale De Escobar, G., and Naranjo, J. R. (2009). The DREAM protein is associated with thyroid enlargement and nodular development. *Mol. Endocrinol.* 23, 862–870.

Rivera-Arconada, I., Benedet, T., Roza, C., Torres, B., Barrio, J., Krzyzanowska, A., Avendano, C., Mellstrom, B., Lopez-Garcia, J. A., and Naranjo, J. R. (2010). DREAM regulates BDNF-dependent spinal sensitization. *Mol. Pain* 6, 95.

Ruiz-Gomez, A., Mellstrom, B., Tornero, D., Morato, E., Savignac, M., Holguin, H., Aurrekoetxea, K., Gonzalez, P., Gonzalez-Garcia, C., Cena, V., Mayor, F. Jr., and Naranjo, J. R. (2007). G protein-coupled receptor kinase 2-mediated phosphorylation of downstream regulatory element antagonist modulator regulates membrane trafficking of Kv4.2 potassium channel. *J. Biol. Chem.* 282, 1205–1215.

Savignac, M., Mellstrom, B., Bebin, A. G., Oliveros, J. C., Delpy, L., Pinaud, E., and Naranjo, J. R. (2010). Increased B cell proliferation and reduced Ig production in DREAM transgenic mice. *J. Immunol.* 185, 7527–7536.

Savignac, M., Pintado, B., Gutierrez-Adan, A., Palczewska, M., Mellstrom, B., and Naranjo, J. R. (2005). Transcriptional repressor DREAM regulates T-lymphocyte proliferation and cytokine gene expression. *EMBO J.* 24, 3555–3564.

Scsucova, S., Palacios, D., Savignac, M., Mellstrom, B., Naranjo, J. R., and Aranda, A. (2005). The repressor DREAM acts as a transcriptional activator on Vitamin D and retinoic acid response elements. *Nucleic Acids Res.* 33, 2269–2279.

Thomsen, M. B., Wang, C., Ozgen, N., Wang, H. G., Rosen, M. R., and Pitt, G. S. (2009). Accessory subunit KChIP2 modulates the cardiac L-type calcium current. *Circ. Res.* 104, 1382–1389.

Trockenbacher, A., Suckow, V., Foerster, J., Winter, J., Krauss, S., Ropers, H. H., Schneider, R., and Schweiger, S. (2001). MID1, mutated in Opitz syndrome, encodes an ubiquitin ligase that targets phosphatase 2A for degradation. *Nat. Genet.* 29, 287–294.

Winter, J., Lehmann, T., Krauss, S., Trockenbacher, A., Kijas, Z., Foerster, J., Suckow, V., Yaspo, M. L., Kulozik, A., Kalscheuer, V., Schneider, R., and Schweiger, S. (2004). Regulation of the MID1 protein function is finetuned by a complex pattern of alternative splicing. *Hum. Genet.* 114, 541–552.

Wu, L. J., Mellstrom, B., Wang, H., Ren, M., Domingo, S., Kim, S. S., Li, X. Y., Chen, T., Naranjo, J. R., and Zhuo, M. (2010). DREAM (Downstream Regulatory Element Antagonist Modulator) contributes to synaptic depression and contextual fear memory. *Mol. Brain* 3, 3.

Zaidi, N. F., Kuplast, K. G., Washicosky, K. J., Kajiwara, Y., Buxbaum, J. D., and Wasco, W. (2006). Calsenilin interacts with transcriptional co-repressor C-terminal binding protein(s). *J. Neurochem.* 98, 1290–1301.

Zhang, Y., Su, P., Liang, P., Liu, T., Liu, X., Liu, X. Y., Zhang, B., Han, T., Zhu, Y. B., Yin, D. M., Li, J., Zhou, Z., Wang, K. W., and Wang, Y. (2010). The DREAM protein negatively regulates the NMDA receptor through interaction with the NR1 subunit. *J. Neurosci.* 30, 7575–7586.

Conflict of Interest Statement: The authors declare that the research was conducted in the absence of any commercial or financial relationships that could be construed as a potential conflict of interest.

Received: 03 February 2012; paper pending published: 27 February 2012; accepted: 11 April 2012; published online: 03 May 2012.

Citation: Dierssen M, Fedrizzi L, Gomez-Villafuertes R, de Lagran MM, Gutierrez-Adan A, Sahún I, Pintado B, Oliveros JC, Dopazo XM, Gonzalez P, Brini M, Mellström B, Carafoli E and Naranjo JR (2012) Reduced Mid1 expression and delayed neuromotor development in daDREAM transgenic mice. Front. Mol. Neurosci. ***5****:58. doi: 10.3389/fnmol.2012.00058*

APPENDIX

Table A1 | Functional annotation of over-represented candidate genes according to Gene Ontology (Cellular components).

GO ID	Term	Probe ID	*P*-value	FDR
GO:0005925	Focal adhesion	1417654_at	0.0134524	0.045738
GO:0005615	Etracellular space	1449340_at, 1460049_s_at	0.0050619	0.0286841
GO:0015630	Microtubule cytoskeleton	1438239_at	0.0116782	0.0496325
GO:0043034	Costamere	1417654_at	0.0024424	0.0207604
GO:0042612	MHC class I protein complex	1425545_x_at	0.00211703	0.0359896

Table A2 | Functional annotation of over-represented candidate genes according to Gene Ontology (Biological process).

GO ID	Term	Probe ID	*P*-value	FDR
GO:0007389	Pattern specification process	1449340_at	0.0142579	0.0161589
GO:0016055	Wnt receptor signaling pathway	1449340_at	0.0262754	0.0262754
GO:0042475	Odontogenesis of dentin-containing tooth	1449340_at	0.00731229	0.0088792
GO:0006955	Immune response	1425545_x_at	0.0243609	0.0258834
GO:0032874	Positive regulation of stress-activated MAPK cascade	1438239_at	0.00211703	0.00514137
GO:0030514	Negative regulation of BMP signaling pathway	1449340_at	0.00471748	0.0066831
GO:0051894	Positive regulation of focal adhesion assembly	1417654_at	0.000977557	0.00415462
GO:0090398	Cellular senescence	1460049_s_at	0.00130323	0.00443099
GO:0051496	Positive regulation of stress fiber assembly	1417654_at	0.00227973	0.00484442
GO:0070314	G1 to G0 transition	1460049_s_at	0.000488878	0.00415546
GO:0045860	Positive regulation of protein kinase activity	1417654_at	0.00504214	0.00659357
GO:0007026	Negative regulation of microtubule depolymerization	1438239_at	0.00260505	0.00492065
GO:0019882	Antigen processing and presentation	1425545_x_at	0.00471748	0.0066831
GO:0008054	Cyclin catabolic process	1460049_s_at	0.000651793	0.00369349
GO:0002474	Antigen processing and presentation of peptide antigen via MHC class I	1425545_x_at	0.00195432	0.00553723
GO:0001916	Positive regulation of T-cell mediated cytotoxicity	1425545_x_at	0.00276768	0.00470505
GO:0002485	Antigen processing and presentation of endogenous peptide antigen via MHC class I via ER pathway, TAP-dependent	1425545_x_at	0.000488878	0.00415546

frontiers in
MOLECULAR NEUROSCIENCE

REVIEW ARTICLE
published: 15 March 2012
doi: 10.3389/fnmol.2012.00025

Three functional facets of calbindin D-28k

Hartmut Schmidt*

Medical Faculty, Carl-Ludwig Institute for Physiology, University of Leipzig, Leipzig, Germany

Edited by:
Beat Schwaller, University of Fribourg, Switzerland

Reviewed by:
Guido C. Faas, University of California, USA
Olivier Caillard, INSERM, France
Jaroslaw J. Barski, Medical University of Silesia, Poland

****Correspondence:***
Hartmut Schmidt, Medical Faculty, Carl-Ludwig Institute for Physiology, University of Leipzig, Liebigstr. 27, 04103 Leipzig, Germany.
e-mail: hartmut.schmidt@medizin.uni-leipzig.de

Many neurons of the vertebrate central nervous system (CNS) express the Ca^{2+} binding protein calbindin D-28k (CB), including important projection neurons like cerebellar Purkinje cells but also neocortical interneurons. CB has moderate cytoplasmic mobility and comprises at least four EF-hands that function in Ca^{2+} binding with rapid to intermediate kinetics and affinity. Classically it was viewed as a pure Ca^{2+} buffer important for neuronal survival. This view was extended by showing that CB is a critical determinant in the control of synaptic Ca^{2+} dynamics, presumably with strong impact on plasticity and information processing. Already 30 years ago, *in vitro* studies suggested that CB could have an additional Ca^{2+} sensor function, like its prominent acquaintance calmodulin (CaM). More recent work substantiated this hypothesis, revealing direct CB interactions with several target proteins. Different from a classical sensor, however, CB appears to interact with its targets both, in its Ca^{2+}-loaded and Ca^{2+}-free forms. Finally, CB has been shown to be involved in buffered transport of Ca^{2+}, in neurons but also in kidney. Thus, CB serves a threefold function as buffer, transporter and likely as a non-canonical sensor.

Keywords: calcium, sensor, transporter, buffer, synaptic plasticity, neurons, transmitter release

INTRODUCTION

Despite the wealth of information on expression patterns of Ca^{2+} binding proteins (CaBPs), their functional significance is only slowly emerging. In particular, this is due to their complex interplay with other Ca^{2+} controlling mechanisms and the inherent technical difficulties in studying biophysical properties of individual proteins (Neher, 2000), including the differentiation between Ca^{2+}-buffer and Ca^{2+}-sensor (da Silva and Reinach, 1991). Buffers are characterized by more or less specific binding/chelating of Ca^{2+} ions without further Ca^{2+}-dependent target interactions. Their function is in the control of the spatiotemporal extent of Ca^{2+} signaling domains (Augustine et al., 2003; Eggermann et al., 2012). Sensors, on the other hand, undergo additional characteristic conformational changes upon Ca^{2+}-binding, resulting in exposure of hydrophobic surfaces necessary for binding and subsequent regulation of downstream effectors (Ikura, 1996; Schwaller, 2008, 2010). Their functional significance lies in both, the control of intracellular free Ca^{2+} ($[Ca^{2+}]_i$) and in triggering Ca^{2+}-dependent downstream signaling.

In consequence, characterization of a CaBP requires determination of several biophysical parameters (**Table 1**), including affinity and kinetics of Ca^{2+}-binding, intracellular mobility, structural and conformational analysis, and the identification of binding partners. Following some general remarks on buffering, I will review advances in gathering biophysical parameters of CB that allowed deducing its functional facets, with emphasis on its neuronal function.

SOME GENERAL ASPECTS OF BUFFERING

Dissociation constants (K_D) of proton buffers are optimized to clamp pH at 7–7.4 in living tissue by bidirectional buffering of free protons to a concentration of ~100 nM. $[Ca^{2+}]_i$ in resting cells is similar, however, contrasting to pH buffers, K_D values of most CaBPs are well above $[Ca^{2+}]_i$; a notable exception is parvalbumin (PV, $K_{D,Ca}$ ~9 nM; Lee et al., 2000b). Thus, under resting conditions most binding sites are unoccupied by Ca^{2+}, such that CaBPs limit increases in $[Ca^{2+}]_i$ from the resting level rather than clamping $[Ca^{2+}]_i$ at a given level, i.e., they act as unidirectional buffers. This can even be augmented by an additional Mg^{2+} affinity, which reduces the effective affinity for Ca^{2+} due to competition or a necessity for preceding Mg^{2+} unbinding (**Figure 1**).

Neuronal Ca^{2+} signals are typically short lived and the amount of Ca^{2+} bound to a specific buffer can substantially deviate from the steady state value (Markram et al., 1998). Non-equilibrium conditions require a kinetic description of Ca^{2+} binding by forward (k_{on}) and backward (k_{off}) rates, values that could be quantified only recently due to a notable technical advance (Nägerl et al., 2000; Faas et al., 2007, 2011).

I will close these general remarks with a note on the ambiguous term "saturation." In biochemistry, saturation refers to the fraction of total binding sites occupied at a given time. In chemistry, it often marks the 100% occupancy, probably the most intuitive meaning. In descriptions of Ca^{2+} dynamics saturation is often used to mark the deviation from linearity. A linear signaling process has the property that the combined effects of two or more elementary events result in a response which is given by the sum of the individual responses. This is the case if increases in $[Ca^{2+}]_i$ are much smaller than K_D of the buffer(s). Ca^{2+} kinetics become more complex if the increase in $[Ca^{2+}]_i$ approaches K_D (Neher, 1998a), i.e., saturation of a CaBP occurs around its half-occupancy.

Ca^{2+} BINDING AND MOBILITY

CB has six EF-hands, of which one or two are non-functioning in metal binding (Leathers et al., 1990; Åkerfeldt et al., 1996;

Table 1 | Properties of calbindin D-28k.

Parameter[a]	Value	References/Notes
Amino acids	260–261	Celio et al., 1996, species specific
Molecular weight	29–30 kDa	Celio et al., 1996
Diffusion coefficients in		
Water	$>100\,\mu m^2 s^{-1}$	Gabso et al., 1997
Spiny dendrites of Purkinje neurons	$20 \pm 2\,\mu m^2 s^{-1}$	Schmidt et al., 2005*
Intracellular concentration in		
Purkinje neurons	100 to $<360\,\mu M$	Kosaka et al., 1993; Maeda et al., 1999
Somata of Purkinje neurons	$208 \pm 42\,\mu M$	Hackney et al., 2005
Hippocampal granule cells	$0–40\,\mu M$	Müller et al., 2005[a]
CA1 pyramidal neurons	$45 \pm 2\,\mu M$	Müller et al., 2005
CA3 interneurons	$47 \pm 6\,\mu M$	Müller et al., 2005
Rat inner hair cells	$40–125\,\mu M$	Hackney et al., 2005[b]
Rat outer hair cells	$57–197\,\mu M$	Hackney et al., 2005[b]
Binding sites		Leathers et al., 1990; Åkerfeldt et al., 1996; Berggård et al., 2002a[c]
Total	6	
Functional	4	Mixed Ca^{2+}/Mg^{2+} binding sites; the remaining 2 EF hands do not bind Ca^{2+} (EF-2) or with a very low affinity (EF-6)
Metal binding		
Mg^{2+} $K_{D,Mg}$	$714\,\mu M$	Berggård et al., 2002a
Ca^{2+} $K_{D,Ca}$	393 nM	Faas et al., 2011
k_{on}	$75\,\mu M^{-1}s^{-1}$	Faas et al., 2011
k_{off}	$29.5\,s^{-1}$	Faas et al., 2011
Cooperativity		
n_H	1.2–1.3	presumably Mg^{2+} dependent[d]
Binding to *myo*-inositol monophosphatase		Berggård et al., 2002b
K_D	$0.9\,\mu M$	Berggård et al., 2002b
k_{off}	0.08 (0.06–0.1)[#] s^{-1}	Schmidt et al., 2005, Purkinje neurons

** Errors as SEM, unless stated otherwise.*

[a] Developmentally-regulated differences.

[b] Field of view averages, disregarding strong developmental differences and differences between apical and basal cells.

[c] Unless otherwise noted all following parameters were obtained from cuvette measurements.

[d] Hill coefficient was estimated by Faas et al. (2011) based on data from Berggård et al. (2002a).

[#] Interquartile range.

Berggård et al., 2002a; Cedervall et al., 2005; Kojetin et al., 2006). EF-2 is consistently viewed as non-metal binding while EF-6 may have a very low Ca^{2+} affinity (Åkerfeldt et al., 1996; Cedervall et al., 2005). EF-1, 3, 4, 5 are mixed metal binding sites, however, with much higher affinity for Ca^{2+} (393 nM; Faas et al., 2011) than for Mg^{2+} (714 μM; Berggård et al., 2002a). Thus, under physiological conditions ($[Mg^{2+}]_i$ ~600 μM) CB will function predominantly as a Ca^{2+} buffer. In resting neurons ($[Ca^{2+}]_i$ ~50 nM, $[Mg^{2+}]_i$ ~600 μM), it will be loaded by approx. ten percent with Ca^{2+} and 45% with Mg^{2+} (**Figure 1**; Berggård et al., 2002a). Compared to the related PV, the presence of Mg^{2+} produces only a minor shift in the apparent $K_{D,Ca}$ of CB (**Figure 1**), while it appears to increase cooperativity in Ca^{2+} binding (Berggård et al., 2002a); however, cooperativity is still negligible, with an estimated Hill coefficient (n_H) of ~1.25 (Faas et al., 2011).

Disregarding cooperativity, CB binds Ca^{2+} with rapid to intermediate kinetics (k_{on} $75\,\mu M^{-1}s^{-1}$) and medium (393 nM) affinity (Faas et al., 2011; **Table 1**). Its on-rates are between those of EGTA (k_{on} $10\,\mu M^{-1}s^{-1}$, K_D 70 nM; Nägerl et al., 2000; Meinrenken et al., 2002) and BAPTA (k_{on} $400\,\mu M^{-1}s^{-1}$, K_D 220 nM; Naraghi, 1997; Naraghi and Neher, 1997; Meinrenken et al., 2002), while its affinity is closer to BAPTA. Typically, these properties endow CB to function as a major determinant of neuronal Ca^{2+} kinetics (Airaksinen et al., 1997; Barski et al., 2003; Schmidt et al., 2003).

The diffusion of CB has been quantified in spiny dendrites of cerebellar Purkinje neurons (PNs). Apart from a smaller immobilized fraction (see below), CB diffused with an apparent diffusion coefficient (D) of $20\,\mu m^2/s$ between spines and parent dendrites (Schmidt et al., 2005). This is ~2-fold slower than the diffusional mobility of PV in the same cellular compartments, but identical to the D of a mobile calmodulin (CaM) fraction in HEK293 cells (Kim et al., 2004) and in spiny dendrites of PNs (Schmidt et al., 2007). To my knowledge there is no quantification of aqueous CB

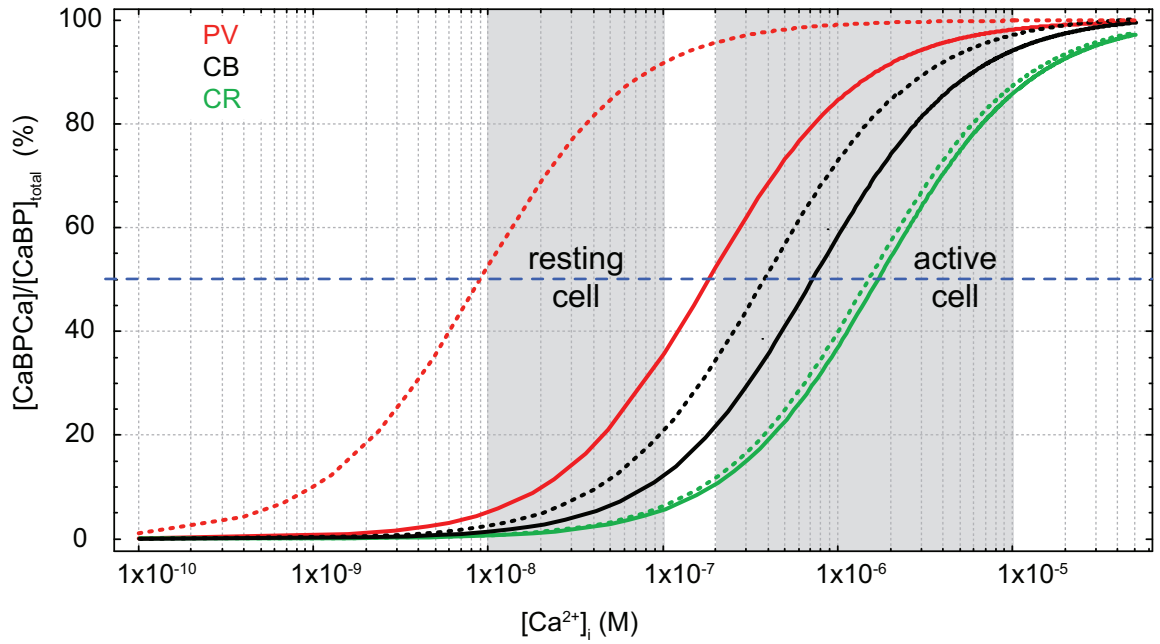

FIGURE 1 | Effects of Mg^{2+} on Ca^{2+} binding. Simulated steady-state Ca^{2+}-binding curves of the Ca^{2+} binding proteins (CaBP) parvalbumin (PV, red, $K_{D,Ca}$ 9 nM, $K_{D,Mg}$ 31 μM), calbindin (CB, black, average $K_{D,Ca}$ 393 nM, $K_{D,Mg}$ 714 μM; cf. **Table 1**), and calretinin (CR, green, average $K_{D,Ca}$ 1.5 μM, $K_{D,Mg}$ 4.5 mM) in the absence of Mg^{2+} (dotted lines) and in the presence of 600 μM Mg^{2+} (solid lines).

diffusion, but it might be estimated to be $>100\,\mu m^2/s$ (Gabso et al., 1997).

BUFFER OR SENSOR?

In vitro studies from the 80th and 90th already suggested that CB might have an additional Ca^{2+} sensor function. It was shown to activate isolated erythrocyte membrane Ca^{2+}-Mg^{2+} -ATPases (Morgan et al., 1986) and cyclic nucleotide phosphodiesterases (Reisner et al., 1992); in centrifugation studies of different tissues CB was found not only in the cytoplasmatic fractions but also in membrane/organelle containing fractions (Hubbard and McHugh, 1995; Winsky and Kuźnicki, 1995). The CB content in the membrane fractions was decreased in samples prepared or incubated in low Ca^{2+} (Winsky and Kuźnicki, 1995).

Three studies from the group of S. Linse (Berggård et al., 2000, 2002a,b) laid the foundation for substantiating the sensor hypothesis: They found that CB underwent substantial conformational rearrangements upon Ca^{2+}-binding and protonation, likely exposing EF-2, but not upon Mg^{2+}-binding. These changes went beyond the moderate redistributions in Mg^{2+}-induced cooperativity in Ca^{2+}-binding (see above). Unlike classical sensors CB had exposed hydrophobic regions also in its Ca^{2+}-free (apo-) conformation, which is thermodynamically unfavorable under aqueous conditions, thus, suggesting additional Ca^{2+}-independent interactions with target proteins. Subsequently, CB was shown to interact with *myo*-inositol monophosphatase-1 (IMPase), a key enzyme in the IP3 second messenger pathway (see below) both, in its apo- and Ca^{2+}-bound form with low affinity (K_D ~0.9 μM). Finally, they identified a 12 amino-acid motive as the putative CB binding domain of IMPase.

Another CB ligand identified is Ran-binding-protein-M (RanBPM), a small GTPase involved in nuclear transport processes and microtubule formation (Lutz et al., 2003). Using NMR, it was shown that RanBPM interacted with Ca^{2+} loaded CB. Finally, CB was found to inhibit caspase-3 in osteoblastic cells independent of Ca^{2+}, thereby, suppressing apoptosis (Bellido et al., 2000). Caspases are important enzymes in apoptosis, with activation of caspase-3 triggering the common executive pathway of cell death (Grütter, 2000; Yuan and Yankner, 2000; Yan and Shi, 2005). In central nervous system (CNS), incorrect execution of death pathways is thought to be associated with severe disorders including Chorea Huntington and Alzheimer disease. The finding that CB markedly reduces caspase-3 activity is particularly noteworthy in this context, since it might act as a neuroprotective agent.

So far, only *in vitro* studies showed a sensor function of CB. The CB-IMPase interaction was demonstrated *in situ* in PNs in acute slices (Schmidt et al., 2005). In multi-photon fluorescence recovery after photobleaching experiments a fraction of dye-labeled CB (~20–30%) was found to be immobilized for >1 s in spines and dendrites, but not in smooth parts of axons. Use of the above peptide sequence from IMPase in a competition assay led to significant relief from immobilization, suggesting that CB indeed interacted with IMPase in PNs. Further experiments showed that the interaction was influenced by synaptic activation associated with increased $[Ca^{2+}]_i$.

A detailed NMR analysis of CB structure (Kojetin et al., 2006), completing earlier work (Klaus et al., 1999; Berggård et al., 2000, 2002a,b; Venters et al., 2003; Venyaminov et al., 2004; Vanbelle et al., 2005), confirmed that upon Ca^{2+} binding CB adopts

discrete hydrophobic states but also has exposed hydrophobic surfaces in its apo-form. In addition, the regions mediating the interactions with RanBPM, IMPase, Caspase-3 and also its pro-domain were mapped.

Finally, in kidney CB was found to associate with TRPV5 channels which are involved in Ca^{2+} reabsorption from the urea (Lambers et al., 2006). The family of TRP channels is extraordinarily large with several members being abundantly expressed in the CNS. While it is temping to speculate on further direct CB interactions with Ca^{2+}-conductances in neurons, experimental evidence is missing.

Taken together, there is growing evidence that CB not only functions as Ca^{2+}-buffer but also binds to and regulates a variety of target proteins, including membrane ATPases, IMPase, RanBPM, procaspase-3, caspase-3, and TRPV5. Unlike canonical Ca^{2+}-sensors, however, CB likely interacts in Ca^{2+}-free and Ca^{2+}-occupied form with its targets.

FUNCTIONAL ASPECTS OF CB

CB appears to fulfill three functions: First, it functions as a mobile or partly immobilized Ca^{2+}-buffer with medium kinetics and affinity—buffer function. Second, it functions in buffered Ca^{2+}-diffusion—transport function. Finally, it interacts with target proteins likely both, in its apo- and Ca^{2+}-loaded form—sensor-like function.

BUFFER FUNCTION

In neurons expressing CB, it makes a major contribution to the total buffer capacitance (Fierro and Llano, 1996; Jackson and Redman, 2003; but see Faas et al. (2011) for an alternative view on CA1 spines in the presumed presence of large amounts of CaM). In dendrites and spines, CB clips the peak amplitude of synaptically induced Ca^{2+} transients, speeds their initial decay kinetics and prolongs their later phase (Airaksinen et al., 1997; Schmidt et al., 2003, 2007), while the rise time of the Ca^{2+} transients remained essentially unaffected (Koster et al., 1995; Schmidt et al., 2003). Thus, in postsynaptic structures CB induces characteristic biphasic decay kinetics of volume averaged Ca^{2+} transients and controls their amplitude.

Long lasting alterations of synaptic weight, like long-term potentiation (LTP) or depression (LTD) comprise strong Ca^{2+}-dependent postsynaptic components. LTP in CA1 pyramidal neurons with reduced CB content could be induced normally but its maintenance was affected, leading to impaired spatial learning (Molinari et al., 1996). Whether this is attributable to altered Ca^{2+}-signaling in the absence of CB or a direct target modulation by CB remained unclear. Lack of CB results also in deficits in motor coordination (Airaksinen et al., 1997; Barski et al., 2003), which is consistent with the strong CB expression in cerebellar cortex and its impact on synaptically mediated Ca^{2+} transients. However, parallel-fiber (PF) LTD in PNs lacking CB was normal and also Ca^{2+}-signals mediated via activation of metabotropic glutamate receptors (mGluRs), known to be required in LTD induction (Daniel et al., 1998; Ito, 2001), were unaltered compared to the WT (Barski et al., 2003). It remained elusive, however, why rapid Ca^{2+} transients mediated by climbing-fiber and PF inputs were affected by lack of CB, whereas longer lasting, mGluR mediated Ca^{2+}-signals were not (cf. discussion in Barski et al., 2003 for a possible explanation). Given that the conditional knock-outs used in the study are not affected by compensations for lack of CB (Vecellio et al., 2000; Kreiner et al., 2010), the answer may involve the as yet not further characterized CB-IMPase interaction (Schmidt et al., 2005; cf. below).

In presynaptic terminals, relevant Ca^{2+}-signaling domains and their topographical relationships to Ca^{2+} dependent processes are well defined (Neher, 1998b; Augustine et al., 2003; Eggermann et al., 2012). However, the function of individual CaBPs has been rarely specified, although they are generally believed to be crucial in regulating transmitter release and short-term plasticity. Specifically, it has been postulated that saturation of CB underlies a form of paired pulse facilitation (PPF) at neocortical interneuron to pyramidal neuron synapses, hippocampal mossy-fiber to CA-3 synapses (Blatow et al., 2003), and recurrent PN synapses (Orduz and Llano, 2007). This form of PPF has been termed "pseudofacilitation" (Rozov et al., 2001) in order to distinguish it from more classical mechanisms like residual Ca^{2+} (Zucker and Stockbridge, 1983; Connor et al., 1986), Ca^{2+} remaining bound to the release sensor or a facilitation sensor ("active Ca^{2+}"; Katz and Miledi, 1968; Yamada and Zucker, 1992; Atluri and Regehr, 1996) or Ca^{2+} dependent facilitation of Ca^{2+}-currents (CDF; Lee et al., 1999, 2000a; Tsujimoto et al., 2002; for more detail see, e.g., Neher, 1998b; Zucker and Regehr, 2002; Stevens, 2003). In pseudofacilitation a substantial amount of Ca^{2+} entering the presynapse during the first action potential (AP) is thought to be buffered by CB, thereby, reducing the initial release probability but also saturating CB, which in turn results in increased $[Ca^{2+}]_i$ during the second AP and potentiated release (Neher, 1998b; Rozov et al., 2001; Blatow et al., 2003; Felmy et al., 2003). Albeit direct evidence for CB saturation is scarce and Ca^{2+} imaging experiments from CB containing versus CB deficient presynaptic terminals are lacking, the hypothesis is consistent with conclusions drawn from experiments with BAPTA (Rozov et al., 2001). However, Ca^{2+} binding by endogenous CaBPs can be more complex than binding by exogenous buffers, as exemplified recently for PV (Caillard et al., 2000; Eggermann et al., 2012; Eggermann and Jonas, 2012). Thus, more direct evidence for saturation is desirable.

CDF and its counterpart Ca^{2+}-dependent inactivation (CDI) are Ca^{2+} driven feedback mechanisms regulating voltage operated $Ca_v2.1$ (P/Q type) Ca^{2+}-channels. CDF is mediated by Ca^{2+} loaded CaM or NCS-1 (Lee et al., 1999, 2000a; Tsujimoto et al., 2002), while CB only affected CDI but not CDF. Different from the CaM and NCS-1 effects on CDF, CB effects on CDI were essentially consistent with its buffering action and did not require the assumption of a Ca^{2+}-sensor function (Kreiner and Lee, 2006).

TRANSPORT FUNCTION

Beyond Ca^{2+} transporting epithelia (Bronner and Stein, 1988; Bronner, 1989; Koster et al., 1995; Lambers et al., 2006), buffered Ca^{2+} transport by CB has recently also been suggested between activated spines and their parent dendritic shafts (Schmidt et al., 2007; Schmidt and Eilers, 2009). Although spill-over of Ca^{2+} from spines into dendrites had been reported before by several

groups (Majewska et al., 2000; Holthoff et al., 2002; Schmidt et al., 2003), these experimental observations were significantly influenced by the action of Ca^{2+} dyes (Sabatini et al., 2002; Schmidt et al., 2003) and in the majority view spine necks remained substantial diffusion barriers for second messengers, making spines biochemically isolated compartments (Gamble and Koch, 1987; Zador et al., 1990; Müller and Connor, 1991; Svoboda et al., 1996; Sabatini et al., 2002). An analysis of spine Ca^{2+} dynamics under minimally perturbed conditions, however, confirmed that indeed most spines of pyramidal neurons allow a sizeable Ca^{2+} efflux that was tightly regulated by the geometry of the spine neck (Noguchi et al., 2005). Consecutively, it was shown that in PNs the majority of Ca^{2+} left the spine bound to CB (Schmidt et al., 2007), with the buffered efflux again being tightly controlled by the spine neck geometry (Schmidt and Eilers, 2009). This diffusional coupling drove a spatial summation process in which coincident activity of neighboring spines was integrated in the dendrite with the potential to activate dendritic CaM. This biochemical summation might exist in parallel to the classical summation of electrical signals in dendrites, possibly with reciprocal interaction (Nemri and Ghisovan, 2007).

Despite buffered Ca^{2+} transport, even neurons expressing large amounts of CB can retain Ca^{2+} signals that are spatially restricted to activated dendritic branches (Eilers et al., 1995, 1997) Although significant Ca^{2+} transport out of the active branches indeed occurred, it was outweighed by Ca^{2+} extrusion along the dendrite. This close interplay between diffusion and extrusion defined the capability of Ca^{2+} to spread between dendritic branches (Schmidt et al., 2011).

SENSOR-LIKE FUNCTION

In this final function-section, I will focus on the neuronal CB-IMPase interaction. IMPase catalyzes the hydrolysis of *myo*-inositol-1(or 4)-monophosphate to form free *myo*-inositol, the resource for IP3 and DAG second messengers. CB was shown to bind IMPase *in vitro* (Berggård et al., 2002b) and in PNs (Schmidt et al., 2005) with a K_D of ∼0.9 μM and an off-rate of ∼0.08 s^{-1} (**Table 1**). *In vitro*, apo- and Ca^{2+}-bound CB activated IMPase similarity up to 250-fold. The activation was most pronounced under conditions that otherwise were associated with very low IMPase activity, precisely at reduced pH and at low substrate concentration. In spiny dendrites, binding of CB to IMPase was apparent at resting Ca^{2+} levels but further amplified by synaptic activation associated with increases in intracellular Ca^{2+} in a frequency dependent way. Thus, while the *in vitro* interaction appeared essentially independent of Ca^{2+}, in dendrites it is likely boosted by increasing Ca^{2+} levels.

Still unresolved is the impact of the CB-IMPase interaction on dendritic IP3 mediated Ca^{2+}-signaling. Two scenarios would be conceivable: First, the increased IMPase activity speeds the degradation of IP and could, in consequence, result in accelerated IP3 degradation and in reduced Ca^{2+}-signals. Second, increased IMPase activity could result in an accelerated source substance supply for IP3 production and consequently in increased IP3 levels and amplified Ca^{2+}-signaling. Considering that IP3 mediated Ca^{2+}-signals in dendrites of PN-specific CB knock-outs were, despite the absence of a major buffer, unaltered compared to the WT (Barski et al., 2003) this argues in favor of the second scenario.

CONCLUDING REMARKS

I reviewed evidence for a threefold function of CB, consisting of a sensor-like and a transport function in addition to buffering of Ca^{2+}. Different from a canonical Ca^{2+}-sensor, CB appears to bind its targets in Ca^{2+}-occupied and Ca^{2+}-free conformation. Spino-dendritic Ca^{2+}-coupling and its regulation by the geometry of the spine neck were shown for pyramidal as well as PNs. In the latter the coupling was essentially mediated by CB. The control of this coupling via the spine neck, which itself undergoes use-dependent regulation, will increase the computational capacitance of dendrites. Despite growing evidence for these two additional functions, decades of investigation on CB mainly underlined its importance as a Ca^{2+}-buffer.

ACKNOWLEDGMENTS

I thank Oliver Arendt for critical reading of the manuscript. This work was supported by the DFG (EI 341/4–2).

REFERENCES

Airaksinen, M. S., Eilers, J., Garaschuk, O., Thoenen, H., Konnerth, A., and Meyer, M. (1997). Ataxia and altered dendritic calcium signalling in mice carrying a targeted nullmutation of the calbindin D28k gene. *Proc. Natl. Acad. Sci. U.S.A.* 94, 1488–1493.

Åkerfeldt, K. S., Coyne, A. N., Wilk, R. R., Thulin, E., and Linse, S. (1996). Ca^{2+}-binding stoichiometry of calbindin D28k as assessed by spectroscopic analyses of synthetic peptide fragments. *Biochemistry* 35, 3662–3669.

Atluri, P. P., and Regehr, W. G. (1996). Determinants of the time course of facilitation at the granule cell to Purkinje cell synapse. *J. Neurosci.* 16, 5661–5671.

Augustine, G. J., Santamaria, F., and Tanaka, K. (2003). Local calcium signaling in neurons. *Neuron* 40, 331–346.

Barski, J. J., Hartmann, J., Rose, C. R., Hoebeek, F., Mörl, K., Noll-Hussong, M., De Zeeuw, C. I., Konnerth, A., and Meyer, M. (2003). Calbindin in cerebellar Purkinje cells is a critical determinant of the precision of motor coordination. *J. Neurosci.* 23, 3469–3477.

Bellido, T., Huening, M., Raval-Pandya, M., Manolagas, S. C., and Christakos, S. (2000). Calbindin-D28k is expressed in osteoblastic cells and suppresses their apoptosis by inhibiting caspase-3 activity. *J. Biol. Chem.* 275, 26328–26332.

Berggård, T., Miron, S., Önnerfjord, P., Thulin, E., Åkerfeldt, K. S., Enghild, J. J., Akke, M., and Linse, S. (2002a). Calbindin D28k exhibits properties characteristic of a Ca^{2+} sensor. *J. Biol. Chem.* 277, 16662–16672.

Berggård, T., Szczepankiewicz, O., Thulin, E., and Linse, S. (2002b). Myo-inositol monophosphatase is an activated target of calbindin D28k. *J. Biol. Chem.* 277, 41954–41959.

Berggård, T., Silow, M., Thulin, E., and Linse, S. (2000). Ca^{2+}- and H^{+}-dependent conformational changes of calbindin D28k. *Biochemistry* 39, 6864–6873.

Blatow, M., Caputi, A., Burnashev, N., Monyer, H., and Rozov, A. (2003). Ca^{2+} buffer saturation underlies paired pulse facilitation in calbindin-d28k-containing terminals. *Neuron* 38, 79–88.

Bronner, F. (1989). Renal calcium transport: mechanisms and regulation-an overview. *Am. J. Physiol.* 257, F707–F711.

Bronner, F., and Stein, W. D. (1988). CaBPr facilitates intracellular diffusion for Ca pumping in distal convoluted tubule. *Am. J. Physiol.* 255, F558–F562.

Caillard, O., Moreno, H., Schwaller, B., Llano, I., Celio, M. R., and Marty, A. (2000). Role of the calcium-binding protein parvalbumin in short-term

synaptic plasticity. *Proc. Natl. Acad. Sci. U.S.A.* 97, 13372–13377.

Cedervall, T., Andre, I., Selah, C., Robblee, J. P., Krecioch, P. C., Fairman, R., Linse, S., and Akerfeldt, K. S. (2005). Calbindin D28k EF-hand ligand binding and oligomerization: four high-affinity sites--three modes of action. *Biochemistry* 44, 13522–13532.

Celio, M. R., Pauls, T., and Schwaller, B. (1996). *Guidebook to the Calcium-Binding Proteins*. Oxford: Sambrook & Tooze Publication at Oxford University Press.

Connor, J. A., Kretz, R., and Shapiro, E. (1986). Calcium levels measured in a presynaptic neurone of Aplysia under conditions that modulate transmitter release. *J. Physiol.* 375, 625–642.

da Silva, A. C., and Reinach, F. C. (1991). Calcium binding induces conformational changes in muscle regulatory proteins. *Trends Biochem. Sci.* 16, 53–57.

Daniel, H., Levenes, C., and Crepél, F. (1998). Cellular mechanisms of cerebellar LTD. *Trends Neurosci.* 21, 401–407.

Eggermann, E., Bucurenciu, I., Goswami, S. P., and Jonas, P. (2012). Nanodomain coupling between Ca^{2+} channels and sensors of exocytosis at fast mammalian synapses. *Nat. Rev. Neurosci.* 13, 7–21.

Eggermann, E., and Jonas, P. (2012). How the 'slow' Ca^{2+} buffer parvalbumin affects transmitter release in nanodomain-coupling regimes. *Nat. Neurosci.* 15, 20–22.

Eilers, J., Augustine, G. J., and Konnerth, A. (1995). Subthreshold synaptic Ca^{2+} signalling in fine dendrites and spines of cerebellar Purkinje neurons. *Nature* 373, 155–158.

Eilers, J., Takechi, H., Finch, E. A., Augustine, G. J., and Konnerth, A. (1997). Local dendritic Ca^{2+} signaling induces cerebellar LTD. *Learn. Mem.* 3, 159–168.

Faas, G. C., Raghavachari, S., Lisman, J. E., and Mody, I. (2011). Calmodulin as a direct detector of Ca^{2+} signals. *Nat. Neurosci.* 14, 301–306.

Faas, G. C., Schwaller, B., Vergara, J. L., and Mody, I. (2007). Resolving the fast kinetics of cooperative binding: Ca^{2+} buffering by calretinin. *PLoS Biol.* 5, 2646–2660. doi: 10.1371/journal.pbio.0050311

Felmy, F., Neher, E., and Schneggenburger, R. (2003). Probing the intracellular calcium sensitivity of transmitter release during synaptic facilitation. *Neuron* 37, 801–811.

Fierro, L., and Llano, I. (1996). High endogenous calcium buffering in Purkinje cells from rat cerebellar slices. *J. Physiol.* 496, 617–625.

Gabso, M., Neher, E., and Spira, M. E. (1997). Low mobility of the Ca^{2+} buffers in axons of cultured Aplysia neurons. *Neuron* 18, 473–481.

Gamble, E., and Koch, C. (1987). The dynamics of free calcium in dendritic spines in response to repetitive synaptic input. *Science* 236, 1311–1315.

Grütter, M. G. (2000). Caspases: key players in programmed cell death. *Curr. Opin. Struct. Biol.* 10, 649–655.

Hackney, C. M., Mahendrasingam, S., Penn, A., and Fettiplace, R. (2005). The concentrations of calcium buffering proteins in mammalian cochlear hair cells. *J. Neurosci.* 25, 7867–7875.

Holthoff, K., Tsay, D., and Yuste, R. (2002). Calcium dynamics of spines depend on their dendritic location. *Neuron* 33, 425–437.

Hubbard, M. J., and McHugh, N. J. (1995). Calbindin28kDa and calbindin30kDa (calretinin) are substantially localised in the particulate fraction of rat brain. *FEBS Lett.* 374, 333–337.

Ikura, M. (1996). Calcium binding and conformational response in EF-hand proteins. *Trends Biochem. Sci.* 21, 14–17.

Ito, M. (2001). Cerebellar long-term depression: characterization, signal transduction, and functional roles. *Physiol. Rev.* 81, 1143–1195.

Jackson, M. B., and Redman, S. J. (2003). Calcium dynamics, buffering, and buffer saturation in the boutons of dentate granule-cell axons in the hilus. *J. Neurosci.* 23, 1612–1621.

Katz, B., and Miledi, R. (1968). The role of calcium in neuromuscular facilitation. *J. Physiol.* 195, 481–492.

Kim, S. A., Heinze, K. G., Waxham, M. N., and Schwille, P. (2004). Intracellular calmodulin availability accessed with two-photon cross-correlation. *Proc. Natl. Acad. Sci. U.S.A.* 101, 105–110.

Klaus, W., Grzesiek, S., Labhardt, A. M., Buchwald, P., Hunziker, W., Gross, M. D., and Kallick, D. A. (1999). NMR investigation and secondary structure of domains I and II of rat brain calbindin D28k (1–93). *Eur. J. Biochem.* 262, 933–938.

Kojetin, D. J., Venters, R. A., Kordys, D. R., Thompson, R. J., Kumar, R., and Cavanagh, J. (2006). Structure, binding interface and hydrophobic transitions of Ca^{2+}-loaded calbindin-D28K. *Nat. Struct. Mol. Biol.* 13, 641–647.

Kosaka, T., Kosaka, K., Nakayama, T., Hunziker, W., and Heizmann, C. W. (1993). Axons and axon terminals of cerebellar Purkinje cells and basket cells have higher levels of parvalbumin immunoreactivity than somata and dendrites: quantitative analysis by immunogold labeling. *Exp. Brain Res.* 93, 483–491.

Koster, H. P., Hartog, A., Van Os, C. H., and Bindels, R. J. (1995). Calbindin-D28K facilitates cytosolic calcium diffusion without interfering with calcium signaling. *Cell Calcium* 18, 187–196.

Kreiner, L., Christel, C. J., Benveniste, M., Schwaller, B., and Lee, A. (2010). Compensatory regulation of Cav2.1 Ca^{2+} channels in cerebellar Purkinje neurons lacking parvalbumin and calbindin D-28k. *J. Neurophysiol.* 103, 371–381.

Kreiner, L., and Lee, A. (2006). Endogenous and exogenous Ca^{2+} buffers differentially modulate Ca^{2+}-dependent inactivation of Cav2.1 Ca^{2+} channels. *J. Biol. Chem.* 281, 4691–4698.

Lambers, T. T., Mahieu, F., Oancea, E., Hoofd, L., De Lange, F., Mensenkamp, A. R., Voets, T., Nilius, B., Clapham, D. E., Hoenderop, J. G., and Bindels, R. J. (2006). Calbindin-D28k dynamically controls TRPV5-mediated Ca^{2+} transport. *Embo J.* 25, 2978–2988.

Leathers, V. L., Linse, S., Forsen, S., and Norman, A. W. (1990). Calbindin-D28k, a 1 alpha,25-dihydroxyvitamin D3-induced calcium-binding protein, binds five or six Ca^{2+} ions with high affinity. *J. Biol. Chem.* 265, 9838–9841.

Lee, A., Scheuer, T., and Catterall, W. A. (2000a). Ca^{2+}/calmodulin-dependent facilitation and inactivation of P/Q-type Ca^{2+} channels. *J. Neurosci.* 20, 6830–6838.

Lee, S-H., Schwaller, B., and Neher, E. (2000b). Kinetics of Ca^{2+} binding to parvalbumin in bovine chromaffin cells: implications for Ca^{2+} transients of neuronal dendrites. *J. Physiol.* 525, 419–432.

Lee, A., Wong, S. T., Gallagher, D., Li, B., Storm, D. R., Scheuer, T., and Catterall, W. A. (1999). Ca^{2+}/calmodulin binds to and modulates P/Q-type calcium channels. *Nature* 399, 155–159.

Lutz, W., Frank, E. M., Craig, T. A., Thompson, R., Venters, R. A., Kojetin, D., Cavanagh, J., and Kumar, R. (2003). Calbindin D28K interacts with Ran-binding protein M: identification of interacting domains by NMR spectroscopy. *Biochem. Biophys. Res. Commun.* 303, 1186–1192.

Maeda, H., Ellis-Davies, G. C., Ito, K., Miyashita, Y., and Kasai, H. (1999). Supralinear Ca^{2+} signaling by cooperative and mobile Ca^{2+} buffering in Purkinje neurons. *Neuron* 24, 989–1002.

Majewska, A., Brown, E., Ross, J., and Yuste, R. (2000). Mechanisms of calcium decay kinetics in hippocampal spines: role of spine calcium pumps and calcium diffusion through the spine neck in biochemical compartmentalization. *J. Neurosci.* 20, 1722–1734.

Markram, H., Roth, A., and Helmchen, F. (1998). Competitive calcium binding: implications for dendritic calcium signaling. *J. Comput. Neurosci.* 5, 331–348.

Meinrenken, C. J., Borst, J. G., and Sakmann, B. (2002). Calcium secretion coupling at calyx of held governed by nonuniform channel-vesicle topography. *J. Neurosci.* 22, 1648–1667.

Molinari, S., Battini, R., Ferrari, S., Pozzi, L., Killcross, A. S., Robbins, T. W., Jouvenceau, A., Billard, J. M., Dutar, P., Lamour, Y., Baker, W. A., Cox, H., and Emson, P. C. (1996). Deficits in memory and hippocampal long-term potentiation in mice with reduced calbindin D28K expression. *Proc. Natl. Acad. Sci. U.S.A.* 93, 8028–8033.

Morgan, D. W., Welton, A. F., Heick, A. E., and Christakos, S. (1986). Specific *in vitro* activation of Ca, Mg-ATPase by vitamin D-dependent rat renal calcium binding protein (calbindin D28K). *Biochem. Biophys. Res. Commun.* 138, 547–553.

Müller, W., and Connor, J. A. (1991). Dendritic spines as individual neuronal compartments for synaptic Ca^{2+} responses. *Nature* 354, 73–76.

Müller, A., Kukley, M., Stausberg, P., Beck, H., Müller, W., and Dietrich, D. (2005). Endogenous Ca^{2+} buffer concentration and Ca^{2+} microdomains in hippocampal neurons. *J. Neurosci.* 25, 558–565.

Nägerl, U. V., Novo, D., Mody, I., and Vergara, J. L. (2000). Binding kinetics of calbindin-D28k determined by flash photolysis of caged Ca^{2+}. *Biophys. J.* 79, 3009–3018.

Naraghi, M. (1997). T-jump study of calcium binding kinetics of calcium chelators. *Cell Calcium* 22, 255–268.

Naraghi, M., and Neher, E. (1997). Linearized buffered Ca^{2+} diffusion in microdomains and its implications for calculation of Ca^{2+} at

the mouth of a calcium channel. *J. Neurosci.* 17, 6961–6973.
Neher, E. (1998a). Usefulness and limitations of linear approximations to the understanding of Ca++ signals. *Cell Calcium* 24, 345–357.
Neher, E. (1998b). Vesicle pools and Ca^{2+} microdomains: new tools for understanding their roles in neurotransmitter release. *Neuron* 20, 389–399.
Neher, E. (2000). Calcium buffers in flash-light. *Biophys. J.* 79, 2783–2784.
Nemri, A., and Ghisovan, N. (2007). Dendritic spines: it takes two to make an impression. *J. Physiol.* 582, 15–16.
Noguchi, J., Matsuzaki, M., Ellis-Davies, G. C., and Kasai, H. (2005). Spine-neck geometry determines NMDA receptor-dependent Ca^{2+} signaling in dendrites. *Neuron* 46, 609–622.
Orduz, D., and Llano, I. (2007). Recurrent axon collaterals underlie facilitating synapses between cerebellar Purkinje cells. *Proc. Natl. Acad. Sci. U.S.A.* 104, 17831–17836.
Reisner, P. D., Christakos, S., and Vanaman, T. C. (1992). *In vitro* enzyme activation with calbindin-D28k, the vitamin D-dependent 28 kDa calcium binding protein. *FEBS Lett.* 297, 127–131.
Rozov, A., Burnashev, N., Sakmann, B., and Neher, E. (2001). Transmitter release modulation by intracellular Ca^{2+} buffers in facilitating and depressing nerve terminals of pyramidal cells in layer 2/3 of the rat neocortex indicates a target cell-specific difference in presynaptic calcium dynamics. *J. Physiol.* 531, 807–826.
Sabatini, B. L., Oertner, T. G., and Svoboda, K. (2002). The life cycle of Ca^{2+} ions in dendritic spines. *Neuron* 33, 439–452.
Schmidt, H., Arendt, O., and Eilers, J. (2011). Diffusion and extrusion shape standing calcium gradients during ongoing parallel fiber activity in dendrites of Purkinje neurons. *Cerebellum* doi: 10.1007/s12311-010-0246-x. [Epub ahead of print].
Schmidt, H., and Eilers, J. (2009). Spine neck geometry determines spino-dendritic cross-talk in the presence of mobile endogenous calcium binding proteins. *J. Comput. Neurosci.* 27, 229–243.
Schmidt, H., Kunerth, S., Wilms, C., Strotmann, R., and Eilers, J. (2007). Spino-dendritic cross-talk in rodent Purkinje neurons mediated by endogenous Ca^{2+}-binding proteins. *J. Physiol.* 581, 619–629.
Schmidt, H., Schwaller, B., and Eilers, J. (2005). Calbindin D28k targets myo-inositol monophosphatase in spines and dendrites of cerebellar Purkinje neurons. *Proc. Natl. Acad. Sci. U.S.A.* 102, 5850–5855.
Schmidt, H., Stiefel, K., Racay, P., Schwaller, B., and Eilers, J. (2003). Mutational analysis of dendritic Ca^{2+} kinetics in rodent Purkinje cells: role of parvalbumin and calbindin D28k. *J. Physiol.* 551, 13–32.
Schwaller, B. (2008). The continuing disappearance of "pure" Ca^{2+} buffers. *Cell. Mol. Life Sci.* 66, 275–300.
Schwaller, B. (2010). Cytosolic Ca^{2+} buffers. *Cold Spring Harb. Perspect. Biol.* 2, a004051.
Stevens, C. F. (2003). Neurotransmitter release at central synapses. *Neuron* 40, 381–388.
Svoboda, K., Tank, D. W., and Denk, W. (1996). Direct measurement of coupling between dendritic spines and shafts. *Science* 272, 716–719.
Tsujimoto, T., Jeromin, A., Saitoh, N., Roder, J. C., and Takahashi, T. (2002). Neuronal calcium sensor 1 and activity-dependent facilitation of P/Q-type calcium currents at presynaptic nerve terminals. *Science* 295, 2276–2279.
Vanbelle, C., Halgand, F., Cedervall, T., Thulin, E., Akerfeldt, K. S., Laprevote, O., and Linse, S. (2005). Deamidation and disulfide bridge formation in human calbindin D28k with effects on calcium binding. *Protein Sci.* 14, 968–979.
Vecellio, M., Schwaller, B., Meyer, M., Hunziker, W., and Celio, M. R. (2000). Alterations in Purkinje cell spines of calbindin D-28 k and parvalbumin knock-out mice. *Eur. J. Neurosci.* 12, 945–954.
Venters, R. A., Benson, L. M., Craig, T. A., Paul, K. H., Kordys, D. R., Thompson, R., Naylor, S., Kumar, R., and Cavanagh, J. (2003). The effects of Ca^{2+} binding on the conformation of calbindin D28K: a nuclear magnetic resonance and microelectrospray mass spectrometry study. *Anal. Biochem.* 317, 59–66.
Venyaminov, S. Y., Klimtchuk, E. S., Bajzer, Z., and Craig, T. A. (2004). Changes in structure and stability of calbindin-D(28K) upon calcium binding. *Anal. Biochem.* 334, 97–105.
Winsky, L., and Kuźnicki, J. (1995). Distribution of calretinin, calbindin D28k, and parvalbumin in subcellular fractions of rat cerebellum: effects of calcium. *J. Neurochem.* 65, 381–388.
Yamada, W. M., and Zucker, R. S. (1992). Time course of transmitter release calculated from simulations of a calcium diffusion model. *Biophys. J.* 61, 671–682.
Yan, N., and Shi, Y. (2005). Mechanisms of apoptosis through structural biology. *Annu. Rev. Cell Dev. Biol.* 21, 35–56.
Yuan, J., and Yankner, B. A. (2000). Apoptosis in the nervous system. *Nature* 407, 802–809.
Zador, A., Koch, C., and Brown, T. H. (1990). Biophysical model of a Hebbian synapse. *Proc. Natl. Acad. Sci. U.S.A.* 87, 6718–6722.
Zucker, R. S., and Regehr, W. G. (2002). Short-term synaptic plasticity. *Annu. Rev. Physiol.* 64, 355–405.
Zucker, R. S., and Stockbridge, N. (1983). Presynaptic calcium diffusion and the time courses of transmitter release and synaptic facilitation at the squid giant synapse. *J. Neurosci.* 3, 1263–1269.

Conflict of Interest Statement: The author declares that the research was conducted in the absence of any commercial or financial relationships that could be construed as a potential conflict of interest.

Received: 12 January 2012; paper pending published: 30 January 2012; accepted: 14 February 2012; published online: 15 March 2012.
Citation: Schmidt H (2012) Three functional facets of calbindin D-28k. Front. Mol. Neurosci. 5:25. doi: 10.3389/fnmol.2012.00025

frontiers in
MOLECULAR NEUROSCIENCE

ORIGINAL RESEARCH ARTICLE
published: 10 July 2012
doi: 10.3389/fnmol.2012.00078

Control of neuronal excitability by calcium binding proteins: a new mathematical model for striatal fast-spiking interneurons

D. P. Bischop*, D. Orduz, L. Lambot, S. N. Schiffmann and D. Gall

Laboratoire de Neurophysiologie, Faculté de Médecine, Université Libre de Bruxelles, Bruxelles, Belgium

Edited by:
Beat Schwaller, University of Fribourg, Switzerland

Reviewed by:
Guido C. Faas, University of California, USA
Hartmut Schmidt, University of Leipzig, Germany

****Correspondence:***
D. P. Bischop, Laboratoire de Neurophysiologie (CP601), Faculté de Médecine, Université Libre de Bruxelles, Route de Lennik 808, B-1070 Bruxelles, Belgium.
e-mail: dobischo@ulb.ac.be

Calcium binding proteins, such as parvalbumin (PV), are abundantly expressed in distinctive patterns in the central nervous system but their physiological function remains poorly understood. Notably, at the level of the striatum, where PV is only expressed in the fast-spiking (FS) interneurons. FS interneurons form an inhibitory network modulating the output of the striatum by synchronizing medium-sized spiny neurons (MSN). So far the existing conductance-based computational models for FS neurons did not allow the study of the coupling between PV concentration and electrical activity. In the present paper, we propose a new mathematical model for the striatal FS interneurons that includes apamin-sensitive small conductance Ca^{2+}-dependent K^+ channels (SK) and the presence of a calcium buffer. Our results show that a variation in the concentration of PV can modulate substantially the intrinsic excitability of the FS interneurons and therefore may be involved in the information processing at the striatal level.

Keywords: calcium dynamics, parvalbumin, striatal fast-spiking interneurons, excitability, mathematical model

INTRODUCTION

Calcium regulates many cellular processes, including hormone secretion, neurotransmitter release, ionic channel permeability, and gene transcription. The cytosolic calcium proteins are classified in trigger or buffer proteins (Schwaller, 2009). Trigger proteins, such as calmodulin, change their conformation upon binding Ca^{2+}, as opposed to buffer proteins (e.g., calretinin, calbindin, or parvalbumin) which bind Ca^{2+} as its concentration increases within a cell and are thought to mainly act as passive modulators of the cytosolic calcium level. Nevertheless, it has been suggested that calbindin also acts as a Ca^{2+} sensor (Schmidt et al., 2005; Lambers et al., 2006). Moreover at the neuronal level, several results have shown that calcium buffers play a key functional role in the control of the neuronal firing. More precisely, it has been shown that the concentration of calretinin, acting as a fast calcium buffer, controls the excitability of cerebellar granule cells, through the activation of high-conductance voltage- and Ca^{2+}-activated K^+ (BK) channels (Gall et al., 2003, 2005; Bearzatto et al., 2006). Furthermore changes in the buffer concentration can dramatically affect the electrical discharge pattern of cerebellar granule cells, hence allowing transitions between regular firing and different types of bursting (Roussel et al., 2006).

PV is a member of the EF-hand calcium binding proteins family and it has two mixed Ca^{2+}/Mg^{2+} binding sites. PV binds Mg^{2+} with medium affinity ($K_{D,Mg} \sim 5$–$500\ \mu$M) and Ca^{2+} with high affinity ($K_{D,Ca} \sim 5$–100 nM; Schwaller, 2009). Under basal $[Ca^{2+}]_i$ (100 nM), the majority of PV's binding sites (>80%) are occupied by Mg^{2+}. The binding of Ca^{2+} is determined by the slow Mg^{2+} off-rate (Schwaller, 2009). For this reason, PV is considered as a slow buffer similar to the synthetic chelator EGTA. However recent studies show that at high concentration and in certain physiological conditions, PV might also act as a fast buffer, similarly to the synthetic chelator BAPTA (Franconville et al., 2011; Eggermann and Jonas, 2012). In the striatum, PV is selectively expressed in the population of FS interneurons. Striatal FS interneurons exert a strong inhibitory control over MSN, the principal neurons of the striatum. FS interneurons can fire regular trains of action potentials (AP) at frequencies ranging from 20 to 200 Hz, with little spike-frequency adaptation. They can also exhibit stuttering firing patterns consisting of brief bursts of AP separated by quiescent periods, which are characterized by subthreshold membrane potential oscillations (Tepper et al., 2010). The FS interneuron firing patterns result from the expression of a specific set of voltage-gated channels (Zhang and McBain, 1995; Martina and Jonas, 1997; Erisir et al., 1999). For example, voltage-gated potassium channels of Kv3 type are responsible for the fast repolarization and short duration of AP (Rudy and McBain, 2001). We have strong indications for the presence of apamin-sensitive small conductance (SK) Ca^{2+}-dependent K^+ channels, that are known to be coupled to voltage-gated Ca^{2+} channels (Stocker, 2004). SK channels are voltage independent and are activated at free Ca^{2+} concentrations in the range of 300–700 nM (Hirschberg et al., 1998; Xia et al., 1998). In rat striatal fast-spiking interneurons, blockade of BK channels by iberiotoxin has no effect on action potential duration (Sciamanna and Wilson, 2011), hence SK channels are strong candidates for the observed spike-frequency adaptation in FS neurons (Maingret et al., 2008). The presence of this calcium-activated ionic conductance could provide a way for parvalbumin to control the discharge pattern of the FSI. In fact, in cerebellar granule cells, it has been shown that calretinin, a fast calcium buffer, modulates the excitability of cerebellar granule cells through the activation of BK channels (Gall et al., 2003).

In this study, we propose a new conductance-based computational model for striatal FS interneurons that includes the influence of PV and the presence of SK channels providing coupling between excitability and calcium dynamics during the spike generation. This model allows us to investigate the effect of variations in the concentration of PV on striatal FS interneurons activity. We show that excitability of FS neurons depends on PV concentration and that this regulatory effect occurs in a similar way for fast and slow buffers.

MATERIALS AND METHODS

FS NEURON COMPUTATIONAL MODEL

Our computational model is adapted from the conductance-based model of Erisir (Erisir et al., 1999) of a FS neocortical interneuron. The ionic currents of the Erisir model consist of a fast transient Na^+ current I_{Na}, a fast delayed rectifier potassium current of Kv3.1 type I_{Kv3}, a slow delayed rectifier potassium current of Kv1.3 type I_{Kv1} and a passive leak current I_{leak}. We add to this model a HVA calcium current I_{Ca} (Stocker, 2004) and a SK potassium current, I_{SK}. Charge conservation governs the membrane potential dynamics through the following equation:

$$C_m \frac{dV}{dt} = -I_{Na} - I_{Kv1} - I_{Kv3} - I_{Ca} - I_{SK} - I_{leak} + I_{app} \quad (1)$$

where C_m, V are the membrane capacitance and potential of the FS neuron, I_{app} is an external applied current. The ionic currents are given by:

$$I_{Na} = g_{Na} m_\infty^3 h\,(V - V_{Na}) \quad (2)$$
$$I_{Kv1} = g_{Kv1} n_1^4\,(V - V_K) \quad (3)$$
$$I_{Kv3} = g_{Kv3} n_3^2\,(V - V_K) \quad (4)$$
$$I_{SK} = g_{SK} k^2\,(V - V_K) \quad (5)$$
$$I_{Ca} = g_{Ca} a_\infty^2\,(V - V_{Ca}) \quad (6)$$
$$I_{leak} = g_{leak}\,(V - V_{leak}) \quad (7)$$

where m and h are respectively the activation and inactivation gating variables of the I_{Na} current, n_1, n_3, k, a are respectively the activation variables of I_{Kv1}, I_{Kv3}, I_{SK}, I_{Ca} currents. The kinetic of the m and a activation variables are considered fast compared to the other gating variables and are set to their steady-state value $m = m_\infty(V)$, $a = a_\infty(V)$. The membrane capacitance was set to 30 pF, the leak conductance g_{leak} to 2.5 nS and the leak reversal potential to −68 mV, to match the known experimental membrane capacitance (25–30 pF), membrane resistance (400 MΩ), and resting membrane potential (−70 mV). The other reversal potentials are $V_{Na} = 74$ mV, $V_K = -90$ mV, $V_{Ca} = 80$ mV, and the maximal ionic conductances are $g_{Na} = 700$ nS, $g_{Kv1} = 2$ nS, $g_{Kv3} = 300$ nS, $g_{Ca} = 30$ nS, $g_{SK} = 2$ nS. The dynamic of the other gating variables (excepted k) are governed by:

$$\frac{dx}{dt} = \alpha_x(V)(1 - x) - \beta_x(V)x \quad (8)$$
$$x_\infty = \frac{\alpha_x}{\alpha_x + \beta_x} \quad (9)$$
$$\tau_x = \frac{1}{\alpha_x + \beta_x} \quad (10)$$

where $x = h, n_1, n_3$. The kinetics of the α_x, β_x are exactly as published in Mancilla et al. (2007). The kinetics of the a variable was adapted from Roussel et al. (2006) and follows:

$$a_\infty = \frac{1}{1 + exp\left(\frac{-6-V}{7.775}\right)} \quad (11)$$
$$\tau_a = \frac{1}{\frac{8.0}{1+exp(-0.072(V-5))} + \frac{0.1(V+8.9)}{exp(0.2(V+8.9))-1}} \quad (12)$$

The k activation variable for SK channels is Ca^{2+} dependent and voltage independent. The equation for its time evolution was taken from Goldberg et al. (2009):

$$\frac{dk}{dt} = \frac{\left(k_\infty\left(\left[Ca^{2+}\right]_i\right) - k\right)}{\tau_k} \quad (13)$$
$$k_\infty = \frac{\left[\mathrm{Ca}^{2+}\right]_i}{K_{SK} + \left[\mathrm{Ca}^{2+}\right]_i} \quad (14)$$
$$\tau_k = \frac{1}{K_{SK} + \left[\mathrm{Ca}^{2+}\right]_i} \quad (15)$$

where $K_{SK} = k_{off,sk}/k_{on,sk}$. The values of $k_{on,sk} = 0.4\,\mu\mathrm{M}^{-1}\,\mathrm{ms}^{-1}$ (Ca^{2+}-binding rate) and $k_{off,sk} = 0.2\,\mathrm{ms}^{-1}$ (from Goldberg et al., 2009). In presence of PV, the coupling of the calcium dynamic is done via the following equations:

$$\frac{d\left[\mathrm{Ca}^{2+}\right]_i}{dt} = -\frac{I_{Ca}}{2FAd} - \gamma\left(\left[\mathrm{Ca}^{2+}\right]_i - \left[\mathrm{Ca}^{2+}\right]_{rest}\right) - \frac{d[PVCa]_i}{dt} \quad (16)$$
$$\frac{d[PVCa]_i}{dt} = k_{on,ca}\left[\mathrm{Ca}^{2+}\right]_i[PV]_i - k_{off,ca}[PVCa]_i \quad (17)$$
$$\frac{d[PVMg]_i}{dt} = k_{on,mg}\left[\mathrm{Mg}^{2+}\right]_i[PV]_i - k_{off,mg}[PVMg]_i \quad (18)$$

where $[Ca^{2+}]_i$ and $[PV]_i$ represent respectively the free intracellular Ca^{2+} concentration and the concentration of free PV. $[PVCa]_i$ and $[PVMg]_i$ are the concentration of PV bound to Ca^{2+} and Mg^{2+}. The total PV concentration $[PV]_T = [PV]_i + [PVCa]_i + [PVMg]_i$. We assume that $[Mg^{2+}]_i$ is constant as in (Lee et al., 2000). $[Mg^{2+}]_i$ was set to 500 μM in agreement with the values found within neurons (300–600 μM; Li-Smerin et al., 2001). The association and dissociation constant of PV with Ca^{2+} and Mg^{2+} are $k_{on,ca} = 0.1\,\mu\mathrm{M}^{-1}\,\mathrm{ms}^{-1}$, $k_{off,ca} = 0.001\,\mathrm{ms}^{-1}$, and $k_{on,mg} = 0.0008\,\mu\mathrm{M}^{-1}\,\mathrm{ms}^{-1}$, $k_{off,mg} = 0.025\,\mathrm{ms}^{-1}$ (Lee et al., 2000). We consider Ca^{2+} fluxes across a shell of thickness $d = 0.2\,\mu$m under cell surface (area $A = 3000\,\mu\mathrm{m}^2$). The inward flux is $-I_{Ca}/2FAd$ (F is the Faraday constant). The term $\gamma([Ca^{2+}]_i - [Ca^{2+}]_{rest})$ is the clearance mechanism associated with the Ca^{2+} fluxes across the plasma membrane or storage organelles ($\gamma = 1\,\mathrm{ms}^{-1}$, $[Ca^{2+}]_{rest} = 0.07\,\mu$M). In presence of the slow or fast buffer, the coupling of the calcium dynamic is done

via the following equations:

$$\frac{d\left[\mathrm{Ca}^{2+}\right]_i}{dt} = -\frac{I_{Ca}}{2FAd} - \gamma\left(\left[\mathrm{Ca}^{2+}\right]_i - \left[\mathrm{Ca}^{2+}\right]_{rest}\right) - \frac{d[BCa]_i}{dt} \quad (19)$$

$$\frac{d[BCa]_i}{dt} = k_{on}\left[Ca^{2+}\right]_i[B]_i - k_{off}[BCa]_i \quad (20)$$

where $[B]_i$, $[BCa]_i$ are the concentration of free and bound buffer (slow or fast). The total buffer concentration $[B]_T = [B]_i + [BCa]_i$. The list of model parameters are shown in **Table 1**. Numerical simulations traces are obtained after an initial integration of 4 s. The equations of the model are numerically solved using a fourth-order Runge–Kutta integration method (Press et al., 1992). The bifurcation diagram was built with the software XPPAUT 6.10 (Free Software Foundation Inc., Cambridge, USA).

RESULTS

EXPERIMENTAL RELEVANCE OF FS NEURON COMPUTATIONAL MODEL

We use a computational model, based on experimental data, to investigate how Ca^{2+} buffering by PV affects striatal FS interneuron excitability. Striatal FS neurons selectively express the slow calcium buffer PV (Kawaguchi et al., 1995). We have strong evidence that they also possess apamin-sensitive small conductance SK channels. Therefore we propose a FS interneuron model, adapted from Erisir et al. (1999), that includes the presence of SK channels and of PV calcium binding proteins. Since PV possesses mixed Ca^{2+}/Mg^{2+} binding sites, we take into account in our model the competition between Ca^{2+} and Mg^{2+} for PV binding sites (see Materials and Methods). Until recently, parvalbumin was considered as a slow calcium buffer similar to the synthetic chelator EGTA (Schwaller, 2009) but new evidence shows that under certain physiological conditions, at high concentration, PV may act as a fast calcium buffer similar to the synthetic chelator BAPTA (Franconville et al., 2011; Eggermann and Jonas, 2012). Therefore we have included three buffering conditions in our study: PV with its mixed Ca^{2+}/Mg^{2+} binding sites, a slow buffer similar to EGTA, and a fast buffer similar to the metal-free form PV. For these three buffering conditions, we have studied the effect of the calcium buffer on the excitability of FS neurons, for different buffer concentrations. In our model, the slow calcium buffer has a $K_D = 0.1\ \mu$M and a $k_{on} = 0.01\ \mu\mathrm{M}^{-1}\ \mathrm{ms}^{-1}$ similar to EGTA (Schwaller et al., 2002; Schwaller, 2009). The fast calcium buffer has a $K_D = 0.01\ \mu$M and a $k_{on} = 0.1\ \mu\mathrm{M}^{-1}\ \mathrm{ms}^{-1}$ similar to those of metal-free form PV (Eberhard and Erne, 1994; Lee et al., 2000).

Figure 1A shows a bifurcation diagram of our FS model, with PV as calcium buffer, where the bifurcation parameter is the applied current (I_{app}). Our model generates stable oscillations in the physiological range. A supercritical Hopf bifurcation (HB) at $I_{app} = 44$ pA gives rise to a small window of periodic solutions that lose stability at $I_{app} = 45$ pA. For $I_{app} > 44$ pA there is a branch of unstable periodic solutions that ends at a saddle-node of limit cycle (SNLC), for $I_{app} = 68$ pA. For $I_{app} = I_{SNLC}$, a branch of stable

Table 1 | Model parameters.

Definition	Parameters	Values	Reference
Sodium conductance	g_{Na}	700 nS	
Sodium reversal potential	V_{Na}	74 mV	Jolivet et al. (2004)
$Kv1$ potassium conductance	g_{Kv1}	2 nS	
$Kv3$ potassium conductance	g_{Kv3}	300 nS	
SK potassium conductance	g_{SK}	2 nS	
Potassium reversal potential	V_K	−90 mV	Jolivet et al. (2004)
SK affinity for calcium	K_{SK}	0.5 μM	Goldberg et al. (2009)
Calcium conductance	g_{Ca}	30 nS	
Calcium reversal potential	V_{Ca}	80 mV	Roussel et al. (2006)
Membrane capacitance	C_m	30 pF	
Leak conductance	g_{leak}	2.5 nS	
Leak reversal potential	V_{leak}	−68 mV	
Ca^{2+} extrusion rate	γ	1 ms^{-1}	
Shell thickness	d	0.2 μm	
Mg^{2+} concentration	$[Mg^{2+}]_i$	500 μM	Li-Smerin et al. (2001)
Resting Ca^{2+} concentration	$[Ca^{2+}]_{rest}$	0.07 μM	
Cell surface	A	3000 $\mu\mathrm{m}^2$	
Ca^{2+} binding rate to PV	$k_{on,ca}$	0.1 $\mu\mathrm{M}^{-1}\ \mathrm{ms}^{-1}$	Lee et al. (2000)
PV affinity for Ca^{2+}	$K_{D,ca}$	0.01 μM	Eberhard and Erne (1994)
Mg^{2+} unbinding rate from PV	$k_{off,mg}$	0.025 ms^{-1}	Lee et al. (2000)
PV affinity for Mg^{2+}	$k_{D,mg}$	31 μM	Eberhard and Erne (1994)
Ca^{2+} binding rate (fast buffer)	k_{on}	0.1 $\mu\mathrm{M}^{-1}\ \mathrm{ms}^{-1}$	Lee et al. (2000)
Affinity for Ca^{2+} (fast buffer)	K_D	0.01 μM	Eberhard and Erne (1994)
Ca^{2+} binding (slow buffer)	k_{on}	0.01 $\mu\mathrm{M}^{-1}\ \mathrm{ms}^{-1}$	Schwaller et al. (2002)
Affinity for Ca^{2+} (slow buffer)	K_D	0.1 μM	Schwaller et al. (2002)

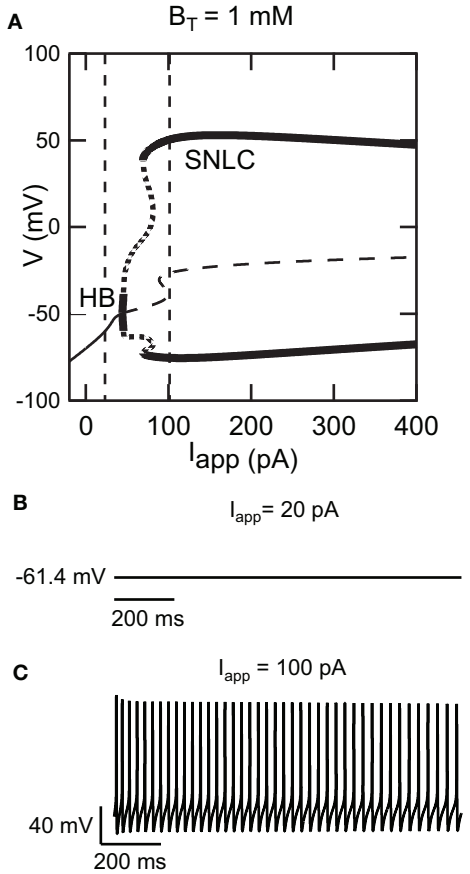

FIGURE 1 | Dynamical behavior of the FS interneuron computational model. (A) Bifurcation diagram of our fast-spiking neuron model ($B_T = 1000\,\mu$M) representing voltage in function of applied current I_{app}. As applied current increases from 0 pA, a branch of stable steady-states (thin solid curve) ends at a Hopf bifurcation (HB) point ($I_{app} \approx 40$ pA), giving rise to a branch of unstable periodic orbits (thick dotted line) and a branch of unstable steady-states at (thin dashed line) $I_{app} \approx 40$ pA. As the applied current increases further a branch of stable periodic solutions emerges from a saddle-node on a limit cycle (SNLC). Stable periodic solutions exist for $I_{app} > 69$ pA. **(B)** Time series showing a stable steady-state solution at $I_{app} = 20$ pA and **(C)** stable periodic solution at $I_{app} = 100$ pA [the corresponding current values are displayed as dashed vertical lines in the bifurcation diagram shown in **(A)**].

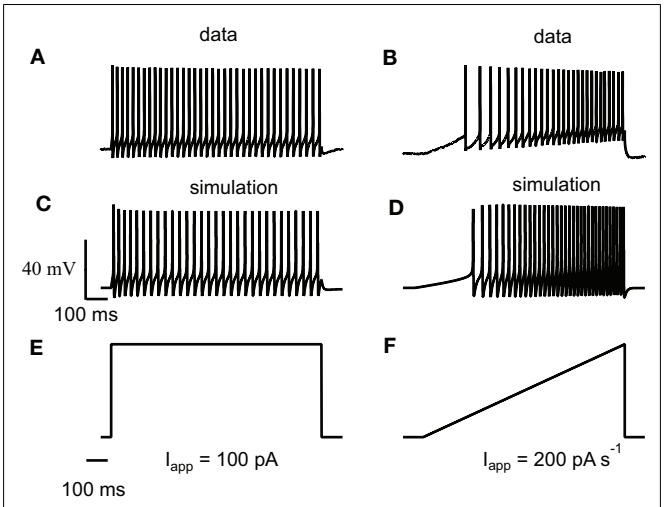

FIGURE 2 | Experimental relevance of the FS neuron computational model. (A) Train of action potentials evoked in a striatal FS interneuron in response to a step and a ramp current injection during whole-cell recordings. During 1 s step of 100 pA the average spiking frequency is 36 Hz and the firing exhibits adaptation. **(B)** Whole-cell recording during a 1-s ramp of 200 pA s^{-1}. Our model is adapted from Erisir et al. (1999) to include Ca^{2+}, SK currents, and an endogenous calcium buffer. **(C,D)** Numerical simulations obtained with similar current protocols. The average spiking frequency in **(C)** is 31 Hz. The step and ramp current protocols used for the above experiment and simulation are shown in **(E,F)**. Experimental and simulated voltage traces exhibit similar firing patterns for both protocols demonstrating the quantitative aspect of the proposed computational model.

periodic solutions emerges. From that point the amplitude of the oscillations decreases as the applied current, I_{app}, increases and the repetitive firing disappears at a supercritical Hopf bifurcation (not shown). A stable steady-state time series at $I_{app} = 20$ pA and a stable periodic solution obtained at $I_{app} = 100$ pA are shown in **Figures 1B,C**. Both the slow (similar to EGTA) and the fast (similar to the metal-free form PV) show a similar bifurcation diagram (data not shown). From a dynamical point of view, neurons are classified in two broad classes: class 1 and class 2 excitability (Izhikevich, 2007). Neurons in class 1 can fire at an arbitrary low frequency, depending on the strength of the applied current, while for neurons of class 2, the onset of oscillations starts at a non-zero frequency. Class 1 neurons can encode continuously the strength of an incoming stimulus in their firing frequency, while class 2 neurons will sense whether the strength of the stimulus is above a threshold. It has been shown experimentally that FS neurons share properties of class 2 neurons (Tateno et al., 2004). Accordingly, the electrical behavior of our FS model displays the typical dynamical behavior of class 2 neurons as the periodic firing originates from a Hopf bifurcation. In addition, typical experimental voltage traces obtained during whole-cell recording and the corresponding results of the numerical simulations are shown in **Figure 2** for two different protocols: 1 s step current of 100 pA and 1 s ramp current injection of 200 pA s^{-1}. In **Figure 2A** the FS interneuron fires at a typical frequency of 36 Hz whereas the result of the simulation gives a frequency of 31 Hz for the same protocol (1 s step current of 100 pA). Experimental and simulated voltage traces exhibit similar firing patterns for both protocols demonstrating the quantitative aspect of the proposed theoretical model.

SUMMATION OF $[Ca^{2+}]_i$ TRANSIENTS DURING TRAINS OF ACTION POTENTIAL

During a train of AP, $[Ca^{2+}]_i$ increases due to the summation of $[Ca^{2+}]_i$ transients. For trains of AP of sufficiently long duration, $[Ca^{2+}]_i$ will reach a steady-state plateau level and fluctuate between a lower and upper level. At steady-state, calcium influx and clearance mechanisms compensate (Helmchen et al., 1996; Neher, 1998). During train of action potentials, evoked by 5 s depolarizing step current of 100 pA, we have investigated the time course to reach the steady-state using three buffering conditions. In

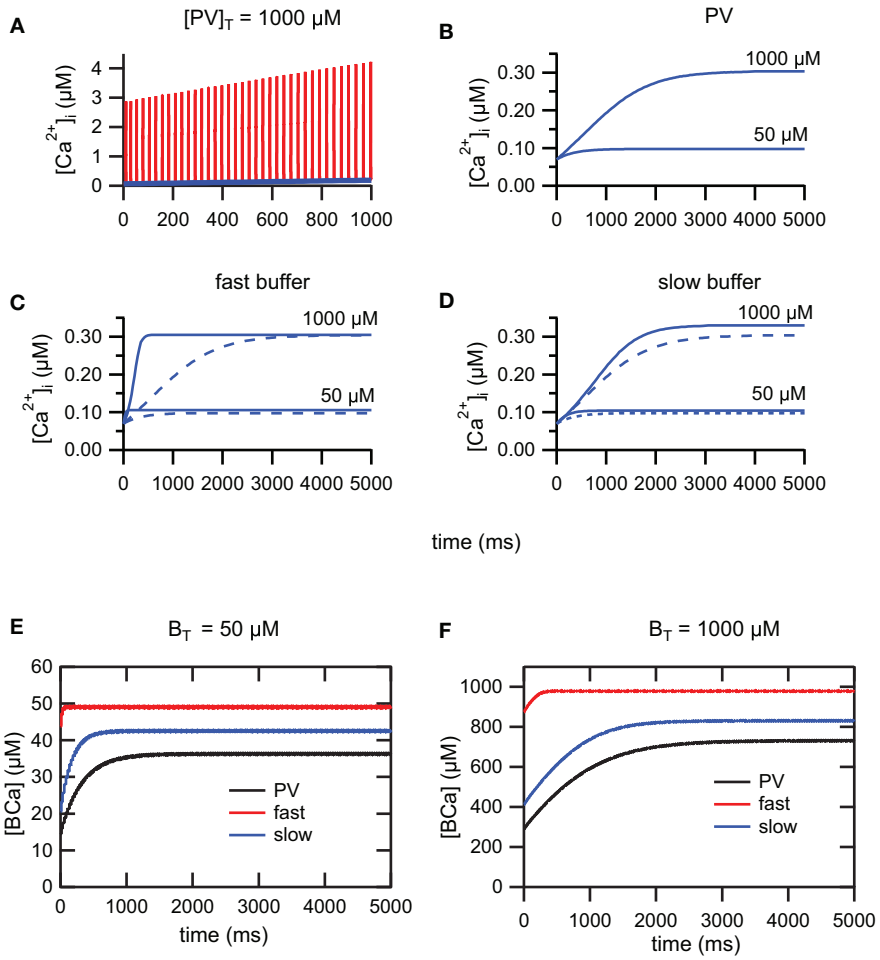

FIGURE 3 | Summation of $[Ca^{2+}]_i$ transients during train of action potentials. (A) Summation (red) and lower envelope (blue) of $[Ca^{2+}]_i$ transients for the PV system ($I_{app} = 100$ pA). **(B)** The time course of the lower envelope in the presence of PV. The time to reach the steady-state is delayed and the plateau level increases as the PV concentration increases. $[Ca^{2+}]_i$ scales in **(A,B)** are different. **(C)** Due to saturation of the fast buffer, the time to reach the steady-state is faster for the fast buffer system (solid curve) compared to the PV system (dashed curve). Once PV is saturated with Ca^{2+}, the PV system follows the time course of the fast buffer system. **(D)** For trains of action potentials of short duration, the time course of the PV system (dashed curve) follows the time course of the slow buffer system (solid curve). **(E,F)** Buffer occupancy vs. time. As for the Ca^{2+} transients, the buffer occupancy oscillates between lower and upper envelopes (not visible at this scale). The PV and slow buffer system will partially saturate after a few hundred milliseconds, whereas the fast buffer system is already saturated from early on. **(E)** $B_T = 50\,\mu$M and **(F)** $B_T = 1000\,\mu$M.

the first condition, we have simulated PV with mixed Ca^{2+}/Mg^{2+} binding sites. In the second and third conditions, we have simulated respectively a slow buffer similar to EGTA and a fast buffer similar to the metal-free form of PV. **Figure 3A** shows the summation and lower envelope of $[Ca^{2+}]_i$ transients, in the presence of PV, during the first 1000 ms of a train of action potentials ($I_{app} = 100$ pA). The time course of the lower envelopes of $[Ca^{2+}]_i$ transients in the presence of PV is shown in **Figure 3B**. As previously demonstrated (Lee et al., 2000), the time to reach the steady-state is delayed and the plateau level increases as the PV concentration increases. A similar behavior is observed for the slow and fast buffer systems (**Figures 3C,D**). For the fast buffer the time to reach the steady-state is shorter than the time for the slow buffer (**Figure 3C**). Moreover, for trains of AP of short duration, the envelope of Ca^{2+} transients follows a similar time course both for PV and the slow buffer (**Figure 3D**). Whereas for trains of AP of longer duration, once PV is saturated with Ca^{2+}, the lower envelope of Ca^{2+} transients follows a similar time course both for PV and the fast buffer (**Figure 3C**). In **Figures 3E,F**, the plots of the buffer occupancy show that PV and the slow buffer partially saturate after a few hundred of milliseconds, whereas the fast buffer system is already saturated at this time. The lower envelope of $[Ca^{2+}]_i$ transients determines the Ca^{2+} available for the activation of SK channels during the interspike intervals and therefore the modulation of the firing frequency. In the following section, we study the effect of different calcium buffer concentrations on the excitability of FS neurons. Using 5 s step current of 100 pA, we only account for Ca^{2+} transients occurring at the steady-state plateau level during the 4th and 5th second of the train. The duration of the step current was chosen to allow Ca^{2+} transients and

spike-frequency adaptation, occurring during trains of AP, to reach their steady-state.

REGULATION OF FS EXCITABILITY BY FAST AND SLOW CALCIUM BUFFERS

We have investigated the effect of different calcium buffer concentrations on FS excitability for PV, the slow and fast buffer systems. Previous studies have shown that the somatic PV concentration ranges from 0.8 to 70.6 μM in hippocampal dentate gyrus basket cells and from 55 to 1788 μM in cerebellar basket cells (Eggermann and Jonas, 2012). In the simulations, we have used a 5-s long depolarizing current of 100 pA and buffer concentration ranging between 0 and 1500 μM. For PV, we observe a decrease in excitability as the total buffer concentration PV_T increases from 50 to 1000 μM (**Figure 4A**). As the buffer concentration increases from 0 to 1500 μM, the mean frequency spiking drops from 39 to 30 Hz (**Figure 4B**). We have observed a similar behavior for the slow and fast buffer (**Figure 4B**). This demonstrates that changes in the level of parvalbumin concentration changes the firing rate of the FS interneurons. This regulatory effect occurs in a similar way for the fast and slow buffers.

To understand the change in firing frequencies, we have investigated the effect of the buffer concentration on the activation of the SK current. We have considered the amplitude of the I_{SK} current, the amplitude, and decay time of the Ca^{2+} transients. To avoid the effect of summation of Ca^{2+} transients, only those transients occurring at the steady-state plateau level were taken into consideration. For low PV concentrations, the decay time of the calcium transients is slower than the decay time at high PV concentration. Moreover, at low PV concentration, the amplitude of Ca^{2+} transients are higher than the amplitude at high PV concentration (**Figure 5A**). Between two AP, the intracellular calcium concentration drops to 0.1 μM (low buffer concentration, $PV_T = 50\ \mu$M) and 0.3 μM (high buffer concentration, $PV_T = 1000\ \mu$M). This value of 0.3 μM is sufficient to activate a significative fraction of the SK channels that have a K_D for calcium of 300–700 nM (Hirschberg et al., 1998; Xia et al., 1998). The amplitude of the I_{SK} current is relatively constant between two AP at low PV concentration (15 pA) while it slowly increases from 19 to 35 pA at high PV concentration (**Figure 5B**). This also increases the duration of the AHP and therefore reduces the firing frequency. **Figures 5C–F** show the results for the slow and fast buffers. As for PV, the residual calcium level between two action potentials is higher at high buffer concentration. It will activate more SK channels, increase the duration of the AHP, and decrease the firing frequency. The time course of the other ionic currents were similar when the buffer concentration was increased in the PV, slow, and fast buffering conditions (not shown).

DISCUSSION

In this paper, we present a new conductance-based single compartment computational model for striatal FS interneurons. Our model is adapted from the model of Erisir et al. (1999) for FS neocortical interneurons. It differs from the former model (and its modifications by Golomb et al., 2007; Ermentrout and Wechselberger, 2009) in that it includes the presence of a calcium buffer protein similar to PV. The dynamic of the calcium buffer is included in the FS model of Erisir et al. (1999) by the addition of a HVA calcium current and a SK current. Our model differs also from other FS models (Jolivet et al., 2004; Lewis and Rinzel, 2004; Mancilla et al., 2007) in that it preserves the dynamic of neurons belonging to class 2 excitability, as it is the case experimentally for FS neurons (Tateno et al., 2004).

PV is considered as a slow buffer similar to EGTA, but recent results show that it can behave like BAPTA, under physiological condition, at high concentration (Franconville et al., 2011; Eggermann and Jonas, 2012). Therefore, we have investigated the effect of PV and the effect of a calcium buffer in both cases, slow and fast binding kinetics. Our results show that calcium buffers, through modulation of the level of residual $[Ca^{2+}]_i$ and its coupling to SK channels during a train of action potentials, control the excitability of FS interneurons. The SK current activation depends on the level of residual $[Ca^{2+}]_i$ between AP. The residual Ca^{2+} concentration increases with buffer concentration, as the calcium buffer can act as a source of calcium ions during that period. Therefore the SK current between AP increases with buffer concentration leading to lower firing frequencies due to prolonged AHP. Our results show that this provides a very robust mechanism for controlling the excitability of FS interneurons. In our simulation, we have used high concentration of PV, such as 1000 μM. Such a high value of buffer concentration is exceptional and so far it has only been found in cerebellar basket cells (Eggermann and Jonas, 2012). Nevertheless our main conclusion does not rely on this specific value of PV concentration. As it is shown in **Figure 4B**, the firing

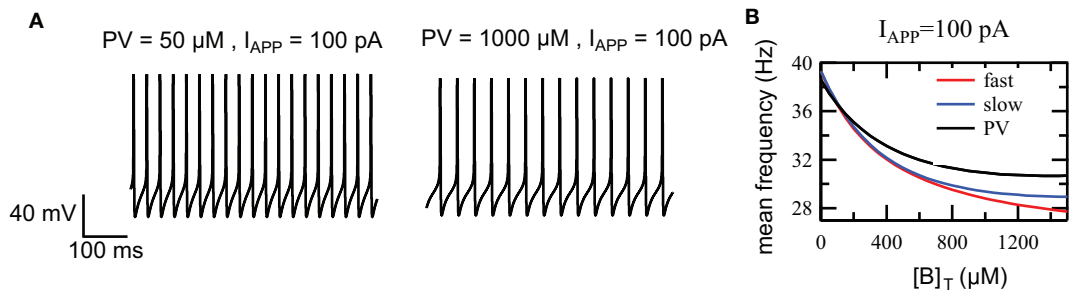

FIGURE 4 | Effect of the PV concentration on the intrinsic excitability in the FS cell model. (A) The response of the FS cell model to injection of 100 pA depolarizing current for a buffer concentration $PV_T = 50\ \mu$M and $PV_T = 1000\ \mu$M. **(B)** Firing frequency vs. buffer concentration. The mean firing frequency decreases as the buffer concentration increases (PV: black, slow buffer: blue, fast buffer: red).

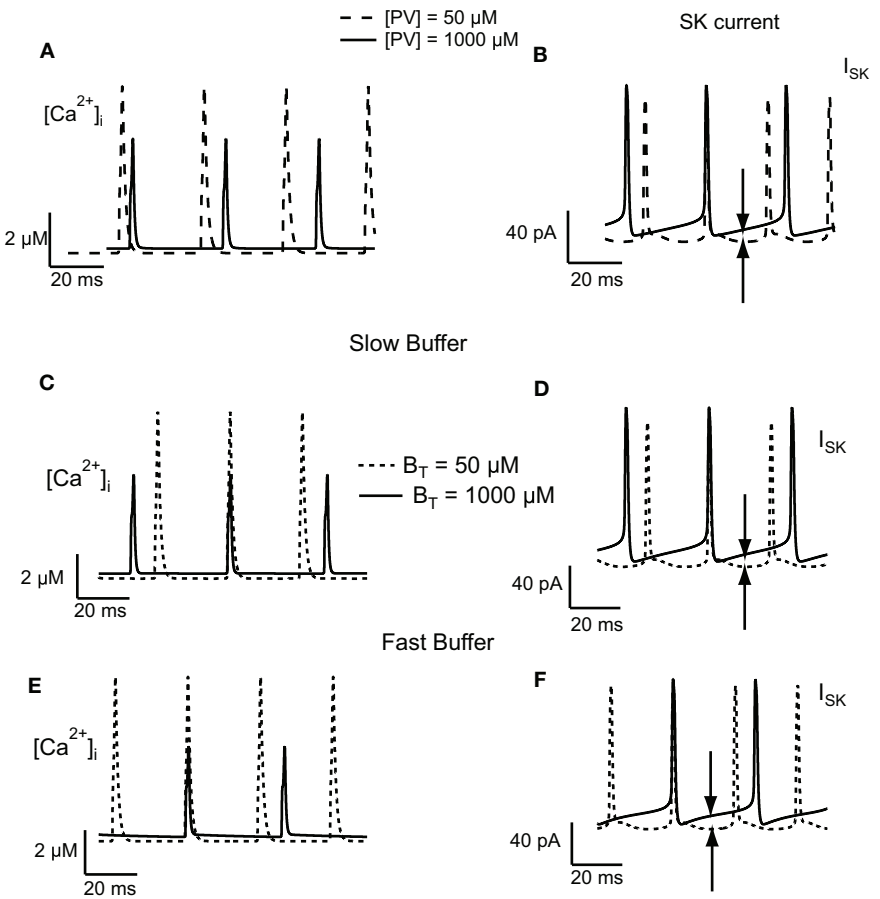

FIGURE 5 | Effect of buffer concentration on the activation of the SK current in the FS cell model. Calcium transients obtained in response to injection of 100 pA depolarizing current for PV **(A)**, slow **(C)**, and fast **(E)** buffers. The calcium transients have a slower decay and have a higher peak value at low buffer concentration. Between two action potentials, at high buffer concentration, the residual calcium level is higher than the level at low buffer concentration. **(B,D,F)** This results in a greater activation of SK channels (indicated by the arrows in the figure), increasing the duration of the AHP, and therefore decreasing the firing frequency.

frequency decreases as the buffer concentration increases from 0 to 1500 μM. This means that a similar decrease in the frequency of firing will be observed if the buffer concentration is raised from 10 to 50 μM, in the PV concentration range found in hippocampal basket cells (Eggermann and Jonas, 2012). Moreover, the regulation by the calcium buffer concentration appears to produce similar effects for PV, fast, and slow calcium buffers. In addition, it appears not to depend on the type of Ca^{2+}-activated K^+ conductance providing coupling between excitability and Ca^{2+} dynamics, as the regulation appears to be same in our FS interneuron model and in cerebellar granule cells where this effect is mediated by BK channels (Gall et al., 2003).

During a train of AP, $[Ca^{2+}]_i$ increases due to the summation of Ca^{2+} transients. For sufficiently long trains of AP, $[Ca^{2+}]_i$ will reach a steady-state plateau and fluctuate between a lower and an upper level. During the accumulation phase of Ca^{2+}, we have observed a faster initial decay and higher amplitude of the Ca^{2+} transients for the slow buffer (data not shown; Markram et al., 1998). The differences in the Ca^{2+} transients between the slow and fast buffers attenuate at the steady-state plateau level where PV, slow, and fast buffers are already saturated. In agreement with previous published work (Helmchen et al., 1996; Lee et al., 2000) our model predicts a build-up in Ca^{2+} and different degrees of buffer occupancy in the three conditions (PV, slow, and fast buffers; **Figures 3E,F**). In our model, the summation of Ca^{2+} transients is responsible for the spike-frequency adaptation through the progressive activation of SK channels. Due to supralinear summation, the fast buffer saturates rapidly whereas PV and the slow buffer lead to a slow build-up in Ca^{2+}. This implies that: for trains of AP of short duration, the neuron containing a fast buffer will display spike-frequency adaptation, whereas neurons containing PV or a slow buffer will display little or no spike-frequency adaptation. Those effects will be more pronounced at a higher buffer concentration than at a lower buffer concentration (**Figures 3B–D**).

The purpose of our model was to propose a basic mechanism for the regulation of excitability of FS neurons by calcium buffering. Despite the use of a single compartment model with a limited set of conductances and currents, the simplicity of our model and the use of buffers with different kinetics validates

our simulations to other neuronal types. Indeed, the proposed mechanism will remain valid providing that the mechanisms of excitability remain the same, as in FS neurons, and that the conductance of the Ca^{2+}-activated K^+ channels is sufficient to obtain a strong coupling between excitability and Ca^{2+} dynamics during the spike generation. A possible improvement in our model would be to explore the competitive binding between different calcium binding partners by considering Ca^{2+} diffusion, immobile, and mobile buffers (Markram et al., 1998). Parvalbumin is considered as a slow mobile buffer and SK channels form a complex with calmodulin and act as high affinity, fast Ca^{2+} binding partners (Stocker, 2004). Moreover, it is has been shown that in acutely dissociated CA1 hippocampal pyramidal neurons, SK channels are tightly coupled with L-type calcium channels, within a distance of 50–150 nm (Marrion and Tavalin, 1998). This spatial coupling of SK channels and Ca^{2+} sources promotes the formation of nano or microdomains that can modify the efficiency of calcium buffering depending on the mobility and affinity of the calcium buffers. If the Ca^{2+} sensor is within ∼20–50 nm of the Ca^{2+} source, a high affinity calcium buffer like BAPTA and not the slow EGTA will be able to interfere with the Ca^{2+} signaling. While if the Ca^{2+} sensor and Ca^{2+} source are located in microdomains (between 50 nm and a few hundred nanometers) both BAPTA and EGTA will interfere with the Ca^{2+} signaling (Neher, 1998; Fakler and Adelman, 2008).

In addition to their already documented role in Ca^{2+} homeostasis, Ca^{2+}-binding proteins appear to play an active role in modulating neuronal intrinsic excitability. Although, information storage is usually believed to be mediated by long-term modifications in the strength of synaptic transmission, activity-dependent changes in the neuronal intrinsic excitability also occur, causing forms of non-synaptic plasticity (Aizenman and Linden, 2000; Armano et al., 2000). Changes in the calcium buffering capacity might have an effect on this regulation. This could be the result of changes in the localization or in the level of expression of Ca^{2+} binding proteins. The mathematical model we present here provides a valuable tool for the investigation of the functional role of parvalbumin in the regulation of the activity of the striatal FS interneurons. This study paves the way for further theoretical work to assess the impact of calcium buffering on the activity of the striatal FS interneurons network.

ACKNOWLEDGMENTS

Laurie Lambot was supported by a doctoral fellowship from Fonds pour la formation à la Recherche dans l'Industrie et dans l'Agriculture, FRIA, Belgium. David Orduz was supported by a postdoctoral fellowship from Fonds de la Recherche Scientifique, FRS-FNRS, Belgium. This study was also supported by Fondation Médicale Reine Elisabeth (FMRE-Belgium), FRS–FNRS (Belgium), research funds from ULB and Action de Recherche Concertée from the CFWB. The authors would like to thank Dr. Frédéric Bollet-Quivogne for his helpful comments on this manuscript.

REFERENCES

Aizenman, C. D., and Linden, D. (2000). Rapid, synaptically driven increase in the intrinsic excitability of cerebellar deep nuclear neurons. *Nat. Neurosci.* 3, 109–111.

Armano, S., Rossi, P., Taglietti, V., and D'Angelo, E. (2000). Long term potentiation of intrinsic excitability at the mossy fiber-granule cell synapse of rat cerebellum. *J. Neurosci.* 20, 5208–5216.

Bearzatto, B., Servais, L., Roussel, C., Gall, D., Baba-Aïssa, F., Schurmans, S., de Kerchove d'Exaerde, A., Cheron, G., and Schiffmann, S. N. (2006). Targeted calretinin expression in granule cells of calretinin-null mice restores normal cerebellar functions. *FASEB J.* 20, 380–382.

Eberhard, M., and Erne, P. (1994). Calcium and magnesium binding to rat parvalbumin. *Eur. J. Biochem.* 222, 21–26.

Eggermann, E., and Jonas, P. (2012). How the 'slow' Ca(2+) buffer parvalbumin affects transmitter release in nanodomain-coupling regimes. *Nat. Neurosci.* 15, 20–22.

Erisir, A., Lau, D., Rudy, B., and Leonard, C. S. (1999). Function of specific K(+) channels in sustained high-frequency firing of fast-spiking neocortical interneurons. *J. Neurophysiol.* 82, 2476–2489.

Ermentrout, B., and Wechselberger, M. (2009). Canards, clusters, and synchronization in a weakly coupled interneuron model. *SIAM J. Appl. Dyn. Syst.* 8, 253–278.

Fakler, B., and Adelman, J. P. (2008). Control of K(Ca) channels by calcium nano/microdomains. *Neuron* 59, 873–881.

Franconville, R., Revet, G., Astorga, G., Schwaller, B., and Llano, I. (2011). Somatic calcium level reports integrated spiking activity of cerebellar interneurons in vitro and in vivo. *J. Neurophysiol.* 106, 1793–1805.

Gall, D., Roussel, C., Nieus, T., Cheron, G., Servais, L., D'Angelo, E., and Schiffmann, S. N. (2005). Role of calcium binding proteins in the control of cerebellar granule cell neuronal excitability: experimental and modeling studies. *Prog. Brain Res.* 148, 321–328.

Gall, D., Roussel, C., Susa, I., D'Angelo, E., Rossi, P., Bearzatto, B., Galas, M. C., Blum, D., Schurmans, S., and Schiffmann, S. N. (2003). Altered neuronal excitability in cerebellar granule cells of mice lacking calretinin. *J. Neurosci.* 23, 9320–9327.

Goldberg, J. A., Teagarden, M. A., Foehring, R. C., and Wilson, C. J. (2009). Nonequilibrium calcium dynamics regulate the autonomous firing pattern of rat striatal cholinergic interneurons. *J. Neurosci.* 29, 8396–8407.

Golomb, D., Donner, K., Shacham, L., Shlosberg, D., Amitai, Y., and Hansel, D. (2007). Mechanisms of firing patterns in fast-spiking cortical interneurons. *PLoS Comput. Biol.* 3, e156. doi:10.1371/journal.pcbi.0030156

Helmchen, F., Imoto, K., and Sakmann, B. (1996). Ca2+ buffering and action potential-evoked Ca2+ signaling in dendrites of pyramidal neurons. *Biophys. J.* 70, 1069–1081.

Hirschberg, B., Maylie, J., Adelman, J. P., and Marrion, N. V. (1998). Gating of recombinant small-conductance ca-activated K+ channels by calcium. *J. Gen. Physiol.* 111, 565–581.

Izhikevich, E. (2007). *Dynamical Systems in Neuroscience: The Geometry of Excitability and Bursting.* Cambridge, MA: MIT Press.

Jolivet, R., Lewis, T. J., and Gerstner, W. (2004). Generalized integrate-and-fire models of neuronal activity approximate spike trains of a detailed model to a high degree of accuracy. *J. Neurophysiol.* 92, 959–976.

Kawaguchi, Y., Wilson, C. J., Augood, S. J., and Emson, P. C. (1995). Striatal interneurones: chemical, physiological and morphological characterization. *Trends Neurosci.* 18, 527–535.

Lambers, T. T., Mahieu, F., Oancea, E., Hoofd, L., de Lange, F., Mensenkamp, A. R., Voets, T., Nilius, B., Clapham, D. E., Hoenderop, J. G., and Bindels, R. J. (2006). Calbindin-d28k dynamically controls trpv5-mediated Ca2+ transport. *EMBO J.* 25, 2978–2988.

Lee, S. H., Schwaller, B., and Neher, E. (2000). Kinetics of Ca2+ binding to parvalbumin in bovine chromaffin cells: implications for [Ca2+] transients of neuronal dendrites. *J. Physiol. (Lond.)* 525(Pt 2), 419–432.

Lewis, T. J., and Rinzel, J. (2004). Dendritic effects in networks of electrically coupled fast-spiking interneurons. *Neurocomputing* 58–60, 145–150.

Li-Smerin, Y., Levitan, E. S., and Johnson, J. W. (2001). Free intracellular Mg(2+) concentration and inhibition of NMDA responses in cultured rat neurons. *J. Physiol. (Lond.)* 533(Pt 3), 729–743.

Maingret, F., Coste, B., Hao, J., Giamarchi, A., Allen, D., Crest, M., Litchfield, D. W., Adelman, J. P., and Delmas, P. (2008). Neurotransmitter modulation of small-conductance Ca2+-activated K+ channels by regulation of Ca2+ gating. *Neuron* 59, 439–449.

Mancilla, J. G., Lewis, T. J., Pinto, D. J., Rinzel, J., and Connors, B. W. (2007). Synchronization of electrically coupled pairs of inhibitory interneurons in neocortex. *J. Neurosci.* 27, 2058–2073.

Markram, H., Roth, A., and Helmchen, F. (1998). Competitive calcium binding: implications for dendritic calcium signaling. *J. Comput. Neurosci.* 5, 331–348.

Marrion, N. V., and Tavalin, S. J. (1998). Selective activation of Ca2+-activated K+ channels by colocalized Ca2+ channels in hippocampal neurons. *Nature* 395, 900–905.

Martina, M., and Jonas, P. (1997). Functional differences in Na+ channel gating between fast-spiking interneurones and principal neurones of rat hippocampus. *J. Physiol. (Lond.)* 505(Pt 3), 593–603.

Neher, E. (1998). Usefulness and limitations of linear approximations to the understanding of Ca++ signals. *Cell Calcium* 24, 345–357.

Press, W. H., Flannery, B. P., Teukolsky, S. A., and Vetterling, W. T. (1992). *Numerical Recipes in C*, 2nd Edn. Cambridge: Cambridge University Press.

Roussel, C., Erneux, T., Schiffmann, S. N., and Gall, D. (2006). Modulation of neuronal excitability by intracellular calcium buffering: from spiking to bursting. *Cell Calcium* 39, 455–466.

Rudy, B., and McBain, C. J. (2001). Kv3 channels: voltage-gated K+ channels designed for high-frequency repetitive firing. *Trends Neurosci.* 24, 517–526.

Schmidt, H., Schwaller, B., and Eilers, J. (2005). Calbindin d28k targets myo-inositol monophosphatase in spines and dendrites of cerebellar Purkinje neurons. *Proc. Natl. Acad. Sci. U.S.A.* 102, 5850–5855.

Schwaller, B. (2009). The continuing disappearance of "pure" Ca2+ buffers. *Cell. Mol. Life Sci.* 66, 275–300.

Schwaller, B., Meyer, M., and Schiffmann, S. (2002). 'New' functions for 'old' proteins: the role of the calcium-binding proteins calbindin d-28k, calretinin and parvalbumin, in cerebellar physiology studies with knockout mice. *Cerebellum* 1, 241–258.

Sciamanna, G., and Wilson, C. J. (2011). The ionic mechanism of gamma resonance in rat striatal fast-spiking neurons. *J. Neurophysiol.* 106, 2936–2949.

Stocker, M. (2004). Ca(2+)-activated K+ channels: molecular determinants and function of the sk family. *Nat. Rev. Neurosci.* 5, 758–770.

Tateno, T., Harsch, A., and Robinson, H. P. C. (2004). Threshold firing frequency-current relationships of neurons in rat somatosensory cortex: type 1 and type 2 dynamics. *J. Neurophysiol.* 92, 2283–2294.

Tepper, J. M., Tecuapetla, F., Koós, T., and Ibáñez-Sandoval, O. (2010). Heterogeneity and diversity of striatal gabaergic interneurons. *Front. Neuroanat.* 4:150. doi:10.3389/fnana.2010.00150

Xia, X. M., Fakler, B., Rivard, A., Wayman, G., Johnson-Pais, T., Keen, J. E., Ishii, T., Hirschberg, B., Bond, C. T., Lutsenko, S., Maylie, J., and Adelman, J. P. (1998). Mechanism of calcium gating in small-conductance calcium-activated potassium channels. *Nature* 395, 503–507.

Zhang, L., and McBain, C. J. (1995). Potassium conductances underlying repolarization and after-hyperpolarization in rat CA1 hippocampal interneurones. *J. Physiol. (Lond.)* 488(Pt 3), 661–672.

Conflict of Interest Statement: The authors declare that the research was conducted in the absence of any commercial or financial relationships that could be construed as a potential conflict of interest.

Received: 09 March 2012; accepted: 18 June 2012; published online: 11 July 2012.

*Citation: Bischop DP, Orduz D, Lambot L, Schiffmann SN and Gall D (2012) Control of neuronal excitability by calcium binding proteins: a new mathematical model for striatal fast-spiking interneurons. Front. Mol. Neurosci. **5**:78. doi: 10.3389/fnmol.2012.00078*

frontiers in
MOLECULAR NEUROSCIENCE

ORIGINAL RESEARCH ARTICLE
published: 23 April 2012
doi: 10.3389/fnmol.2012.00056

Absence of the calcium-binding protein calretinin, not of calbindin D-28k, causes a permanent impairment of murine adult hippocampal neurogenesis

Kiran Todkar, Alessandra L. Scotti and Beat Schwaller*

Unit of Anatomy, Department of Medicine, University of Fribourg, Fribourg, Switzerland

Edited by:
Michael R. Kreutz, Leibniz-Institute for Neurobiology, Germany

Reviewed by:
Miou Zhou, University of California Los Angeles, CA, USA
Jose R. Naranjo, Centro Nacional de Biotecnología, Spain
Cordula Nitsch, University of Basel, Switzerland

***Correspondence:**
Beat Schwaller, Unit of Anatomy, Department of Medicine, University of Fribourg, Route Albert-Gockel 1, CH-1700 Fribourg, Switzerland.
e-mail: beat.schwaller@unifr.ch

Calretinin (CR) and calbindin D-28k (CB) are cytosolic EF-hand Ca^{2+}-binding proteins and function as Ca^{2+} buffers affecting the spatiotemporal aspects of Ca^{2+} transients and possibly also as Ca^{2+} sensors modulating signaling cascades. In the adult hippocampal circuitry, CR and CB are expressed in specific principal neurons and subsets of interneurons. In addition, CR is transiently expressed within the neurogenic dentate gyrus (DG) niche. CR and CB expression during adult neurogenesis mark critical transition stages, onset of differentiation for CR, and the switch to adult-like connectivity for CB. Absence of either protein during these stages in null-mutant mice may have functional consequences and contribute to some aspects of the identified phenotypes. We report the impact of CR- and CB-deficiency on the proliferation and differentiation of progenitor cells within the subgranular zone (SGZ) neurogenic niche of the DG. Effects were evaluated (1) two and four weeks postnatally, during the transition period of the proliferative matrix to the adult state, and (2) in adult animals (3 months) to trace possible permanent changes in adult neurogenesis. The absence of CB from differentiated DG granule cells has no retrograde effect on the proliferative activity of progenitor cells, nor affects survival or migration/differentiation of newborn neurons in the adult DG including the SGZ. On the contrary, lack of CR from immature early postmitotic granule cells causes an early loss in proliferative capacity of the SGZ that is maintained into adult age, when it has a further impact on the migration/survival of newborn granule cells. The transient CR expression at the onset of adult neurogenesis differentiation may thus have two functions: (1) to serve as a self-maintenance signal for the pool of cells at the same stage of neurogenesis contributing to their survival/differentiation, and (2) it may contribute to retrograde signaling required for maintenance of the progenitor pool.

Keywords: calcium-binding, adult neurogenesis, dentate gyrus, calretinin, calbindin, calcium buffer, calcium sensor, subgranular zone

INTRODUCTION

Adult neurogenesis is the process of generating functional neurons from adult neuronal precursors. It requires the regulated, adaptive maintenance of a neurogenic proliferative matrix beyond prenatal and perinatal development into adult life (Altman and Bayer, 1990a). In the mammalian CNS this is accomplished in the subventricular zone and the subgranular zone (SGZ). The SGZ is located in the dentate gyrus (DG) of the hippocampus, along the lower border of the granule cell layer (GCL). Within the SGZ new excitatory granule neurons are born to migrate and synaptically integrate within the adjacent principal neuron layer of the DG (Kempermann, 2011; Ming and Song, 2011). The pool of proliferating cells in the DG neurogenic niche is heterogeneous, consisting of few slowly dividing putative stem cells and numerous generations of progenitors with different and changing cell cycle rates, which eventually develop into postmitotic immature neurons. Putative stem cells characteristically express glial fibrillary acidic protein (GFAP), nestin, and brain lipid-binding protein (BLBP), while the progenitor pool can be distinguished by the expression of Tbr2, polysialylated neural cell adhesion molecule (PSA-NCAM) and doublecortin (DCX). Intermediate transitional stages are consistently present, characterized by proliferating cells typically expressing both nestin and DCX (Brown et al., 2003; Ming and Song, 2011; von Bohlen Und Halbach, 2011). Before cell cycle exit, progenitors realign their processes in a vertical direction and leave the SGZ to migrate a short distance into the lower granular layer at the border of the SGZ. The critical phase of cell cycle exit correlates with the onset of transient expression of the Ca^{2+}-binding protein calretinin (CR) (Ming and Song, 2011; von Bohlen Und Halbach, 2011).

Abbreviations: BLBP, brain lipid-binding protein; BrdU, bromodeoxyuridine; CB, calbindin D-28k; CR, calretinin; DAPI, 4′,6′-diamidino-2-phenylindole; DCX, doublecortin; DG, dentate gyrus; GABA, gamma amino butyric acid; GCL, granule cell layer; GFAP, glial fibrillary acidic protein; IHC, immunohistochemistry; LTP, long-term potentiation; ML, molecular layer; PCNA, proliferating cell nuclear antigen; PSA-NCAM, polysialylated neural cell adhesion molecule; ROI, region of interest; SDS, sodium dodecyl sulfate; SGZ, subgranular zone; TCF-4, T-cell-specific transcription factor 4; WT, wild type.

Put on a timeline, most of the dividing progenitors labeled by a bromodeoxyuridine (BrdU) pulse will become CR-positive immature neurons within a week from BrdU injection. CR expression continues on average for an additional 2–3 weeks, but the percentage of BrdU and CR-positive cells then rapidly decreases (Brandt et al., 2003). Differentiating immature neurons are largely influenced by depolarizing gamma amino butyric acid (GABA) currents during the second week from birth (Ge et al., 2006): they rapidly grow axons toward the CA3 target region, ramify and grow dendrites toward the molecular layer (ML). By the end of the second week, immature granule cells receive synaptic glutamatergic input from perforant path terminals and release glutamate onto CA3 pyramidal cells (Faulkner et al., 2008; Ge et al., 2008). Synaptic targeting gradually continues and is refined over the next two weeks. The final step of synaptic integration consists in the targeting by basket and axo-axonic GABA-ergic synapses at about the end of the fourth week (Esposito et al., 2005). By this time most granule cells express the Ca^{2+}-binding protein calbindin D-28k (CB) (Kempermann et al., 1997; Brandt et al., 2003), considered as a marker of their differentiated state (Ming and Song, 2011; von Bohlen Und Halbach, 2011). Both the proliferation and the differentiation stages are orchestrated by manifold interwoven signals aiming to maintain homeostasis and thus to preserve function of adult neurogenesis and related behavior (Kempermann, 2011; Ming and Song, 2011). It is interesting to note that the way immature neurons convey information from the entorhinal cortex to the CA3 region is qualitatively different from that of mature granule cells. Undifferentiated young neurons are more excitable and more prone to spread information to both the contralateral and distant ipsilateral DG, because they lack a strong inhibitory input and are densely connected to the hilar mossy cells commissural associational system (Henze and Buzsaki, 2007; Deng et al., 2009; Mongiat et al., 2009). In addition young granule cells are preferentially activated by specific stimuli and appear to strongly inhibit mature granule cells on their turn (Ge et al., 2008; Ming and Song, 2011; Toni and Sultan, 2011). Thus, mature and immature granule cells may represent two parallel information highways to the same target with different functions (Aimone et al., 2011; Ming and Song, 2011). There is accumulating evidence that, at a circuitry level, perforant path long-term potentiation (LTP) primarily relies on young adult born granule cells, suggesting that adult neurogenesis endows the DG with the potential for plasticity that this region requires to accomplish tasks like the continuous encoding of new memories and the discrimination between new and familiar information throughout life (Treves et al., 2008; Aimone et al., 2011; Ming and Song, 2011).

CR and CB belong to the large family of cytosolic EF-hand Ca^{2+}-binding proteins, which bind Ca^{2+} ions with high affinity. They are well-known to function as Ca^{2+} buffers influencing the spatiotemporal aspects of Ca^{2+} transients within the cytosol (Schwaller, 2010). Recent evidence hints toward an additional/alternative role for CB and CR as Ca^{2+} sensors, capable of influencing signaling cascades in response to intracellular Ca^{2+} transients (Schwaller, 2009). Recent studies in mice lacking CB and CR by gene targeting confirm previous reports, indicating that both proteins are critical for many physiological properties (excitability, efficacy of synaptic release, resistance to hypoxia/ischemia) of the neuron expressing them and their absence may disrupt network function in some brain regions eventually affecting behavior (Schiffmann et al., 1999; Cheron et al., 2004; Schwaller et al., 2004; Farre-Castany et al., 2007; Stadler et al., 2010).

Evidence on the impact of CB or CR loss on hippocampal and, in particular, DG function is poor. In CB-deficient mice, hippocampal functional reserve appears curtailed: the normal asymptomatic age-dependent decline in DG metabolism, as estimated by rCBV, is significantly accelerated and is accompanied by a deficit in hippocampus-dependent learning in the active place avoidance task (Moreno et al., 2011). In addition, CB with its fast Ca^{2+}-binding properties is pivotal for mature granule cell function within the hippocampal system as reported before (for details, see Schwaller, 2010). In CR-deficient mice, LTP is selectively impaired in the DG, but not the CA1 region. The disturbed DG synaptic plasticity is attributed to the absence of CR from the local hilar mossy cells resulting in changes in excitability of the DG network. Contrarily to what was reported for CB-deficient mice, the deficit at the circuitry level in $CR^{-/-}$ mice does not seem to affect hippocampal-dependent spatial learning in the Morris water maze (Schurmans et al., 1997; Gurden et al., 1998). CB and CR are normally expressed in many different neuronal types within the hippocampal circuitry including subsets of interneurons and the observed deficit at the phenotype level may therefore depend on which neurons are affected the most and how their "malfunction" may act additive or synergistic. CR and CB expression during the process of adult neurogenesis mark critical transition stages, i.e., onset of differentiation for CR and the shift to adult-like connectivity for CB. The absence of the respective Ca^{2+} sensor/buffer at these stages may well have functional consequences and contribute to the reported phenotypes. In this study, we investigated whether the constitutive absence of either CR or CB would have any consequences on the balance between proliferation and differentiation within the SGZ neurogenic niche of the DG. We decided to examine the different genotypes (I) at young age (P14 and P28), during the important transition period of the proliferative matrix into the adult state, and (II) in adult animals (12–14 weeks of age) to trace probable permanent changes.

MATERIALS AND METHODS

ANIMALS

Thirty CR-deficient ($CR^{-/-}$) mice (Schurmans et al., 1997) and thirty CB-deficient ($CB^{-/-}$) mice (Airaksinen et al., 1997) backcrossed to C57BL/6J for 10 generations and thus considered as congenic to C57BL/6J were used for the experiments. C57BL/6J wild type (WT) animals ($n = 30$) were used as control. Animals were bred and housed in a SPF facility under adequate temperature (23°C) and humidity (60%) control with a 12 h/12 h light/dark cycle (light onset at 7 a.m.) and provided with free access to water and food. Animals were sacrificed at 2, 4, and 14 weeks of age under deep anesthesia with 0.1% Eutha 77 in physiological saline (Essex Animal Health, Friesoythe, Germany). Cervical dislocation and fresh dissection of the brain was used for biochemistry experiments ($n = 8$ per genotype); transcardial perfusion fixation with buffered paraformaldehyde for morphology

($n = 22$ per genotype). All experiments were performed with permission of the local animal care committee and according to the present Swiss law and the EU Directive (86/609/EEC) and Appendix A of the Council of Europe Convention ETS123, EU decree 2001–486 Decree 214/97.

SUBSTANCE ADMINISTRATION

The thymidine analogue BrdU was administered intraperitoneally to mice to label proliferating cells. BrdU is taken up by cells undergoing DNA synthesis and can be visualized *post-hoc* by immunohistochemistry (IHC) techniques. The BrdU solution for injection was prepared in sterile saline at 20 mg/ml and the dose injected was of 2 mg/10 g mouse for the proliferation assay and of 1 mg/10 g mouse for the differentiation assay, respectively.

Proliferation in the DG stem cell niche was estimated in 2 weeks old mice ($n = 6$ per genotype) by sacrificing animals 24 h after a single dose BrdU injection. Long-term survival and differentiation of dividing cells in the niche was estimated in adult 12 weeks old mice ($n = 5$ per genotype). These mice were injected once a day for three consecutive days and sacrificed for analysis 2 weeks after the last BrdU injection.

BIOCHEMISTRY (WESTERN BLOT ANALYSIS)

Five animals per group were used for the analysis at 2 weeks of age and three per group were sacrificed at 4 weeks of age. The whole hippocampus was dissected out of the fresh brain in ice-cold 0.9% NaCl and stored at −75°C to prevent protein degradation until further processing. Tissue samples were lysed with 250 µl of RIPA buffer (Plumpe et al., 2006), homogenized and the protein concentration was measured with protein DC assay (Bio-Rad Laboratories, Inc., USA). The whole-cell extract was used for Western blotting. Samples were prepared by denaturing the protein lysates in Laemmli buffer and loaded on sodium dodecyl sulphate (SDS)-polyacrylamide gels (12%) for separation. Proteins of interest had molecular weights in the range of 29 kDa–40 kDa (CR: 30 kDa; CB: 28 kDa; proliferating cell nuclear antigen (PCNA): 36 kDa; DCX: 40 kDa); 10–15 µg protein extracts were loaded on 1 mm thick gels. After transfer to a nitrocellulose membrane (Bio-Rad), a Ponceau Red staining was performed and documented (BIOCAPT software) to test for uniform loading and transfer of protein samples. After destaining, the membranes were incubated first in blocking buffer (Odissey, LI-COR GmbH, Germany) and then overnight with the primary antibody diluted 1:1000 in the same buffer. The following antibodies were used: mouse anti PCNA (Chemicon); goat anti DCX C-18 (Santa Cruz Biotechnology); rabbit anti CR 7696 and rabbit anti CB 38a (both Swant).

The appropriate secondary antibody was selected depending on the emission wavelength (IRDye 680, IRDye 800; Odissey) and the source of the primary antibody. Secondary antibodies were all diluted 1:5000. The Odyssey image analyzer was used to scan images at different intensities. Densitometric analysis was performed with the GeneTools software (Syngene, CA, UK). The intensity of a specific protein band was normalized to the intensity of the Ponceau Red staining of the same lane. The mean optical density ratio value for the WT samples was set as 100% and those of $CR^{-/-}$ and $CB^{-/-}$ mice were normalized to the WT values. All statistical analyzes were performed with student's *T*-test, two samples, using the Welch correction for unequal variances whenever necessary (Prism, Graphpad). The level of significance was assumed to be $p < 0.05$.

IMMUNOHISTOCHEMISTRY

Animals perfused at 2 weeks of age were 10 per genotype; those perfused at 4 weeks of age were 4 per genotype and those sacrificed at 14 weeks of age were 8 per genotype (numbers include the mice used for BrdU injections). After transcardial perfusion fixation, the brains were dissected out of the skull and postfixed with gentle shaking in the same fixative solution (4% paraformaldehyde in 0.1 M phosphate buffer, pH 7.3) for 24 h at 4°C. They were then transferred to a 0.1 M Tris-buffered saline solution containing 18% sucrose and 0.01% Na-azide for cryoprotection and were kept at 4°C until they sank to the bottom of the vial. Serial coronal sections, 40 µm thick, were cut with a freezing microtome (Reichert-Jung, Nussloch, Germany) and collected in six wells plates at a 240 µm interval (i.e., each section within a well is 240 µm apart from the previous/next section). The primary antibodies used and their dilutions are as follows: mouse anti PCNA 1:500 (Chemicon); mouse anti BrdU 1:100 (Dakocytomation); mouse anti T-cell-specific transcription factor 4 (TCF-4) 1:50 (Abnova); goat anti DCX C-18 1:250 (Santa Cruz Biotechnology); rabbit anti CR 1:1000 and rabbit anti CB 1:2500 (both Swant). Pretreatments differed from antibody to antibody. In general, sections were permeabilized with Triton X-100 (0.1–0.3% in phosphate buffered saline for 1–2 h) to facilitate penetration of the reagents. PCNA and TCF-4 immunolabelings required antigen retrieval pretreatment with 0.01 M citric buffer. This treatment was performed at 120°C in a steamer for the PCNA labeling and at 80°C in a dry oven for the TCF-4 labeling. The antigen retrieval step for the DCX labeling was carried out in 0.3% hydrogen peroxide in phosphate buffered saline for 30 min at room temperature. To improve the binding of the anti BrdU antibody a 30 min treatment with 2 M HCl, in a 37°C water bath, was performed in order to partially denaturate DNA (Brown et al., 2003). Antibodies were diluted either in 2% horse serum or 10% bovine serum and incubated overnight in the cold room (4°C) with gentle shaking. For single labeling and visualization with the diaminobenzidine dye, we used biotinylated secondary antibodies and the avidin-biotin peroxidase technique (ABC kit, Rectolab SA). A subset of those sections labeled for nuclear antigens (BrdU and PCNA) were counterstained with the hematoxylin-eosin stain. Sections were dehydrated in increasing ethanol concentrations and xylene and then coverslipped with Entellan. For multiple labeling, fluorochrome conjugated secondary antibodies were used instead and the mounted sections were coverslipped in glycerol supplemented with an antifade reagent (Invitrogen cat. No. S2828). Note that for the multiple immunofluorescence labeling we avoided parallel incubation of the antibodies and preferred a serial labeling protocol to minimize cross-reaction risks. A subset of the double-labeled sections was additionally counterstained with the nuclear stain 4′,6-diamidino-2-phenylindole (DAPI) (1 µg/ml). Images were taken on an upright ZEISS light contrast microscope or

on an inverse Leica SP5 confocal microscope equipped with the following laser excitation lines: 405 nm, 488 nm and 633 nm.

To quantify the changes in signal intensity of DCX within the dendrites and the perikarya of newborn granule cells, we chose fluorochrome-labeled sections of 4 weeks old WT and $CR^{-/-}$ mice ($n = 4$ per genotype). Measurements were performed on selected images with the same magnification using the software Image J (Tony Collins, 2009 release www.macbiophotonics.ca/imagej/). Eight bit images (1024 × 1024 pixels) were viewed with the lookup table HiLo, which displays the zero values blue and the 255 white values red. A region of interest (ROI) of 80 × 80 pixels was defined within the hilus of the DG and used for background subtraction from the ROI. DCX-labeled dendrites were outlined within the granular layer and the ML of the DG (10–30 profiles per image). DCX-labeled cell bodies were selected within the SGZ (6–15 profiles per image). Mean intensity, area in square pixels and the fraction of the area displaying intensity values above background were measured for each profile. A dendrite to soma intensity ratio per image was calculated using the corrected total mean density values per pixel of the dendritic and the somatic profiles. Statistics were performed as described above for Western blot analysis.

MORPHOMETRIC ANALYSIS

Nuclei immunolabeled for PCNA or TCF-4 in the GCL and the SGZ of the hippocampal DG were counted in 2 weeks and 4 weeks old animals, to quantify putatively dividing cells in the cells in the DG stem cell niche. The mean density of PCNA-positive nuclei was additionally determined in adult mice of 14 weeks of age. The analysis was restricted to the septal hippocampus and cells were counted in three coronal sections per animal (bregma levels −1.46; −2.00; −2.30 ± 0.05 mm) for a total of six hippocampal regions per animal. The length of the SGZ was measured for each hippocampus and density values were expressed as the number of cells per mm length, pooled and averaged. This value was used then for group statistics. BrdU counts to estimate proliferative activity in the septal SGZ were only performed in 2 weeks old animals and analyzed as described for PCNA and TCF-4.

To study the survival/differentiation of the SGZ progeny in 14 weeks old animals sacrificed 2 weeks after the last BrdU injection, we determined the total number of BrdU-positive cells in the SGZ along its whole septotemporal extent. Cells were counted in eight serial coronal sections approx. two hundred and forty micrometer apart from each other (bregma level −1.22 to −3.20 ± 0.05 mm) for a total of 16 hippocampal regions. The sum of these values was calculated and extrapolated to the total number of BrdU-labeled SGZ/DG cells per brain multiplying it by 6 (since only every sixth section had effectively been counted). Since however, cell location was not limited to the SGZ, but also included the DG, subset counts were performed in the following regions: (1) the SGZ, between the inner border of the GCL and the hilus; (2) GCL corresponding to the cell band and (3) GCL/ML corresponding to the outer border of the GCL (see **Figure 6C**). Statistical analysis was performed with the Prism software (Graph Pad, USA). Statistical comparisons between genotypes were performed with student's *T*-test, two samples, correcting for unequal variances whenever necessary (Welch correction). Statistical comparisons within WT, or mutants at different time points were performed by one-way ANOVA using the Tukey test as a *post-hoc* test. The level of significance was assumed to be $p < 0.05$.

RESULTS

DENTATE GYRUS MORPHOGENESIS IS NORMAL IN THE ABSENCE OF CR AND CB

The first observation in both null-mutant strains ($CR^{-/-}$ and $CB^{-/-}$) was that the general appearance of the DG is normal as shown in **Figures 1**, **3**, **6** and **7**. The thickness (height) of the GCL is normal, as well as the morphology of the mature granule cells (CB-ir in WT and $CR^{-/-}$ mice) and the not-yet fully differentiated ones bordering to the SGZ (CB-negative in WT and $CR^{-/-}$ mice). The length and shape of the GCL/SGZ did not differ in mutant mice in comparison to WT animals, neither in young (2–4 weeks) animals nor in adults (12–14 weeks). Thus, both DG blades properly form during late embryonic and early postnatal development and the two proteins seem not to be involved in the control of this developmental process.

LOW PROLIFERATIVE CAPACITY IN THE SGZ OF YOUNG (P14) $CR^{-/-}$ MICE IS MAINTAINED INTO ADULT LIFE

To screen for changes in the SGZ in $CR^{-/-}$ mice, we first examined the protein content, the signal intensity and distribution of DCX and CB in 2 and 4 weeks old animals. At 2 weeks of age, morphogenesis of the infrapyramidal blade of the DG is well completed, the proliferative matrix has rearranged along the SGZ and implementation of the inner third of the adult DG is ongoing, a gradual process that lasts till the end of the first postnatal month (Altman and Bayer, 1990a,b; Li and Pleasure, 2005). DCX expression within the DG SGZ is characteristic for proliferating progenitors and to a minor extent for early postmitotic neurons (Brown et al., 2003; Ming and Song, 2011; von Bohlen Und Halbach, 2011). On the other hand CB is a marker for mature granule cells (Baimbridge et al., 1992; von Bohlen Und Halbach, 2011). The large majority of newborn neurons express CB by the fourth week past their birth (Kempermann et al., 1997; Brandt et al., 2003). DCX and CB protein contents in whole hippocampal lysates were not different in $CR^{-/-}$ mice (**Figures 1A,B**). As expected for 2–4 weeks old animals, CB labeling did not encompass the whole width of the DG (**Figure 1C**). A clear gradient existed between the mature strong CB-ir GCL neurons and the young CB-negative neurons located within the lower third of the GCL, at the border to the SGZ; this is best seen in the merged (DAPI/CB/DCX) image of **Figure 1C**. CB staining intensity was rather variable between sections from different mice. Changes in the labeling intensity with time or between genotypes were not consistent and probably reflect individual variability in CB expression during this phase of adjustment and definitive maturation of the DG (Altman and Bayer, 1990a,b; Li and Pleasure, 2005). The DCX staining intensity within the SGZ, GCL and ML was consistently decreased in 2 weeks and 4 weeks old $CR^{-/-}$ mutants as compared to WT. The signal appeared particularly low within the dendrites in the 4 weeks old $CR^{-/-}$ group, as if DCX would preferentially label the cell bodies rather than the processes (**Figure 1C**). To validate this we determined

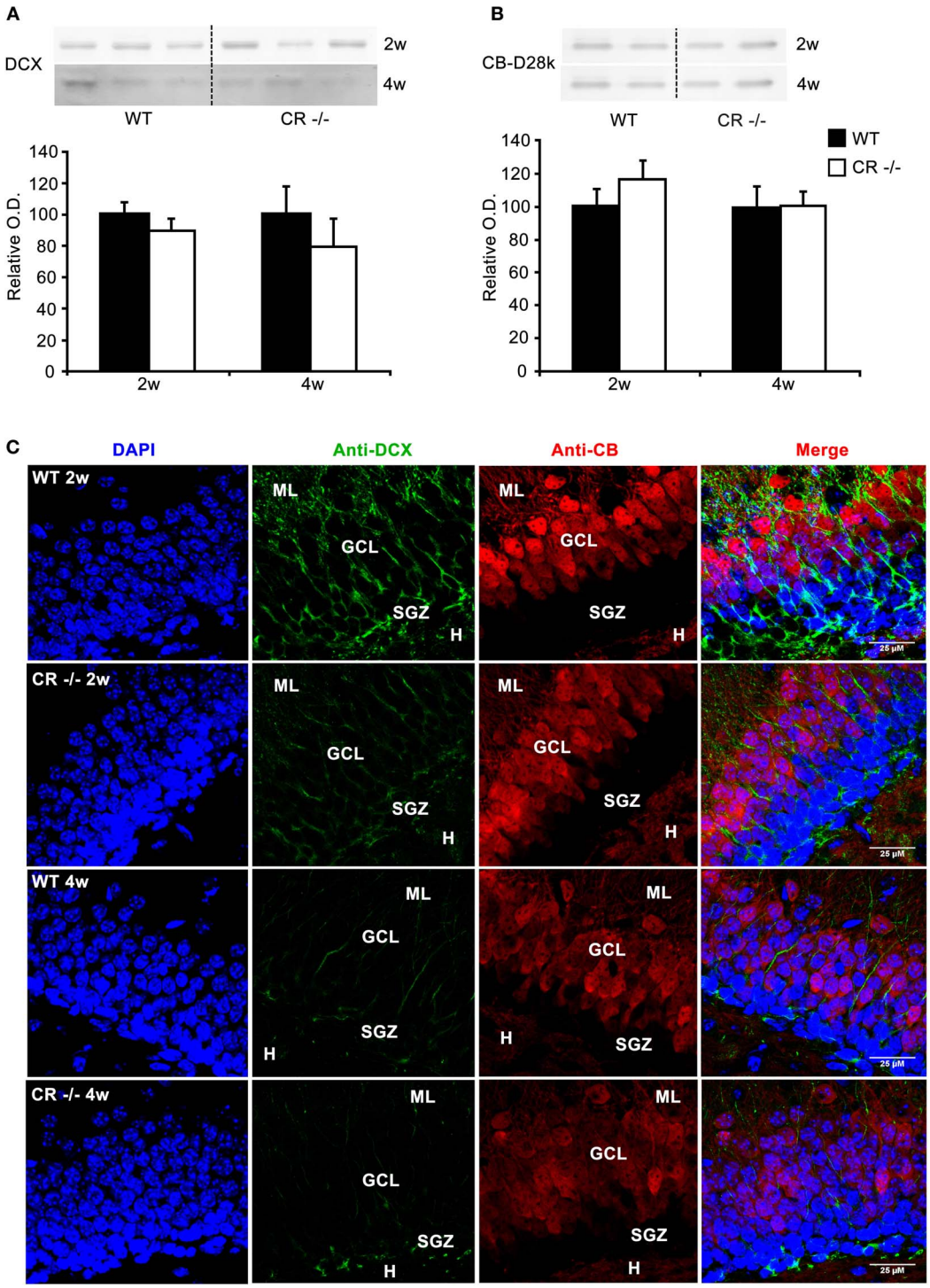

FIGURE 1 | Changes in DCX-immunoreactivity in cells in the GCL at 2 and 4 weeks in CR$^{-/-}$ mice. (A) Representative Western blots for DCX of whole hippocampi from 3 WT and 3 CR$^{-/-}$ mice at the age of 2 and 4 weeks (2w, 4w; upper panel). Densitometric analysis (lower panel) show that global DCX protein levels are not different between WT and CR$^{-/-}$ (2w: $n = 5$ per genotype; 4w: $n = 3$ per genotype). **(B)** Absence of CR does not affect hippocampal CB expression levels (2w $n = 5$ per genotype; 4w $n = 3$ per genotype). **(C)** Double immunolabeling with DCX (green) and CB (red) on sections from 2 and 4 weeks old mice counterstained with DAPI (blue). Note the weaker staining for DCX in both cell somata and processes in 2 weeks old CR$^{-/-}$ mice. The differences in intensity in the cell bodies between WT and CR$^{-/-}$ mice appear to level out within the two following weeks. However, in 4 weeks old CR$^{-/-}$ mice DCX-immunoreactivity remains weak in the dendritic processes. CB labeling intensity of granule cells is rather variable and is not linked to either age or genotype, for details see Results. Scale bar: 25 µm. Abbreviations: CR: calretinin, GCL: granule cell layer, H: hilus region, ML: molecular layer, O.D: optical density, SGZ: subgranular zone, w: week.

the intensity values per pixel of dendritic profiles and cell bodies in selected images of each group at this age. Mean ratio values of DCX intensity (dendritic/somatic) amounted to 0.52 ± 0.05 for WT and were significantly reduced to 0.26 ± 0.05 in $CR^{-/-}$ ($p = 0.015$). Selective confinement or redistribution of DCX to the cell bodies observed in $CR^{-/-}$ mice may well occur without affecting total protein content and may reflect changes in the regulation of DCX binding to the cytoskeleton critical for its functions (Bilimoria et al., 2010; Jin et al., 2010).

Since most DCX-labeled cells within the SGZ belong to cycling progenitors rather than to early postmitotic neurons (von Bohlen Und Halbach, 2011), we decided to further explore functional changes in this population by investigating the proliferative activity in the DG SGZ of $CR^{-/-}$ mice. We adopted PCNA, a well-known marker for dividing cells (Miyachi et al., 1978; Ino and Chiba, 2000). Western blots of whole hippocampus lysates of $CR^{-/-}$ and WT mice revealed a decrease in protein content in $CR^{-/-}$ mice. Densitometric analysis evidenced a significant decrease of 35% in PCNA protein content in 4-weeks old animals ($p < 0.05$), but not in 2-weeks old ones (**Figure 2**).

We looked, therefore, for more localized and detailed changes by IHC in young (2–4 weeks old) as well as in adult animals (14 weeks). PCNA-immunoreactive (-ir) cells were mostly distributed in the SGZ of the DG below the GCL (**Figure 3A**). These proliferating cells may correspond in part to the few radial glia cells with putative stem cell function as well as to the more numerous and more rapidly cycling granule cell progenitors (Ino and Chiba, 2000). Since the number of PCNA-positive cells decreased with increasing age in both genotypes (**Figure 3A**), we determined their density in three coronal sections through the septal/dorsal DG for comparisons (**Figure 3B**). Density estimates

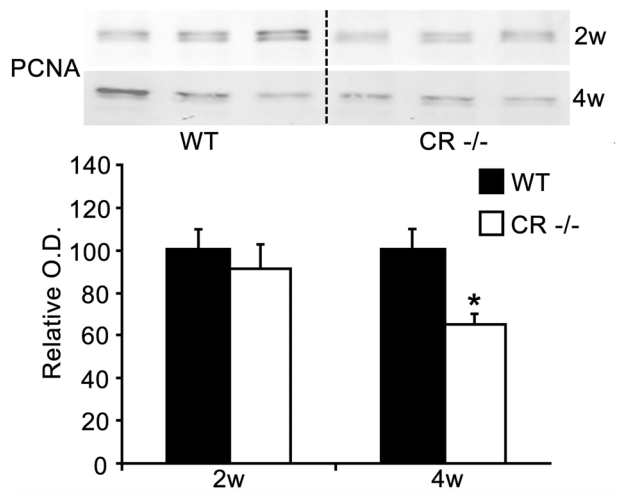

FIGURE 2 | Reduction in expression of hippocampal PCNA in 4 weeks old $CR^{-/-}$. Upper panel: representative Western blots of whole hippocampi from 3 WT and three $CR^{-/-}$ mice. Staining with the PCNA antibody resulted in two specific bands and for the quantification of PCNA (lower panel), both signals were summed up. Normalized densitometric optical density values (mean ± sem, $n = 5$ per genotype at 2 weeks and $n = 3$ at 4 weeks) are shown. A significant decrease of about 35% of PCNA is detectable in 4 weeks old $CR^{-/-}$ mice (*$p < 0.05$).

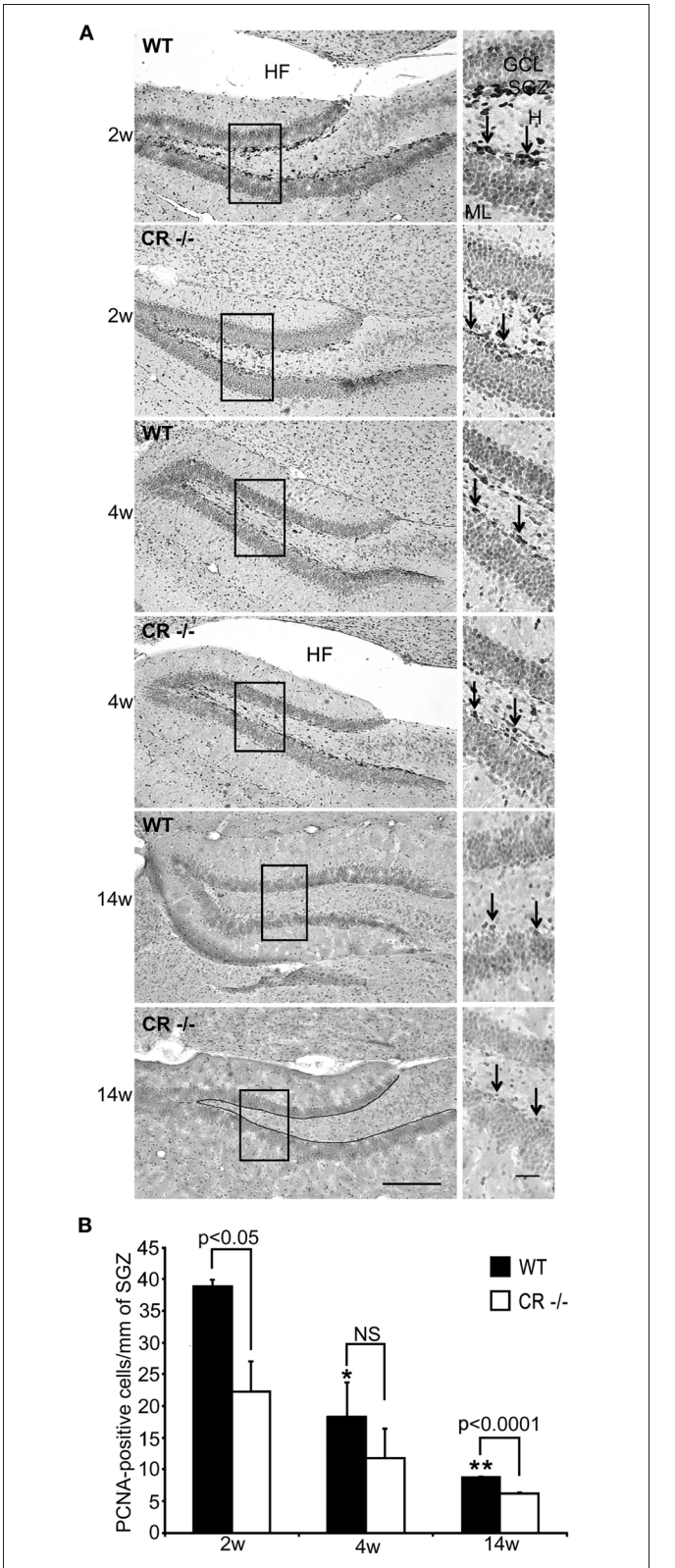

FIGURE 3 | Density of PCNA-ir cells in the septal DG stem cell niche is reduced in $CR^{-/-}$ mice. (A) Representative sections from the DG of WT and $CR^{-/-}$ mice immunostained for PCNA and counterstained.

(Continued)

FIGURE 3 | Continued
High-resolution micrographs (scale bar: 10 μm) accompany each overview (scale bar: 100 μm) and correspond to the boxed areas. At the age of 2 weeks PCNA-ir cells (arrows in insets) are numerous and well visible, both in WT and $CR^{-/-}$ mice. They are located in the SGZ at the inner border of the GCL. Positive cells appear less distinct and are less numerous with increasing age. The line drawn in the bottom overview image exemplifies the length measurements and marks the zone selected for the cell counts. **(B)** Density estimates of PCNA-ir cells are highest in 2 weeks old WT animals and significantly decrease at 4 and 14 weeks (*4w vs. 2w $p < 0.05$; **14w vs. 2w $p < 0.01$). A similar time-dependent decrease is also observed in $CR^{-/-}$ mice, although differences did not reach statistical significance. Note that the density of PCNA-ir cells is significantly lower in $CR^{-/-}$ as compared to WT animals at 2 weeks (−40%) and 14 weeks (−30%). $N = 3$ for both genotypes at each data point. Abbreviations: see **Figure 1**; HF: hippocampal fissure.

of mitotically active cells were highest in young WT animals (2 weeks) and significantly decreased by 50% within the 2 successive weeks ($p < 0.05$). A further significant loss of 52% followed between the first and the third postnatal month of life ($p < 0.01$). A similar, time-dependent decrease was also seen in sections from $CR^{-/-}$ mice, although not reaching statistical significance. Strikingly, the density of PCNA-ir cells was significantly lower in $CR^{-/-}$ mice as compared to WT animals at 2 weeks (−40%) and 14 weeks (−30%).

We then used alternative markers to confirm and explore in more detail this early decrease in proliferative matrix occurring in $CR^{-/-}$ mice. The BrdU uptake into dividing cells was tested in 2 weeks old WT and $CR^{-/-}$ mice, which were sacrificed 24 h after a single intraperitoneal BrdU injection. BrdU-ir nuclei within the SGZ of both WT and $CR^{-/-}$ were more intensely labeled as compared to the PCNA labeling (**Figure 4A**, compare with **Figure 3A**). In absolute terms, the number of BrdU-positive, i.e., dividing cells in the SGZ was larger than the number of PCNA-ir neurons in 2 weeks old WT animals (compare **Figure 4B** and **Figure 3B**). Quantification of BrdU-labeled dividing cells in the SGZ of WT and $CR^{-/-}$ mice showed a significant reduction in $CR^{-/-}$mice by about 25% (**Figure 4B**; $p < 0.03$), analogous to the reduction observed by PCNA staining.

TCF-4 was selected in 2 weeks and 4 weeks old mice as an additional marker for proliferating neuronal progenitor cells in the SGZ to consolidate the PCNA and BrdU data. TCF-4 is a basic-helix-loop-helix transcription factor activated by the canonical Wnt signaling pathway (Clevers, 2006). In the postnatal and adult DG, TCF-4 is expressed in DCX-positive granule cell progenitors (Lie et al., 2005; Kuwabara et al., 2009). In both WT and $CR^{-/-}$ sections, TCF-4 immunoreactivity was rather weak, but restricted to specific nuclei of cells located in the SGZ (**Figure 5A**). Quantification of TCF-4-positive nuclei showed a significant decrease (−26%, **Figure 5B**) in 2 weeks old $CR^{-/-}$ mice, thus in line with the PCNA and BrdU results. As for the PCNA staining (**Figure 3B**), no significant differences between genotypes persisted in 4 weeks old mice.

Altogether these data strongly suggest that $CR^{-/-}$ mice present a defect in proliferative capacity in the SGZ of the DG. Loss of proliferative activity is particularly evident and consistent at the early age of 2 weeks and seems to be maintained into adult life.

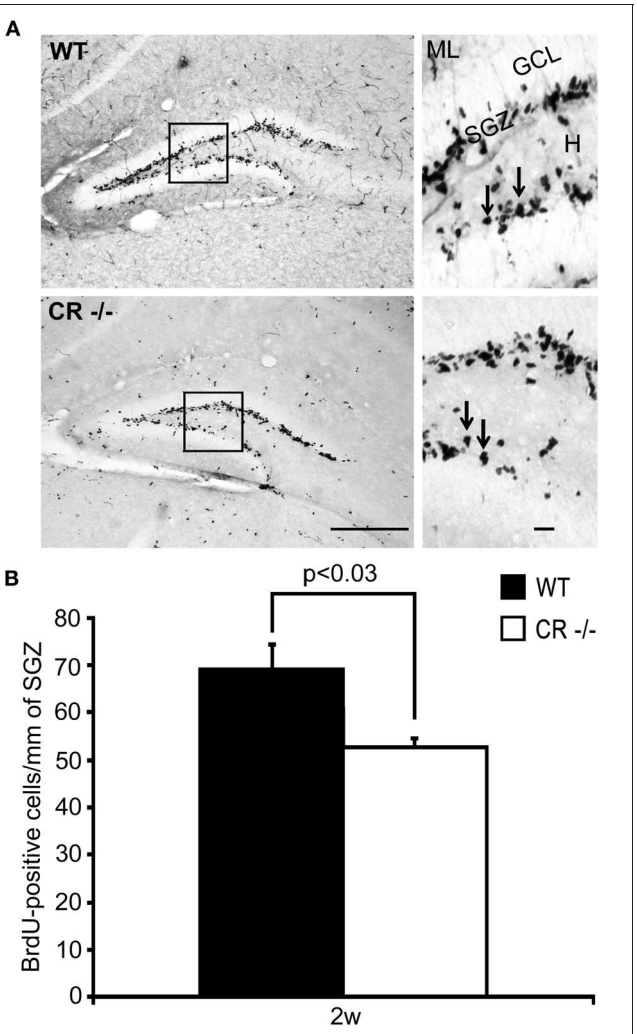

FIGURE 4 | Density of BrdU-ir cells in the septal DG stem cell niche is decreased in 2 weeks old $CR^{-/-}$ mice. (A) Overview of the distribution of BrdU-ir cells in the SGZ of the DG in WT (upper panel) and $CR^{-/-}$ (lower panel) mice. High-resolution micrographs (scale bar: 10 μm) correspond to the boxed areas in the overviews (scale bar: 100 μm). Arrows point to individual labeled cells. **(B)** Estimate of proliferating cells in the DG neurogenic niche, determined 24 h after a single BrdU pulse. Density estimates of BrdU-labeled cells are significantly reduced (−24%) in 2 weeks old $CR^{-/-}$ ($n = 4$) mice as compared to WT ($n = 6$). Abbreviations: see **Figure 1**.

LOW PROLIFERATIVE CAPACITY IN THE ADULT SGZ OF $CR^{-/-}$ MICE AFFECTS SURVIVAL OF NEWBORN GRANULE CELLS AND SLOWS DOWN THEIR MIGRATION INTO THE GCL

To explore more in detail the consequences of such a loss in proliferative capacity at adult age we performed a BrdU differentiation assay and evaluated the 2 week survival/differentiation capacity of cells born in the SGZ at 12 weeks of age. BrdU-ir cells detected with this protocol were sparser in both WT and in $CR^{-/-}$ mice, compared to those detected by the proliferation assay performed at 2 weeks of age (**Figure 6A**, compare with **Figure 4A**). We thus counted the BrdU-positive nuclei in serial sections along the whole septotemporal extent of the DG to determine differences

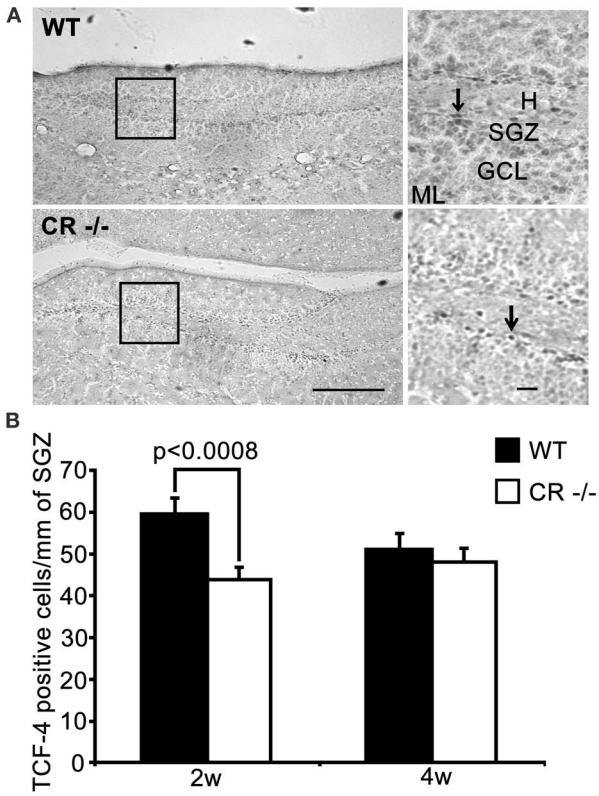

FIGURE 5 | TCF-4-ir cells responsive to proliferative signals are significantly decreased in the SGZ of 2 weeks old CR$^{-/-}$ mice. **(A)** Overview of the distribution of TCF-4 positive cells in the SGZ of the DG in WT (upper panel) and CR$^{-/-}$ (lower panel) mice. High-resolution micrographs (scale bar: 10 μm) correspond to the boxed areas in the overviews (scale bar: 100 μm). Arrows point to individual TCF-4-ir cells. **(B)** The density estimates of the putative progenitor pool expressing TCF-4 differ significantly in 2 weeks old mice (−26.6% of WT in CR$^{-/-}$). The initial decrease in TCF-4-ir cells does not persist in 4 weeks old CR$^{-/-}$ mice. $N = 4$ per genotype and age. Abbreviations: see **Figure 1**.

in the mean total number between genotypes. We found that the survival and differentiation of newborn cells in the adult SGZ niche of CR$^{-/-}$ mice was significantly reduced by a factor of 2 as compared to WT (**Figure 6B**). In WT about 53% of the nuclei were localized in the SGZ, while in CR$^{-/-}$ mice this fraction amounted to 64%. Those BrdU-ir nuclei located within the GCL amounted to 36% for WT and corresponded to only 28% of the total in CR$^{-/-}$. Similarly, the relative fraction of BrdU-ir cells close to the ML was smaller in CR$^{-/-}$ mice (8%) as compared to the 11% of WT (**Figures 6C–D**). These data suggest that migration of progenitor cells out of the SGZ into the inner GCL is hampered in the absence of CR, affecting in turn the migration process of differentiating granule cells throughout the GCL. To further explore this possibility, values for WT and CR$^{-/-}$ presented in **Figure 6D** were normalized within each genotype, plotted against the relative migration (**Figure 6E**) and the slope of the linear regression was taken as a proxy measure for migration, i.e., the steeper the slope, the lower cell migration. The slope for CR$^{-/-}$ mice was approximately 40% larger (−56.8 in CR$^{-/-}$ vs. −41.3 in WT) supporting the hypothesis of slower/reduced migration of newly generated granule cells. Overall, the mean cell number of BrdU-ir cells was significantly lower at each location in CR$^{-/-}$ mice as compared to WT animals ($p < 0.02$–0.05; **Figures 6C–D**). These data indicate that the prolonged failure in proliferative activity into adult age observed in the SGZ of CR$^{-/-}$ may negatively influence the survival of postmitotic neurons.

Double labeling of BrdU and CR, respectively CB was performed to evaluate the extent of differentiation that these newborn cells generally undergo in WT mice in the time period of 2 weeks after the last BrdU injection. BrdU-positive nuclei were not found to colocalize with CB-ir mature granule cells (**Figure 6F**), while BrdU and CR co-localization in immature granule cells distributed at the inner border of the GCL was observed at a variable rate (39 ± 21%; e.g., **Figure 6G**), in agreement with the reported temporal expression patterns for BrdU-labeled, CR-positive neurons in WT mice (approx. 30% at 2.5 weeks; Kempermann et al., 1997; Brandt et al., 2003). In CR$^{-/-}$ mice, the approximate timeline of appearance of CB in new granule cells was similar as in WT mice, i.e., no CB and BrdU co-localization was seen (data not shown). Thus, we conclude that the impaired migration process of the fewer cells in the CR$^{-/-}$ 2 weeks after birth is likely more affected than their differentiation as measured in terms of average time to onset of CB expression.

NO EVIDENCE FOR CHANGES IN THE PROLIFERATIVE ACTIVITY OR CELL SURVIVAL IN THE SGZ OF CB$^{-/-}$ MICE

Since CB is expressed in mature granule cells, we investigated whether its absence in CB$^{-/-}$ mice also entails alterations in postnatal neurogenesis. We analyzed the total amount, the relative distribution and staining intensity in the SGZ of 2 weeks and 4 weeks old mice for DCX, as in the CR$^{-/-}$ mice. A weaker DCX staining mostly confined to cell bodies was observed in CB$^{-/-}$ mice, a staining pattern strongly reminiscent of the one present in CR$^{-/-}$ mice (compare **Figure 7A** with **Figure 1C**); in line with results in CR$^{-/-}$ mice, DCX protein levels were not different between WT and CB$^{-/-}$ mice (data not shown). In CB$^{-/-}$ mice we used CR IHC to check the overall morphology of the subpopulation of postmitotic neurons that partly also express DCX. Neither immunostaining signal intensity and distribution (**Figure 7A**) nor CR protein expression levels (**Figure 7B**) were different between CB$^{-/-}$ and WT mice.

PCNA-ir cells in the SGZ showed a significant age-dependent decrease in both WT and CB$^{-/-}$ mice, most pronounced in the period from 2–4 weeks. A decrease in the density of PCNA-ir cells was observed only at the earliest time point (2 weeks) in CB$^{-/-}$ mice in comparison to WT animals. So contrarily to what we observed in CR$^{-/-}$ animals, a long-term recovery of the proliferative capacity occurred in CB$^{-/-}$ mice (**Figure 8A**). Noteworthy, the BrdU proliferation assay at 2 weeks did not reveal significant differences between genotypes (**Figure 8B**, for details, see discussion). Analysis of the 2 weeks survival/differentiation assays (same as those reported for CR$^{-/-}$ mice in **Figure 6**) did not show any differences between CB$^{-/-}$ and WT mice (**Figure 8C**). Accordingly, no differences with respect to the relative distribution of BrdU-ir cells in the different compartments SGZ, GCL, and GCL/ML were detected (data not shown); the values largely corresponded to those reported for WT in **Figure 6D**.

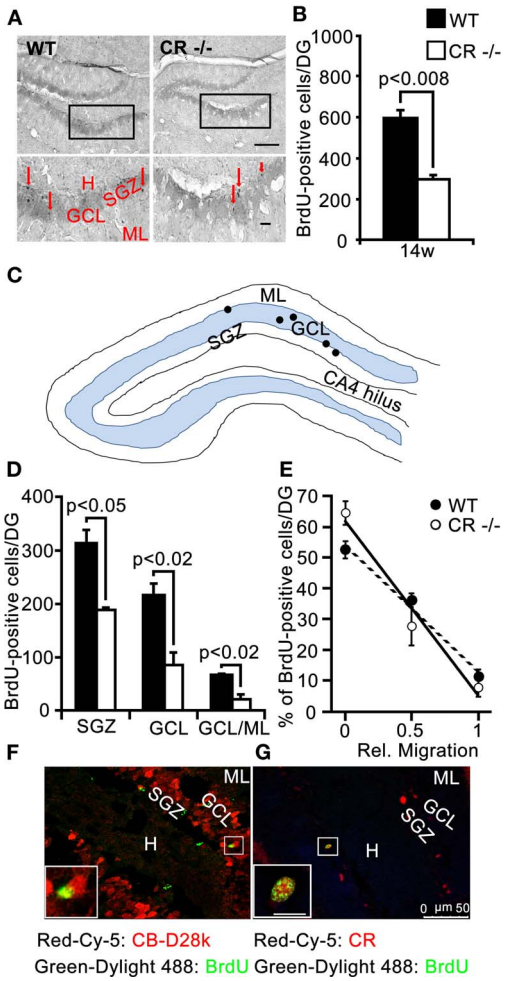

FIGURE 6 | BrdU differentiation assay: survival of newborn cells is significantly reduced in adult (14w) CR$^{-/-}$ mice and the migration into the GCL is impaired. (A) Overview of the distribution of BrdU-ir cells in the DG of WT (left panel) and CR$^{-/-}$ (right panel) mice. High-resolution micrographs (lower images, scale bar: 10 µm) correspond to the boxed areas in the overviews (scale bar: 100 µm). Red arrows point to individual BrdU-ir cells. **(B)** Bar graph plotting the mean total number of BrdU-ir cells determined along the whole septotemporal extent of the DG, 2 weeks after 3 daily BrdU pulses in adult 3 months old animals. The survival of newborn cells in CR$^{-/-}$ is significantly reduced by a factor of 2 as compared to WT (−50%, $n = 3$ per genotype). **(C)** Drawing of the DG (not scaled) exemplifying the layer distribution of BrdU-ir cells (black dots) 2 weeks after the last marker injection. **(D)** Layer specific counts of BrdU-ir nuclei are plotted for the two genotypes. In CR$^{-/-}$ the mean cell number is significantly lower than in WT at each location. **(E)** Relative distribution of BrdU-ir cells in SGZ (rel. migration: 0), in the GCL (rel. migration: 0.5) and in the border region GCL/ML (rel. migration: 1) of WT and CR$^{-/-}$ mice. The slopes of the linear regression curves ($r^2 = -0.99$ for both genotypes) served as a proxy measure for migration of newborn granule cells. The steeper slope in CR$^{-/-}$ mice is indicative of slower/reduced migration. **(F–G)** Double labeling of BrdU and CB **(F)** or BrdU and CR **(G)** in the DG of a representative adult WT animal evaluated 2 weeks after the last BrdU injection. BrdU-ir nuclei never colocalize with CB-ir granule cells **(F)**; CR is expressed in approx. one third of BrdU-ir cells. Due to the low number of BrdU-ir cells per section, rarely more than 1–2 double-labeled cells are observed on a given section; they are located at the inner border of the GCL **(G)**. Scale bar: 50 µm. Boxed areas are shown enlarged as insets at the left bottom of the micrographs (scale bar: 10 µm). Abbreviations: see **Figure 1**.

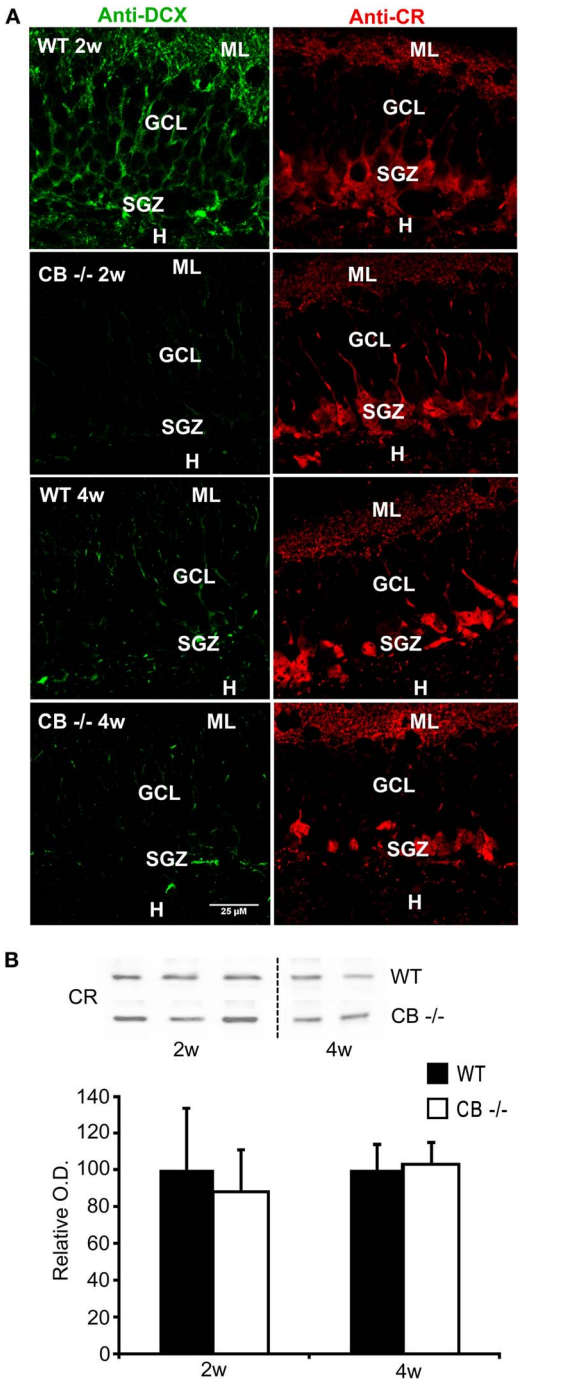

FIGURE 7 | No reduction in DCX and CR expression levels, but in DCX staining in 2–4 weeks old mice lacking CB. (A) Double immunolabeling with DCX (green, left panel) and CR (red, right panel). The images show details of the GCL and the SGZ for the 2 genotypes at 2 and 4 weeks. Note that the changes in DCX labeling intensity and intracellular signal distribution are the same as described for the CR$^{-/-}$ in comparison to WT (**Figure 1**). No qualitative differences in CR-ir cells are visible between WT and CB$^{-/-}$ at the two different time points. Scale bar: 25 µm. **(B)** Representative Western blots for CR from WT and CB$^{-/-}$ mice at the age of 2 and 4 weeks. Densitometric analysis reveals no differences between genotypes (2w: $n = 5$ per genotype; 4w: $n = 3$ per genotype). Abbreviations: see **Figure 1**.

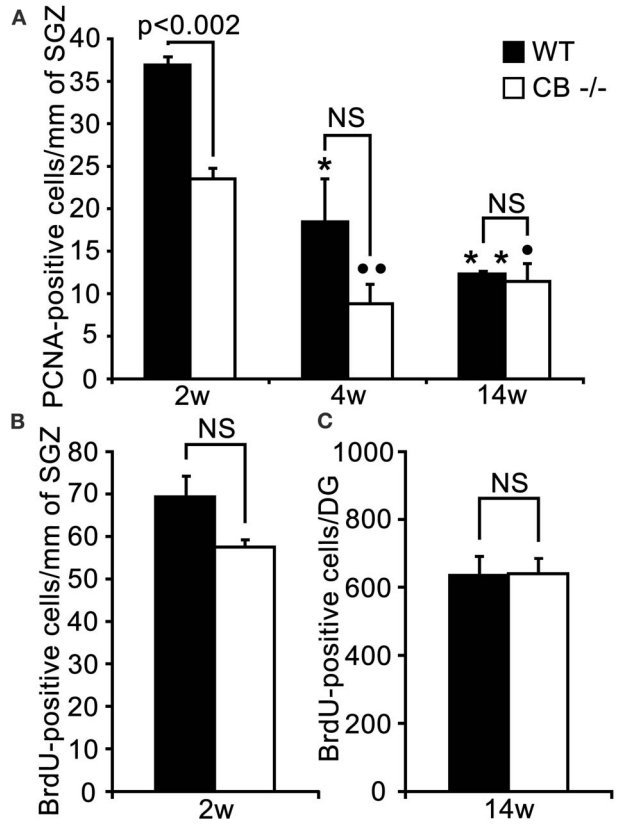

FIGURE 8 | An early putative deficit in proliferative activity in the DG cell stem niche of 2 weeks old CB$^{-/-}$ mice has no effect on survival/differentiation of granule cells in adult (14w) mice. (A) Density estimates of PCNA-ir cells in the septal extent of the SGZ of WT and CB$^{-/-}$ mice. PCNA-ir cell density is highest in young (2 weeks) WT animals and decreases steadily and significantly in the successive 2 weeks. At the adult age of 3 months the density is reduced to one third of the initial value (*$p < 0.05$ 4w vs. 2w; **$p < 0.01$ 14w vs. 2w). In CB$^{-/-}$ mice a significant decrease is only observed from 2 to 4 weeks, while no changes occur from 4 to 14 weeks (°°$p < 0.01$ 4w vs. 2w and °$p < 0.05$ 14w vs. 2w). The initial reduction in the density of PCNA-ir cells observed in 2 weeks old CB$^{-/-}$ mice is not maintained at later time points (4w and 14w). $N = 3$ for both genotypes and ages. **(B)** Density of BrdU-ir nuclei determined 24 h after a single BrdU pulse in the septal SGZ. The small decrease in the density of BrdU-ir nuclei in 2 weeks old CB$^{-/-}$ mice (20%) is not significant ($n = 6$ mice per genotype). **(C)** Mean total number of BrdU-ir cells estimated along the whole septotemporal extent of the DG, 2 weeks after 3 daily BrdU pulses in adult 3 months old animals. The survival of newborn cells in CB$^{-/-}$ mice does not differ from WT mice ($n = 3$ per genotype).

These data indicate that loss of CB expression from DG granule cells as well as from the few hippocampal CB-ir interneurons (Gulyas and Freund, 1996) has no significant effect on the proliferative activity of progenitor cells nor affects survival and/or migration of newborn neurons within the adult SGZ.

DISCUSSION

We studied the impact that the constitutive absence of the Ca^{2+}-binding proteins CR and CB, mutually expressed at different stages of maturation of granule cells, may have on the proliferation and differentiation within the SGZ neurogenic niche of the DG in null-mutant mice. Effects were evaluated at young age (2 weeks and 4 weeks) and in adult animals (3 months). The constitutive absence of CB expression from differentiated DG granule cells has no retrograde effect on the proliferative activity of progenitor cells, nor affects survival or migration/differentiation of newborn neurons in the adult DG including the SGZ. On the contrary, lack of CR from immature early postmitotic granule cells, causes an early loss in proliferative capacity of the SGZ that is maintained into adult age, when it has a further impact on the migration/survival of newborn granule cells.

ABSENCE OF CR EXPRESSION IN NEWBORN GRANULE CELLS IMPAIRS THE PRECEDING PROGENITOR PROLIFERATION PHASE

DCX is a microtubule-associated protein that promotes their polymerization. In the SGZ of the DG, DCX is transiently expressed in proliferating neural progenitors and in early postmitotic neurons expressing CR and NeuN (Brandt et al., 2003; Brown et al., 2003; von Bohlen Und Halbach, 2011). Thus, the pool of DCX-positive cells also includes to a minor extent cells exiting the cell cycle to become immature granule cells. Whole hippocampal DCX protein levels were similar in 2 and 4 weeks old CR$^{-/-}$ and CB$^{-/-}$ mice and did not differ from WT ones. However, compared to WT animals, differences in DCX distribution were evident at the morphological level: in 4 weeks old mutant mice, in particular, the intensity per pixel was significantly weaker in processes than in the cell bodies. DCX plays an active role in cytoskeletal assembly and process growth in immature neurons (Bilimoria et al., 2010; Jin et al., 2010). Such redistribution from dendritic processes to the cell body may therefore reflect a decrease of the cytoskeletal scaffold resulting in less and/or impaired growth of neuronal processes. Reduced process growth may eventually limit the capacity of sensing modulatory cues from the neighboring environment promoting targeting, network integration and survival. However, the changes in DCX-ir varied between genotypes and even between animals from the same genotype suggesting rapid redistribution dynamics and/or large inter-individual variety. A more detailed, possibly *in vitro* approach might be necessary to further investigate the putative role of DCX localization in neurogenesis in CR$^{-/-}$ and CB$^{-/-}$ mice.

To address more directly the putative role of CR and CB in postnatal neurogenesis, PCNA and TCF-4 expression, as well as BrdU incorporation 24 h post injection were investigated. PCNA is a sliding clamp processivity factor, essential for fast replication of DNA during the S-phase of the cell cycle (Mathews et al., 1984). Therefore it is a well-known marker for dividing cells (Miyachi et al., 1978; Ino and Chiba, 2000); used as a complement or as an alternative to the classical 24 h BrdU proliferation assay. In line with previous reports (Ben Abdallah et al., 2010; Knoth et al., 2010), the density of proliferating cells in the SGZ considerably decreased with increasing age in WT mice. In 2 weeks old CR$^{-/-}$ mice densities of PCNA-ir and of BrdU-ir cells were much lower than in WT mice indicating a loss of the proliferating pool. Of note, in all experiments, the differences in density between WT and knockout mice were larger for PCNA-ir cells than for BrdU-ir cells (e.g., **Figure 3B** vs. **Figure 4B**). In the case of PCNA-ir, we reason that the lower contrast between the specific

immunolabeling and the counterstaining led to an overestimation of differences. The BrdU-ir instead presented a better signal-to-background contrast and thus reflects more accurately the real differences between genotypes.

TCF-4 is a basic-helix-loop helix transcription factor that mediates Wnt signaling by binding β-catenin and is considered to control downstream genes promoting cell proliferation and maintenance of the stem cell phenotype (Clevers, 2006). However, binding of additional proteins to the β-catenin/TCF-4 complex within the nucleus may alternatively result in cell cycle exit and induction of differentiation programs (Teo et al., 2005; Teo and Kahn, 2010). Modulation of Wnt signaling plays a prominent role in CNS development (Michaelidis and Lie, 2008) and is critical for DG development. Its disruption causes the proliferative activity to stop prematurely and results in DG aplasia or hypoplasia (Galceran et al., 2000; Zhou et al., 2004). In the postnatal and adult DG, Wnt is secreted by astrocytes and continues to regulate the balance between proliferation and differentiation. TCF-4 is expressed within the SGZ, where it often colocalizes with DCX (Lie et al., 2005; Kuwabara et al., 2009). These cells may therefore correspond to the largely DCX-positive progenitor pool. Thus, we assumed a significant overlap between TCF-4-ir cells and the population determined by PCNA staining and BrdU incorporation. In accordance with the latter results, the density of TCF-4 positive cells was clearly decreased in 2 weeks old $CR^{-/-}$ and the effect (–27% compared to WT) was in the same range as for PCNA staining (–39%) and BrdU incorporation (–24%). Therefore, the loss of proliferative capacity observed with PCNA and BrdU IHC in 2 weeks old $CR^{-/-}$ appears to affect progenitor cells that are sensitive to the Wnt signaling cascade and its modulators and which are about to decide on their fate (either reenter or exit the cell cycle).

Results in 4 weeks old $CR^{-/-}$ mice were less conclusive. The densities of PNCA-ir and TCF-4-ir cells were almost indistinguishable from those in WT mice, although the values were still slightly smaller. This may reflect an attempt to compensate the earlier loss of proliferative capacity. However, the significant reduction in whole hippocampal PCNA protein levels observed at this age rather suggests that compensation is not achieved. Adult neurogenesis is considered as a process that may be influenced at many different stages of neuronal development and showing a high degree of plasticity (Kempermann, 2011). Thus, it is not surprising that the initially rather large differences seen at 2 weeks in the absence of CR did not extend to the age of 4 weeks. The apparent inconsistencies with respect to PCNA, i.e., a decrease in PCNA-ir cells without significant changes in protein levels at 2 weeks and the opposite finding at 4 weeks may be the result of the low number of animals analyzed per group and of the larger variability in signal intensities of the PCNA Western blots. Considering all the investigated markers (TCF-4, PCNA, BrdU) we can conclude that the absence of CR expression in early postmitotic granule cells at the age of 2 weeks negatively affects neurogenesis, namely the preceding progenitor proliferation phase.

Once morphogenesis of the infrapyramidal blade of the DG is accomplished by the end of the first postnatal week, the proliferative matrix remains quite active for the following 2–3 weeks. During this time period more granule cells are added to the network, i.e., to the inner third of the DG (Altman and Bayer, 1990a,b; Li and Pleasure, 2005). Meanwhile the proliferating pool in the SGZ changes and rearranges into the prospective adult state: the strictly genetic/intrinsic control-active during development is implemented with additional extrinsic modulatory cues derived from the functional DG network, e.g., synaptic activity and its dependent signaling as well as the overall metabolic state (Kempermann, 2011). It has been proposed that this transition period would be better-termed "childhood" or "adolescence" neurogenesis (Knoth et al., 2010). It is well possible that during this sensitive period of transition to adult neurogenesis, early postmitotic neurons may be the source of some extrinsic modulatory signals, which influence in a feedback mode the cycling activity of the progenitor pool. Within the adult SGZ, CR expression seems restricted to postmitotic cells, i.e., CR co-expression in BrdU-ir cells is never observed early (4 h) after BrdU injection (Brandt et al., 2003). In maturing granule cells, CR probably functions as a Ca^{2+} buffer and/or sensor during Ca^{2+} transients occurring in concomitance with the onset of synaptic activity and linked to the GABA-dependent depolarizing currents (Ge et al., 2006). It is plausible that within the Ca^{2+} signaling network typical of this stage (Jagasia et al., 2009; Merz et al., 2011) retrograde signals may be generated to regulate an antecedent phase. Speculatively, it could be assumed that during the time period of transient CR expression immature granule cells give a feedback to the progenitor pool with regard to their successful differentiation progress, thus regulating cell fate decision toward cell cycle reentry and further proliferation/amplification. CR deficiency in mutants would then hamper feedback signaling and eventually deliver instructions to the progenitor pool to regulate cell fate decision in the opposite direction. This would result in a more frequent/precocious cell cycle exit and eventually endanger amplification of the progenitor pool, thus exhausting the proliferative matrix. According to this scenario, the decrease in TCF-4 expressing cells observed in $CR^{-/-}$ mice suggests that such regulatory feedback may interfere with the Wnt/β-catenin-TCF-4 signaling cascade, which is critical for cell fate decisions both during embryonic DG morphogenesis (Galceran et al., 2000; Zhou et al., 2004), as well as adult neurogenesis (Lie et al., 2005; Kuwabara et al., 2009). Further experiments are required to investigate the nature of the putative diffusible signals and to identifying the Wnt/β-catenin-TCF-4 cascade as a possible target.

ABSENCE OF CR IN NEWBORN GRANULE CELLS SEVERELY DECREASES THEIR SURVIVAL AND LIKELY AFFECTS THE MIGRATION PROCESS

We further examined adult animals, because by this time the lifelong steady-state levels of proliferation and differentiation typical of adult neurogenesis have been accomplished (Ben Abdallah et al., 2010; Knoth et al., 2010; Kempermann, 2011). In both WT and $CR^{-/-}$ mice, the density of PCNA-ir cells was much lower than in 2 weeks old animals and a clear difference (−30%) in the density of PCNA-ir putative progenitor cells was observed in mice lacking CR. Thus, the deficit in proliferative capacity of the SGZ was maintained in adult $CR^{-/-}$ mice. To test whether

such a permanent decrease in the progenitor pool would have any consequences on the survival and differentiation of newborn neurons in adult mice a BrdU differentiation essay was performed. The number and distribution of BrdU-positive cells within the SGZ and the GCL were determined 2 weeks after administration of the substance in adult mice. BrdU-labeled neurons were reduced by a factor of two in $CR^{-/-}$ as compared to WT mice. A period of 2 weeks is not sufficient for BrdU-ir cells to express CB, since it generally takes 4 weeks for newborn granule cells to express it (Kempermann et al., 1997). Transient CR expression reaches a maximum 1 week from birth of a newly generated granule cell; 2.5 and 4 weeks after birth, the percentage of BrdU-ir cells expressing CR is reduced to approximately 30 and 5%, respectively, (Brandt et al., 2003). Since we did not observe changes in $CR^{-/-}$ mice regarding this timeline, we assume that most BrdU-ir cells detected in the survival/differentiation assay correspond to postmitotic neurons in the phase of active process growth and synaptogenesis (Ge et al., 2006; Toni and Sultan, 2011). Thus, the survival of the pool of newborn immature granule cells is drastically reduced in $CR^{-/-}$ mice.

Detailed analysis of the relative position of the BrdU-ir cells within the height of the adult SGZ and GCL in WT and $CR^{-/-}$ mice revealed that in $CR^{-/-}$ a larger percentage of neurons remained confined to the SGZ. Accordingly the relative fraction of newborn cells distributed within the GCL was decreased. Migration out of the SGZ into the GCL seems to occur in 2 steps. In a first step, which is accomplished while exiting the cell cycle, all cells move out of the SGZ to reach the inner GCL. Then postmitotic cells further migrate within the GCL to different extents (Ming and Song, 2011; von Bohlen Und Halbach, 2011). Thus, we may conclude that those newborn cells detectable in the $CR^{-/-}$ by this assay exhibit a deficit in the migration process.

Critical prerequisites for the successful accomplishment of the different maturation steps are the GABA-mediated depolarization (Ge et al., 2006) and the related activation of CREB signaling (Merz et al., 2011). If the depolarizing effects of GABA are lost or CREB phosphorylation is reduced at this stage, then survival of the newborn neurons is at risk (Jagasia et al., 2009). As mentioned earlier, the presence of CR in newborn neurons largely coincides with the phase of sensitivity to the GABA-dependent depolarizing currents. Many studies *in vivo* and *in vitro* have demonstrated that Ca^{2+} buffers such as CR can affect processes like protein phosphorylation and/or dephosphorylation mediated by Ca^{2+}/CaM-dependent kinases or calcineurin, respectively, (Schwaller, 2010). CR may thus modulate depolarization-induced Ca^{2+} transients and subsequently affect CREB phosphorylation and in turn CREB-dependent activation of downstream targets promoting survival and further differentiation of newborn neurons (Merz et al., 2011). The specific and time-locked expression of CR at the onset of the differentiation stage in adult neurogenesis may thus play (1) a role on the self-maintenance signal for the pool of cells at the same stage contributing to their survival/differentiation, and (2) may contribute (as a retrograde signal) to the maintenance of the progenitor pool. Loss of CR-mediated signaling would then reduce survival and eventually the size of the differentiating pool and compromise the proliferative function of progenitors.

PHYSIOLOGICAL IMPLICATIONS OF CR'S ABSENCE IN DG PROGENITORS

What would be the consequences of the hypothesized dual role of CR in terms of network function and of hippocampal dependent behavior? If we consider that in $CR^{-/-}$ mice the pool of immature granule cells which is particularly prone to exhibit synaptic plasticity (Deng et al., 2009; Mongiat et al., 2009) is only one half of that present in WT animals, then some effects at the network level are rather plausible. Thus, the deficient LTP induction specific to the DG of $CR^{-/-}$ mice (Schurmans et al., 1997) may well depend in part on the deficit in the number of immature granule cells and not solely on the loss of CR's Ca^{2+} buffering/sensing properties from terminals of the hilar mossy cell commissural associational pathway. An elegant approach to test this hypothesis would be to repeat the DG LTP study in mutants, where CR expression is only ablated in maturing granule cells. Numerous experimental and theoretical studies have accumulated in the last decades on the specific role of the DG within the hippocampal formation and its function at the behavioral level (Aimone et al., 2011). There is also increasing evidence that only a particular subset of hippocampal-dependent learning and their related behavioral tasks critically relies on normal adult neurogenesis (Treves et al., 2008; Aimone et al., 2011; Ming and Song, 2011). These are more likely tasks requiring encoding and association of events separated by time, rather than spatial learning tasks like those developed for the Morris water maze (Shors et al., 2001, 2002). Some impairment in spatial learning can also be detected, when adult neurogenesis is impaired, provided the time factor attains more relevance e.g., long-term retrieval in the water maze over days (Snyder et al., 2005). The behavioral tasks (spatial learning in the water maze and 24 h retrieval) as described in Schurmans et al. (1997) may therefore not be the ideal way to test the role of maturing neurons in learning and memory in $CR^{-/-}$ animals.

Loss of proliferative capacity as shown here for $CR^{-/-}$ mice, may also have additive effects on the hypothesized deficits in LTP and DG-dependent learning and memory tasks. Cells not generated during early postnatal neurogenesis are then lacking at the stage of maturation and integration into the mature network and consequently curtailing the neurogenic reserve of the DG (Kempermann, 2008). We thus hypothesize that such deficits will worsen with age and either *per se* or in concomitance with neurodegenerative challenges will cause severe behavioral impairments much earlier in $CR^{-/-}$ than in WT mice.

ACKNOWLEDGMENTS

We would like to thank Simone Eichenberger, Dr. Sylvie Ducreux and Dr. Zoltan Mészár for technical assistance and W. Blum and Dr. T. Henzi, all from Anatomy, University of Fribourg for the critical reading of the manuscript. We would like to thank Dr. Olivier Raineteau, University of Zurich for the kind gift of TCF-4 antibody. This work was supported by the Swiss National Science Foundation (grant # 130680 to Beat Schwaller).

REFERENCES

Aimone, J. B., Deng, W., and Gage, F. H. (2011). Resolving new memories: a critical look at the dentate gyrus, adult neurogenesis, and pattern separation. *Neuron* 70, 589–596.

Airaksinen, M. S., Eilers, J., Garaschuk, O., Thoenen, H., Konnerth, A., and Meyer, M. (1997). Ataxia and altered dendritic calcium signaling in mice carrying a targeted null mutation of the calbindin D28k gene. *Proc. Natl. Acad. Sci. U.S.A.* 94, 1488–1493.

Altman, J., and Bayer, S. A. (1990a). Migration and distribution of two populations of hippocampal granule cell precursors during the perinatal and postnatal periods. *J. Comp. Neurol.* 301, 365–381.

Altman, J., and Bayer, S. A. (1990b). Mosaic organization of the hippocampal neuroepithelium and the multiple germinal sources of dentate granule cells. *J. Comp. Neurol.* 301, 325–342.

Baimbridge, K. G., Celio, M. R., and Rogers, J. H. (1992). Calcium-binding proteins in the nervous system. *Trends Neurosci.* 15, 303–308.

Ben Abdallah, N. M., Slomianka, L., Vyssotski, A. L., and Lipp, H. P. (2010). Early age-related changes in adult hippocampal neurogenesis in C57 mice. *Neurobiol. Aging* 31, 151–161.

Bilimoria, P. M., de La Torre-Ubieta, L., Ikeuchi, Y., Becker, E. B., Reiner, O., and Bonni, A. (2010). A JIP3-regulated GSK3beta/DCX signaling pathway restricts axon branching. *J. Neurosci.* 30, 16766–16776.

Brandt, M. D., Jessberger, S., Steiner, B., Kronenberg, G., Reuter, K., Bick-Sander, A., von der Behrens, W., and Kempermann, G. (2003). Transient calretinin expression defines early postmitotic step of neuronal differentiation in adult hippocampal neurogenesis of mice. *Mol. Cell. Neurosci.* 24, 603–613.

Brown, J. P., Couillard-Despres, S., Cooper-Kuhn, C. M., Winkler, J., Aigner, L., and Kuhn, H. G. (2003). Transient expression of doublecortin during adult neurogenesis. *J. Comp. Neurol.* 467, 1–10.

Cheron, G., Gall, D., Servais, L., Dan, B., Maex, R., and Schiffmann, S. N. (2004). Inactivation of calcium-binding protein genes induces 160 Hz oscillations in the cerebellar cortex of alert mice. *J. Neurosci.* 24, 434–441.

Clevers, H. (2006). Wnt/beta-catenin signaling in development and disease. *Cell* 127, 469–480.

Deng, W., Saxe, M. D., Gallina, I. S., and Gage, F. H. (2009). Adult-born hippocampal dentate granule cells undergoing maturation modulate learning and memory in the brain. *J. Neurosci.* 29, 13532–13542.

Esposito, M. S., Piatti, V. C., Laplagne, D. A., Morgenstern, N. A., Ferrari, C. C., Pitossi, F. J., and Schinder, A. F. (2005). Neuronal differentiation in the adult hippocampus recapitulates embryonic development. *J. Neurosci.* 25, 10074–10086.

Farre-Castany, M. A., Schwaller, B., Gregory, P., Barski, J., Mariethoz, C., Eriksson, J. L., Tetko, I. V., Wolfer, D., Celio, M. R., Schmutz, I., Albrecht, U., and Villa, A. E. (2007). Differences in locomotor behavior revealed in mice deficient for the calcium-binding proteins parvalbumin, calbindin D-28k or both. *Behav. Brain Res.* 178, 250–261.

Faulkner, R. L., Jang, M. H., Liu, X. B., Duan, X., Sailor, K. A., Kim, J. Y., Ge, S., Jones, E. G., Ming, G. L., Song, H., and Cheng, H. J. (2008). Development of hippocampal mossy fiber synaptic outputs by new neurons in the adult brain. *Proc. Natl. Acad. Sci. U.S.A.* 105, 14157–14162.

Galceran, J., Miyashita-Lin, E. M., Devaney, E., Rubenstein, J. L., and Grosschedl, R. (2000). Hippocampus development and generation of dentate gyrus granule cells is regulated by LEF1. *Development* 127, 469–482.

Ge, S., Goh, E. L., Sailor, K. A., Kitabatake, Y., Ming, G. L., and Song, H. (2006). GABA regulates synaptic integration of newly generated neurons in the adult brain. *Nature* 439, 589–593.

Ge, S., Sailor, K. A., Ming, G. L., and Song, H. (2008). Synaptic integration and plasticity of new neurons in the adult hippocampus. *J. Physiol.* 586, 3759–3765.

Gulyas, A. I., and Freund, T. F. (1996). Pyramidal cell dendrites are the primary targets of calbindin D28k-immunoreactive interneurons in the hippocampus. *Hippocampus* 6, 525–534.

Gurden, H., Schiffmann, S. N., Lemaire, M., Bohme, G. A., Parmentier, M., and Schurmans, S. (1998). Calretinin expression as a critical component in the control of dentate gyrus long-term potentiation induction in mice. *Eur. J. Neurosci.* 10, 3029–3033.

Henze, D. A., and Buzsaki, G. (2007). Hilar mossy cells: functional identification and activity *in vivo*. *Prog. Brain Res.* 163, 199–216.

Ino, H., and Chiba, T. (2000). Expression of proliferating cell nuclear antigen (PCNA) in the adult and developing mouse nervous system. *Brain Res. Mol. Brain Res.* 78, 163–174.

Jagasia, R., Steib, K., Englberger, E., Herold, S., Faus-Kessler, T., Saxe, M., Gage, F. H., Song, H., and Lie, D. C. (2009). GABA-cAMP response element-binding protein signaling regulates maturation and survival of newly generated neurons in the adult hippocampus. *J. Neurosci.* 29, 7966–7977.

Jin, J., Suzuki, H., Hirai, S., Mikoshiba, K., and Ohshima, T. (2010). JNK phosphorylates Ser332 of doublecortin and regulates its function in neurite extension and neuronal migration. *Dev. Neurobiol.* 70, 929–942.

Kempermann, G. (2008). The neurogenic reserve hypothesis: what is adult hippocampal neurogenesis good for? *Trends Neurosci.* 31, 163–169.

Kempermann, G. (2011). Seven principles in the regulation of adult neurogenesis. *Eur. J. Neurosci.* 33, 1018–1024.

Kempermann, G., Kuhn, H. G., and Gage, F. H. (1997). Genetic influence on neurogenesis in the dentate gyrus of adult mice. *Proc. Natl. Acad. Sci. U.S.A.* 94, 10409–10414.

Knoth, R., Singec, I., Ditter, M., Pantazis, G., Capetian, P., Meyer, R. P., Horvat, V., Volk, B., and Kempermann, G. (2010). Murine features of neurogenesis in the human hippocampus across the lifespan from 0 to 100 years. *PLoS One* 5:e8809. doi: 10.1371/journal.pone.0008809

Kuwabara, T., Hsieh, J., Muotri, A., Yeo, G., Warashina, M., Lie, D. C., Moore, L., Nakashima, K., Asashima, M., and Gage, F. H. (2009). Wnt-mediated activation of NeuroD1 and retro-elements during adult neurogenesis. *Nat. Neurosci.* 12, 1097–1105.

Li, G., and Pleasure, S. J. (2005). Morphogenesis of the dentate gyrus: what we are learning from mouse mutants. *Dev. Neurosci.* 27, 93–99.

Lie, D. C., Colamarino, S. A., Song, H. J., Desire, L., Mira, H., Consiglio, A., Lein, E. S., Jessberger, S., Lansford, H., Dearie, A. R., and Gage, F. H. (2005). Wnt signalling regulates adult hippocampal neurogenesis. *Nature* 437, 1370–1375.

Mathews, M. B., Bernstein, R. M., Franza, B. R. Jr., and Garrels, J. I. (1984). Identity of the proliferating cell nuclear antigen and cyclin. *Nature* 309, 374–376.

Merz, K., Herold, S., and Lie, D. C. (2011). CREB in adult neurogenesis–master and partner in the development of adult-born neurons? *Eur. J. Neurosci.* 33, 1078–1086.

Michaelidis, T. M., and Lie, D. C. (2008). Wnt signaling and neural stem cells: caught in the Wnt web. *Cell Tissue Res.* 331, 193–210.

Ming, G. L., and Song, H. (2011). Adult neurogenesis in the mammalian brain: significant answers and significant questions. *Neuron* 70, 687–702.

Miyachi, K., Fritzler, M. J., and Tan, E. M. (1978). Autoantibody to a nuclear antigen in proliferating cells. *J. Immunol.* 121, 2228–2234.

Mongiat, L. A., Esposito, M. S., Lombardi, G., and Schinder, A. F. (2009). Reliable activation of immature neurons in the adult hippocampus. *PLoS One* 4:e5320. doi: 10.1371/journal.pone.0005320

Moreno, H., Burghardt, N. S., Vela, D., Mascotti, J., Hua, F., Fenton, A. A., Schwaller, B., and Small, S. A. (2011). Reductions in the calcium-buffering protein calbindin correlate with age-related hippocampal metabolic decline. *Hippocampus*. doi: 10.1002/hipo.20957. [Epub ahead of print].

Plumpe, T., Ehninger, D., Steiner, B., Klempin, F., Jessberger, S., Brandt, M., Romer, B., Rodriguez, G. R., Kronenberg, G., and Kempermann, G. (2006). Variability of doublecortin-associated dendrite maturation in adult hippocampal neurogenesis is independent of the regulation of precursor cell proliferation. *BMC Neurosci.* 7, 77.

Schiffmann, S. N., Cheron, G., Lohof, A., D'alcantara, P., Meyer, M., Parmentier, M., and Schurmans, S. (1999). Impaired motor coordination and Purkinje cell excitability in mice lacking calretinin. *Proc. Natl. Acad. Sci. U.S.A.* 96, 5257–5262.

Schurmans, S., Schiffmann, S. N., Gurden, H., Lemaire, M., Lipp, H. P., Schwam, V., Pochet, R., Imperato, A., Bohme, G. A., and Parmentier, M. (1997). Impaired long-term potentiation induction in dentate gyrus of calretinin-deficient mice. *Proc. Natl. Acad. Sci. U.S.A.* 94, 10415–10420.

Schwaller, B. (2009). The continuing disappearance of "pure" Ca^{2+} buffers. *Cell. Mol. Life Sci.* 66, 275–300.

Schwaller, B. (2010). Cytosolic Ca^{2+} buffers. *Cold Spring Harb. Perspect. Biol.* 2, a004051.

Schwaller, B., Tetko, I. V., Tandon, P., Silveira, D. C., Vreugdenhil, M.,

Henzi, T., Potier, M. C., Celio, M. R., and Villa, A. E. (2004). Parvalbumin deficiency affects network properties resulting in increased susceptibility to epileptic seizures. *Mol. Cell. Neurosci.* 25, 650–663.

Shors, T. J., Miesegaes, G., Beylin, A., Zhao, M., Rydel, T., and Gould, E. (2001). Neurogenesis in the adult is involved in the formation of trace memories. *Nature* 410, 372–376.

Shors, T. J., Townsend, D. A., Zhao, M., Kozorovitskiy, Y., and Gould, E. (2002). Neurogenesis may relate to some but not all types of hippocampal-dependent learning. *Hippocampus* 12, 578–584.

Snyder, J. S., Hong, N. S., Mcdonald, R. J., and Wojtowicz, J. M. (2005). A role for adult neurogenesis in spatial long-term memory. *Neuroscience* 130, 843–852.

Stadler, F., Schmutz, I., Schwaller, B., and Albrecht, U. (2010). Lack of calbindin-D28k alters response of the murine circadian clock to light. *Chronobiol. Int.* 27, 68–82.

Teo, J. L., and Kahn, M. (2010). The Wnt signaling pathway in cellular proliferation and differentiation: a tale of two coactivators. *Adv. Drug Deliv. Rev.* 62, 1149–1155.

Teo, J. L., Ma, H., Nguyen, C., Lam, C., and Kahn, M. (2005). Specific inhibition of CBP/beta-catenin interaction rescues defects in neuronal differentiation caused by a presenilin-1 mutation. *Proc. Natl. Acad. Sci. U.S.A.* 102, 12171–12176.

Toni, N., and Sultan, S. (2011). Synapse formation on adult-born hippocampal neurons. *Eur. J. Neurosci.* 33, 1062–1068.

Treves, A., Tashiro, A., Witter, M. E., and Moser, E. I. (2008). What is the mammalian dentate gyrus good for? *Neuroscience* 154, 1155–1172.

von Bohlen Und Halbach, O. (2011). Immunohistological markers for proliferative events, gliogenesis, and neurogenesis within the adult hippocampus. *Cell Tissue Res.* 345, 1–19.

Zhou, C. J., Zhao, C., and Pleasure, S. J. (2004). Wnt signaling mutants have decreased dentate granule cell production and radial glial scaffolding abnormalities. *J. Neurosci.* 24, 121–126.

Conflict of Interest Statement: The authors declare that the research was conducted in the absence of any commercial or financial relationships that could be construed as a potential conflict of interest.

Received: 20 February 2012; paper pending published: 09 March 2012; accepted: 05 April 2012; published online: 23 April 2012.

*Citation: Todkar K, Scotti AL and Schwaller B (2012) Absence of the calcium-binding protein calretinin, not of calbindin D-28k, causes a permanent impairment of murine adult hippocampal neurogenesis. Front. Mol. Neurosci. **5**:56. doi: 10.3389/fnmol.2012.00056*

frontiers in
MOLECULAR NEUROSCIENCE

ORIGINAL RESEARCH ARTICLE
published: 06 August 2012
doi: 10.3389/fnmol.2012.00084

Novel insights into the distribution and functional aspects of the calcium binding protein Secretagogin from studies on rat brain and primary neuronal cell culture

Magdalena Maj*[1], *Ivan Milenkovic*[2,3], *Jan Bauer*[4], *Tord Berggård*[5], *Martina Veit*[2], *Aysegül Ilhan-Mutlu*[1], *Ludwig Wagner*[1] *and Verena Tretter*[2]

[1] *Department of Internal Medicine III, Division of Nephrology and Dialysis, Medizinische Universität Wien, Vienna, Austria*
[2] *Department of Biochemistry and Molecular Biology, Center for Brain Research, Medizinische Universität Wien, Vienna, Austria*
[3] *Institute of Neurology, Medizinische Universität Wien, Vienna, Austria*
[4] *Department of Neuroimmunology, Center for Brain Research, Medizinische Universität Wien, Vienna, Austria*
[5] *Alligator Bioscience, Lund, Sweden*

Edited by:
Michael R. Kreutz, Leibniz-Institute for Neurobiology, Germany

Reviewed by:
Michael R. Kreutz, Leibniz-Institute for Neurobiology, Germany
Beat Schwaller, University of Fribourg, Switzerland

***Correspondence:**
Verena Tretter, Department for Biochemistry and Molecular Biology, Center for Brain Research, Medizinische Universität Wien (Medical University Vienna), Spitalgasse 4, 1090 Vienna, Austria.
e-mail: eva.tretter@meduniwien.ac.at

Secretagogin is a calcium binding protein (CBP) highly expressed in neuroendocrine cells. It has been shown to be involved in insulin secretion from pancreatic beta cells and is a strong candidate as a biomarker for endocrine tumors, stroke, and eventually psychiatric conditions. Secretagogin has been hypothesized to exert a neuroprotective role in neurodegenerative diseases like Alzheimer's disease. The expression pattern of Secretagogin is not conserved from rodents to humans. We used brain tissue and primary neuronal cell cultures from rat to further characterize this CBP in rodents and to perform a few functional assays *in vitro*. Immunohistochemistry on rat brain slices revealed a high density of Secretagogin-positive cells in distinct brain regions. Secretagogin was found in the cytosol or associated with subcellular compartments. We tested primary neuronal cultures for their suitability as model systems to further investigate functional properties of Secretagogin. These cultures can easily be manipulated by treatment with drugs or by transfection with test constructs interfering with signaling cascades that might be linked to the cellular function of Secretagogin. We show that, like in pancreatic beta cells and insulinoma cell lines, also in neurons the expression level of Secretagogin is dependent on extracellular insulin and glucose. Further, we show also for rat brain neuronal tissue that Secretagogin interacts with the microtubule-associated protein Tau and that this interaction is dependent on Ca^{2+}. Future studies should aim to study in further detail the molecular properties and function of Secretagogin in individual neuronal cell types, in particular the subcellular localization and trafficking of this protein and a possible active secretion by neurons.

Keywords: Secretagogin, calcium binding proteins, neuronal cell marker, insulin

INTRODUCTION

Calcium (Ca^{2+}) is a universal second messenger, which plays a crucial role in signal transduction in many fundamental physiological processes. In the central nervous system (CNS) calcium signaling is utilized by neurons to control membrane excitability, neurotransmitter release, gene expression, cellular growth, differentiation, and cell death. Different variants of high transient and local Ca^{2+} concentrations in neurons play an important role in information processing (Niggli and Shirokova, 2007). Intracellular Ca^{2+} waves are also observed in glia cells, a finding that currently reshapes the known role of glia cells from neuronal supporters to active signal transmitting cells (Dityatev and Rusakov, 2011).

Calcium binding proteins (CBPs) therefore play a pivotal role in sensing and transducing these signals into cellular responses like the modulation of ion channel or receptor function, enzyme activity, neurotransmitter release, and many more (Yanez et al., 2012). The huge number of identified CBPs relates to their different roles and substrate specificity. N-terminal myristoylation and specific protein–protein interactions mediate their subcellular targeting and substrate specificity. Calcium also plays an important role in the secretory pathway of neurons regulating processes like vesicle budding and fusion, vesicle trafficking between Golgi stacks, TGN sorting, and the regulation of SNARE proteins. Some CBPs like calmodulin are possibly present in all neuronal cell types. Other known neuronal CBPs (nCBPs) are present only in certain subpopulations of neurons (Mikhaylova et al., 2011). From the functional point of view two major groups of nCBPs have traditionally been distinguished: Ca^{2+} buffers, which bind Ca^{2+} with high affinity without undergoing major conformational changes, and Ca^{2+} sensors (NCS), which need higher Ca^{2+} pulses for activation and undergo substantial conformational changes upon binding to Ca^{2+}. These activated states lead to the exposure of

Abbreviations: CBP, calcium binding protein; nCBP, neuronal calcium binding protein; NCS, neuronal calcium sensor; SCGN, Secretagogin (human); Scgn, Secretagogin (rat).

interaction motifs with downstream targets and frequently initiate signal transduction cascades (Burgoyne and Haynes, 2012). One of the best-known and well-studied examples also in this respect is again calmodulin. The distinction between calcium buffers and calcium sensors is still valid from a functional viewpoint, but it becomes increasingly difficult to assign individual CBPs selectively to one or the other group. The more experimental evidence is available, the more it becomes clear that CBPs might have dual or more functional properties (Schwaller, 2009; Mikhaylova et al., 2011).

A large body of evidence has indicated that unbalanced Ca^{2+} homeostasis contributes to the development of neurological and neurodegenerative diseases (Braunewell, 2005; Yu et al., 2009; Demuro et al., 2010; Hermes et al., 2010; Camandola and Mattson, 2011).

Nonetheless, several mechanisms have been developed to control Ca^{2+} homeostasis and to prevent cellular damage. Among these are also nCBPs, which have been reported to display altered levels in neurodegenerative disorders (Steiner et al., 2011). Apart from this role in homeostasis, a major task of many nCBPs is in active signal transduction, where our current knowledge is restricted to only few representatives and is still frequently rudimentary.

Most nCBPs exhibit a tissue specific expression pattern in the mammalian brain. Therefore, they have been used as cell type specific markers before other ways of identification of cell types in the CNS became available (Klausberger et al., 2003). Novel nCBPs are discovered on a regular basis mostly by proteomic screens, each of them with different developmental and cell type specific expression patterns.

A more recently identified CBP is Secretagogin, a multi-faceted protein that is highly expressed in pancreatic beta cells, cells of the gastrointestinal tract as well as in neuroendocrine cells of the CNS (Wagner et al., 2000; Gartner et al., 2001; Mulder et al., 2009). Secretagogin contains six EF-hand motifs as potential Ca^{2+} binding sites, some of which seem to be non-functional. Structural analysis have revealed some similarities with the Ca^{2+} sensor calmodulin (Bitto et al., 2009). Secretagogin undergoes conformational changes upon Ca^{2+} binding indicating a potential role as a Ca^{2+} sensor in specialized cells (Rogstam et al., 2007). Broad screenings by protein arrays have led to the identification of a variety of Secretagogin interaction partners that are associated with vesicle fusion (like SNAP-23, SNAP-25, ARFGAP2, DOC2alpha, rootletin), trafficking (tubulin, KIF5B), enzymatic activity (DDAH-2, ATP-synthase), and one onco-protein (myeloid leukemia factor 2; Rogstam et al., 2007;Bauer et al., 2011a,b). Secretagogin has received considerable attention due to its significance in insulin secretion from pancreatic beta cells and as a potential biomarker for the diagnosis of stroke and distinct tumors of endocrine origin such as adenocarcinomas of the stomach, pancreas, prostate, colorectum, kidney, and lung small cell carcinoma in the blood of patients (Gartner et al., 2001; Lai et al., 2006; Adolf et al., 2007; Ilhan et al., 2011; Zurek and Fedora, 2012). Albeit performed studies on Secretagogin its function is still unclear. By *in silico* gene analysis it was previously found that the Secretagogin gene-promoter sequence might respond to glucose (Skovhus et al., 2006).

Human and mouse brain has been examined to some extent for Secretagogin expression in previous studies (Attems et al., 2008;Mulder et al., 2009, 2010). As the regional expression pattern turned out to differ significantly between species, we now chose to characterize the expression of Secretagogin in rat brain to compare with previous studies on mouse and human brain. In order to perform functional studies we were looking for a primary cell culture system that expresses endogenous Secretagogin at a high level and chose the well-established primary culture system of rat embryonic hippocampal and cortical neurons for *in vitro* studies to get a hint of the expression dynamics and functional aspects of the protein. The tight connection between glucose and insulin, which is also a basic neuronal trophic factor, let us ask, whether insulin and glucose levels influence the expression of Secretagogin in neuronal cells.

Our cell culture system proved to be a suitable model system to perform more functional assays in the future, last but not least, because interference of signaling cascades by drug treatment and tracking the fate and trafficking of proteins by transfection of these neurons with test constructs (like dominant negative or non-functional variants of proteins, fluorescent tagged versions of the protein, and subcellular markers) is technically easy to perform and analysis by common biochemical and cell biological techniques promises relevant results. The *in vitro* studies can be extended to neuronal cultures derived from other brain areas that express high levels of endogenous Secretagogin in order to investigate cell type specific functional similarities or differences of this protein.

Since the recent clinical studies on Secretagogin revealed its potential implication as a novel blood and cerebrospinal fluid biomarker, further knowledge on this protein is of major interest also from the medical point of view.

MATERIALS AND METHODS

PRODUCTION AND PURIFICATION OF SECRETAGOGIN PROTEIN

Human and rat Secretagogin protein was produced and purified the same way as described previously in Wagner et al. (2000) and Gartner et al. (2007), respectively. In brief, the entire coding sequence of the human/rat Secretagogin gene was amplified by PCR using primers with *Eco*RI and *Bam*HI at the flanking end and subsequently cloned into the pGEX-1λT expression vector. The coding sequence for Secretagogin in this construct is located downstream of the coding sequence for glutathione *S*-transferase separated from GST by a thrombin cleavage site. These constructs (GST-SCGN and GST-Scgn) were transformed into *Escherichia coli* BL21, and after colony selection transformed bacteria were grown overnight at 37˚C. The next morning the culture was diluted 1:5 and expression of the fusion proteins was induced by addition of isopropyl-β-D-thiogalactoside (final conc. 10 mM) followed by incubation for 3 h at 31˚C on a rotating shaker. Afterwards the bacteria were pelleted, sonicated in ice-cold PBS containing 0.1% Triton X-100, and a mix of protease inhibitors. The bacterial lysate was precleared by centrifugation at 12,000 rpm for 10 min and equilibrated glutathione-Sepharose 4B beads were added to the obtained supernatant and mixed for 30 min at 4˚C under constant rotation. Following three washes of protein-bound beads with cold PBS, full-length Secretagogin was released by thrombin

cleavage. The reaction was incubated for 3 h at RT on a rotating platform, centrifuged at 1500 rpm, and the resulting supernatant containing Secretagogin (human or rat) was tested by SDS-PAGE gel-electrophoresis in order to evaluate the presence of full-length protein. After protein quantification the purified Secretagogin protein was frozen at −80˚C until further use.

ANTIBODIES

Rabbit anti-SCGN antiserum was generated against recombinant Secretagogin protein as described previously and cross-reacts with the rat ortholog (Wagner et al., 2000; Gartner et al., 2001). We used dilutions of 1:1000 for immunohistochemistry and 1:5000 for immunoblotting.

The following commercial antibodies were used for immunofluorescence or other techniques as indicated: rabbit anti-pan-TAU (Cat. No. A 0024, DakoCytomation, Denmark, Glostrup) dil. 1:5000 for immunoblotting; mouse anti-Parvalbumin (Cat. No. PVG214, Swant, Switzerland) dil. 1:3000; mouse anti-Calbindin D28k (Cat. No.300, Swant, Switzerland) dil. 1:10,000; mouse anti-Calretinin (Cat. No. 6B3, Swant, Switzerland) dil. 1:5000; mouse anti-GRP78 (which was a kind gift from the lab of Prof. Johannes Berger) dil. 1:100; mouse anti-GM130 (Cat. No. 560257, BD Biosciences, Franklin Lakes, NJ) dil. 1:100; mouse monoclonal anti-β-actin (AC-15; Cat. No. NB600-501, Novus Biologicals, Littleton, CO, USA) for Western blot controls dil. 1:5000. Secondary antibodies and nuclear staining: DyLight488 goat anti-mouse (Cat. No. 115-485-1460, Jackson ImmunoResearch, Suffolk, UK) dil. 1:400; DyLight488 donkey anti-rabbit (Cat. No. 711-485-1520, Jackson ImmunoResearch) dil. 1:400; Cy3 goat anti-rabbit (Cat. No. 111-166-003, Jackson ImmunoResearch) dil. 1:500; DyLight649 donkey anti-guinea pig (Cat. No. 706-495-148, Jackson ImmunoResearch) dil. 1:400; DyLight649 donkey anti-rabbit (Cat. No. 111-196-003, Jackson ImmunoResearch) dil. 1:400; TO-PRO (Cat. no. T-3605, Invitrogen) dil. 1:500; DAPI (Sigma Cat. No. D8417) final conc. 1 μg/ml in PBS.

RABBIT ANTI-SCGN ANTISERUM SPECIFICITY TEST

In order to confirm specificity of our rabbit anti-human SCGN antiserum against rat-Scgn, the recombinant purified protein (rat-Scgn, 267 amino acid residues) was pre-incubated with anti-SCGN antibody. The reaction was performed at room temperature for 2 h. The resultant solution containing antibody/antigen complexes was centrifuged at 13,000 rpm for 15 min at 4˚C. The supernatant was then used in parallel with native untreated antibody for staining of sections of fixed rat brain. Immunofluorescence staining and imaging was performed as indicated below. The experiment was carried out in duplicates.

Further evidence for antiserum specificity was obtained from a stable cell line expressing human Secretagogin. Jurkat cells were transfected with full-length human Secretagogin encoding plasmid pZeoSV2. Cells, that had stably incorporated the plasmid in the genome and were expressing the protein at a high level were chosen for further experiments.

Protein G-Sepharose beads were used to bind rabbit anti-Scgn antiserum. After washing, beads were incubated with lysates from sham-transfected and SCGN-expressing Jurkat cells. Following three washing steps with 0.1% Tween 20 in PBS (TPBS), beads were eluted in 50 mM triethanolamine, 150 mM NaCl, 0.1% Tween 20, pH 11.2. Eluted fractions were neutralized and loaded onto a 10% SDS-PAGE gel and transferred to nitrocellulose using a semi-dry blotting device. Blotted membranes were blocked and exposed to biotinylated rabbit anti-SCGN antibody followed by incubation with Streptavidine/HRP for 30 min. Each incubation step was followed by two washes with TPBS for 10 min. The blot was finally developed with chemiluminescent reagent and bands were visualized with a Lumi Imager F1.

IMMUNOHISTOCHEMISTRY OF RAT BRAIN SLICES

Six-week-old rats were deeply anesthetized with Equithesin and perfused transcardially with 0.9% NaCl, followed by a mixture of 4% paraformaldehyde, and 15% picric acid in 0.1 M phosphate buffer (PB; pH 7.2–7.4) using a peristaltic pump. Brains were left *in situ* for 10–15 min, removed, and kept in 0.1 M PB with 0.05% sodium azide for a few days at 4˚C. Serial coronal sections of 50 μm were cut on the vibratome. Sections were kept in PB containing 0.05% sodium azide at 4˚C until staining.

Immunofluorescence experiments were carried out according to previously published procedures (Klausberger et al., 2003; Vasiljevic et al., 2011). Briefly, free-floating sections were incubated in 0.1% Triton X-100/PB for 30 min, blocked in 20% normal horse serum diluted in Tris-buffered saline (50 mM Tris, pH 7.2, 0.85% NaCl) for 2 h, and then incubated in a solution containing a mixture of primary antibodies (rabbit anti-Secretagogin antibody, dil. 1:5000; mouse monoclonal anti-Parvalbumin antibody; mouse monoclonal anti-Calbindin D28k antibody; mouse monoclonal anti-Calretinin antibody) for 48 h at 4˚C. Sections were washed and subsequently incubated for 4 h at room temperature with appropriate secondary antibodies conjugated either to Alexa Fluor 488 (anti-rabbit; Invitrogen Molecular Probes, dil. 1:1000) or Cy3 (anti-mouse; Jackson ImmunoResearch Laboratories, dil. 1:400). All antibodies were diluted in TBS containing 0.1% Triton X-100 and 1% normal horse serum. After washing in TBS (50 mM Tris buffer, pH 7.4), sections were mounted in Aqua PolyMount (Polysciences Europe, Eppelheim, Germany), and left to polymerize at 4˚C over night. Sections were examined with a Leica TCS SP5 II confocal microscope (Leica Microsystems GmbH, Wetzlar, Germany). All antibodies were tested for optimal dilution, and secondary antibodies were tested for cross-reactivity and non-specific staining.

IMMUNOHISTOCHEMISTRY OF HUMAN SAMPLES

Brain tissue obtained from routine autopsy was fixed in 4% Formalin and embedded in paraffin as a routine procedure for the process of pathological specimens. Tissue sections of 4 mm were deparaffinized with xylol, passed through a graded ethanol series and finally washed in distilled water. Endogenous peroxidase was blocked with 3% H_2O_2 in methanol for 10 min. Following antigen retrieval in citrate buffer, pH 6.0 for 60 min at 96˚C, slides were washed in Tris-buffered saline (TBS), and blocked with 10% FCS for 10 min. The primary antibody was applied for 2 h. After washing the slide for 10 min in PBS the secondary antibody was applied and incubated for 1.5 h at RT. Following two washing steps for 10 min at RT in PBS, the chromogenic substrate DAB was

applied (EnVision ™Kit DakoCytomation K5007) and the reaction was stopped after 10 min by washing the slide with tap water. As a counterstain Mayer's Hemalaun was used for 30 s, which was washed off by tap water. Finally, slides were exposed to 0.45 M HCl in 70% EtOH followed by a further wash in water. Sections were dehydrated in acetyl butyrate and mounted with a coverslip. Images were taken using a Leica Aristoplan microscope.

PRIMARY RAT CELL CULTURE

Primary neuronal cultures were prepared from rat E18 embryos (pregnant Sprague-Dawley rats were purchased from Charles River, Germany). Procedures were carried out in accordance with animal care guidelines of the Medical University of Vienna, Austria. Cultures were essentially prepared as neuron/glia co-cultures as described previously with modifications (Brewer et al., 1993). Hippocampus and cortex were dissected and individually trypsinized at 37˚C in a 10 mM HEPES buffered Hank's balanced salt solution (HBSS; GIBCO Life Technologies, NY, USA). Tissues were washed three times with ice-cold HBSS and dissociated by trituration. Cortical neurons were additionally sieved through 100 and 70 μm filters (Falcon). Neurons were plated at a density of ∼52,500 cells/cm^2 into 24-well culture plates. For Western blot analysis and real-time quantitative PCR (RT-qPCR) six-well culture plates were seeded at the same density. Cells were left to attach overnight in MEM medium containing 10% horse serum, 1 mM sodium pyruvate (all from GIBCO), 1.2% D-glucose (Sigma), 100 U/ml penicillin together with 100 μg/ml streptomycin (GIBCO). All surfaces were coated with a solution of 0.5 mg/ml poly-L-lysine (MW 30,000–70,000; Sigma) in 0.05 M sodium borate, pH 8.0 overnight at room temperature and were washed thoroughly with distilled water before adding the culture medium. Cultures were maintained in an incubator with 5% CO_2 at 37˚C during the whole culturing period. After attachment of cells, the medium was replaced by serum-free Neurobasal medium (GIBCO) supplemented with 2% v/v B-27 (Invitrogen), 2 mM glutamine (GIBCO), 1.2% D-glucose (Sigma), 100 U/ml penicillin, and 100 μg/ml streptomycin.

Hippocampal neurons were used for experiments mostly between 14 and 22 DIV (days *in vitro*), whereas cortical neurons were used at 7 DIV.

CELL CULTURE CONDITIONS FOR STUDIES WITH INSULIN

Hippocampal neurons were grown in six-well culture plates either in normal Neurobasal medium supplemented with 2%v/v B-27, 2 mM glutamine, 1.2% D-glucose, 100 U/ml penicillin and 100 μg/ml streptomycin, or in insulin-free medium consisting of Neurobasal medium and all ingredients such as indicated above, except commercially available insulin-free B-27 (Cat. No. 05-0129SA, GIBCO). For insulin deprivation experiments neurons were initially grown in standard Neurobasal medium in order to support optimal growth. At 18 DIV, one third of medium was replaced with pre-warmed insulin-free medium. This procedure was repeated on the following 2 days. On the fourth day neurons were harvested using TRIzol reagent (Cat. No. T9424, Sigma, Germany) to stabilize the mRNA and samples were frozen at −80˚C until further proceeding. For insulin boost experiments 21 DIV neurons grown in standard Neurobasal medium were challenged once with 100 μg/ml of insulin (Cat. No. I9278, Sigma, Germany) added to the growth medium for 1, 4, and 24 h. After the individual time periods, neurons were again harvested with TRIzol reagent. Additionally, we cultured hippocampal neurons in insulin-free medium from 0 DIV onward in comparison with the same batch of cells in standard growth medium and harvested the cells at 21 DIV using TRIzol reagent.

ISOLATION OF mRNA FROM RODENT AND HUMAN BRAIN SAMPLES

Three rats were sacrificed and their brains were isolated. Tissues were immediately shock frozen in liquid nitrogen. Subsequently, different brain regions (cerebellum, hippocampus, striatum, frontal cortex, parietal cortex, olfactory bulb) were dissected under the microscope.

For human samples tissues were obtained from the Pathology Department, Medical University of Vienna, Austria in agreement with the Ethical Committee of the Medical University of Vienna (EK: 987/2010). Samples were from three male individuals 62, 73, and 70 years of age, who have died of lung cancer, chronic obstructive airway disease and myocardial infarction, respectively.

About 30 mg of each human brain tissue (cerebellum, frontal cortex, parietal cortex, occipital lobe, temporal cortex, hippocampus, olfactory bulb, thalamus, hypothalamus, stem ganglia) was put into TRIzol reagent and RNA was isolated as described below.

REAL-TIME QUANTITATIVE PCR

RNA (from neuronal cells or brain tissues stabilized with TRIzol reagent) was extracted using chloroform-isopropanol with phase-separation by centrifugation. Subsequently, 1 μg of total RNA was reverse-transcribed (1 h, 55˚C) using MLV reverse transcriptase (Invitrogen). The diluted (1:3) cDNA was used as a template together with TaqMan 2xMasterMix (Lot: N10545, Applied Biosystems) and with TaqMan probes specific for rat-Scgn (No. Rn01529973_m1), human-SCGN (No. Hs00907373_m1), rat-Tau (No: Rn01495715_m1), rat-SNAP-25 (No. Rn00578534_m1), rat-Syt-1 (No. Rn00436852_m1), rat-Sgk (N0. Rn00570285_m1), and rat-Ins-1 (No: Rn02121433_g1). The RT-qPCR measurement was carried out at the StepOnePlus Fast Real-Time PCR System (Applied Biosystems). Expression values were calculated according to the ΔΔCT method or with calculation of the copy number using rat-Scgn plasmid as standard. As housekeeping genes, the TaqMan Ubc probe (No. Rn01789812_g1) was used for samples from neuronal cell cultures and the Gapdh probe (No: Rn01775763_g1 for rat, Hs02758991_g1 for human) was used in brain samples.

GST PULL-DOWN ASSAY FROM RAT BRAIN

GST pull-down assays were performed essentially in the same manner as described in (Maj et al., 2010). Briefly, human GST-SCGN fusion protein or GST only was loaded onto Glutathione-Sepharose 4B beads (Cat. No.17-0756-01, Healthcare Biosciences). Whole rat brain tissue was homogenized and 200 mg was lysed in 2000 μl TPBS including 1 mM PMSF in Lysing Matrix A (MP Biomedicals Cat.nr. 6910-050) tubes using the Precellys 24 lysis and homogenization device set at 5000 for 20 s. The resultant lysate was centrifuged at 12,000 × *g* for 10 min and incubated with GST- and GST-SCGN-Sepharose beads according to Maj et al. (2010).

In brief, 35 μl of beads were incubated with 400 μl of lysate at 4°C for 90 min under constant rotation. In order to test for calcium dependence of the interaction between Secretagogin and Tau protein, we used different concentrations of EDTA (0, 2.5, 5.0, 7.5, and 10.0 mM) in the lysate upon incubation with GST-SCGN-Sepharose beads. After three washes with TPBS including 1 mM PMSF bound proteins were eluted with 10 mM EDTA. The eluates were then further processed for Western blot analysis. 15% of the lysate used for pull-downs was loaded as input control.

IMMUNOPRECIPITATION

PureProteom protein G magnetic beads (100 μl, Millipore) were washed in PBS and loaded with D24 mAb by incubation at RT for 60 min under constant rotation (negative control: unrelated isotype mAb) and afterwards washed with 0.2 M sodium borate pH 9.0. Antibodies bound to the beads were chemically crosslinked using 40 mM dimethyl pimelidate dihydrochloride (DMP, Sigma) for 1 h at RT. Excess of DMP was neutralized with 0.2 M ethanolamine pH 8.0 followed by washes with PBS. Before use, beads were pre-eluted with 0.1 M glycine pH 2.0.

For immunoprecipitation, antibody-coupled beads were incubated with brain extract (prepared as for GST pull-down experiments) and incubated at 4°C for 2 h under constant rotation. After three washes with TPBS, bound protein was eluted with 100 mM glycine pH 2.0. Eluates were loaded onto SDS-PAGE, transferred onto nitrocellulose and developed with rabbit anti-SCGN and anti-pan-Tau, respectively.

SUBCELLULAR FRACTIONATION ON A SUCROSE GRADIENT

One-hundred milligrams of whole rat tissue were homogenized in 1.7 ml sucrose buffer (250 mM sucrose, 20 mM Tris/HCl pH 7.4, 1 mM EDTA, protease inhibitors). Cell nuclei and large aggregates were pelleted by centrifugation at 10,000 × *g* for 10 min. The entire supernatant was loaded onto a discontinuous sucrose gradient in polyAllomer centrifuge tubes (14 mm × 95 mm, Beckman). Following centrifugation (2 h at 4°C) at 40,000 rpm using a SW40 Ti rotor in a L-80 ultracentrifuge, the gradient was fractionated in 500 μl aliquots using a peristaltic pump starting at the bottom of the tube. Individual fractions were subjected to immunoblotting using antibodies for Scgn, SNAP-25, α-tubulin, and pan-Tau.

RESULTS

EXPRESSION OF SECRETAGOGIN IN THE MAMMALIAN BRAIN

Expression of Secretagogin has been found at the highest level in pancreatic beta cells and in neuroendocrine cells of the CNS (Wagner et al., 2000; Gartner et al., 2001; Attems and Jellinger, 2006; Mulder et al., 2010). Studies on mouse and human brain tissue indicated a varying expression pattern in mice and men. However, until now no detailed comparative analysis of the Secretagogin distribution in mammalian brain has been presented. We used quantitative real-time PCR (RT-qPCR) to measure relative Secretagogin mRNA levels in different major areas of rat brain and compared it to tissue from the corresponding areas in human brain (**Figure 1**). Interestingly, while human brain reveals an expression maximum in the cerebellum (**Figure 1A**), in rat brain by far the highest expression of Secretagogin is found in the olfactory bulb (**Figure 1B**). This is also the case in mouse brain (Mulder et al., 2009). Significant expression of Secretagogin is also found in the hippocampus of humans and rodents confirming previous studies (Gartner et al., 2001; Attems et al., 2007; Mulder et al., 2009). The same pattern translates into differences of protein expression especially with regard to expression maxima in cerebellum and olfactory bulb respectively, which we confirmed by Western blotting also for human and rat brain (Inserts in **Figures 1A,B**). Differences between mRNA levels and protein have been found in other areas with lower expression levels. β-actin was used as internal standard. For all of our immunological studies we used a rabbit polyclonal anti-SCGN antibody generated in our lab. The antibody specificity has been tested for individual applications, like Western blotting, immunocytochemistry of fixed cells in culture, and immunohistochemistry on paraffin-embedded human and rat tissue and paraformaldehyde-fixed rat tissue (**Figures 2A,B**).

CELL TYPE SPECIFIC EXPRESSION OF SECRETAGOGIN IN HUMAN CEREBELLUM AND RAT OLFACTORY BULB

The neuronal circuits and cell identities are well defined in cerebellum and olfactory bulb. In order to investigate the distribution of Secretagogin in the different cell types of human cerebellum and rat olfactory bulb we performed immunohistochemistry from paraffin-embedded slices of the respective tissues. Human cerebellum reveals especially high Secretagogin expression in the molecular layer (**Figure 3A**). Positive neurons have previously been identified as interneurons of the basket and stellate cell type (Gartner et al., 2001). Purkinje cell bodies are faintly staining positive, granule cells are free from intracellular Secretagogin staining, while interneurons of the granule cell layer are Secretagogin-positive (**Figures 3A,C**). A contribution of a small cross-reactivity of our Secretagogin antibody to faint stainings (like in Purkinje cell bodies) cannot be fully excluded.

The outer part of the olfactory bulb is also organized in well defined cell layers. In rat, many neurites (probably dendrites and axons) and some cell bodies stain positive in the glomerular layer and in the external plexiform layer. However, within the granular cell layer mainly cell bodies and only few neurites are Secretagogin-positive. From the routine experience with our antibody we consider the faint staining of mitral cell bodies as slightly positive for Secretagogin. But a staining due to weak cross-reactivity again cannot be fully excluded (**Figures 3B,D**).

HOTSPOTS OF SECRETAGOGIN-POSITIVE CELLS IN SPECIALIZED AREAS OF RAT BRAIN

As previous studies describe Secretagogin in the mouse and human nervous system, we extended our investigations to rat brain. Although both mice and rats are rodents, differences in Secretagogin distribution cannot be excluded. Also, recent studies on mouse focused only on special areas in the mouse brain (Mulder et al., 2009, 2010).

Therefore we stained coronal sections from rat brain with anti-Secretagogin antibody and counterstained with hematoxylin (**Figure 4**). Secretagogin-positive (Scgn+) cells frequently occur in cell clusters in addition to positive cells scattered over larger areas. As described for mouse, also in rats peripheral cell layers of the olfactory bulb are Scgn+. When choosing a more lateral layers in addition to the cell layers described in **Figure 3**,

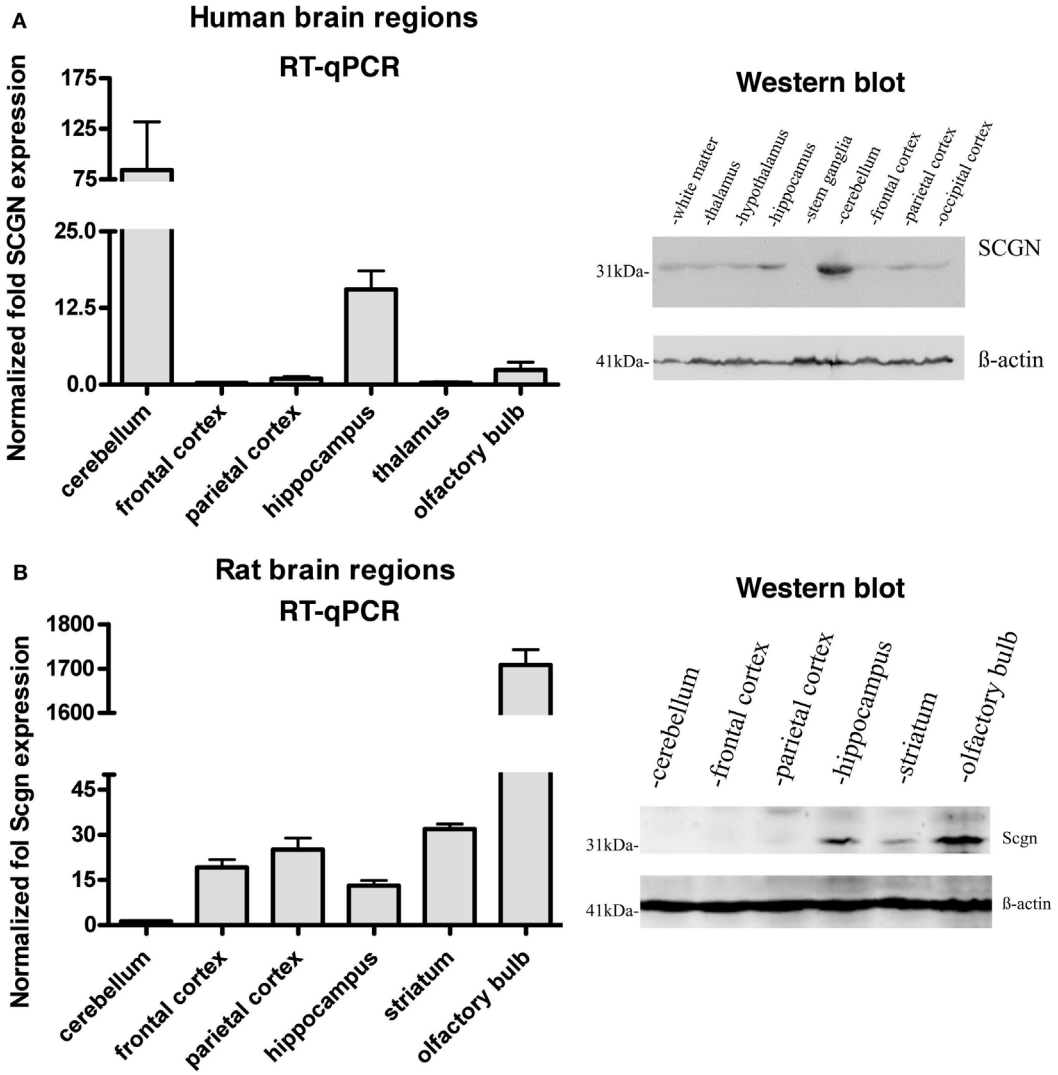

FIGURE 1 | Expression of Secretagogin in different regions of human and rat brain. Tissues from different brain areas were analyzed for relative Secretagogin gene and protein expression by RT-qPCR and Western blotting. **(A)** Human post-mortem tissues from three individuals were analyzed with regard to the following specific brain regions: cerebellum, frontal cortex, parietal cortex, hippocampus, thalamus, and olfactory bulb. Western blot analysis was performed from tissue of white matter, thalamus, hypothalamus, hippocampus, stem ganglia, cerebellum, frontal cortex, parietal cortex, and occipital cortex. Equal protein loading was verified by staining with β-actin antibody. **(B)** Rat brain tissues from three adult rats were dissected and analyzed from cerebellum, frontal cortex, parietal cortex, hippocampus, striatum, and olfactory bulb. A representative Western blot of equal amounts of protein from cerebellum, frontal cortex, parietal cortex, hippocampus, striatum, and olfactory bulb is shown on the right. β-actin immunostaining was again used as loading control.

seemingly unordered patches of strong Scgn+ cells were observed (**Figure 4A**). Moving in caudal direction we found strong staining lining the surface above the optic nerve (**Figure 4B**). Further positive nuclei are the supraoptic nuclei on both sides of the optic chiasm and the suprachiasmatic nuclei of the hypothalamus (**Figure 4C**). In addition some islets of clustered cells can be seen in this figure, which we could not unambiguously attribute to a defined anatomical structure (arrows). A highlighted area is also the paraventricular nucleus (**Figure 4D**). Prominent Secretagogin staining has been observed in hippocampal areas CA1–CA3, with almost no staining in dentate gyrus (**Figure 4E**). A magnification of an area in CA1 reveals staining of hippocampal pyramidal cell bodies and more positive intercalated interneurons as defined later in co-stainings with antibodies for marker proteins in **Figure 5** (**Figure 4E1**). Moving further in caudal direction again accumulations of strongly stained cells were detected in the outer cortex around the posterolateral cortical amygdaloid area (**Figure 4F**). A magnification of the positive cell patch reveals strong staining of neuronal processes in this area (**Figure 4F1**). Further a meshwork of positive processes with some scattered Scgn+ cells is observed in the basal ganglia with caudate putamen shown in (**Figure 4G**). Patches of positive cells are seen at the beginning

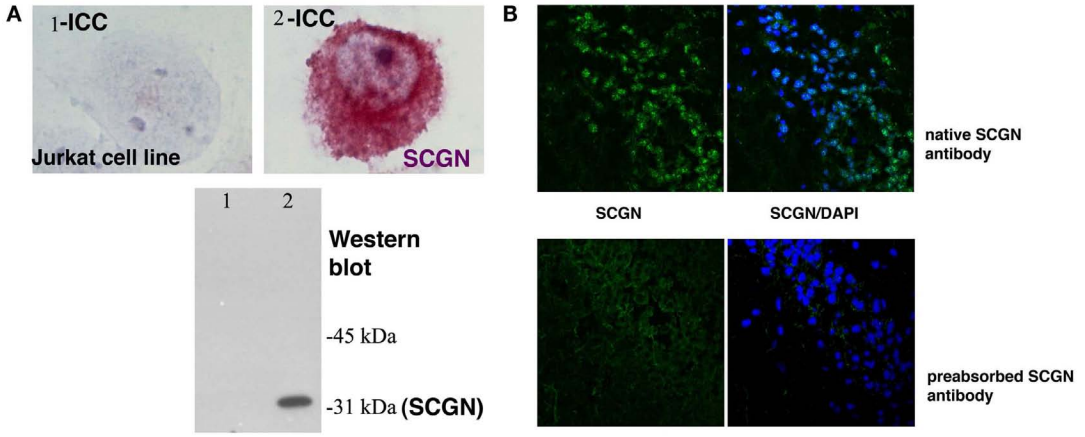

FIGURE 2 | Secretagogin antibody specificity. (A) A Jurkat cell line (1) was stably transfected with human Secretagogin (2). Immunocytochemistry and Western blot analysis from cell lysates reveal the specificity of the antibody in this heterologous cell line for both techniques. **(B)** Secretagogin antibody specificity test on rat brain slices: our Secretagogin antibody was used to stain rat brain slices in the CA1 region of the hippocampus without (upper panel) and with pre-absorption (lower panel) with purified antigen. Secretagogin staining is shown in green and nuclear staining (DAPI) in blue.

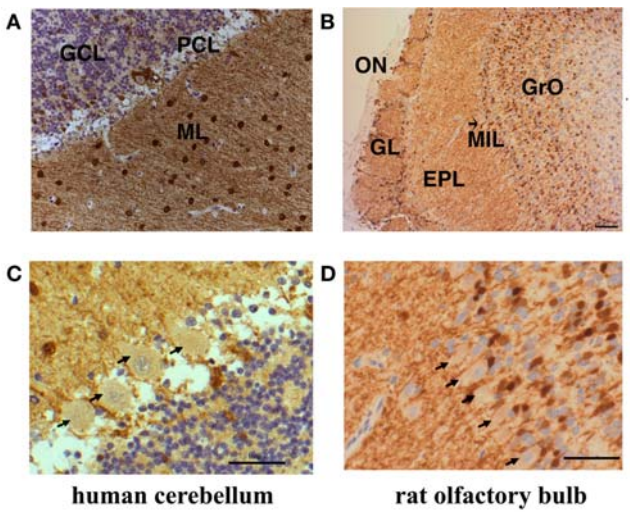

FIGURE 3 | Subcellular distribution of Secretagogin-positive cells in human cerebellum and rat olfactory bulb. Paraffin sections from human cerebellum **(A)** and rat olfactory bulb **(B)** were processed for Secretagogin immunoreactivity (DAB staining in brown) and counterstained with Mayer's Hemalaun (blue). Human cerebellum reveals positive Secretagogin staining of interneurons in the molecular layer (ML) and the granule cell layer (GCL). Granule cells are immuno-negative and Purkinje cells bodies revealed faint positive staining (PCL). Actual expression of Secretagogin in Purkinje cells would need verification by single cell analysis. The rat olfactory bulb shows Secretagogin-positive cells in the glomerular layer (GL), the external plexiform layer (EPL), and the granular cell layer (GrO). The mitral cell bodies (indicated by an arrow, MIL) seem to be very weakly positive. Scale bars: 200 μm. Magnifications of the human Purkinje cell layer and rat mitral cells are shown in **(C,D)** respectively. Principal cells are indicated by arrows. Scale bars: 20 μm.

of the hippocampal formation close to the ventricle. The same figure reveals Scgn+ cells in the habenular region, which is located ventral to the hippocampus, again near the ventricle (**Figure 4H**). The lateral amygdala nucleus reveals also quite a few positive cells (not shown). Two nuclei, arrays of surface lining cells and scattered Scgn+ cells were found in the medulla oblongata (**Figure 4I** and magnification in **Figure 4I1**). Finally we also found the superior colliculus as a Scgn+ area (**Figure 4J**). Larger magnifications of Scgn+ cells in different areas are shown in (**Figures 4K,E1**).

SECRETAGOGIN AND OTHER CALCIUM BINDING PROTEINS

Coronal sections revealing the hippocampal formation were co-stained for Secretagogin and other known CBPs like Parvalbumin, Calbindin D28k, and Calretinin (**Figure 5**).

The antibodies mostly recognized different cell populations with occasional overlaps like co-expression of Parvalbumin and Secretagogin in interneurons of the CA1-3 regions (**Figures 5A–C**), and Calbindin-Secretagogin co-expression in young, possibly migrating cells (**Figure 5D**). Frequently, patches of Secretagogin-positive cells are in close vicinity of patches of neurons that stain positive for another CPB. This can nicely be shown in the habenula, where large groups of Secretagogin-positive cells are flanked by groups of Calbindin or Calretinin-positive cells (**Figures 5E,F**).

SUBCELLULAR LOCALIZATION OF SECRETAGOGIN

We observed some degree of colocalization of Parvalbumin-positive (inter-)neurons with Secretagogin in rat hippocampus. But cells, that co-expressed Parvalbumin and Secretagogin mostly revealed a different subcellular staining pattern for both proteins (**Figures 5A–C**). While Parvalbumin always stained the soma homogenously, Secretagogin frequently seemed to be accumulated on subcellular structures (**Figure 5C**). In order to visualize the different subcellular distribution we performed a high resolution z-stack with a confocal microscope of a Parvalbumin/Secretagogin-positive cell from a rat brain slice in the CA1 region of the hippocampus and show the three-dimensional reconstruction in a movie (see Movie S1 in Supplementary Material).

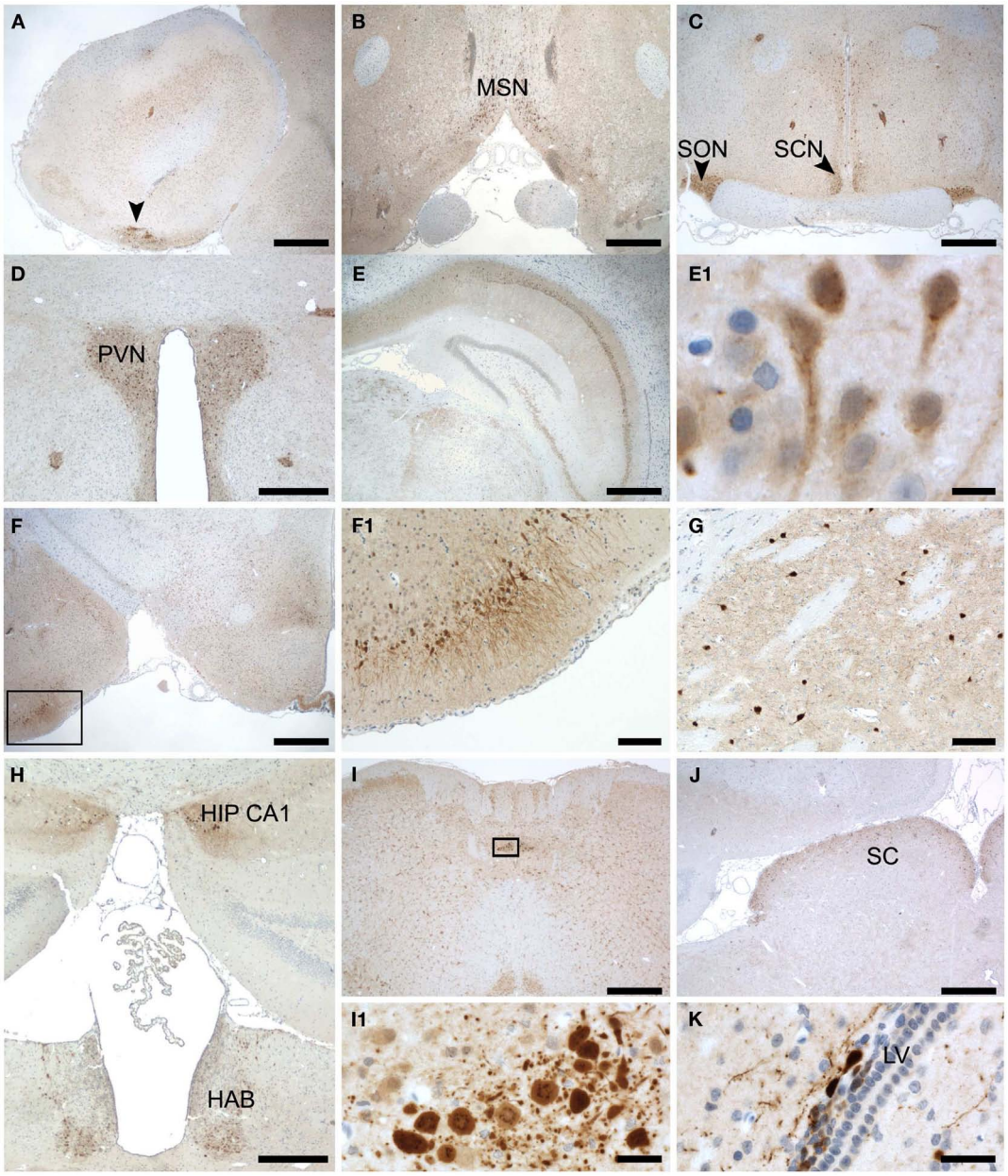

FIGURE 4 | Subregional expression of Secretagogin in rat brain. Representative sections from rat brain were stained for Secretagogin immunoreactivity and counterstained with hematoxylin. Panels represent the following brain areas: **(A)** olfactory bulb, arrow pointing to a patch of strong Scgn+ cells. Scale bar: 500 μm. **(B)** Medial septal nucleus. Scale bar: 500 μm. **(C)** Supraoptic nucleus (SON) and Suprachiasmatic nucleus (SCN). Scale bar: 500 μm. **(D)** Paraventricular nucleus (PVN). Scale bar: 400 μm. **(E)** Hippocampus. Scale bar: 500 μm. **(E1)** Magnification of hippocampal neurons in CA1. Scale bar: 10 μm. **(F)** Lateral amygdaloid nucleus (indicated by box). Scale bar: 500 μm. **(F1)** Magnification of the region indicated in **(F)**. Scale bar: 100 μm. **(G)** Cells in caudate putamen. Scale bar: 100 μm. **(H)** Panel reveals two Scgn+ areas: beginning of hippocampal CA1 region (HIP CA1) and habenula (HAB). Scale bar: 400 μm. **(I)** Medulla oblongata. Scale bar: 500 μm. **(I1)** Magnification of a strongly Scgn+ nucleus in medulla oblongata as indicated in **(I)**. Scale bar: 25 μm. **(J)** Superior colliculus (SC). Scale bar: 500 μm. **(K)** Cells around the lateral ventricle. Scale bar: 25 μm.

To further investigate the structures, that Secretagogin seems to be associated with, we stained for compartmental maker proteins localized in the ER or Golgi apparatus. The marker GM130 is an intracellular peripheral membrane protein associated with the cis-Golgi network and vesicles derived from ER and associated with cis-Golgi. We found, that Secretagogin frequently stained clusters in immediate apposition to GM130 clusters. In contrast, Secretagogin clusters seemed not to be spatially associated with staining for the ER marker GRP78 (**Figure 6**). The close localization of Secretagogin and GM130 is again visualized in a three-dimensional reconstruction based on z-stack imaging (see Movie S2 in Supplementary Material).

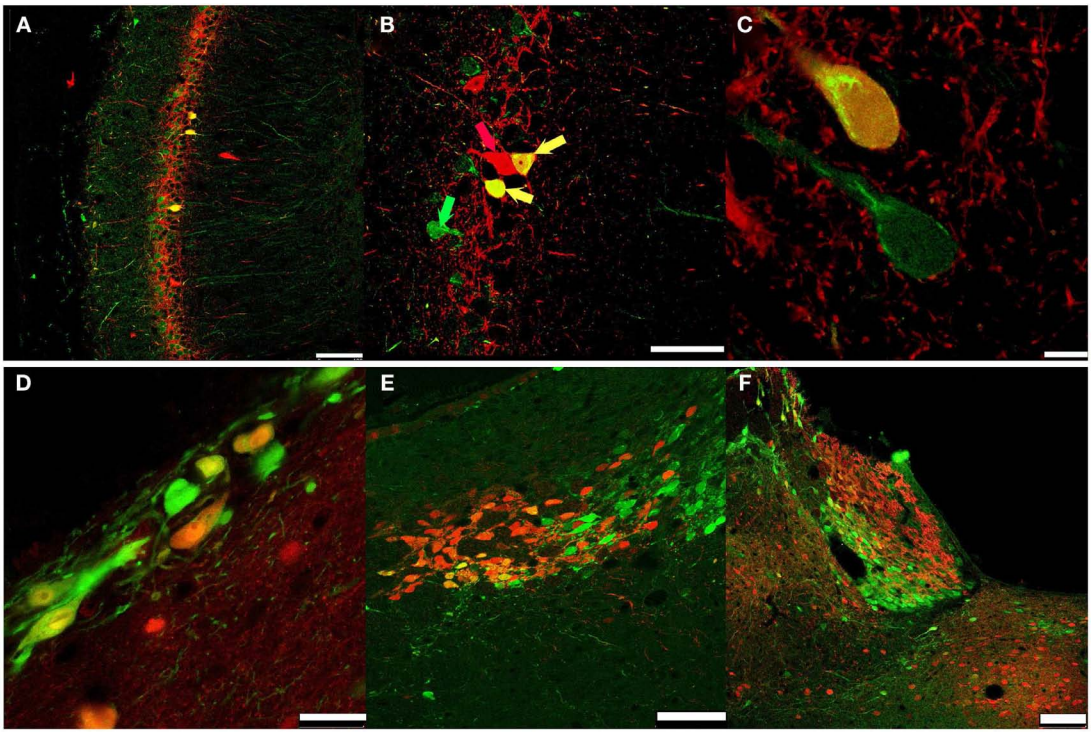

FIGURE 5 | Secretagogin and other CBPs. PFA-fixed rat brain slices were immunostained for Secretagogin (Scgn: green) and other CBPs (red) and processed for immunofluorescence. **(A-C)** Hippocampal CA1 region: Secretagogin (green), Parvalbumin (PV, red). **(A)** Scale bar: 100 μm**. (B)** Arrows indicate co-expression of Scgn and PV; green arrow: Scgn only, red arrow: PV only; yellow arrow: co-expression of Scgn and PV in a single neuron. Scale bar: 50 μm. **(C)** Larger magnification of Scgn/PV co-expressing neurons indicates a distinct subcellular distribution. Scale bar: 7.5 μm. **(D)** Secretagogin-positive neurons near the ventricle. Secretagogin (green), Calbindin D28k (red). Scale bar: 25 μm. **(E)** Habenula: Secretagogin (green), Calbindin D28k (red). Scale bar: 75 μm. **(F)** Habenula: Secretagogin (green), Calretinin (red). Scale bar: 100 μm.

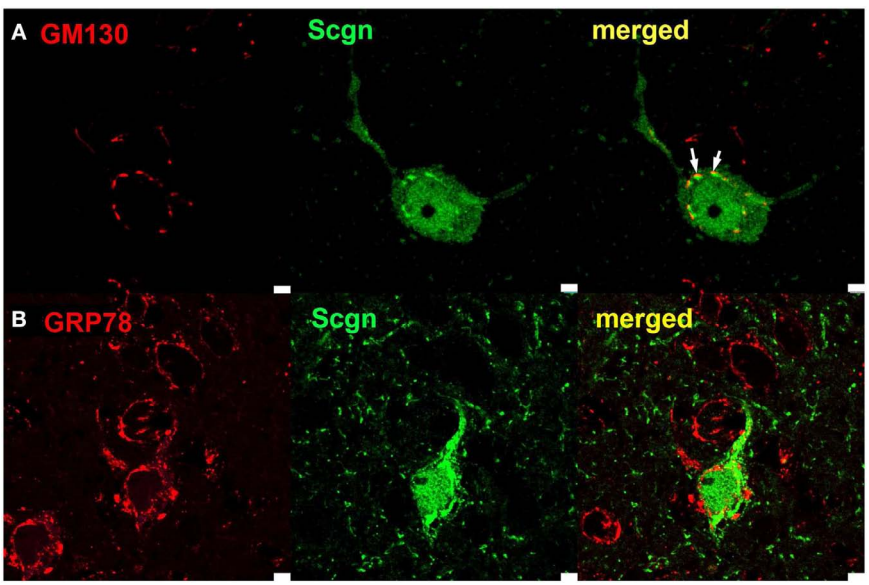

FIGURE 6 | Subcellular localization of Secretagogin. Rat brain slices were processed for immunofluorescence with anti-Secretagogin antibody (green) and antibodies for marker proteins of subcellular compartments (red): **(A)** GM130 (for cis-Golgi compartments) and **(B)** GRP78 (for Endoplasmatic Reticulum). White arrows in upper panel indicate close spatial apposition of Secretagogin clusters and GM130. Scale bar: 10 μm.

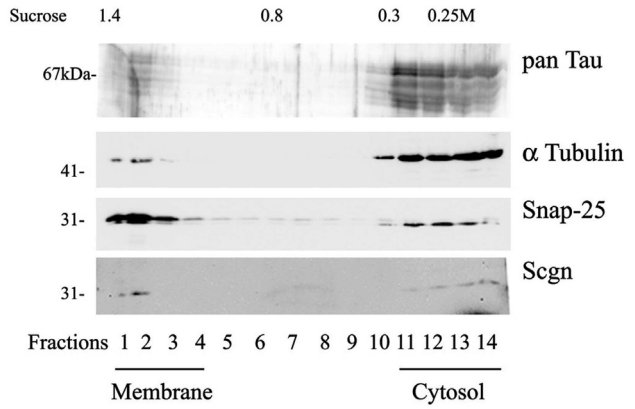

FIGURE 7 | Fractionation of rat hippocampal extract by sucrose density gradient. The fractionation and sampling was done as described in the methods section. Fractions were immunoblotted and proteins detected with antibodies for Tau protein (pan-Tau), alpha-tubulin, synaptic vesicle-associated protein SNAP-25 and Secretagogin. Fractions of high density hold the membrane-associated components and fractions with lower sucrose concentration contain soluble proteins of the cytosol. Calculated sucrose concentrations of collected aliquots are indicated on top of the panel. The experiment was repeated three times with similar results.

We also used sucrose density centrifugation of rat hippocampal tissue extracts to separate membrane-bound proteins from soluble proteins. Secretagogin was found in the membrane-fraction as well as in the cytosolic fraction (**Figure 7**).

SECRETAGOGIN AND TAU PROTEIN

Secretagogin has previously been shown to interact with an isoform of Tau in an insulinoma cell type (Maj et al., 2010). We now investigated, if this interaction is also present in rat brain. We immunoprecipitated Secretagogin from brain extracts and performed a Western blot. The co-precipitation of Tau was confirmed by incubation with a pan-Tau antibody (**Figure 8A**).

The dependence of this interaction on the presence of Ca^{2+} was verified with an *in vitro* pull-down assay. A GST-fusion protein of full-length Secretagogin was incubated with rat brain extracts in the absence or presence of different concentrations of EDTA. Tau protein could only be found to be associated with GST-SCGN in the complete absence of EDTA, indicating the Ca^{2+}-dependence of this interaction (**Figure 8B**).

INSULIN REGULATES SECRETAGOGIN EXPRESSION *IN VITRO*

Insulin is a conventional growth factor for cultured cells. A vast number of publications deals with the roles of insulin in the nervous system affecting neuronal growth, neuroprotection, neurotransmitter release, activation of Ca^{2+} channels, and more (Unger et al., 1991; Zhao and Alkon, 2001). On the other hand, Secretagogin has been discovered and is now well-established as Ca^{2+} sensor in insulin secretion from pancreatic beta cells (Wagner et al., 2000). Interestingly, Secretagogin mRNA transcript levels are significantly higher in a pancreatic tissue obtained from Goto–Kakizaki rats (an animal model for type 2 diabetes) when compared to non-diabetic control Wistar rats (Bazwinsky-Wutschke et al., 2010). On this basis, we aimed to investigate the effects of insulin on the expression of Secretagogin in a rat primary neuronal cell culture.

Hippocampal neurons were grown in standard Neurobasal medium with B-27 supplement (with a basal insulin concentration of 40 pg/ml in the final medium as indicated in the data sheet of the manufacturer). When synaptogenesis was finished, a strong insulin boost (final concentration: 100 μg/ml) or a gentle – but almost complete – insulin deprivation was performed as described in the Section "Materials and Methods."

Insulin deprivation from normal culture medium over 3 days caused a significant decline in Secretagogin gene expression level to as little as 20% of control levels already on the first day after feeding with insulin-free Neurobasal/B-27 medium (**Figure 9A**), whereas a single insulin boost caused a steady highly significant increase in its expression levels after 24 h (**Figure 9B**). In addition, we measured the mRNA level of other proteins similarly involved in exocytosis processes, such as SNAP-25 and synaptotagmin-1. These levels were also significantly increased by the insulin boost (not shown). All measurements were related to housekeeping genes.

As insulin is a major control factor of the energy status, we also checked if addition of a high glucose concentration to the medium has an effect on Secretagogin gene expression level. We expected that the effect of glucose would be rather fast, as it is readily taken up by cells via transporters and metabolized quite fast. One hour after the addition of glucose to a final concentration of 50 mM we harvested the cells and determined the expression level of endogenous Secretagogin mRNA, which had significantly declined by 56%. The data from the glucose-boost experiments show that glucose decreases Secretagogin expression (**Figure 9C**).

DISCUSSION

In the present study we report novel immunocytochemistry and functional data of the CBP Secretagogin in the context of neuronal cells. Secretagogin has been shown to be involved in insulin release from pancreatic beta cells, but it is also highly expressed in neurons – another type of excitable cells. Studies in flies have revealed that the pancreatic islet has evolutionarily developed from an ancestral insulin-producing neuron (Rulifson et al., 2002; Craft and Watson, 2004). The intrinsic properties of the protein might be similar in different locations, but the functional aspects most probably have evolved independently in the endocrine and nervous system. A large number of CBPs exist with different molecular properties. Some CBPs have been used as markers for neuronal cell types especially to group the enormous heterogeneity of cells in the nervous system before other measurable characteristics like unambiguous morphologies or firing patterns became accessible. More recently, those CBPs received focused attention with regard to their individual functional properties. Their very limited co-localization indicates, that different cell types might tune the expression according to their needs based on the molecular properties of the CBPs.

Secretagogin belongs to a family of hexa EF-hand CBPs and is capable of binding four Ca^{2+} ions at physiological intracellular Ca^{2+} levels with a binding affinity of Ca^{2+} similar to

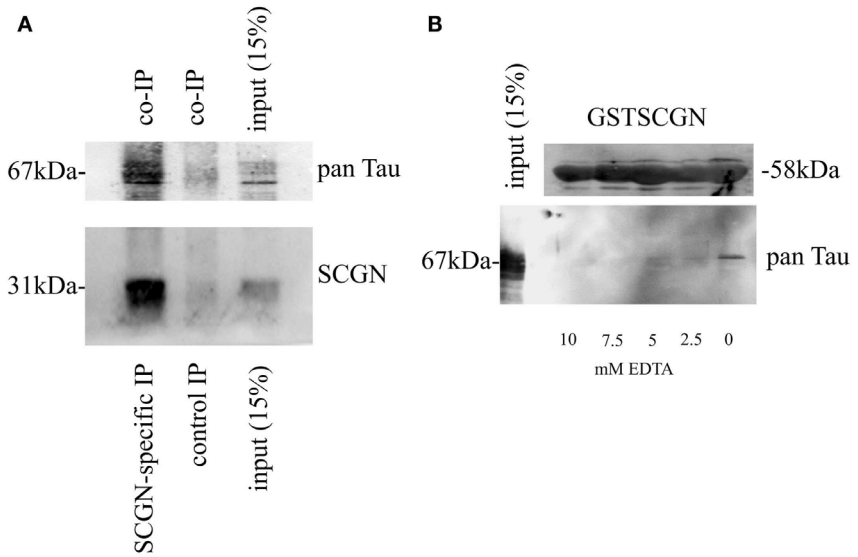

FIGURE 8 | Calcium-dependent association of Secretagogin with Tau protein. (A) Immunoprecipitation from brain extracts using anti-Secretagogin antibody followed by immunoblot with pan-Tau antibody (upper panel) and anti-Secretagogin antibody (lower panel). The input-lane contains 15% of the whole extract used for immunoprecipitation. For a negative control an equal amount of an unrelated antibody was used for the immunoprecipitation. **(B)** Pull-down experiment from rat brain using GST-SCGN fusion protein in the presence or absence of EDTA. Upper panel: Coomassie staining of GST-SCGN fusion protein, which was used for pull-down assays. Lower panel: Immunoblot with pan-Tau antibody. The input-lane contains 15% of the extract used for individual pull-down experiments. All experiments were repeated at least three times.

other nCBPs (Rogstam et al., 2007). High Secretagogin expression was reported not only in the pancreatic tissue, but also in subpopulations of developing or adult neurons (Gartner et al., 2001; Mulder et al., 2009, 2010). As the expression of Secretagogin is restricted to specialized brain areas, it is especially motivating to research for a context of Secretagogin expression and functional aspects of these neuronal populations in the organism. Intrinsic mechanisms of activation (also with regard to Mg^{2+} as a co-factor), subcellular location, and target protein specificity as investigated also for other CBPs are important parameters in this regard (Rogstam et al., 2007; Schmidt, 2012).

In this study we characterized the distribution of Secretagogin immunoreactivity in rat brain and in specialized areas from human brain. The unique, but distinct Secretagogin expression pattern within human and rodent brain presumably underlines the existence of complex and refined mechanisms of Ca^{2+} signaling. This goes hand in hand with the expression of neuronal insulin and insulin receptors. Apart from entering the CNS via the blood-brain barrier by a receptor-mediated transport process, insulin expression is also found directly from cells of the CNS. In rodents insulin binding is especially high in the olfactory bulb, the cerebral cortex, hippocampus, hypothalamus, amygdala, and septum (Baskin et al., 1987). Insulin receptors are also found in the substantia nigra, basal ganglia, and frontal cortex (Unger et al., 1991; Craft and Watson, 2004). By immunohistochemistry we could show a high expression of Secretagogin not only in the olfactory bulb and the hippocampal pyramidal cell layer, but also in the basal ganglia, and with extreme density in major nuclei of the hypothalamus (in the neurosecretory neurons of the supraoptical nucleus, the suprachiasmatic nucleus controlling circadian rhythms, and the paraventricular nucleus involved in the control of food-intake), the habenula, the amygdala, the medulla oblongata, and the superior colliculus. Many neurons in the hypothalamus release peptide hormones like oxytocin, vasopressin, vasoactive intestinal peptide, anti-diuretic hormone, and others that are released into the blood as well or act directly within the brain on receptors on the surface of other neurons. Many of these areas have some functional similarities and are interconnected. In analogy to insulin-releasing pancreatic beta cells, a role of Secretagogin in neuronal hormone-release or glucose metabolism can be hypothetically anticipated. The habenula is a phylogenetically old area receiving input from the limbic system, the pineal gland, and the basal ganglia. The habenula is thought to play a part in many basic processes. It is a relay area for olfactory stimuli and is thought to be involved in processing of external stress, decision-making, and also sleep (Hikosaka, 2010). The habenula seems to be especially activated during experiences that are associated with unpleasant events, the absence or opposite of reward, and even punishment. In rat models of depression the glucose metabolism in the lateral habenula has been shown to be elevated. Secretagogin knock-out mice would be an extremely interesting model system for investigating the role of this CPB in more complex brain-body functions.

In relation to other CBPs, we observed only a restricted overlap of Secretagogin with Parvalbumin and Calbindin D28k in some areas. Even in cells expressing Secretagogin together with another CBP, the time course of expression or the subcellular localization might be different in development, different phases of brain activity or metabolic states. A role of Secretagogin in developing or not

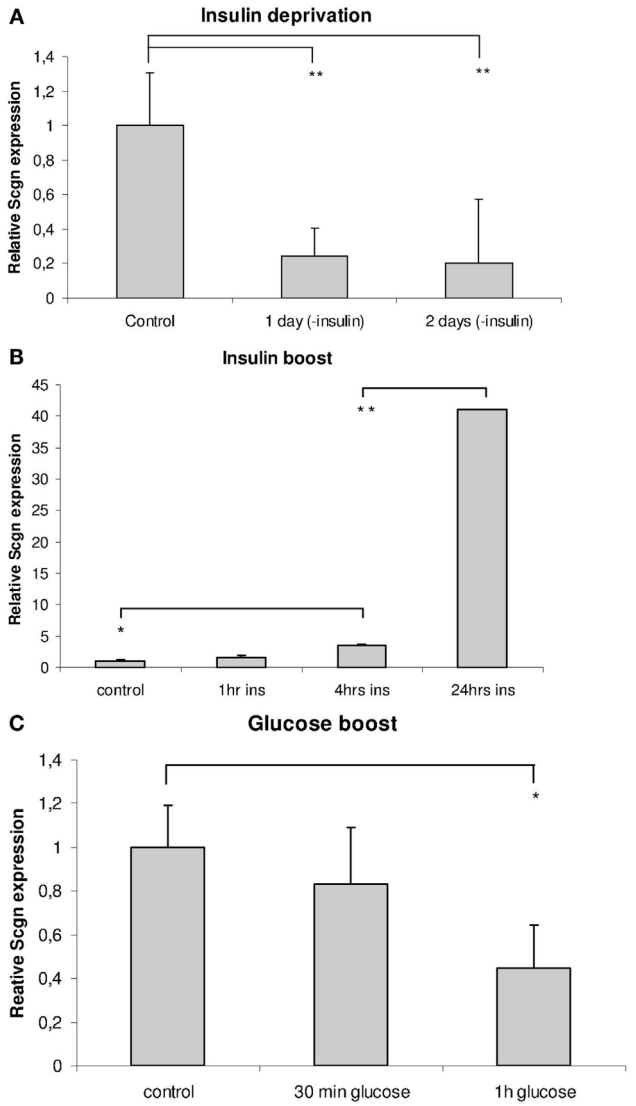

FIGURE 9 | Insulin and glucose regulate Secretagogin expression in neuronal cell culture. Hippocampal neurons in culture were subjected to insulin deprivation or challenged with an insulin- or glucose-boost and analyzed for Secretagogin expression at 21 DIV. Relative amounts of Secretagogin mRNA were determined by RT-qPCR after insulin deprivation **(A)**, insulin boost **(B)**, and glucose boost **(C)** at different time points after treatment ($n = 3$).

terminally differentiated neurons has been proposed and shown previously in some areas like the olfactory bulb (Mulder et al., 2009, 2010). In our studies we also observed Secretagogin-positive neurons, that are probably not terminally differentiated in areas known to contain migrating neurons (as shown in **Figure 4K**) and sometimes also in areas with few other neuronal cell bodies like the corpus callosum (not shown). We think, that this issue needs a detailed study on its own. It might be possible, that neurons also switch the expression of their CBPs in the course of development.

In mature neurons of the CA1 pyramidal cell layer a compartmental association of Secretagogin could be observed in rat brain slices. Secretagogin does neither possess a classical signal peptidase cleavage site that would be a sign for targeting to the ER nor a consensus site for myristoylation for membrane attachment like in many other CBPs. However, we could show a direct opposition of strong Secretagogin and GM130 immunoreactivity indicating an association with cis-Golgi vesicles or compartments. The exact identification of these compartments and the form of interaction needs further investigations.

It is accepted knowledge that Ca^{2+} homeostasis is shifted during normal aging and is especially disturbed in many neurodegenerative disorders. Thus the intimate connection between intracellular Ca^{2+} levels and diseases of the CNS reinforces the importance of maintaining the delicate balance of Ca^{2+} levels within the brain, and the important role of CBPs in this matter. Of special interest with regard to Alzheimer's disease further studies on the Secretagogin-Tau interaction *in vitro* should not be neglected. A neuroprotective role of Secretagogin in the human hippocampus has been previously suggested, as Secretagogin expressing neurons have been shown to be free of the pathological hyperphosphorylated form of Tau in AD brains (Attems et al., 2008). In particular the Secretagogin expression level in human hippocampus from AD patients versus healthy individuals seems to remain unchanged for longer periods of the developing illness, implying that these neurons might be more resistant to pathological deregulation and cell death (Attems et al., 2008). A causal link between Secretagogin expression and neuroprotection has not been shown. But also, if this hypothesis holds true, a contribution of other factors might as well play a significant role. Unpublished observations indicated that Secretagogin seems to be upregulated in cells close to amyloid plaques what can be interpreted as a protective adaptation with the aim of regeneration. This promising hints have led to further studies on the communication between Secretagogin and Tau using transgenic animals (Attems et al., 2011). The (P301L) Tau transgenic mice are a model system for the Tau-pathological aspects in AD in the absence of Aβ plaques. Interestingly, overexpression of this mutant (pathological form of) Tau protein significantly reduced Secretagogin expression in the brains of these mice.

As Secretagogin has been shown to be involved in insulin release from pancreatic cells, a possible link between Secretagogin and insulin in the brain can be imagined. Insulin together with insulin growth factor-1 (IGF-1) belongs to the main growth factors *in situ*, and therefore it is also added to the medium for neuronal cell culturing *in vitro*. The downstream signaling cascades are relatively well known. On the other hand, Secretagogin not only influences insulin synthesis in and secretion from endocrine cells, but it might also play a role in energy household and metabolism. Here we show that Secretagogin expression is increased in response to insulin *in vitro* supporting the idea that levels of Secretagogin could be regulated by circulating insulin or via different factors influencing insulin signaling pathways in the brain under normal and pathological conditions.

In this study we provide new insights into the expression patterns of Secretagogin in rodent's (rat) brain that should help to formulate new hypotheses concerning the role of this CBP in the

nervous system. Neuronal cell culture systems have meanwhile undergone further technical advancement and protocols are available for many more cell types of the CNS compared to the recent past. These primary neurons *in vitro* can be simple model systems to study the cellular functions and dynamics of Secretagogin. A high translational relevance of further knowledge on this protein is already apparent.

ACKNOWLEDGMENTS

M. Maj has been supported by the "Jubiläumsfonds der Österreichischen National bank," Austria (Grant Nr 13402). We thank Drs. Balint Lasztoci, Milos Vasiljevic, and Marco Treven for helpful discussions, Mirnes Bajric, Daniel Maurer, Marianne Leißer, Ulrike Köck, Sabine Thomas, and Irene Leisser for excellent assistance with cultures and immunohistochemistry. We thank Prof. Werner Sieghart for providing access to facilities and support.

SUPPLEMENTARY MATERIAL

The Supplementary Material for this article can be found online at http://www.frontiersin.org/Molecular_Neuroscience/10.3389/fnmol.2012.00084/abstract

Movie S1 | Three-dimensional reconstruction of a hippocampal interneuron co-expressing Parvalbumin and Secretagogin. Rat brain slices were immunostained for Secretagogin (green) and Parvalbumin (red). Z-stacks were taken on a Leica confocal microscope from a Parvalbumin-positive interneuron in the CA1 region of the hippocampus co-expressing Secretagogin. The different subcellular distribution of both CBPs becomes clearly visible.

Movie S2 | Subcellular association of Secretagogin with cis-Golgi marker GM130. Rat brain slices were immunostained for Secretagogin (green) and GM130 (red). Z-stacks were taken on a Leica confocal microscope and recombined in a three-dimensional reconstruction of the cell. A non-random spatial proximity of compartment- or subcellular structure-associated Secretagogin and GM130 becomes evident.

REFERENCES

Adolf, K., Wagner, L., Bergh, A., Stattin, P., Ottosen, P., Borre, M., Birkenkamp-Demtroder, K., Orntoft, T. F., and Torring, N. (2007). Secretagogin is a new neuroendocrine marker in the human prostate. *Prostate* 67, 472–484.

Attems, J., Ittner, A., Jellinger, K., Nitsch, R. M., Maj, M., Wagner, L., Gotz, J., and Heikenwalder, M. (2011). Reduced secretagogin expression in the hippocampus of P301L tau transgenic mice. *J. Neural Transm.* 118, 737–745.

Attems, J., and Jellinger, K. A. (2006). Olfactory tau pathology in Alzheimer disease and mild cognitive impairment. *Clin. Neuropathol.* 25, 265–271.

Attems, J., Preusser, M., Grosinger-Quass, M., Wagner, L., Lintner, F., and Jellinger, K. (2008). Calcium-binding protein secretagogin-expressing neurones in the human hippocampus are largely resistant to neurodegeneration in Alzheimer's disease. *Neuropathol. Appl. Neurobiol.* 34, 23–32.

Attems, J., Quass, M., Gartner, W., Nabokikh, A., Wagner, L., Steurer, S., Arbes, S., Lintner, F., and Jellinger, K. (2007). Immunoreactivity of calcium binding protein secretagogin in the human hippocampus is restricted to pyramidal neurons. *Exp. Gerontol.* 42, 215–222.

Baskin, D. G., Figlewicz, D. P., Woods, S. C., Porte, D. Jr., and Dorsa, D. M. (1987). Insulin in the brain. *Annu. Rev. Physiol.* 49, 335–347.

Bauer, M., Maj, M., Wagner, L., Cahill, D. J., Linse, S., and O'Connell, D. J. (2011a). Protein networks involved in vesicle fusion, transport, and storage revealed by array-based proteomics. *Methods Mol. Biol.* 781, 47–58.

Bauer, M. C., O'Connell, D. J., Maj, M., Wagner, L., Cahill, D. J., and Linse, S. (2011b). Identification of a high-affinity network of secretagogin-binding proteins involved in vesicle secretion. *Mol. Biosyst.* 7, 2196–2204.

Bazwinsky-Wutschke, I., Wolgast, S., Muhlbauer, E., and Peschke, E. (2010). Distribution patterns of calcium-binding proteins in pancreatic tissue of non-diabetic as well as type 2 diabetic rats and in rat insulinoma beta-cells (INS-1). *Histochem. Cell Biol.* 134, 115–127.

Bitto, E., Bingman, C. A., Bittova, L., Frederick, R. O., Fox, B. G., and Phillips, G. N. Jr. (2009). X-ray structure of *Danio rerio* secretagogin: a hexa-EF-hand calcium sensor. *Proteins* 76, 477–483.

Braunewell, K. H. (2005). The darker side of Ca2+ signaling by neuronal Ca2+-sensor proteins: from Alzheimer's disease to cancer. *Trends Pharmacol. Sci.* 26, 345–351.

Brewer, G. J., Torricelli, J. R., Evege, E. K., and Price, P. J. (1993). Optimized survival of hippocampal neurons in B27-supplemented Neurobasal, a new serum-free medium combination. *J. Neurosci. Res.* 35, 567–576.

Burgoyne, R. D., and Haynes, L. P. (2012). Understanding the physiological roles of the neuronal calcium sensor proteins. *Mol. Brain* 5, 2.

Camandola, S., and Mattson, M. P. (2011). Aberrant subcellular neuronal calcium regulation in aging and Alzheimer's disease. *Biochim. Biophys. Acta* 1813, 965–973.

Craft, S., and Watson, G. S. (2004). Insulin and neurodegenerative disease: shared and specific mechanisms. *Lancet Neurol.* 3, 169–178.

Demuro, A., Parker, I., and Stutzmann, G. E. (2010). Calcium signaling and amyloid toxicity in Alzheimer disease. *J. Biol. Chem.* 285, 12463–12468.

Dityatev, A., and Rusakov, D. A. (2011). Molecular signals of plasticity at the tetrapartite synapse. *Curr. Opin. Neurobiol.* 21, 353–359.

Gartner, W., Lang, W., Leutmetzer, F., Domanovits, H., Waldhausl, W., and Wagner, L. (2001). Cerebral expression and serum detectability of secretagogin, a recently cloned EF-hand Ca(2+)-binding protein. *Cereb. Cortex* 11, 1161–1169.

Gartner, W., Vila, G., Daneva, T., Nabokikh, A., Koc-Saral, F., Ilhan, A., Majdic, O., Luger, A., and Wagner, L. (2007). New functional aspects of the neuroendocrine marker secretagogin based on the characterization of its rat homolog. *Am. J. Physiol. Metab.* 293, E347–E354.

Hermes, M., Eichhoff, G., and Garaschuk, O. (2010). Intracellular calcium signalling in Alzheimer's disease. *J. Cell. Mol. Med.* 14, 30–41.

Hikosaka, O. (2010). The habenula: from stress evasion to value-based decision-making. *Nat. Rev. Neurosci.* 11, 503–513.

Ilhan, A., Neziri, D., Maj, M., Mazal, P. R., Susani, M., Base, W., Gartner, W., and Wagner, L. (2011). Expression of secretagogin in clear-cell renal cell carcinomas is associated with a high metastasis rate. *Hum. Pathol.* 42, 641–648.

Klausberger, T., Magill, P. J., Marton, L. F., Roberts, J. D., Cobden, P. M., Buzsaki, G., and Somogyi, P. (2003). Brain-state- and cell-type-specific firing of hippocampal interneurons in vivo. *Nature* 421, 844–848.

Lai, M., Lu, B., Xing, X., Xu, E., Ren, G., and Huang, Q. (2006). Secretagogin, a novel neuroendocrine marker, has a distinct expression pattern from chromogranin A. *Virchows Arch.* 449, 402–409.

Maj, M., Gartner, W., Ilhan, A., Neziri, D., Attems, J., and Wagner, L. (2010). Expression of TAU in insulin-secreting cells and its interaction with the calcium-binding protein secretagogin. *J. Endocrinol.* 205, 25–36.

Mikhaylova, M., Hradsky, J., and Kreutz, M. R. (2011). Between promiscuity and specificity: novel roles of EF-hand calcium sensors in neuronal Ca2+ signalling. *J. Neurochem.* 118, 695–713.

Mulder, J., Spence, L., Tortoriello, G., Dinieri, J. A., Uhlen, M., Shui, B., Kotlikoff, M. I., Yanagawa, Y., Aujard, F., Hokfelt, T., Hurd, Y. L., and Harkany, T. (2010). Secretagogin is a Ca2+-binding protein identifying prospective extended amygdala neurons in the developing mammalian telencephalon. *Eur. J. Neurosci.* 31, 2166–2177.

Mulder, J., Zilberter, M., Spence, L., Tortoriello, G., Uhlen, M., Yanagawa, Y., Aujard, F., Hokfelt, T., and Harkany, T. (2009). Secretagogin is a Ca2+-binding protein specifying subpopulations of telencephalic neurons. *Proc. Natl. Acad. Sci. U.S.A.* 106, 22492–22497.

Niggli, E., and Shirokova, N. (2007). A guide to sparkology: the taxonomy of elementary cellular Ca2+ signaling events. *Cell Calcium* 42, 379–387.

Rogstam, A., Linse, S., Lindqvist, A., James, P., Wagner, L., and Berggard, T. (2007). Binding of calcium ions and SNAP-25 to the hexa EF-hand protein secretagogin. *Biochem. J.* 401, 353–363.

Rulifson, E. J., Kim, S. K., and Nusse, R. (2002). Ablation of insulin-producing neurons in flies: growth and diabetic phenotypes. *Science* 296, 1118–1120.

Schmidt, H. (2012). Three functional facets of calbindin D-28k. *Front. Mol. Neurosci.* 5:25. doi:10.3389/fnmol.2012.00025

Schwaller, B. (2009). The continuing disappearance of "pure" Ca2+ buffers. *Cell. Mol. Life Sci.* 66, 275–300.

Skovhus, K. V., Bergholdt, R., Erichsen, C., Sparre, T., Nerup, J., Karlsen, A. E., and Pociot, F. (2006). Identification and characterization of secretagogin promoter activity. *Scand. J. Immunol.* 64, 639–645.

Steiner, J., Bogerts, B., Schroeter, M. L., and Bernstein, H. G. (2011). S100B protein in neurodegenerative disorders. *Clin. Chem. Lab. Med.* 49, 409–424.

Unger, J. W., Livingston, J. N., and Moss, A. M. (1991). Insulin receptors in the central nervous system: localization, signalling mechanisms and functional aspects. *Prog. Neurobiol.* 36, 343–362.

Vasiljevic, M., Heisler, F. F., Hausrat, T. J., Fehr, S., Milenkovic, I., Kneussel, M., and Sieghart, W. (2011). Spatiotemporal expression analysis of the calcium-binding protein calumenin in the rodent brain. *Neuroscience* 202, 29–41.

Wagner, L., Oliyarnyk, O., Gartner, W., Nowotny, P., Groeger, M., Kaserer, K., Waldhausl, W., and Pasternack, M. S. (2000). Cloning and expression of secretagogin, a novel neuroendocrine- and pancreatic islet of Langerhans-specific Ca2+-binding protein. *J. Biol. Chem.* 275, 24740–24751.

Yanez, M., Gil-Longo, J., and Campos-Toimil, M. (2012). Calcium binding proteins. *Adv. Exp. Med. Biol.* 740, 461–482.

Yu, J. T., Chang, R. C., and Tan, L. (2009). Calcium dysregulation in Alzheimer's disease: from mechanisms to therapeutic opportunities. *Prog. Neurobiol.* 89, 240–255.

Zhao, W. Q., and Alkon, D. L. (2001). Role of insulin and insulin receptor in learning and memory. *Mol. Cell. Endocrinol.* 177, 125–134.

Zurek, J., and Fedora, M. (2012). The usefulness of S100B, NSE, GFAP, NF-H, secretagogin and Hsp70 as a predictive biomarker of outcome in children with traumatic brain injury. *Acta Neurochir. (Wien)* 154, 93–103.

Conflict of Interest Statement: The authors declare that the research was conducted in the absence of any commercial or financial relationships that could be construed as a potential conflict of interest.

Received: 31 January 2012; accepted: 17 July 2012; published online: 06 August 2012.

*Citation: Maj M, Milenkovic I, Bauer J, Berggård T, Veit M, Ilhan-Mutlu A, Wagner L and Tretter V (2012) Novel insights into the distribution and functional aspects of the calcium binding protein Secretagogin from studies on rat brain and primary neuronal cell culture. Front. Mol. Neurosci. **5**:84. doi: 10.3389/fnmol.2012.00084*

Advantages of publishing in Frontiers

OPEN ACCESS
Articles are free to read, for greatest visibility

COLLABORATIVE PEER-REVIEW
Designed to be rigorous – yet also collaborative, fair and constructive

FAST PUBLICATION
Average 85 days from submission to publication (across all journals)

COPYRIGHT TO AUTHORS
No limit to article distribution and re-use

TRANSPARENT
Editors and reviewers acknowledged by name on published articles

SUPPORT
By our Swiss-based editorial team

IMPACT METRICS
Advanced metrics track your article's impact

GLOBAL SPREAD
5'100'000+ monthly article views and downloads

LOOP RESEARCH NETWORK
Our network increases readership for your article

Frontiers
EPFL Innovation Park, Building I • 1015 Lausanne • Switzerland
Tel +41 21 510 17 00 • Fax +41 21 510 17 01 • info@frontiersin.org
www.frontiersin.org

Find us on